

Sustainable Civil Infrastructures

Leslie Struble  
Gabriele Tebaldi *Editors*

# Materials for Sustainable Infrastructure

Proceedings of the 1st GeoMEast  
International Congress and Exhibition,  
Egypt 2017 on Sustainable  
Civil Infrastructures



 Springer

# **Sustainable Civil Infrastructures**

## **Editor-in-chief**

Hany Farouk Shehata, Cairo, Egypt

## **Advisory Board**

Dar-Hao Chen, Texas, USA

Khalid M. El-Zahaby, Giza, Egypt



### *About this Series*

Sustainable Infrastructure impacts our well-being and day-to-day lives. The infrastructures we are building today will shape our lives tomorrow. The complex and diverse nature of the impacts due to weather extremes on transportation and civil infrastructures can be seen in our roadways, bridges, and buildings. Extreme summer temperatures, droughts, flash floods, and rising numbers of freeze-thaw cycles pose challenges for civil infrastructure and can endanger public safety. We constantly hear how civil infrastructures need constant attention, preservation, and upgrading. Such improvements and developments would obviously benefit from our desired book series that provide sustainable engineering materials and designs. The economic impact is huge and much research has been conducted worldwide. The future holds many opportunities, not only for researchers in a given country, but also for the worldwide field engineers who apply and implement these technologies. We believe that no approach can succeed if it does not unite the efforts of various engineering disciplines from all over the world under one umbrella to offer a beacon of modern solutions to the global infrastructure. Experts from the various engineering disciplines around the globe will participate in this series, including: Geotechnical, Geological, Geoscience, Petroleum, Structural, Transportation, Bridge, Infrastructure, Energy, Architectural, Chemical and Materials, and other related Engineering disciplines.

More information about this series at <http://www.springer.com/series/15140>

Leslie Struble · Gabriele Tebaldi  
Editors

# Materials for Sustainable Infrastructure

Proceedings of the 1st GeoMEast International  
Congress and Exhibition, Egypt 2017  
on Sustainable Civil Infrastructures



*Editors*

Leslie Struble  
University of Illinois at Urbana-Champaign  
Urbana-Champaign, IL  
USA

Gabriele Tebaldi  
Department of Civil and Environmental  
Engineering and Architecture  
University of Parma  
Parma  
Italy

ISSN 2366-3405

Sustainable Civil Infrastructures

ISBN 978-3-319-61632-2

DOI 10.1007/978-3-319-61633-9

ISSN 2366-3413 (electronic)

ISBN 978-3-319-61633-9 (eBook)

Library of Congress Control Number: 2017946467

© Springer International Publishing AG 2018

This work is subject to copyright. All rights are reserved by the Publisher, whether the whole or part of the material is concerned, specifically the rights of translation, reprinting, reuse of illustrations, recitation, broadcasting, reproduction on microfilms or in any other physical way, and transmission or information storage and retrieval, electronic adaptation, computer software, or by similar or dissimilar methodology now known or hereafter developed.

The use of general descriptive names, registered names, trademarks, service marks, etc. in this publication does not imply, even in the absence of a specific statement, that such names are exempt from the relevant protective laws and regulations and therefore free for general use.

The publisher, the authors and the editors are safe to assume that the advice and information in this book are believed to be true and accurate at the date of publication. Neither the publisher nor the authors or the editors give a warranty, express or implied, with respect to the material contained herein or for any errors or omissions that may have been made. The publisher remains neutral with regard to jurisdictional claims in published maps and institutional affiliations.

Printed on acid-free paper

This Springer imprint is published by Springer Nature

The registered company is Springer International Publishing AG

The registered company address is: Gewerbestrasse 11, 6330 Cham, Switzerland

# Preface

Toward building sustainable and longer civil infrastructures, the engineering community around the globe continues undertaking research and development to improve existing design, modeling, and analytical capability. Such initiatives are also the core mission of the Soil-Structure Interaction Group in Egypt (SSIGE) to contribute to the ongoing research toward sustainable infrastructure. This conference series “GeoMEast International Congress and Exhibition” is one of these initiatives.

Ancient peoples built their structures to withstand the test of time. If we think in the same way, our current projects will be a heritage for future generations. In this context, an urgent need has quickly motivated the SSIGE and its friends around the globe to start a new congress series that can bring together researchers and practitioners to pursue “Sustainable Civil Infrastructures.” The GeoMEast 2017 is a unique forum in the Middle East and Africa that transfers from the innovation in research into the practical wisdom to serve directly the practitioners of the industry.

More than eight hundred abstracts were received for the first edition of this conference series “GeoMEast 2017” in response to the Call for Papers. The abstracts were reviewed by the Organizing and Scientific Committees. All papers were reviewed following the same procedure and at the same technical standards of practice of the TRB, ASCE, ICE, ISSMGE, IGS, IAEG, DFI, ISAP, ISCP, ITA, ISHMII, PDCA, IUGS, ICC, and other professional organizations who have supported the technical program of the GeoMEast 2017. All papers received a minimum of two full reviews coordinated by various chairs and supervised by the volume editors through the Editorial Manager of the SUCI “Sustainable Civil Infrastructure” book series. As a result, 15 volumes have been formed of the final +320 accepted papers. The authors of the accepted papers have addressed all the comments of the reviewers to the satisfaction of the chairs, the volume editors, and the proceedings editor. It is hoped that readers of this proceedings of the GeoMEast 2017 will be stimulated and inspired by the wide range of papers written by a distinguished group of national and international authors.

Publication of this quality of technical papers would not have been possible without the dedication and professionalism of the anonymous papers reviewers. The names of these reviewers appear in the acknowledgment that follows. For any additional reviewers whose names were inadvertently missed, we offer our sincere apologies.

We are thankful to Dr. Hany Farouk Shehata, Dr. Nabil Khelifi, Dr. Khalid M. ElZahaby, Dr. Mohamed F. Shehata, and to all the distinguished volume editors of the proceedings of the GeoMEast 2017. Appreciation is extended to the authors and track chairs for their significant contributions. Thanks are also extended to Springer for their coordination and enthusiastic support to this conference. The editors acknowledge the assistance of Ms. Janet Sterritt-Brunner, Mr. Arulmurugan Venkatasalam in the final production of the 15 edited volumes “Proceedings of GeoMEast 2017”.

*The original version of the book was revised:  
For detailed information please see Erratum.  
The erratum to the book is available at  
[https://doi.org/10.1007/978-3-319-61633-9\\_25](https://doi.org/10.1007/978-3-319-61633-9_25)*

# Contents

<b>Evaluation of Non-nuclear Alternatives to Replace the Nuclear Density Gauge During Compaction Quality Control of Unbound Pavement Layers</b> .....	1
Ayman W. Ali, Yusuf Mehta, Manuel Celaya, and Giri Venkateela	
<b>Quantifying the Mechanistic and Economic Impacts of Using Asphalt Rubber Mixtures</b> .....	16
Mena Souliman, Ragaa Abd El-Hakim, Mark Davis, and Lubinda Walubita	
<b>Fuzzy Logic Based Modeling for Pavement Characterization</b> .....	27
Mercado Pérez José Luis and Beltrán Calvo Gloria Inés	
<b>Impact of a Poly-olefin Based Additive on Bitumen and Asphalt Mix Performance</b> .....	46
Jan Valentin, Lucie Benešová, and Tereza Valentová	
<b>Influence of Mix Parameters on Development of Sulfur Modified Bituminous Paving Mixes with Sand</b> .....	65
Subhashree Jena, Mahabir Panda, and Prasanta Kumar Bhuyan	
<b>Effect of Spray Dryer Absorber as Mix Enhancers on HMA Performance</b> .....	80
Clayton Cloutier, Emil G. Bautista, Ahmed F. Faheem, and Konstantin Sobolev	
<b>Impact Load Test on Conventional and Roller Compactor Steel Fiber Reinforced Concrete Pavement</b> .....	96
Zainab A. AL-Kaissi, Ahmed S.D. Al-Ridha, and Rusul Raed Abdull-Hussain	
<b>Study on Mixing Proportion for AC-13C Asphalt Mixture and Construction Control</b> .....	121
Wu Jing and Wu Li	

<b>Study of Radioactive Characteristics of Cement Pastes Blended with GGBFS</b> . . . . .	130
Ahmed S. Ouda	
<b>Optimum Partial Replacement of Cement by Rice Husk Ash and Fly Ash Based on Complete Consumption of Calcium Hydroxide</b> . . . . .	145
Winai Ouypornprasert, Narong Traitruengtatsana, and Kong Kamollertvara	
<b>Freeze-Thaw Durability of Air-Entrained Concrete Incorporating Natural and Recycled Concrete Aggregate Mixtures</b> . . . . .	185
Prabir K. Kolay, Salman Sulaiman, Sanjeev Kumar, and Vijay K. Puri	
<b>Use of Rice Husk Ash (RHA) as a Sustainable Cementitious Material for Concrete Construction</b> . . . . .	197
Mohammad Badrul Ahsan and Zahid Hossain	
<b>Behavior of SCC Incorporating Granulated Blast Furnace Slag and Ground Clay Brick Powders at High Temperatures</b> . . . . .	211
M.H. Seleem, A.A.M. Badawy, S.A. Ahmed, and A.A. Elakhras	
<b>Investigation on the Effect of Anti Stripping Additives on the Moisture Sensitivity of Bituminous Concrete</b> . . . . .	228
A.U. Ravi Shankar, Goutham Sarang, B.M. Lekha, and Calvin Carlton-Carew	
<b>The Strength of Lightly Cemented Power Plant Ash</b> . . . . .	240
Felix N. Okonta, Thabo Falayi, and Roshuma Makhado	
<b>Determination of Indirect Tensile Strength of Bituminous Concrete Mix Prepared Using Stone Dust and Cement as Filler Materials</b> . . . . .	249
Lokesh Gupta and G. Suresh	
<b>Sustainable Application of Quarry Byproducts Mixed with Large Size Unconventional Aggregates for Improved Performance</b> . . . . .	262
Issam Qamhia, Hasan Kazmee, Erol Tutumluer, and Hasan Ozer	
<b>Membrane-Forming Performance and Application of Emulsion Wax Curing Agent (EWCA) for Cement Concrete Curing</b> . . . . .	274
Jian-Bo Yuan, Jia-Liang Yao, Hui-Cong Wang, and Ming-Jie Qu	
<b>Thermoelasticity, Superelasticity and Nanoscale Aspects of Structural Transformations in Shape Memory Alloys</b> . . . . .	287
Osman Adiguzel	
<b>Mechanical Behavior of Hydraulic Concrete to Extreme Service Temperatures: The Influence of the Particle Size</b> . . . . .	294
Kenouza Yamina	



**Thermal Properties of Base-Course Material Containing Recycled Glass Under Dry and Wet Condition** . . . . . 306  
Youness Berraha, Michel Vaillancourt, and Daniel Perraton

**Evaluation of Using Waste Road Construction Materials with Additives in Warm Mix Asphalt** . . . . . 322  
Abdelzaher E.A. Mostafa, Mohamed S. Ouf, and Hala H. Abdel Fatah

**Developing New Design Criteria of Asphalt Pavement Mix Using Nano-Materials and Polymer-Materials** . . . . . 335  
Abdelzaher E.A. Mostafa, Waleed M.F. Tawhed, Mohamed R. Elshahat, and Alaa G. Sherif

**The Application Analysis of Fly Ash in Magnesium Phosphate Cement.** . . . . . 348  
Rui Huang and Xiangxing Kong

**Erratum to: Materials for Sustainable Infrastructure** . . . . . E1  
Leslie Struble and Gabriele Tebaldi

**Author Index.** . . . . . 353

# Evaluation of Non-nuclear Alternatives to Replace the Nuclear Density Gauge During Compaction Quality Control of Unbound Pavement Layers

Ayman W. Ali<sup>1</sup>(✉), Yusuf Mehta<sup>1</sup>, Manuel Celaya<sup>2</sup>,  
and Giri Venkiteela<sup>3</sup>

<sup>1</sup> Center for Research and Education in Advanced Transportation Engineering Systems (CREATEs), Rowan University, Glassboro, NJ, USA  
{alia, mehta}@rowan.edu

<sup>2</sup> Advanced Infrastructure Design (AID), Trenton, NJ, USA  
mcelaya@aidpe.com

<sup>3</sup> NJDOT Bureau of Research, Trenton, NJ, USA  
giri.venkiteela@dot.nj.gov

**Abstract.** Pavement performance is highly dependent on several factors that include: structural adequacy, material properties, traffic loading, and construction quality. The quality of subgrade or base/subbase compaction also significantly affects the performance of pavements; predominantly flexible pavements. In particular, the majority of the distresses in flexible pavements are mainly attributed to the compaction defect in these layers. In current practice, the compaction quality of these layers is usually quantified using the nuclear density gauge (NDG). However, several concerns arise due to the use of the NDG. This study was initiated with the aim of evaluating the sensitivity of the parameters measured using non-nuclear methods/devices to moisture content, compaction effort, testing time after compaction, and aggregate type. To fulfill this objective, a laboratory procedure for compacting large samples was developed. This procedure facilitated testing using three non-nuclear devices: Briaud compaction device (BCD), light weight falling deflectometer (LWD), and dynamic cone penetrometer (DCP). Four types of aggregates, two subgrade soils, one dense graded aggregate, and one recycled concrete aggregates, were selected to comprehensively cover a wide range of subgrade and base/subbase materials. Each device was evaluated for accuracy and repeatability. The sensitivity of the results measured from each device to moisture content, compaction effort applied, and testing time was also evaluated. Based on testing results, it was concluded that the DCP was most sensitive to detecting changes in the measured parameters. In addition, precision of the DCP was similar to other non-nuclear devices.

## 1 Introduction

Naturally existing soil and quarry-produced aggregates play a crucial role in highway infrastructure. These materials are typically used to construct base or subbase layers in rigid and flexible pavements. During the construction of these pavements, it is essential

to properly compact base/subbase and subgrade materials to suitable density levels. This is primarily because the performance of rigid or flexible pavements is highly dependent on the quality of the compacted subgrade and unbound base/subbase layers. In other words, any compaction defects in these layers typically result in distresses in the upper hot mix asphalt (HMA) or Portland cement concrete (PCC) layers.

In practice, highway agencies employ specifications that rely on selecting a specific aggregate type and a minimum density level (e.g., 95% of the Proctor maximum dry density). The density requirement is determined using the nuclear density gauge (NDG) method, which is currently considered the primary tool for measuring density of compacted base/subbase and subgrade layers. As an example, the New Jersey Department of Transportation (NJDOT) currently uses the NDG for assessing the compaction quality for Embankments, Aggregate and Base Courses, and Foundation/Backfill of Structures (New Jersey Department of Transportation 2007). The popularity of the NDG is mainly due to its portability, ease of use, accuracy, and timely results.

Despite the popularity and advantages of the NDG, there are several concerns and safety risks associated with using this device. Strict regulations for using the NDG require specific transportation and storage methods/procedures only appropriate for nuclear devices. These regulations also require having trained licensed personnel to operate the NDG, making the NDG onerous and expensive. In addition, when using the NDG, the operator may be exposed to harmful radiation; thus, the NDG can pose a safety risk. Furthermore, the NDG only measures a density value as opposed to a modulus or design-specific value. From a design perspective, the engineer uses an assumed modulus value for designing pavement structures, while in the field the quality is controlled using a density value. This results in a gap between the mechanistic empirical pavement design stage and the quality control stage during the construction of pavement structures. Therefore, it is highly desirable to evaluate other methods/devices that can replace the NDG and provide design engineers with design-specific measurements that can help in avoiding over/under designed pavements.

In current literature, several studies were conducted to evaluate modulus-based methods as tools for evaluating unbound subgrade and base/subbase pavement layers. For instance, Nazarian et al. (2014) developed a modulus-based construction specification for compaction of earthwork and unbound aggregates. The laboratory and field-testing was conducted on three fine-grained soils, two sandy materials, and two unbound granular base materials at different target moisture contents and densities to determine construction parameters of each geomaterial as well as establish relationships between field and laboratory moduli. Both laboratory and field tests were used to calibrate modulus prediction models developed for the study. Based on the results from the laboratory testing and structural models a draft specification was proposed. The proposed specifications was tested and improved through continuous testing on construction projects.

Lenke et al. (2003) evaluated the potential for using the GeoGauge as an alternative to the NDG for compaction control. According to the researchers, the GeoGauge measures the modulus of compacted layers. Lenke et al. (2003) also reported that the GeoGauge's ability to obtain target values for stiffness in the laboratory was elusive.

This was due to the dynamic nature of the measurements obtained using this device. In addition, Lenke et al. (2003) reported that future specifications for compaction using the GeoGauge may require specific controls of moisture and requirements concerning compaction equipment with stiffness monitoring.

Alshibli et al. (2005) examined the potential for using the light weight falling deflectometer (LWD) and GeoGauge as quality control/quality assurance (Qc/Qa) devices for testing compacted subgrades. These devices along with the static plate load test (PLT) and the dynamic cone penetrometer (DCP) were used to conduct testing on samples compacted in the laboratory. Based on their testing results, it was reported that both the LWD and GeoGauge can be used to determine elastic modulus and stiffness of these compacted layers.

Nazzal et al. (2007) evaluated the LWD for measuring in-situ modulus of pavement layers and subgrade. Nine sections were constructed and tested using the Prima 100 model-LWD. FWD, PLT, and DCP tests were also utilized as reference measurements. The depth influence of the LWD was also examined. In addition, linear regression models were developed to relate LWD modulus with results of the FWD, PLT moduli, and DCP penetration rates. It was concluded that the FWD, PLT, and DCP could predict LWD values within a certain confidence. They also reported that the laboratory results indicated an influence depth between 10.6 in. to 11 in. (270 mm to 280 mm) for the LWD.

Kim et al. (2007) evaluated in-situ modulus of compacted subgrade layers using a portable falling weight deflectometer (PFWD) and PLT tests. Two highway construction site sections were utilized in their study for testing. Based on the results, a reasonable linear correlation between the dynamic deflection modulus and the coefficient of subgrade reaction of well-compacted subgrades was reported. In addition, the dynamic deflection moduli were not significantly affected by variation in the falling energies.

In summary, there is a consensus among researchers that alternative non-nuclear in-situ devices would provide useful parameters for controlling the quality of compacted subgrade and base/subbase layers. However, the majority of literature (e.g., Alshibli et al. 2005; Nazzal et al. (2007); Kim et al. (2007); Abu-Farsakh et al. (2005); Hearth et al. (2005); Chan et al. (2005); Weidinger et al. (2005) mainly focused on using the non-nuclear devices for measuring pavement layers moduli values without regard to the quality of layers compaction. In addition, these studies correlated the non-nuclear devices' results to the plate load test and not the results obtained from the NDG. Furthermore, the studies did not comprehensively evaluate the effect of aggregate type, moisture content, compaction effort, and delayed testing time on the results obtained from these devices. In order to fill this gap, this paper focuses on evaluating these factors on the non-nuclear devices.

## 2 Goal and Objectives

The goal of this paper is to determine the sensitivity of the parameters measured using non-nuclear methods/devices to moisture content, compaction effort, testing time after compaction, and aggregate type. This constitutes a step towards determining the feasibility of the non-nuclear devices as a quality acceptance tool to assess in-situ compaction levels of unbound materials. The specific objectives of this study are summarized as follows:

- Develop a procedure for compacting large and representative samples in the laboratory; and,
- Evaluate the effect of moisture content and compaction effort on results obtained from non-nuclear devices of four soils, two fine graded and two dense graded.

### 3 Materials Description

In this study, four aggregate types were selected to facilitate evaluating the impact of aggregate type on testing results. The selected aggregates included: (1) two subgrade soils: natural sand 1 (NAT-1) and natural sand 2, (NAT-2) and (2) two base/subbase materials: dense graded aggregates (DGA) and recycled concrete aggregates (RCA). The particle size distribution for each aggregate type was determined along with their moisture-density relationships (Proctor test). Figure 1 shows the particle size distribution obtained for NAT-1, NAT-2, DGA, and RCA materials, respectively. From this figure, both subgrade soils were gap-graded while both base/subbase aggregates were well-graded. Testing using the modified proctor test yielded average optimum moisture content (OMC) of 9.7% and maximum dry density (MDD) of 110 lbs./ft.<sup>3</sup> for NAT-1. An OMC of 9.65% and maximum dry density of 120 lbs./ft.<sup>3</sup> was obtained for NAT-2. DGA material had an average of 8.7% OMC achieving a maximum dry density of 125 lbs./ft.<sup>3</sup>. The RCA had an OMC of 10.7% and maximum dry density of 138 lbs./ft.<sup>3</sup>

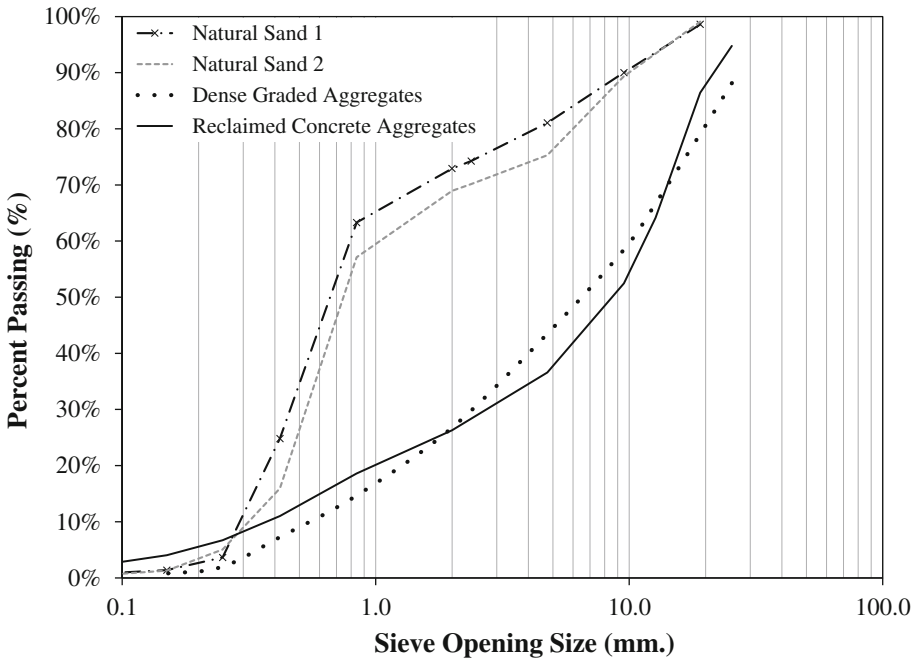


Fig. 1. Particle size distributions obtained for selected aggregates

## 4 Selected Non-nuclear Methods/Devices

Three non-nuclear devices were selected for evaluation in this study. These non-nuclear devices included: (1) Briaud compaction device (BCD), (2) light weight falling deflectometer (LWD), and (3) dynamic cone penetrometer (DCP). A brief description of these devices is provided in the following subsections.

### 4.1 Briaud Compaction Device (BCD)

The BCD is a tool that measures the modulus of compacted aggregate layers. To operate the device it is first placed on top of the tested layer. The operator then gradually applies a load of 50-lbs magnitude onto the device. A 6-in. diameter plate at the bottom of the device is retrofitted with radial and axial strain gauges that measure the plate's deformation as the load is applied. According to the device manufacturer it is recommended that four measurements be taken 90° apart at one testing location for a better reading (Briaud et al. 2009). The collected measurements are then automatically stored for retrieval at a later time.

### 4.2 Light Weight Falling Deflectometer (LWD)

The LWD is another device that measures the modulus of compacted aggregate layers. Similar to the BCD, this device is first placed on top of the layer being tested. A standard weight of 22-lbs is then dropped freely onto a bearing plate from a specified height (2.3 ft.). The operation of the test applies three seating load drops followed by three deflection measuring loads. The 7.8 in. bearing plate contains geophone sensors that measure the aggregate layer's deflections from the impact of the falling weight. The device automatically outputs and stores the measured deflection values and estimated layer modulus value. In this study, the LWD was selected due to its portability, ease of use, timely collected modulus/deflection results Nazzal et al. (2007).

### 4.3 Dynamic Cone Penetrometer (DCP)

The DCP is the third device evaluated in this study. It is operated by first placing the tip of a pushing rod on top of the testing location. A standard hammer weight of 17.6 lbs. is then dropped from a height of 22.6 in. and the number of hammer blows and depth of soil penetrated is recorded. The DCP results are usually normalized with penetration depth. Therefore, it can be hypothesized that the higher number of blows required to penetrate 1 in. of soil the better is the compaction applied Abu-Farsakh et al. (2005). The DCP utilized in this study was retrofitted with an automatic ruler that recorded and stored penetrated depth and number of blows applied.

## **5 Laboratory Compaction Procedure**

In order to evaluate the three selected non-nuclear devices and the NDG, a procedure for compacting large aggregate samples in the laboratory was developed. This compaction procedure was necessary in order to compare/correlate the results obtained using the non-nuclear devices and the NDG while simulating field compaction. The Proctor moisture-density relationships obtained for each aggregate type were utilized to compact samples at different dry densities when changing the moisture content. This was essential for evaluating the effect of the aggregate's moisture content on collected results. A detailed description of the laboratory sample compaction procedure implemented is presented in the following step-by-step structure:

### **5.1 Step 1: Drying of Material Below Targeted Values**

This step involved placing the aggregates on an open floor in the laboratory for air-drying under ambient temperature for a week prior to compaction. During this week, the aggregate were raked frequently to ensure uniform drying. The quantity of aggregates placed at one time for compacting two samples was approximately 1,000 lbs. It is worth mentioning that this step was conducted to ensure that the present moisture content in the aggregates was lower than the targeted moisture content and not to completely dry the aggregates.

### **5.2 Step 2: Determine Moisture Content**

On the day of compaction, five to six samples were collected from the air-dried aggregates. The weight of the wet aggregate in each sample was determined and the samples were dried in an oven preheated to 300 °F, for about 1 h. After drying, an average moisture content was calculated and used in determining the amount of water needed to reach the targeted aggregate moisture content. As an example, if the present moisture content in the aggregates was 2% and the targeted moisture content was 8%, an amount of 6 lbs. of water was needed for every 100 lbs. of aggregates in order to reach 8% moisture content.

### **5.3 Step 3: Mix Water to Reach Targeted Moisture Content**

In this step, the quantity of water needed to reach the targeted moisture content was mixed with the aggregates using a concrete mixer for 5 min to ensure a uniform water distribution within the aggregates. Moisture samples were collected after completing the mixing process to confirm that the targeted moisture content was reached. The targeted moisture contents were varied depending on the specific objective of the compaction. More details can be found in the testing plan section.

#### **5.4 Step 4: Compact Aggregates**

The compaction process involved placing the moist aggregates into a large aluminum mold having a length of 24 in., a width of 17 in., and a depth of 12 in. The aggregates were placed in three consecutive 4-inch thick lifts. For each lift a specific amount of aggregates was placed as determined through the aggregate Proctor moisture-density relationship and mold/lift dimensions and the moisture content being targeted. For instance, if the OMC was the targeted value, the Proctor MDD was utilized in computing the required weight per lift using the well-known density-mass-volume relationship. This procedure for determining the lift weight was implemented for the samples prepared with the objective of evaluating the impact of moisture content on testing results. However, for the case of samples prepared for evaluating the effect of various compaction efforts, density values significantly higher/lower than the MDD were used in computing the required lift weight.

Once the required lift weight was placed into the mold, either a manual steel tamper or a jackhammer was used to compact the aggregates. When the aggregates reached a thickness of 4 in. the compaction process was deemed to be complete. This process was repeated until the entire 12-inch thick mold was filled with aggregates.

#### **5.5 Step 5: Verify Quality of Compaction**

The quality of the compaction procedure was verified using the data collected throughout the compaction process. As mentioned previously, moisture samples were collected after mixing the aggregates with water in the mixer (Step 3). These samples were used to verify whether the targeted moisture content was reached after mixing. In addition, density testing using the NDG was also conducted (after compaction was completed) to ensure the desired density was achieved. This was completed by comparing the NDG density values to those computed using the three lifts weights and mold volume. The actual moisture contents collected for the compacted samples were within  $\pm 0.5\%$  of the targeted moisture content. The actual density values, as measured using the NDG, were also found to be within  $\pm 5$  lbs./ft.<sup>3</sup> of their targeted density values for all aggregate types. Based on these results the implemented compaction procedure was deemed satisfactory for purposes of this study.

### **6 Testing Plan**

The testing plan prepared for this study involved evaluating the effect of aggregate type, moisture content, and compaction efforts on testing results obtained from the NDG and the non-nuclear devices. To evaluate the effect of moisture content, three moisture levels were selected; these included the OMC, 2% higher than OMC, and 2% lower than OMC. The corresponding densities, as determined using the Proctor moisture-density relationships, were then used to determine the weight required for each lift during compaction. In addition, for each aggregate type two large samples were compacted at each of the moisture contents. The compacted samples were then tested using the NDG, BCD, LWD, and DCP devices immediately (i.e., within 1 h),



24 h, and 48 h after completion of compaction. This testing scheme was implemented to evaluate the effect of delayed testing on the results collected from these devices.

In order to evaluate the impact of different compaction efforts on testing results, three density levels were selected to compact samples at constant moisture content (i.e., OMC). Initially, the Proctor test moisture-density relationships were developed using lower/higher compaction efforts (i.e., 50% lower/higher blows than standard number of blows) to obtain the density value needed to prepare samples at lower/higher compaction efforts. However, these relationships yielded densities that were within  $\pm 5$  lbs./ft.<sup>3</sup> of the values determined using the Proctor standard number of blows. To ensure truly applying distinctive compaction efforts, density levels were selected based on the density results obtained through testing at the Proctor MDD. These include the Proctor MDD, 5 to 20 lbs./ft.<sup>3</sup> higher than MDD, and 5 to 10 lbs./ft.<sup>3</sup> lower than MDD. The specific density values and their corresponding moisture values used to evaluate the effect of moisture content and compaction effort on testing results for each material are presented in Table 1 below.

**Table 1.** Targeted Moisture and Density Values Utilized for Compacting the Four Aggregate Types.

Experiment	Level tested	NAT-1	NAT-2	DGA	RCA
Effect of moisture content (%)	2% Below OMC	7.7	7.7	6.7	8.7
	Opt. Moist. Cont.	9.7	9.7	8.7	10.7
	2% Above OMC	11.7	11.7	10.7	12.7
Effect of compaction effort <sup>a</sup> (lbs./ft. <sup>3</sup> )	Below MDD	105	105	115	115
	Max. Dry Density	112	120	125	125
	Above MDD	120	135	145	130

<sup>a</sup>Moisture contents were kept constant at OMC

## 7 Results and Discussion

This section presents the results collected for samples compacted at different moisture contents and density levels. The impact of moisture contents and compaction efforts on the testing results obtained from the NDG and the non-nuclear devices are also presented. In addition, this section presents the outcome of the multi-factor Analysis of Variance (MANOVA) conducted using the Statistical Package for Social Sciences (SPSS) software to evaluate the significance of these impacts. All error bars shown in the figures represent a 95% confidence interval of the mean.

### 7.1 Effect of Moisture Content

Figure 2 presents the results obtained from testing compacted samples prepared at different moisture contents using the NDG, and non-nuclear devices. Figure 2a presents the density values obtained for all aggregate types. As can be seen from this

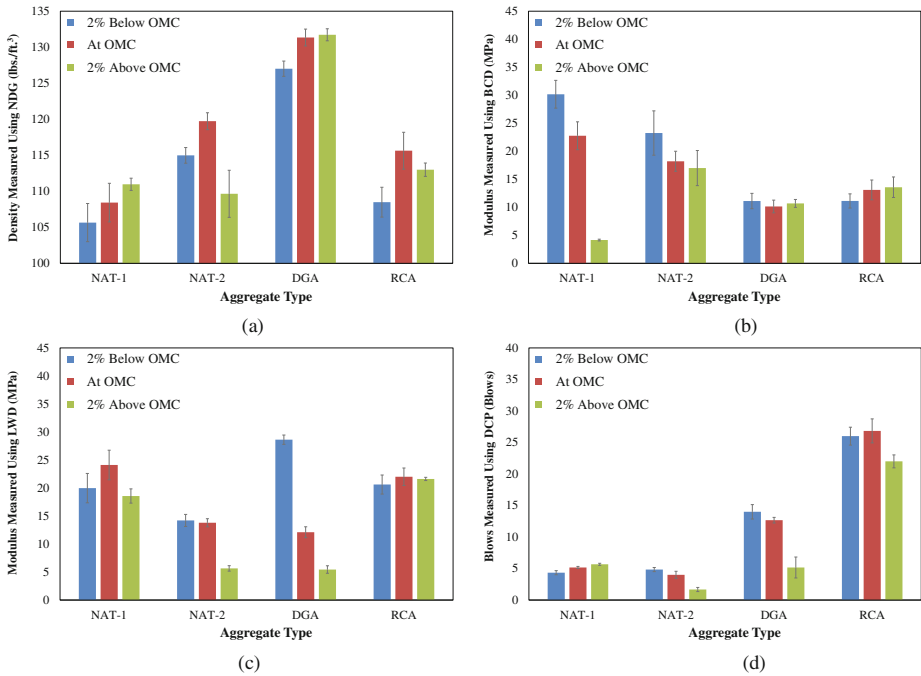


**Fig. 2.** Effect of moisture content on testing results: (a) NDG results, (b) BCD results, (c) LWD results, and (d) DCP result

figure, the NDG density values for samples compacted at moisture contents 2% above and 2% below OMC were lower than those compacted at OMC. This was expected since it is a similar trend that is seen in laboratory developed Proctor moisture-density relationships. This trend was observed only for NAT-2 and RCA aggregates. In the case of NAT-1 and DGA, the density values for samples at 2% above OMC were slightly higher (within 2 lbs./ft<sup>3</sup>) than those for samples compacted at OMC and 2% below OMC. Although this contradicts the expected moisture-density relationship trend, it is believed that the NDG might not be sensitive enough to capture differences in density when increasing/decreasing the moisture by 2%. The results presented in Fig. 2a also show that the NDG measured densities for the NAT-1 samples compacted at OMC ranged between 105 to 112 lbs./ft<sup>3</sup>, which is overlapping with the results obtained for the 2% above OMC samples. The Proctor moisture-density relationships for this material also showed variability within 3 lbs./ft<sup>3</sup> when the moisture was increased/decreased by 2% higher or lower than OMC. A similar observation was made for DGA aggregates.

The modulus results obtained using the BCD are presented in Fig. 2b. As shown in this figure, the modulus values for NAT-1 and NAT-2 decreased with the increase in aggregates' moisture content. For DGA and RCA aggregates, the modulus values increased when the moisture content increased. These observations generally might indicate that the BCD was sensitive to the changes in moisture content within the

samples. It is noted that the four modulus values, collected using the BCD from one location within the sample, varied significantly (between 5 and 35 MPa as shown in Fig. 2b) for all aggregates. In addition, this high variability might be the reason why the DGA and RCA data is not showing a similar trend to that seen for NAT-1 and NAT-2. The modulus values (Fig. 2b) for the natural sand materials (NAT-1 and NAT-2) and dense graded aggregates (DGA and RCA) were similar to each other. However, the modulus values of the sands (between 15 and 30 MPa) were significantly greater than the dense graded aggregates (between 7 and 11 MPa). These observations indicate that the BCD was able to capture differences between the aggregate types.

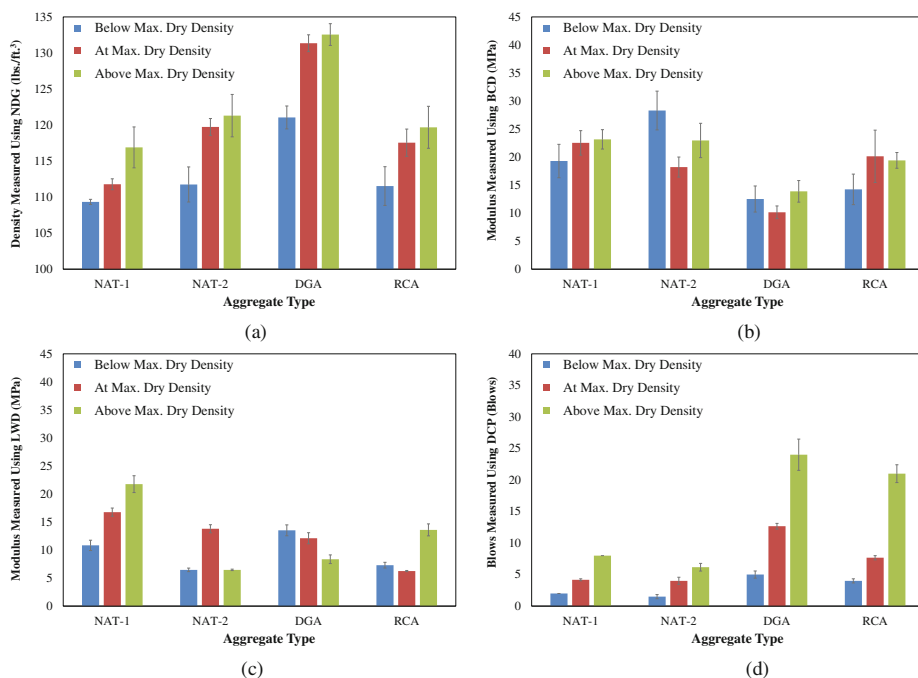
Moreover, as can be seen from Fig. 2c, NAT-1 and RCA had similar modulus values from LWD for all moisture contents (i.e., 2% below OMC, at OMC, and 2% above OMC). This might indicate that the LWD was not influenced by the changes (up to  $\pm 2\%$  of OMC) in the samples' moisture content. In the case of NAT-2 and DGA, the LWD modulus values decreased with the increase in moisture content. For these particular aggregates, the results suggest that the LWD was able to capture the change in modulus as the moisture content increased. In addition to the factors considered (aggregate type and moisture content), it is noted that the results of the LWD might have been influenced by mold size; explaining the mixed trends observed. In literature, Nazzal et al. (2007) reported the influence depth of the LWD ranges between 10.6 to 11 inches. The mold (12 inch thick and 17 inches wide) used in this study was larger than the influence zone determined by Nazzal et al. (2007); however, since it is not significantly larger (about 1 inch larger) the results might be influenced by the mold. Finally, the results presented in Fig. 2c show that the LWD was capable of capturing the differences between samples prepared using the selected aggregates.

Figure 2d presents the DCP number of blows required to penetrate the 1-ft. thickness of the compacted samples. As shown in this figure, the required DCP blow count for all aggregates were slightly decreasing (from 15 to 5 blows for DGA) with the increase in the samples' moisture content. This was expected due to the lubrication effect of the water, that helps reduce the friction resistance of the penetrating cone. This observation also suggests that the DCP might be influenced by the change in the moisture content (up to 2% below/above OMC). Figure 2d also shows that the DCP values for the two natural sand aggregates were lower than the dense graded aggregates (i.e., DGA or RCA). The natural sand materials had DCP values on between 1 and 6 blows while the DGA and RCA aggregates had values between 12 and 26. This was expected since the DGA and RCA aggregate consisted of larger sized particles and had a well-graded dense gradation. These observations indicate that the DCP is capable of capturing the difference between aggregates.

Overall, the results presented in Fig. 2 suggest that the DCP was the only device that can be classified as statistically significant to capture all the differences between the compacted samples (i.e., capturing the effect of moisture content). The results for both the BCD and LWD devices were for the most part similar and were not influenced by the change in moisture content for up to  $\pm 2\%$  from OMC.

### 7.2 Effect of Compaction Effort

Figure 3 presents the results conducted on samples prepared at varying density levels (i.e., at MDD, above MDD, and below MDD). Figure 3a presents the NDG density results for all aggregate type considered. As can be seen from this figure, the NDG density values for all aggregate types were the lowest at density levels below MDD and highest at levels at above MDD. This was expected because the densities of the samples were increasing; therefore the NDG values should have increased as well. The results also show, for all aggregates, that the differences between the NDG density values at MDD levels and above MDD levels were within 3 lbs./ft<sup>3</sup>. It should be noted; however, that when compacting samples for the above MDD density levels a jackhammer was used to ensure higher targeted densities were achieved. Therefore, the results might suggest that the NDG was not capable of capturing the differences between MDD and above MDD.



**Fig. 3.** Effect of compaction effort on testing results: (a) NDG results, (b) BCD results, (c) LWD results, and (d) DCP results

The BCD modulus values for the samples compacted using different compaction efforts are presented in Fig. 3b. As shown in this figure, the modulus values for all density levels were relatively similar (i.e., within 5 MPa) indicating that the BCD was not able to capture the differences between the compaction efforts applied. In addition, by comparing the BCD modulus values for the natural sand materials (gap-graded) with

the dense graded aggregates (DGA and RCA), it can be seen that NAT-1 and NAT-2 aggregates had similar modulus values (around 20 MPa) but different than those obtained for DGA and RCA aggregates (around 10 to 15 MPa). These observations might suggest that the BCD was able to capture the differences in aggregate size and gradation.

Figure 3c illustrates the LWD modulus values obtained for samples compacted at different density levels. As demonstrated in this figure, the trends observed were dependent on aggregate type. Meaning, the modulus values for the NAT-1 and NAT-2 (gap-graded) were higher for samples compacted at MDD than those below MDD. This was expected since modulus increases as the compaction effort applied increases. In the case of DGA and RCA (dense graded) the modulus values obtained for samples compacted at MDD and below MDD were similar (i.e., within 5 MPa). This might suggest that the LWD is influenced by the aggregate type. As observed from the LWD results obtained by varying moisture, NAT-2 and DGA modulus values decreased with an increase in compaction effort. Based on these findings, it is concluded that the LWD is able to detect changes in compaction effort. In the case of NAT-1 and RCA modulus values increased as compaction increased. These results suggest that the LWD was able to capture the change in modulus with an increase in compaction. As previously mentioned, the mixed trends obtained at above MDD can be attributed to the LWD being influenced by mold size.

The DCP number of blows required to penetrate the 1-ft. thick samples are shown in Fig. 3d. As can be seen from this figure, the DCP blows increased with the increase in compaction effort for all aggregates; indicating that the DCP was capturing the differences in compaction levels applied. This trend was expected because the denser the aggregate structure is the harder (i.e., higher number of blows) it is to penetrate. It can also be observed from Fig. 3d that the DCP values obtained for the natural sand aggregates were lower than those obtained for the dense graded aggregates. This difference is more significant at higher compaction levels than lower compaction levels. Based on these observations, it is concluded that the DCP was capable of capturing the difference between the aggregate types.

In summary, similar to the discussion presented for the effect of moisture content, the results presented in Fig. 3 show that the DCP appears to be the most sensitive of the three non-nuclear devices to the different compaction efforts applied.

## 8 Precision of Measurements

The standard error of the mean (SEM) was calculated for data collected immediately after compaction and it was determined as a percentage of the mean (Table 2). The SEM was based on the standard deviation (STD) of results at each moisture content tested (i.e. 2% below, at OMC and 2% below) divided by the square root of the total amount of replicates measured from each device. In our case, we had six replicates. The SEM provides insight on the variability of the sample mean. The data showed that the variability of all non-nuclear devices were similar (range of 5–8%) to each other. However, they were greater than that of the Nuclear Density Gauge, which had a standard error of the mean of 1%. In addition, the variability at different moisture

**Table 2.** Standard Error of the Mean of the Results (expressed as a percentage of the mean value) Measured from all Devices.

	Standard error of the mean of NDG, %			Average error of all materials, %
	2% Below	OMC	2% Above	
				1%
NAT-1	2%	2%	1%	
NAT-2	1%	1%	2%	
DGA	1%	1%	0%	
RCA	1%	2%	1%	
Average	1%	1%	1%	
<i>Standard Error of the Mean of BCD, %</i>				
	2% Below	OMC	2% Above	8%
NAT-1	6%	8%	3%	
NAT-2	12%	7%	13%	
DGA	9%	8%	5%	
RCA	8%	10%	10%	
Average	9%	8%	8%	
<i>Standard Error of the Mean of LWD, %</i>				
	2% Below	OMC	2% Above	5%
NAT-1	9%	8%	5%	
NAT-2	5%	4%	6%	
DGA	2%	6%	9%	
RCA	6%	4%	1%	
Average	6%	5%	5%	
<i>Standard Error of the Mean of DCP, %</i>				
	2% Below	OMC	2% Above	7%
NAT-1	5%	2%	2%	
NAT-2	5%	10%	14%	
DGA	6%	3%	23%	
RCA	4%	5%	3%	
Average	5%	5%	11%	

contents was similar for NDG, BCD and LWD. On the other hand, DCP blows at 2% above OMC had slightly variability (by an algebraic difference of 6%). This indicates that moisture content within 2% of OMC has minimal impact on measured values, except in the case of DCP where excess moisture causes the DCP blows to become more variable.

## 9 Conclusions

Based on the collected testing results and the subsequent statistical analysis results, the following conclusions were drawn:

- The laboratory procedure developed for compacting large samples was found to be satisfactory. The actual moisture contents and densities were within  $\pm 0.5\%$  and  $\pm 5$  lbs./ft<sup>3</sup> of their targeted values, respectively.
- The moisture content within the compacted samples (up to  $\pm 2\%$  of OMC) was sensitive to parameters measured from all devices evaluated. The Dynamic Cone Penetrometer (DCP) was the most suitable device for capturing the change in moisture contents within the samples while all other devices showed mixed trends within their results, specifically when preparing samples at 2% below and 2% above OMC.
- Based on the comparison of the standard error of the mean results, variability was similar for all non-nuclear devices. In addition, DCP showed higher variability when the soils had higher moisture content than the OMC.
- All of the parameters measured from these four devices were able to distinguish between the four aggregate types.

**Acknowledgments.** The authors would like to acknowledge the New Jersey Department of Transportation for funding the study presented in this paper. The findings reflect the views of the authors who are responsible for the facts and accuracy of the data presented. The contents do not reflect the official views or policies of the New Jersey Department of Transportation. This paper does not constitute a standard, specification, or regulation.

## References

- Abu-Farsakh, M., Nazzal, M., Alshibli, K., Seyman, E.: Application of DCP in pavement construction control. In *Transportation Research Record: Journal of the Transportation Research Board*, No. 1913, Transportation Research Board of the National Academies, Washington, D.C., pp. 53–61 (2005)
- Alshibli, K., Abu-Farsakh, M., Seyman, E.: Laboratory evaluation of the Geogauge and light falling weight deflectometer as a construction control tool. *ASCE J. Mater. Civil Eng.* **17**(5), 560–569 (2005)
- Briaud, J.-L., Rhee, K., Saez, D.: The BCD: a new instrument for compaction control. In *Transportation Research Record: Journal of the Transportation Research Board*, Transportation Research Board of the National Academies, Washington D.C. (2009)
- Chan, E.E., Champion, F.C., Chang, J.C., Hannon, J.B., Forsyth, R.A.: Improved performance criteria for use in nuclear gage specifications. California Department of Transportation (1975)
- Hearth, A., Mohammad, L., Gaspard, K., Gudishala, R., Abu-Farsakh, M.: The use of dynamic cone penetrometer to predict resilient modulus of subgrade soils. Report No. FHWA-LAW-417, FHWA, Washington, DC (2007)
- Kim, J., Kang, H., Kim, D., Park, D., Kim, W.: Evaluation of in situ modulus of compacted subgrades using portable falling weight deflectometer and plate-bearing load test. *J. Mater. Civil Eng.* **19**(6), 492–499 (2007)
- Lenke, L., McKeen, R., Grush, M.: Laboratory evaluation of Geogauge for compaction control. In *Transportation Research Record: Journal of Transportation Research Board*, No. 1849, Transportation Research Board of the National Academies, Washington, D.C., pp. 20–30 (2003)

- Nazarian, S., Mazari, M., Abdallah, I., Puppala, A.J., Mohammad, L.N., Abu-Farsakh, M.Y.: Modulus-based construction specification for compaction of earthwork and unbound aggregates. NCHRP Report 10–84. In Transportation Research Record: Journal of the Transportation Research Board, No. 10–84, Transportation Research Board of the National Academies, Washington, D.C. (2014)
- Nazzal, M., Abu-Farsakh, M., Alshibli, K., Mohammad, N.: Evaluation the LFWD device for in situ measurement of elastic modulus of pavement layers. In Transportation Research Record: Journal of the Transportation Research Board, No. 2016, Transportation Research Board of the National Academies, Washing D.C., pp. 13–22 (2007)
- New Jersey Department of Transportation. Standard Specifications for Road and Bridge Construction. New Jersey (2007). [www.state.nj.us/transportation/eng/specs/2007/Division.shtml](http://www.state.nj.us/transportation/eng/specs/2007/Division.shtml). Accessed 1 May 2015
- Weidinger, D.A.: Laboratory evaluation of the briard compaction device. J. Geotechn. Geoenviron. Eng. **135**(10), 1543–1546 (2009)



# Quantifying the Mechanistic and Economic Impacts of Using Asphalt Rubber Mixtures

Mena Souliman<sup>1</sup>(✉), Ragaa Abd El-Hakim<sup>2</sup>, Mark Davis<sup>3</sup>,  
and Lubinda Walubita<sup>4</sup>

<sup>1</sup> Department of Civil Engineering, The University of Texas at Tyler,  
3900 University Blvd, RBS 1008, Tyler, TX 75701, USA  
msouliman@uttyler.edu

<sup>2</sup> Public Works Engineering Department, Faculty of Engineering,  
Tanta University, Tanta, Egypt  
ragaa.abdelhakim@f-eng.tanta.edu.eg

<sup>3</sup> Department of Civil Engineering, The University of Texas at Tyler,  
3900 University Blvd, Tyler, TX 75701, USA

<sup>4</sup> TTI, The Texas A&M University System, 3135 TAMU, College Station  
TX 77843-3135, USA  
L-Walubita@tti.tamu.edu

**Abstract.** As far as hot mix asphalt pavement goes, tension at the bottom layer of the HMA layer creates the most issues for pavement engineers. Adding rubber to asphalt mix has the ability to extend the life of a pavement and provide an end use to old tires that would otherwise end up in a landfill. It is already known that the initial construction cost of an asphalt rubber mix will be higher than that of a conventional mix, but the purpose of this paper is to see if the reduced layer thickness and improved fatigue life will offset the initial cost. After completing a mechanistic analysis using the FHWA software package named 3D Move, the pavement thickness required to last for 50,000,000 cycles (estimated endurance limit) is much less for the asphalt rubber mixes as opposed to the reference hot mix asphalt. The cost to construct one lane mile of the reference mix pavement designed for 70 mph traffic was \$171,530.88 while the asphalt rubber mix at 70 mph came out to be \$157,059.70. This is a \$14,471.18 difference. Additionally, the cost to construct one lane mile of the reference mix pavement designed for 10 mph traffic was \$231,932.76, while the asphalt rubber mix at 10 mph came out to be \$200,162.55. This is a \$31,770.21 price difference. Overall, analysis showed that AR modified asphalt mixtures exhibited significantly lower cost of pavement per 1000 cycles of fatigue life per mile compared to conventional HMA mixture.

## 1 Literature Review

To understand why there is an essential need for a more durable and tension resisting pavement material, it is important to understand what is already known about pavement distresses. Important parameters like pavement structure, load speed, load configuration, and bituminous material temperature need to be considered when selecting an appropriate pavement design for a certain geographical region. The bottom of the HMA

layer and at the interface is referred to as the prime location where fatigue cracking will occur, and load magnitude and configuration is one of the main factors that can cause fatigue cracking. Ambassa et al. (2013) supports the Equivalency Factor as an important parameter to be taken into account when predicting pavement performance.

Moreno and Rubio (2012) specifically look at the grading curve of aggregates used in mix design along with the nature of the aggregate. Properties like absorption, specific gravity, bulk specific gravity, and saturated surface dry specific gravity can all be used to characterize aggregates. LTPP (Long Term Pavement Performance) provides soil classification data for base materials and subgrade of pavement structures in the United States and Canada, making it possible to look at similar parameters in studies, meaning that actual laboratory work and field samples does not necessarily need to be taken. Moreno and Rubio (2012) specifically site that the main cause of fatigue failure is from traffic loading and thermal related influences.

Adding rubber to asphalt has the ability to extend the life of a pavement and provide an end use to old tires that would otherwise end up in a landfill. As far as hot mix asphalt pavement goes, tension at the bottom layer of the HMA layer creates the most issues for pavement engineers. Although pavement performs poorly in tension, adding rubber to the asphalt mix has been proven to help in this area. Quoting Souliman and Eifert (2015), “results from the beam fatigue tests indicated that the AR gap graded mixtures would have much longer fatigue life compared with the reference (conventional) mixtures”. Souliman and Eifert (2015) proved that when evaluating asphalt rubber and conventional hot mix asphalt mixtures based on their performance and economic feasibility, the cost of using asphalt rubber mixtures was lower than hot mix asphalt for the entire life of the pavement. Only layers of 4 in and 8 in were considered in that study, but the groundwork was laid to do more in depth future studies. In that paper, it was also noted that as the vehicle speed decreases, the cost per 1000 miles increased.

When considering the performance of pavement, it is very important to look at what is called the endurance limit. “If the pavement thickness is controlled so that the strain at the bottom of the asphalt layer is kept below the endurance limit, the pavement would endure indefinite load repetitions and would not experience bottom-up fatigue cracking” Souliman et al. (2015). Additionally, Souliman et al. (2013) states that “A hyperbolic function between stress ratio and number of load cycles was developed. The asymptote of this curve parallel to the load cycle axis indicates that there is a stress level below which the number of cycles to failure does not proportionally increase with decreasing stress, thus the material tends to have unlimited fatigue life”. This is an important idea when considering pavement life, and provides much of the theory behind the study presented in this paper.

The basic principal of the current study is that if the strains are below the endurance limit at the bottom of the asphaltic layer, the pavement has the ability to possibly heal itself between cycles of loading and unloading according to Souliman et al. (2015). If a pavement possessed the ability to heal itself, it would stand to reason that it would last longer. When comparing conventional hot mix asphalt to rubberized asphalt, there is a potential that the thickness of the HMA layer will not need to be as high with the

asphalt rubber mixes. It is already known that the initial construction cost of an asphalt rubber mix will be higher than that of a conventional mix, but the purpose of this paper in part is to see if the reduced layer thickness and improved fatigue life will offset the initial cost via a comprehensive mechanistic and cost analyses.

## 2 Background

In 2008, the cooperation between Arizona State University (ASU) and the Swedish Road Administration (SRA) started by testing conventional and Asphalt rubber-gap-graded mixtures placed on Malmo E6 External Ring Road in Sweden. In 2009, the cooperation between SRA and ASU continued to test three types of gap-graded mixtures: conventional, Asphalt Rubber-modified mixtures, as well as polymer modified asphalt mixtures placed on highway E18 between the interchanges JärvaKrog and Bergshamra in the Stockholm area of Sweden.

Rice specific gravities and beam specimens were prepared according to the Strategic Highway Research Program (SHRP) and the American Association of State Highway and Transportation Officials (AASHTO): SHRP M-009 and AASHTO T321-03 (equivalent European test standards are: EN12697-24 A to D). Air voids, thickness and bulk specific gravities were measured for each test specimen and the samples were stored in plastic bags in preparation for the testing program. The designated road section within the construction project had three asphalt mixtures: a Reference gap-graded mixture (designation: ABS 16 70/100) used as a control, a Rubber-modified mixture (designation: GAP 16) that contained approximately 20% ground tire rubber (crumb rubber) and another polymer modified asphalt mixtures which is out of the scope of this paper. Test sections were located in fast lanes on highway E18 between the Järva-Krog & Bergshamra interchanges. The Swedish Road Administration provided information stating that the field compaction/ air voids for the three mixtures was around 3.0% to reduce any potential for moisture damage. The original mix designs were done using the Marshall Mix design method.

Previous publications showed that asphalt rubber mixture had a superior fatigue resistance performance over the conventional HMA mixture as shown in Fig. 1 (Souliman and Kaloush 2010). In addition, asphalt rubber mixtures have been widely accepted by the pavement community as an alternative to conventional asphalt mixtures to reduce bottom-up fatigue cracking due to its flexibility especially at low temperatures (Mobasher et al. 1997; Kaloush et al. 2010; Zborowski and Kaloush 2011; Rodezno and Kaloush 2011). The fatigue-resistant nature of asphalt rubber allows the designer to use a thinner layer to reach the endurance limit as compared to conventional asphalt mixtures as shown from other studies (Xiao et al. 2009, 2011). This hypothesis was the motive for this study. The remaining unanswered question is: do AR mixtures represent a cost effective solution to resist fatigue cracking compared to conventional HMA mixtures?

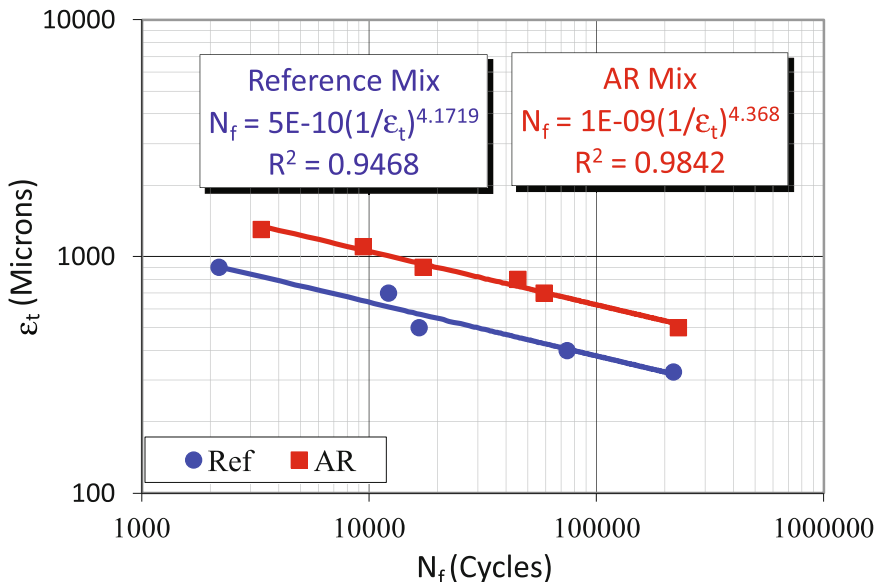


**Fig. 1.** Fatigue life comparison between reference conventional mixture and AR mixture at 21 °C using N<sub>f</sub> at 50% of the initial stiffness (Souliman and Kaloush 2010)

### 3 Research Methodology

In this paper, the reference conventional mixture and the AR mixtures are compared in order to quantify the mechanistic and economic impacts of using asphalt rubber mixtures. Table 1 shows the reported average aggregate gradations for each mixture And the in-situ mixture properties of the Stockholm pavement test sections, which includes % binder content by mass of the mix, Marshall Percent void content by volume of the mix, and maximum theoretical specific gravity of the mixes estimated at ASU laboratories. The base bitumen used was Pen 70/100 and rubber was called GAP 16.

**Table 1.** Average aggregate gradations and mixture characteristics, Stockholm Highway

	Sieve size (mm)	Reference Conventional	AR
Gradation (% Passing by mass of each sieve)	22.4	100	100
	16	98	98
	11.2	65	68
	8	38	44
	4	23	24
	2	21	22
	0.063	10.5	7.5
Binder Content (%)		5.9	8.7
Air Voids (%)		2.6	2.4
G <sub>mm</sub>		2.4642	2.3588

Using 3D Move, a mechanistic-empirical analysis was performed on the asphalt rubber and reference hot mix asphalt to evaluate the performance of each. Each iteration/run of the study involved changing dynamic modulus (depending on which mix was being evaluated), phase angle (only when the dynamic modulus changed), superpave binder grade (only changed from asphalt rubber to reference mix), speed, layer thickness, and finally the response points for each run. A summary of the process is displayed in the figure below.

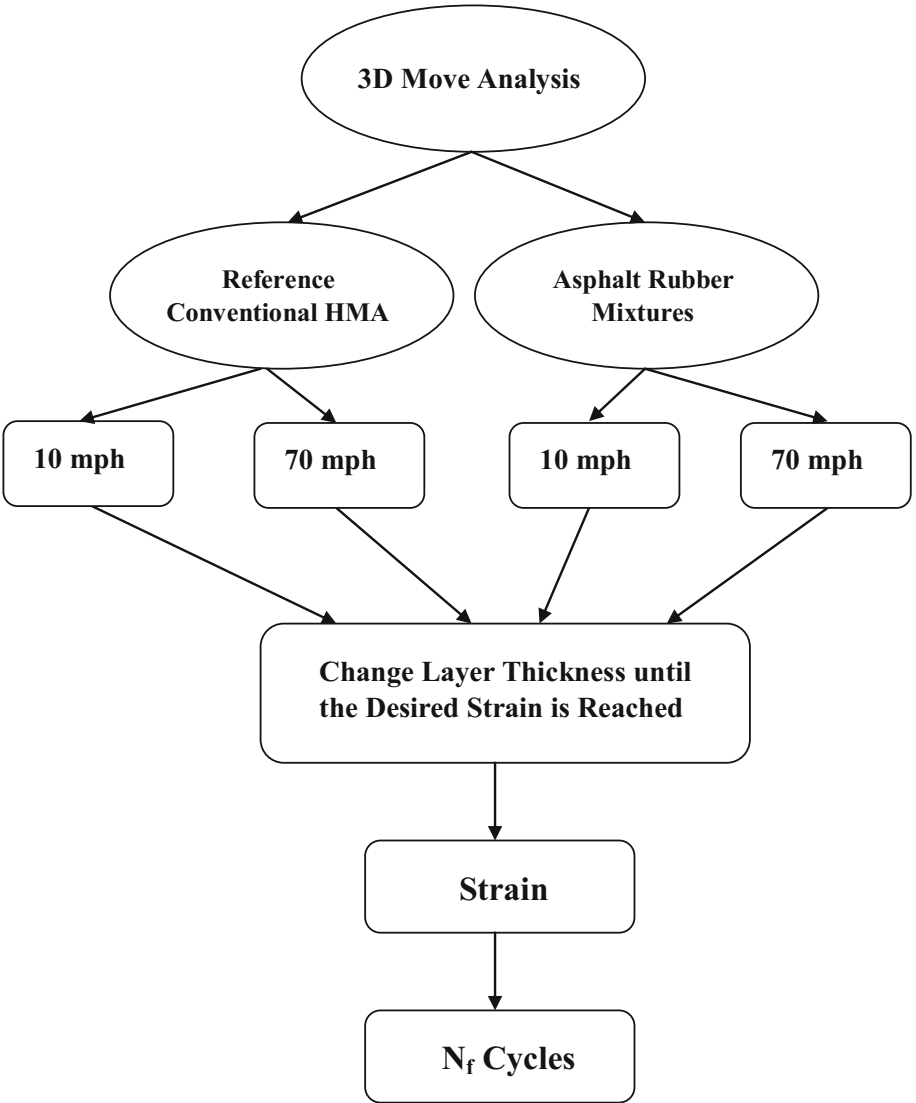


Fig. 2. Analysis flowchart

Figure 2 depicts the exact steps that were followed in the study for the 3D move analysis. The step where the pavement layer is changed was performed multiple times (10 times for some settings) until the desired strain in the pavement layer was achieved. In order to calculate the required strain for each asphalt mix, fatigue life prediction Eq. (1) was used.

$$N_f = k_1 \left( \frac{1}{e_t} \right)^{k_2} \quad (1)$$

where

- $N_f$ : The fatigue life, or number of load cycles to failure
- $e_t$ : Tensile strain
- $k_1$  and  $k_2$ : Regression Coefficients

The  $k_1$  and  $k_2$  values were known from (Souliman and Kaloush 2010). For the asphalt rubber mix,  $k_1 = 1 \times 10^{-9}$  and  $k_2 = 4.37$ . For the reference mix,  $k_1 = 5 \times 10^{-10}$  and  $k_2 = 4.17$ . Since it was known that the desired fatigue life of the pavement was 50,000,000, the fatigue life of an asphalt concrete layer equation could be solved to find strain. The strain that was being looked for in the reference mix was 84  $\mu$ , while the strain in the asphalt rubber mix was 151  $\mu$ . When the appropriate pavement thicknesses have been selected based on the calculated strains, a cost analysis can be performed.

## 4 Mechanistic Analysis

3D move Mechanistic analysis was performed for the two investigated mixtures using different pavement thicknesses based on two speeds, 70 mph and 10 mph. The following figures represent the findings of the 3D move mechanistic analysis in the form of a relationship between pavement thickness, in. and number of load cycles to failure,  $N_f$ . The findings will be presented in the order of Reference hot mix asphalt at 70 mph, Reference hot mix asphalt at 10 mph, Asphalt rubber mix at 70 mph, and finally Asphalt rubber mix at 10 mph.

Above, the results for the Reference Mix at 70 mph are depicted in Fig. 3. Also on the graph, a horizontal line intersecting the  $N_f$ -Thick line has been plotted, and represents the exact pavement thickness at a life of 50,000,000 cycles. It can be noted that 5.4 in. is required to reach the endurance limit.

For the asphalt reference mix at 10 mph, the same type of analysis was performed. The main objective was to obtain a pavement thickness at 50,000,000 cycles. As demonstrated in Fig. 4, the pavement thickness required to last for that number of cycles was 7.3 in. This is about 1.9 in. in thickness difference, which is to be expected with lower speeds due to the increased strain at the bottom of the HMA layer (Fig. 5).

For the asphalt rubber mix at 70 mph, the pavement thickness would need to be 3.85 in. to last for 50,000,000 Load cycles. It's important to note again that the

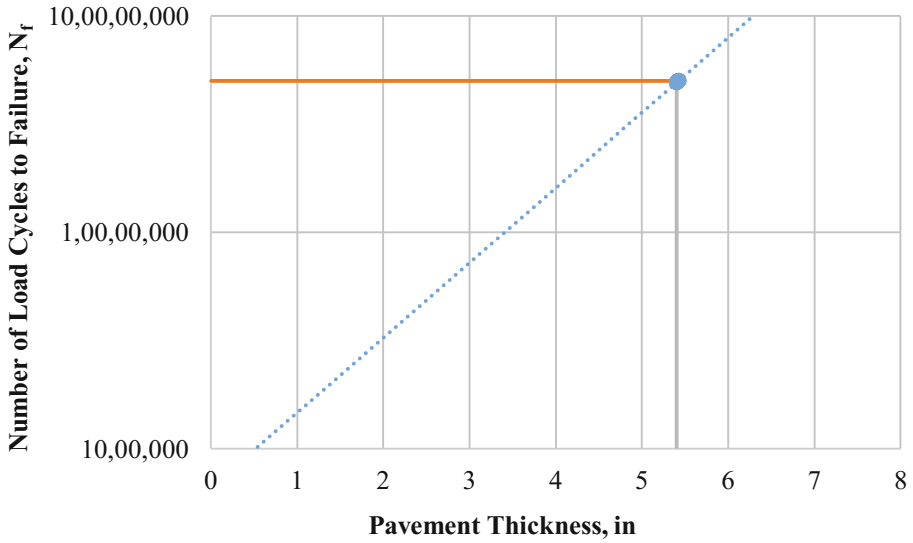


Fig. 3. Relationship between Pavement Thickness, in. and Number of Load Cycles to Failure,  $N_f$ , for Reference Mix at 70 mph

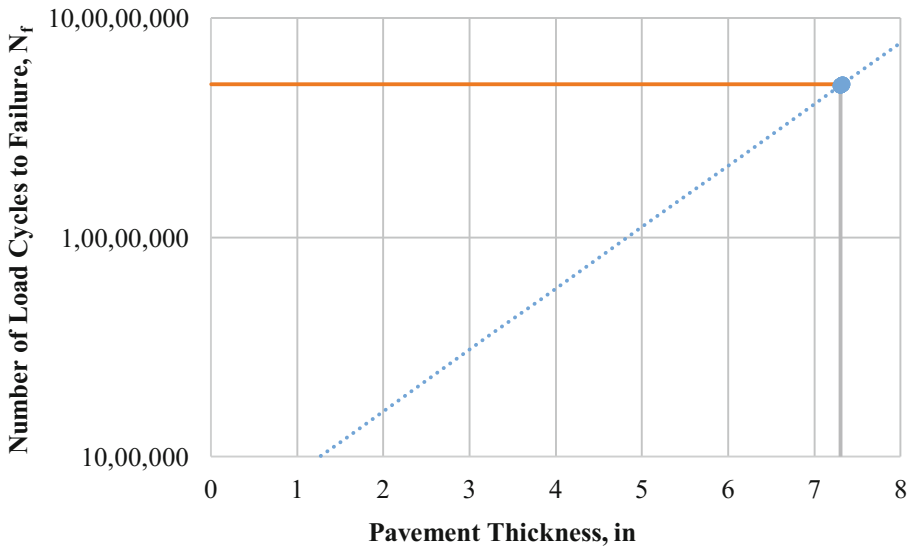


Fig. 4. Relationship between Pavement Thickness, in. and Number of Load Cycles to Failure,  $N_f$ , for Reference Mix at 10 mph

pavement thickness required for the reference mix at speed of 70 mph was 5.40 in. with a life of 50,000,000 Load cycles. The difference in required pavement thickness is 1.55 in. (Fig. 6).

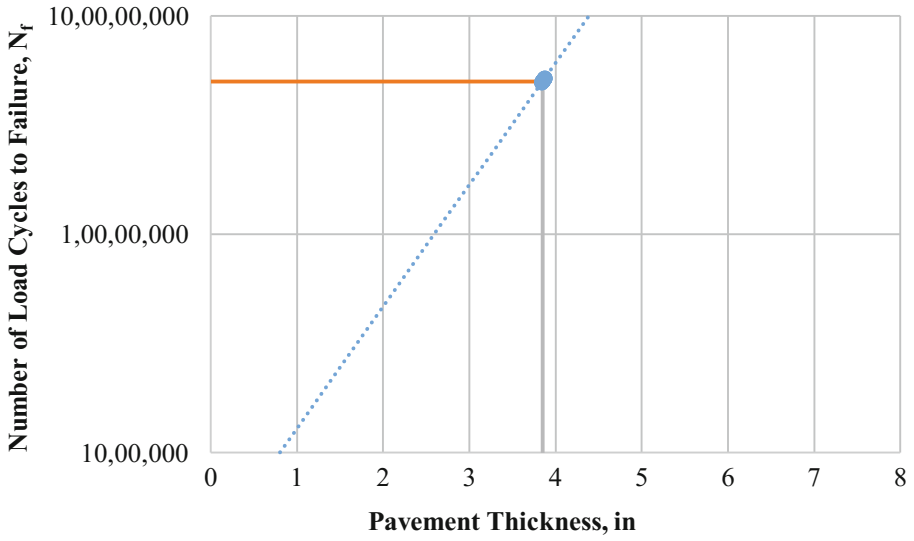


Fig. 5. Relationship between Pavement Thickness, in. and Number of Load Cycles to Failure,  $N_f$ , for Asphalt Rubber Mix at 70 mph

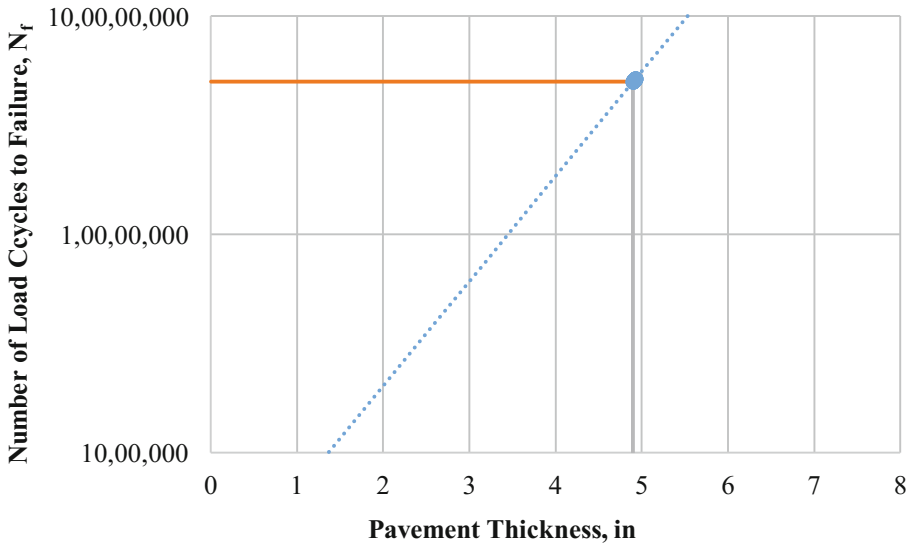


Fig. 6. Relationship between Pavement Thickness, in. and Number of Load Cycles to Failure,  $N_f$ , for Asphalt Rubber Mix at 10 mph



Finally, for the asphalt rubber mix at speed of 10 mph, the required pavement thickness is 4.90 in. in order to last for 50,000,000 cycles. Once again, this is 2.40 in. less required for the reference mix at speed of 10 mph. A final summary of the pavement thicknesses and the associated fatigue life is summarized in the table below (Table 2).

**Table 2.** Summary of pavement thickness results

Mix type	Thickness corresponding to endurance limit at 50 million cycles to failure (in)
RM at 70 mph	5.40
RM at 10 mph	7.30
AR at 70 mph	3.85
AR at 10 mph	4.90

## 5 Cost Comparison Based on Fatigue Performance

In order to evaluate the economic value of AR and reference HMA mixtures based on fatigue performances, a pavement section of 1.6 km (1 mile which is equal to 1760 yards) with 4.57 m (15 feet which is equal to 5 yards) wide single lane was considered. Based on the assumed density of 110 lb/sq-yd-in, the required quantities for paving the required pavement layer thickness for each case for the investigated mixtures are as follows:

- RM 70 mph:  $5.421 \text{ in.} \times \frac{110\text{lb}}{\text{yd}^2\text{in}} \times 1760 \text{ yd} \times 5 \text{ yd} = (5,247,528 \text{ Ib}) 2,624 \text{ tons}$
- RM 10 mph:  $7.329 \text{ in.} \times \frac{110\text{lb}}{\text{yd}^2\text{in}} \times 1760 \text{ yd} \times 5 \text{ yd} = (7,094,472 \text{ Ib}) 3,548 \text{ tons}$
- AR 70 mph:  $3.847 \text{ in.} \times \frac{110\text{lb}}{\text{yd}^2\text{in}} \times 1760 \text{ yd} \times 5 \text{ yd} = (3,723,896 \text{ Ib}) 1,862 \text{ tons}$
- AR 10 mph:  $4.901 \text{ in.} \times \frac{110\text{lb}}{\text{yd}^2\text{in}} \times 1760 \text{ yd} \times 5 \text{ yd} = (4,744,168 \text{ Ib}) 2,373 \text{ tons}$

The cost of production of 100 tons of HMA mixture can be calculated as follows:

- Optimum binder content in the mixture = 4.5% by total weight of mixture.
- Quantity of binder required = 4.5 tons
- Quantity of aggregates = 95.5 tons
- Total cost of binder @ \$600/ton binder =  $4.5 \times 600 = \$2,700$
- Total cost of aggregates @ \$14/ton aggregate =  $95.5 \times 14 = \$1,337$
- Cost of plant and equipment lump sum for 100 tons of HMA mixture = \$2,500
- Total cost for the production of 100 tons of the HMA mixture =
- $\$2,700 + \$1,337 + \$2500 = \$6,537$
- Therefore, the cost of HMA per ton = \$65.37

The additional cost for AR mixtures per ton was estimated to be around \$18.98 based on the AASHTO Crumb Rubber Modified (CRM) 1993 cost survey conducted by Steiner (1993). Therefore, the estimated cost of one ton of asphalt rubber is \$65.37 (Cost of HMA per ton) + \$18.98 = \$84.35 per ton. Knowing the cost of the HMA and

AR mixtures per ton, the required cost to pave 1.6 km (1 mile) of the pavement section with various mixtures were calculated as follows:

- RM 70 mph:  $\$65.37 \times 2,624 \text{ tons} = \$171,530.88$
- RM 10 mph:  $\$65.37 \times 3,548 \text{ tons} = \$231,932.76$
- AR 70 mph:  $\$84.35 \times 1,862 \text{ tons} = \$157,059.70$
- AR 10 mph:  $\$84.35 \times 2,373 \text{ tons} = \$200,162.55$

Combining the cost of the pavement per mile with the fatigue lives from the mechanistic-empirical analyses, the costs of 1000 cycles of fatigue life per pavement mile were calculated for the AR mixtures and their corresponding reference conventional HMA mixtures. This cost figure was derived by dividing the total cost of the 1-mile pavement section by the number of 1000 cycles to fatigue failure (i.e. N/1000 as summarized the next few lines). In other words, the cost of a 1.6 km (1-mile) pavement section for every 1000 cycles of fatigue life were determined as follows:

- RM 70 mph:  $\$171,530.88/(50,015,735/1,000) = \$3.43$
- RM 10 mph:  $\$231,932.76/(50,018,958/1,000) = \$4.64$
- AR 70 mph:  $\$157,059.70/(50,020,673/1,000) = \$3.14$
- AR 10 mph:  $\$200,162.55/(50,021,863/1,000) = \$4.00$

## 6 Summary and Conclusions

This paper investigated the mechanistic and economic impacts of using asphalt rubber mixtures. In order to quantify the economic value of using rubber, mechanistic analysis was performed using 3D move program on both reference and asphalt rubber mixtures for different thicknesses, and changed speed. From the results of 3D move, the required pavement thicknesses for asphalt rubber mixtures versus reference HMA mixtures for different speed rates were calculated. After the completion of the 3D move mechanistic analysis, the following conclusions were derived:

- The pavement thickness required to last for 50,000,000 cycles is much less for the asphalt rubber mixes as opposed to the reference hot mix asphalt.
- The cost to construct one lane mile of the reference mix pavement designed for 70 mph traffic was \$171,530.88 while the asphalt rubber mix at 70 mph came out to be \$157,059.70. This is a \$14,471.18 difference.
- Additionally, the cost to construct one lane mile of the reference mix pavement designed for 10 mph traffic was \$231,932.76, while the asphalt rubber mix at 10 mph came out to be \$200,162.55. This is a \$31,770.21 price difference.
- The cost for pavements constructed at 70 mph were at a lower cost per 1,000 cycles per mile was less than that of 10 mph.
- The cost for pavements constructed with asphalt rubber concrete mixtures were at a lower cost per 1,000 cycles per mile in comparison with that of reference conventional HMA (8.43% and 13.7% reduction in cost for speeds of 70 mph and 10 mph respectively).

Based off the results, the asphalt rubber not only adds fatigue resistance to the pavement, it also provides a more economical choice in the long term of the pavement mixture.

## References

- Ambassa, Z., Allou, F., Petit, C., Eko, R.M.: Fatigue Life Prediction of an asphalt pavement subjected to multiple axle loading with viscoelastic FEM. *Constr. Build. Mater.* **43**, 443–452 (2013). ScienceDirect. Web. 24 March 2015
- Kaloush, K.E., Biligiri, K.P., Zeiada, W.A., Rodezno, M.C., Souliman, M.I., Reed, J.X., Stempihar, J.J.: Laboratory evaluation of rubber & polymer modified bituminous mixtures constructed in Stockholm. Final Report Submitted to Swedish Road Administration, Vägverket, 405 33 Göteborg, Kruthusgatan 17, Sweden (2010)
- Mobasher, B., Mamlouk, M., Lin, H.: Evaluation of crack propagation properties of asphalt mixtures. *J. Transp. Eng. ASCE* **123**(5), 405–413 (1997). doi:[10.1061/\(ASCE\)0733-947X\(1997\)123:5\(405\)](https://doi.org/10.1061/(ASCE)0733-947X(1997)123:5(405))
- Moreno, F., Rubio, M.C.: Effect of aggregate nature on the fatigue-cracking behavior of halt mixes. *Mater. Des.* **47**, 61–67 (2012). ScienceDirect. Web. 24 March 2015
- Rodezno, M.C., Kaloush, K.E.: Implementation of asphalt-rubber mixes into the mechanistic empirical pavement design guide. *Road Mater. Pavement Design* **12**(2), 423–439 (2011). doi:[10.1080/14680629.2011.9695252](https://doi.org/10.1080/14680629.2011.9695252). [Lavoisier.]
- Souliman, M.I., Eifert, A.: Impact of Added Rubber on the Mechanical, Mechanistic, and Economical Attributes of Asphaltic Mixtures. Hardcopy, 1 November 2015
- Souliman, M.I., Mamlouk, M., Kaloush, K.E.: Preliminary Prediction of Endurance Limit for Asphalt Rubber Mixtures Due to Healing. Copy. Accessed 31 Nov 2015
- Souliman, M.I., Zeiada, W., Mamlouk, M., Kaloush, K.: Fatigue endurance limit for HMA based on healing. “Asphalt Pavement Technology” *J. Assoc. Asphalt Paving Technol.* **82**, 503 (2013)
- Xiao, F., Amirkhanian, S., Juang, H.: Prediction of fatigue life of rubberized asphalt concrete mixtures containing reclaimed asphalt pavement using artificial neural networks. *J. Mater. Civ. Eng.* **21**(6), 253–261 (2009). doi:[10.1061/\(ASCE\)0899-1561\(2009\)21:6\(253\)](https://doi.org/10.1061/(ASCE)0899-1561(2009)21:6(253))
- Xiao, F., Zhao, W., Amirkhanian, S.: Laboratory investigation of fatigue characteristics of rubberized asphalt mixtures containing warm asphalt additives at a low temperature. *J. Test. Eval.* **39**(2), 290–295 (2011)
- Zborowski, A., Kaloush, K.: A fracture energy approach to model the thermal cracking performance of asphalt rubber mixtures. *Road Mater. Pavements Design J.* **12**(2), 377–395 (2011). doi:[10.3166/rmpd.12.377-395](https://doi.org/10.3166/rmpd.12.377-395)

# Fuzzy Logic Based Modeling for Pavement Characterization

Mercado Pérez José Luis<sup>1</sup>(✉) and Beltrán Calvo Gloria Inés<sup>2</sup>

<sup>1</sup> Universidad Nacional de Colombia, Bogotá, Colombia  
jlmercadop@unal.edu.do

<sup>2</sup> Department of Civil and Agricultural Engineering,  
Universidad Nacional de Colombia, Bogotá, Colombia  
gibeltranc@unal.edu.co

**Abstract.** Maintenance decisions of existing pavements are highly dependent on stiffness and deterioration conditions, throughout their operation. A methodology based on non-conventional fuzzy logic is proposed in this work to evaluate the structural, functional and deterioration conditions of pavements by Fuzzy Inference Systems (FIS). The developed systems, allowed representing expert knowledge and linguistic variables of subjective and qualitative nature, commonly used to describe the severity levels of deterioration, strength and stiffness; thus FIS can be involved into structural characterization of pavements. Analyses were conducted using a database obtained from field tests performed on several pavement systems of toll roads in Colombia. Information about layer thicknesses, magnitude and severity of structural distresses, parameters and indicators derived from deflection test and International Roughness Index measures (IRI) were used. Results were expressed linguistically to make easier the interpretation and understanding. Based on the high quality of results obtained, it seems reasonable to conclude that the proposed methodology could be used confidently for a pavement characterization and sectorization purposes, with low computational cost.

## 1 Introduction

Traditionally, decision making process related to conservation and maintenance of existing pavements, involves intuition and experience, whose results are affected by any kind of uncertainty. Thus, there is a need to explore techniques that allow to optimize processes, given the large number of factors involved (multicriterion analysis), the wide variety of conservation and maintenance solutions, the costs for any made mistake and the promptness required in decision making.

Based on successful experiences in the field of artificial intelligence, there has been a huge interest worldwide in applying non-conventional methods for pavement evaluation. Some examples are reported in the work of Mahmood et al. (2013), Koduru et al. (2010), Arliansyah et al. (2003), Beltrán (2012) and Moazami et al. (2011).

In this work, Fuzzy Logic tools were used to deal with subjective variables, like pavement condition (poor, fair, good and very good) or linguistic variables like conservation and maintenance solutions (rebuild, overlay and so on). The purpose is to design Fuzzy Inference Systems (FIS), which combines the computational tools

capacity and available technical information, with human expert knowledge and experience in pavement evaluation. Thus, this knowledge can be automatized and used in making decisions for conservation and maintenance in later cases.

Five FIS were developed to provide a methodology able to automatically infer stiffness, deterioration and functional condition of pavement, as well as conservation and maintenance decisions in sectors with structural deficiencies.

In order to obtain good, reasonable and quick solutions, design and validation of FIS were emphasized; for that purpose, non-destructive survey data for a specific case study was used. It is expected that results obtained allow both the realistically reflect of pavement condition and the characterization of any road, with a desired detail level at any point or section.

### Fuzzy Logic Basis

Non-formal logic involves fuzzy concepts of abstract imprecise nature used to describe some attributes of a system or phenomenon. For instance, stiffness can be expressed in real numbers, but it is usually expressed as high, medium or low. Fuzzy Logic (FL) provides a framework for managing qualitative information that implies some degree of uncertainty and subjectivity, so that it can be formulated and processed in computational tools, in similar way to human reasoning.

Zadeh (1965) introduced the concept of fuzzy sets to describe attributes of any variable. Each attribute is defined by a set of real values, and each value is associated to a grade of “true” or grade of membership with its respective set. The grade of membership to a set is expressed as a function that takes values between 0 and 1, creating a gradual transition between no membership (0) and total membership (1).

The above can be expressed with a function  $\mu_{mf}(x)$ , where  $\mu$  is the grade of membership; mf is the membership function’s name and x are the possible values that take the represented variable.

Membership functions could have different shapes: triangular, trapezoidal, Gaussian, among others; the former is the simplest function for computational purposes. Selection and definition of the values for membership functions depends on the knowledge we have about the variable of interest.

Figure 1 shows an example of fuzzy representation for variable named “% affected area by cracks”, with its associated attributes. Horizontal axe represents the physic domain of numerical values for each possible category.

Interpretation of membership functions can be described as follows: when cracked area is 0, the low condition membership function takes a value of 1 ( $\mu_{low}(0\%) = 1$ ); when the affected area increases to 5%, membership to low condition gradually decreases until it reaches a null value ( $\mu_{low}(5\%) = 0$ ).

It is observed that membership functions can be overlapped; hence some values of the domain can be related to different attributes, three in Fig. 1. For example, when cracked area is 2.5%, the low condition membership function takes a value of 0.5 ( $\mu_{low}(2.5\%) = 0.5$ ) and the medium membership function takes a valued of 0,5 as well ( $\mu_{medium}(2.5\%) = 0.5$ ). In those cases, intermediate conditions are generated, for example, fairly light and moderately severe.

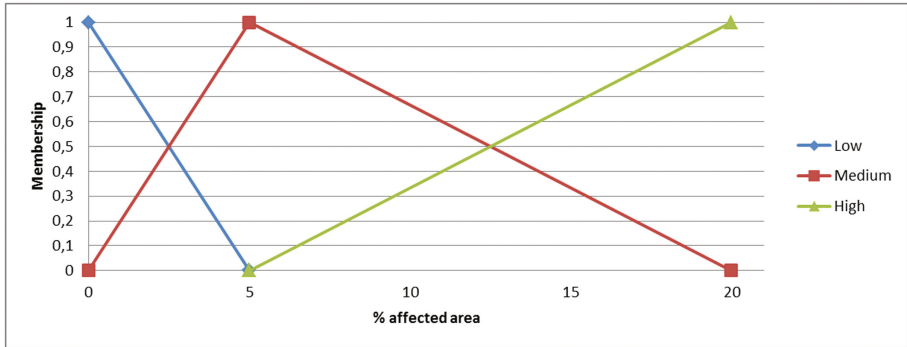


**Fig. 1.** Fuzzy representation for a variable.

Fuzzy sets can be defined by inference rules, formed by premises and consequences as IF ... AND/OR ... THEN .....rules (for example IF cracking OR deformation is light THEN condition is good). Also, the consequences can be expressed in fuzzy terms, with categories, membership functions and physic domain previously defined.

To represent the logic operator OR between premises, it is introduced a basic union operation between fuzzy sets, generating aggregation or maximum implication (max). Meanwhile, operator AND implies intersection between fuzzy sets, generating minimum aggregation (min).

In problems where solutions depend on several variables, which have many attributes, it can be proposed fuzzy inference systems (FIS) which are capable of processing multiple rules.

For this particular work, it is used the system proposed by Mamdani and Assilian (1975) composed by:

- Database that contain associated terms to input variables.
- Rule sets that articulate variables.
- “Fuzzification” interface where each input variable and rule component are expresses as fuzzy sets.
- Inference rules that allows obtaining a reasonable consequence.
- Inference system outputs formed by aggregation of consequences of each rule activated simultaneously in the system.
- “Defuzzification” interface to obtain a scalar number that represents the fuzzy set in the output.

Fuzzy Inference Systems generally work in three main steps, as follows:

- One or several variables are assigned to one or more fuzzy sets, trough membership functions. This process is known as “Fuzzification”.
- Evaluation of inference rules related to the variables of the first step. The results are a fuzzy inference that can involve several variables.
- Finally, values from fuzzy inference are transformed into a scalar number that represents the model output and is associated to a unique decision. This action is known as “Defuzzification”.

Figure 2 shows the structure previously described.

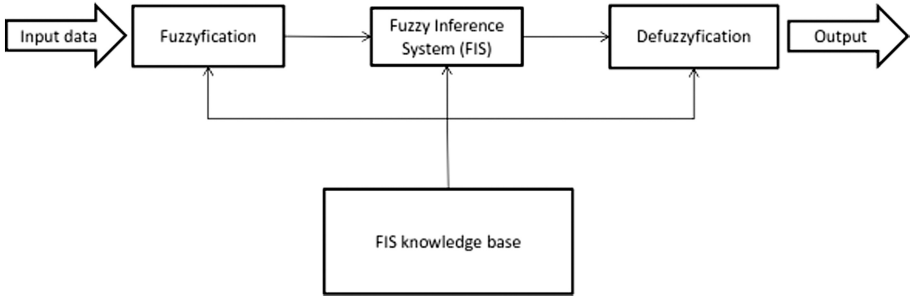


Fig. 2. Fuzzy inference system structure.

There are several methods to make “Defuzzyfication”. Most used are centre of gravity, area bisector, among others. Following example shows the way this process is done. For a FIS of three rules it is obtained the results represented by shade area in Fig. 3. “Defuzzyfication” consist in transforming this area in a numerical value. In this case, two methods were used: centre of gravity and area bisector.

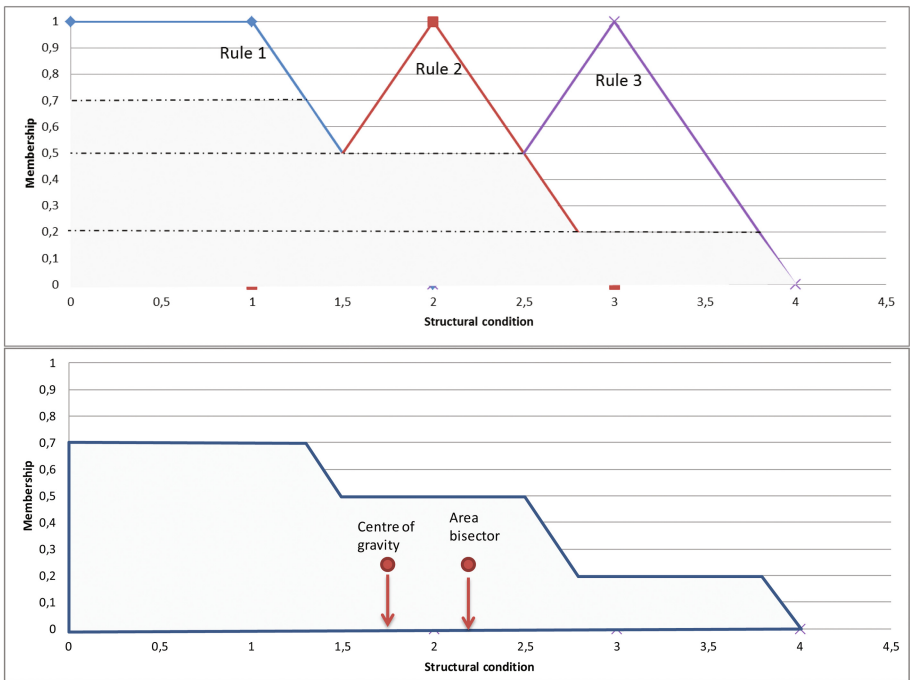


Fig. 3. Inference and defuzzyfication in Mandami FIS.

FIS knowledge base is formed by input variables, membership functions, inference rules and outputs or results of the system. Since Fuzzy Logic is an artificial intelligence tool, that tries to automatize expert knowledge, main source for this base is precisely practical experience and studies in the field of study.

### Applied Case

A 44 km length roads were selected to develop the system proposed. The pavement systems are composed by layer of asphalt concrete above layer of granular material. Figure 4 shows pavement structures.

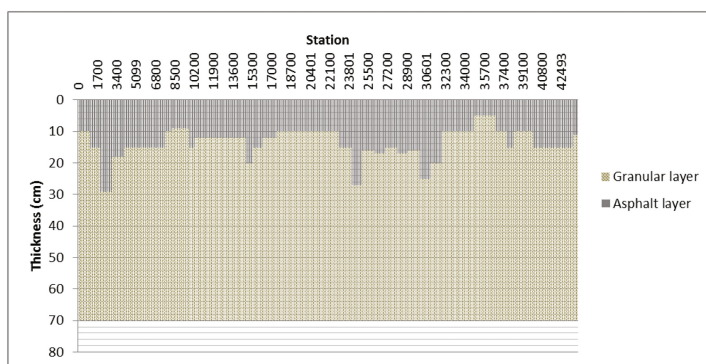


Fig. 4. Structural system in the road analyzed.

Database for this study was formed by information collected from the field, through non-destructive test, including functional and structural parameters.

Functional parameters measured are: international roughness index (IRI) and surface damages that do not affect the structural behavior, like transverse cracks, edge fissures, potholes, raveling, bleeding and polishing. Although, information about friction was not available for the case study, this parameter was included in the system, for future evaluations.

With regard to structural behavior, the parameters evaluated were classified into two groups: deterioration and stiffness. Deterioration was evaluated by means of damages related to structural behavior: rutting, longitudinal cracks and alligator cracks. Information on the location, extent and severity of the damage mentioned were available.

For stiffness evaluation, we considered the following variables: maximum deflection ( $D_0$ ), indicators of structural capacity proposed by Horak and Emery (2006) based on deflection bowl (BLI, MLI and LLI), the structural number (SN) proposed by the AASHTO-93, moduli of asphalt layers (AC), granular material layer (GR) and subgrade (SG).

In this case, information of deflections is critical for estimating the aforementioned structural parameters. Measurements were conducted every 100 m and have been processed in section of 1 km, in order to facilitate the presentation and interpretation of



the results. Deflection measurements attempt to simulate the load on pavement by an equivalent of 8.2 ton vehicle axis, by measuring the response in vertical displacements. It has been found that the size and shape of these displacement profile, known as deflection bowl, is related to layer stiffness and the structural behavior of pavement.

This measurement is performed with devices such as the Falling Weight Deflectometer (FWD) or Heavy Weight Deflectometer (HWD). These devices apply a pulse of surface load, whose magnitude varies between 0.7 and 16 tons in the FWD and between 2.7 and 24.5 tons in the HWD; the idea is to reproduce the representative load of heavy vehicles on a road. The load is applied in free fall on a circular plate, which can be rigid or segmented depending on the equipment used. Figure 5 shows the sensors arrangement used for recording deflections in the illustrated case study. Through seven sensors located at different distances from the axis of load application, the deflections were measured ( $D_0, D_1, \dots, D_6$ ), which define the profile of displacement or deflection bowl.

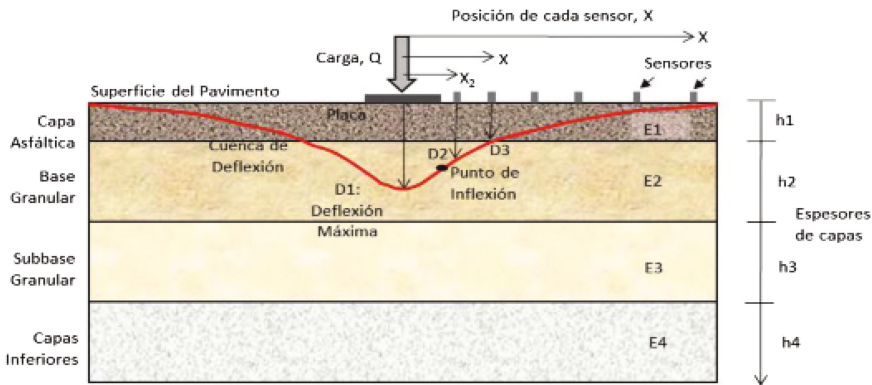


Fig. 5. Deflection test and deflection bowl.

Through these tests, elastic moduli of pavement layers can be estimated by back calculation techniques. Additionally, there are several structural indices derived from deflection bowls. For this work, we considered the maximum deflection ( $D_{max}$  or  $D_0$ ) recorded by the sensor located just below the axis load; shape indices proposed by Horak and Emery (2006), determined by the following expressions, where  $D_{0,3}$ ,  $D_{0,6}$  and  $D_{0,9}$  deflections are measured at 0.3, 0.6 and 0.9 m from axis load respectively.

$$BLI = D_0 - D_{0,3} \text{ (associated with the rigidity of the surface and base layers)}$$

$$MLI = D_{0,3} - D_{0,6} \text{ (related to the stiffness of the sub-base layer)}$$

$$LLI = D_{0,6} - D_{0,9} \text{ (stiffness indicator of the lower layers)}$$

Effective structural number ( $SN_{eff}$ ) is determined from the formula recommended by the AASHTO-93:

$$SN_{\text{eff}} = 0.0045D\sqrt[3]{Ep} \quad (1)$$

Where:

$E_p$ : is the equivalent pavement module.

$D$ : is the total thickness of the pavement structure, measured in inches.

Equivalent modulus is determined by the AASHTO-93 methodology, using data obtained from deflection measurements, following equation:

$$d_0 = 1.5P.a \left( \frac{1}{MR\sqrt{1 + \left(\frac{D^3}{a} \sqrt{\frac{E_p}{MR}}\right)^2}} + \frac{1 - \frac{1}{MR\sqrt{1 + \left(\frac{D}{a}\right)^2}}}{E_p} \right) \quad (2)$$

Where:

$d_0$ : central deflection.

$P$ : pressure load plate, psi. (82.3 psi)

$a$ : radio load plate, inches (5.9 in)

$D$ : total thickness of pavement layers on the subgrade (inches)

$MR$ : resilient modulus of subgrade (psi)

$E_p$ : effective module of the pavement (psi)

Resilient subgrade modulus can be determined from the deflections obtained with deflectometer (FWD), by the following expression:

$$Mr = \frac{0.24P}{D_r \cdot r} \quad (3)$$

Where:

$MR$ : resilient modulus of subgrade (psi)

$P$ : applied load (pounds)

$D_r$ : deflection measured at a distance  $r$  from the center of the load plate (inches)

$r$ : distance from the center of the load plate (inches)

### Design of Inference Systems

To perform the evaluation and characterization of pavement condition, five FIS were designed. All of them are formed by inputs, outputs and inference rules. Inputs and outputs were defined by membership functions; trapezoidal shape were selected to represent them, taking into account previous experiences from other studies (Beltrán 2012).

### *Stiffness Evaluation FIS*

To evaluate stiffness of pavement layers the following parameters were used:  $D_0$ , the BLI, MLI and LLI indices, structural number (SN) and the layers moduli (Eac (asphalt concrete), Egr (granular layer) and Esg (subgrade)). The combination of these parameters allows identifying structural problems and its possible solutions.

For peak deflection ( $D_0$ ), categories like low, moderate, high and very high, were defined; BLI, MLI and LLI were categorized as adequate, at risk and severe; SN number was ranked as very good, good, fair and poor; while for layers modules, high, medium and low categories were used. The rating ranges and its representation as fuzzy sets were defined based on a review of national and international literature and experience in toll roads in Colombia.

Linking the above variables, the following categories to qualify the stiffness of pavement systems were established as high, medium, low and very low. A scale from 0 to 10 was defined, from worst to best condition stiffness. Table 1 shows all inference rules defined. Figure 6 shows the FIS designed for stiffness evaluation.

### *Deterioration Evaluation FIS*

Input parameters selected for deterioration evaluation were rutting, longitudinal fatigue cracks and alligator cracks. In the case of rutting categories as very good, good, fair and poor were used; while fatigue cracks and alligator cracks were classified as low, medium and high. Rating ranges and its fuzzy sets representation were defined based on a review of national and international literature.

Joining these variables possible, deterioration ratings were defined as good condition, low rutting, low cracking, medium cracking, severe cracking, medium rutting, severe rutting and failed. A scale from 0 to 10 is defined, from worst to best deterioration condition. Table 2 shows all inference rules defined and Fig. 7 shows resulting FIS for deterioration evaluation.

### *Structural Evaluation FIS*

To merging results of stiffness and deterioration evaluation FISs, structural condition evaluation was derived through the following categories, which are closely related to maintenance strategies: failed pavement 2, failed pavement 1, regular pavement 3, regular pavement 2, regular pavement 1, medium pavement 3, medium pavement 2, medium pavement 1 and good pavement. A scale from 0 to 10 was defined, from worse to best structural condition. Table 3 shows the inference rules proposed and Fig. 8 shows the FIS designed for structural evaluation.

### *Functional Evaluation FIS*

To evaluate pavement functional condition the following input variables were used: IRI, transverse and edge cracks, potholes, raveling, bleeding and polishing. For IRI categories like poor, fair, good and very good were used. Meanwhile, for surface damage, that does not affect structural behavior, were classified as high, medium and low. The rating ranges and its representation as fuzzy sets were defined based on a review of national and international literature and experience in toll roads in Colombia.

Linking the above variables, the following categories for functional condition were defined: bad surface, regular surface and good surface. A scale from 0 to 5 was defined,

**Table 1.** Inference rules to evaluate stiffness.

IF	Rating	AND	Rating	Category
D <sub>0</sub> (mm)	Low	SN	Very good or Good	High
			Fair or Poor	Medium
	Moderate		Very good or Good	High
			Fair or Poor	Medium
	High		Very good or Good	Low
	Fair or Poor			
	Very High		Very good or Good	
			Fair or Poor	Very low
BLI (mm) or MLI (mm) or LLI (mm)	Adequate	D <sub>0</sub> (mm)	Low or Moderate	High
			High	Medium
			Very High	Low
	At Risk		Low or Moderate	Medium
			High or Very High	Low
	Severe		Low	Low
			Moderate or High or Very High	Very low
			High	
Eac or Egr or Esg	High	D <sub>0</sub> (mm)	Low or Moderate	High
			High	Medium
			Very High	Low
	Medium		Low or Moderate	Medium
			High or Very High	Low
	Low		Low	Low
			Moderate or High or Very High	Very low
			High	
Eac	High	BLI (D <sub>max</sub> - D <sub>0.3</sub> )	Adequate or At risk	High
			Severe	Medium
	Medium		Adequate or At risk	Medium
			Severe	Low
	Low		Adequate	Low
At risk or Severe	Very low			
Egr	High	MLI (D <sub>0.3</sub> - D <sub>0.6</sub> )	Adequate or At risk	High
			Severe	Medium
	Medium		Adequate or At risk	Medium
			Severe	Low
	Low		Adequate	Low
At risk or Severe	Very low			
Esg	High	LLI (D <sub>0.6</sub> - D <sub>0.9</sub> )	Adequate or At risk	High
			Severe	Medium
	Medium		Adequate or At risk	Medium
			Severe	Low
	Low		Adequate	Low
At risk or Severe	Very low			

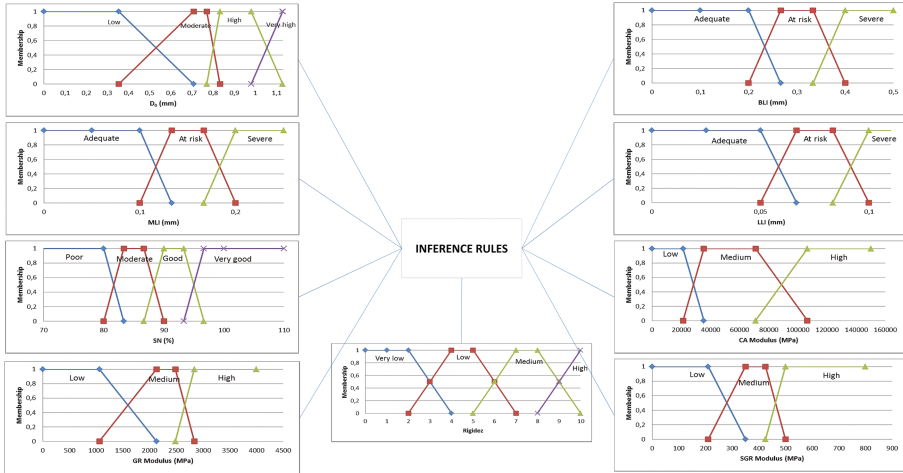


Fig. 6. Fuzzy inference system to evaluate stiffness.

Table 2. Inference rules to evaluate deterioration.

IF	Rating	AND	Rating	OR	Rating	Category
Rutting	Very good	Cracking	Low	Alligator cracks	Low	Good condition
	Good					
	Fair					
Rutting	Very good	Cracking	Medium	Alligator cracks	Medium	Low cracking
	Good					
	Fair					
Rutting	Very good	Cracking	High	Alligator cracks	High	Severe cracking
	Good					
	Fair					
Rutting	Poor	Cracking	Low	Alligator cracks	Low	Medium rutting
			Medium		Medium	Severe rutting
			High		High	Failed

from worst to best condition. Table 4 shows all inference rules defined and Fig. 9 shows the FIS designed for functional evaluation.

*Decision Making FIS - Maintenance and Conservation*

To define the most convenient pavement maintenance strategies, results of the structural and functional evaluation were combined, defining the following interventions: total reconstruction and subgrade improvement, AC and GR layers reconstruction, pavement recycling and new CA layer/milling and AC replacement, milling and AC overlay, AC overlay, milling and microsurfacing, cracks sealing/patching/BST (Bituminous surface

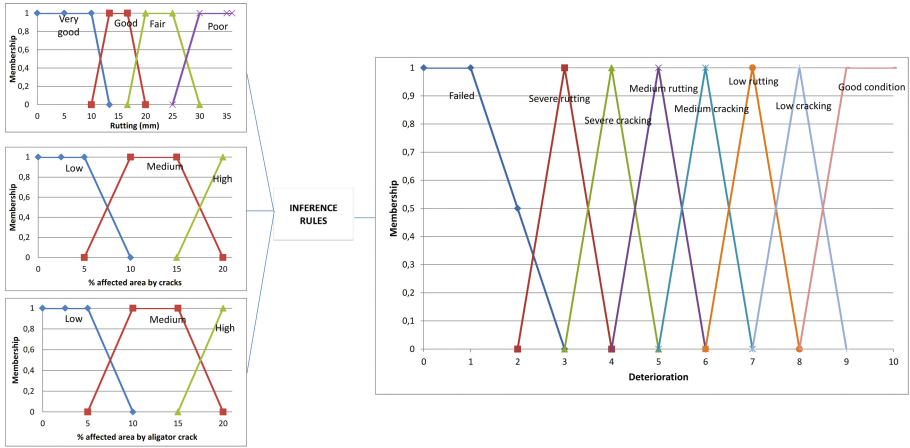


**Fig. 7.** Fuzzy inference system to evaluate deterioration.

**Table 3.** Inference rules to evaluate structural condition.

Stiffness	Deterioration	Structural condition
High	Good condition	Good pavement
High or Medium	Low cracking	Medium pavement 1
	Low rutting	
High	Medium cracking	Medium pavement 2
High or Medium	Medium rutting	Medium pavement 3
	Severe rutting	
High	Severe cracking	
High or Medium	Failed	Regular pavement 2
Medium	Good condition	Medium pavement 1
Medium	Medium cracking	Regular pavement 1
Medium or Low	Severe cracking	Regular pavement 2
Low or very low	Good condition or Low cracking	Medium pavement 1
Low or very low	Medium cracking	Regular pavement 2
	Low rutting	
Low	Medium rutting	Medium pavement 3
	Severe rutting	Regular pavement 1
	Failed	Regular pavement 3
	Failed	
Very low	Low rutting	Regular pavement 1
	Severe cracking	Failed pavement 1
	Medium rutting	
	Severe rutting	Failed pavement 2
	Failed	

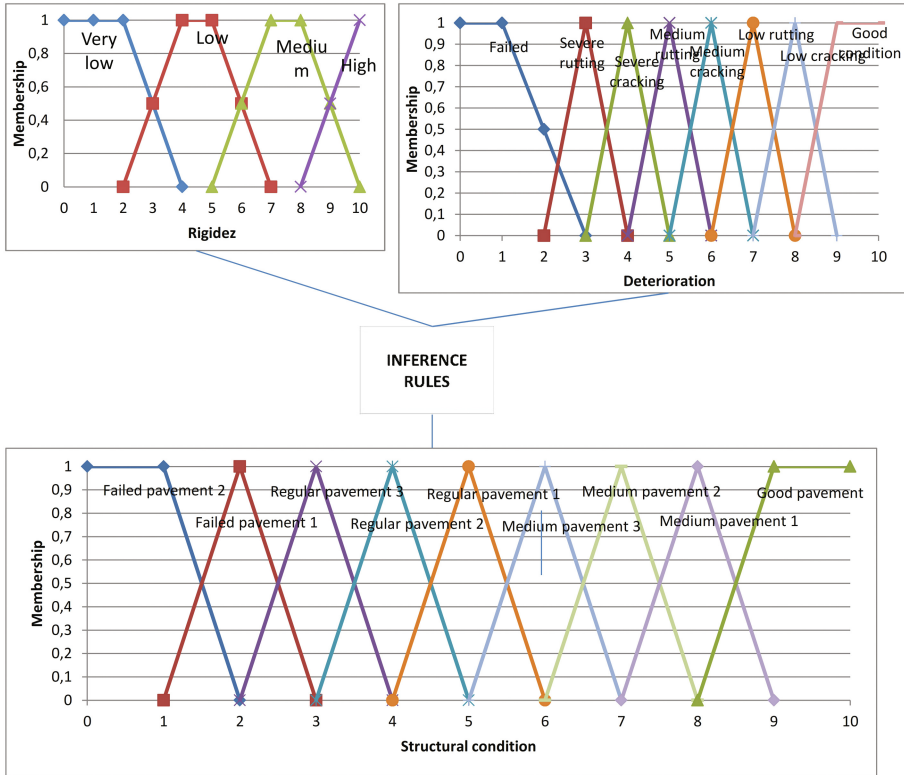


Fig. 8. Fuzzy inference system to evaluate structural condition.

Table 4. Inference rules to evaluate functional condition.

IF	Rating	AND	Rating	Category
IRI (m/Km)	Poor	Functional damage	High	Bad surface
			Medium	
			Low	Regular surface
	Fair		High	Bad surface
			Medium	
			Low	Regular surface
	Good		High	Good surface
			Medium	
			Low	
	Very good		High	Regular surface
			Medium	Good surface
			Low	

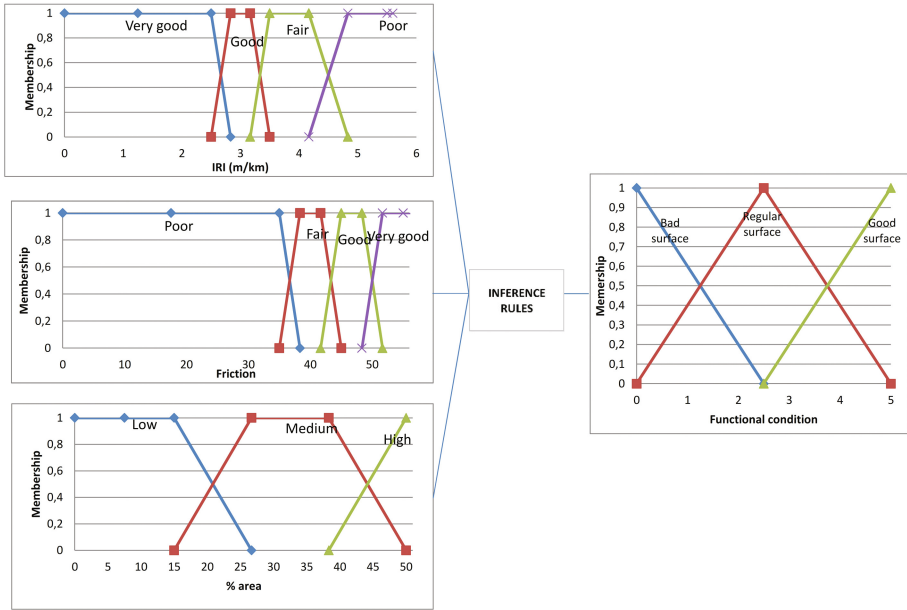


Fig. 9. Fuzzy inference system to evaluate functional condition.

treatment), cracks sealing/patching/microsurfacing, cracks sealing/patching, BST, microsurfacing, routine maintenance/monitoring and not intervention.

A scale for general condition of pavement from 0 to 10 was defined, where 0 represents a pavement that requires total reconstruction and 10 a pavement that do not requires intervention. For ratings between 5 and 9, maintenance strategies were focused on the correction of functional and minor structural damage. For ratings between 1 and 5, maintenance strategies were focused on restoring the structural pavement condition. Maintenance strategies were based on the recommendations of the entities responsible for road management in Colombia, as National Institution of Roads (INVIAS) and National Agency of Infrastructure (ANI). Table 5 shows all inference rules defined and Fig. 10 shows the FIS designed for decision making.

**Results Analysis**

A computational tool in MATLAB® was developed for the FIS proposed, which allowed the evaluation of a large amount of data in just a few seconds. MATLAB® is based on matrixes, data, functions and algorithms. It has two basics components, MATLAB® y Simulink ®. Main software allows to be complemented with an additional package named toolboxes. One of these tools is the Fuzzy Logic Toolbox, which contain functions and applications to analyze, design and perform simulations of systems based on Fuzzy Logic. This tool allows implementing complex system through simple inference rule, with a graphic interface user-friendly.



**Table 5.** Inference rules to evaluate to make decisions for maintenance and conservation.

Structural category	Functional category		
	Good surface	Regular surface	Bad surface
Good pavement	Not intervention	Microsurfacing	BST
Medium pavement 1	Routine maintenance/monitoring	Microsurfacing	BST
Medium pavement 2	Cracks sealing/patching	Cracks sealing/patching/microsurfacing	Cracks sealing/patching/BST
Medium pavement 3	Milling and microsurfacing	Milling and microsurfacing	Milling and microsurfacing or BST
Regular pavement 1	AC overlay	AC overlay	AC overlay
Regular pavement 2	Pavement recycling and new CA layer/milling and AC replacement	Pavement recycling and new CA layer/milling and AC replacement	Pavement recycling and new CA layer/milling and AC replacement
Regular pavement 3	Milling and AC overlay	Milling and AC overlay	Milling and AC overlay
Failed pavement 1	AC and GR layers reconstruction	AC and GR layers reconstruction	AC and GR layers reconstruction
Failed pavement 2	Total reconstruction and subgrade improvement	Total reconstruction and subgrade improvement	Total reconstruction and subgrade improvement

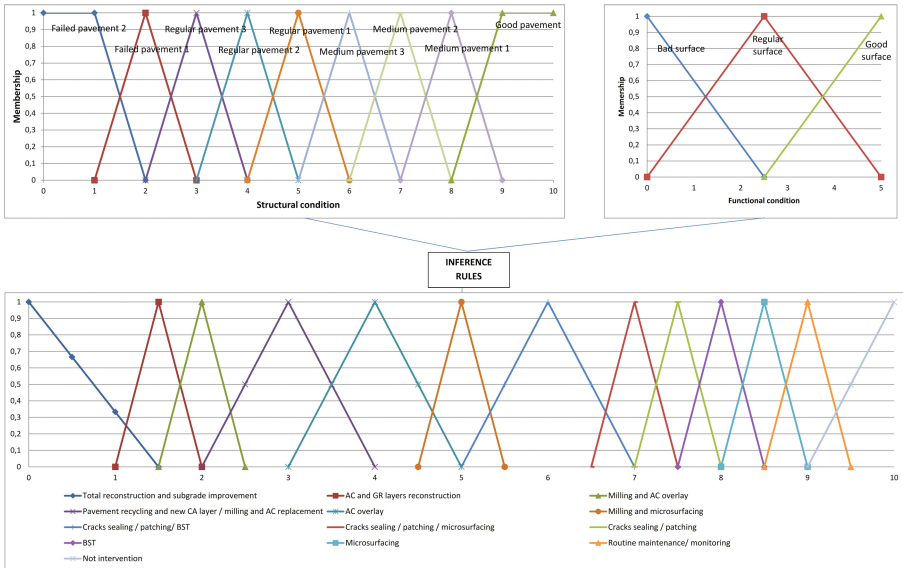


**Fig. 10.** Fuzzy inference system to make decision.

Fuzzy Logic toolbox works with vectors, where an input vector is analyzed with the defined inference rules, obtaining an output vector (numerical value). Software has the following editing components:

- FIS editor.
- The membership function editor.
- Rule editor.
- The rule viewer.
- The surface viewer.

Figure 11 shows the views of software component.

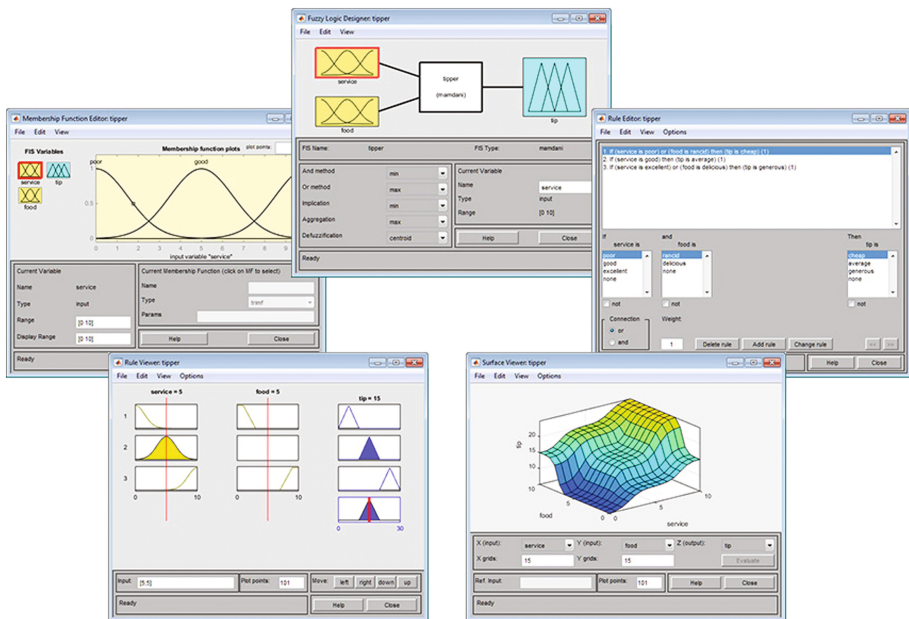


**Fig. 11.** Fuzzy Logic toolbox views. Membership function editor (Top left), FIS editor (center), Rule editor (Top right), Rule viewer (bottom left) and Surface viewer (bottom right). Source: [www.mathworks.com](http://www.mathworks.com)

Input data were entered into sections of 1 km in length. Variation of the condition for each criteria evaluated is shown in Figs. 12 and 13. Functional condition had a rating categorized as regular along the entire road, influenced by the values of IRI, since the percentages of area affected by functional damage were low.

With regard to structural rating, results of stiffness were classified as medium along the road. For deterioration condition was observed a significant variation in the rating, which can be used to establish similar behavior sectors that can help to simplify the analysis. In this case, maintenance and conservation strategies were considered every kilometer, in order to observe the behavior of results.

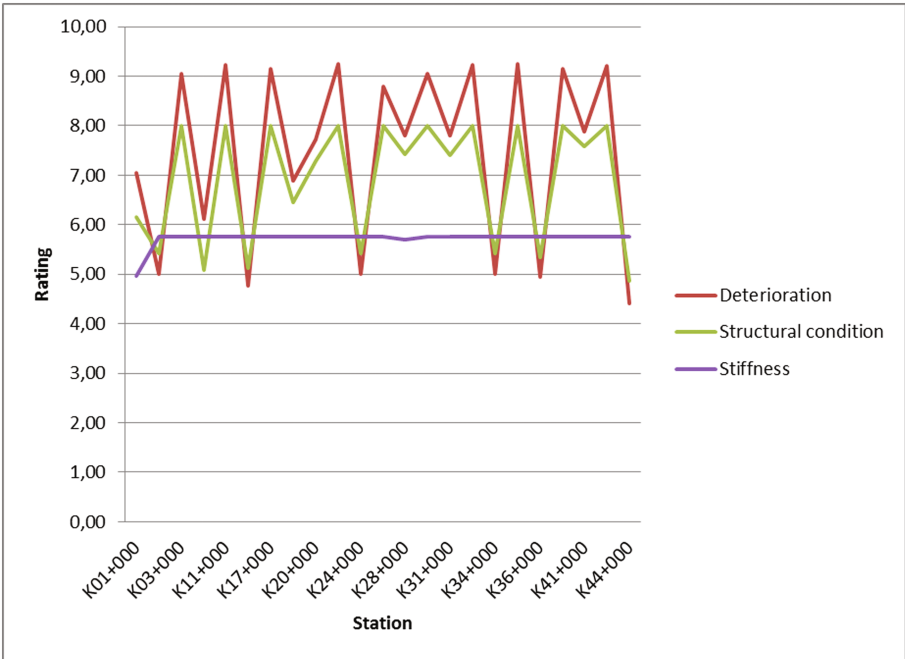


Fig. 12. Variation of structural pavement condition.

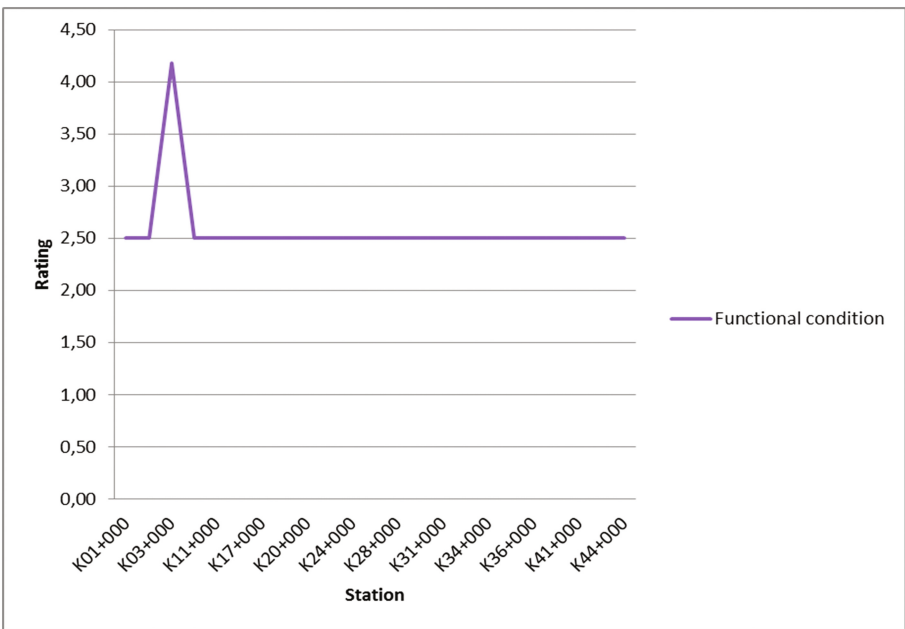


Fig. 13. Variation of functional pavement condition.

**Table 6.** Results obtained for evaluated road.

Start station	End station	Stiffness	Deterioration	Structural condition	Functional condition	Recommended intervention
K00+000	K01+000	Low	Low rutting	Medium pavement 3	Regular surface	Cracks sealing/patching/BST
K01+000	K02+000	Low	Medium rutting	Regular pavement 1	Regular surface	AC overlay
K02+000	K03+000	Low	Good condition	Medium pavement 1	Good surface	Routine maintenance/monitoring
K03+000	K04+000	Low	Medium cracking	Regular pavement 1	Regular surface	AC overlay
K04+000	K11+000	Low	Good condition	Medium pavement 1	Regular surface	Microsurfacing
K11+000	K12+000	Low	Medium rutting	Regular pavement 1	Regular surface	AC overlay
K12+000	K17+000	Low	Good condition	Medium pavement 1	Regular surface	Microsurfacing
K17+000	K19+000	Low	Low rutting	Medium pavement 3	Regular surface	Cracks sealing/patching/BST
K19+000	K20+000	Low	Low cracking	Medium pavement 2	Regular surface	Cracks sealing/patching
K20+000	K23+000	Low	Good condition	Medium pavement 1	Regular surface	Microsurfacing
K23+000	K24+000	Low	Medium rutting	Regular pavement 1	Regular surface	AC overlay
K24+000	K27+000	Low	Good condition	Medium pavement 1	Regular surface	Microsurfacing
K27+000	K28+000	Low	Low cracking	Medium pavement 2	Regular surface	Cracks sealing/patching
K28+000	K29+000	Low	Good condition	Medium pavement 1	Regular surface	Microsurfacing
K29+000	K31+000	Low	Low cracking	Medium pavement 2	Regular surface	Cracks sealing/patching
K31+000	K32+000	Low	Good condition	Medium pavement 1	Regular surface	Microsurfacing
K32+000	K34+000	Low	Medium rutting	Regular pavement 1	Regular surface	AC overlay
K34+000	K35+000	Low	Good condition	Medium pavement 1	Regular surface	Microsurfacing
K35+000	K36+000	Low	Medium rutting	Regular pavement 1	Regular surface	AC overlay
K36+000	K40+000	Low	Good condition	Medium pavement 1	Regular surface	Microsurfacing
K40+000	K41+000	Low	Low cracking	Medium pavement 1	Regular surface	BST
K41+000	K42+000	Low	Good condition	Medium pavement 1	Regular surface	Microsurfacing
K42+000	K44+000	Low	Severe cracking	Regular pavement 1	Regular surface	AC overlay

Road condition was generally good and strategies were focused on improving the functional condition. Microsurfacing and BST were the main strategies proposed. There were some sections where structural condition must be improved and construction of an AC overlay was recommended.

Results were similar to the strategies recommended by ANI that for this section were recommended activities of partial maintenance, BST and repair of damages, and milling and replacement of asphalt layer.

Table 6 shows interventions obtained.

## 2 Conclusions

Fuzzy inference systems proposed were able to combine structural and functional condition parameters to define maintenance and conservation strategies. The developed system allows to involving criteria used by agencies in charge of pavement management in Colombia, to generate a more rigorous and less uncertainty analysis.

For the case study, a uniform stiffness condition classified as medium was obtained. The same situation occurred in functional evaluation, where a regular surface condition defined by the results of IRI, was obtained. In this particular case, there were not available friction measurements, but this variable can be involved for future evaluations.

Deterioration evaluation system, defined by the existing pavement damage, showed the largest variation in this case study. Deterioration evaluation FIS was defined based on the predominant damage (cracking and rutting), which allowed to associate it with the most convenient maintenance strategy.

For the case study, good structural pavement condition was obtained, so that interventions were mostly focused on repairing the functional condition, with some sectors that required structural intervention. An AC overlay was recommended for those sectors.

FIS proposed offer the advantage of being flexible and dynamic, allowing to involve additional variables, thus achieving greater precision in the results. Use of MATLAB® as a computer tool is a great advantage because it allows the evaluation of a large amount of data in a short time, optimizing the resources used. Thus, long extension road networks evaluation is possible.

It is concluded that fuzzy logic is an effective tool to optimize pavement evaluation processes and decision making for conservation and maintenance strategies, allowing systematizing expert and practical knowledge. Accuracy and representativeness of the results depends on the quantity and quality of available information and knowledge and experience in pavement management, in the cases where there is interest in applying this technique.

**Acknowledgments.** We thank H&F Ingenieria who provided measures information used to validate and test the proposed system.

## References

- AASHTO. AASHTO guide for design of pavement structures (1993)
- Arliansyah, J., Maruyama, T., Takahashi, O.: A development of fuzzy pavement condition assesment. *JSCE* **746**, 275–285 (2003)
- Beltrán, G.: Evaluación Estructural de Pavimentos Flexibles con Métodos de Inteligencia Artificial y Auscultación No Destructiva. Universidad Nacional Autónoma de México (2012)
- Koduru, H.K., Xiao, F., Amirkhani, S.N., Juang, C.H.: Using fuzzy logic and expert system approaches in evaluating flexible pavement distress: case study. *J. Transp. Eng.* **136**(2), 149–157 (2010)
- Horak, E., y Emery, S.: Falling weight deflectometer bowl parameters as analysis tool for pavement structural evaluations. In: 22nd Australian Road Research Board International Conference, Australia (2006)
- Mahmood, M., Rahman, M., Nolle, L., Mathavan, S.: A fuzzy logic approach for pavement section classification. *Int. J. Pavement Res. Technol.* **6**(5), 620–626 (2013)
- Moazami, D., Behbahani, H., Muniandy, R.: Pavement rehabilitation and maintenance prioritization of urban roads using fuzzy logic. *Expert Syst. Appl.* **38**(10), 12869–12879 (2011)
- Zadeh, L.: Fuzzy sets. *Inf. Control* **8**(3), 338–353 (1965)

# Impact of a Poly-olefin Based Additive on Bitumen and Asphalt Mix Performance

Jan Valentin<sup>(✉)</sup>, Lucie Benešová, and Tereza Valentová

Faculty of Civil Engineering, Czech Technical University in Prague,  
Prague, Czech Republic  
jan.valentin@fsv.cvut.cz

**Abstract.** Based on the comparison of the selected characteristics of laboratory prepared modified binders, different version of bituminous binders with added poly-olefin based additive (VP) alone or in combination with SBS polymer were assessed. The basic type of bitumen used for the modification was a paving grade 50/70 to which 5 M% and 6 M% or only 1 M% but in combination with a selected type of SBS (quantity of 3 M%) were added. Frequency sweep test (complex shear modulus) and MSCR test was done on virgin and aged binders. Additionally assessed binder variants were used in a SMA mixture and bitumen properties were compared with performance behavior of the mixture – mainly stiffness, water susceptibility and resistance to permanent deformations.

## 1 Introduction

This paper focuses on the comparison of the effects of selected additives modified by poly-olefin based agent or the combination of this additive with SBS polymer. At the same time the paper summarizes laboratory results of SMA asphalt mixtures where these variants were used. Stone mastic asphalt mixture (SMA) are used for decades in wearing courses of asphalt pavements predominantly for highly loaded surfacing of roads, motorways and expressways. These mixtures if compared to traditional asphalt concretes are characterized by a gap-graded grading curve and higher bitumen content. The gap-graded curve secures a very strong mineral skeleton based on coarse aggregates, which is bond by asphalt mastic formed by bitumen, limestone filler and fine aggregates. Thanks to this composition SMA mixtures can very well resist the traffic loading and have high resistance to permanent deformation and resistance to crack propagation. From the viewpoint of traffic safety it is also important to highlight the typical surface texture with improved roughness and macrotexture (due to the used aggregate grading), which secures good skid resistance properties and therefore also a high comfort to the drivers and in connection with specific attenuation of traffic also some noise abatement (NAPA Practice 1999). SMA mixtures are designed and tested according to the national appendices of EN 13108-5. The standard requires in the Czech Republic for initial type testing determination of volumetric properties of the mixture, resistance to permanent deformation and bitumen drainage ratio. Other characteristics or parameters are not required.

One of the first projects that dealt with the modification by the poly-olefin modifier was a 5-year study (Wardlaw 1992), that was performed to investigate the behavior of asphalt mixtures containing plastic and latex modifiers. The research included laboratory experiments to characterize the materials and five field trials, which were built in different climatic regions of the United States. These field trials were built to test the constructability of pavements using these asphalt modifiers and to provide sites to monitor the long-term performance of these mixtures. Laboratory results showed that the effectiveness of these modifiers was very dependent upon the source of the bitumen used in the mixtures. The modifiers seemed to provide higher mixture stiffness at higher temperatures which possibly indicated a greater resistance to permanent deformation, while maintaining about the same characteristics as conventional mixtures at low temperatures. Another consistent tendency in the field data is the difference between the laboratory molded test specimens results and the core samples results. The laboratory test specimens consistently had a greater resilient modulus than the core specimens.

Another article (Zhu 2014) summarized the distribution of polymers and mentioned poly-olefins. As an important category of plastomers, poly-olefin is one of the earliest used modifiers for bitumen. Various poly-olefin-based materials, including high-density polyethylene (HDPE), low-density polyethylene (LDPE), linear low-density polyethylene (LLDPE), IPP and APP, have been studied for application in bitumen modification due to the relatively low cost and the benefits they might bring. Those used materials were usually found to result in high stiffness and good rutting resistance of modified bitumen, although they are quite different in chemical structure and properties. However, those used poly-olefin-based materials failed to significantly improve the elasticity of bitumen. In addition to this, the regular long chains of those modifiers give them a high tendency to pack closely and crystallize, which could lead to a lack of interaction between bitumen and poly-olefin and result in the instability of the modified bitumen.

Using amorphous poly alpha olefin (APAO) improves the high temperature performances of bituminous binders according to the article (Wei 2013). In this article bituminous binders were modified with two different APAOs and added content of 4 M % of bitumen. The effect of APAO on the rheological properties of bituminous binders was investigated. Conclusions of investigation were, that the addition of APAO reduces the temperature susceptibility of bituminous binders. On the other hand the addition of APAO increases the viscosity of modified bituminous binder at high temperatures. In addition, BBR results demonstrate that additional APAO has negative effects on the creep stiffness and creep rate.

The reported results indicate that poly-alpha-olefin modified binders and the mixture have a good low-temperature flexibility, high-temperature stability and anti-ageing property (Kong 2005). This was proven by the further presented research partly.

The addition of poly-alpha-olefin into base bitumen improves the short-term ageing characteristics and the mixing of poly-alpha-olefin with base bitumen do not have any chemical reaction (Wei 2014). In this article two types of APAOs with different viscosities were selected. It is found that APAO improves the high-temperature performance and reduced the temperature susceptibility of the modified bituminous binder. However, APAO has negative effect on the low-temperature performance of modified bituminous binder.



The last aspect which is typical mainly for SMA mixtures, but in a similar way also for porous asphalts, is the necessity to use suitable type of fibers, which act as so called binder carriers and baffle the drainage of higher content of used bitumen. This blocks the segregation of the mixture and guarantees high quality of the SMA from the production until the mixture is paved and compacted. Within the further assessed SMA mixtures in the Czech Republic typical cellulose fiber S-CEL G7 was used compare with an improved type of cellulose fiber, identified as F3000, which is protected by a Czech based patent.

## 2 Production of Bituminous Binders

The basic type of bituminous binder used for the modification was a paving grade bitumen 50/70 from a Czech refinery to which 5 M% and 6 M% or just 1 M% of poly-alpha-olefin (PAO) based additive was added (Fig. 1). In the case of 1 M% this was in combination with SBS polymer (with a dosage of 3 M%). Poly-alfa-olefin is a special wax made by powdering technique that improves the viscosity and workability of the material in which being added and has good adhesion and high thermal stability. The modified binders were aged in the laboratory conditions by thin-film oven test (TFOT) according to EN 12607-2 and by rolling thin-film oven test (RTFOT) according to EN 12607-1 both simulating short-term bitumen ageing. The laboratory simulations followed the procedures given in both standards. At the same time PAV (pressure ageing vessel) method according to EN 14769 was performed after TFOT to simulate long-term bitumen ageing. The marking and detailed description of the variants assessed is indicated in Table 1. The bituminous binder of each tested variant, using paving grade bitumen 50/70, was mixed at 150 °C for 30–40 min using laboratory stirrer (type IKA C-MAG HS7), with an angular velocity of 350–400 revolutions/min. In the case of bitumen modified by SBS polymer, the mixing temperature amounted to 170 °C for at least 60 min with mixing speed of 450 revolutions per minute.



**Fig. 1.** Applied additive poly-alpha-olefin

**Table 1.** Identification of tested bituminous binders

Bituminous binder	Designation
50/70	50/70
PMB 25/55-55	PMB
50/70 + 5% poly-alpha-olefin	5% PAO
50/70 + 6% poly-alpha-olefin	6% PAO
3% SBS a 1% poly-alpha-olefin	SBS + PAO

### 3 Selected Test Methods of Bituminous Binders

Standard empirical testing defined for unaged, polymer-modified bituminous binders in EN 14023 and test methods for assessment of selected functional characteristics were applied to compare the performance-related properties of bituminous binders modified by polymer or amorphous poly-alpha-olefin additive.

#### 3.1 Basic Characteristics of Bituminous Binders

The basic empirical characteristics, including the loss of volatiles after ageing, are summarised in Table 2 and in Fig. 2. The comparison of standard requirements is derived from the specifications listed in EN 14023 (Bitumen and bituminous binders – Specification framework for polymer modified bituminous binders) for individual PMB types.

**Table 2.** Results of basic empirical tests of assessed binders

Designation	Penetration [0.1 mm]	Softening point [°C]	Penetration index [-]	Elastic recovery [%]	Mass loss of volatiles	
					TFOT [%]	TFOT + PAV [%]
50/70	64.0	48.4	-1.0	–	–	–
PMB	41.0	57.9	0.1	74.9	–	–
5% PAO	42.0	65.8	1.7	22.1	0.12	0.59
6% PAO	38.8	72.0	2.5	20.2	0.08	0.64
SBS + PAO	36.3	73.8	2.6	83.8	-0.01	0.40

Standard paving grade bitumen 50/70 was chosen as the basic bituminous binder and EN 12591 indicates a softening point interval of 46–54 °C and penetration range of 50–70 dmm for this bitumen. The used reference binder met both requirements. According to these basic criteria, a rough assessment of the effect of additives applied can be made. Comparing penetration and softening point of assessed activated or modified bituminous binders, a significant impact of the additives was noticed in contrast to the values of reference/control bitumen. Penetration decreased in all cases by 20 dmm at least. When a higher quantity of PAO is applied, penetration decreases while the softening point increases; for SBS application, the reduction is even more noticeable.

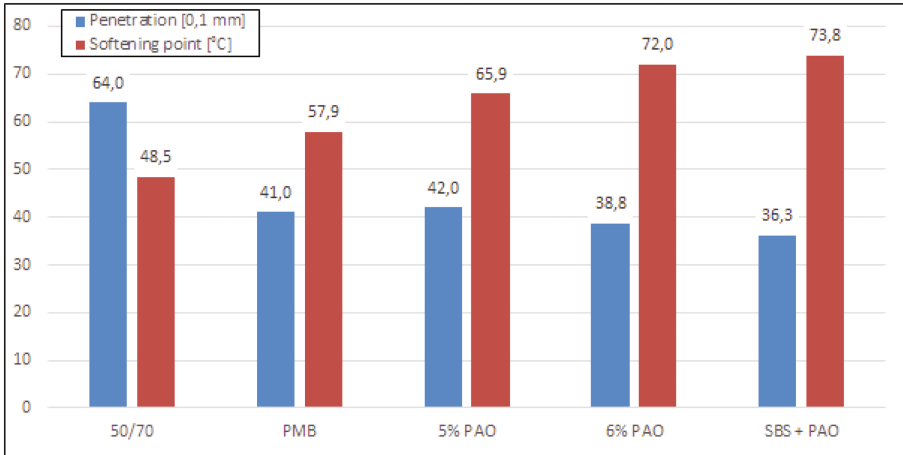


**Fig. 2.** Results of bitumen penetration and softening point test

Elastic recovery represents a fast and simple test the result of which is used to indicate the level of flexible properties of modified bituminous binders. The test was conducted with virgin and aged samples. For all virgin binders it was possible to extend the test samples to the 200 mm length at 25 °C, which is required by the standard. When the test was conducted with aged binders, they always failed prematurely. No assessed bitumen elongated after long-term ageing to even 100 mm. The elastic recovery measured after 30 min from elongation and subsequent cutting of the sample, is very low when PAO is applied (with both dosages). In the case of the version with SBS, the percentage of recovery is the best, exceeding even after PAV ageing 50%.

After short-term ageing, the difference of the softening point for PMB 25/55-65 should be lower than 10 °C, which was met by all binders without any problem. However, it is obvious that this condition was met by binders with SBS even after long-term ageing which points out a very good resistance to ageing in case of this binder. The positive impact of a higher quantity of PAO is reflected here as well, since 6% PAO records an 11 °C difference in the softening point of virgin bitumen and binders after TFOT + PAV while binders with 5% PAO demonstrate a 17 °C difference. Similar conclusions can be made on the basis of mass loss of volatiles after ageing.

### 3.2 Oscillation Frequency Sweep Test and Complex Shear Modulus Determination

In a common oscillation test, the measurement is taken with constant shear stress ( $\tau = 2000$  Pa) within a loading frequency interval of 0.1–10 Hz and thermal range of 20–60 °C, which is called the “frequency sweep” (FS). Based on earlier findings and conclusions of the SHRP (US research program), the frequency of 1.59 Hz is a very

important value which, according to the Van der Poel nomogram, roughly corresponds with the shear effect of traffic load at 90 km/h, or load duration of 0.13 s.

The main obtained characteristics of the complex shear modulus describe the resistance of the material to permanent deformation and defines the basic assumptions for the fatigue behaviour thereof. Together with dynamic shear measurement, we can also determine the viscous and elastic behaviour of the binder based on the complex shear modulus components and phase angle determination.

With high resistance of an asphalt mix to deformation, the  $G^*$  should be high,  $\delta$  should be lower if possible, and the  $G^*/\sin(\delta)$  rate should be as high as possible. The  $G^*/\sin(\delta)$  parameter describes the deforming behaviour of the binder; its minimum value required for bitumen was set to 1 kPa within SHRP in the past. The required value applies to virgin bituminous binders under 60 °C. In the case of fatigue behaviour, the  $G^* \times \sin(\delta)$  parameter can be used. Both parameters can be used for information although, in general, this concept of bituminous binder characterisation has been largely abandoned and replaced, at least in the field of deformation behaviour, by the MSCR test concept. This is confirmed by Fig. 3 (low correlation between  $G^*/\sin(\delta)$  and maximum relative rut depth  $PRD_{AIR}$ ) and Fig. 12 (higher correlation between MSCR test and  $PRD_{AIR}$ ).

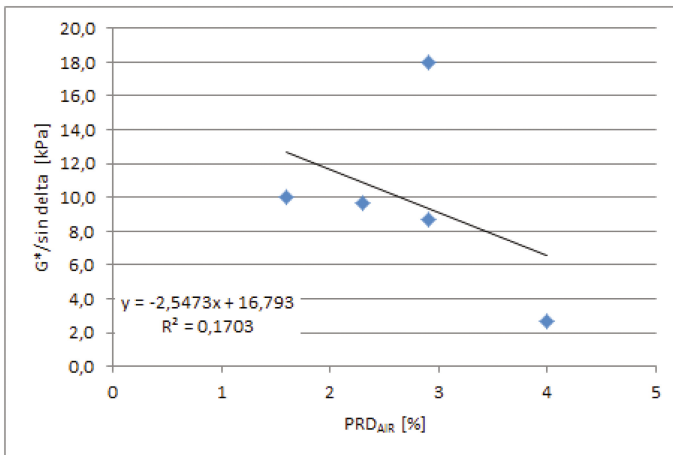


Fig. 3. Correlation between  $PRD_{AIR}$  and  $G^*/\sin(\delta)$

### 3.2.1 Results of Oscillatory Frequency Sweep Test

From the point of view of results evaluation, oscillation dynamic measurements can be divided into two approaches of conducted analysis. In the first case, the shear modulus and phase angle values were assessed for 1.59 Hz and two selected temperatures, 40 °C and 60 °C. The results achieved are indicated in Table 3 and also presents the characteristics of  $G^*/\sin(\delta)$  or  $G^* \times \sin(\delta)$ , which are comprehensible shown in Fig. 4. The requirement of minimum  $G^*/\sin(\delta) > 1$  kPa was met by all assessed binders. When SBS is applied, this characteristic is the highest and, therefore, the likelihood of

**Table 3.** Characteristics of complex shear modulus of tested binders

Designation		40°C				60°C			
		G*	$\delta$	G*/sin( $\delta$ )	G*x sin( $\delta$ )	G*	$\delta$	G*/sin( $\delta$ )	G*x sin( $\delta$ )
		[kPa]	[°]	[kPa]	[kPa]	[kPa]	[°]	[kPa]	[kPa]
50/70	Virgin	49.5	79.3	50.4	48.6	2.7	86.5	2.7	2.7
PMB		93.8	66.6	102.2	86.1	9.5	71.1	10.0	9.0
5% PAO		157.0	63.2	175.9	140.2	8.5	76.4	8.7	8.2
6% PAO		170.5	63.4	190.7	152.4	9.3	75.8	9.6	9.0
SBS + PAO		192.5	58.1	226.6	163.5	16.8	68.8	18.0	15.7
50/70	TFOT	140.0	63.4	156.6	125.2	7.9	78.2	8.0	7.7
5% PAO		406.0	49.8	531.2	310.3	10.7	74.7	11.1	10.3
6% PAO		536.5	46.9	735.1	391.6	21.0	70.7	22.3	19.8
SBS + PAO		369.0	49.3	486.7	279.8	23.4	64.2	26.0	21.1
50/70	TFOT + PAV	530.0	47.3	721.0	389.6	36.0	67.8	38.9	33.3
5% PAO		1050.0	37.9	1708.2	645.4	70.8	63.1	79.4	63.1
6% PAO		815.0	38.5	1308.5	507.6	66.1	60.4	76.0	57.5
SBS + PAO		458.0	46.4	632.2	331.8	40.4	58.5	47.4	34.5
50/70	RTFOT	–	–	–	–	–	–	–	–
5% PAO		353.0	61.2	402.9	309.3	17.2	77.2	17.6	16.7
6% PAO		377.0	59.9	435.7	326.2	16.6	78.3	16.9	16.2

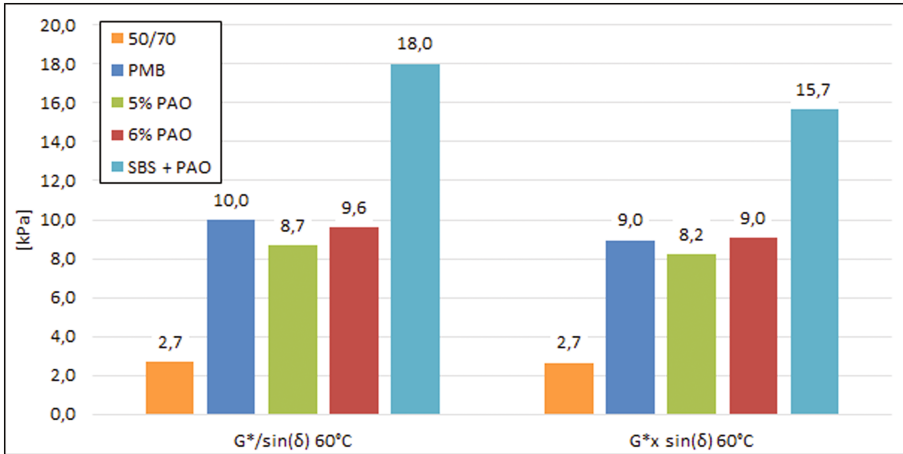


**Fig. 4.** Bitumen performance characteristics according to SHRP

preventing permanent deformation is the highest, too. If only PAO is applied, the characteristic is almost down to one half and the difference in the dose is negligible; according to our expectations, the characteristic improves with larger quantities. However, in comparison to the reference bitumen, a significant improvement was recorded for all variants. The highest G\* and lowest  $\delta$  values for both temperatures were achieved by binders with SBS; this PMB binder verifies the expected more elastic

and better resistant bituminous binder when permanent deformation under higher temperatures is concerned. Almost identical phase angles were noticed for both binders with PAO; these only differ in the complex shear modulus but, again, the difference is not too distinctive. After short-term ageing, it is obvious that the binder with SBS at 60 °C demonstrated almost no change in the characteristics examined. In the case of the variants with PAO, qualitative characteristics increased considerably, particularly for the variant with a higher content of the additive – a certain negative influence of ageing can be seen. After long-term ageing, all of the characteristics measured recorded significant changes for all variants; again, a visibly lowest ageing is shown by the SBS variant. When the  $G^*/\sin(\delta)$  characteristic was compared, the variant with SBS recorded a 2.5 times increase after long-term ageing (when compared to the unaged sample) while the other modified binders had up to 8-times increases.

The other approach chosen to express the oscillation test data assumes that frequency sweeps have been carried out for the temperature range of 20–60 °C with frequencies ranging from 0.1 to 10 Hz for each temperature selected. Subsequently, temperature and time superposition is applied to viscoelastic materials where all values measured are related to the selected temperature which, in the case of the presented results, amounted to 20 °C. This enables to make a very good assessment of the deformation effect of individual binders over a broad frequency interval which facilitates the interpretation of various impacts of traffic load and intensities on the material in the pavement structure. The graphic representation shown as a master curve is presented in Fig. 5.

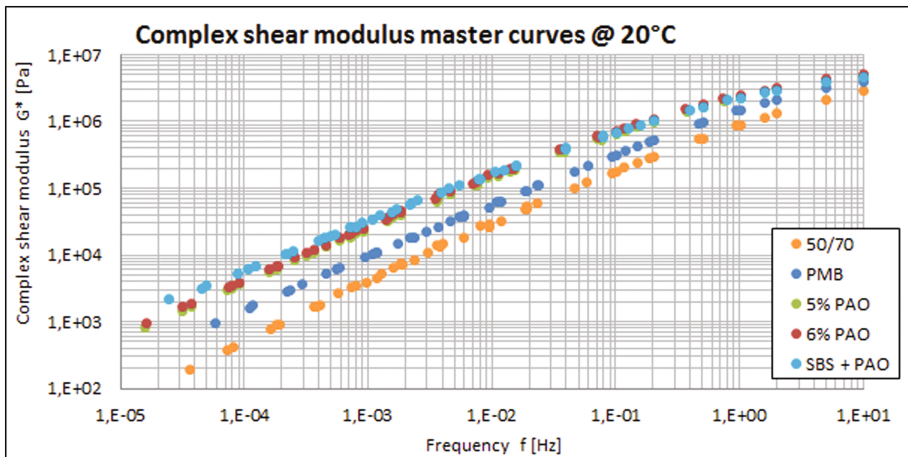
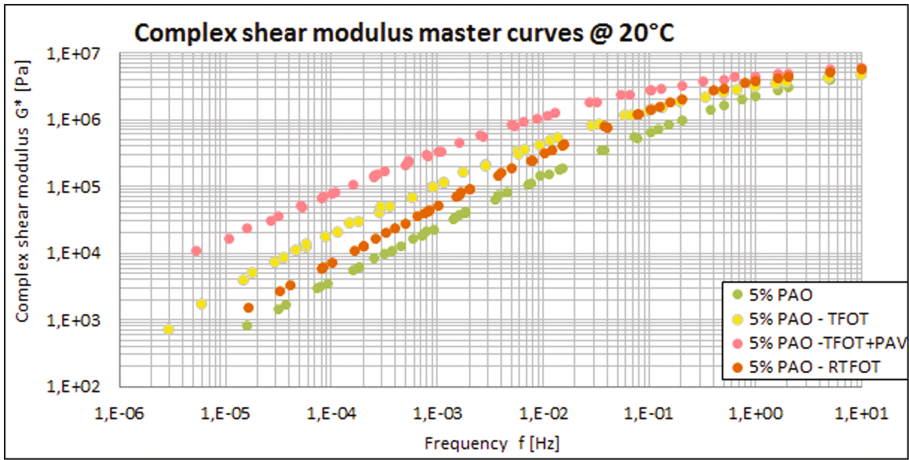


Fig. 5. Complex shear modulus master curves; reference temperature 20 °C

Figure 5, depicts the complex modulus dependence on frequency, reconfirms the highest  $G^*$  for binders with SBS + PAO, which signifies the highest stiffness of the binder, particularly under lower frequencies. Lower frequencies correspond with high temperatures which has a positive effect on bituminous binder stiffness and resistance

against permanent deformation. This claim is also supported by the results of the basic characteristic, SHRP  $G^*/\sin(\delta)$ , which has the highest values for this binder as well. In this figure, all curves of the modified binders are largely similar; therefore, the distinct difference in comparison to the reference binder can be mainly observed.

Figures 6 and 7 exploit two cases of the binders under evaluation to demonstrate the master curve change affected by ageing. The variant with 5% PAO showcases a significant difference after both short- and long-term ageing (the same applies to the



**Fig. 6.** Complex shear modulus master curves for bitumen with 5% PAO; different regimes of ageing

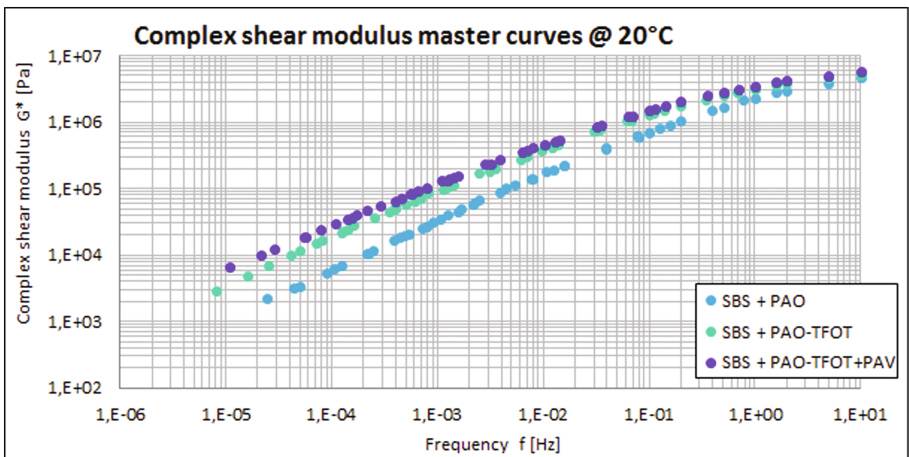


**Fig. 7.** Complex shear modulus master curves for bitumen SBS + PAO; different regimes of ageing

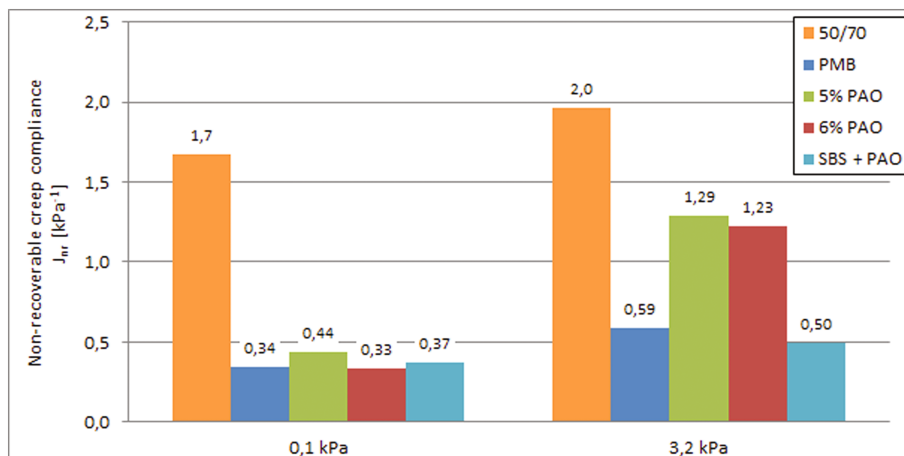


Fig. 8. Irreversible shear compliance of assessed binders,  $T = 60\text{ }^{\circ}\text{C}$

variant with 6% PAO), while the change for the variant SBS + PAO is not as distinctive; again, this confirms improved resistance to ageing of this bitumen variant. This fact is also supported by the smaller total difference between the individual complex shear modulus values for the thermo-oxidative degrading state, particularly for the frequency range of  $10^{-5}$  to 1 Hz.

### 3.3 Multi-stress Creep Recovery Test (MSCR)

Last performed test was the MSCR test determining the bitumen resistance to plastic deformation under elevated operation temperatures. This method determines the percentage of elastic recovery and non-recoverable creep of bituminous binders. The elastic recovery is an indicator of the tested bitumen sample to revert to its original state after multiple stress and relaxation. The percentage expression is used to determine the levels of elastic response and strength dependencies in modified and, possibly, even unmodified bituminous binders where it distinguishes the elasticity levels of the two bituminous binder types very well. The test uses the concept of cumulative material's strain under a constant stress.

The test describes bituminous binder behaviour at a selected temperature ( $60\text{ }^{\circ}\text{C}$ ) and with simultaneous effect of shear stress of 0.1 kPa and 3.2 kPa. The output from the test is the determination of elastic recovery (elasticity) in the bitumen expressed as the non-recoverable shear compliance,  $J_{nr}$ , at the same time. The lower the  $J_{nr}$ , the greater proportion of stress the binder is capable to absorb, being less susceptible to plastic deformation. Based on our findings so far, the informative value required for highly stressed pavements is  $J_{nr}$  of less than  $1\text{ kPa}^{-1}$  after ten cycles at stress of 0.1 kPa and another ten cycles at 3.2 kPa and at a temperature of  $60\text{ }^{\circ}\text{C}$ .



### 3.3.1 Results of MSCR Test

As it is obvious from the results shown in Fig. 8, the expected significant improvement in the values monitored was recorded for all modified binders in comparison to the control bitumen 50/70. For the variants with bitumen 50/70 and lower stress of 0.1 kPa, the values of unaged modified binders are also identical; however, for higher stress, there is a distinctive difference when SBS polymer is applied – this highlights the more significant effects of higher stress on the material. In both cases of application of PAO alone, the maximum value of  $J_{nr} = 1 \text{ kPa}^{-1}$  under 3.2 kPa was exceeded. If the elastic recovery is compared (Fig. 9), the significantly higher elastic recovery in the SBS + PAO variant is obvious which also complies with the values measured in the elastic recover test according to EN 13398.

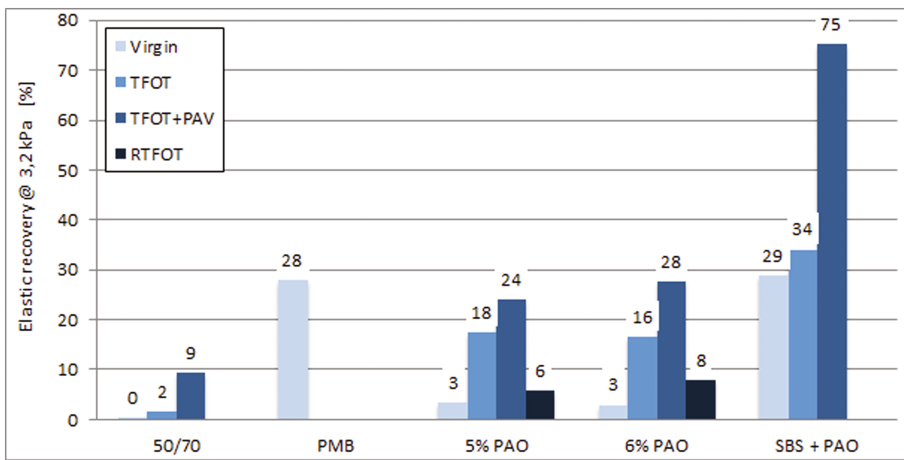
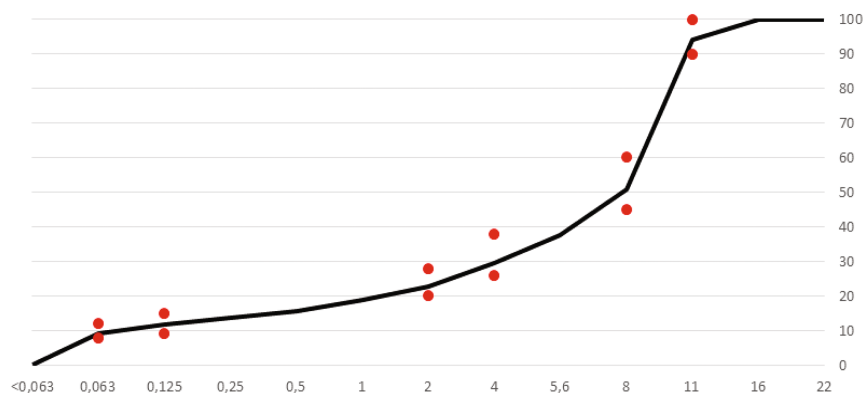


Fig. 9. Elastic recovery of assessed bituminous binders after ageing,  $T = 60 \text{ }^\circ\text{C}$  and stress 3.2 kPa

## 4 Asphalt Mix Design

The selected mix of the SMA 11S type is based on an extensive series of experimental testing conducted at the Faculty of Civil Engineering, Czech Technical University in Prague, since 2014. Particular assessed and described experimental SMA mixtures were always designed with the same grading curve (Fig. 10) and the same bitumen content. The mix consisted of crushed spilite aggregates from the Litice quarry in Western Bohemia. The used limestone filler originates from Velké Hydčice quarry. All mixtures applied 5.8 M% of bituminous binder. The mix composition is summarised in Table 4.



**Fig. 10.** Grading curve of SMA 11S mix

**Table 4.** Mix design of SMA 11S

Aggregate fraction/Mix component	Content in aggregate mix (%)	Content in asphalt mix (%)
Litice 8/11	52	<b>49.0</b>
Litice 4/8	20	<b>18.8</b>
Litice 2/4	5	<b>4.7</b>
Litice 0/2	12	<b>11.3</b>
JMV	11	<b>10.4</b>
Bitumen	–	<b>5.8</b>
Fibers S CEL	–	<b>0.3</b>
<b>TOTAL</b>		100.3

#### 4.1 Variants of the Mix Designs

Table 5 lists the individual variants of SMA mixtures assessed; four reference mixtures were chosen to illustrate the behaviour of the version with standard paving grade bitumen and polymer-modified bitumen (PMB). Moreover, the version either with

**Table 5.** The individual variants of SMA mixes

Mix designation	Description	Bitumen	Type of fibers
A	Reference (control) mix No. 1	50/70	Cellulose fibers F3000
B	Reference (control) mix No. 2	50/70	S-Cel fibers
I	Reference (control) mix No. 3	PMB 25/55-55	Cellulose fibers F3000
J	Reference (control) mix No. 4	PMB 25/55-55	S-Cel fibers
E5	5% poly-alpha-olefin	50/70	S-Cel fibers
E6	6% poly-alpha-olefin	50/70	S-Cel fibers
ES	3% SBS a 1% poly-alpha-olefin	50/70	S-Cel fibers

paving grade bitumen or PMB involved cellulose fibres F3000 (variant A, I) and S-CEL fibres (variant B, J) as well. Three mix versions applied binders containing a poly-alpha-olefin additive (variant E5, E6), and one of these cases involved mixing 3 M% of SBS polymer and 1 M% of PAO in the 50/70 bitumen (variant ES).

## 4.2 Basic Characteristics of Individual Variants of SMA

### 4.2.1 Volumetric Properties

The following values were determined for all asphalt mixtures designed: maximum density of asphalt mix and bulk density of compacted asphalt mix. In compliance with EN 12697-8, the voids content of the asphalt mix was subsequently determined. The results are listed in Table 6. According to the national appendix of standard EN 13108-5 the required limits of voids content for SMA 11S has to be 3.0%–4.5% for design. The control testing then requires 2.0%–6.0%.

**Table 6.** Volumetric characteristics of SMA 11S mixtures

Mix designation	Maximum density (g/cm <sup>3</sup> )	Bulk density (g/cm <sup>3</sup> )	Voids content (%-vol.)
A	2.594	2.530	2.5
B	2.595	2.508	3.4
I	2.594	2.502	3.5
J	2.567	2.478	4.5
E5	2.573	2.477	3.7
E6	2.578	2.467	4.1
ES	2.565	2.488	3.0

The control mix (designation J) demonstrates higher voids content values which is on the upper required limits from the perspective of initial type testing (ITT) as stipulated by the standard. This might be caused by lack of precision during the production as such, and during the determination of bulk and maximum density – in both cases, the values are illogically high. All mixtures are satisfactory from the point of view of control testing. Increased content of PAO results in a slight increase in voids content, while the combination with SBS polymer reduces voids.

## 5 Durability of Asphalt Mixtures

### 5.1 Determination of Water Susceptibility

One of the basic parameters assessed nowadays particularly in case of mixtures for the surface and binder courses is the durability which is generally expressed by the ITR characteristic (indirect tensile strength ratio for saturated and unsaturated specimens prepared by Marshall compactor with  $2 \times 25$  blows). The characteristic is determined in compliance with EN 12697-12. Simultaneously with that, the experimental activities

included monitoring of the modified ITSR which, in case of saturated specimens, is based on the methodology of AASHTO T 283 standard, where specimens are exposed to not only water but also the effects of freezing cycles. In contrast to the US standard, the applied methodology is adjusted, particularly in the sense of compacting the test specimens, using identical approach to that of EN 12697-12. The relevant test specimen set is subsequently saturated with water in the exsicator with the effect of the vacuum and the saturated specimens in plastic wraps are placed in a freezer at  $(-18 \pm 3) \text{ }^\circ\text{C}$  for at least 16 h. After that time, the test specimens are placed in a water bath of  $60 \text{ }^\circ\text{C}$  for another 24 h. The indirect tensile strength (ITS) according to EN 12697-23 is determined for all specimens identically while the specimens are tempered to the test temperature of  $15 \text{ }^\circ\text{C}$  for at least 4 h before the test.

The SMA mix standard EN 13108-5 does not require this type of test. For AC mix types, ITSR in the “S” mix quality class requires at least 80% which was used in this study. As has been discovered in relation to the values according to the AASHTO standard, the ITSR value is then approximately ten percentage points lower – however, this does not apply generally.

### 5.1.1 Results of Water Susceptibility

The results given in Table 7 show with respect to water susceptibility tests not only the benefit of PMB binders but also the benefit of PAO where a condition with minimum strength decrease after water immersion is basically achieved for the selected mixtures. From the point of view of combined effects of water and frost, the mixture with bitumen containing 5% PAO seems to be the most suitable variant. Nevertheless, the remaining two variants of SMA mixture (designation E6 and ES) with binder containing PAO demonstrate also very good values of water susceptibility (Fig. 11).

**Table 7.** Results of water susceptibility of assessed SMA 11S mixtures

Mix designation	ITS <sub>dry</sub>	ITS <sub>EN</sub>	ITS <sub>AASHTO</sub>	ITSR <sub>EN</sub>	ITSR <sub>AASHTO</sub>
	(MPa)	(MPa)	(MPa)	(-)	(-)
A	1.63	1.40	1.55	0.86	0.95
B	1.49	1.32	1.30	0.89	0.88
I	2.13	2.09	2.03	0.98	0.95
J	1.69	1.69	1.73	1.00	1.02
E5	1.23	1.19	1.11	0.96	0.90
E6	1.21	1.20	0.99	0.99	0.82
ES	1.58	1.59	1.36	1.00	0.86

Note: IST<sub>dry</sub> – testing of the indirect tensile strength at dry condition to the test temperature of  $15 \text{ }^\circ\text{C}$  (according to ČSN EN 13108-5)

The values of indirect tensile strength for dry specimens are rather baffling – both SMA mixture variants with 50/70 bitumen and application of PAO score lower values in comparison to the reference mix. Adding cellulose fibers F3000 (variant A, I) leads to increased values of indirect tensile strength.

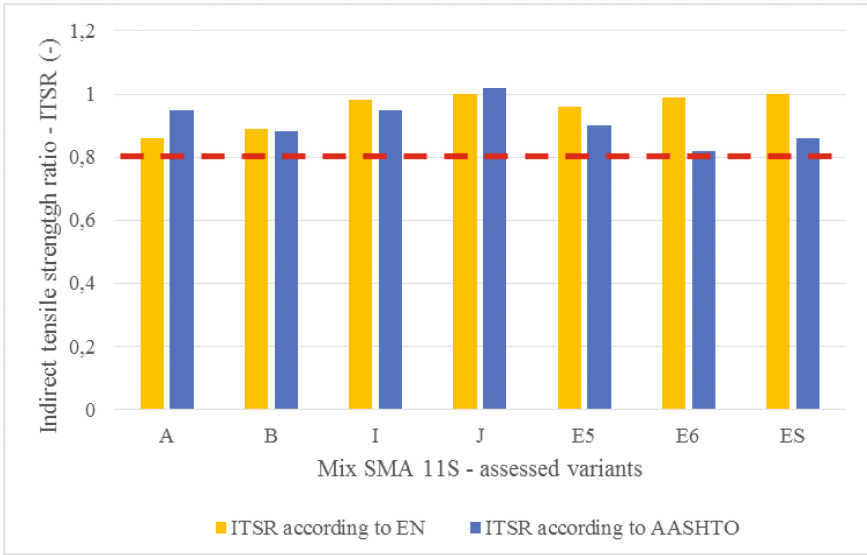


**Fig. 11.** Result of indirect tensile strength ratio for assessed mixtures by EN standard and AASHTO

## 5.2 Determination of Stiffness

The stiffness modulus characteristic was determined by the IT-CY test method in compliance with EN 12697-26 (Annex C) on cylindrical test specimens for 4 selected test temperatures. Test specimens were tested both as unaged asphalt mixtures and as mixtures exposed to laboratory long-term ageing procedure which was carried out with cylindrical test specimens according to prEN 12697-52 (specimens stored at 85 °C for 5 days in air circulated oven).

### 5.2.1 Results of Stiffness Modulus

Table 8 summarizes the results of stiffness determinations conducted on unaged test specimens. Focusing on the key reference temperature at 15 °C, for which the stiffness modulus is used in the Czech Republic in pavement structure design calculations, there is an obvious influence of paving grade bitumen substitution by PMB binder. At the same time, it is also necessary to consider the fact that PMB 25/55-55 was applied. The application of PAO basically generates no improvement; the combination of SBS with PAO even resulted in slight stiffness modulus deterioration not only from the perspective of 15 °C but also in relation to thermal susceptibility. In general, the application of the used additive or modifiers does not result in clearly visible thermal susceptibility changes.

**Table 8.** Stiffness modulus of unaged SMA 11S mixtures at different test temperatures

Mix designation	Stiffness (MPa) at the test temperature				Thermal susceptibility	
	0°C	5°C	15°C	27°C	$S_5/S_{27}$	$S_0/S_{27}$
A	–	17 624	7 320	2 939	6.0	–
B	–	16 642	6 666	2 497	6.7	–
I	–	18 562	10 291	3 903	4.8	–
J	–	15 803	9 319	2 380	6.6	–
E5	18 140	14 966	6 189	2 258	6.6	8.0
E6	18 841	15 793	7 047	2 550	6.2	7.4
ES	17 798	14 908	6 299	2 205	6.8	8.1

**Table 9.** Stiffness modulus of aged SMA 11S mixtures at different test temperatures

Mix designation	Stiffness (MPa) at the test temperature				Thermal susceptibility	
	0°C	5°C	15°C	27°C	$S_0/S_{27}$	$S_5/S_{27}$
A	16 396	16 854	6 535	2 353	7.0	7.2
B	16 877	15 422	5 819	1 764	9.6	8.7
I	18 764	17 236	9 145	3 496	5.4	4.9
J	21 962	19 386	9 234	3 624	6.1	5.3
E5	17 934	–	8 204	3 151	5.7	–
E6	21 593	–	9 026	3 683	5.9	–
ES	18 874	–	8 255	3 453	5.5	–

**Table 10.** Ageing index of asphalt mix stiffness

Mix designation	Stiffness ageing index				Thermal susceptibility index	
	0°C	5°C	15°C	27°C	$S_0/S_{27}$	$S_5/S_{27}$
A	–	0.96	0.89	0.80	–	1.19
B	–	0.93	0.87	0.71	–	1.31
I	–	0.93	0.89	0.90	–	1.04
J	–	1.23	0.99	1.52	–	0.81
E5	0.99	–	1.33	1.40	0.71	–
E6	1.15	–	1.28	1.44	0.79	–
ES	1.06	–	1.31	1.57	0.68	–

The results of stiffness modulus for test specimens subjected to ageing are indicated in Table 9 along with the ageing index characteristic given in Table 10. The results demonstrate that, as has been expected, due to the binder degradation and increased

stiffness, the stiffness modules increase as well. At 15 °C, this elevation rests on average at a 25% level. From the results gained for bituminous binders after ageing it is obvious that binder modified with PAO and SBS is the least ageing susceptible variant. Nevertheless if this result would be compared to the ageing index found for asphalt mixtures such conclusion would not be as evident.

### 5.3 Resistance to Permanent Deformation

Asphalt mix resistance to permanent deformation was tested according to EN 12697-22 with a small test device in air bath using test temperature of 50 °C and loading the test slabs by 10,000 cycles. The national annex to the product standard EN 13108-5 stipulates the requirements for  $PRD_{AIR}$  parameter as 5% and for  $WTS_{AIR}$  by maximum 0.07 for resistance to permanent deformation required in case of SMA mixtures.

#### 5.3.1 Results of Resistance to Permanent Deformation

From the perspective of the results, it can be noted that with the exception of  $WTS_{AIR}$  in the variant B, all variants fit within the required limit values. In most cases, the results fit very comfortably which corresponds with the findings concerning the stiffness results to a certain degree. What is interesting is the fact that 6% of PAO scores identically to the reference mix with paving grade bitumen 50/70; in contrast to that 5% of PAO resulted in a slight deterioration while this variant is fundamentally identical to the SMA mixture where SBS polymer was applied along with 1% of PAO. These results are clearly summarized in Table 11. Resistance to permanent deformation should be considerably dependent on the values  $J_{nr}$  from the MSCR test on bituminous binders. Figure 12 confirms certain dependence, but it is not a strong dependence. The main difference compared with the results of bituminous binders is that the variant with SBS did not prove the best resistance to permanent deformation.

**Table 11.** Resistance of SMA 11S mixtures to permanent deformation

Mix designation	Maximum relative rut depth ( $PRD_{AIR}$ ; %)	Maximum increment of rut depth ( $WTS_{AIR}$ ; mm)	Maximum rut depth after 10,000 cycles (mm)
A	2.3	0.028	1.09
B	4.0	0.080	2.00
I	2.8	0.023	1.24
J	1.6	0.016	0.72
E5	2.9	0.044	1.41
E6	2.3	0.021	1.03
ES	2.9	0.037	1.34

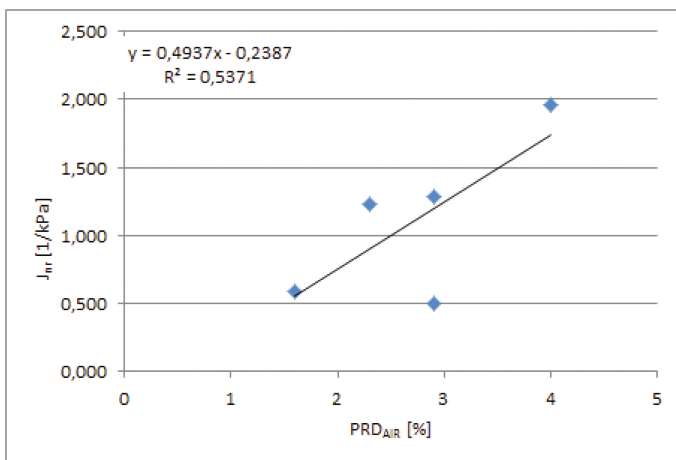


Fig. 12. Correlation between PRD<sub>AIR</sub> and J<sub>nr</sub>

## 6 Conclusions

Within the framework of the experimental assessment of potentials for poly-alpha-olefins (PAO) 3 bituminous binders modified by PAO used in bitumen 50/70 were prepared in the laboratory. The first finding is an overall reduction of penetration and a higher softening point value; this leads us to the question whether the used paving grade 50/70 is ideal for this examination, particularly if the binder is subsequently applied to an SMA-type mix. However, what is more important, is the inter-comparison of the effects of PAO and the PAO + SBS combination when, logically, a significantly more improved behaviour of the bituminous binder modified by SBS can be expected. Especially according to the performance based testing, the difference in the effect of SBS in comparison to PAO is rather great. However, the question remains of what quality would be achieved by a binder if the SBS level were reduced to e.g. 1.5 M% or 2 M% and the quantity of PAO would range from 2 to 3 M%. In general, in relation to the quantities of additives or modifiers added, we have to point out that increasing the proportion of PAO from 5 M% to 6 M% is ineffective both technically and economically.

From the perspective of general use of a binder modified by a PAO addition, the binder obtained might play the role of a certain in-between step if looking on a broad bitumen family between the standard paving grades and PMB binders. The binder possesses improved deformation characteristics. Its behaviour from the point of view of high resistance to ageing is more limited to a certain extent, and its elastic properties are really small.

Focusing on the effects of PAO on asphalt mixtures the results of the empirical tests clearly show that in the case of bulk densities, all the variants behave similarly; they approximate or even score values comparable to the asphalt mixture with PMB applied. With respect to the fact that all mixtures were prepared under standard temperatures (depending on the bitumen applied) and test specimens were compacted at 150 °C or 160 °C (PMB), the results of comparable voids content show that the tested additive



has no distinctive effect on workability improvement. However, this finding should be treated with caution as it might be significantly affected by the quality of the mix composition as such.

In the case of the stiffness test, the mixtures demonstrated no improvement in comparison to the reference mix. Even the thermal susceptibility values are identical to the reference mixtures. According to the water sensitivity test it can be noted that the saturation by water has no impact on any deterioration of indirect tensile strength when test procedure according to the EN standard is applied. The assessment of asphalt mix behaviour from the point of view of resistance to permanent deformation shows, that the results copy the findings for stiffness to a certain extent. If the variants with PAO are compared to standard SMA 11S with polymer modified bitumen, it is logical that the variant with PMB has a slightly better performance.

In general, it can be noted that in some respects, PAO results in improved behavior of SMA mixtures (particularly improved water susceptibility); nevertheless, there are performance-related characteristics where no improvement has been proven, or the mixtures assessed demonstrated identical values at best. It was even not possible to confirm improved workability when PAO was applied. Nonetheless, the above does not mean that the additive is unsuitable or has no use within the road construction industry. From the perspective of used dosage, it might be recommended to seek for applications with maximum 5% of the additive. If an improved effect was sought in combination with polymer modified binder and PAO, it should be recommended focusing rather on verification of such applicability with industrially prepared PMB binders. It might not be true to present the potential of the additive in the way as an equal binder with SBS, especially where the modification is carried out directly by the asphalt mixing plant itself since the laboratory assessments did not prove a justifiable effect.

**Acknowledgments.** This paper was supported by the research project No TA04031255 of the Technology Agency of the Czech Republic.

## References

- Designing and Constructing SMA Mixtures—State-of-the-Practice. National Asphalt Pavement Association (NAPA). Lanham, 57 pp. (1999)
- Kong, L.Y., Zhou, J.C., Li, W.: Experimental research of APAO modified asphalt. *Technol. Hwy. Trans.* **10**, 63–67 (2005)
- Wardlaw, K.R.: *Polymer Modified Asphalt Binders: Laboratory and Field Studies of Polyolefin and Latex Modifiers for Asphalt Mixtures*, ASTM Publication Code Number (PCN) 04-011080-08, 1992, Philadelphia (1992)
- Wei, J., Liu, Z., Zhang, Y.: Rheological properties of amorphous poly alpha olefin (APAO) modified asphalt binders. *Constr. Build. Mater.* **48**, 533–539 (2013). ISSN: 0950-0618
- Wei, J., et al.: Study on the amorphous poly alpha olefin (APAO) modified asphalt binders. *Constr. Build. Mater.* **66**, 105–112 (2014). ISSN: 0950-0618
- Zhu, J., Birgisson, B., Kringos, N.: *Polymer modification of bitumen: advances and challenges*. Division of Highway and Railway Engineering, Department of Transport Science, KTH Royal Institute of Technology, Sweden (2014)

# Influence of Mix Parameters on Development of Sulfur Modified Bituminous Paving Mixes with Sand

Subhashree Jena<sup>(✉)</sup>, Mahabir Panda, and Prasanta Kumar Bhuyan

Department of Civil Engineering,  
National Institute of Technology Rourkela, Rourkela, Odisha, India  
subhashreejena021@gmail.com,  
{mpanda, bhuyanp}@nitrkl.ac.in

**Abstract.** Aggregates obtained from natural stone resources is the main source of infrastructure including road-pavement construction. To keep pace with economic development, rapid industrialization and urbanization, the natural stone resources are being depleted at an alarming rate, which is a major concern for future construction. Keeping this issue in mind, the use of alternative materials to aggregates for construction is a major research interest. Since sand is available abundantly in some places, such as: coastal deltaic plains and desert areas, it is necessary to evaluate the potential of sand as an alternative to the stone aggregates. But, because of its low stability, sand-bituminous mix was not found to be suitable for pavement construction. The advantageous effects of using sulfur with construction materials motivated the authors to develop sand-bitumen mixes modified by locally available commercial sulfur.

This research addressed the procedure to develop the sulfur modified bituminous mixes. Based on an earlier study, a Sand-Sulfur-Bitumen (S-S-B) mix comprising of poorly graded river sand, sulfur and VG 30 bitumen with proportion of 85:10:5 by weight was selected. The influence of mixing parameters such as: mixing sequences, mixing temperature and mixing time on performance characteristics of the mix was evaluated. The characterization of the mix was based on Marshall test due to its easy availability and widely usage for mix design. It was concluded that best results were obtained when the molten sulfur was added to heated sand and mixed for about 90s, followed by mixing of all the ingredients for about two minutes at a mixing temperature of 150°C.

## 1 Introduction

Globally, bituminous pavement constitutes the major share of the road-pavement construction due to its inherent advantages of smooth riding surface and lower initial cost of construction. Most commonly, the wearing coats/upper layers of such pavements are constructed with blend of aggregate and bitumen (bituminous mix) where bitumen provides the adhesion to bind the aggregates together. The rapid developments of road network and many other infrastructure projects have led to a severe depletion in the reserve of natural stone resources. Further, good quality aggregates (especially coarse aggregates) are not easily available or costly which increases the construction cost. Since,

sand is abundantly available in some places; researches on the use of sand in paving mixes as an alternative to aggregates are worth taking up. In this direction, few studies (Fatani and Sultan 1982; Satyakumar and Satheeshchandran 2013) reported the sand-bituminous mix to have high air voids and low stability that restricted its application in paving works. The ability of sulfur to improve the properties of bituminous mixes was studied mostly in the 1970's and 1980's. As a by-product of petro-chemical industries a large quantity of sulfur is produced, along with the coal processing and copper refining in mining sector. Thermopave, a new material consisting of a mixture of sulfur, bitumen and sand was introduced by Shell Canada Limited. Possessing properties comparable to conventional bituminous mixes, Thermopave could be used as an alternative for the same (Saylak and Gallaway 1974). Sulfur, when added to the bituminous mix, not only improved mix workability but showed improved field performance (Hammond et al. 1971). Later, investigation further established the potentiality of sulfur as a paving binder for low grade aggregates and sands to obtain paving mixes, as good as, or better than bitumen (Saylak et al. 1975). In addition, a two-continuous phase sulfur–asphalt composite was developed which was found to be suitable for use as a road repair material (Beaudoin and Sereda 1979). But due to insufficient anti-skid characteristics of native sand, the sand-bitumen-sulfur mixes was recommended to be used for base and binder courses but not as a finished riding surface (Glascok 1976). Along with the dune sand, the use of single-sized crushed aggregates, dense-graded aggregates and/or powdered sulfur in sand-bitumen mixes was reported to improve the engineering properties of the mix (Fatani and Sultan 1982).

This study addressed the feasibility of various mixing techniques that could be used to develop a best possible sand-sulfur-bitumen (S-S-B) mix that would perform satisfactorily when compared with conventional mixes with stone aggregates. Specimens were tested for different mixing sequences as it was anticipated that the homogeneity, workability and strength of the mixture might get affected by the sequence in which the three ingredients were added. Moreover, the temperature required to obtain a homogeneous mix depends upon the characteristics of its constituents. One of the most prominent characteristics of sulfur is the way its viscosity varies with temperature. In general, it can be found that the viscosity of sulfur decreases as the temperature increases above melting point. As the temperature is raised above 160°C, the viscosity rapidly increases (Saylak and Gallaway 1974). On the other hand, the viscosity of bitumen decreases with increase in temperature. Hence, after deciding the best mixing sequence, variables such as mixing time and mixing temperature were optimized for the S-S-B mix and an appropriate mixing procedure for suitable S-S-B mix was determined.

## 2 Experimental Investigations

### 2.1 Materials

The sand used in this study was collected from nearby Koel river bed. As per sieve analysis (Fig. 1) it was found to be almost uniformly graded with a uniformity coefficient of 2.48. The amount of materials passing through 75  $\mu\text{m}$  sieve was nil. The specific gravity of sand was 2.61. The sulfur was of commercial grade, having a specific gravity of

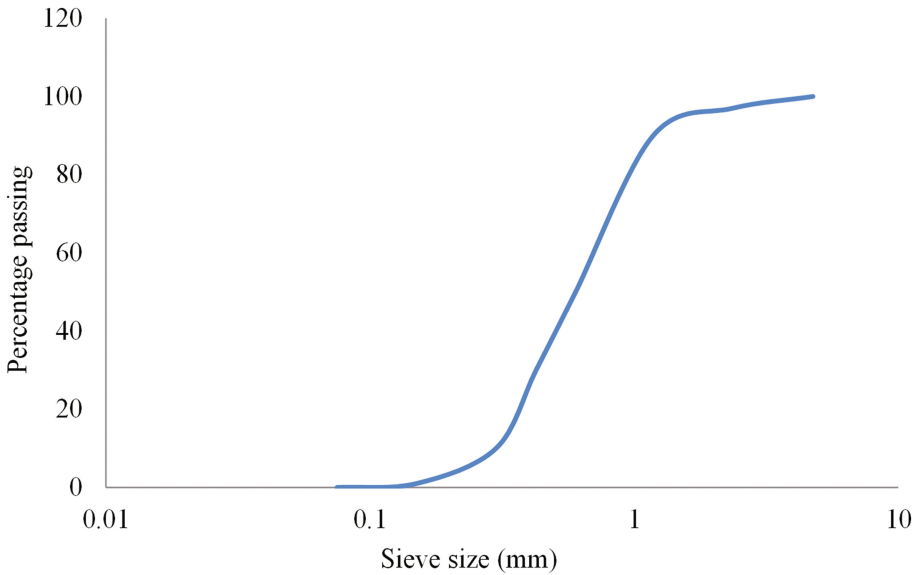


**Fig. 1.** Grain size distribution of river sand used

2.095 and melting point of 116.5°C. Viscosity graded, VG 30 bitumen having a specific gravity of 1.01 and softening point (R&B) of 48°C was used as binder. The important physical properties of the materials used in this study are summarized in Table 1.

**Table 1.** Physical properties of the materials used

Material	Physical Properties	
River Sand	Specific Gravity	2.61
	Coefficient of uniformity	2.48
	Coefficient of curvature	0.81
	Fineness modulus	4.22
	Water Absorption	0.81%
Bitumen	Grade	VG30
	Specific Gravity	1.01
	Penetration at 25°C (0.1 mm)	67
	Softening Point (R&B) (°C)	48
	Ductility (cm)	+100
	Absolute viscosity at 60°C (Poise)	2505
	Kinematic viscosity at 135°C (cSt)	405
Sulfur	Colour	Light Yellow
	Specific Gravity	2.095
	Melting Point	116.5°C

## 2.2 Preparation of S-S-B Mixes

In general, for preparation of S-S-B mix, measured quantity of sand was taken in a steel container and heated to 150°C like normal aggregate. The three ingredients, bitumen (heated to 150°C), sulfur (either in powder form or in a molten state at 140°C) and heated sand were mixed in different mix processing sequences. The mixing temperature was maintained at 150°C. As per Mazumdar and Rao (1985), the proportion of sand-sulfur-bitumen mix (by weight) was maintained at 85:10:5. Thus, specimens were prepared using Marshall method and then, tested in accordance with ASTM D1559 (1989).

## 3 Test Results and Discussions

### 3.1 Mixing Sequences

The three ingredients of the mix; namely sand, bitumen and sulfur were added in six different mix processing sequences as shown in Table 2. In the first sequence, sulfur powder was mixed with heated bitumen and then these two ingredients were thoroughly mixed with heated sand. Second sequence considered mixing of heated bitumen with heated sand and then, sulfur powder with the sand-bitumen mix. In the third sequence, sulfur powder was first mixed with heated sand and then, bitumen was mixed with the sand-sulfur mix. Fourth sequence employed mixing of molten sulfur with heated bitumen and then, these two ingredients were thoroughly mixed with heated sand. The fifth sequence involves mixing of bitumen to heated sand followed by mixing of molten sulfur with the sand-bitumen mix. Lastly, the sixth sequence involves thorough mixing of heated bitumen with the mix of sand and molten sulfur.

**Table 2.** Mixing sequence methods

No.	Sequences
Sequence 1	bitumen + sulfur powder + sand
Sequence 2	sand + bitumen + sulfur powder
Sequence 3	sand + sulfur powder + bitumen
Sequence 4	bitumen + molten sulfur + sand
Sequence 5	sand + bitumen + molten sulfur
Sequence 6	sand + molten sulfur + bitumen

The effects of different mixing sequences on the Marshall properties of the bituminous mixes are presented in Figs. 2, 3, 4 and 5. After a number of trials, it was observed that out of the six different mixing sequences considered, sequence 1 and sequence 4 produced the most unsatisfactory results. For mixes prepared by sequence 1 and sequence 4, the Marshall stability values were found to be 4.90 kN and 5.55 kN respectively, which are much lower than as specified for bituminous surface courses (MoRTH 2013). For all other mixing sequences, there was no significant difference observed in the Marshall properties of the mixes. However, the sixth (last) sequence,

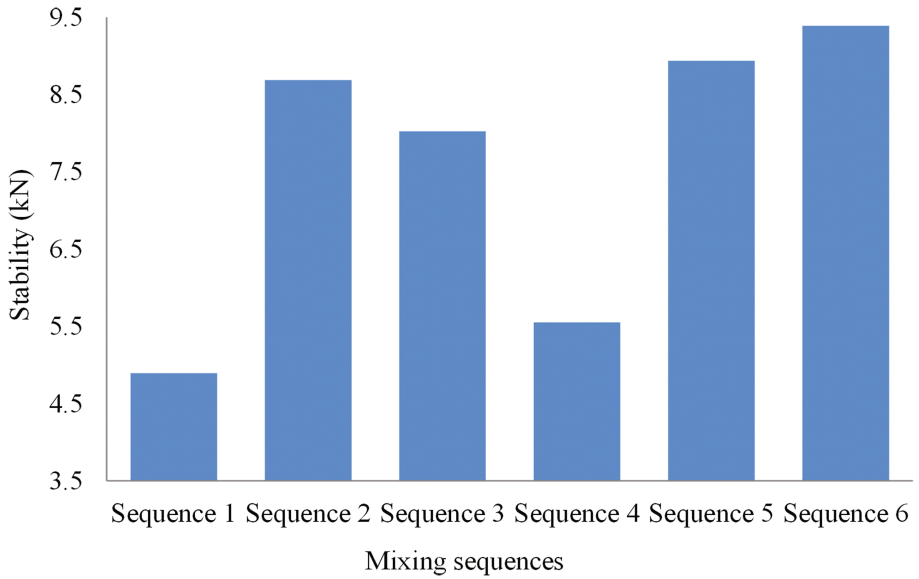


**Fig. 2.** Marshall stability values of mixes prepared as per different mixing sequences

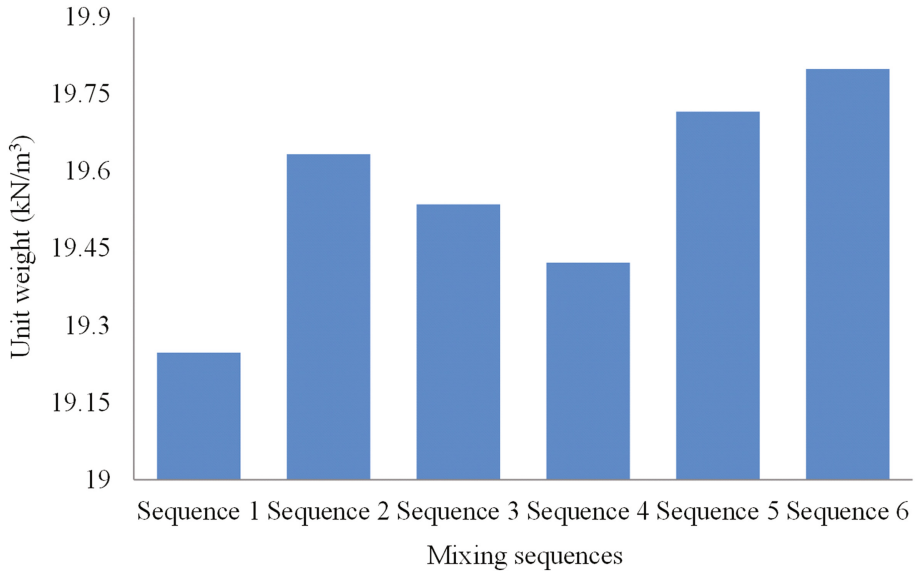


**Fig. 3.** Unit weight values of mixes prepared as per different mixing sequences

i.e., addition of molten sulfur to sand followed by addition of bitumen to the mix, was found to produce the best results. In this sequence, Marshall stability as high as 9.39 kN, flow value of 2.35 mm and air voids of 18.41% were obtained. During

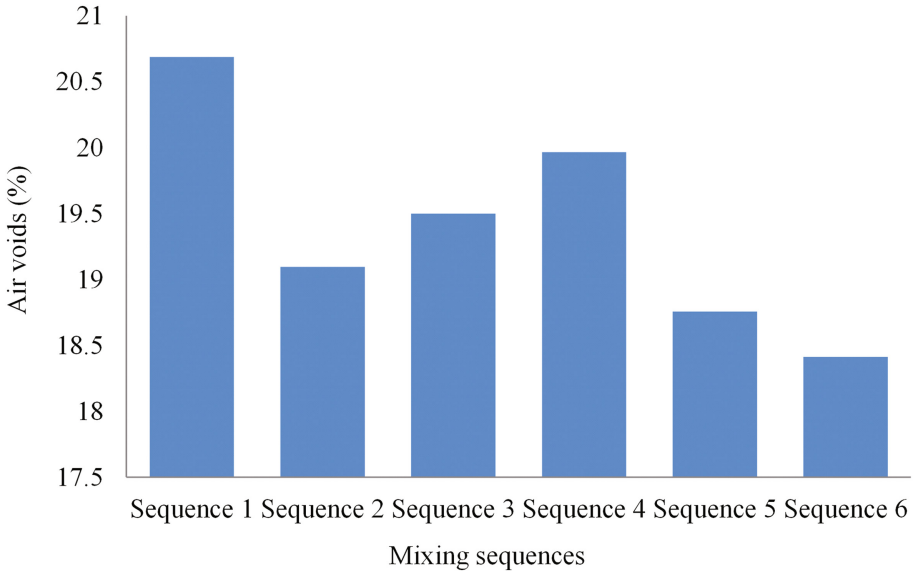


**Fig. 4.** Air voids of mixes prepared as per different mixing sequences

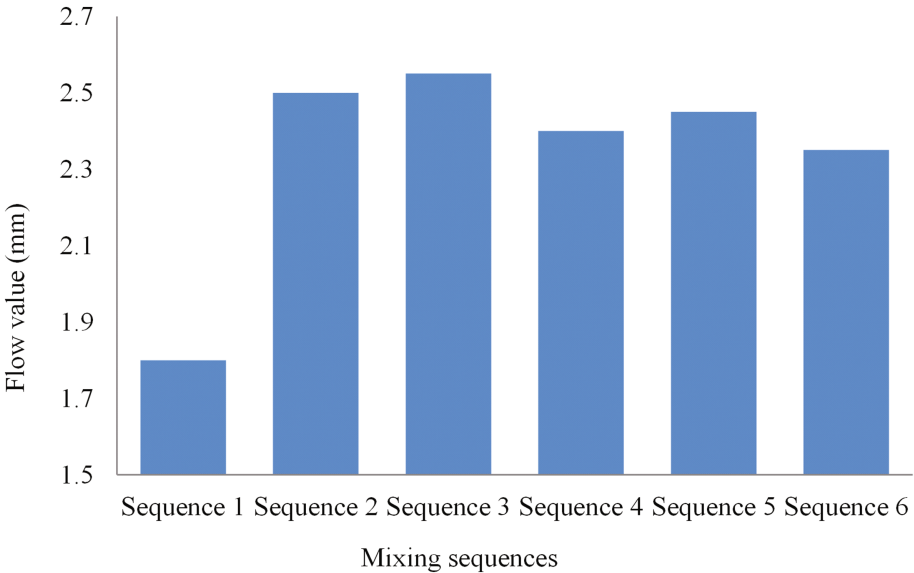


**Fig. 5.** Flow values of mixes prepared as per different mixing sequences

mixing process in the laboratory, addition of molten sulfur to the mix was physically observed to yield relatively better workability as compared to the addition of dry sulfur powder.

### 3.2 Mixing Temperature

After obtaining the best mixing sequence, several mix specimens were prepared under different mix conditions, by varying one parameter at a time while other parameters were kept constant. For the preparation of S-S-B mix, molten sulfur was added to the heated sand and thoroughly mixed for sixty seconds. Next, bitumen heated separately was added to the sand-sulfur mix and then, these three ingredients were mixed thoroughly for two minutes. In this process, the mixing temperature was varied in the range of 140–160°C with an increment of 5°C. The effects of mixing temperatures on the Marshall properties of mix are presented in Figs. 6, 7, 8 and 9. As observed from the influence of the mix temperature on the Marshall flow values of the mixes, the mix became more stiffer with an increase in the temperature of the mix. An optimum value of Marshall stability and air voids content of the mix was obtained at a mixing temperature of 150°C. At a mixing temperature of 140–150°C, Marshall stability increased possibly because the binder had adequate viscosity for mixing the ingredients homogeneously. Any further increase in temperature was observed to have an adverse effect on the workability and strength of the mix as the binder might have higher viscosity than required.

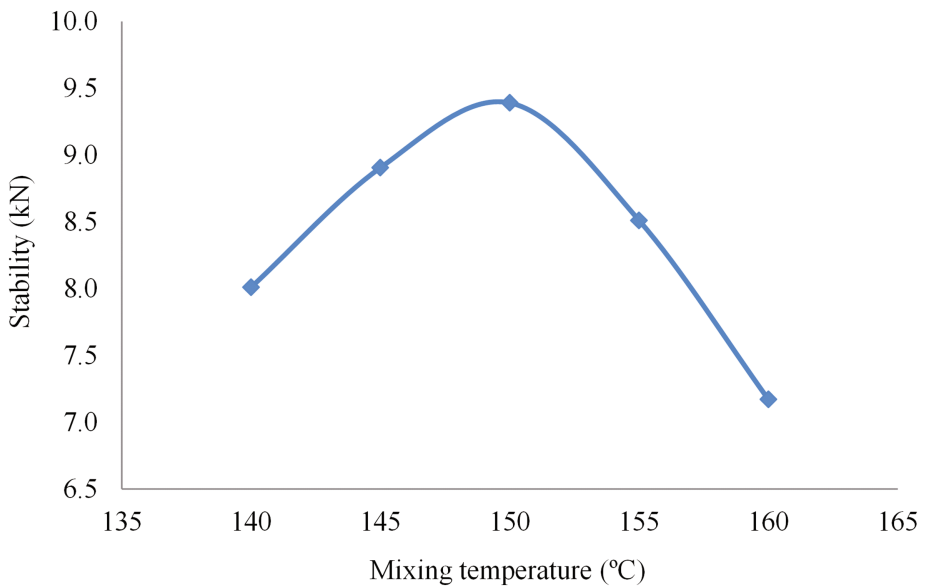


**Fig. 6.** Variation in Marshall stability with mixing temperature



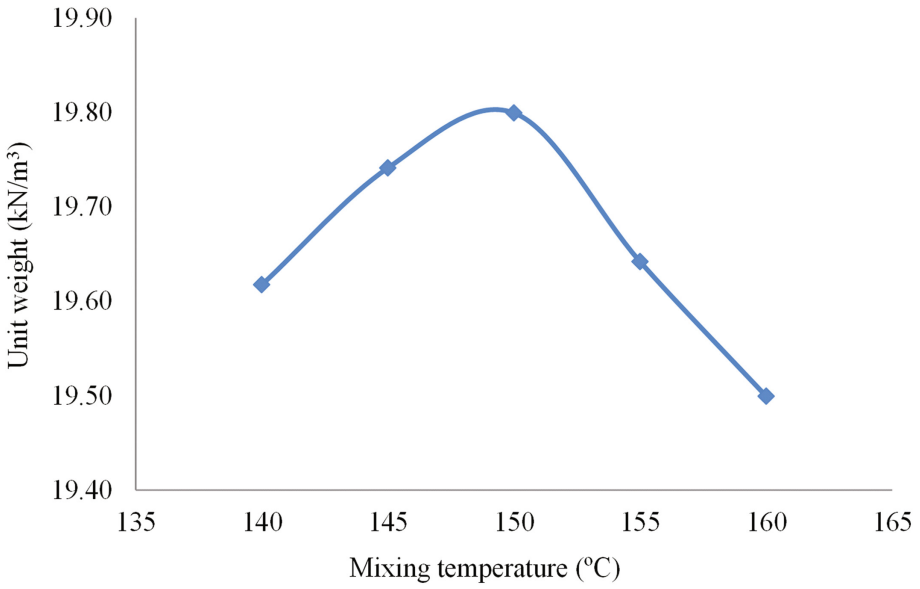


**Fig. 7.** Variation in unit weight with mixing temperature

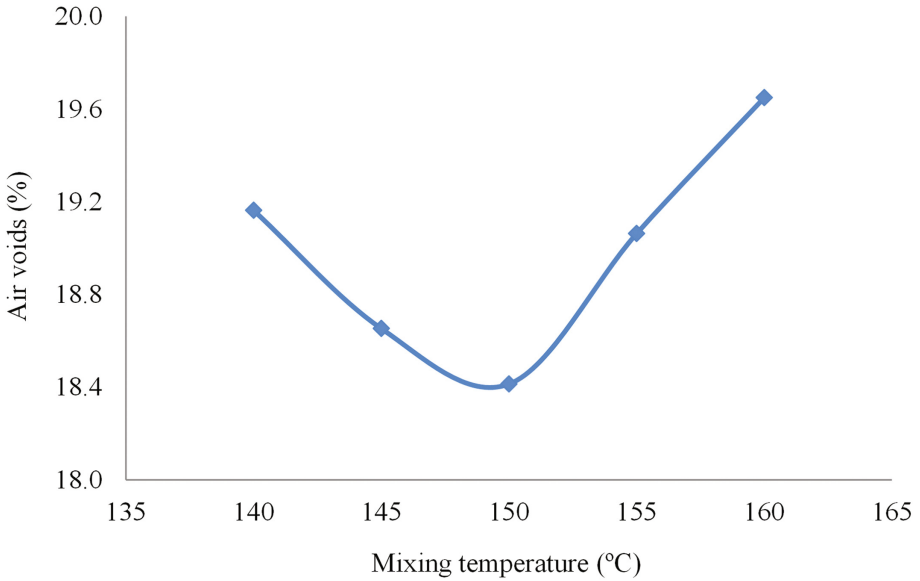


**Fig. 8.** Variation in air voids with mixing temperature

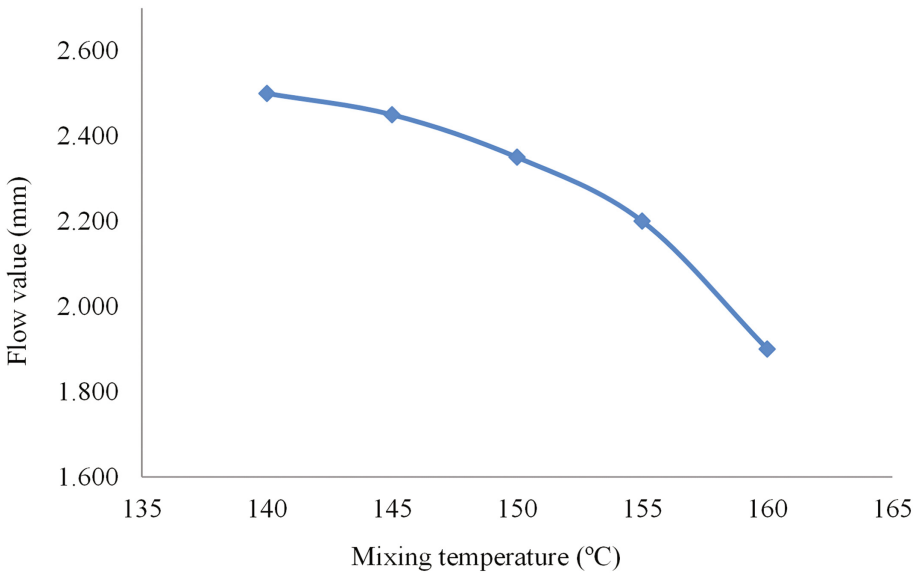


**Fig. 9.** Variation in flow value with mixing temperature

### 3.3 Mixing Time

#### 3.3.1 Mixing Time of Bitumen with Sand-Sulfur Mix

Sulfur in molten state heated to 140°C was added to heated sand and these two ingredients were mixed for about one minute. The mixing time of bitumen with sand-sulfur mix was varied from one to three minutes at a constant mixing temperature of 150°C. The variations in Marshall properties illustrated in Figs. 10, 11, 12 and 13 indicated that the best results were obtained when bitumen was mixed with the sand-sulfur mix for about two minutes.

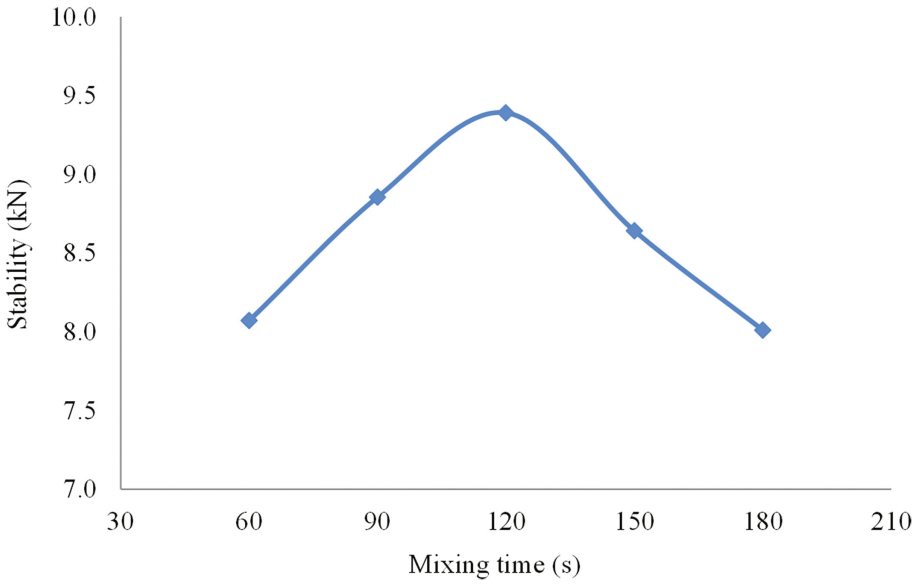


**Fig. 10.** Variation in Marshall stability with mixing time of bitumen with sand-sulfur mix

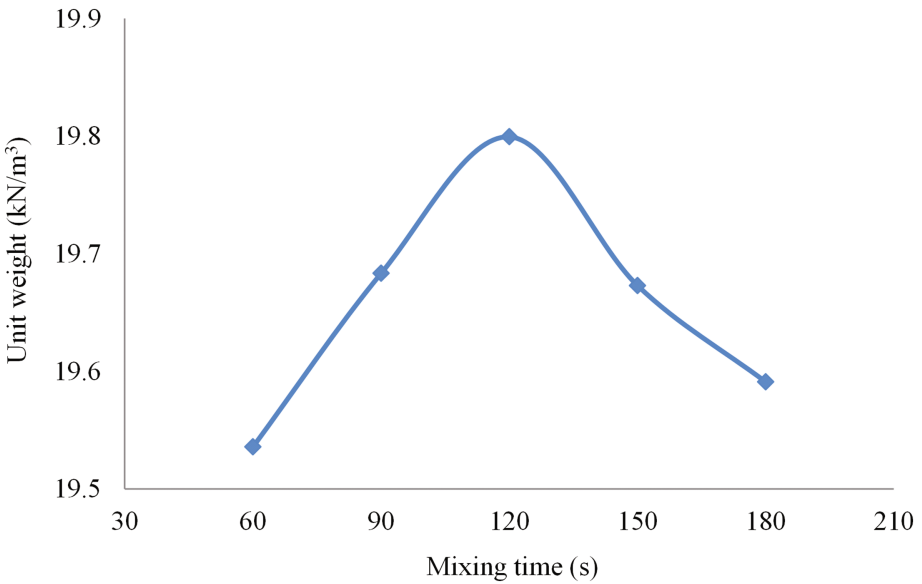


**Fig. 11.** Variation in unit weight with mixing time of bitumen with sand-sulfur mix

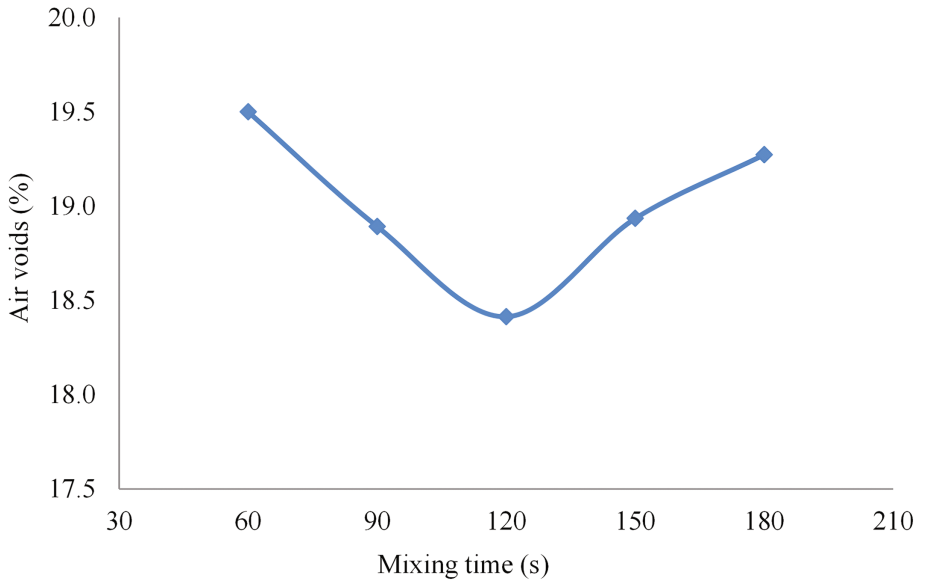


**Fig. 12.** Variation in air voids with mixing time of bitumen with sand-sulfur mix

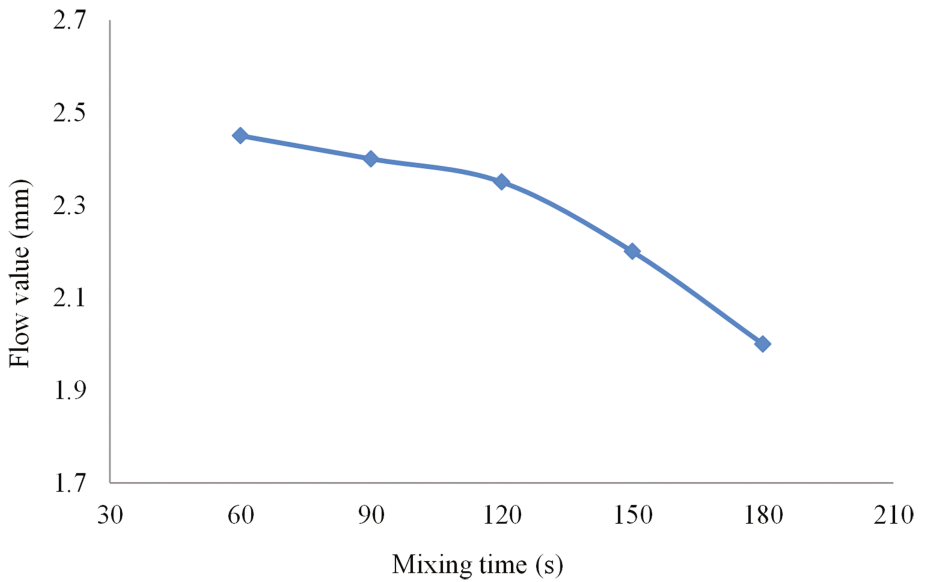


**Fig. 13.** Variation in flow value with mixing time of bitumen with sand-sulfur mix

### 3.3.2 Mixing Time of Sand and Sulfur

The mixing time of heated sand and molten sulfur was varied, followed by mixing of bitumen to the mix for about two minutes at a mixing temperature of 150°C. The effects

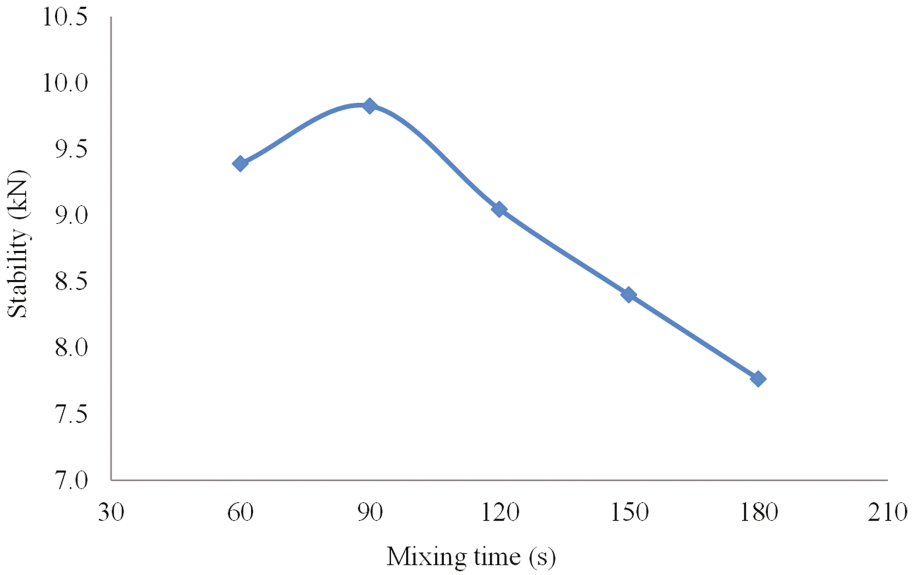


**Fig. 14.** Variation in Marshall stability with mixing time of sand and sulfur

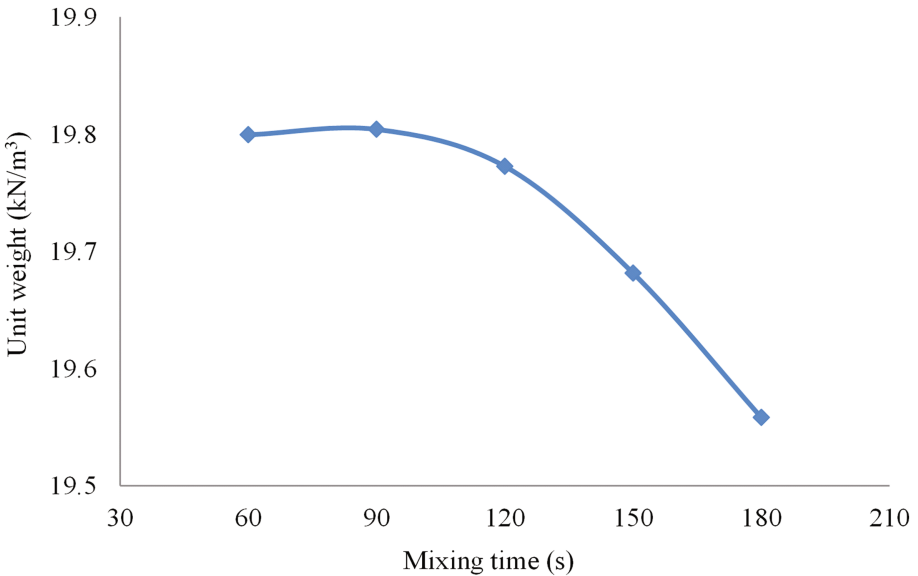


**Fig. 15.** Variation in unit weight with mixing time of sand and sulfur

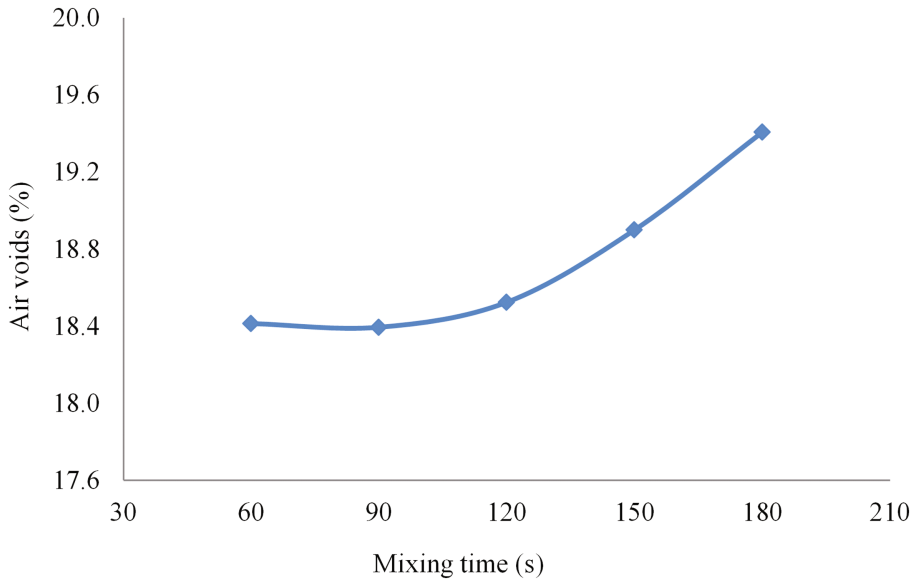


**Fig. 16.** Variation in air voids with mixing time of sand and sulfur

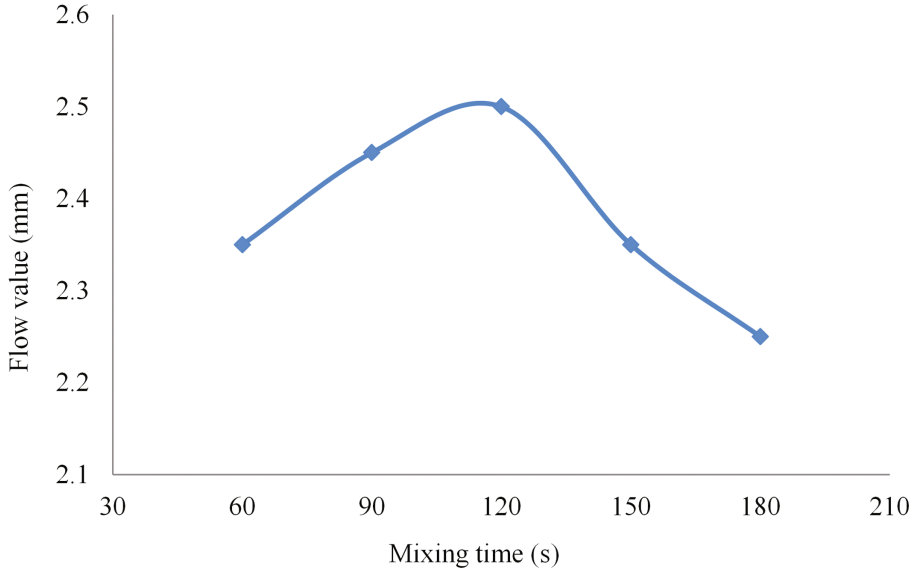


**Fig. 17.** Variation in flow value with mixing time of sand and sulfur

of mixing time of sand and sulfur on the Marshall properties of mixes are shown in Figs. 14, 15, 16 and 17. It was observed that Marshall stability as high as 9.83 kN, flow value of 2.45 mm and air voids of 18.39% were obtained when the sand and sulfur were mixed for about ninety seconds. With increasing mixing time, the Marshall stability values tend to show a decreasing trend. However, marginal differences in the unit weight values of the mixes were observed.

## 4 Conclusions

The influence of mixing parameters such as: mixing sequences, mixing temperature and mixing time were studied and a suitable procedure to achieve a best possible sand-sulfur-bitumen mix was developed. Based on the results of Marshall tests on sand-bitumen mixes involving different mix parameters, the major findings of this were summarized as follows.

- The Marshall characteristics of the mixes were sensitive to the sequence in which the three ingredients of the mix, i.e., sand, bitumen and sulfur were mixed. The mixing sequence involving/entailing addition of molten sulfur to sand, followed by the addition of bitumen to the mix yielded the best Marshall results.
- Selection of mixing temperatures higher than 150°C resulted in inferior workability and hence showed an adverse effect on both the stability and air voids of the mix.
- For better workability and Marshall stability, heated sand and molten sulfur was recommended to be mixed for about ninety seconds. Then heated bitumen should be mixed with the sand-sulfur mix for about two minutes at a mixing temperature of 150°C.
- For mixes with optimum mixing parameters, Marshall stability as high as 9.83 kN and flow value of 2.45 mm were obtained which satisfied the MoRTH (2013) specification of a minimum stability of 9.0 kN and flow value of 2–4 mm for dense bituminous mixes.
- However, use of almost single sized fraction of sand considered as aggregates resulted in higher air voids than the specified limit suggested by MoRTH for bituminous surface courses.
- Overall, it was found that the sand-bitumen mixes prepared with sulfur as an additive can be used as a binder course for all types of roads or even a surface course with a wearing coat such as: seal coat or semi-dense bituminous concrete, for a normally trafficked road.

**Acknowledgments.** The authors gratefully acknowledge the technical and non-technical staff of Highway Engineering Laboratory of National Institute of Technology Rourkela, Odisha, India for their supports during the material collection, specimen preparation and experimentation.

## References

- ASTM D 1559: Test Method for Resistance of Plastic Flow of Bituminous Mixtures Using Marshall Apparatus, American Society for Testing and Materials, Philadelphia, USA (1989)
- Beaudoin, J.J., Sereda, P.J.: A two-continuous-phase sulphur-asphalt composite-development and characterization. *Can. J. Civ. Eng.* **6**(3), 406–412 (1979). doi:[10.1139/l79-053](https://doi.org/10.1139/l79-053)
- Fatani, M.N., Sultan, H.A.: Dune sand-aggregate mixes and dune sand-sulfur mixes for asphalt concrete pavements. *Transportation Research International Documentation*, (No. 843), pp. 72–79, (1982)
- Glascok, L.A.: A Laboratory Evaluation of Sulfur-Asphalt Paving Mixtures. Louisiana Department of Highways, Research and Development Section, Baton Rouge, LA, USA, (No. LA-74-1B (B)-F Final Rpt) (1976)
- Hammond, R., et al.: The use of Sand-Asphalt-Sulphur mixes for road base and surface applications. In: *Proceedings Canadian Technical Asphalt Association*, vol. 16, pp. 27–51 (1971)
- Mazumdar, M., Rao, S.K.: Effect of comparative efforts on sand-asphalt-sulphur mixes. *Can. J. Civ. Eng.* **12**(4), 916–919 (1985). doi:[10.1139/l85-104](https://doi.org/10.1139/l85-104)
- Ministry of Road Transport and Highways (MoRTH): Specifications for Road and Bridge Works, Section 500, Fifth Revision, Indian Roads Congress, New Delhi, India (2013)
- Satyakumar, M., Satheeshchandran, R.: Experimental investigations of effect of Sulphur on Beach Sand-Fly Ash–Asphalt (SFA) paving mixes. *Civ. Eng. Dimension* **15**(1), 36–42 (2013). doi:[10.9744/ced.15.1.36-42](https://doi.org/10.9744/ced.15.1.36-42)
- Saylak, D., Gallaway, B.M.: Beneficial Use of Sulfur in Sulfur-Asphalt Pavements. Texas Transportation Institute, Texas A&M University, College Station, Tex. 77843 (1974)
- Saylak, D., et al.: Beneficial use of sulfur in sulfur-asphalt, pavements. *New uses of sulfur. Adv. Chem. Ser.* **140**, 102–129 (1975). doi:[10.1021/ba-1975-0140.ch007](https://doi.org/10.1021/ba-1975-0140.ch007)



# Effect of Spray Dryer Absorbers as Mix Enhancer on HMA Performance

Clayton Cloutier<sup>1</sup>✉, Emil G. Bautista<sup>2</sup>, Ahmed F. Faheem<sup>3</sup>,  
and Konstantin Sobolev<sup>1</sup>

<sup>1</sup> University of Wisconsin-Milwaukee, Milwaukee, USA  
cloutie5@uwm.edu

<sup>2</sup> GeoTest, Inc., Bellingham, USA

<sup>3</sup> Temple University, Philadelphia, USA

**Abstract.** For many years Coal Combustion Products (CCPs), and, especially fly ash, have been effectively used as a partial replacement of portland cement in different types of concrete, as well as in flowable fills, embankments and soil stabilization. On the other hand, the use of CCPs in asphalt pavements has been very limited. Only few researchers have reported on the benefits of CCPs in asphalt. This research investigates the effect of Spray Dryer Absorber (SDA) CCP on HMA performance with respect to laboratory measured performance indicators at both the mastic and mixture level using a PG58-28 unmodified binder. In this study, two SDA materials and a reference limestone filler was introduced to an asphalt mastic at 0, 5, 15, and 25% by volume. After mastic evaluation, only one of the SDA materials was introduced to an asphalt mix at 10% replacement of the binder by mass and compared to a standard 3 million ESAL control mix. With respect to performance, all mastics and mixtures were tested for aging index, fatigue, and low-temperature thermal cracking resistance. The HMA mix with SDA had the higher resistance to aging where the aging index was significantly lower/reduced than that of the control mix. The same trend was observed for repeated fatigue loading. Overall, the SDA mix outperformed the control HMA. The reported study proves that replacing 10% by mass of the asphalt binder with SDA does not hinder workability, and improves aging resistance, moisture damage resistance, and fatigue life. This implies a significant impact associated with CCPs utilization in flexible pavements rather than landfilling.

## 1 Introduction

Developing a cost-efficient and long-term road infrastructure requires innovative approaches that are both green and environmentally sustainable. Today, building a sustainable, long-lasting, and efficient road infrastructure with little or no repairs is a challenging task, and highly innovative technological breakthroughs are needed.

According to the American Coal Ash Association (ACAA 2015) 117 million tons of Coal Combustion Product (CCP) are being produced but only 52% is currently being utilized in different applications. The remaining 48% goes to landfills. Moreover, only 0.069% of the CCP used is being used as mineral filler in asphalt cement. The utilization is mostly focused on Class C fly ash while high carbon CCPs, such as Spray

Dryer Absorbers (SDA), remain vastly underutilized. Out of approximately 1.31 million tons of SDA produced only 19.3% are currently being use in applications in mining and the oil/gas field services industries. This leaves 80.7% of the material to be disposed in landfills. This trend proves that new markets and innovative uses of CCPs, especially SDA materials, are needed to enhance the utilization of a waste material that otherwise will be stored in landfills.

Spray Dryer Absorbers (SDA) are products of flue gas desulfurization (FGD) processes. The SDA material is used to reduce the sulfur dioxide (SO<sub>2</sub>) emissions from the flue gasses at coal-fired power plants by capturing the SO<sub>2</sub> particles. Slaked lime slurries are incorporated into this process by being sprayed into the flue gas, dried, and then collected. The SDA materials can be collected with fly ash, or these materials can be combined with both fly ash and the lime particulate (EPRI 2007).

Construction materials researchers have extensively investigated the use of by-products such as fly ash to improve the material properties of asphalt (Sobolev and Naik 2005). Fly ash has been used extensively in portland cement concrete technology; however, there are few limited applications in which fly ash has been tested in asphalt pavements (Ali et al. 1996; Churchill and Amirkhanian 1999; Asi and Assa'ad 2005; Faheem and Bahia 2009; Sobolev et al. 2013; Bautista et al. 2015a, b; Cloutier 2016).

Sobolev et al. (2013) reported that the introduction of fly ash into asphalt mixtures (ASHphalt) improves the performance at levels compared with those achieved through polymer modification. This is attributed to the unique spherical, beneficial size distribution and chemical properties of fly ash. The use of fly ash in bitumen based materials is attractive as it improves the performance and reduces costs and environmental impacts (Tapkin 2008). Advantages of fly ash in asphalt include improved mixing, placing and compaction, stability, resistance to water damage, rutting resistance, flexibility, and resistance to freeze-thaw damage (Tapkin 2008).

Bautista et al. (2015a, b) conducted a series of performance tests on asphalt mastics. A large group of CCPs at different concentrations were mixed with different unmodified asphalt binder's sources and on different levels of polymer modifications. They found that most of the influence of the CCPs was not binder dependent. This could be due to the increased sulphur content.

Despite these reported benefits, the application of fly ash in asphalt technology has not been widely utilized. Fly ash in HMA has not been adopted on a commercial scale, and Class C (ASTM C618) fly ash has received most of the research focus. Class F fly ash and other CCPs, such as Spray Dryer Absorber (SDA) material, and non-Spec Ash, have not been thoroughly explored for use in asphalt mixtures.

For this study, two SDA materials were incorporated in asphalt mastics using PG58-28 asphalt binder. The CCP was incorporated in the asphalt mastics at concentrations of 0, 5, 15, and 25% by volume. Later, one of the SDA materials was added to an asphalt mixture by replacing 10% of the asphalt binder by mass. Therefore, for this study the CCP is not viewed as part of the aggregate blend, but rather the part of mastic volume binding the aggregate structure.

## 2 Experimental Program

In this study, both the mastic testing program and the mixture testing program investigated the performance of adding SDA materials with respect of the following indicators: aging resistance, fatigue-cracking resistance, and low-temperature thermal-cracking resistance. Table 1 presents the experimental testing matrix at both the mastic and mixture level.

**Table 1.** Experimental Research testing matrix

Test	Measured indicator		Aging	CCPs	CCP dosage	Replicates per test	Total	
Mastic testing								
Aging comparison	Complex shear modulus, $G^*$		Long-term	SF15 SDA, DL16 SDA, & control	0, 5, 15, 25% (by volume)	2	24	
Fatigue	$G^* \sin \delta$	Intermediate temp.	Long-term			2	24	
Thermal cracking	S and m	Low temp.	Long-term			2	24	
Mixture testing								
Aging comparison	Number of gyrations to compact to 92% $G_{mm}$		Long-term	SF15 SDA & control	10% (by mass)	6	12	
Fatigue	Number of cycles drop in $E^*$ using IDT		Intermediate temp.			Long-term	2	4
Thermal cracking	Fracture energy		Low temp.			Long-term	2	4

### 2.1 Chemical and Physical Properties

Chemical properties were evaluated in accordance to ASTM C618. This standard categorizes different pozzolan materials based on  $Al_2O_3$ , CaO and  $SiO_2$  contents. The SDA materials contain large amounts of calcium oxide and low amounts of silicon dioxide. Table 2 reports on the chemical properties of the SDA materials.

Table 3 shows physical property values for the SDA and limestone filler materials.

**Table 2.** Chemical composition of investigated CCPs

Material ID	Class	$Al_2O_3$	CaO	$Fe_2O_3$	$SiO_2$	$SO_3$	SAF	LOI
SF15	SDA	17.5	28.1	4.4	25.2	14.2	47.1	2.7
DL16	SDA	4.7	51.0	1.2	5.8	33.3	11.7	7.2

\*SAF =  $SiO_2 + Al_2O_3 + Fe_2O_3$

The fraction void test was used in accordance to the European Standard EN 1097-4 to determine Rigden voids. It can be observed that the SDA materials demonstrate higher values of Rigden voids than the limestone filler. Specific gravity was determined by

following the procedure in ASTM D5550 by using the Helium Pycnometer test. SDA materials exhibit lower specific gravities than the limestone filler.

A more extensive research investigation of the chemical and physical properties of

**Table 3.** Physical properties of investigated CCPs and limestone filler

Material ID	Class	Rigden voids, %	Specific gravity
SF15	SDA	30.74	2.33
DL16	SDA	53.14	2.36
Control	Limestone	30.22	2.81

these materials was studied by Bautista et al. (2015a, b).

## 2.2 Mastic Testing

For mastic testing, SF15 SDA and DL16 SDA materials were added to a PG58-28 asphalt binder at concentrations of 0%, 5%, 15%, and 25% replacement of binder by volume. These mastics were then compared to a control mastic which had a reference limestone filler.

Aging resistance was evaluated by comparing the increase in the complex shear modulus,  $G^*$ , which represents the stiffness of the material. The increase in  $G^*$  was determined by using the Dynamic Shear Rheometer (DSR) which compared unaged mastics as well as mastics that were exposed to PAV (Pressure Aging Vessel) aging. Mastics were tested at intermediate temperatures and the aging index was then calculated.

Asphalt mastic fatigue-cracking resistance was evaluated at intermediate pavement service temperatures by using the Dynamic Shear Rheometer (DSR) to calculate the fatigue factor,  $G^* \sin \delta$ . The asphalt mastic was aged in the RTFO and Pressure Aging Vessel (PAV) and then was tested under the dynamic loading at the intermediate pavement service temperature using an 8 mm diameter sample. The fatigue factor had a maximum limit of 5,000 kPa. Similar to unaged materials, for this research, the target strain level for PAV aged materials was reduced to 0.6% so the material was tested in the linear viscoelastic region. The target strain value for PAV aged asphalt binder according to AASHTO T325 is 1%. These strain levels were selected based on limited experiments to assure the linear viscoelastic response.

The Bending Beam Rheometer test was conducted according to the standard AASHTO T313 to evaluate thermal-cracking resistance by measuring the creep stiffness ( $S_t$ ) and the slope of the creep stiffness (m-value). Low temperature cracking is generally found mostly in older, brittle pavements; therefore, the test was performed on the long-term aged material, after Pressure Aging Vessel (PAV).

According to Superpave®, for asphalt binders the creep stiffness  $S_{(t)}$  must not exceed 300 MPa. Also the slope of the creep stiffness is calculated as an indication of the relaxation of the asphalt binder at low temperatures and it is called m-value. The m-value must be at least 0.300. A high m-value is desirable, because the asphalt binder will respond as a material that is less stiff as the temperature decreases and contraction

occurs. The standard states that the stiffness value at 60 s is reported because this correlates to the 2 h of actual traffic loading, resulting in pavement cracking. The test was conducted at the low PG temperature plus 10 °C, and the time temperature superposition was applied to calculate the response at the low PG temperature; this allows for shorter testing times (Ng Puga 2013). Therefore, for PG58-28, the test was conducted at -18 °C rather than -28 °C.

### 2.3 Mixture Testing

For mixture testing, only the SF15 SDA material was introduced to an asphalt mix (due to favorable mastic testing results discussed in Sect. 3) at 10% replacement of the binder by mass and compared to a standard 3 million ESAL control mix. Mixtures prepared for this study used a job mix formula (JMF) approved by the Wisconsin DOT. The mix used a PG58-28 binder and had a nominal maximum aggregate size (NMAS) of 12.5 mm, which is the typical NMAS for surface mixes in Wisconsin. The reference mix design required 5.5% optimum asphalt content. The SDA was assumed as part of the binder mass rather than as an aggregate component. A control mix was used to compare the impact of the added SDA on the performance indicators of mixtures. The control mixes were fabricated according to the JMF at the optimum asphalt content.

The aging resistance was evaluated by comparing the aging index of all the mixtures. The aging index was calculated as the ratio of the number of gyrations to reach 92%  $G_{mm}$  for long-term aged materials versus the number of gyrations to reach 92%  $G_{mm}$  for short-term aged materials. The short-term aged materials were placed in a forced-draft oven for 2 h  $\pm$  5 min at a temperature equal to the mixture's compaction temperature  $\pm$  3 °C. The long-term aged materials were placed in a force-draft oven for 120  $\pm$  0.5 h at a temperature of 85  $\pm$  3 °C. The long-term aging procedure used was in accordance with AASHTO R30-02 and methods adapted by Elwardany et al. (2010).

Fatigue testing was performed as a modified test from AASHTO T322-03, AASHTO T342-11, and methods adapted by Shu et al. (2007). Typical results of fatigue test are reported in Fig. 1. The repeated cyclic loading yield a damage curve that shows early rapid deformation (initial flow) followed by steady state rate of deformation (secondary flow), then when the samples undergo failure the rate of deformation increases again (tertiary flow). The performance parameters for this test are the secondary flow steady rate of deformation.

In addition, the Complex Modulus ( $E^*$ ) of the mixture is calculated as function of the cycle number. The fatigue life of the specimen is selected at the cycle corresponding to 50% drop in  $E^*$ .

For this study, fatigue was evaluated by using a sine wave loading condition, a test temperature of 20  $\pm$  1 °C, a 2% pre-loading condition, a 20% ultimate loading condition, and a frequency of 10 Hz. For all specimens, the same ultimate loading condition of 11.0 kN was used to directly compare the specimens. To evaluate the fatigue cracking resistance, a universal loading frame was used with an environmental chamber with temperature control capability. The samples were of 101.6  $\pm$  2.0 mm diameter by 50.8  $\pm$  2.0 mm thick with duplicates tested. The applied load and vertical displacement was recorded to calculate the needed performance indicators.

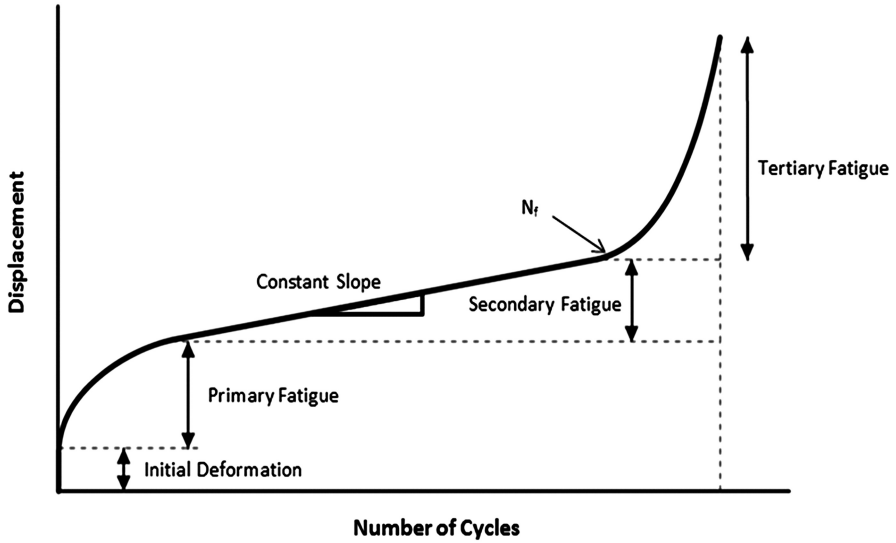


Fig. 1. Typical deformation plot for repeated fatigue loading

The Semi-Circular Bending (SCB) test was used to determine the low-temperature ( $-18\text{ }^{\circ}\text{C}$ ) properties such as Fracture Energy ( $G_f$ ) and Stiffness ( $S$ ). Asphalt mixtures become brittle at low temperatures, and when the developing thermal stresses become too large, the pavement cracks as a result. Therefore, asphalt materials that are too brittle at low temperature are undesirable, whereas materials that are more elastic perform better since these are able to recover from the emerging stresses.  $G_f$  is obtained by dividing the work of fracture (area under the load vs. vertical displacement curve) by the ligament area. The Stiffness ( $S$ ) is represented as the slope of the linear portion of the vertical displacement curve. For this testing, higher values of  $G_f$  are desirable as this demonstrates larger amounts of energy that is necessary to crack the specimen. On the other hand, lower stiffness values are desirable as this demonstrates a more ductile material that can recover from the stresses that are developed due to traffic loads. The SCB test was performed at  $-18\text{ }^{\circ}\text{C}$  by applying a vertical load on the specimen at a rate of  $0.03\text{ mm/min}$ , and the test was done once the load decreases to  $0.5\text{ kN}$ .

### 3 Research, Results, and Discussion

#### 3.1 Mastic Testing

##### 3.1.1 Aging Resistance

In this section the increase in  $G^*$  due to PAV aging for mastics is compared to the increase of  $G^*$  of unaged mastics tested at intermediate temperature to calculate the aging index. The goal of this comparison was to verify that the SDA materials could reduce the extent of the aging as compared to the reference limestone filler. Lower aging indexes demonstrate a reduction (delay) of the aging. Figure 2 indicates that for

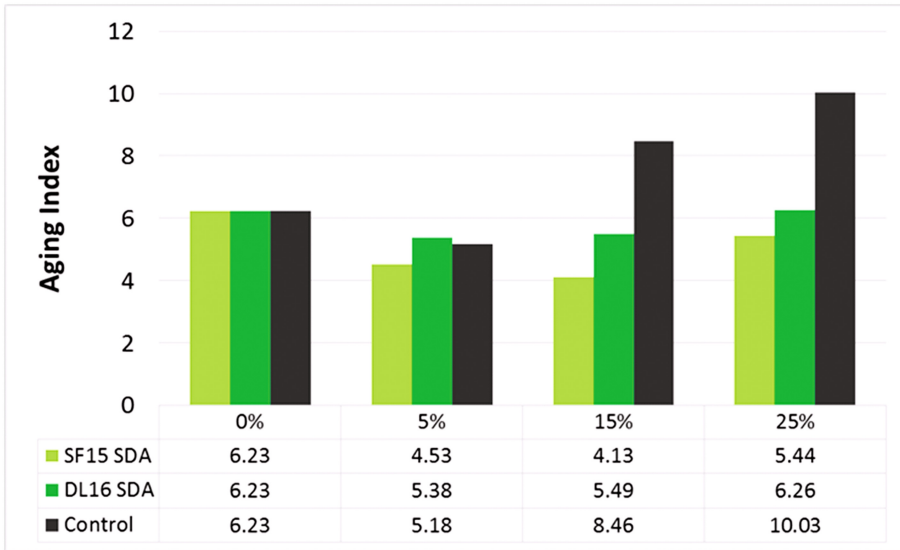


Fig. 2. Aging index for PG58-28 mastics

PG58-28 unmodified binder with SF15 SDA the aging index is less than the aging index for the control mastic with limestone filler at all concentration levels. Figure 2 also shows that DL16 SDA also performed better than the controlled mastic at levels of 15 and 25% concentration levels.

From the aging index results it is evident that the increase in the aging index in mastics with reference limestone filler was proportional to filler concentration indicating that with the increase in concentration, the mastics are more sensitive to aging. It can be concluded at this stage that the addition of the CCP causes some retardation in aging compared to the natural fillers.

Further testing should be conducted to identify the significance of aging retardation and failure mechanisms since most of the cracking in asphalt pavements is attributed to aging. In addition, filler properties will be evaluated to highlight the influencing factors on the reported observations. The inclusion of any particulate is expected to increase the stiffness with increase in concentration. The observed results raise a very important question for future research; how much of the observed increase in  $G^*$  is due to aging compared to particulate inclusion.

### 3.1.2 Fatigue Resistance

The Superpave® binder specification systems use a fatigue factor,  $G^* \sin \delta$ , to measure the fatigue damage resistance of binder at intermediate pavement service temperatures using the DSR.

Figure 3 demonstrate the fatigue damage resistance results for mastics prepared with SDA CCPs and the reference limestone filler combined with PG58-28

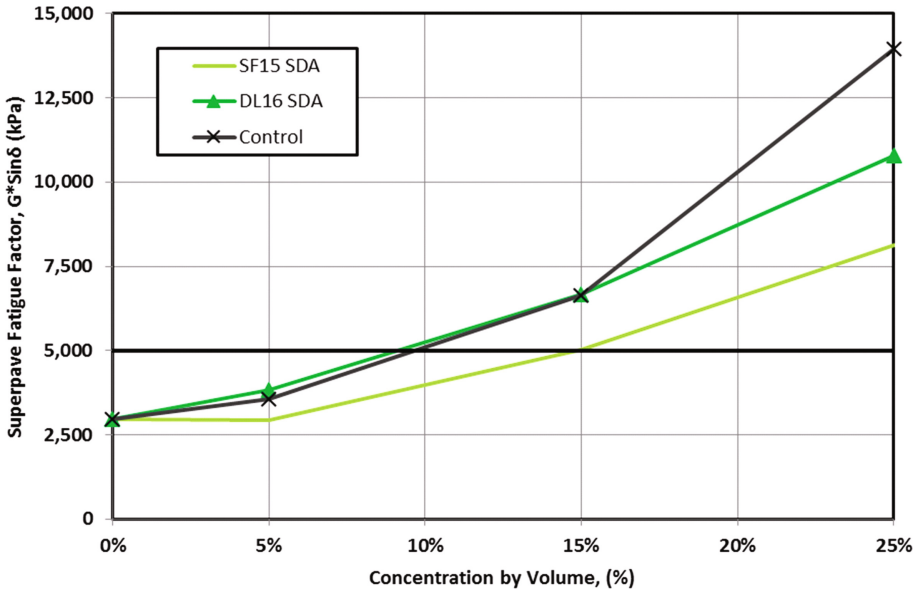


Fig. 3. The effect of SDA CCPs on  $G^* \sin \delta$

(unmodified). The results show that the PG58-28 mastics with up to 15% of SF15 SDA can still meet the binder specifications as this is less than the 5,000 kPa limit.

PG58-28 based mastics had the  $G^* \sin \delta$  results which are lower than the corresponding mastics with reference limestone filler. It is important to note that the reference filler had the most rapid rate of increase. This could indicate that SDA SF15 CCP based mastics are less prone to fatigue damage in terms of  $G^* \sin \delta$  when compared to the reference limestone filler.

A unique behavior was also noticed for mastics with 5% of SF15 SDA. It is evident that the addition of lower dosages of SF15 SDA reduces the intermediate temperature stiffness indicating the potential for the CCP to extend the asphalt binder, especially, in the polymer modified systems.

### 3.1.3 Thermal-Cracking Resistance

The Superpave® binder specification uses the Bending Beam Rheometer (BBR) to measure the asphalt tendency to develop thermal stresses at a specified temperature by measuring the creep stiffness ( $St$ ) and the  $m$ -value. The creep stiffness ( $St$ ) is defined as the binders' resistance to load. If the creep stiffness ( $St$ ) is too high, the asphalt binder behaves in a brittle manner and, therefore, is more prone to cracking at low temperatures.

This section presents the low temperature creep stiffness of mastics. The Bending Beam Rheometer tests were conducted to evaluate the effects of CCPs addition on the resistance to thermal cracking at  $-18^\circ\text{C}$  for asphalt binders. Figure 4 demonstrates the creep stiffness for PG 58-28 (unmodified) mastics.



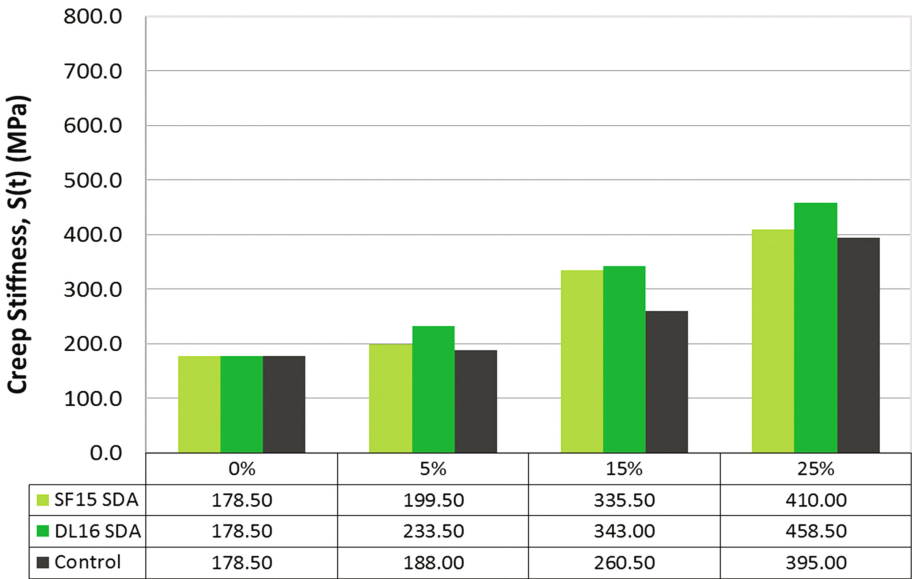


Fig. 4. Creep stiffness for PG58-28 mastics

For mastics with up to 5% of SF15 and DL16 SDA CCPs, the stiffness of all mastics are still within the Superpave® limit for binders of 300 MPa. For the evaluation of the influence of the CCPs, the focus was mostly on the CCP’s ability to maintain the thermal relaxation rather than abiding by the Superpave® limits. This is because it is expected that the stiffness of the binders will increase due to the inclusion of particulates. Therefore, the complete evaluation will include the evaluation of the rate of increase of the stiffness combined with the relaxation modulus (m-value).

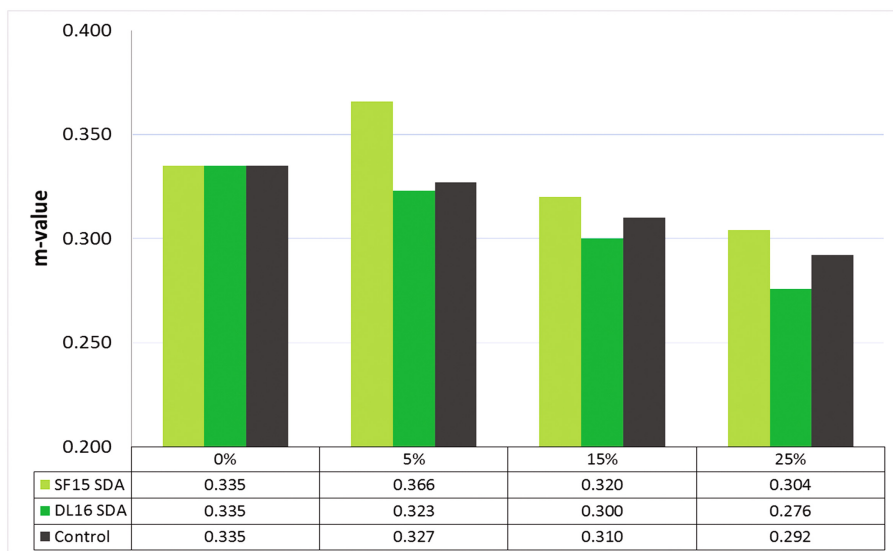
The m-value for mastics prepared are reported in Fig. 5. As stated previously, a higher m-value is desired as this indicates a higher ability to relax the stresses.

Figure 5 indicates that the m-value for PG58-28 unmodified binder blends with SF15 SDA CCPs is higher than that of the control mastics with reference fillers at all concentrations levels. It is evident that the SF15 SDA based mastics had higher creep stiffness than the reference filler mastics. The m-value results demonstrate that these CCPs based mastics can relax the stresses better than the reference filler. It is difficult to analyze the effect of the CCPs on the stiffness limits for the Superpave® as these limits are developed for binders only.

### 3.2 Mixture Testing

#### 3.2.1 Aging Resistance

An aging index was used as a parameter to compare the aging properties of the mixtures. Comparing the material in the short-term and long-term aging conditions was critical because resisting the effects of age-hardening could potentially increase the life expectancy of the material since it would become stiffer at a slower rate. Age hardening



**Fig. 5.** m-value for PG58-28 mastics

increases the stiffness of the material, which means the compaction effort is expected to increase.

The results in Fig. 6 clearly demonstrate that the SDA material aids in aging resistance since the aging index is less than that of the control mixture. This lower value indicates the ability of the SF15 SDA material to decrease the rate at which the mixture ages and this is critical over the pavement's lifecycle. These results demonstrate similar trends shown in Fig. 2 for mastic testing. It is important to note that this approach for mixtures is damage independent and is used only as indication of potential differences in compaction due to aging.

### 3.2.2 Fatigue Resistance

Figure 7a displays the rate of vertical deformation from the secondary fatigue flow of the materials. The results clearly show rapid secondary flow experienced by the control mix as the rate of deformation was  $5.72E-05$  mm/cycle. ASHphalt mixes had much lower rate of deformation with a deformation rate of  $1.76E-05$  mm/cycle. This represents a slower rate of deterioration during the service life for the mixtures with SF15 SDA.

Figure 7b demonstrates the number of cycles that the samples could withstand until 50% drop in  $E^*$ . The results demonstrate that SF15 SDA mixtures performed better since this mixture type lasted for 76,750 cycles. The SDA mixes outperformed the control mix which lasted only 27,250 cycles until failure.

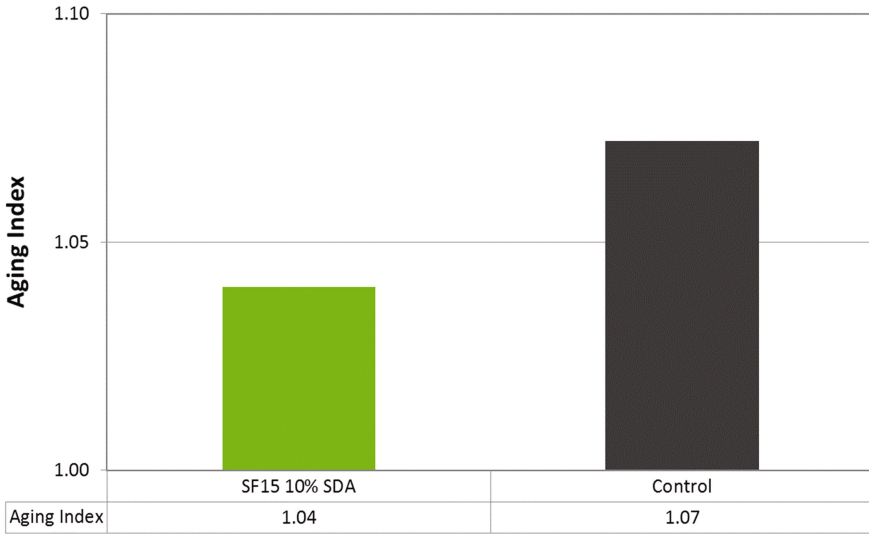


**Fig. 6.** Aging index for SF15 SDA and control mixture

These results represent an increase in fatigue life of the ASHphalt mixes. With the results being consistently in favor of the ASHphalt samples, it can be confidently concluded that mixes with SF15 SDA are much more resistant to fatigue cracking. The results of the fatigue testing are in exact agreement with the mastic trends presented in Fig. 3. This adds confidence that the improvement in the fatigue life is due to the ability of the ASHphalt mastic to resist the embrittlement effect of aging, thus improve fatigue repeated loading.

**3.2.3 Thermal-Cracking Resistance**

Figure 8a demonstrates the Fracture Energy ( $G_f$ ) of the investigated asphalt materials. From the results, it can be seen that the ASHphalt mixtures performed better than the control mixture in terms of  $G_f$ . The SF15 SDA mix outperformed the control as this mixture was able to achieve a  $G_f$  value of  $0.83 \text{ kJ/m}^2$ . These results are extremely significant since this demonstrates improved performance of ASHphalt mixtures at low temperature.

Figure 8b shows the stiffness results from the SCB testing. From these results, it can be seen that the ASHphalt mixtures performed better than the control mixture since the stiffness values were much lower. SF15 SDA mix demonstrated lower stiffness of  $7.54 \text{ kN/mm}$ , whereas the control mixture obtained a higher stiffness of  $14.27 \text{ kN/mm}$ .

These results reveal that the control mixture is much more brittle at the low temperature as compared with the ASHphalt mixtures. In terms of thermal cracking resistance, it can be concluded that ASHphalt mixtures resisted the effects of low-temperature cracking better than the control mixtures for Fracture Energy ( $G_f$ ) and Stiffness ( $S$ ) evaluations. These results prove that adding SF15 SDA to asphalt mixtures can potentially enhance low-temperature thermal cracking resistance. It is

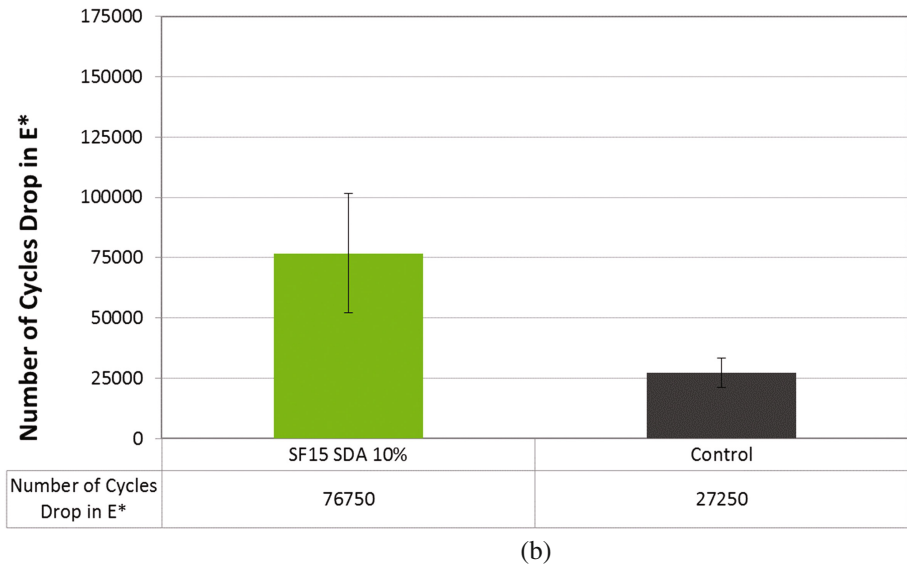
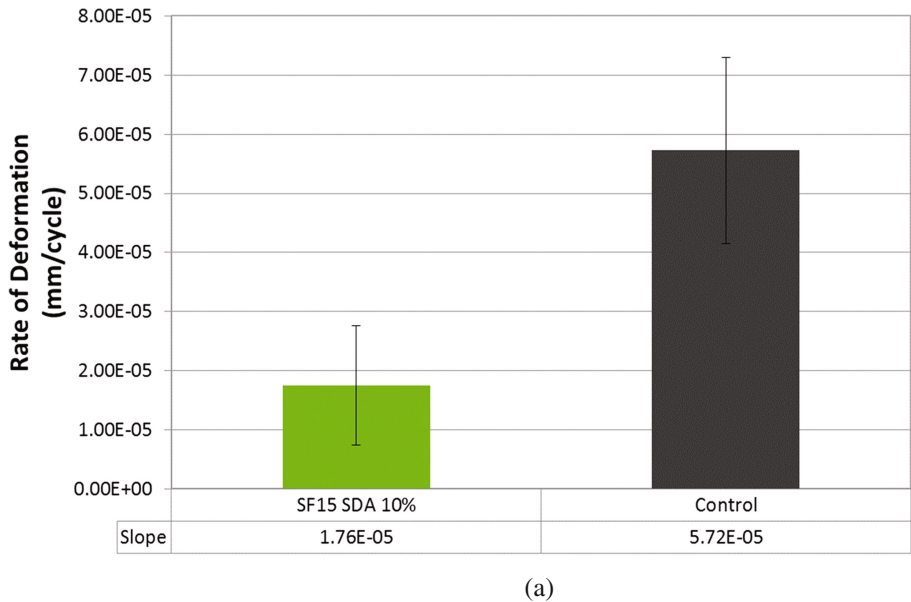
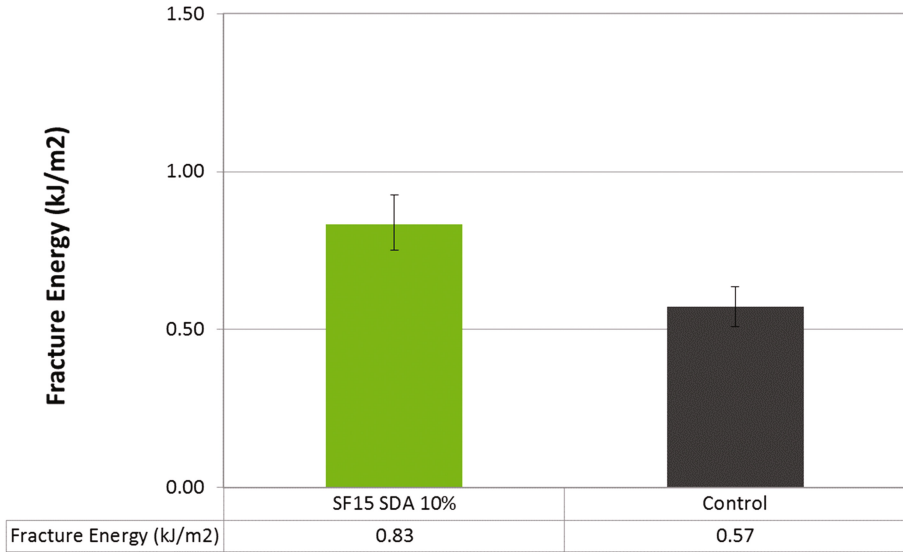
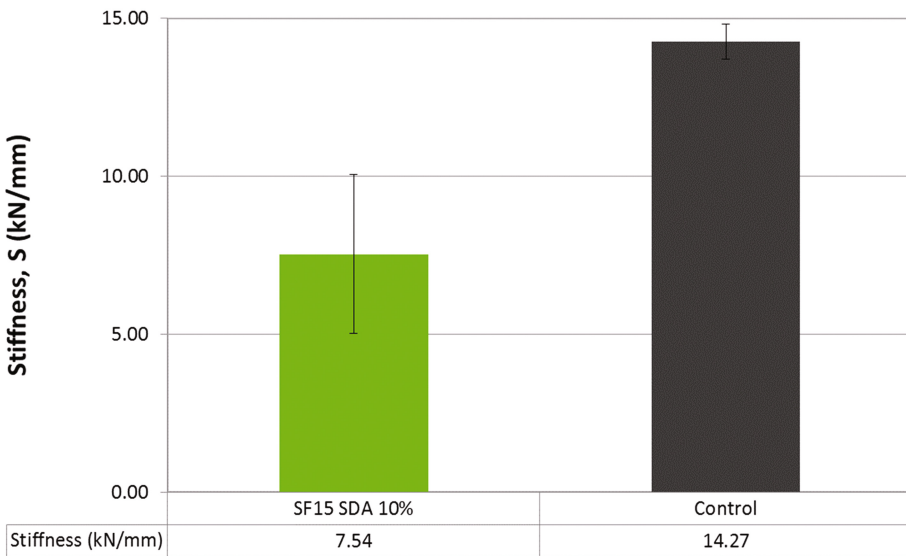


**Fig. 7.** Fatigue testing results; (a) Secondary flow rate of deformation, (b) Fatigue life as measured by 50% drop in  $E^*$

important to note that the stiffness results from the mixture testing did not correlate with the stiffness values obtained for the binders using the BBR. However, the ranking agrees with the m-values obtained. This could be due to the fact that in the mixture testing the samples are characterized based on damage (failure) resistance unlike the



(a)



(b)

**Fig. 8.** Low temperature performance results; (a) Fracture energy ( $G_f$ ), (b) Stiffness ( $S$ )

BBR testing. This means that the m-value (thermal relaxation indicator) is a more suitable performance parameter for damage resistance.

## 4 Conclusion

This study was conducted to examine the effect of two SDA CCPs on the performance of asphalt mastics and one SDA CCP on the performance of asphalt mixtures. The SDA material was incorporated at 0, 5, 15, and 25% by volume for mastics and 10% by mass binder replacement for mixtures. The experimental program demonstrated an impressive potential of these SDA materials as a binder enhancer.

The aging index results showed that the increase in the aging index in mastics with reference limestone filler was proportional to filler concentration. This indicates that as the filler concentration increases, the mastics show more sensitivity to aging. The addition of the SDA CCPs caused some retardation in aging compared to the natural fillers. More specifically, SF15 SDA CCP demonstrated a lower aging index at all concentrations as compared to the limestone filler. For mixture evaluation, the results also demonstrated this trend as the aging index for the SF15 SDA material reduced the effects of aging. This lower aging index value demonstrates the ability of the SF15 SDA material to decrease the rate of aging which is important for the material lifecycle assessment.

Fatigue resistance results demonstrated improved performance for materials with SDA CCPs. Mastic results showed that the SF15 SDA material enhanced fatigue resistance at all concentrations as compared to the mastic with reference limestone filler. The results demonstrated that the addition of SF15 SDA at lower dosages even reduced the intermediate temperature stiffness when compared to the binder without any filler materials and this shows major potential for this CCP. The asphalt mixtures also demonstrated similar trends in that the fatigue resistance increased for mixtures with SF15 SDA materials. The fatigue life measured was significantly higher for the mixtures with the SDA CCP as compared to the control mixtures. The rate of deformation due to fatigue was also lower for the mixtures with SDA material as compared to the control mixtures. This adds confidence that the improvement in the fatigue life is due to the ability of the ASHphalt mastic to resist the embrittlement effect of aging, thus improve fatigue repeated loading.

Thermal cracking results showed that the m-value for mastics with SF15 SDA was higher than that of the control mastics with reference fillers at all concentrations levels. The SF15 SDA mastics had higher creep stiffness than the reference filler mastics. The m-value results demonstrate that these CCPs based mastics can relax the stresses better than the reference filler. Asphalt mixtures with SF15 SDA also demonstrated higher resistance to low temperature cracking since the stiffness of the ASHphalt was significantly lower than the control mix. This decrease in stiffness at low temperatures indicates flexibility under traffic loading which is crucial to the lifecycle of the material. The mixture testing clearly proves that ASHphalt mixes are superior to typical HMA, even when produced at a reduced asphalt content.

These results are extremely significant since this demonstrates improved performance of both mastics and mixtures with SDA materials. Incorporating SDA CCPs in asphalt mixtures has tremendous potential for pavement innovations.

**Acknowledgements.** The authors would like to acknowledge Electric Power Research Institute (EPRI) and We Energies for their financial support and donation of CCP materials. Special thanks are expressed to Valero Benicia and Flint & Hills for supplying the bitumen used for this project.

## References

- AASHTO T 312-15: Standard Method of Test for Preparing and Determining the Density of Asphalt Mixture Specimens by Means of the Superpave Gyrotory Compactor
- Ali, N., Chan, J.S., Simms, S., Bushman, R., Bergan, A.T.: Mechanistic evaluation of fly ash asphalt concrete mixtures. *J. Mater. Civ. Eng.* **8**(1), 19–25 (1996)
- American Coal Ash Association (2015). <https://www.acaa-usa.org>. Accessed 18 Oct 2016
- Asi, I., Assa'ad, A.: Effect of Jordanian oil shale fly ash on asphalt mixes. *J. Mater. Civ. Eng.* **17**(5), 553–559 (2005)
- Bautista, E.G., Flickinger, J., Saha, R., Flores-Vivian, I., Faheem, A.F., Sobolev, K.: Effect of coal combustion by-products addition on high temperature performance of asphalt mastics. *Constr. Build. Mater. J.* **94**, 572–578 (2015a)
- Bautista, E.G., Faheem, A.F., Saha, R., Sobolev, K.: Characterization of damage and aging resistance of asphalt mastics with coal combustion by-products. In: American Society of Civil Engineers (ASCE) International Airfield & Highway Pavements Conference, June 2015 (2015b)
- Bautista, E.G.: Experimental evaluation of the effect of coal combustion products on constructability, damage and aging resistance of asphalt mastics. Doctoral Thesis. University of Wisconsin-Milwaukee (2015)
- Cabrera, J.G., Zoorob, S.: Design of low energy hot rolled asphalt. The Civil Engineering Materials Unit, Department of Civil Engineering, University of Leeds, United Kingdom (1994)
- Churchill, E.V., Amirkhanian, S.N.: Coal ash utilization in asphalt concrete mixtures. *J. Mater. Civ. Eng.* **11**(4), 295–301 (1999)
- Cloutier, C.J.: The effective use of Coal Combustion Products (CCPs) in asphalt pavements. Master's Thesis. University of Wisconsin-Milwaukee (2016)
- Galloway, B.M.: A review of the use of mineral filler in asphalt-aggregate mixtures. In: Fly Ash Applications in 1980 Conference (1980)
- Henning, N.E.: Evaluation of lignite fly ash as a mineral filler in asphaltic concrete. Report No. Item 2 (73). Twin City Testing and Engineering Laboratory, St. Paul, Minnesota (1974)
- EPRI: A Review of Literature Related to the Use of Spray Dryer Absorber Material: Production, Characterization, Utilization Applications, Barriers, and Recommendations. EPRI, Palo Alto, CA and UND EERC CARRC, Grand Forks, ND, 1014915 (2007)
- Faheem, A.F., Bahia, H.U.: Modelling of asphalt mastic in terms of filler-bitumen interaction. *Road Mater. Pavement Des.* **11**(sup1), 281–303 (2009)
- Sankaran, K.S., Rao, D.R.: The influence of the quality of filler in asphaltic paving mixtures. *Indian Roads Congress* **35**, 141–151 (1973)
- Sobolev, K., Ismael, F., Bohler, J., Faheem, A., Covi, A.: Application of Fly Ash in ASHphalt Concrete from Challenges to Opportunities, Milwaukee (2013)
- Sobolev, K., Naik, T.R.: Performance as a factor for sustainability of the cement industry. In: CANMET/ACI International Symposium on Sustainable Development of Cement and Concrete, Toronto, pp. 295–312 (2005)

- Standard Specification for Coal Fly Ash and Raw or Calcined Natural Pozzolan for Use in Concrete. ASTM C618-15. Developed by Subcommittee: [C09.24](#)
- Tons, E. et al.: Fly ash as an asphalt reducer in bituminous base courses. Report prepared by the University of Michigan, The Board of Water and Light. Consumer Power Co. and Detroit Edison Co. Detroit, Michigan (1983)
- Warden, W.B., Hudson, S.B., Howell, H.C.: Evaluation of mineral filler in terms of practical pavement performance. Proc. Assoc. Asph. Paving Technol. **27**(52), 101–110 (1952)



# Impact Load Test on Conventional and Roller Compactor Steel Fiber Reinforced Concrete Pavement

Zainab A. AL-Kaissi<sup>1</sup>(✉), Ahmed S.D. Al-Ridha<sup>2</sup>,  
and Rusul Raed Abdull-Hussain<sup>1</sup>

<sup>1</sup> Highway and Transportation Engineering Department,  
Al-Mustansiriyah University, Baghdad, Iraq  
zainabalkaissi77@googlemail.com

<sup>2</sup> Civil Engineering Department,  
Al-Mustansiriyah University, Baghdad, Iraq  
ahmedsahibdiab@yahoo.com

**Abstract.** The effect of compaction method on steel fiber reinforced concrete pavement (SFRC) has been simulated in this study, a locally manufactured steel roller compactor is designed to simulate steel roller compactor which is commonly used in site for compaction. 0.8 % volume fraction ( $V_f$ ) of steel fiber content is used and compacted using roller compactor in three cases category, case 1: load 10 kg and no. of cycles are 8, 16, 24 cycles. Case 2: initial stage: load 10 kg and no. of cycles are 4, 8, 12 cycles and final stage: load 25 kg and no. of cycles are 4, 8, 12 and finally Case 3: load 25 kg and no. of cycles are 8, 16, 24 cycles. The obtained beam specimens were tested using a locally manufactured impact load apparatus and test results has been compared with steel fiber reinforced concrete beam specimens compacted using conventional compaction method. Test results show that the optimum steel fiber roller compacted concrete beam specimen under impact load test gives 17 blows for first crack and 173 blows for failure while steel fiber reinforced concrete beam specimen compacted using conventional method gives 15 blows for first crack and 110 blows for failure. Material properties have also been improved when using roller compactor by about 9.74%, 8.84% and 4.76% for compression strength, tensile strength and modulus of elasticity respectively.

**Keywords:** Steel fiber reinforced concrete (SFRC) · Roller compactor · Steel fiber roller compacted concrete (SFRCC) · Impact load test

## Abbreviations

SFRC	Steel Fiber Reinforced Concrete
RCC	Roller Compacted Concrete
SFRCC	Steel Fiber Roller Compacted Concrete
PCC	Portland Cement Concrete Pavement

---

The original version of the book was revised: For detailed information please see Erratum. The erratum to the book is available at [https://doi.org/10.1007/978-3-319-61633-9\\_25](https://doi.org/10.1007/978-3-319-61633-9_25)

NCCLR	National Center for Construction Laboratories and Research
$f'_{cu}$	Compressive Strength
$f_t$	Splitting Tensile Strength
$E_c$	Modulus of Elasticity
W/C	Water Cement Ratio
$\sigma_t$	Splitting Tensile Strength
P	Applied Compressive Load
L	Length of Cylinder
D	Diameter of Cylinder
v	Velocity of the Wave, km/sec
L	Distance between Transducers, mm.
t	Traveling Time, $\mu$ sec
$\rho$	Density ( $\text{kg/m}^3$ )
$\nu$	Poisson's Ratio
v	Pulse Velocity (km/s)
$V_f$	Volume Fraction of Steel Fiber
U	Impact Energy
$f_r$	Modulus of rupture

## 1 Introduction

Roller compacted concrete (RCC) is a zero-slump concrete mixture containing of Portland cement, sand and dense-graded aggregate particles. Since it contains a comparatively small quantity of water content, it cannot be placed by the same techniques used for conventional Portland cement concrete (PCC) mixtures. For pavement applications; RCC is usually placed using an asphalt paver as for density is attained through compaction using vibrating roller compactor [1].

Roller-compacted concrete pavements (RCCP) suffers from a number of difficulties. In particular, the application of tie bars or slip bars is challenging, because of the heavy compaction by vibratory roller compactor. As a result, it is known that RCCP is prone to cracking due to drying shrinkage or thermal stress which prevents the placing of pavement slabs with long joint spacing. Nevertheless using steel fiber in concrete pavement offers higher crack resistance and flexural strength, if roller-compacted concrete (RCC) could be given the properties of SFRC, it would offer benefits as a heavy traffic pavement applications concerning its rapid construction and shorter lead time. To achieve adequate bonding between the new and old layer at cold joint, the optimum layer thickness for SFRCC ranges from 20 to 30 cm. the test results shows that with increment of volume percentage of steel fiber in SFRCC mixture from 25–75 %, compressive strength increase from 42.22 MPa to 43.55 MPa, splitting tensile strength increase from 3.89 MPa to 4.95 MPa and flexural strength increase from 6 MPa to 7.4 MPa [2].

The flexural strength of SFRCC for a given consistency is 12.5% to 52.3% higher than that of conventional RCC. The flexural toughness of SFRC with hooked fibers is

0.31 to 1.88 MPa higher than with indented fibers. The toughness of SFRC with long fibers is 1.42 to 2.99 MPa higher than with short fibers. However, accumulation of experimental results with various fiber contents is still needed [3].

## 2 Material Characteristics

### 2.1 Cement

Iraqi Portland cement (type V) of Tasluja Factory is used in the present paper. Tables 1 and 2 show the chemical composition and physical properties of the cement used. This cement is tested and checked according to Iraqi Standard Specification [4].

**Table 1.** Chemical composition of cement (All chemical tests were made by National Center for Construction Laboratories and Research (NCCLR))

Compound composition	Chemical composition	Percentage by weight	IQS 5:1984 limits
Lime	CaO	62.22	–
Silica	SiO <sub>2</sub>	22. 1	–
Alumina	Al <sub>2</sub> O <sub>3</sub>	5.49	–
Iron Oxide	Fe <sub>2</sub> O <sub>3</sub>	3.53	–
Magnesia	MgO	2.24	≤ 5
Sulfate	SO <sub>3</sub>	1.07	≤ 2.5
Loss on Ignition	L.O.I	0.09	≤ 4
Insoluble residue	I.R	0.32	≤ 1.5
Lime saturation factor	L.S.F	0.86	0.66–1.02
Main Compounds (Bogue's equation) percentage by weight of cement			
Tricalcium Silicate (C3S)		38.55	
Dicalcium Silicate (C2S)		33.15	
Tricalcium Aluminate (C3A)		8.58	
Tetracalcium Aluminoferrite (C4AF)		10.73	

**Table 2.** Physical properties of cement (All chemical tests were made by National Center for Construction Laboratories and Research (NCCLR))

Physical properties	Test result	IQS 5:1984 limits
Fineness using Blain Air Permeability Apparatus (m <sup>2</sup> /kg)	310	250 min.
Soundness using Autoclave Method	0.19%	≤ 0.8
Setting Time using Vicat's Instruments		
Initial (hrs:min.)	1:65	45 m min.
Final (hrs:min)	2:46	10 h. Max.
Compressive Strength for Cement Paste Cube 70.7 mm) at		
3 days (MPa)	16.4	15 min.
7 days (MPa)	27	23 min.
28 days (MPa)	35	additional

## 2.2 Fine Aggregate

Natural river sand from Al-Sudoor region is used. Tables 3 and 4 show the grading and physical properties of the fine aggregate respectively that are performed by the National Center for Construction Laboratories and Research (NCCLR).

**Table 3.** Grading of fine aggregate AASHTO T-27.

No.	Sieve size (mm)	% Passing by weight	
		Fine aggregate %	AASHTO T-27-9
1	4.75	96	90–100
2	2.36	90	85–100
3	1.18	83	75–100
4	0.60	70	60–79
5	0.30	31	12–40
6	0.15	6.0	0–10

**Table 4.** Physical properties of fine aggregate. (All Test made by National Center for Construction Laboratories and Research (NCCLR))

No.	Physical properties	Test results	Limits of iraqi specification SCRB, 2003	Test No.
1	Specific gravity	2.65	–	<i>AASHTO T 84</i>
2	Sulfate content	0.08%	≤ 0.5%	
3	Absorption	0.75%	–	<i>AASHTO T 84</i>

## 2.3 Coarse Aggregate

Crushed gravel brought from Al-Niba'ee region is used. The grading and physical properties of coarse aggregate are shown in Tables 5 and 6 respectively. The mid-range of specification is used of aggregate gradation as plotted in Fig. 1.

**Table 5.** Grading of coarse aggregate.

Sieve size (mm)	Coarse aggregate gradation % passing by weight	
	AASHTO M 43, Size No. 67, 2003	Selected gradation of aggregate
25	100	100
19	90–100	95
12	–	–
9.5	20–55	37.5
4.75	0–10	5
2.36	0–5	2.5

**Table 6.** Physical properties of coarse aggregate (All Test made by National Center for Construction Laboratories and Research (NCCLR)).

No.	Physical properties	Test results	Limits of specification	Test No.
1	Specific Gravity	2.6	–	AASHTO T- 85
2	Sulfate Content	0.087%	≤ 0.1%	AASHTO T-290
3	Absorption	0.63%	–	AASHTO T- 85
4	Percent of Passing no.200 by Weight	0.05%	≤ 1%	ASTM C 33/03
5	%Organic Impurities	0.2%	≤ 2%	ASTM C33/03

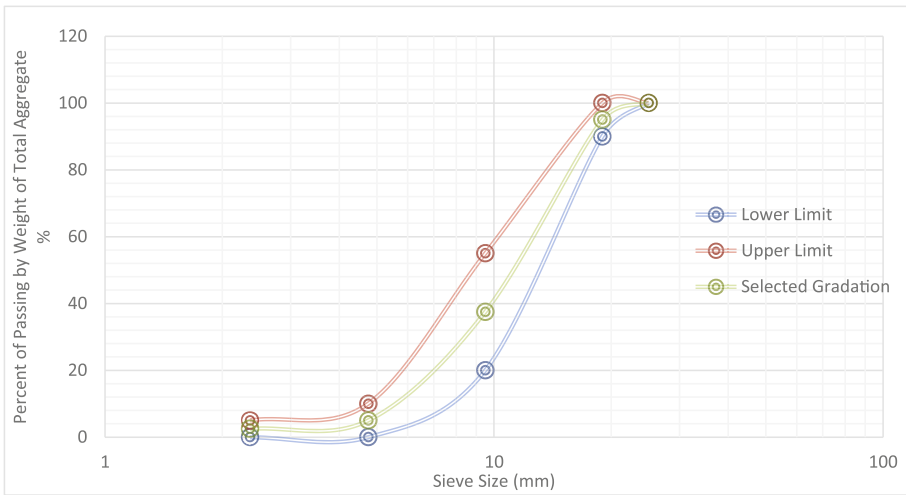


**Fig. 1.** Specification limits and gradation of coarse aggregate.

## 2.4 Water

Potable water of Baghdad is used for casting and curing.


## 2.5 Steel Fiber

Dramix steel fibers manufactured by Bekaert Corporation are used at a 0.4 % and 0.8 % ( $V_f$ ). Table 7 gives properties of the steel fibers.

## 2.6 Fluidifying Additives

Sika ViscoCrete-5930, is a third generation of superplasticizers for concrete and mortar, is used. It meets the requirements for superplasticizers according to ASTM C 494 Types G and F and BS EN 934 Part 2: 2001. Main properties of the used superplasticizers are shown in Table 8.

**Table 7.** Properties of steel fiber (Supplied by the manufacturer).

Commercial Name	Configuration	Property	Specifications
Dramix ZC 50/0.5	 Hooked Ends	Density	7860 kg/m <sup>3</sup>
		Ultimate Strength	1130 MPa
		Modulus of Elasticity	200x10 <sup>3</sup> MPa
		Strain at Proportion Limit	5650 x10 <sup>-6</sup>
		Poisson's Ratio	0.28
		Average Length	50 mm
		Nominal Diameter	0.5 mm
		Aspect Ratio (L/D <sub>f</sub> )	100

**Table 8.** The properties of fluidifying additive (Supplied by the manufacturer).

Appearance	Turbid liquid
Density	1.08 kg/lit _0.005
Basis	Aqueous solution of modified polycarboxylate
Packing	5 kg, 20 kg, 200 kg drums
Benefit	<ul style="list-style-type: none"> <li>• Strong self-compacting behavior</li> <li>• Extremely high water reduction</li> <li>• Excellent flow ability</li> <li>• Increase high early strengths development</li> <li>• Improve shrinkage and creep behavior</li> </ul>
Shelf life	Shelf life at least 12 months from date of production

## 2.7 Subgrade Soil Layer

The subgrade soil consist of a layer of low-plasticity silt and clay (ML and OL) according to Unified Soil Classification System USCS or (A-4) according to AASHTO M 145, which is simulated and contains inside a steel box of 800 mm length, 800 mm width and 350 mm depth and is compacted using 9 kg steel manually operated compactor with rectangular base plate with dimension of 100 × 350 mm, the soil is compacted in three layers at which each layer is compacted inside the box separately. The soil is brought from Bab-Almoadam overpass project. The physical and index properties of soil are shown in Table 9 and are carried in (NCCLR) according to the limits of the Iraq Standard Specification (*SCRB, 2003-R5*).

## 2.8 Concrete Proportions

A common concrete matrix is used in all mixes. The mixing proportion of (cement: sand: aggregate) is 1:2:2 by weight and the water–cement ratio (W/C) is 0.4 with superplasticizer of 0.02% by weight of cement. This mix is based on several trial mixes in order to achieve the most appropriate mix to produce good workability and uniform mixing of concrete without segregation. Steel fiber reinforced concrete is obtained by

**Table 9.** Physical and chemical properties of subgrade (All Test made by National Center for Construction Laboratories and Research (NCCLR)).

Index property	Index value	Limit of <i>SCRB specification R5, 2003</i>	
		Other layers	Finishing layer (upper layer)
Laboratory/Field no.	2685		
Max. Dry Density (gm/cm <sup>3</sup> )	1.763	–	>1.7
Moisture Content (%)	11.7	–	–
Liquid Limit % (L.L)	35	<70	<55
Plasticity Index % (P.I)	7.2	<45	<30
California Bearing Ratio for 95% Compaction (%)	4.1	–	>4
Swelling Ratio (%)	0.9	–	–
TSS (Total Soluble Salts) (%)	2.895	<20	<10
Organic Matter (%)	0.460	<12	<12

adding steel fibers with volume fraction of 0.8%  $V_f$  to the fresh non-fibrous concrete mix, and remixed.

### 3 Experimental Work

#### 3.1 Molds Preparation

Six wooden plywood molds are designed and fabricated for casting all beams. The molds are made of 700 mm length, 100 mm width and 100 mm height and their side pieces are connected by bolts which can easily be removed to strip off the hardened beams after casting. All molds have been well connected, cleaned, oiled, before pouring of concrete mixture into them.

#### 3.2 Mixing

In order to obtain a homogenous concrete mixture with sufficient workability a certain producer used. All batching is done by weight. The concrete is mixed using electrical mixture. The interior surface of the mixture is cleaned and moisturized before placing the materials. First both coarse and fine aggregate placed and mixed for several minute in the mixer after that cement is added, The materials are mixed until a uniform color is obtained, Afterwards half of the water quantity is added and mixed for several minutes too. The fluidifying agent (Visco Crete -5930) quantity is split into two halves, first half is added to the remain water and moved by a sticker till homogenous mixture obtained before adding to the mixer and mixed for 5 min, finally the rest of the fluidifying agent (Visco Crete -5930) quantity is added to the mixer and mixed for about 3 min. When steel fiber is added to the mix it is uniformly distributed by several nodes in the mixer cover.

### 3.3 Casting, Compaction, and Curing

After mixing the SFRC mixture poured into molds in two layers, when each layer laid; the sides of the molds is hammered by rubber driver, to shake the mix and consolidate it into the molds. Then is compacted using a table vibrator compactor in case of normal compaction for about 40 s for each layer. During compaction air bubbles would appear on the surface as an indication of dispossessing unwanted air.

Afterwards the surface of SFRC is leveled off and finished with a trowel, then the specimens are covered to prevent evaporation of water. After 24 hours, the specimens were stripped from the molds and cured in a water bath with 25° temperature for about one month. Since water temperature would be below the desire temperature degree heater is used in cold weather to achieve adequate curing. After that they are took out from the water bath, finally specimens are tested.

Steel fiber concrete mixture is also used for roller compacted concrete with 0.8%  $V_f$  of steel fiber known as SFRCC, after mixing, the steel fiber concrete mixture is poured in one layer into the beam mold and hammered by rubber driver, to shake the mix and consolidate it into the molds. Compaction is carried out as shown in Plate 1 by different weight and number of passes as shown in Table 10, the compaction is done in three different cases as in the following:

**Table 10.** Steel fiber roller compacted concrete cases.

Case 1		Case 2				Case 3	
		Initial stage		Final stage			
Load	No. of cycles	Load	No. of cycles	Load	No. of cycles	Load	No. of cycles
10	8	10	4	25	4	25	8
10	12	10	8	25	8	25	16
10	24	10	12	25	12	25	24

1. Case 1: load 10 kg and no. of cycles are 8, 16, 24 cycles.
2. Case 2: initial stage: load 10 kg and no. of cycles are 4, 8, 12 cycles.  
final stage: load 25 kg and no. of cycles are 4, 8, 12 cycles.
3. Case 3: load 25 kg and no. of cycles are 8, 16, 24 cycles.

Three cube and cylinder specimens are prepared for each beam specimen for conventional SFRC and for SFRCC with certain load and number of passes. As far for cube and cylinder specimens compaction for SFRCC; a locally manufactured apparatus is used, as shown in Plate 2, the steel fiber reinforced concrete mixture is poured into cubes in one layer of 100 mm hammered on sides and compacted, as for cylinders steel fiber reinforced concrete mixture which is applied in two layers each layer of 100 mm, and each layer is hammered and compacted individually. Weight to be applied onto cubes and cylinders differs from weight applied on beam specimens and it is calculated depending on stress applied in contact area between roller compactor and concrete mixture surface.





**Plate 1.** Roller Compacted Concrete.



**Plate 2.** Compaction of Cubes and Cylinders Specimens.

## 4 Strength and Mechanical Properties of Hardened Concrete

### 4.1 Compressive Strength ( $f'_{cu}$ )

The compressive strength test is carried out in Material Laboratory of Faculty of Engineering in Al- Mustansiriya University for both fibrous and non-fibrous concrete [5] using a standard cubes specimens with dimensions  $100 \times 100 \times 100$  mm for length, width, and height respectively, loaded uniaxially using the universal testing machine (ELE, Digital Elect 2000).

### 4.2 Splitting Tensile Strength ( $f_t$ )

Indirect tensile strength is carried out in Material Laboratory of Faculty of Engineering in Al- Mustansiriya University on non-fibrous, and fibrous concrete specimens [6] using standard cylinders specimens with 100 mm diameter and 200 mm height. The test is carried out by placing a cylinder specimen horizontally in the compression testing machine and load is applied until failure occurs. The splitting tensile strength is calculated from the following equation:

$$\sigma_t = \frac{2P}{\pi LD} \quad (1)$$

Where:

$\sigma_t$ : Splitting tensile strength (MPa),

P: Applied compressive load (N),

L: Length of cylinder (mm),

D: Diameter of cylinder (mm).

### 4.3 Modulus of Elasticity ( $E_c$ )

#### 4.3.1 Equation Method

Measurements of static modulus of elasticity of concrete ( $E_c$ ) is determined by obtained compressive strength of concrete and SFRC of cube specimens by conducting compressive strength test and then using the following equation [7];

$$E = 4.73\sqrt{f'_c} \quad (2)$$

Where:

$E$ : Elastic modulus (MPa),

$f'_c$ : Compressive strength of Cylinder (MPa).

While  $f'_c$  can be obtained using the following equation [8];

$$f'_c = 0.8 f_{cu} \quad (3)$$

Where:

$f'c$ : Compressive strength of Cylinder (MPa)

$fcu$ : Compressive strength of Cube (MPa)

### 4.3.2 Ultrasonic Test Method

Portable Ultrasonic Non-destructive Digital Indicating Test (PUNDIT) is used to determine young modulus for concrete beam, cube and cylinder specimens. The device contains two transducers, one as transmitter and the other one as receiver, which used to send and receive frequency. The time that the wave takes to travel is read out and the velocity of wave transport can be calculated using the following equation; [9]

$$v = \frac{L}{t} \quad (4)$$

Where;

$v$  = Velocity of the wave, km/sec.

$L$  = Distance between transducers, mm.

$t$  = Traveling time,  $\mu$  sec.

Then following equation is used to determine young modulus for concrete; [10]

$$E = \rho v^2 \frac{(1 + \nu)(1 - 2\nu)}{(1 - \nu)} \quad (5)$$

Where;

$E$ : Elastic modulus (MPa),

$\rho$ : Density ( $\text{kg/m}^3$ ),

$\nu$ : Pulse velocity (km/s), and

$\nu$ : Poisson's ratio.

## 4.4 Impact Load Measurement

### 4.4.1 Manufactured Apparatus: Impact Load Device

The apparatus for the drop-weight test, as shown in Plate 3, is manufactured in local market to simulate the load repetition applied to concrete pavement on field. The equipment consists of a 2 kg steel cylinder shaped weight load, with diameter of 60 mm and length of 100 mm manually operated falling from 1,450 mm height of steel pipeline containing six holes on its sides near the base plate to prevent air from accumulating and effect the free drop weight from falling with respect to gravity. The distance of base plate edges is 200 mm.



**Plate 3.** Impact Load Apparatus.

#### **4.4.2 Crack Width Measurement**

Crack width is measured using steel roller package containing several steel rulers each with certain width, the rulers width ranging from 0.05-1 mm, the rulers are inserted in the crack and fitted then their sum is calculated to obtain the total crack width.

### **4.5 Roller Compacted Concrete**

#### **4.5.1 Manufactured Apparatus: Roller Compactor**

The apparatus is manufactured in local market and designed to simulate steel roller compactor which is commonly used in the site for compaction as shown in Plate 4. A solid cylinder of 100 mm diameter, 100 mm length and 4.5 kg weight is fixed to the chase and connected from one side to steel column of 200 mm length where load would be applied and from the other side to the roller compactor holder. Finally the overall length of the apparatus is 1000 mm.

#### **4.5.2 Cubes and Cylinders Compactor**

The apparatus is manufactured in local market to compact the SFRC mixture in cube and cylinder specimens as shown in Plate 5, a steel bar of 600 mm length with circular base plate at bottom of 95 mm diameter and two steel plates distance 300 mm from the bottom plate at which load is entered between them.



**Plate 4.** Roller Compactor Apparatus.

## 5 Results and Discussion

### 5.1 Material Properties

Compressive strength, tensile strength and modulus of elasticity are measured at 0.8 %  $V_f$  of SF RCC, Figs. 2 and 3 show the compressive and tensile strength results respectively along with Table 11, it can be notice that beam (E2) has the maximum compressive and tensile strength results which was 62.39 MPa and 10.34 MPa respectively, that can be concluded; compacting SFRC in two layers and increasing load applied magnitude for each layer compaction gives maximum strength for SFRC. While beam specimen (F3) which has the second higher compressive and tensile strength which was 56.43 MPa and 9.51 MPa respectively.

It can be concluded from the previous results that compacting SFRC cube and cylinder specimens in two layers while increasing load magnitude gives maximum values for compressive and tensile strength at which equivalent loads to the loads on beams is applied on cube and cylinder specimens by determining stress values.

The modulus of elasticity is measured using equation method and ultrasonic device and from the obtained results that shown in Table 12; beam specimen (E2) has the maximum value of modulus of elasticity followed by beam specimen (F3); according to compaction technique of applying different incremental loads at two stages (first layer



**Plate 5.** Cube and Cylinder Specimens Compactor.

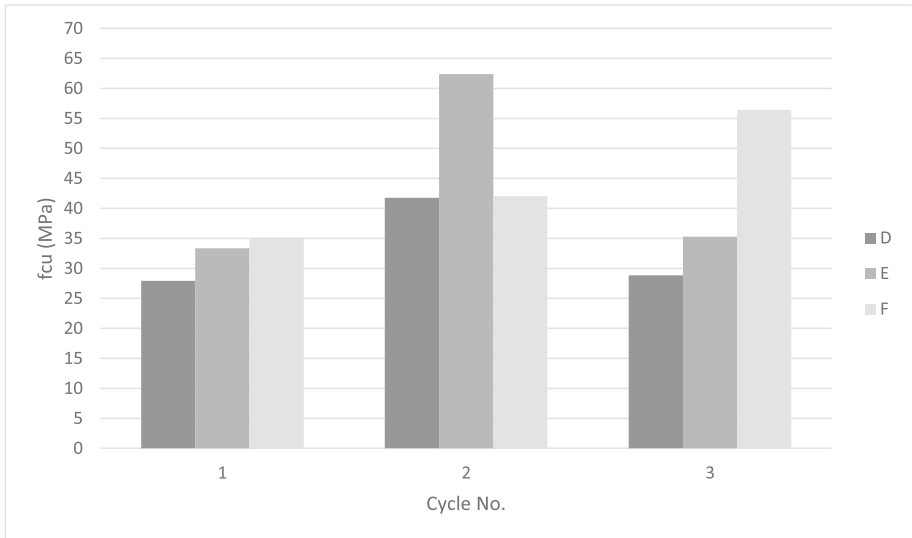


**Fig. 2.** Compressive strength results for roller compacted concrete cube specimens.

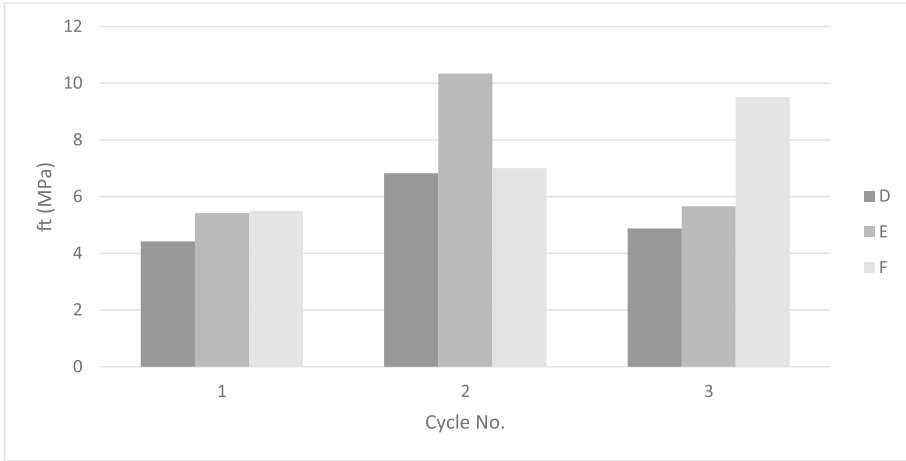


**Fig. 3.** Tensile strength results for roller compacted concrete cylinder specimens.

**Table 11.** Compressive and indirect tensile strength tests results for SF-RCC.

Sample		Compressive strength $f_{cu}$ (MPa)	Indirect tensile strength $f_t$ (MPa)
D	D1	27.93	4.42
	D2	41.76	6.82
	D3	28.85	4.88
E	E1	33.37	5.42
	E2	62.39	10.34
	E3	35.29	5.66
F	F1	35.1	5.5
	F2	42.01	7
	F3	56.425	9.51

**Table 12.** Modulus of elasticity results for SF-RCC.

Sample		$E_c$ equation (GPa)	$E_c$ ultrasonic (GPa)		
			Cube	Cylinder	Beam
D	D1	22.36	33.75	43.63	16.98
	D2	27.34	39.11	46.73	32.78
	D3	22.72	34.01	45.66	30.92
E	E1	24.44	38.46	46.08	37.68
	E2	33.42	45.45	54.00	47.23
	E3	25.13	38.78	46.73	38.41
F	F1	25.06	40.13	46.51	38.22
	F2	27.42	44.63	48.06	33.75
	F3	31.78	45.04	48.98	46.36

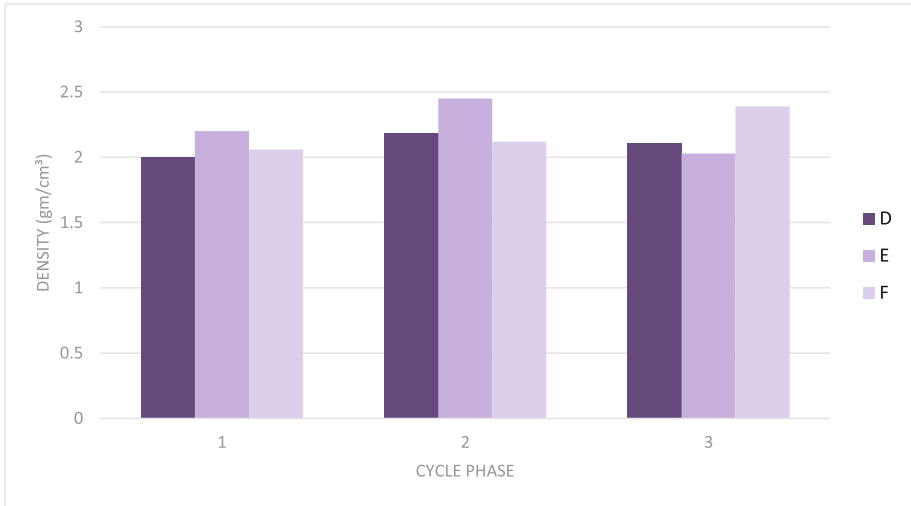


**Fig. 4.** Density for SFRCC beam specimens results.

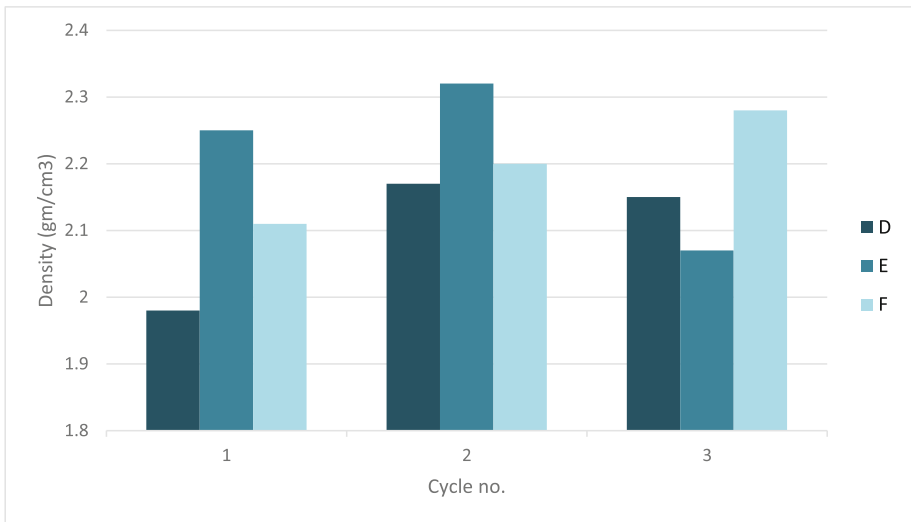


**Fig. 5.** Density for SFRCC cube specimens results.

with 10 kg and 8 passes) and (second layer with 25 kg and 8 passes) enhance the ability of SFRC pavement to deformed elasticity and increased it's stiffness.

Density of SFRC beam, cube and cylinder specimens are illustrated in Figs. 4, 5 and 6 respectively along with Table 13. It can be concluded that beam specimen (E2) has the maximum density followed by beam specimen (F3), which clarify that



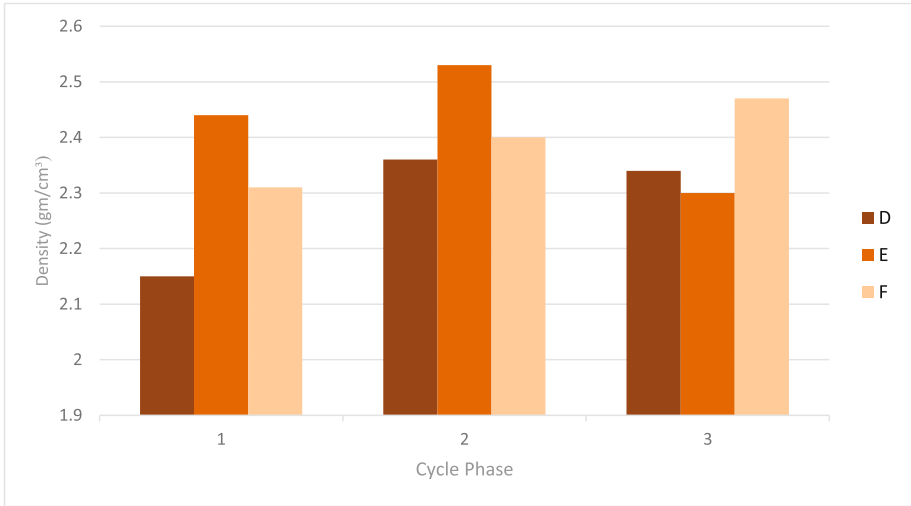


**Fig. 6.** Density for SFRCC cylinder specimens results.

**Table 13.** Density tests results for SF-RCC.

Sample	Density of beams (gm/cm <sup>3</sup> )	Density of cubes (gm/cm <sup>3</sup> )	Density of cylinders (gm/cm <sup>3</sup> )
D	D1	2	1.98
	D2	2.19	2.17
	D3	2.11	2.15
E	E1	2.2	2.25
	E2	2.45	2.32
	E3	2.03	2.07
F	F1	2.06	2.11
	F2	2.12	2.2
	F3	2.39	2.28

$$\text{Density of Beam} = \frac{\text{Weight of Beam}(gm)}{\text{Volume of Beam}(cm^3)}$$

$$\text{Density of Cube, Cylinder} = \frac{\text{Weight in Air}}{\text{Weight in air} - \text{Weight in Water}}$$

compaction technique of applied different incremental loading at two stages (first stage: 10 kg, 8 passes) and (second stage: 25 kg, 8 passes) enhance density of SFRC and eventually increase all material properties of SFRCC.

Compressive strength, tensile strength and modulus of elasticity are measured and compared between beam specimens that have been compacted conventionally of 0.8%  $V_f$  (C) and (E2) that has been compacted using roller compactor as shown in Figs. 7 and 8 for compressive and tensile strength test results respectively and in Table 14 for modulus of elasticity test results.

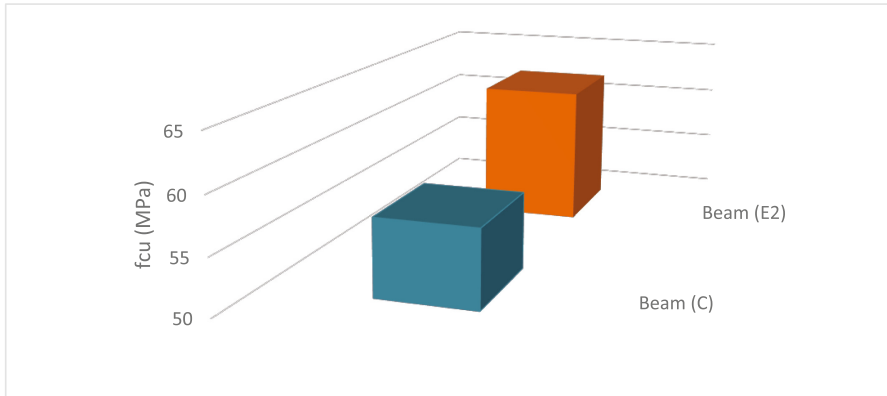


**Fig. 7.** Comparison of Compressive Strength Results for Cube specimens (C) and (E2).

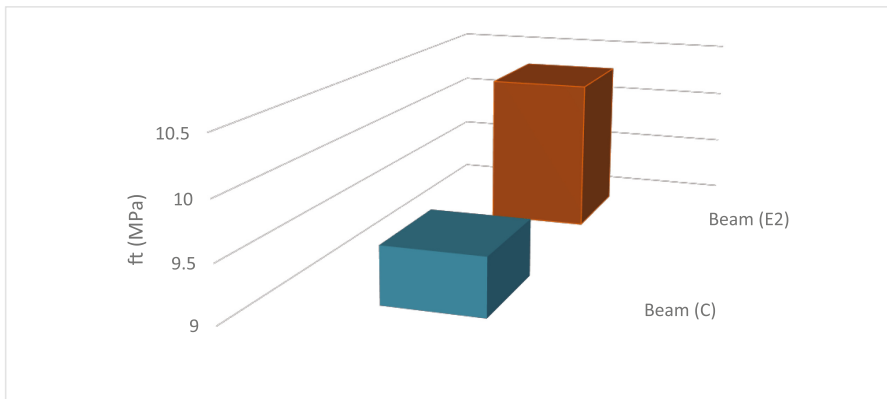


**Fig. 8.** Comparison of Tensile Strength Results for Cylinder specimens (C) and (E2).

**Table 14.** Comparison of modulus of elasticity results for (C) and (E2).

Sample	Ec equation (GPa)	Ec ultrasonic (GPa)		
		Cube	Cylinder	Beam
C	31.90	44.63	51.39	43.94
E2	33.42	45.45	54.00	47.23

According to the previous test results compressive strength increased from 56.85 MPa for cube specimen (C) to 62.39 MPa for cube specimen (E2) resulting in increasing of about 9.74%, while tensile strength increased from 9.5 MPa for cylinder specimen (C) to 10.34 MPa for cylinder specimen (E2) resulting in increasing of about 8.84% while modulus of elasticity for Ec equation increased by about 4.76% and for ultrasonic test results increased by factor of increasing 1.84%, 5.08% and 7.49% for

**Table 15.** Comparison of Density Results for specimens (C) and (E2).

Sample	C			E2		
	Beam	Cube	Cylinder	Beam	Cube	Cylinder
Density	2.43	2.21	2.45	2.45	2.32	2.53

cube, cylinder and beam specimens respectively, that shows compacting SFRC using roller compactor improve material properties strength of SFRC rather than compaction using vibrator table.

Density Comparison between beam, cube and cylinder specimens of (C) and (E2) cases are shown in Table 15. Comparison shows that, density is increased by about 0.82%, 4.98% and 3.27% for beam, cube and cylinder specimens respectively, which confirms the conclusion that, compaction of SFRC using roller compactor is more efficient and gives higher strength to SFRC pavement rather than using conventional vibratory compaction technique.

Comparison also has been carried out between modulus of rupture and pavement thickness for both beam specimens (C) and (E2) at which modulus of rupture ( $f_r$ ) is calculated using the most commonly equation that relate compressive strength of plain concrete to modulus of rupture [11];

$$f_r = 0.62\sqrt{f'_c}. \quad (6)$$

Where:

$f_r$  = Modulus of rupture (MPa)

$f'_c$  = Compressive strength (MPa)

While modulus of rupture for SFRC is calculated using the following equation; [12]

$$f_r = 0.99\sqrt{f'_c} + 3.83V_f \quad (7)$$

Where:

$f_r$  = Modulus of rupture (MPa)

$f'_c$  = Compressive strength (MPa)

$V_f$  = Volume fraction of steel fiber

Thickness has been determined using (AASHTO Method) [13] as shown in Table 16 test results show that SFRC pavement thickness would be decreased by about 4.09%; when using roller compactor instead of conventional compaction technique.

**Table 16.** Comparison of Thickness Results for specimens (C) and (E2).

Sample	Modulus of rupture ( $f_r$ ) (MPa)	Thickness (mm)	Percentage of decrease (%)
C	9.74	178	–
E2	10.06	171	4.09

## 5.2 Impact Load Test

9 Specimens of roller compacted steel fiber reinforced concrete beams with 0.8 %  $V_f$  are tested using impact load apparatus. Each beam specimen is compacted using different load and number of load cycles as illustrated in Table 17.

**Table 17.** Impact energy results for roller compacted SFRC beam specimens.

Beam	No. of blows		Impact energy (kN. mm)	
	First crack	Failure	First crack	Failure
D1	3	27	87.09	783.81
D2	4	38	116.12	1103.14
D3	5	36	145.15	1045.08
E1	4	32	116.12	928.96
E2	17	173	493.51	5022.19
E3	7	35	203.21	1016.05
F1	5	33	145.15	957.99
F2	8	39	232.24	1132.17
F3	10	70	290.3	2032.1

Impact load test results are shown in Figs. 9 and 10 for first crack and failure respectively. It can be noticed that beam specimen (E2) is reported for maximum number of blows of first crack which is 17 blows; in which beam specimen (E2) is compacted in two layers of 50 mm each, 10 kg with 8 passes is applied on the first layer and 25 kg with 8 cycles is applied on the second layer. While beam specimen (F3) is reported to be the next beam for maximum number of blows for first crack which is about 10 blows, beam specimen (F3) is compacted in one layer of 100 mm, load applied is 25 kg and 24 passes.

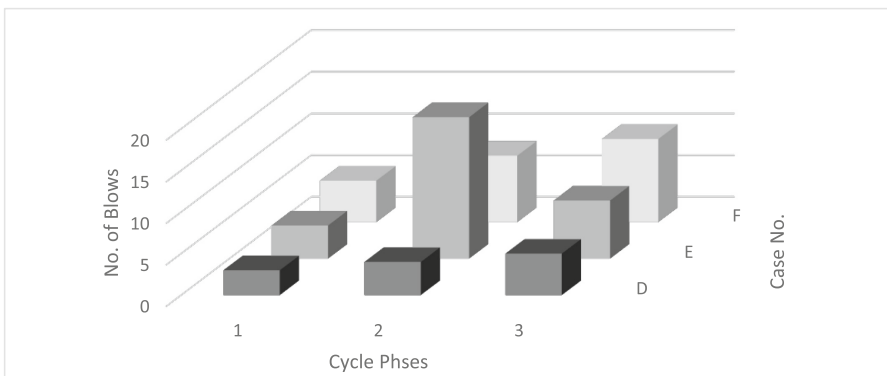


**Fig. 9.** Impact load test results for roller compacted concrete beams at first crack.

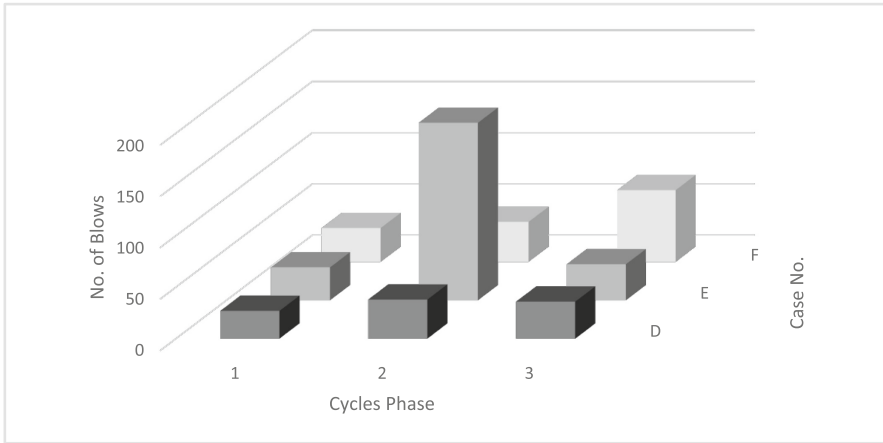


**Fig. 10.** Impact load test for roller compacted concrete beam specimens at failure.

As it can be seen that beam specimen (E2) has maximum number of blows 173 blows at failure due to its high strength as compared to the others; this indicated that compaction in two layers with different incremental loading value is more efficient and enhance high strength and performance with long life by increasing load magnitude at failure, reduce first crack appearance and hence minimal maintenance. Plate 6 shows all beam specimen for roller compaction technique.



**Plate 6.** Failed Beam Specimens Roller Compacted SFRC under Impact Load Test.

Impact energy is illustrated in Table 15 at which energy required to introduce first crack and failure to beam specimen (E2) is higher than the others, due to its high

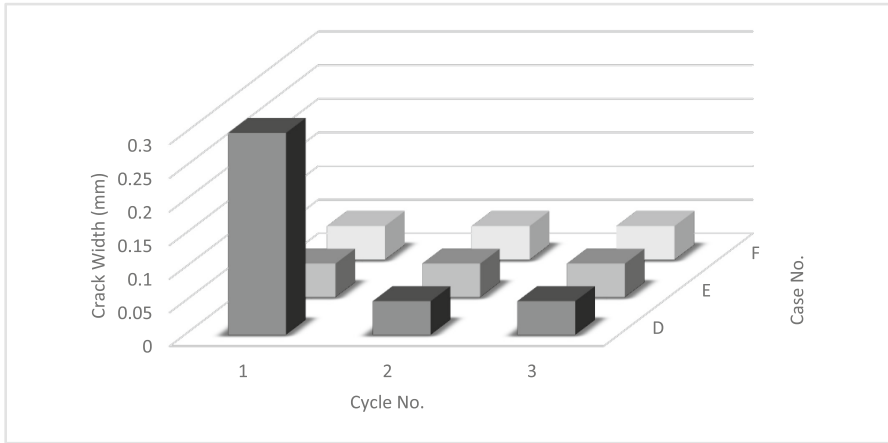


**Fig. 11.** Crack width results for impact load test on roller compacted concrete beam specimens at first crack.

number of blows which directly proportional to impact energy which is 493.51 kN.mm at first crack and 5022.19 kN.mm at failure. At which (U) is equal to 29.03 kN.mm [14].

As for Crack width results for first crack and failure are shown in Figs. 11 and 12 respectively. It can be notice from the obtained results that cracks width at first crack have no significant difference except beam specimen (D1) that difference may be reported as a results of low applied loading 10 kg and number of passes 8 cycles as compared to the other specimens.

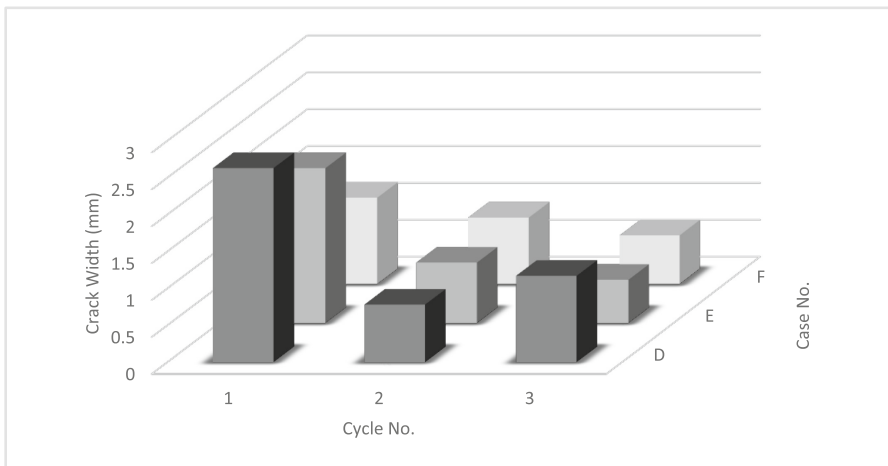


**Fig. 12.** Crack width results for impact load test on roller compacted concrete beam specimens at failure.

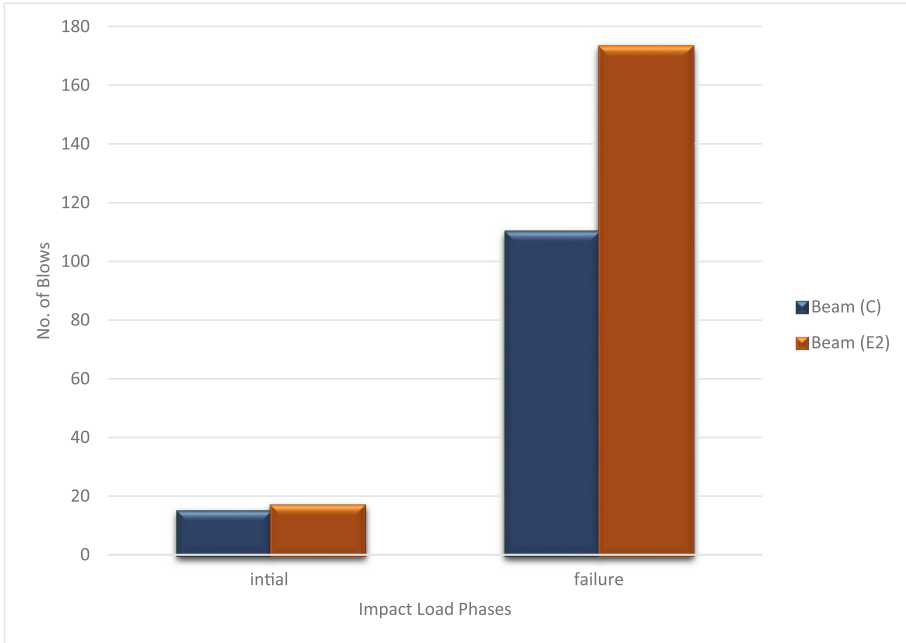


**Fig. 13.** Comparison between Beam specimens (C) and (E2) at Impact Load Test Results.

Crack width at failure also have no significant difference although maximum crack width can be seen in first cycle (D1, E1, F1) due to low applied loading which is about 10 kg as compared to the other specimens regardless of number of passes.

Comparison has been carried out for impact load test results between SFRC beam specimens with 0.8%  $V_f$  of steel fiber that have been compacted using two different compaction techniques; vibrator; (beam specimen C) and roller compacter (beam specimen E2). Impact load test is carried out for both beam specimens although the test for beam specimen (C) is carried out after 150 days and for (E2) beam specimen after 30 days, beam specimen (E2) gives higher values for number of blows for first crack and failure as shown in Fig. 13.

Impact energy required to introduce first crack and failure for beam specimens (C) and (E2) are shown in Table 18 and since impact energy is directly proportional to number of blows, it's greater for beam specimen (E2).

**Table 18.** Impact Energy Results for (C) and (E2) Beam specimens.

Beam	No. of blows		Impact energy (kN. mm)	
	First crack	Failure	First crack	Failure
C	15	110	435.45	3193.3
E2	17	173	493.51	5022.19

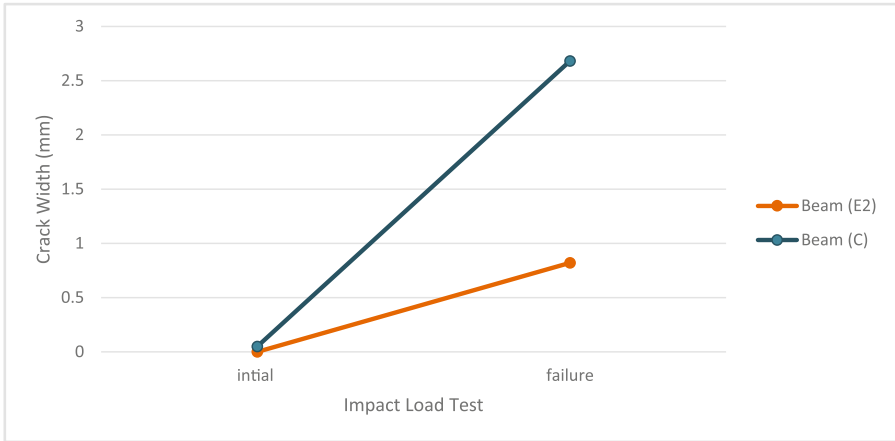


**Fig. 14.** Comparison between crack width at impact load test for beam specimens (C) and (E2).

As for crack width it can be seen in Fig. 14 that although beam specimen (E2) has more number of blows but its crack width is smaller than beam specimen (C) due to high bonding strength in beam specimen (E2) when using roller compactor.

## 6 Conclusions

1. Roller compacted steel fiber reinforced concrete beam specimen (E2) which has been compacted in two layers (first layer with 10 kg and 8 passes, second layer with 25 kg and 8 passes) and with 0.8%  $V_f$  of steel fiber has the maximum number of blows at impact load test; 173 blows at failure due to its high strength related to the existing of steel fiber; this indicated that compaction in two layers with different incremental loading value is more efficient and enhance high strength and performance with long life by increasing load magnitude at failure, reduce first crack appearance and hence minimal maintenance.
2. The modulus of elasticity for roller compacted specimens is measured using equation method and ultrasonic device and from the obtained results beam specimen (E2) has the maximum value of modulus of elasticity; according to compaction technique of applying different incremental loads at two stages (first layer with 10 kg and 8 passes) and (second layer with 25 kg and 8 passes) enhance the ability of SFRC pavement to deformed elasticity and increased it's stiffness.
3. Comparison between SFRC beam specimens with 0.8 %  $V_f$  of steel fiber that have been compacted using two different compaction techniques; vibrator; (beam specimen C) and roller compactor (beam specimen E2) at impact load test show that beam specimen (E2) gives higher values for number of blows for first and failure crack with 15, 17 blows for beams specimen (C, E2) respectively at first crack and 110, 173 blows for beams specimen (C, E2) respectively at failure.



4. Comparison shows that density of specimens (C) and (E2) is increased by about 0.82%, 4.98% and 3.27% for beam, cube and cylinder specimens respectively, which confirm the conclusion that compaction of SFRC using roller compactor is more efficient and give higher strength to SFRC pavement rather than using conventional vibratory compaction technique.
5. Comparison between modulus of rupture and pavement thickness for both beam specimens (C) and (E2) show that SFRC pavement thickness would be decreased with 4.09%; when using roller compactor is used instead of conventional compaction technique.

## References

1. Halsted, G.E.: Roller-compacted concrete pavements for highways and streets. In: Portland Cement Association the Advances in Pavement Design and Construction Session of the 2009 Annual Conference of the Transportation Association of Canada Vancouver, British (2009)
2. Kumar, V.D.R., KrishnaRao, S., Panduranga Rao, B.: A study on properties of steel fibre reinforced roller compacted concrete. *Int. J. Eng. Sci. Emerg. Technol.* **6**, 221-227 (2013)
3. Kagaya, M., Suzuki, T., Kokubun, S., Tokuda, H.: A study on mix proportions and properties of steel fiber reinforced roller-compacted concrete for pavements. Translation from Proceedings of JSCE, No.669/V-50 (2001)
4. Iraqi Standard Specification I.Q.S. No. 5, 1984 requirements. المواصفات العراقية (1984)  
رقم (5) للإسمنت, الجهاز المركزي للتقييس والسيطرة النوعية. بغداد, عام
5. American Association of State Highway and Transportation Officials (AASHTO T 22). Standard Method of Test for Compressive Strength of cube concrete specimens. Washington, D.C (2010)
6. American Association of State Highway and Transportation Officials (AASHTO T 198-02), Standard Method of Test for Splitting Tensile Strength of Cylindrical Concrete Specimens. Washington, D.C (2010)
7. Building code requirements for structural concrete and commentary: ACI Committee: 318. American concrete Institute, Farmington Hills, Michigan (2000)
8. American Association of State Highway and Transportation Officials (AASHTO T 22). Standard Method of Test for Compressive Strength of cube concrete specimens. Washington, D.C (2010)
9. Ali, B.A.H.: Assessment of Concrete Compressive Strength by Ultrasonic Non-Distractive Test. M.Sc. Thesis, Department of Civil Engineering, University of Baghdad (2008)
10. British Standards Institution: Testing Concrete. Recommendations for Measurement of Velocity of Ultrasonic Pulses in Concrete, Milton Keynes: BS188, part203 (1988)
11. Salem, R.M., Burdette, E.G., Mike Jackson, N.: Interrelationship of Physical Properties of Concrete Made with Recycled Aggregates. TRB Annual Meeting. (ACI, 1999) (2003)
12. Karl, K.-W., Lee, D.H., Hwang, J.-H., Kim, K.S., Il-Sup Choi: Revision on material strength of steel fiber-reinforced concrete. *Int. J. Concrete Struct. Mater.* **5**(2), 87-96 (2011). (ACI, 1992)
13. Huang, Y.H.: Pavement Analysis and Design, 2nd (edn.). University of Kentucky (2004)
14. Ali, A.H., Yasin, M.H.: Influence of mix proportions on the impact resistance of high strength concrete. *J. Eng. Dev.* **18**(3) (2014). ISSN 1813-7822

# Study on Mixing Proportion for AC-13C Asphalt Mixture and Construction Control

Wu Jing<sup>1,2(✉)</sup> and Wu Li<sup>2</sup>

<sup>1</sup> School of Civil Engineering, Hubei Engineering University,  
Xiaogan, Hubei, China  
wu.jingpaper@163.com

<sup>2</sup> School of Engineering, China University of Geosciences,  
Wuhan, Hubei, China

**Abstract.** With good waterproof performance and high stability under high temperature, SBS modified AC-13C asphalt mixture can meet the requirements in highway construction nowadays. In this article, the Loudi test highway section is mainly used to carry out discussions on the design and test of the production mix proportion for AC-13C asphalt mixture, and at the same time studies are carried out for the construction methods such as mixing and rolling, to further improve highway pavement quality.

**Keywords:** AC-13C · Asphalt mixture · Mix proportion · Construction control

## 1 Introduction

With continual development of economy and technology, urbanization is increased day by day, and higher requirements on highway construction speed and quality are raised. Due to its economy and convenience, SBS modified asphalt construction technology is widely used in highway construction. However, due to different effects resulted from indoor mixing and on-site mixing as well as different mineral specifications and gradation change, usually there are differences from the design requirements when carrying out gradation for the mixture in accordance with the target mix proportion during construction, and therefore, the production mix proportion must be designed for asphalt mixture before production. In this article, the test data in Loudi test highway section are used to introduce the mix proportion design schemes and construction quality control measures for AC-13C asphalt mixture.

## 2 About the Project

Loudi test highway section is located in a continental subtropical monsoon humid climate zone, with four distinct seasons, and in summer, it is hot and rainy, and in winter, it is warm, and the annual average air temperature is between 16–18 °C, and the annual precipitation is between 1200–1700 mm. The highway pavement consists of two layers: a 34 cm thick reinforced cement concrete layer and a 16 cm thick cement stabilized crushed stone base layer.

### 3 Material Inspection

To ensure high performance of asphalt highway pavement structure, the quality of all the raw materials must be checked to ensure that the raw materials are qualified.

#### 3.1 Asphalt

AC-13C asphalt was used, which has such advantages as low needle penetration, good bonding performance, high stability under high temperature, and good ductility under low temperature. Through special tests, all the indexes of the asphalt meet the requirements in Standard JTG F40-2004 Technical Specifications for Construction of Highway Asphalt Pavements. The test results are shown in Table 1:

**Table 1.** Test results of AC-13C asphalt

Item of test	Unit	Technical index	Test result	Conclusion
Needle penetration (25 °C, 100 g, 5 s)	0.1 mm	40–60	58	Pass
Ductility (5 °C, 5 cm/min)	cm	≥ 20	35	Pass
Softening point (T <sub>R&amp;B</sub> )	°C	≥ 60	68	Pass
Residue after RTFOT	Quality loss	%	±1.0	Pass
	Needle penetration ratio after heating (25 °C)	%	≥ 65	Pass
	Ductility (5 cm/min, 5 °C)	cm	≥ 15	19.0

#### 3.2 Filler

The filler for the highway section consists of cement and mineral powder, and all the mineral powder was prepared by grinding water repellent limestone, and the maximum metric particle size of crushed stones used in cement stabilized crushed stone base layer was 26.5 mm, and the crushed stones must be hard, durable and clean and has a good bonding performance. The particles must meet the requirements in Table 2.

The material for the base layer is higher than 4.75 mm, and coarse aggregate is classified into three grades, i.e.: 19–26.5 mm, 9.5–19 mm, and 4.75–9.5 mm, and

**Table 2.** Range of gradation for porous cement stabilized crushed stone base

Mesh size	Passing percent
31.5	100
26.5	95–100
13.2	25–60
4.75	0–10
2.36	0–5
0.075	0–2

coarse aggregate of these three particle grades should be separately stored. The highway in the material storage area and the mixing area must be hardened to prevent mixing mud. For particles with a size below 0.6 mm in the aggregate, tests for liquid limit index and plastic limit index must be carried out, and the liquid limit index must be lower than 28%, and the plastic limit index must be lower than 9.

The crushing value for aggregate should not be higher than 30%, and the content of needle and strip shaped aggregate should not be higher than 20%.

### 3.3 Hot Aggregate

For the test highway section, intermittent mixing plant is used, and the mesh gauge of the vibration screen is 3 mm, 6 mm, 11 mm and 19 mm, and when the cold aggregate in the mixing plant is screened for a second time, the size of hot aggregate obtained is 11–19 mm, 6–11 mm, 3–6 mm, and 0–3 mm, and the test results are shown in Table 3.

**Table 3.** Test results of hot aggregate

Item		Specification of mineral material			
		0–3 mm stone chips	3–6 mm rubbles	6–11 mm rubbles	11–19 mm rubbles
		Hot aggregate passing percent (%)			
Mesh size (mm)	16.00	100.0	100.0	100.0	100.0
	13.20	100.0	100.0	100.0	67.0
	9.50	100.0	100.0	76.8	6.1
	4.75	100.0	84.2	7.1	0.4
	2.36	81.2	12.8	1.7	0.2
	1.18	51.8	3.8	1.1	0.2
	0.60	29.8	1.2	0.7	0.2
	0.30	14.8	0.9	0.6	0.2
	0.15	8.5	0.8	0.4	0.2
	0.075	3.3	0.4	0.2	0.1
Specific gravity (g/cm <sup>3</sup> )	Apparent specific gravity	2.559	2.618	2.601	2.619
	Bulk specific gravity	–	2.456	2.449	2.458

### 3.4 Determination of Proportion in Hot Aggregate Bin

The target mix proportion for the asphalt mixture should be consistent with the requirements in Standard JTG F40-2004 Technical Specifications for Construction of Highway Asphalt Pavements, and moreover, when preparing asphalt mixture, the requirements in the above standard must also be met in the process of design of the production mix proportion, and at the same time the production requirements in the

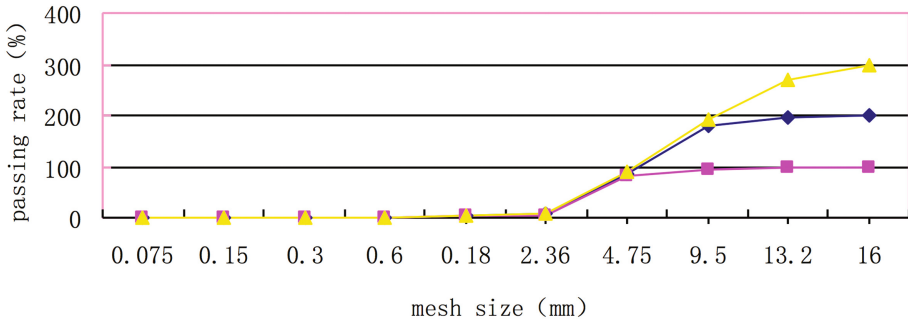


Fig. 1. Curve of mixing of mineral material

construction drawings must be met. It is required to be consistent with the target mix gradation required in production. With the above data, the mixing results of the asphalt mixture are shown in Fig. 1.

### 3.5 Design of Asphalt Content

In the process of designing the production mix proportion for the asphalt mixture, normally  $\pm 0.3\%$  of the optimum asphalt content determined in the target mix proportion is used to carry out Marshall (4.3%, 4.6%, and 4.9%), and one optimum asphalt content within the production mix proportion of the asphalt mixture is determined with the test results. As the production mix proportion for the highway section is substantially consistent with the target mix proportion in design, to ensure more accurate test results, we used  $\pm 0.1\%$  of the target mix proportion in the Marshall test, that is to say, in the tests, the asphalt content was 4.4%, 4.5%, 4.6%, 4.7% and 4.8%.

## 3.6 Marshall Test

### 3.6.1 Test of Mechanical Indexes

Marshall tests were carried out by following the mix proportions for the hot aggregate determined above, and for the asphalt content, references were made to the requirements in Standard JTG 052-2000 Test Procedures for Asphalt and Asphalt Mixtures for Highway Engineering, and the maximum specific gravity was provided by the laboratory of the construction organization. The test results are shown in Table 4.

### 3.6.2 Test Characteristics

Draw plots with the test results obtained in the above tests, with the horizontal ordinate representing the asphalt content, and with the vertical ordinate representing the compacted bulk specific gravity, porosity, voidage, saturation, stability, and flow value respectively, to show the curve relationship between the individual indexes and the content of asphalt, and plots as shown in Fig. 2 are obtained.

**Table 4.** Test results in Marshall tests for AC-13C asphalt mixture in Loudi test

Content of asphalt (%)	Thickness of test piece (mm)	Compacted bulk specific gravity ( $\text{g}/\text{cm}^3$ )	Maximum specific gravity actually measured ( $\text{g}/\text{cm}^3$ )	Porosity (%)	Voidage (%)	Saturation (%)	Stability (kN)	Flow value (0.1 mm)
4.8	64.1	2.450	2.551	4.0	15.3	74.1	14.6	35.4
4.7	63.2	2.450	2.558	4.2	15.3	72.6	14.1	35.0
4.6	63.6	2.465	2.561	3.8	14.7	74.5	18.7	40.9
4.5	62.6	2.493	2.597	4.0	14.8	73.1	19.2	38.3
4.4	67.0	2.445	2.601	6.0	16.4	63.4	14.3	34.9

### 3.6.3 Determination of Optimum Asphalt Content

- (1) Determination of  $OAC_1$ : From plots in Fig. 2, the corresponding maximum value of the compacted bulk specific gravity, the voidage and the stability in the plots is obtained, and the asphalt content corresponding to these maximum values is 4.46%, 4.44% and 4.53%, and we take the arithmetic mean value calculated with these three indexes as  $OAC_1$ , and the calculation is conducted with the following formula:

$$OAC_1 = (\alpha_1 + \alpha_2 + \alpha_3)/3 = 4.48\% \quad (1)$$

- (2) Determination of  $OAC_2$ : From plots in Fig. 2, we know that when the various Marshall mechanical indexes meet the requirements in the technical specifications (not including VMA), the asphalt content should be in the range between 4.2%–5.2%, and we take the mean value of the maximum value and the minimum value in the content range as  $OAC_2$ , and the calculation is conducted with the following formula:

$$OAC_2 = (OAC_{\min} + OAC_{\max})/2 = 4.7\% \quad (2)$$

- (3) Determination of  $OAC$ : We take the arithmetic mean value obtained from  $OAC_1$  and  $OAC_2$  above as the value of  $OAC$ , the optimum asphalt content, and the calculation is conducted with the following formula:

$$OAC = (OAC_1 + OAC_2)/2 = 4.59\% \quad (3)$$

At the same time, we can see from the plots in Fig. 2 that, for  $OAC$ , the optimum asphalt content, all the corresponding mechanical indexes such as porosity, voidage and flow value meet the requirement in Marshall test.

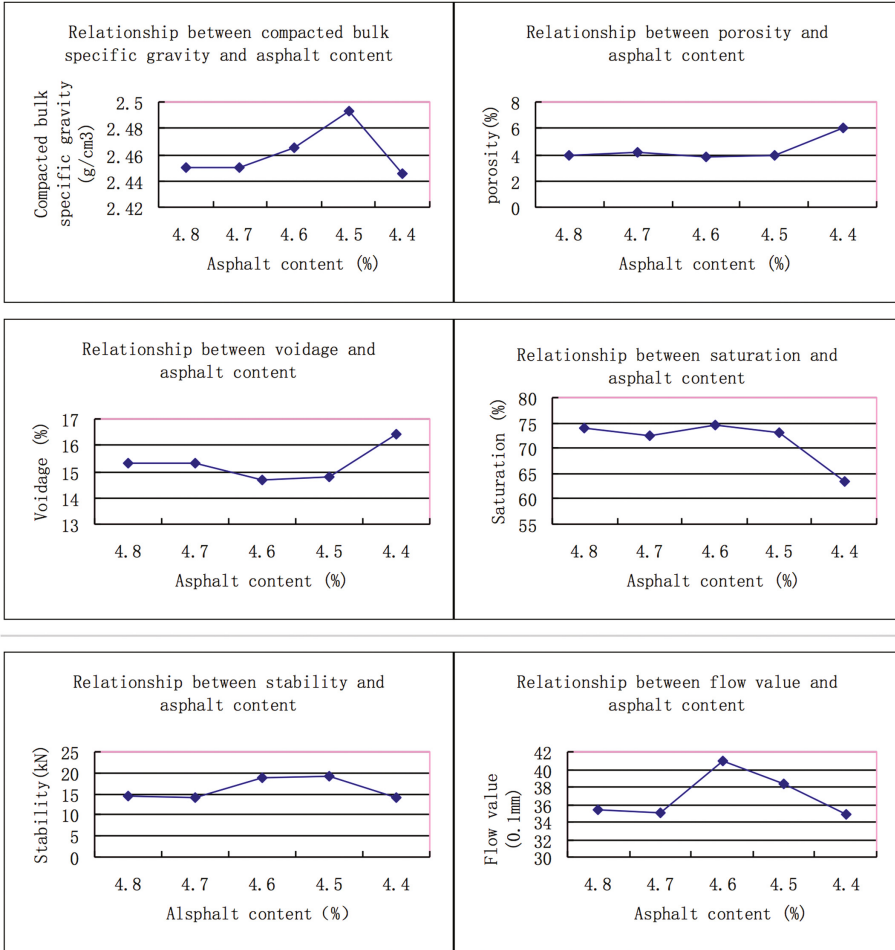


Fig. 2. Characteristic plots in the tests

### 3.7 Design and Test of the Mix Proportion

As for the design and test of the mix proportion, we followed the optimum asphalt content determined according to the calculations above under standard test conditions, and the tests were carried out by testing the water stability and high temperature stability for the mix proportion, and the test results are as follows:

According to test, when the asphalt mixture is prepared at 4.59%, the optimum proportion of stone and asphalt, Marshall residual stability test meets the requirements in the specifications. Moreover, the result of stability test under high temperature is 3,860 times/mm, and the high temperature stability also meets the requirements in the specifications.

### 3.8 Test Conclusions

With the mix proportion for asphalt mixture designed with the source data in the construction of Loudi highway section, we carried out tests for them, and took the climate and environment features as well as the construction experiences in Loudi into consideration to determine that the optimum proportion of stone and asphalt in asphalt mixture is 4.59%.

## 4 Construction Processes and Quality Control

### 4.1 Mixing

- (1) Before mixing, the materials in the mixing site can be used for paving for 3–5 days.
- (2) Before mixing every day, check the water content in the aggregate in each area in the site, calculate the mix proportion for the day, and the total content of added water and natural water should be slightly higher than the optimum water content. The actual cement quantity can be about 0.5% higher than the cement quantity determined when designing the materials for the mixture, but the cement quantity actually used and the actual cement quantity in the bottom base layer spot checked on site should be less than 4.0%; and the cement quantity in the base layer should be less than 6.0% (the cement quantity in PCC and CRC base layer can be 6.0%). Meanwhile, when adequately evaluating the surplus strength of construction, start from control by reducing the construction deviation, but do not increase the strength by increasing the quantity of cement used.
- (3) When starting to mix every day, take samples from the feeding conveyor belt of the mixer when mixture is fed to check whether the design mix proportion is met, and when formal production is carried out, check the mixing every 1–2 h, and spot check whether the mix proportion and water content are changed. During work under high temperature, the water content in the morning and in the evening should be different, and adjustment should be made in time according to change of temperature.
- (4) Equip a mixture bin with a flap-panel funnel, and directly feed mixture from the funnel into trucks and transport. When loading mixture, move the transport truck back and forth, and load mixture by three times, with the height of loaded mixture not higher than 1.5 m to prevent mixture separation. At the same time, take measures to reduce the drop distance when loading mixture.

### 4.2 Rolling

- (1) Use three-wheeled or dual steel wheeled roller and vibration roller for rolling immediately after every paver, and note to roll slightly firstly and forcefully later and statically first and dynamically later, and roll normally for 50 m–80 m every



time. The rolled sections must be clearly marked, and clear boundary marks must be set, and supervisor must be available nearby.

- (2) During rolling, follow the procedures and processes determined in the trial paved highway section. Note to use sufficiently stable rolling, and cause no waving and shift during vibration rolling. When compacting, first compact stably (with suitable number of times of rolling, and with the compactness reaching 90%)→Start slight vibration rolling→Then carry out heavy vibration rolling. A nucleonic instrument can be used to check the compactness on site, and when failed, re-compact (note to check the compacting time). When the rolling is completed, use sand replacement method to test the compactness (Table 5).
- (3) When rolling with rollers, 1/2 wheel width should be overlapped.
- (4) When the roller is reversed and the gear is shifted, operate smoothly, never move the bottom base layer or the base layer, and when initial compaction is completed in rolling for the first time, try to return along the previous route after reversing, and gears are shifted on compacted sections, and when gears are shifted and roller is reversed on the end which is not rolled, the positions must be staggered to form serrations, and where individual swellings occur, workers should be appointed to level.
- (5) The recommended driving speed of the roller when rolling is 1.5–1.7 km/h for the 1<sup>st</sup> and 2<sup>nd</sup> time of rolling, and the speed is 1.8–2.2 km/h for every subsequent time of rolling.
- (6) During the period of constructing the base layer, if the mixture quantity and the number of rolling devices are sufficient, when the bottom layer is rolled for about 100–150 m, the starting position which was just rolled can be immediately returned, and cement and crushed stones on the upper layer can be immediately paved continuously, but the upper layer must be rolled before initial cement coagulation of the bottom layer. Where it has no time to complete such work, this construction method cannot be used. When this method is used, there are advantages as follows: The upper and bottom layer can be bonded well, and there is no need to spray pure liquid cement or dry cement.
- (7) Rollers must be parked in a staggered way and with an interval of 3 m, and it is better to park them on a rolled highway section, to prevent any damage to the base layer structure.
- (8) Never turn around and brake the roller on any highway section which has been rolled or is being rolled, to ensure that the stable aggregate layer pavement is not damaged.

Ninth, the rolling should be completed before initial cement coagulation and within the delay time determined in tests, and the required compactness should be reached.

**Table 5.** Test of residual stability of mix proportion

Optimum proportion of stone and asphalt	Stability when the test piece is immersed in water for 0.5 h (KN)	Stability when the test piece is immersed in water for 48 h (KN)	Residual stability (%)
4.59%	12.3	15	16

### 4.3 Setting Transverse Seam

- (1) When paving cement stabilized mixture, work must be carried out constantly with no interruption. When any work is discontinued for over 2 h due to any reason, a transverse seam should be set; and after completion of work every day, the cross section of the seam commenced the next day should also be set with a transverse seam; and when passing through bridges and culverts, in particular open culverts and open passages, a transverse seam should be set on both sides, and it is better to fit the transverse seam on the base layer and the bottom base layer with the end of the bridge end transition slab. Pay special attention to the rolling of the cement stabilized aggregate before the bridge end transition slab.
- (2) Where the paving is interrupted for over 2 h and no transverse seam is set, the uncompacted mixture near and under the paver should be removed, and the end which has been rolled and compacted and of which the elevation and levelness meet the requirements is evacuated so that level is perpendicular to the center line of the highway and the cross section is perpendicular to the pavement, and then new mixture is paved.

## 5 Conclusions

In highway construction, whether the target mix proportion can realize the production mix proportion and the mix proportion during production construction can be controlled are closely related, and for highway engineering, the individual indexes for asphalt highway pavement can be increased through tests designed for mix proportion for asphalt mixture, so the highway is more suitable for the climate and environmental need in the region and the service quality of highway is further improved.

## References

1. Wu, D., Guo, P., Han, J.: Application of orthogonal experiment method in SMA-16 mix proportion design. *J. Hefei Univ. Technol. (Nat. Sci.)* (02) (2011)
2. Peng, J.: A study on design of mix proportion of asphalt mixture in South Region of Qinghai Province. *Qinghai Traffic Technol.* (01) (2013)
3. Wang, S.: Discussions on design of mix proportion of asphalt mixture in highway maintenance and repair engineering for Rongwei Expressway. *Guide Sci-Tech Mag.* (32) (2011)
4. Yu, M., Wu, G.: A study on design of mix proportion for dry rubber modified asphalt mixture. *J. Build. Mater.* (01) (2014)
5. Li, Z.: A study on design method of mix proportion for asphalt mixture in permafrost regions. *Highway* (02) (2009)

# Study of Radioactive Characteristics of Cement Pastes Blended with GGBFS

Ahmed S. Ouda<sup>1,2</sup>(✉)

<sup>1</sup> Concrete Chemistry and Building Materials, Housing & Building National Research Center, Dokki, Giza, Egypt

<sup>2</sup> Department of Chemistry, University College of Taimaa, Tabuk University, Tabuk, Kingdom of Saudi Arabia  
Ahmed.Kamel56@yahoo.com

**Abstract.** This paper reports an experimental study carried out to investigate the effects of ground granulated blast-furnace slag (GGBFS) on radiation attenuation and mechanical properties of blended cements. Five cement mixtures were prepared with 0%, 10%, 15%, 30% and 40% of slag replacing the cement content and having water to cement ratio of 0.3, 0.29, 0.28 and 0.27 by weight, respectively. The cement pastes were tested for compressive strength after water curing at 1, 3, 7 and 28 days. The various hydration products were identified using x-ray diffraction (XRD), differential thermal analysis (DTA) and scanning electron microscope (SEM) techniques. In the same context, the radiation attenuation coefficients expressed as linear attenuation coefficient,  $\mu$ , of the investigated specimens were also determined after 28 days of hydration. The utilized radiation source comprised  $^{137}\text{Cs}$  radioactive element with photon energy of 0.662 MeV. In a similar manner, HVL and TVL for the tested samples were obtained. From the investigation, it has been revealed that the partial replacement of OPC on average 30% slag significantly increased compressive strength than the neat mixture at 28 days of curing. Although the enhancement of compressive strength upon replacing OPC with GGBFS, however the results of radiation parameters showed no significant effect of slag substitution on the attenuation of  $\gamma$ -rays.

**Keywords:** Blended cements · Linear attenuation coefficient · Half-value thickness · Tenth-value thickness

## 1 Introduction

Because of the wide application of nuclear science and technology in various fields as nuclear power plant, therefore, adequate and effective shielding is a prerequisite for the installation of such nuclear facilities to keep the radiation exposure below the dose limits recommended by the International Commission on Radiological Protection (ICRP). Shielding from gamma rays is more difficult than others because gamma photons have no mass and charge and hold high-energy, they can readily penetrate into the matter [1]. The photon interaction with the matter depends on its energy and the density of the shielding material [2]. The radiation shielding properties of a material are presented in terms of the linear attenuation coefficient ( $\mu$ ), which is defined as the

probability of a radiation interacting with a material per unit path length [3], and it is considered the most important quantity characterizing the penetration and diffusion of  $\gamma$ -rays in a medium. Its magnitude depends on the incident photon energy, the atomic number and the density ( $\rho$ ) of the shielding materials [3]. Several works have been performed to obtain linear attenuation coefficients (l) theoretically and experimentally for different elements, compounds and mixtures [4], for different building materials [5], for concretes [6, 7] and for some aqueous solutions [8]. Concrete is a good radiation protector material because it has the characteristics which necessary to weaken the  $\gamma$  rays and neutrons [9]. The use of concrete for radiation shield is more focused on the nuclear requirements, not strength. Medium quality concrete is sufficient to achieve the strength of radiation shield, while the concrete of high- density can better resists the radiation. Quantity of material radiation includes: (1). Rate of exposure, which is defined as the ratio of number of photons after passing through thickness of protection material with the number of initial photons; (2). Coefficient of attenuation, which is a microscopic latitudes side, while the physical meaning of the latitudes sides (cross section) is the probability to absorb or scatter radiation. Gamma rays are attenuated in proportion to the atomic masses of the material. It is thus advantageous to make a gamma-ray shield of the densest material economically feasible [10]. In radiation shielding, absorbent material's properties must be well known. Shielding material must have high density, high radiation attenuation coefficient and structural properties like high strength.

Nuclear installations such as nuclear power reactors, particle accelerators, hot cells for radioisotopes production and radioactive waste conditioning facility, require shielding for radiation protection. This can be achieved by substituting concrete aggregates with some industrial by-products. Metallurgical slags which are produced as industrial by-products, if accumulated, are considered as hazardous waste materials from an environmental point of view. Most of these slags such as blast furnace slag, steel slag, copper slag and lead slag are used as aggregates in concrete components [11]. Mahdy et al. [12] used concretes containing magnetite as aggregate and mixed with three levels of silicafume to investigate the compressive strength and shielding properties. They concluded that magnetite as an aggregate and silica fume as a mineral admixture for concrete improve its compressive strength as well as its shielding properties. Portland cement is the main cementitious component of conventional concrete. The chemical composition of cement paste depends on the type of cement used in construction. Portland cement is the most commonly used cement for concrete shielding structures. Other cements with different chemical compositions are available but have not been used in construction of nuclear power plant concrete [9].

Many studies indicate that radiation affects the microstructure of cement paste. Lowinska-Kluge and Piszora [12] conducted a study on the microstructure of cement paste under various doses of gamma radiation using SEM. They concluded that pseudomorphoses had taken place after a dose of 130 MGy and that the microstructure of cement paste was changed significantly by the gamma radiation. Behaviors of cement paste and aggregate are known to differ under irradiation conditions: cement paste tends to contract slightly and aggregates tend to expand. Several researchers developed concrete properties to suit the shielding requirements. They mostly concentrate on

reducing the water contents or using other cementitious materials such as blast furnace slag, silica fume and polymeric compounds in addition to Portland cement [14, 15].

Ground granulated blast furnace (GGBFS) is a non-metallic material consisting essentially of silicates and alumino silicates of calcium [16]. It has been used as a supplementary cementitious material in Portland cement concrete, either as a mineral admixture or as a component of blended cement [17]. The partial replacement of ordinary Portland cement with GGBFS improves strength and durability of concrete by creating a denser matrix and thereby enhancing the service life of concrete structures. According to Hwang and Lin [18], GGBFS has the potential to replace cement in high percentages because of its in-built cementitious property.

In this study, the influences of replacing OPC with GGBFS on the mechanical properties of cement pastes were investigated. Also, the radiological properties of blended mixtures were studied by measuring the attenuation of  $\gamma$ - rays using radiation source comprised  $^{137}\text{Cs}$  with photon energy of 0.662 meV. The obtained hydration products were identified using XRD, DTA and SEM techniques.

## 2 Experimental Details

### 2.1 Materials and Mix Proportions

Type I cement (42.5 N) with surface area of  $2415 \text{ cm}^2 \text{ kg}^{-1}$  in compliance with the requirements of ASTM C150 [19], was used in the preparation of blended cements, obtained from Suez Cement Company, Egypt. GGBFS with surface area of  $4000 \text{ cm}^2 \text{ kg}^{-1}$  was provided by Iron and Steel Company, Egypt. The chemical composition of ordinary Portland cement- OPC and GGBFS as conducted by XRF Spectrometer PW 1400 is presented in Table 1.

**Table 1.** Chemical composition of the starting materials

Oxides, %	OPC	GGBFS
$\text{SiO}_2$	21.26	37.81
$\text{Al}_2\text{O}_3$	4.49	13.14
$\text{Fe}_2\text{O}_3$	3.49	0.23
CaO	63.81	38.70
MgO	2.02	7.11
$\text{SO}_3$	3.11	1.19
$\text{Na}_2\text{O}$	0.14	1.03
$\text{K}_2\text{O}$	0.09	0.19
$\text{TiO}_2$	–	0.40
BaO	–	–
$\text{P}_2\text{O}_5$	–	0.17
L.O.I.	1.57	–
Total	99.98	99.97

For studying the effects of GGBFS as a supplementary cementing material on the properties of OPC either mechanical or radiological, five blended cement pastes designated as S0, S10, S15, S30 and S40 were prepared by the partial substitution of OPC with GGBFS at proportions of 0%, 10%, 15%, 30% and 40%. The w/b ratios for all mixtures were determined according to ASTM C187 [20] and had the values 0.3, 0.29 and 0.28 and 0.27 by weight, respectively. The details of mixture proportions are given in Table 2.

**Table 2.** Proportioning of blended cement mixtures, (%)

Mixture ID	OPC	GGBFS
S0	100	–
S10	90	10
S15	85	15
S30	70	30
S40	60	40

## 2.2 Specimen Preparation and Test Method

The dry mixtures were proportioned and mixed using a bench-mounted mixer of 5 L capacity to ensure complete homogeneity. Subsequently the required amount of mixing water was poured to the dry specimen. Continuous and vigorous mixing was conducted for 5 min. The specimens were cast in three layers into 25 × 25 × 25 mm cubic steel molds, then pressed until each layer being consolidated using a vibrating table. After the top layer was compacted, the surface of the paste was smoothed by the aid of thin edged trowel. After casting, the specimens were covered with wet burlap and polyethylene sheets, and then kept in the laboratory at room temperature for 24 h. After demolding, they were cured in tap water until the time of testing.

## 2.3 Compressive Strength Measurements

The hardened mixtures are subjected to the compressive strength test after 1, 3, 7 and 28 days of water curing according to ASTM C109 [21]. For stopping hydration process, crushed portions were stored in a solution of 1:1 methanol/acetone by volume for 24 h, then dried at 70 °C for 1 h and kept in an air-tight bottle.

## 2.4 X-ray Diffraction

The XRD analysis was carried out using a Philips PW 1050/70 Diffractometer. The data were identified according to the XRD software (pdf-2: database on CD-Release 2005). For conducting test, samples were passed through a 63 µm sieve.

## 2.5 Differential Thermal Analysis (DTA)

DTA was carried out by heating the sample in nitrogen atmosphere upto 1000 °C with a heating rate of 20 °C/min using a DT-50 Thermal Analyzer (Schimadzu Co- Kyoto, Japan).

## 2.6 SEM Investigation

The microstructure of the hardened blended cement mortars was studied using SEM Inspect S (FEI Company, Holland) equipped with an energy dispersive X-ray analyzer (EDX). The data generated by EDX analysis consist of spectra showing peaks corresponding to the elements making up the true composition of the sample being analyzed. Elemental mapping of a sample and image analysis are also possible.

## 2.7 Gamma- Ray Attenuation Measurements

The linear attenuation coefficients of blended cements have been measured using the gamma spectrometer which contains sodium iodide NaI (TI) scintillation detector [22]. The signals from detector were amplified and recorded by a Multi-Channel-Analyzer which communicates with Computer. The linear attenuation coefficients ( $\mu$ ) were determined by measuring the transmission of  $\gamma$ -rays through specimens of dimensions  $10 \times 10 \times 10$  cm and the  $\gamma$ -rays were obtained experimentally using  $^{137}\text{Cs}$  radioactive elements with photon energies of 0.662 MeV as standard sources with activities in micro curie (5 mCi). After 28 days of water curing, samples were taken out and left to oven dry at 105 °C with method used by Yilmaz et al. [23], subsequently each sample is arranged in front of a collimated beam obtained from gamma ray source for about 20 min. The linear attenuation coefficients ( $\mu$ ) were extracted from the mass attenuation coefficients ( $\mu/\rho$ ) calculated using a computer program named XCOM in a wide range of photon energies.

$$\mu = \left(\frac{1}{x}\right) \ln\left(\frac{N_0}{N}\right) \quad (1)$$

Where N and N<sub>0</sub> are the background subtracted number of counts recorded in detector with and without material between detector and source respectively and x is the material thickness (10 cm).

The half value layer (HVL) or the tenth value layer (TVL) of a material is used to describe the effectiveness of  $\gamma$ -ray shielding. Those can be calculated using equations below [24]:

$$\text{HVL} = \frac{\ln 2}{\mu} \quad (2)$$

$$\text{TVL} = \frac{\ln 10}{\mu} \quad (3)$$

### 3 Results and Discussion

#### 3.1 Compressive Strength Development

The variation in compressive strength for all blended mixtures as a function of curing time at 1, 3, 7 and 28 days is graphically plotted in Fig. 1. The compressive strength increases with curing time for all blends, as a result of the continuous of hydration process with formation of hydration products that accumulates closing up some of available pore volumes giving more strength. The incorporation of high ratios of GGBFS in the cement pastes produces lower values of compressive strength at preliminary ages up to 7 days as compared to the neat OPC. This decrease can be caused by slower hydration reaction of slag than that of OPC, besides its latent hydraulic properties; however the compressive strength increases at later ages, due to the formation of extra amounts of crystalline calcium silicate hydrate (C-S-H) produced from the pozzolanic reaction between  $\text{Ca(OH)}_2$  from OPC and amorphous  $\text{SiO}_2$  of slag, that fills the large capillary voids in matrix, resulting in improved compressive strength [25]. This process of transformation is referred as “pore size refinement” [26]. The inclusion of 10% GGBFS (S10) in the blend matrix slightly enhanced 28-day compressive strength by nearly 0.7%, whereas the compressive strength has improved by about 3.5% at incorporation of 15% (S15). As it is also evident from the results that the partial replacement of OPC with 30% GGBFS (S30) significantly increased compressive strength by approximately 7.5%. The enhancement in compressive strength of the blended pastes is mainly attributed to the precipitation of additional amounts of

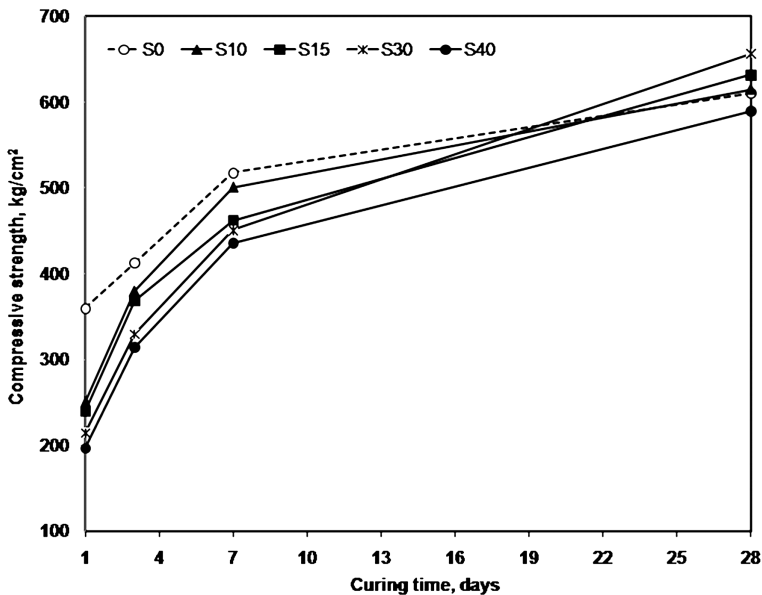


Fig. 1. Compressive strength development of cement pastes incorporating different ratios of ground granulated blast furnace slag after 28 days of water curing



secondary C-S-H gel and calcium aluminate hydrate (C-A-H) from the pozzolanic reaction in OPC-GGBFS system within the available pore volumes located in cement matrix. This gel is less dense and has more volume than primary C-S-H gel. Therefore it fills all the pores inside the cement matrix and makes it more impermeable with a consequent increase in compressive strength [26]. In contrast, the partial replacement of OPC with 40% GGBFS (S40) causes a marked decrease in the compressive strength values at all ages of hydration as compared to the neat OPC paste, as it had achieved a 45%, 24%, 13% and 3.5% lower compressive strength values at curing ages 1, 3, 7 and 28 days, respectively than the corresponding reference blend (S0). This decrease may be attributed to a reduction in OPC content that is responsible for the decrease in the amount of formed hydration products, mainly as C-S-H, which represents the main hydration product of the hardened cement pastes in addition to the dilution effect of OPC component with higher volumes of slag [27]. Finally, it can be concluded that the mixture incorporating 30% GGBFS as a partial replacement of OPC showed the highest compressive strength among all mixtures at curing age of 28 days, pointing out the effect of adding slag in enhancing the mechanical performance of cement pastes.

### 3.2 X-ray Diffraction (XRD)

The XRD patterns of cement mixtures incorporating 0%, 10%, 15%, 30% and 40% GGBFS and hydrated for 28 days in water are graphically represented in Fig. 2. Through the patterns, major peaks of portlandite (P) which are the expected product formed by OPC hydration along with calcium silicate hydrate (C-S-H), ettringite (E),

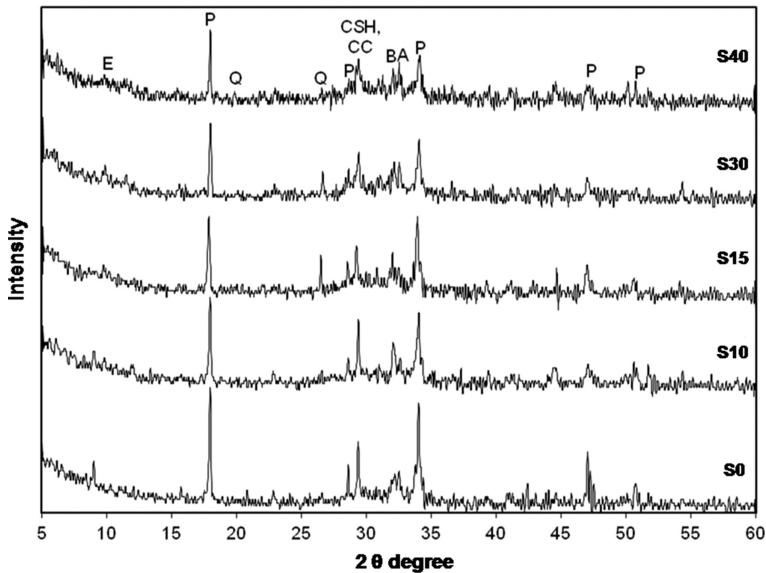
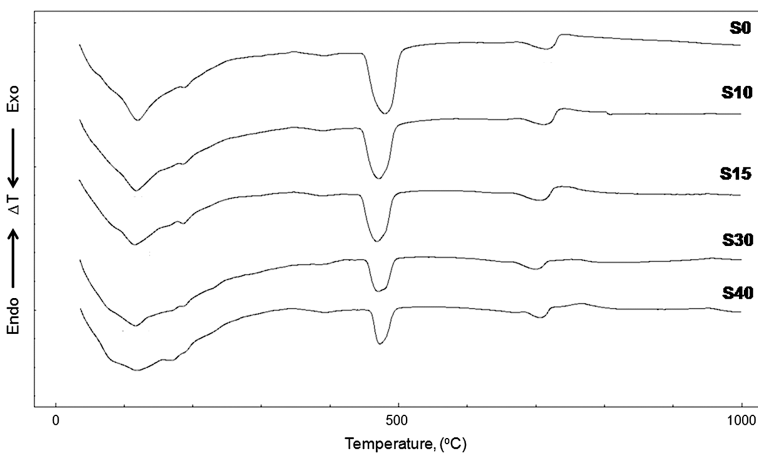


Fig. 2. X-ray diffraction patterns of cement pastes incorporating different ratios of ground granulated blast furnace slag after 28 days of water curing

calcium carbonate ( $CC'$ ), quartz (Q) as a main constituent of slag as well unhydrated cement phases (A is alite ( $C_3S$ ), B is belite ( $\beta-C_2S$ )) are detected. The patterns demonstrated that the intensity of the main peaks of portlandite located at  $2\theta$  of 17.97, 28.75 and 34.13 was diminished as GGBFS content increased, which in turn reflects the incidence of a pozzolanic reaction arising from the consumption of portlandite with the amorphous silicates of slag forming additional amounts of C-S-H phases. Obviously, ettringite phase was also observed in all blends and its intensity is sharply decreased with increasing GGBFS content, due to the consumption of free lime as well as the dilution of OPC by slag. On the other hand, peak intensity of C-S-H phase is decreased with the increase of slag than the neat mixture. Peaks of  $CC'$  overlapped with C-S-H were also detected for all mixtures. Likewise, residual un-hydrated larnite- $\beta-C_2S$  phases were also appeared even after 28 days of hydration; this is due to the rate of hydration of  $\beta-C_2S$  is slower than  $C_3S$ . In spite of the progress of hydration reaction, however the total amount of portlandite available for pozzolanic reaction has not yet been consumed, suggesting that the rate of consumption of free lime by blast furnace slag is too small at early ages, due to the latent hydraulic nature of slag material.

### 3.3 Differential Thermal Analysis (DTA)

Typical plots of DTA curves for cement pastes containing 0%, 10%, 15%, 30% and 40% GGBFS after curing in water for 28 days are given in Fig. 3. From the DTA thermograms, it was observed that five characteristic endothermic peaks located at 120, 187, 394, 480 and 715 °C are detected. The endotherms around 200 °C correspond to the decomposition of the nearly amorphous hydrates, mainly C-S-H as well as sulphoaluminate hydrates [28]. The temperature at which these compounds lose water depends upon the available  $CaO:SiO_2$  ratio in the hydrated cement matrix. The decomposition of ettringite and/or monosulphate occurs at lower temperature and is



**Fig. 3.** DTA thermograms of cement pastes incorporating different ratios of ground granulated blast furnace slag after 28 days of water curing

overlapped by the C-S-H [29]. The peak area of C-S-H increases with GGBFS content up to 30%. Whilst, the endotherms observed around 394 °C may be denotes to the decomposition of hydrogarnet or be characterizing the decomposition of calcium aluminate silicate hydrate (CASH) and calcium aluminate hydrate (CAH) [30]. The sharp endotherms occurred around 480 °C indicates the dehydroxylation of portlandite- $\text{Ca}(\text{OH})_2$  formed during OPC hydration [31]. It was observed that the intensity of portlandite peaks decreases sharply with increasing slag content. The reduction in  $[\text{Ca}(\text{OH})_2]$  content indicates its consumption during pozzolanic reaction or may be the dilution of Portland cement by the slag. On the other hand, endotherms located around 715 °C represents the decarbonation of  $\text{CaCO}_3$  and the intensity of peaks decrease with increase slag content in the blends.

### 3.4 Microstructural Analysis by SEM

Figure 4 showed the results of SEM analysis of the hardened cement pastes made of 0%, 15%, 30% and 40% GGBFS as a partial replacement of OPC after hydration in water for 28 days. The microstructure of the reference OPC paste as in Fig. 4a showed that the hydration products are formed and distributed all over the surface of the cement matrix. The hydration products existed mainly in the form of gel C-S-H(I) identified by its short needle-like form and some massive layers of  $\text{Ca}(\text{OH})_2$  identified by the fine-grained without crystal form distributed entirely in different regions of the cementitious matrix that have totally filled up capillary pore system in some areas, leaving others free of calcium hydroxide (CH). Likewise the micrographs indicated the presence of some voids permeate the microstructure. The partial replacement of OPC with 15% GGBFS accelerates the hydration phases ( $\text{C}_3\text{S}$  and  $\text{C}_2\text{S}$ ) with sequential formation of massive hexagonal layers of calcium hydroxide and homogeneous well distributed foil-like C-S-H(II) phases that filled most of the available pore volume (Fig. 4b).

Also, as shown in Fig. 4b, the SEM micrographs appeared relatively dense and homogenous with close texture structure that has relatively high compressive strength than its original OPC micrographs after 28 days of curing. Further increasing GGBFS content in the matrix up to 30% (Fig. 4c) led to a relatively dense and compact microstructure in addition to more reduction in the un-hydrated GGBFS particles, indicating that most of the available hydrated lime from OPC is consumed by slag's amorphous silica content to form additional amounts of secondary crystalline C-S-H phases that filled up the capillary pores inside the matrix, resulting in an extra enhancement in the specimen's morphology as compared to the microstructure of OPC paste (Fig. 4a) as well the reduction of CH may be due to the dilution of OPC by slag. On the opposite side, increasing the replacement of GGBFS up to 40% on the expense of OPC as described in Fig. 4d, led to a relatively permeable and less compact microstructure with pronounced formation of short fine-needle like ettringite, this hydration phase spread all over the surface of matrix, in addition to it filled the large pore voids. Finally, it can be concluded that high level replacement of GGBFS reduces the CH content librated from OPC hydration as a result of the dilution effect of OPC; which in turn resulted in the reduction of compressive strength of the blend at early ages than the corresponding S0 mix.

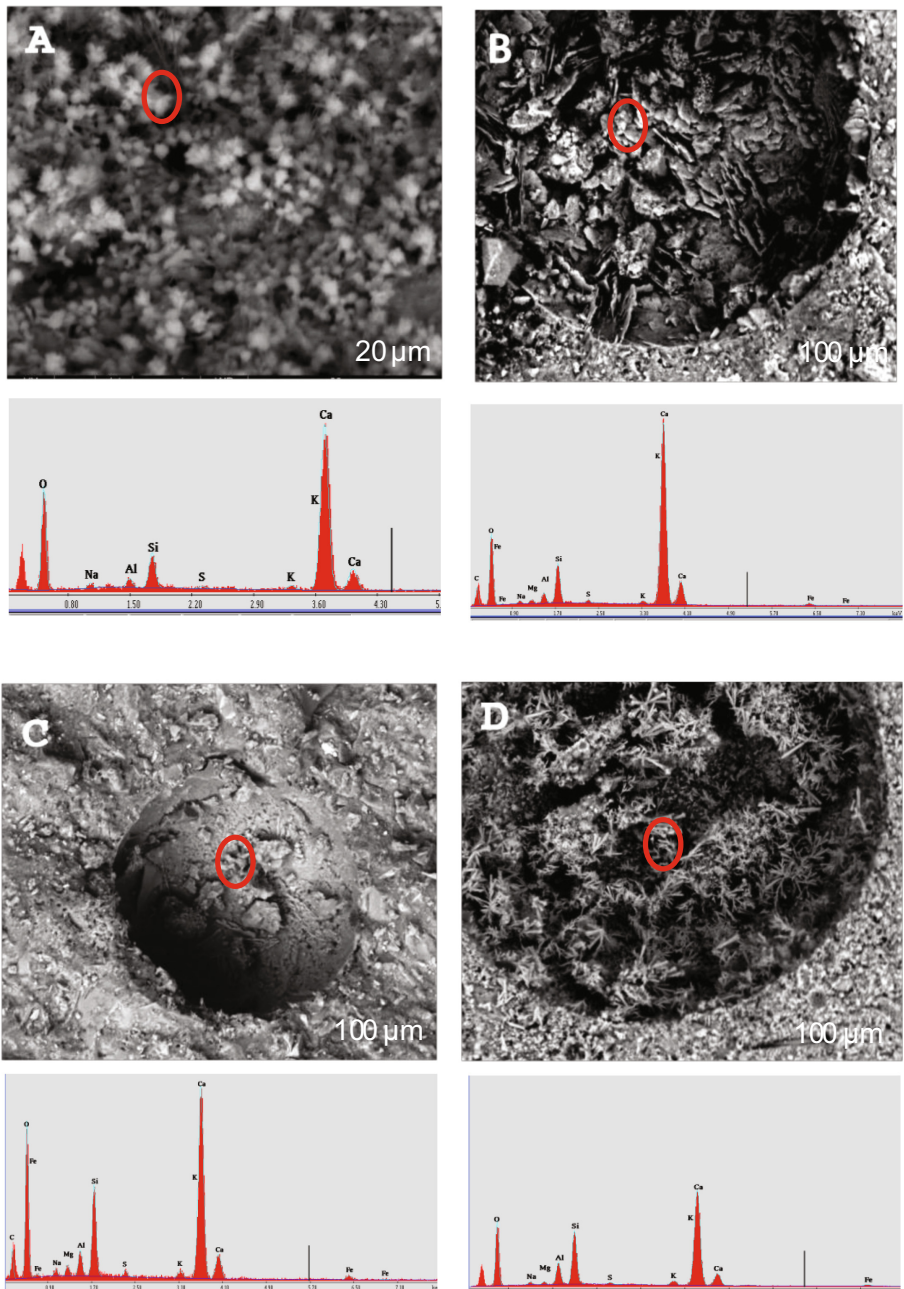


**Fig. 4.** SEM micrographs of cement pastes incorporating different ratios of ground granulated blast furnace slag after 28 days of water curing; (A) S0, (B) S15, (C) S30 and (D) S40

### 3.5 Gamma-ray Shielding Using $^{137}\text{Cs}$ Source

The values of measured of linear attenuation coefficient,  $\mu$ , in the field of  $\gamma$ -rays emitted by  $^{137}\text{Cs}$  at a given photon energy of 662 keV for the blended cements containing 0%, 15%, 30% and 40% GGBFS after hydration up to 28 days are graphically presented in Fig. 5. It has been reported that the linear attenuation coefficients decreased drastically with increasing concentration of GGBFS content in the blend. The reference mixture designated as S0 exhibited attenuation for gamma irradiation amounted to  $0.294\text{ cm}^{-1}$ . As it is also evident from Fig. 5 the inclusion of 10% GGBFS reduced the linear attenuation by approximately 2%, whereas it decreased by an average of 3% at inclusion of 15%. As shown in Fig. 5, displayed that the higher the GGBFS content the lower the linear attenuation coefficient. The mixture containing 30% slag as a replacement showed lower value to the linear attenuation coefficient was estimated at 6% than the neat S0 paste. The same trend was observed for S40 when OPC was partially replaced with GGBFS up to 40%, since the linear attenuation coefficient of this mixture revealed approximately 8% times lower than the corresponding S0 paste. The decrease in linear attenuation coefficients for blended pastes may be associated with the dilution effect of OPC with high contents of GGBFS, besides the differences in specific gravities between OPC and GGBFS, where the latter presents lower specific gravity than OPC, which in turn affects the density of mixtures. The decrease in linear attenuation coefficient with the increase of slag content confirms a dependence on the material density and hence the provision of better shielding from  $\gamma$ -rays [32]. However, it can be seen from the results presented in Fig. 5 that partial replacement of GGBFS in cement pastes is not an option to be used for the purposes of gamma-radiation shielding.

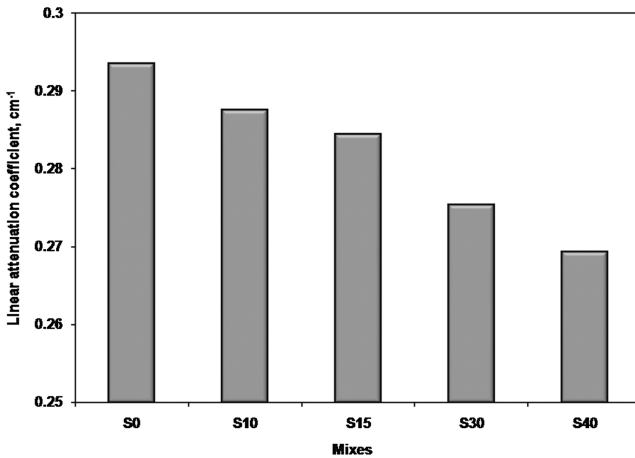


**Fig. 5.** The linear attenuation coefficients of cement pastes incorporating different ratios of ground granulated blast furnace slag after 28 days of water curing at photon energy of 662 keV for  $^{137}\text{Cs}$  source

### 3.6 Half and Tenth Thicknesses (HVT & TVT)

Another parameter that is related to the linear attenuation coefficient,  $\mu$  is called the half-value thickness, HVT, which is defined as the depth of shielding where the intensity of the primary photon beam is reduced by 50%. In similar fashion, the tenth-value thickness, TVT, is the depth required to reduce the photon intensity to one-tenth [33]. Half value thickness plays an important role on radiation shielding. The variations in HVT and TVT of blended cement pastes containing 0%, 15%, 30% and 40% GGBFS after hydration up to 28 days in the field of gamma rays at photon energy of 662 keV irradiated by  $^{137}\text{Cs}$  are graphically represented in Figs. 6 and 7, respectively. Comparing Figs. 5, 6 and 7, it can be clearly noted that the HVT and TVT are inversely proportional to the linear attenuation coefficient values. Consequently, the values of both HVT and TVT are significantly increased with increasing of slag content up to 40%, where S40 mixture demonstrated the highest values relative to the S0 mixture that displayed the lowest values at the same dose of 662 keV. The HVT and TVT of the other blends (S10, S15 and S30) are gradually increased with increasing GGBFS content. The inclusion of 10% slag in the cement matrix enhanced the HVT and TVT on average 2% and the insertion of 15% enhanced them by approximately 3%. The same trend was observed for mixture S30, as it enhanced HVT and TVT by approximately 7% relative to the S0 paste. Figures 5 and 6 indicated also that the thickness increases as the density of pastes decreases, due to the dilution effect of the cementitious matrix by high volumes of slag. Finally, it can be said that blended cements with GGBFS had a negative effect on the attenuation of gamma-rays at photon energy dose of 662 keV, thus the slag-loaded cements would not be preferred as materials in building construction against  $\gamma$ - radiation.

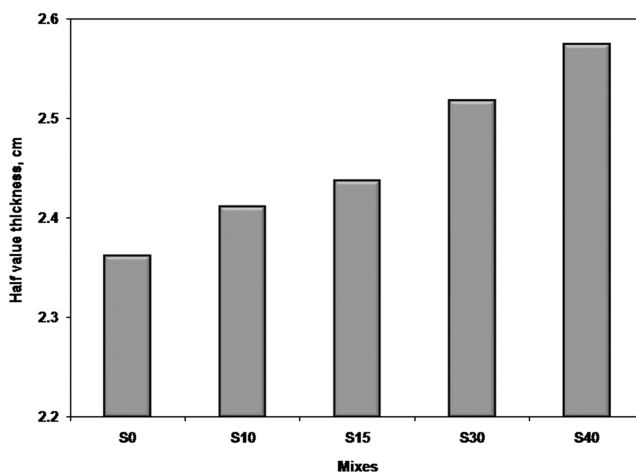


**Fig. 6.** Half-value thickness of cement pastes incorporating different ratios of ground granulated blast furnace slag after 28 days of water curing at photon energy of 662 keV for  $^{137}\text{Cs}$  source

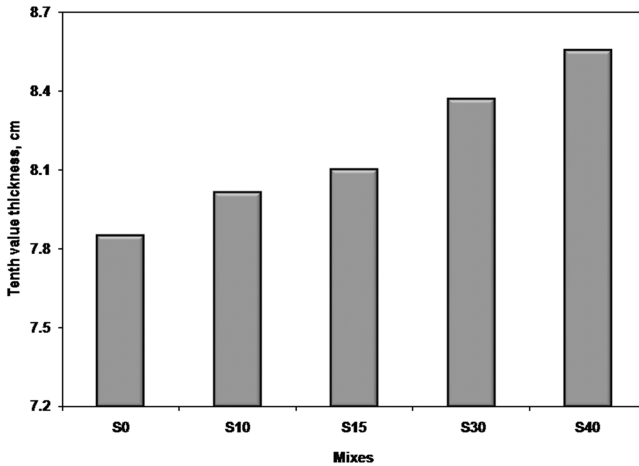


**Fig. 7.** Tenth-value thickness of cement pastes incorporating different ratios of ground granulated blast furnace slag after 28 days of water curing at photon energy of 662 keV for  $^{137}\text{Cs}$  source

## 4 Conclusions

Based on the experimental results obtained from the undertaken study, the following conclusions can be summarized as follows:

1. The replacement of OPC with GGBFS in the preparation of blended cement led to an increase in the compressive strength after 28 days of water curing. The replacements at an average of 10%, 15% and 30% by weight enhanced it by approximately 0.7%, 3.5% and 7.5% folds, respectively comparing to the corresponding neat ordinary mixture of slag-free.
2. The inclusion of 40% GGBFS in the blend decreases the compressive strength at all hydration ages relative to the reference S0 paste. This tendency can be attributed to the hydraulic activity of the slag is less than of the OPC, Which had an impact in reducing the amount of hydration products, mainly as C-S-H, which represents the main binding centers of the hardened cement pastes.
3. From results it is clear that, with variation in slag content, there is no change in linear attenuation coefficients for all the studied mixtures at photon energy of 662 keV irradiated by  $^{137}\text{Cs}$  source; meaning that slag has no obvious effect for enhancement of the shielding efficiency of cement against  $\gamma$ -rays in the thin thickness shield of 10 cm.
4. Whereas the attenuation of gamma rays depends primarily on the density of matter and as a result of the variation in specific gravities between OPC and GGBFS, it can be concluded that the slag-loaded cements are not suitable in building applications against  $\gamma$ - radiation.

## References

1. Akkurt, I., Mavi, B., Akkurt, A., Basyigit, C., Kilincarslan, S., Yalim, H.: Study on Z-dependence of partial and total mass attenuation coefficients. *J. Quant. Spectrosc. Radiat. Transf.* **94**, 379–385 (2005)
2. Kallan, M.F.: *Concrete Radiation Shielding*. Longman Scientific and Technical, New York (1989)
3. Wood, J.: *Computational Methods in Reactor Shielding*. Pergamon Press, New York (1982)
4. Hubbell, J.H.: Photon mass attenuation and energy absorption coefficients from 1 keV to 20 MeV. *Int. J. Appl. Radiat. Isot.* **33**(11), 1269–1290 (1982)
5. Akkurt, I., Basyigit, C., Kilincarslan, S.: The photon attenuation coefficients of barite, Marble and limra. *Ann. Nucl. Eng.* **31**(5), 577–582 (2004)
6. Bashter, I.I.: Calculation of radiation attenuation coefficients for shielding concretes. *Ann. Nucl. Eng.* **24**(17), 1389–1401 (1997)
7. El-Sayed Abdo, A.: Calculation of the cross-sections for fast neutrons and gamma-rays in concrete shields. *Ann. Nucl. Eng.* **29**(16), 1977–1988 (2002)
8. Singh, K., Gagandeep, K., Sandhu, G.K., Lark, B.S.: Interaction of photons with some solutions. *Rad. Phys. Chem.* **61**(3–6), 537–540 (2001)
9. Mehta, P.K., Monteiro, P.J.M.: *Concrete Microstructure, Properties and Materials*, 2nd edn. Prentice Hall Inc., New Jersey (1993)
10. Walker, R.L., Grotenhuis, M.A.: Summary of shielding constants for concrete, ANL-6443 Reactor Technology (TID-4500. 16th (edn.) Amended), AEC Research and Development Report (1961)
11. Ermichev, S.G., Shapovalov, V.I., Sviridov, N.V., Orlov, V.K., Sergeev, V.M., Semyenov, A.G., Visik, A.M., Maslov, A.A., Demin, A.V., Petrov, D.D., Noskov, V.V., Sorokin, V.I., Uferov, O.I., Ornl, L.D., Ridge, O.: High-density concrete with ceramic aggregate based on depleted uranium dioxide, IHLRWM, Las Vegas, NV, 30 April–4 May, pp. 880–884 (2006)
12. Mahdy, M., Speare, P.R.S., Abdel-Reheem, A.H.: Shielding properties of heavyweight, high strength concrete. In: 2nd Material Specialty Conference of the Canadian Society for Civil Engineering, 5–8 June (2002)
13. Kluge, A.L., Piszora, P.: Effect of gamma irradiation on cement composites observed with XRD and SEM methods in the range of radiation Dose 0–1409 MGy. *Acta Phys. Pol., A* **114**(2), 399–411 (2008)
14. Gencil, O., Brostow, W., Ozel, C., Filiz, M.: Concretes containing hematite for use as shielding barriers. *Mater. Sci.* **16**(3), 249–256 (2010)
15. Gencil, O., Brostow, W., Ozel, C., Filiz, M.: An investigation on the concrete properties containing colemanite. *Int. J. Phys. Sci.* **5**(3), 216–225 (2010)
16. Siliceous by-products for use in concrete, Final Report, RILEM Technical Reports 73-SBC RILEM Committee, 21(1), pp. 69–80 (1988)
17. Shi, C., Qian, J.: High performance cementing materials from industrial slags—a review. *Resour. Conserv. Recycl.* **29**(3), 195–207 (2000)
18. Hwang, C.L., Lin, C.Y.: Strength development of blended blast furnace slag cement mortars. In: Malhotra, V.M. (ed.) *Proceedings of the 2nd International Conference on Fly Ash, Silica Fume, Slag and Natural Pozzolana in Concrete*, SP-91, pp. 1323–1340. American Concrete Institute, Farmington Hills, Mich (1986)
19. ASTM C150, Standard Specification for Portland Cement (2015)
20. ASTM C187, Standard Test Method for Amount of Water Required for Normal Consistency of Hydraulic Cement Paste (2011)



21. ASTM C109, Standard Test Method for Compressive Strength of Hydraulic Cement Mortars (Using 2-in. or [50-mm] Cube Specimens) (2013)
22. Akkurt, I.: Effective atomic and electron numbers of some steels at different energies. *Ann. Nucl. Eng.* **36**(11–12), 1702–1705 (2009)
23. Yilmaz, E., Baltas, H., Kiris, E., Ustabas, I., Cevik, U., El-Khayatt, A.M.: Gamma ray and neutron shielding properties of some concrete materials. *Ann. Nucl. Eng.* **38**(10), 2204–2212 (2011)
24. Akkurt, I., Akyildirim, H., Mavi, B., Kilincarslan, S., Basyigit, C.: Gamma-ray shielding properties of concrete including barite at different energies. *Prog. Nucl. Eng.* **52**(7), 620–623 (2010)
25. Islam, M.M., Islam, M.S., Mondal, B.C., Islam, M.R.: Strength behavior of concrete using slag with cement in sea water environment. *J. Civ. Eng. (IEB)* **38**(2), 129–140 (2010)
26. Bakker, R.F.M.: Permeability of blended cement concretes. In: *Proceedings of the First CANMET/ACI International Conference on Fly Ash, Silica Fume, Slag and other Mineral Products in Concrete-SP-79*, ACI, Detroit., pp. 589–606 (1983)
27. Amin, M.S., El-Gamal, S.M.A., Abo-El-Enein, S.A., El-Hosiny, F.I., Ramadan, M.: Physico-chemical characteristics of blended cement pastes containing electric arc furnace slag with and without silica fume. *J. HBRC* **11**(3), 321–327 (2015)
28. Lea, F.M.: *The Chemistry of Cement and Concrete*, 4th edn, p. 184. Edward Arnold, London (1974)
29. Heikal, M., Helmy, I., El-Didamony, H., Abd El-Raouf, F.: Electrical properties, physico-chemical and mechanical characteristics of fly ash-limestone-filled pozzolanic cement. *Ceram. Silik.* **48**(2), 49–58 (2004)
30. Ubbriaco, P., Calabrese, D.: Solidification and stabilization of cement paste containing fly ash from municipal waste. *Thermochim. Acta* **321**(1–2), 143–150 (1998)
31. Singh, S.P.: Use of thermo analytical techniques in the study of hydration of cement. In: *Proceedings of the National Conference on Thermal Analysis, 1*, BARC, Mumbai, 69 (2002)
32. Akkurt, I., Akyıldırım, H., Mavi, B., Kilincarslan, S., Basyigit, C.: Radiation shielding of concrete containing zeolite. *Radiat. Meas.* **45**, 827–830 (2010)
33. El-Dakrouy, A., Gasser, M.S.: Effects of SF and Ilmenite on the Chemical. Mech. Radiat. Behav. Matrices Used Solidification Wastes, *Nature Sci.* **10**(5), 92–99 (2010)

# Optimum Partial Replacement of Cement by Rice Husk Ash and Fly Ash Based on Complete Consumption of Calcium Hydroxide

Winai Ouypornprasert<sup>1</sup>(✉), Narong Traitruengtatsana<sup>2</sup>,  
and Kong Kamollertvara<sup>3</sup>

<sup>1</sup> Department of Civil Engineering, Rangsit University, PathumThani, Thailand  
owinai@yahoo.com

<sup>2</sup> RDI Center, Asia Group (1999) Co. Ltd., Bangkok, Thailand

<sup>3</sup> Asia Group (1999) Co. Ltd., Bangkok, Thailand

**Abstract.** The objective of this technical paper was to propose the optimum partial replacement of cement (PRC) by rice husk ash (RHA) and fly ash (FA) based on the complete consumption (CC) of calcium hydroxide (CH) from hydration and the strength activity index (SAI) based on equivalent calcium silicate hydrate (C-S-H) as well as the propagation of uncertainty due to randomness inherent in main chemical compositions in cement, RHA and FA. Firstly the hydration and pozzolanic reactions as well as stoichiometry were reviewed. Then the optimum PRC by RHA and FA based on CC of CH was formulated.

The long-term SAI would be proposed based on equivalent C-S-H. Contribution to strength by calcium aluminate hydrate and calcium ferrite hydrate would be transformed to equivalent C-S-H. Based on the reasons mentioned above and the given values of strength for the age of 360 days, the long-term SAI could be defined. This concept could be extended for the SAI at any age based on Bogue's curve and nano-structures of C-H-S gel.

After that the propagation of uncertainty due to main chemical compositions in cement, RHA and FA was discussed. The linear characteristic of the gradient of a function was derived for an estimate. Monte-Carlo simulations together with Goodness-Of-Fit tests were proposed for the better estimates. The reliability analyses for applying the suitable PRC were reviewed.

Finally an applicability of the concepts mentioned above based on statistical data of materials available was demonstrated. The results from analyses were consistent with the tested results by the authors and other researchers. The results of this study provided guidelines of suitable utilization of RHA and FA for PRC. It was interesting to note that these concepts could be extended to optimize PRC by combination of other types of pozzolan which were described in the other papers of the authors.

## 1 Introduction

Cement content in concrete is the main cost for the concrete production. The reduction of cement content in concrete mix proportion would lower the cost of concrete and would increase the competitiveness in marketing. Therefore the probabilistic concrete mix design for mass production of concrete has been commercially applied (Kamollertvara and Ouypornprasert 2015). Dumrongsil et al. (2000) studied the suitable partial replacement of cement by rice husk ash (RHA). In this study the optimum replacement of cement by RHA was derived by the concept of calcium oxide equivalent. Results showed that the values of compressive strength of concrete mixed with RHA of the age less than 28 days tend to be lower than those of concrete mixed with Ordinary Portland Cement (OPC). However with suitable replacements of cement by RHA the values of compressive strength of concrete can be higher than those of ordinary concrete even at the early age (Habeeb and Mahmud 2010). The major reason might be the heat of hydration of cement mixed with pozzolan could surpass that of OPC (Langan et al. 2002).

In this technical paper the optimum replacement of cement by RHA and fly ash based on stoichiometry of the complete consumption of calcium hydroxide from hydration of cement and pozzolanic reactions of pozzolanic substances as well as the long-term strength activity index based on Equivalent Strength of Calcium Silicate Hydrates (C-S-H) would be proposed. This concept could be extended for the strength activity index at any age based on nano-structures of C-S-H gel. Since the chemical compositions of cement and RHA might vary because of the production process, propagation of uncertainty with respect to main chemical compositions would also be discussed. To assure the quality of concrete mixed with RHA the suitable replacement of cement by RHA should be determined with the target confidence interval. Once the particular replacement would be selected the distribution of the long-term strength activity index could be obtained. Then reliability of the selected replacement could be determined accurately by Monte-Carlo simulations or approximately by the advanced First-Order Second-Moment (FOSM) method. The applicability of the proposed formulations could be demonstrated by a set of data available in hand.

## 2 Chemical Reactions and Stoichiometry

### 2.1 General Remarks

It is usual for the cement chemist to use the following abbreviations for discussions about hydration reactions of cement and pozzolanic reactions of pozzolan: *C* for calcium oxide ( $CaO$ ), *S* for silicon dioxide ( $SiO_2$ ), *H* for water ( $H_2O$ ), *A* for aluminum oxide ( $Al_2O_3$ ), *F* for ferric oxide ( $Fe_2O_3$ ), *CH* for calcium hydroxide ( $Ca(OH)_2$ ),  $C_3S$  for tricalcium silicate ( $3CaO \cdot SiO_2$ ),  $C_2S$  for dicalcium silicate ( $2CaO \cdot SiO_2$ ),  $C_3A$  for tricalcium aluminate ( $3CaO \cdot Al_2O_3$ ),  $C_4AF$  for tetracalcium aluminoferrite ( $4CaO \cdot Al_2O_3 \cdot Fe_2O_3$ ),  $C_3S_2H_3$  or  $C - S - H$  for calcium silicate hydrate ( $3CaO \cdot 2SiO_2 \cdot 3H_2O$ ),  $C_3AH_6$  for calcium aluminate hydrate ( $3CaO \cdot Al_2O_3 \cdot 6H_2O$ ) and  $C_3FH_6$  for calcium ferrite hydrate ( $3CaO \cdot Fe_2O_3 \cdot 6H_2O$ ). They are summarized in Table 1.

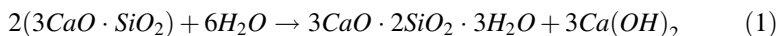
**Table 1.** Abbreviations for hydration of cement and pozzolanic reactions

Abbreviation	Technical term (Chemical formula)
<i>C</i>	calcium oxide ( $CaO$ )
<i>S</i>	silicon dioxide ( $SiO_2$ )
<i>H</i>	water ( $H_2O$ )
<i>A</i>	aluminium oxide ( $Al_2O_3$ )
<i>F</i>	ferric oxide ( $Fe_2O_3$ )
<i>CH</i>	calcium hydroxide ( $Ca(OH)_2$ )
$C_3S$	tricalcium silicate ( $3CaO \cdot SiO_2$ )
$C_2S$	dicalcium silicate ( $2CaO \cdot SiO_2$ )
$C_3A$	tricalcium aluminate ( $3CaO \cdot Al_2O_3$ )
$C_4AF$	tetracalcium alumino ferrite ( $4CaO \cdot Al_2O_3 \cdot Fe_2O_3$ )
$C_3S_2H_3$ or $C - S - H$	calcium silicate hydrate ( $3CaO \cdot 2SiO_2 \cdot 3H_2O$ )
$C_3AH_6$	calcium aluminate hydrate ( $3CaO \cdot Al_2O_3 \cdot 6H_2O$ )
$C_3FH_6$	calcium ferrite hydrate ( $3CaO \cdot Fe_2O_3 \cdot 6H_2O$ )

## 2.2 Hydration, Pozzolanic Reactions and Stoichiometry

### 2.2.1 Hydration

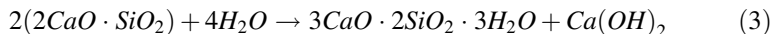
- (1) Hydration of Tricalcium Silicate ( $C_3S$ )



or



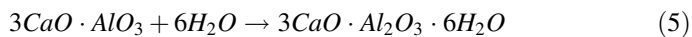
- (2) Hydration of Dicalcium Silicate ( $C_2S$ )



or

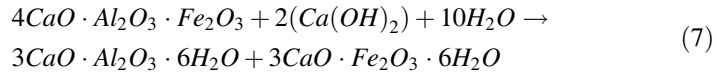


- (3) Hydration of Tricalcium Aluminate ( $C_3A$ )

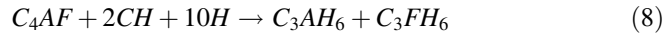
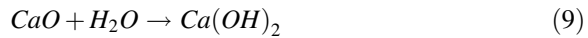


or

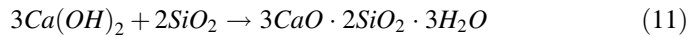


(4) Hydration of Tetracalcium Alumino Ferrite ( $C_4AF$ )

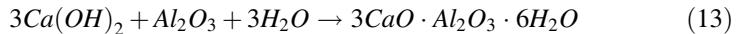
or

**2.2.2 Pozzolanic Reactions**(1) Additional Calcium Hydroxide from Calcium Oxide ( $CaO$ ) in Pozzolan

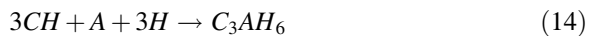
or

(2) Pozzolanic Reaction of Silicon Dioxide ( $SiO_2$ )

or

(3) Pozzolanic Reaction of Aluminum Oxide ( $Al_2O_3$ )

or

**2.2.3 Rate of Pozzolanic Reactions**

Chansawang and Ouypornprasert (2017) studied that rate of pozzolanic reactions of nano silica, nano aluminium oxide, RHA and fly ash by the complexometric titration technique with EDTA (ethylenediaminetetraacetic acid). The indicator was Eriochrome Black T. Figure 1 showed the quantity of  $Ca^{2+}$  reacted in the  $Ca(OH)_2$  solution after elapsed time. It could be concluded that RHA could react with  $Ca(OH)_2$  much faster than that of fly ash (FA).

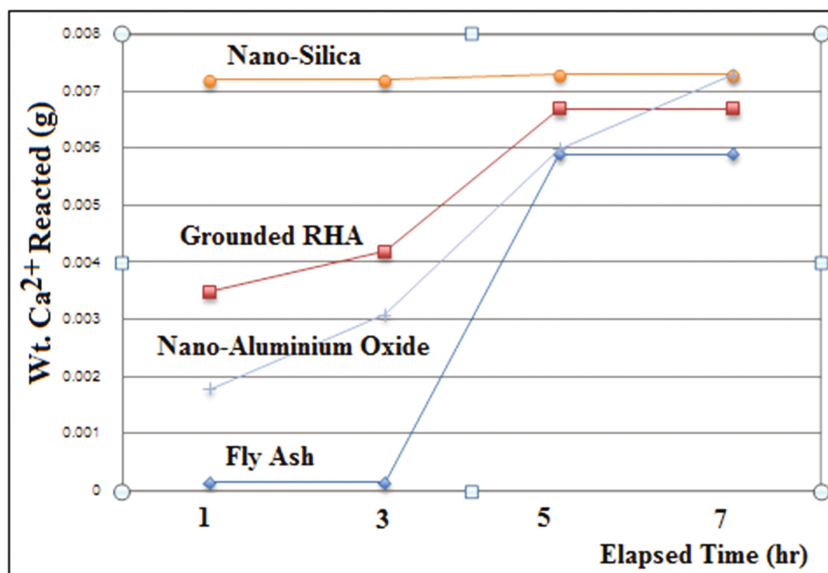


Fig. 1. Rate of pozzolanic reactions

### 2.3 Stoichiometry

Atomic- and molecular weights of all substances related in stoichiometry of hydration- and pozzolanic reactions are summarized in Table 2, 3 and 4. This information will be used throughout the following discussions.

Table 2. Atomic weight of elements related in hydration and pozzolanic reactions

Element	<i>H</i>	<i>O</i>	<i>Al</i>	<i>Si</i>	<i>Ca</i>	<i>Fe</i>
Atomic weight	1	16.00	26.98	28.09	40.08	55.85

Table 3. Molecular weight of main chemical components in cement, rice husk ash and fly ash

Compound	$C_3S$	$C_2S$	$C_3A$	$C_4AF$	$CaO$	$SiO_2$	$Al_2O_3$	$Fe_2O_3$
Molecular weight (g/mol)	228.2	172.2	270.0	483.1	56.1	60.1	102.0	156.7

Table 4. Molecular weight of chemical components related in hydration and pozzolanic reactions

Chemical components	$H_2O$	$Ca(OH)_2$	$C_3S_2H_3$	$C_3AH_6$	$C_3FH_6$
Molecular weight (g/mol)	18.0	74.1	228.2	378.1	432.8

**Table 5.** Statistical properties of main chemical oxide compositions in cement, rice husk ash and fly ash

Chemical components	Fractional		Coefficient of variation (stand. dev./ mean)
	Mean	Standard deviation	
$C_3S$	0.60877	0.01170	0.0192
$C_2S$	0.14857	0.01169	0.0787
$C_3A$	0.08473	0.00283	0.0334
$C_4AF$	0.10293	0.00064	0.0062
$CaO$ (RHA)	0.0074	0.00283	0.3824
$SiO_2$ (RHA) <sup>a</sup>	0.74638	0.08844	0.1185
$Al_2O_3$ (RHA)	0.0021	0.00173	0.8238
$CaO$ (FA)	0.2127	0.08788	0.4132
$SiO_2$ (FA)	0.3583	0.10444	0.2915
$Al_2O_3$ (FA)	0.2127	0.05763	0.2709

Remarks <sup>a</sup> reactive silica, rice husk ash from western part of Thailand, fly ash from Mae Moh (Thailand)

### 2.4 Optimum Replacement of Cement by Rice Husk Ash and Fly Ash

In this technical paper the optimum replacement of cement by rice husk ash (RHA) and fly ash (FA) will be considered by the complete consumption of calcium hydroxide ( $CH$ ) from hydration reactions of main minerals in cement by the main chemical compositions in RHA (Table 6).

Let  $fC_r, fS_r$  and  $fA_r$  be the fraction of  $C, S$  and  $A$  in RHA, respectively,  $fC_f, fS_f$  and  $fA_f$  be the fraction of  $C, S$  and  $A$  in FA (Fly Ash), respectively,  $r_t, r_f$  and  $r_r$  be the

**Table 6.** Sensitivity of optimum replacement of cement by rice husk ash with respect to uncertainty

Chemical components	Error propagation		Error propagation (part. deriv. × std. dev.)
	Partial derivative	Standard deviation	
$C_3S$	0.2397	0.01170	0.0028
$C_2S$	0.1059	0.01169	0.0012
$C_4AF$	-0.1511	0.00283	-0.0001
$CaO$ (RHA)	0	0.00064	0
$SiO_2$ (RHA) <sup>a</sup>	0	0.00283	0
$Al_2O_3$ (RHA)	0	0.08844	0
$CaO$ (FA)	0.1405	0.00173	0.0004
$SiO_2$ (FA)	-0.1968	0.08788	-0.0017
$Al_2O_3$ (FA)	-0.1160	0.10444	-0.0002

Remarks <sup>a</sup> reactive silica, rice husk ash from western part of Thailand, fly ash from Mae Moh (Thailand)

partial replacement of cement by RHA and FA, by FA and by RHA, respectively. Then the fractional calcium hydroxide ( $fCH$ ) from hydration reactions of cement in unit weight replaced by RHA and FA with the ratio  $r_i$  would be  $fCH \cdot (1 - r_i)$ .

$$fCH = fC_3S \cdot r_{CH-C_3S} + fC_2S \cdot r_{CH-C_2S} - fC_4AF \cdot r_{CH-C_4AF} \tag{15}$$

Where  $fC_3S$ ,  $fC_2S$  and  $fC_4AF$  are the fraction of  $C_3S$ ,  $C_2S$  and  $C_4AF$  in cement per unit weight, respectively.  $r_{CH-C_3S}$ ,  $r_{CH-C_2S}$  and  $r_{CH-C_4AF}$  are the ratios of  $CH$  from the hydration reactions of  $C_3S$ ,  $C_2S$  and  $fC_4AF$ , respectively. Their values are:

$$r_{CH-C_3S} = \frac{3 \cdot w_{CH}}{2 \cdot w_{C_3S}} = 0.48678 \tag{16}$$

$$r_{CH-C_2S} = \frac{w_{CH}}{2 \cdot w_{C_2S}} = 0.21509 \tag{17}$$

$$r_{CH-C_4AF} = \frac{2 \cdot w_{CH}}{w_{C_4AF}} = 0.30677 \tag{18}$$

Where  $w_{CH}$ ,  $w_{C_3S}$ ,  $w_{C_2S}$  and  $w_{C_4AF}$  are molecular weight of  $CH$ ,  $C_3S$ ,  $C_2S$  and  $C_4AF$ , respectively (See Table 2 and 3).

Since calcium oxide ( $CaO$ ) in RHA and FA can be soluble in water and yield calcium hydroxide as shown in Eqs. (9) and (10) and the  $SiO_2$  content in RHA is usually much more than  $CaO$ , it might be assumed that amount of  $SiO_2$  in RHA and FA is always more than the amount required for the pozzolanic reaction with  $CaO$  in RHA and FA itself, there will be adequate residual amount of  $SiO_2$  to react with the residual calcium hydroxide from hydration of cement (see Eqs. (11) and (12)). Aluminum oxide ( $Al_2O_3$ ) in RHA and FA can also react with the residual calcium hydroxide from hydration of cement (see Eqs. (13) and (14)).

The residual  $CH$  from Eq. (15) can be completely consumed in pozzolanic reactions with  $SiO_2$  and  $Al_2O_3$  as shown in Eq. (19).

$$(1 - r_i) \cdot fCH = (fS_f - fC_f \cdot r_{CS}) \cdot r_{SCH} \cdot r_f + (fS_r - fC_r \cdot r_{CS}) \cdot r_{SCH} \cdot r_r + (fA_f \cdot r_f + fA_r \cdot r_r) \cdot r_{ACH} \tag{19}$$

Let

$$fS'_f = fS_f - fC_f \cdot r_{CS} \tag{20}$$

and

$$fS'_r = fS_r - fC_r \cdot r_{CS} \tag{21}$$

Where  $r_{CS}$  is the ratio by weight of  $C$  to  $S$  for complete pozzolanic reactions of  $SiO_2$  whose value is given in Eq. (22).



$$r_{CS} = \frac{3 \cdot w_C}{2 \cdot w_S} = 1.40063 \quad (22)$$

Where  $w_C$  and  $w_S$  are the molecular weights of  $C$  and  $S$ , respectively (see Table 2). Then Eq. (19) reduces to:

$$(1 - r_t) \cdot fCH = (fS'_f \cdot r_f + fS'_r \cdot r_t) \cdot r_{SCH} - fS'_r \cdot r_f \cdot r_{SCH} + (fA_f \cdot r_f + fA_r \cdot (r_t - r_f)) \cdot r_{ACH} \quad (23)$$

$$(1 - r_t) \cdot fCH = fS'_f \cdot (r_t - r_r) \cdot r_{SCH} + fS'_r \cdot r_r \cdot r_{SCH} + (fA_r \cdot r_r + fA_f \cdot (r_t - r_r)) \cdot r_{ACH} \quad (24)$$

Where  $r_{SCH}$  and  $r_{ACH}$  are the ratios of molecular weights that calcium hydroxide reacts with silicon dioxide and aluminium oxide, respectively. Their values are shown in Eqs. (25) and (26), respectively.

$$r_{SCH} = \frac{3 \cdot w_{CH}}{2 \cdot w_S} = 1.84986 \quad (25)$$

$$r_{ACH} = \frac{3 \cdot w_{CH}}{w_A} = 2.17941 \quad (26)$$

Then  $r_f$  can be rewritten from Eq. (23) as shown in Eq. (27).

$$r_f = \frac{(1 - r_t) \cdot fCH - (fS'_r \cdot r_{SCH} + fA_r \cdot r_{ACH}) \cdot r_t}{(fS'_f - fS'_r) \cdot r_{SCH} + (fA_f - fA_r) \cdot r_{ACH}} \quad (27)$$

Similarly  $r_r$  can be rewritten from Eq. (24) as shown in Eq. (28).

$$r_r = \frac{(1 - r_t) \cdot fCH - (fS'_f \cdot r_{SCH} + fA_f \cdot r_{ACH}) \cdot r_t}{(fS'_r - fS'_f) \cdot r_{SCH} + (fA_r - fA_f) \cdot r_{ACH}} \quad (28)$$

In the case of cement is replaced by RHA only (no FA)  $r_r = r_t$  and  $r_f = 0$ :

$$r_t = r_r = \frac{fCH}{fCH + fS'_r \cdot r_{SCH} + fA_r \cdot r_{ACH}} \quad (29)$$

In the case of cement is replaced by FA only (no RHA)  $r_f = r_t$  and  $r_r = 0$ :

$$r_t = r_f = \frac{fCH}{fCH + fS'_f \cdot r_{SCH} + fA_f \cdot r_{ACH}} \quad (30)$$

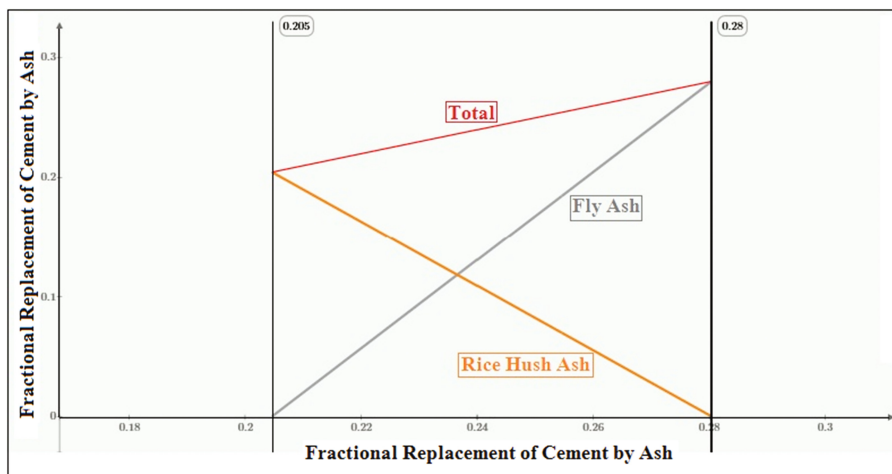


Fig. 2. Optimum replacement of rice husk ash and fly ash for replacement of cement

Optimum partial replacement of cement by mixed ash of RHA and FA is shown in Fig. 2. It can be seen that the optimum fractional replacement of cement by rice husk ash is much lower than that of fly ash. There is a straight line connected between the two optimum points. The diagonal lines show the fractional replacement for each type of pozzolan.

## 2.5 The Whole Range of Cement Replacement by Rice Husk Ash and Fly Ash

For the practical application it is also interesting to determine the chemical reactions and the consequences in the range of the cement replacement below and above the point of complete consumption of calcium hydroxide (CC). For the sake of further discussions the fractional replacement of cement by ash below the point of complete consumption should be called the state of the incomplete consumption (IC); whereas the fractional replacement of cement by ash beyond the point of complete consumption should be called the state of the beyond-complete consumption (BC). In the range of IC until CC all ash should be consumed. Otherwise ash should be partially consumed.

## 3 Strength Activity Index

### 3.1 Long-Term Strength Activity Index

#### 3.1.1 Complete Consumption of Calcium Hydroxide

Strength of cement paste is mainly contributed by C-S-H from  $C_3S$  and  $C_2S$ . Additional contributions are from  $C_3AH_6$ , the product of  $C_3A$  and  $C_4AF$ . With rice husk ash and fly ash in binder C-S-H and  $C_3AH_6$  from pozzolanic reactions have not been clearly understood in the term of rate of reactions as well as the strength development. It was

concluded that C-S-H from pozzolanic reactions had the same structure as C-S-H from hydration of cement (Taylor 1997). However, at the early age of cement paste the rate of hydration of  $C_2S$  as well as the strength development is much slower than developed from  $C_3S$ . Fortunately the long-term strength of C-S-H developed from  $C_2S$  is insignificantly lower than that from  $C_3S$ , the long-term strength of C-S-H from the pozzolanic reaction could be assumed to be the average strength of C-S-H from  $C_3S$  and  $C_2S$  without significant errors. Furthermore the contribution of  $C_3AH_6$  from the hydration of cement and pozzolanic reactions take minor contribution to the overall strength of binder. Therefore the strength of  $C_3AH_6$  can be assumed equal for both type of reactions. Based on the reasons mentioned above and the given values of strength for the age of 360 days (Bogue 1955) the long-term strength activity index ( $SAI$ ) can be defined as the strength of binder paste over the strength of cement paste at the age of 360 days as shown below:

$$SAI = \frac{fa \cdot (1 - r_t) + \frac{1}{2wSiO_2} (fS_r \cdot r_r + fS_f \cdot r_f) \cdot \alpha\beta + \frac{1}{wAl_2O_3} (fA_r \cdot r_r + fA_f \cdot r_f) \cdot \gamma_s}{fa} \quad (31)$$

$$fa = \frac{1}{2} \cdot \left( \frac{fC_3S}{wC_3S} \cdot \alpha_s + \frac{fC_2S}{wC_2S} \cdot \beta_s \right) + \left( \frac{fC_3A}{wC_3A} \right) \cdot \gamma_s + \left( \frac{fC_4AF}{wC_4A} \right) \cdot \delta_s \quad (32)$$

Where  $\alpha_s = 72.0$ ,  $\beta_s = 71.265$ ,  $\gamma_s = 8.082$  and  $\delta_s = 5.143$ . Ouyornprasert et al. (2016) suggested that for long-term strength activity index  $\alpha\beta$  could be determined by taking the average of without a significant error i.e.  $\alpha\beta = 71.6325$ , since the long-term values of  $\alpha_s$  and  $\beta_s$  are very close to each other.

### 3.1.2 Incomplete Consumption of Calcium Hydroxide

In this range of replacement all ash should be consumed. Equations (31) and (32) are still valid for determining the values of strength activity index.

### 3.1.3 Beyond-Complete Consumption of Calcium Hydroxide

In this range of replacement not all ash should be consumed. Again, only Eq. (32) is still valid for determining the contribution of  $SAI$  from cement, but  $SAI$  should be determined from different conditions based on: (1) the total pozzolan and the calcium hydroxide remained from hydration of cement plus additional calcium hydroxide produced from pozzolan (CHc), (2) calcium oxide content from pozzolan (CHC), (3) aluminium oxide from pozzolan (CHA) and (4) the total pozzolanic content from pozzolan (CHP). These quantities can be determined from Eqs. (33)–(36), respectively.

$$CHc = \frac{1}{2} \left( \frac{3fC_3S}{wC_3S} + \frac{fC_2S}{wC_2S} - \frac{4fC_4AF}{wC_4A} \right) \cdot (1 - r_t) + \frac{1}{wCaO} \cdot (fC_r \cdot r_r + fC_f \cdot r_f) \quad (33)$$

$$CHC = \frac{3}{2wSiO_2} \cdot (fS_r \cdot r_r + fS_f \cdot r_f) \quad (34)$$

$$CHA = \frac{3}{wAl_2O_3} \cdot (fA_r \cdot r_r + fA_f \cdot r_f) \tag{35}$$

$$CHP = \frac{3}{2wSiO_2} \cdot (fS_r \cdot r_r + fS_f \cdot r_f) + \frac{3}{wAl_2O_3} \cdot (fA_r \cdot r_r + fA_f \cdot r_f) \tag{36}$$

- (i) For  $CHC \leq CHc$  and  $CHA \leq CHc - CHC$ ,  $SAI$  should be determined from Eq. (37).

$$SAI = \frac{fa \cdot (1 - r_t) + \frac{1}{3} \cdot CHC \cdot \alpha\beta + \frac{1}{3} \cdot CHA \cdot \gamma}{fa} \tag{37}$$

- (ii) For  $CHC \leq CHc$  and  $CHA > CHc - CHC$ ,  $SAI$  should be determined from Eq. (38).

$$SAI = \frac{fa \cdot (1 - r_t) + \frac{1}{3} \cdot CHC \cdot \alpha\beta + \frac{1}{3} \cdot (CHc - CHC) \cdot \gamma}{fa} \tag{38}$$

- (iii) For  $CHC \geq CHc$ ,  $SAI$  should be determined from Eq. (39).

$$SAI = \frac{fa \cdot (1 - r_t) + \frac{1}{3} \cdot CHC \cdot \alpha\beta}{fa} \tag{39}$$

### 3.2 Diagram of the Long-Term Strength Activity Index

Based on  $SAI$  at state of IC (Incomplete Consumption), CC (Complete Consumption) and BC (Beyond-Complete Consumption) using Eqs. (31)–(39) a diagram for the long-term strength activity index with respect to the fractional replacement of cement by ash could be constructed.

Within the range of IC the calcium hydroxide produced by hydration and dissolution of CaO in ash will not be used up. The values of  $SAI$  can be determined by Eq. (31). It could be observed that once  $r_t$  or  $r_r + r_f$  is fixed, Eq. (31) is linear with respect to  $r_t$  up to the point of CC.

Within the range of BC additional pozzolanic reaction is still possible. A typical diagram for the long-term  $SAI$  can be shown in Fig. 3. For the ash with high silica content the contributions of CaO and Alumina to  $SAI$  approaches zero. The values of  $SAI$  determined from Eqs. (37), (38) and (39) are nearly equal. Therefore the value of  $SAI$  will decrease linearly with respect to the fractional replacement of cement by ash. For the ash with high content of CaO the point of CC will shift to the right considerably. Just right to the point of CC the value of  $SAI$  will drop abruptly. Within the range of BC, again the value of  $SAI$  will change linearly with respect to the fractional replacement of cement by ash.

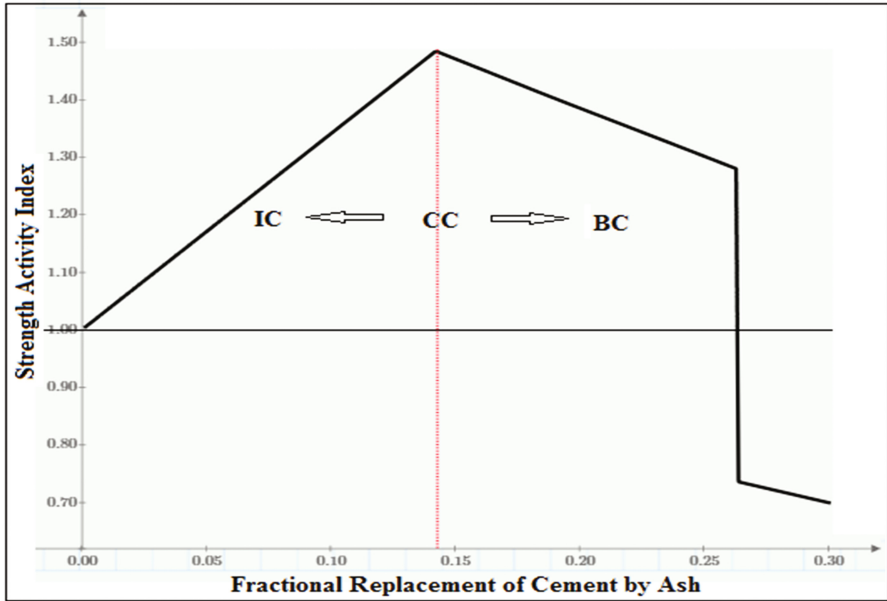


Fig. 3. SAI diagram for partial replacement of cement by RHA or SF

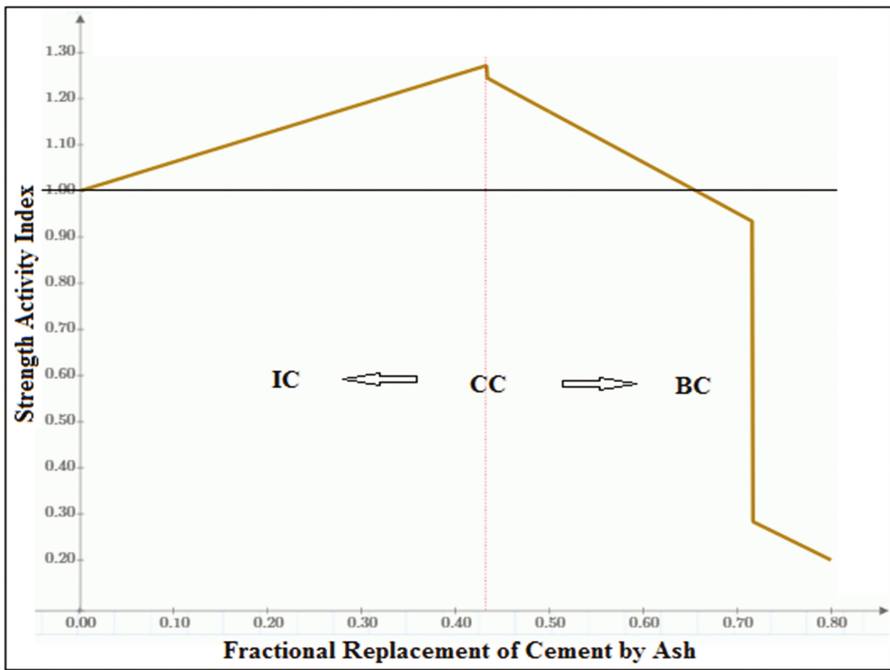


Fig. 4. SAI diagram for partial replacement of cement by FA

### 3.2.1 Effects of Silica Content on the Long-Term SAI Diagram

It should be noted that rice husk ash can contain very high content of reactive silica, but very low contents of calcium oxide and alumina. Furthermore its chemical composition is quite similar to silica fume. A set of hypothetical ashes with high content of silica are assumed. Thus, the effects of silica content in ash can be shown in Fig. 5. It could be observed that the higher the silica content in ash, the higher the peak of the strength activity index at CC, the steeper the slope of the SAI curve in the IC range, but the lower the fractional replacement of cement by ash at CC with the constant slope of SAI curve within the BC range.

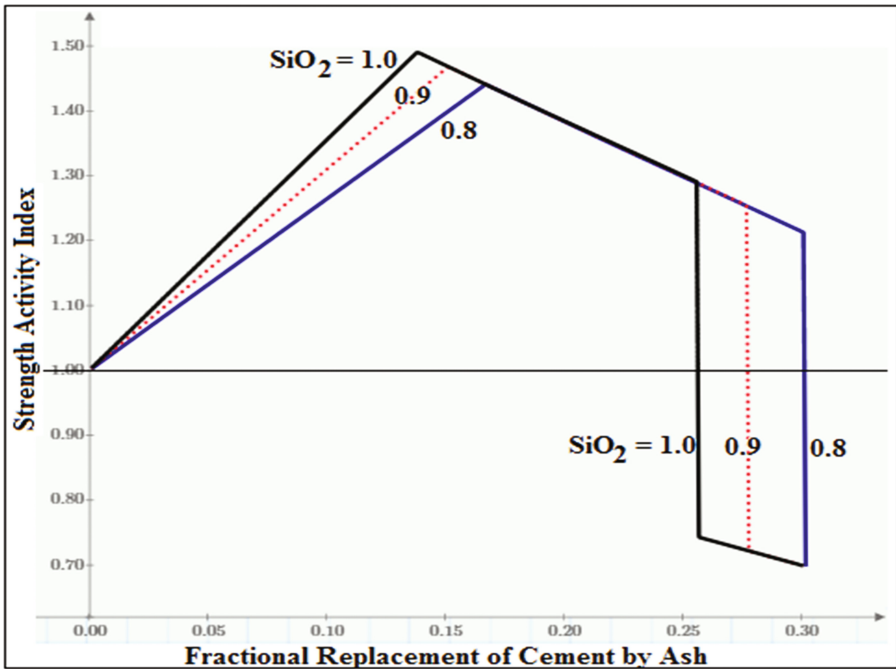


Fig. 5. Effect of silica content in ash on the long-term SAI diagram

### 3.2.2 Effects of Calcium Oxide Content on the Long-Term SAI Diagram

Class F fly ash may contain small CaO content; whereas Class C fly ash may contain high content of CaO. Therefore a set of hypothetical ashes with various contents of silica are assumed. Thus, the effects of CaO content in ash can be shown in Fig. 6. It could be observed that the higher the CaO content in ash, the higher the peak of the SAI at CC, the higher the fractional replacement of cement by ash at CC, the wider the range of possible replacement, the flatter the slope of the SAI curve in the IC range and the BC range.

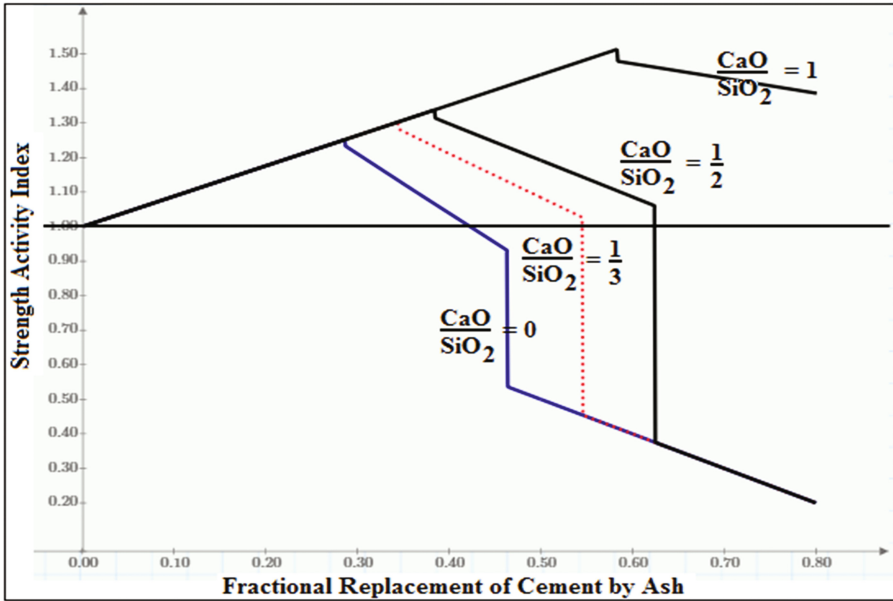


Fig. 6. Effect of alumina content in ash on the long-term SAI diagram

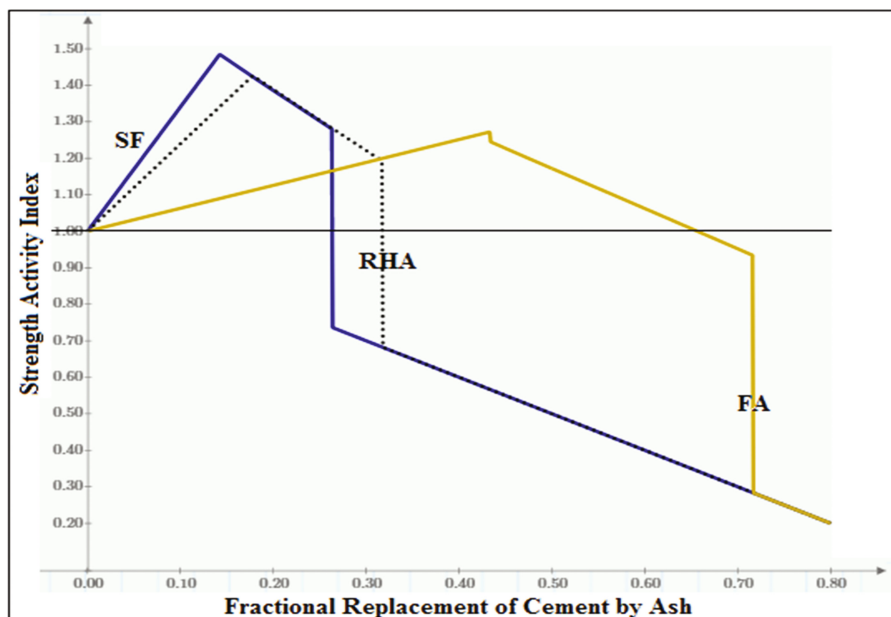
### 3.2.3 SAI Diagram for Rice Husk Ask, Fly Ash and Mixed Ashes

Figure 7 compares the diagrams of the long-term SAI with respect to the total fractional replacement of cement by rice husk ash, fly ash and mixed ashes of rice husk ash and fly ash. It should be observed that the peak value of SAI for the cement replacement by rice husk ash is higher than that of fly ash, but the fractional cement replacement by rice husk ash is much lower than that of fly ash. There is a line connecting these two peaks. This line represents the point of CC for mixed ashes of rice husk ash and fly ash. For a given value of the total fractional cement replacement by mixed ashes the optimum ratio of rice husk ash and fly ash can be determined from Eqs. (28) and (27), respectively.

Since any type of ash may contain some amount of CaO, silica and alumina, it should be represented best in term of mixed ash. Thus, the typical diagram for the long-term SAI of mixed ash may have the shape like that shown in Fig. 4.

### 3.3 Strength Activity Index for Any Age

The long-term strength activity index can be extended for predicting strength activity index for different ages and different surface areas. The coefficients could be obtained by curve fitting of data from tests carried out by many investigators such as Habeeb and Mahmud (2010), Le and Ludwig (2016), Khalil et al. (2014), Nawaz et al. (2016) and Chatveera and Nimityongskul (1994). Details will be out of the scope of this technical paper and will be discussed in the authors' complete research project (2017).



**Fig. 7.** Long-term strength activity index against total fractional replacement of cement by rice husk ash and fly ash

For the strength activity index at other ages the values of strength of C-S-H from  $C_3S$  and  $C_2S$  are rather different at early ages. However the difference in values would decrease with the increasing age. Since the development of strength of C-S-H products from pozzolanic reactions of pozzolan is still not clear, it should be studied extensively so that we can use rice husk ash and fly ash in partial replacement of cement more appropriately and with more confidence. To demonstrate how the strength activity index at other ages could be extended, again the values of strength of main minerals in cement were measured directly from Bogue's curve (Bogue 1955). For the short-term cases, however,  $\beta_s$  could be much lower than  $\alpha_s$ , for example at the age of 28 days  $\alpha_s = 47.76$ ,  $\beta_s = 5.89$ ,  $\gamma_s = 4.58$  and  $\delta_s = 2.77$ . Therefore a closer look for the value of  $\alpha\beta$  should be considered.

### 3.3.1 Effects of CaO/SiO<sub>2</sub> Ratio on Nano-structures of C-S-H and Strength Activity Index

Taylor (1986) showed that the Ca/Si ratio effected on the form of nanostructure of C-S-H. The chain of Jennite would be formed with the Ca/Si ratio in the range of 1.6–2.2. Whereas the chain of Tobermorite could be formed with the Ca/Si ratio in the range of 0.8–1.2. Taylor (1997) summarized from results of many researchers that C-S-H type I was the fibrous nanostructure and C-S-H type II was the honeycombs nanostructure. From the compositional standpoint Jennite and the C-S-H (II) are closer to C-S-H gel than 1.4 nm Tobermorite and C-S-H (I). Skinner et al. (2010) concluded



from the total X-ray scattering measurements for the nanostructure of C-S-H in cement that the C-S-H component in hydrated tricalcium silicate was similar to C-S-H (I).

Furthermore James and Rao (1986) claimed that the  $\text{CaO}/\text{SiO}_2$  ratio of 0.65 was the lower limit for the forward pozzolanic reaction. Based on the concept of complete consumption of calcium hydroxide proposed by the authors the  $\text{CaO}/\text{SiO}_2$  ratio of 1.40 is within the forward pozzolanic reaction. For the sake of further discussions we should convert the  $\text{Ca}/\text{Si}$  ratios to the  $\text{CaO}/\text{SiO}_2$  ratios by the factor of 0.654. The relationship between  $\text{CaO}/\text{SiO}_2$  and the fractional replacement of cement by ash – nanostructures of C-S-H is shown in Fig. 8. Based on the reasons shown above the  $\alpha$ s strength activity index (SAI) will be selected to represent tricalcium silicate, C-S-H (I), and Tobermorite. Whereas the  $\beta$ s SAI will be selected to represent dicalcium silicate, C-S-H (II), and Jennite.

Figure 8 showed the relationship between the  $\text{CaO}/\text{SiO}_2$  ratio and the fractional replacement of cement by ash in view of the consumption of calcium hydroxide. At the point of the complete consumption (CC) of calcium hydroxide (CH) the  $\text{CaO}/\text{SiO}_2$  ratio = 1.4 corresponds clearly to the Tobermorite and SAI. With the  $\text{CaO}/\text{SiO}_2$  ratio above this point the  $\text{CaO}/\text{SiO}_2$  ratio increases rapidly with the decrease of the replacement of cement and the pozzolanic reaction proceed rapidly and the SAI is, again,  $\beta$ s. Above the upper limit of the  $\text{CaO}/\text{SiO}_2$  ratio = 1.439 the SAI is assumed constant at  $\beta$ s. This interval of  $\text{CaO}/\text{SiO}_2$  ratio above CC should be called the interval of incomplete consumption of calcium hydroxide (IC). Below the complete con-

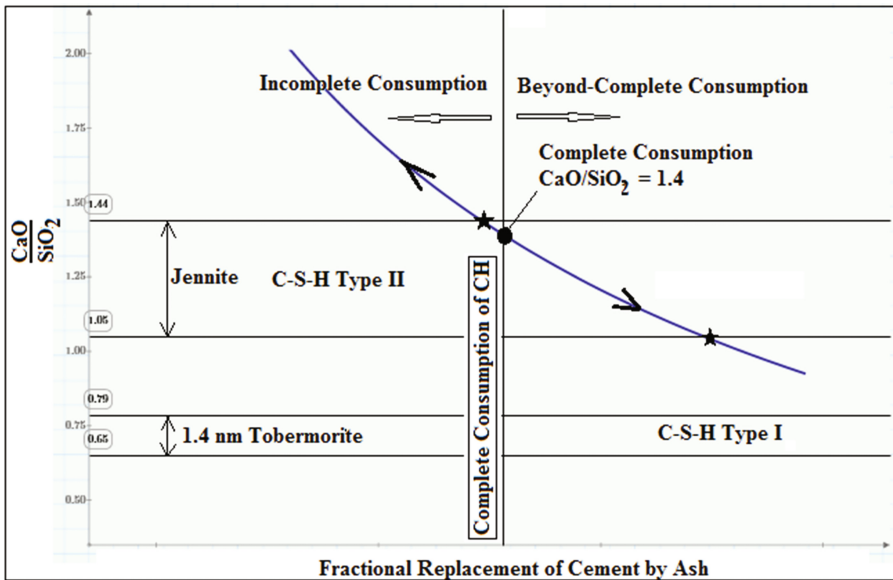


**Fig. 8.** Relationship between  $\text{CaO}/\text{SiO}_2$  and fractional replacement of cement by ash – nanostructures of C-S-H

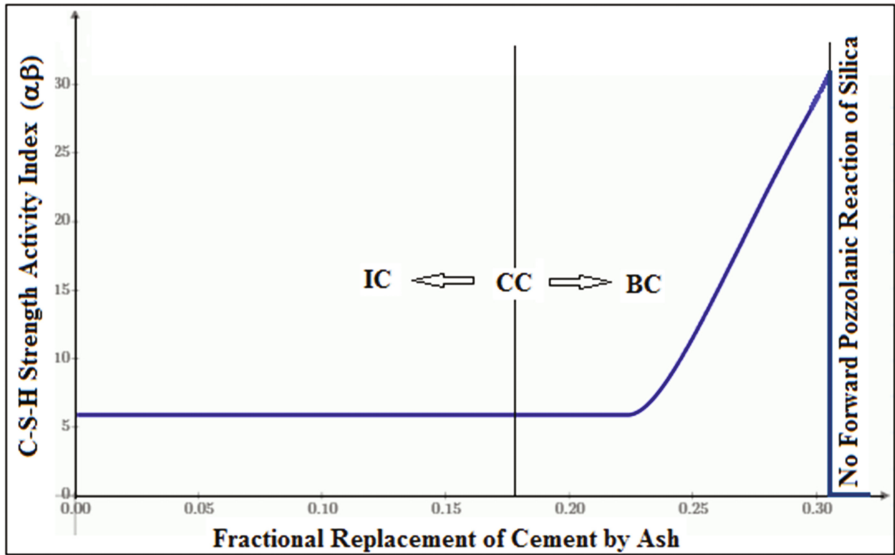


Fig. 9. Relationship between C-S-H strength activity index ( $\alpha\beta$ ) and fractional replacement of cement by ash at the age 28 days

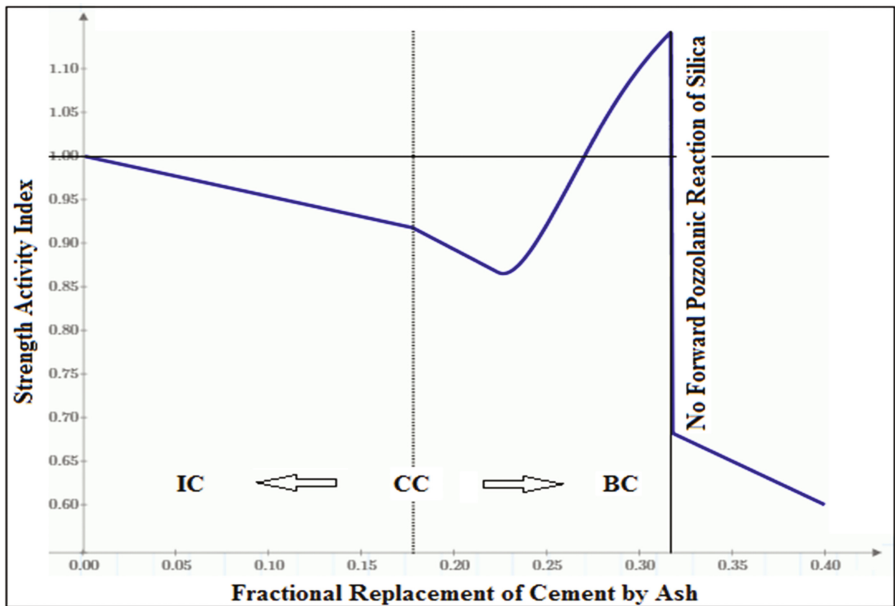


Fig. 10. Relationship between SAI and fractional replacement of cement by ash at the age 28 days

consumption of CH the CaO/SiO<sub>2</sub> ratio decreases slowly with the increment of the cement replacement by ash. This interval should be called beyond-complete consumption of CH (BC). The lower bound for the βs SAI occurs at the CaO/SiO<sub>2</sub> ratio = 1.047. The αs SAI is in the interval of the CaO/SiO<sub>2</sub> ratio of (0.523, 0.785). It is interesting to note that the lower bound of forward pozzolanic reaction of 0.65 lies within this interval. The practical values of cement replacement by ash are far above this limit. The linear extension is assumed for the αβ SAI for the gap of the CaO/SiO<sub>2</sub> ratios of (0.785,1.047). Based on these assumptions the average αβ SAI for the whole range of the pozzolanic reaction for ash or mixed ashes could be determined. The relationship of the αβ SAI and C-S-H SAI to the fractional replacement of cement by ash could be depicted in Figs. 9 and 10, respectively.

### 3.3.2 Other Factors Effecting Strength Activity Index

Hydration reaction, formation of calcium hydroxide by dissolving calcium oxide (quicklime) in water and pozzolanic reactions of silica and alumina are all exothermic reactions. Langan et al. (2002), Tokyay et al. (2010) and Över (2012) concluded that the presence of silica fume, fly ash, rice husk ash and other types of pozzolan could accelerate or retard heat evolution in hydration of Portland cement at the early age. Therefore it may result in increasing and decreasing of strength activity index at the early age. A diagram for the long-term strength activity index with respect to the fractional replacement of cement by ash could be compared with the corresponding diagram for the earlier ages as shown in Fig. 11.

Many other factors may also effect on the strength activity index of cement paste mixed with ash such as chemical composition of and Portland cement and ash, physical

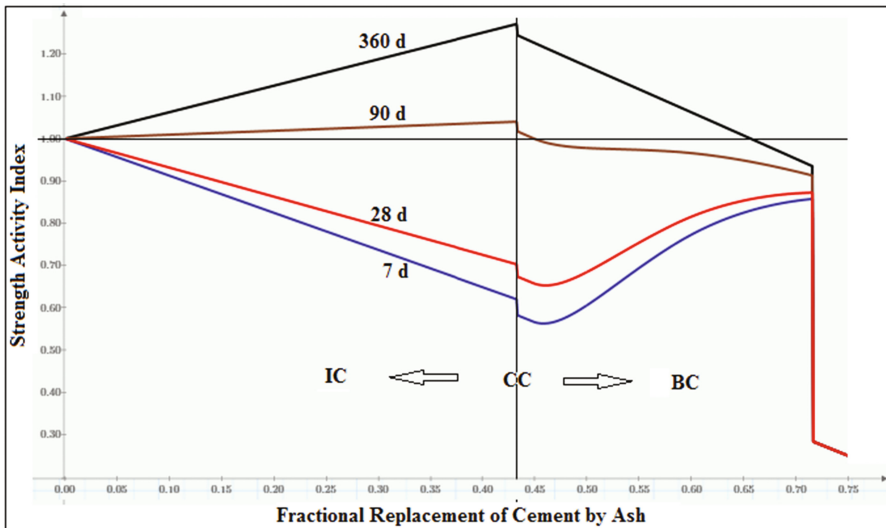


Fig. 11. Scenario of SAI diagram for par. replacement of cement by pozzolan

properties of ash such as shape of particles, particle size distribution, fineness modulus or surface area of cement and ash, heat evolution of hydration, type and dose of superplasticizer and environmental conditions. All these factors are, however, out of scope of this technical paper.

Uncertainty in chemical composition of and Portland cement and ash can also effect on the strength activity index and will be discussed in a following subsection.

### 3.4 Short-Term and Long-Term SAI Diagrams for Rice Husk Ask, Fly Ash and Mixed Ashes

Long-term SAI for rice husk ash and fly ash could be understood in view of diagrams shown in Figs. 3 and 4, respectively. Furthermore the scenario of SAI diagrams at several ages for rice husk ash or fly ash or any type of pozzolan is depicted in Fig. 11. It can be seen clearly that the older the age, the higher would be the values in the SAI diagram.

### 3.5 Results from the Authors

A series of tests for specimens of cement mortars mixed with silica fume, rice husk ash and fly ash have been carried out. The ordinary Portland cement type I was used. The range of fractional replacement of cement by pozzolan covered IC, CC and BC. The water binder ratios were in the range of 0.4–0.5. The mortar specimens were in the size of a  $50 \times 50 \times 50 \text{ mm}^3$  cube. All specimens were controlled by  $110 \pm 5\%$  of the flow table test. No high range reducing is added for the controlled specimens and the specimens with cement replacement by fly ash. However, small amount of high range water reducing agent were added for the specimens with cement replacement by silica fume or rice husk ash to achieve the controlled flow. All specimens were cured in filtered underground water.

The main chemical compositions of cement were  $\text{C}_3\text{S}$  (60.88%),  $\text{C}_2\text{S}$  (14.86%),  $\text{C}_3\text{A}$  (8.47%) and  $\text{C}_4\text{AF}$  (10.29%). Three ash samples SF, RHA and FA composed of silica ( $\text{SiO}_2$ ) 89.36, 74.64 and 35.83%, respectively, alumina ( $\text{Al}_2\text{O}_3$ ) 0.42, 0.21 and 21.27%, respectively, and CaO 0.45, 0.74 and 16.17%, respectively.

Some of these results within the range of IC were plotted against the short-term – and long-term SAI diagrams as shown in Figs. 12, 13 and 14 for silica fume, rice husk ash and fly ash, respectively. More results within the range of BC were referred to Ouypornprasert et al. (2017).

It should be observed that the values of SAI for the tested results could be a slightly higher or lower than the corresponding predicted values at the same age from the models. However, all the actual values of SAI were still far below the corresponding long-term predicted values from the models. The deviations from the proposed SAI diagrams could be explained by results from other researchers, some of which were summarized in the following.

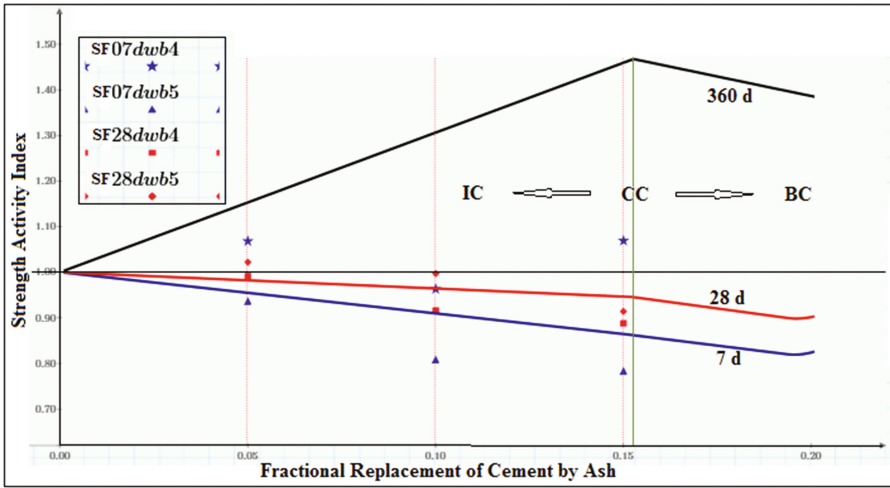


Fig. 12. Comparison between the tested SAI with the SAI diagram for SF

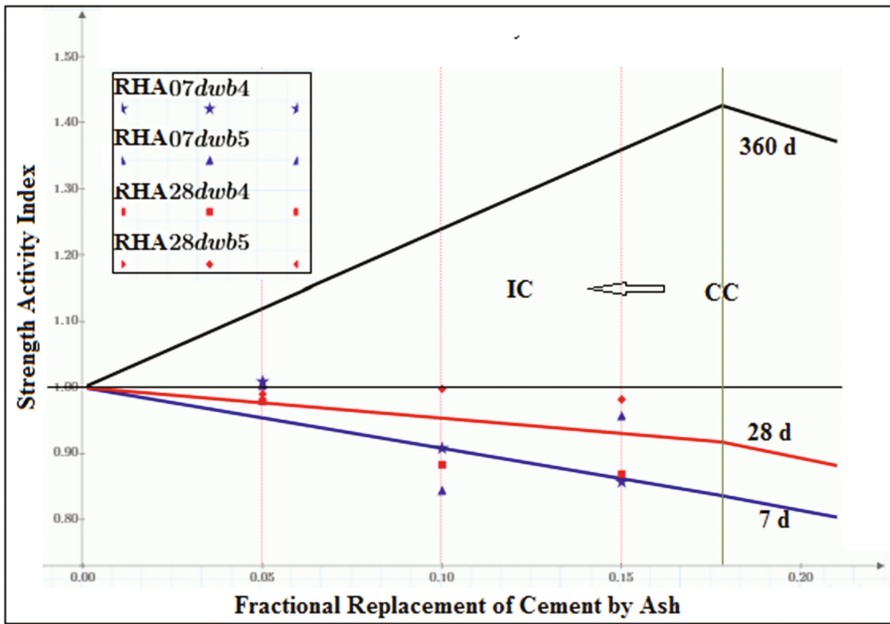


Fig. 13. Comparison between the tested SAI with the SAI diagram for RHA

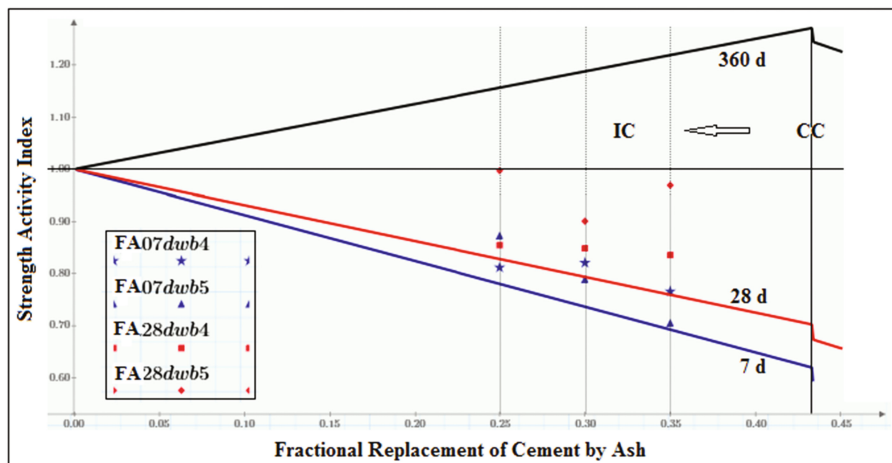


Fig. 14. Comparison between the tested SAI with the SAI diagram for FA

### 3.6 Results from Other Researchers

Results from other researchers could be compared only in cases that enough necessary data for analyses were given. Some results of comparisons were discussed below.

#### 3.6.1 Cement Paste - Barley Husk Ash, Rice Husk Ash and Coal Fly Ash

Khalil et al. (2014) tested a series of cement paste specimens of  $1'' \times 1'' \times 1''$  cubes. The water content of consistency was determined for each set of the specimens. The ordinary Portland cement Type I was used. No high range water reducing agent was added. Barley husk ash, rice husk ash and coal fly ash was screened through 0.125 mm standard sieve. The consistency and the setting time of fresh pastes were tested according to ISO 9597:1989. The fractional replacement of cement by barley husk ash (BHA), rice husk ash (RHA) or coal fly ash (CFA) was in the range of 0.05–0.30. The water demand for standard consistency linearly increased with an increment of cement replacement level by BHA, RHA, or CFA, this was due to the relatively higher specific surface area of the ashes (11,000–12,000  $\text{cm}^2/\text{g}$ ) than the OPC (3,100  $\text{cm}^2/\text{g}$ ) in addition to the hygroscopic nature of the ashes which consume relatively higher amounts of mixing water.

The main chemical compositions of cement necessary for Bogue's equation were CaO (64.62%),  $\text{SiO}_2$  (20.63%),  $\text{Fe}_2\text{O}_3$  (6.88%),  $\text{Al}_2\text{O}_3$  (1.54%) and  $\text{SO}_3$  (1.21%). Three ash samples BHA, RHA, and CFA composed mainly of silica ( $\text{SiO}_2$ ) 79.298, 64.948 and 60.402%, respectively, and alumina ( $\text{Al}_2\text{O}_3$ ) 8.775, 11.830 and 11.00%, besides little content of CaO.

At a fixed fractional replacement of cement by ash a noticeable improvement in compressive strength was observed as the curing time (age of hydration) increased from 3 to 7 to 28 days, beyond which (at 90 days) the improvement in strength was less significant. The values of the strength activity index for the specimens at the age of 90 days were plotted against the short-term and long-term *SAI* diagrams proposed as

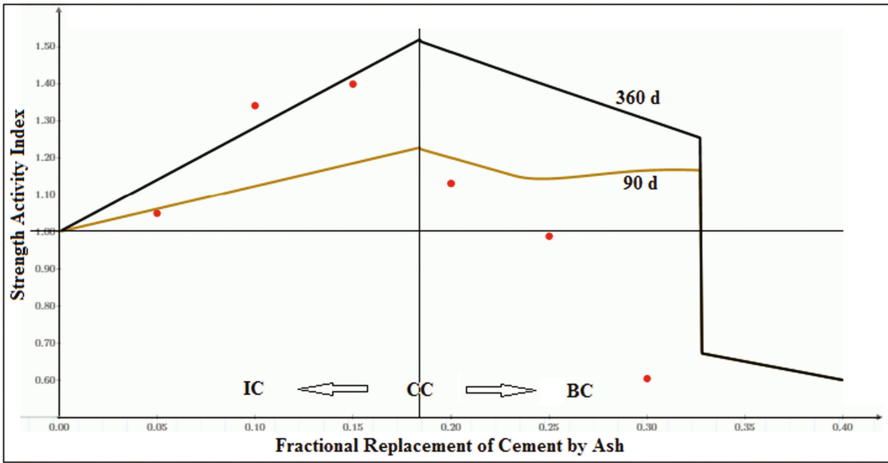


**Fig. 15.** Comparison between the tested results by Khalil et al. (2014) with the SAI diagram - barley husk ash

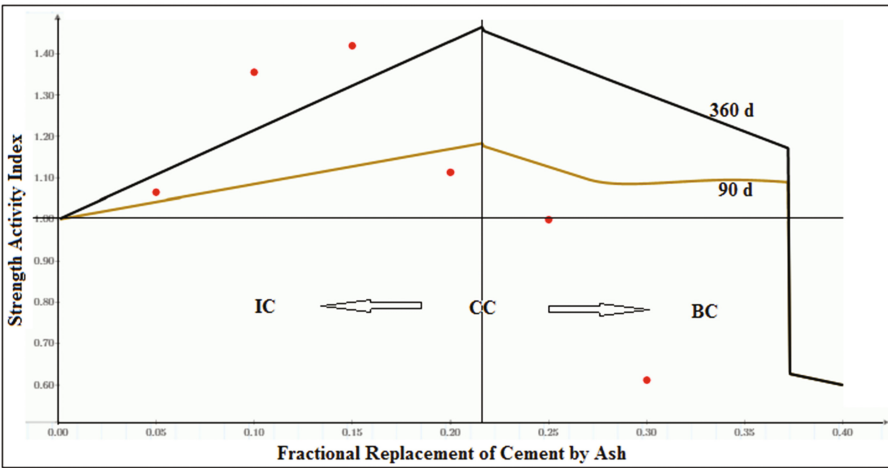


**Fig. 16.** Comparison between the tested results at the age 90 days by Khalil et al. (2014) with the SAI diagram - rice husk ash

shown in Figs. 15, 16 and 17 for barley husk ash, rice husk ash and coal fly ash, respectively. It could be observed that the values of SAI from tested results were much higher than the corresponding values from the model within the range of IC, but much lower in the range of BC.

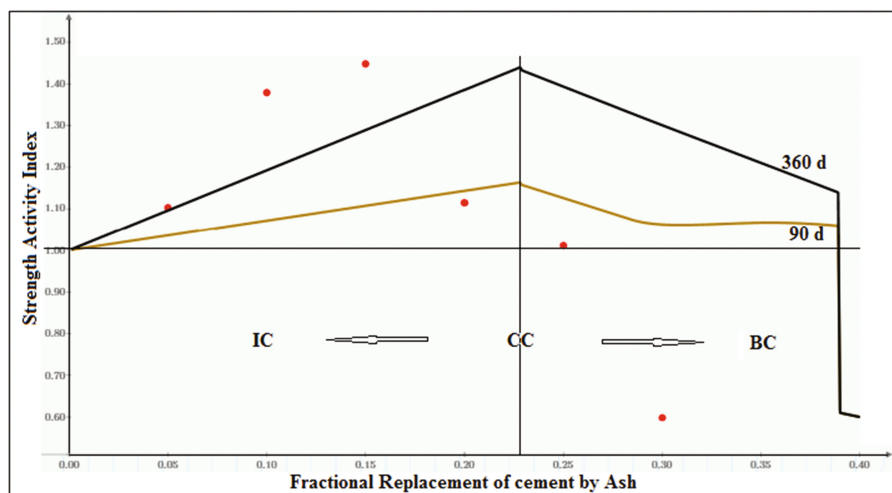


**Fig. 17.** Comparison between the tested results at the age 90 days by Khalil et al. (2014) with the SAI diagram – coal fly ash

### 3.6.2 Cement Paste – Nanosilica and Silica Fume

Qing et al. (2007) tested a series of cement paste specimens of 25 mm × 25 mm × 25 mm cubes. The water content of consistency was determined for each set of the specimens. The ordinary Portland cement (42.5 grade, Blaine specific surface 310 m<sup>2</sup>/kg) complying with Chinese standard (GB 175) was used. A commercial sulphated melamine formaldehyde polymer (liquid solution, water content 70%) with special gravity 1.2 g/cm<sup>3</sup> and water reduction up to 20% was used. Tap water was used in all experiments. For all the pastes, a cement plus addition:water:superplasticizer ratio of 1:0.22:0.025 was used. The fractional replacement of cement by pozzolan was not greater than 0.05.

The main chemical compositions of cement necessary for Bogue's equation were CaO (64.27%), SiO<sub>2</sub> (21.05%), Fe<sub>2</sub>O<sub>3</sub> (4.03%), Al<sub>2</sub>O<sub>3</sub> (5.56%) and SO<sub>3</sub> (0.75%). Two pozzolan samples nanosilica and silica fume composed mainly of amorphous state of silica (SiO<sub>2</sub>) 99.9 and 92.1%, respectively. They possessed variable contents of alumina (Al<sub>2</sub>O<sub>3</sub>) 0 and 2.04%, besides negligible content of CaO.

The values of the strength activity index for the specimens at the age of 1, 3, 28 and 60 days were plotted against the short-term and long-term SAI diagrams as shown in Figs. 18 and 19 for nanosilica and silica fume, respectively. It should be observed that the values of SAI from the tested results were much higher than the corresponding values. These might be due to the addition of high amount of superplasticizer as shown by Chatveera and Nimityongsakul (1994b). Furthermore the particle size of silica fume was much smaller than OPC and the filler effect occurred. This effect was more pronounced in the case of nanosilica.



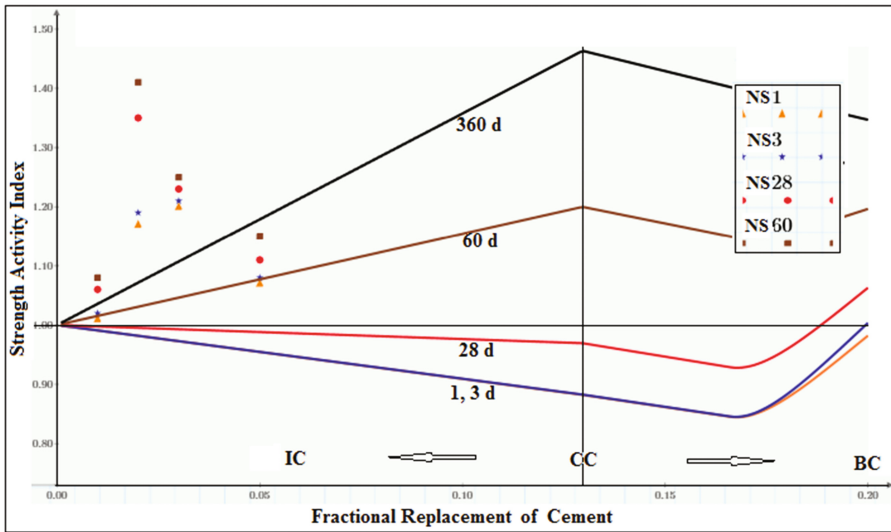


**Fig. 18.** Comparison between the tested results at the age 1, 3, 28 and 60 days by Qing et al. (2007) with the SAI diagram – nanosilica

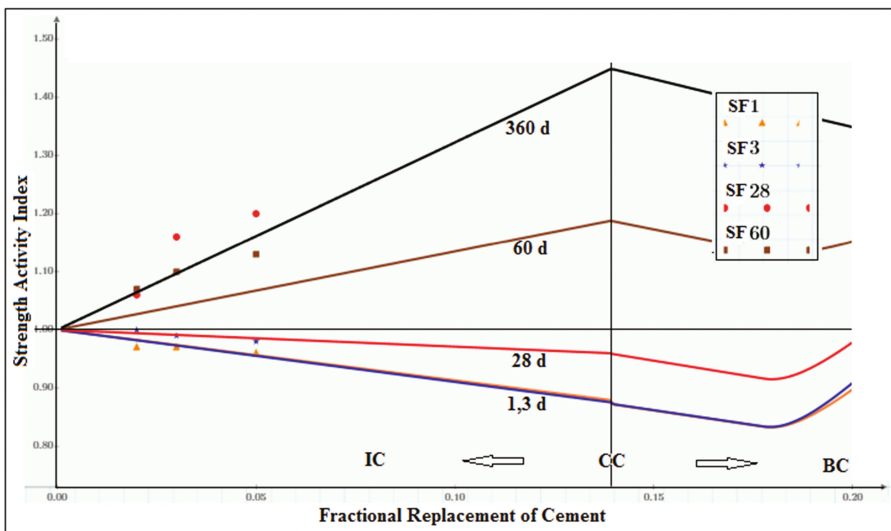


**Fig. 19.** Comparison between the tested results at the age 1, 3, 28 and 60 days by Qing et al. (2007) with the SAI diagram – silica fume

### 3.6.3 Mortar - Rice Husk Ash and Fly Ash

Chatveera and Nimityongskul (1994a) studied the influence of artificial pozzolanas on mechanical behavior of high strength concrete. Two sources of river sand were used. The values of fineness modulus were 3.37 and 2.39.

The main chemical compositions of cement necessary for Bogue’s equation were CaO (63.8%), SiO<sub>2</sub> (20.2%), Fe<sub>2</sub>O<sub>3</sub> (2.9%), Al<sub>2</sub>O<sub>3</sub> (5.4%) and SO<sub>3</sub> (2.6%). Two ash samples RHA, and FA composed mainly of silica (SiO<sub>2</sub>) 97.27 and 33.62%, respectively, alumina (Al<sub>2</sub>O<sub>3</sub>) 0.54 and 15.08%, respectively, and CaO 1.09 and 23.96%, respectively.

The fractional replacement of cement by rice husk ash or fly ash was fixed to 0.30. The water-binder ratios for the ordinary cement, cement mixed with RHA and cement mixed with FA were 0.28, 0.42 and 0.38, respectively.

The values of the strength activity index for the specimens without superplaticizer at the age of 3, 7, 28 and 56 days were plotted against the short-term – and long-term SAI diagrams for rice husk ash and fly ash as shown in Figs. 22 and 23, respectively.

It should be observed from Fig. 20 that the fractional replacement of cement by RHA = 0.3 was in the range of BC and the values of SAI of mortars mixed with RHA agreed very well with the corresponding values from the model. These results confirmed the claim of no forward pozzolanic reaction of silica at the CaO/SiO<sub>2</sub> ratio of 0.65. From Fig. 21, however, the values of SAI from the tested results for cement mixed with FA were quite scattered. The values of the compressive strength of the specimens with higher value of fineness modulus were much lower than those with the lower value of fineness modulus. On the contrary the values of SAI of the specimens with higher value of fineness modulus were much higher than those with the lower value of fineness modulus.

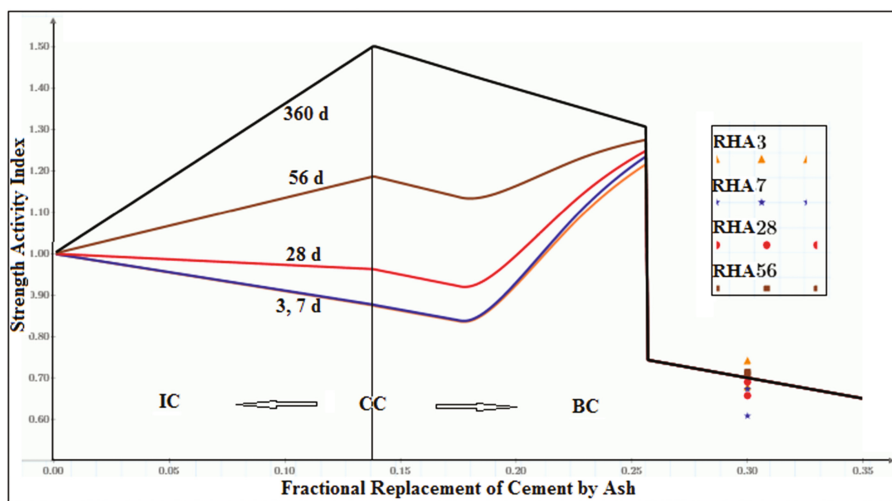


Fig. 20. Comparison between the tested results at the age 3, 7, 28 and 56 days by Chatveera and Nimityongskul (1994a) with the SAI diagram – rice husk ash

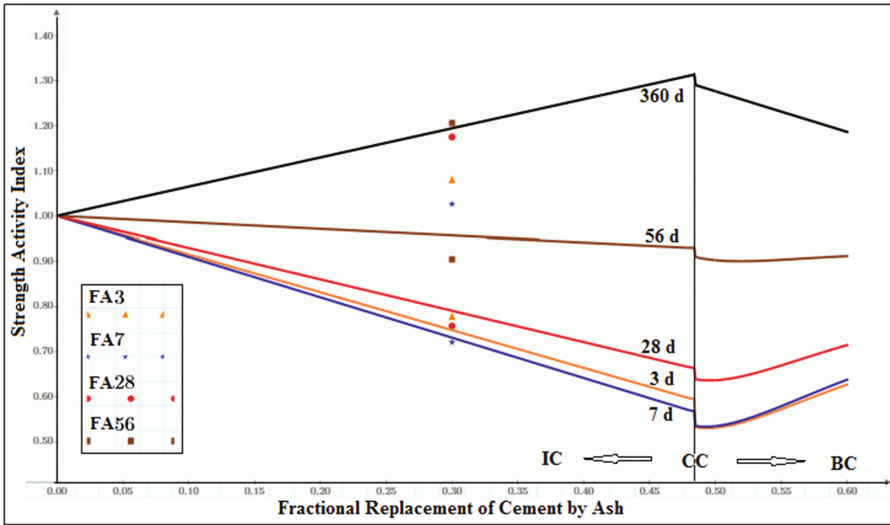


Fig. 21. Comparison between the tested results at the age 3, 7, 28 and 56 days by Chatveera and Nimityongskul (1994a) with the SAI diagram – fly ash

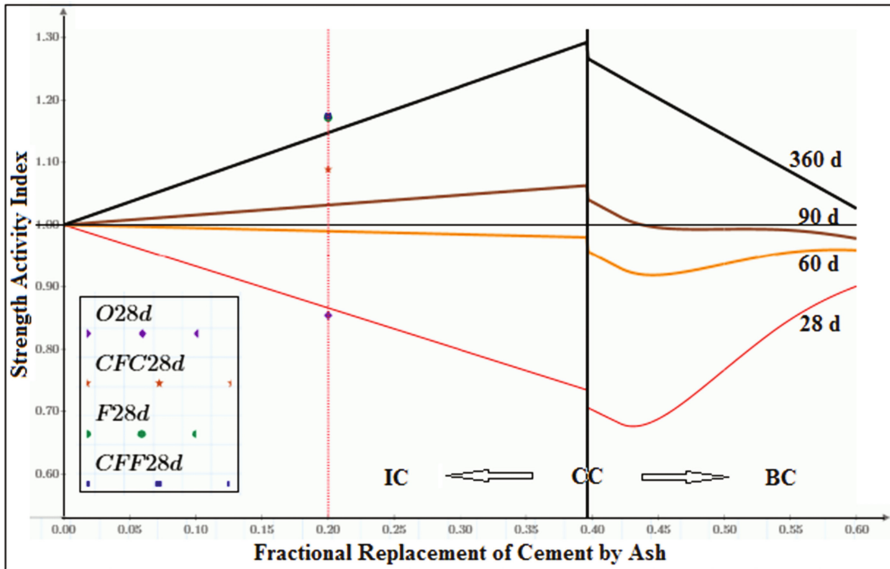
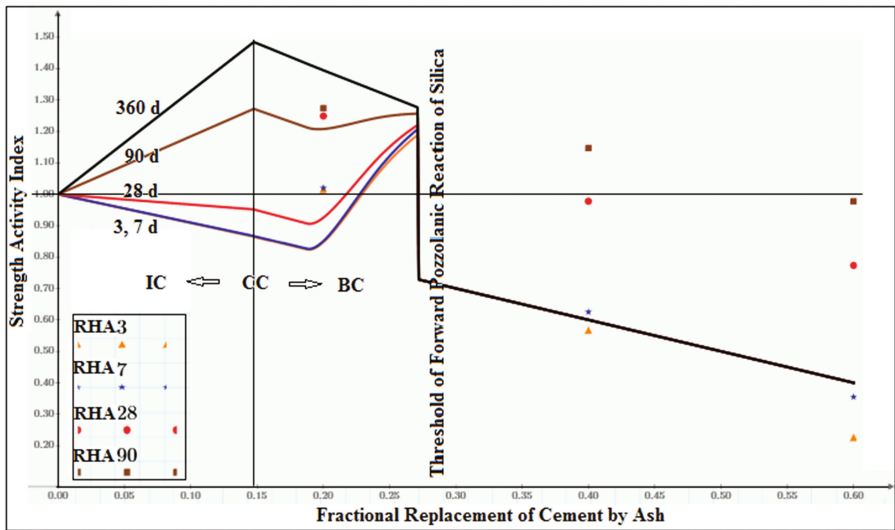


Fig. 22. Comparison between the tested results at the age 28 days by Jaturapitakkul et al. (1999) with the SAI diagram – fly ash



**Fig. 23.** Comparison between the tested results at the age 28 days by Chatveera and Nimityongskul (1994b) with the SAI diagram – rice husk ash

### 3.6.4 Mortar - Effect of Particle Size of Fly Ash

Jaturapitakkul et al. (1999) studied the strength activity index of ground coarse fly ash with cement. The ordinary Portland cement Type I was used. The control samples were prepared with the proportion cement to sand of 1:2.75 by weight and with the water to cement ratio of 0.64. For the other samples the cement was replaced by fly ash 20% by weight. The ratios of water to cementitious material (cement+fly ash) for the other samples were varied between 0.60–0.69, depending on the fineness of fly ash, to maintain flow of mortar between  $110 \pm 5\%$  in accordance with ASTM C 230. The standard mortar cubes of  $50 \times 50 \times 50 \text{ mm}^3$  were cast in brass molds and the mortars were removed from the molds after 24 h. The compressive strength of the mortars was performed as prescribed by ASTM C 109 at 24 h, 3, 7, 14, 28, 60, and 90 days of curing.

The main chemical compositions of cement necessary for Bogue's equation were CaO (64.99%), SiO<sub>2</sub> (20.62%), Fe<sub>2</sub>O<sub>3</sub> (3.1%), Al<sub>2</sub>O<sub>3</sub> (5.22%) and SO<sub>3</sub> (2.7%). The original coarse fly ash from Mae Moh Amphur composed of silica (SiO<sub>2</sub>) 45.94%, alumina (Al<sub>2</sub>O<sub>3</sub>) 25.62% and CaO 9.39%. The original coarse fly ash was grounded, processed and classified with respect to the processes. The major change was the particle size distributions, not the chemical composition. The mean particle size of OPC was 16.0 μ. Whereas the mean particle sizes for the original fly ash (O), Fly Ash (CFC), Fly Ash (F) and Fly Ash (CFF) were 50.0, 19.5, 18.0 and 5.0 μ, respectively.

The values of the strength activity index for the specimens at the age of 28 days were plotted against the short-term – and long-term SAI diagrams for fly ash as shown in Fig. 22. It should be observed that the value of SAI for Fly Ash (O) was very close to the corresponding value from the model. Whereas the values of SAI for the other classes of Fly Ash were much higher than the corresponding value from the model. The

main reason was the mean particle sizes of Fly Ash were nearly equal or lower than that of OPC. In these cases filler effect of fly ash accelerated the precipitation of C-S-H gel on the interface surface area.

### 3.6.5 Mortar – High Volume Cement Replacement and Effect of Superplasticizer - Rice Husk Ash and Fly Ash

Chatveera and Nimityongskul (1994b) studied the strength activity index for high volume replacement of cement by rice husk ash and fly ash as well as for the effect of superplasticizer. The ordinary Portland cement Type I was used. The control samples were prepared with the proportion cement to sand of 1:2.75 by weight and with the water to cement ratio of 0.64. The flow of mortar was controlled between  $110 \pm 5\%$  in accordance with ASTM C 230. The standard mortar cubes of  $50 \times 50 \times 50 \text{ mm}^3$  were cast in brass molds and the mortars were removed from the molds after 24 h. The compressive strength of the mortars was performed as prescribed by ASTM C 109 at the age of 7, 14, 28, 60 and 90 days. The fractional replacement of cement by ash or mixed ash was in the range of 0–0.6. In this studied the original rice husk ash was grounded and the particle size of RHA was much lower than that of OPC.

The main chemical compositions of cement necessary for Bogue's equation were CaO (63.8%), SiO<sub>2</sub> (20.2%), Fe<sub>2</sub>O<sub>3</sub> (2.9%), Al<sub>2</sub>O<sub>3</sub> (5.4%) and SO<sub>3</sub> (2.6%). Two ash samples RHA, and FA composed mainly of silica (SiO<sub>2</sub>) 89.9 and 15.1%, respectively, alumina (Al<sub>2</sub>O<sub>3</sub>) 0.5 and 7.0%, respectively, and CaO 0.5 and 33.0%, respectively.

The values of SAI for the specimens without superplasticizer were plotted against the short-term and long-term SAI diagrams for rice husk ash and fly ash as shown in Figs. 23 and 24, respectively.

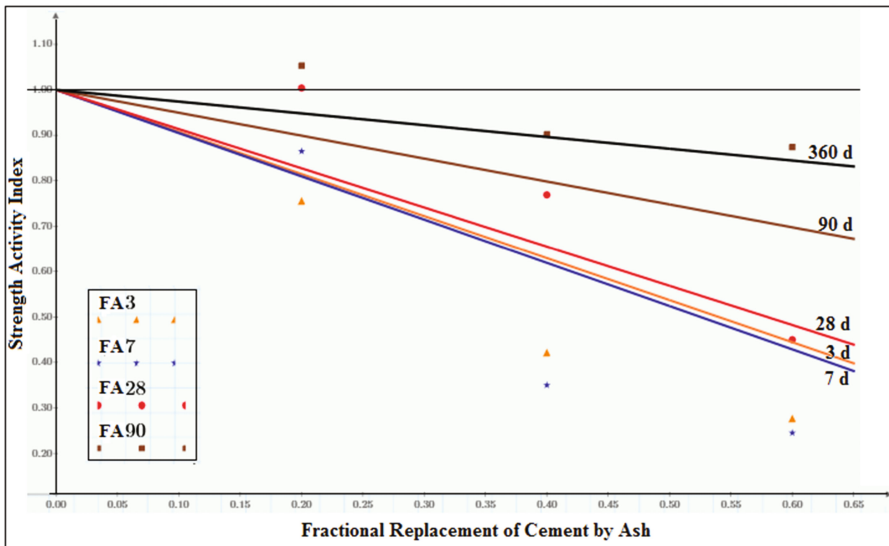
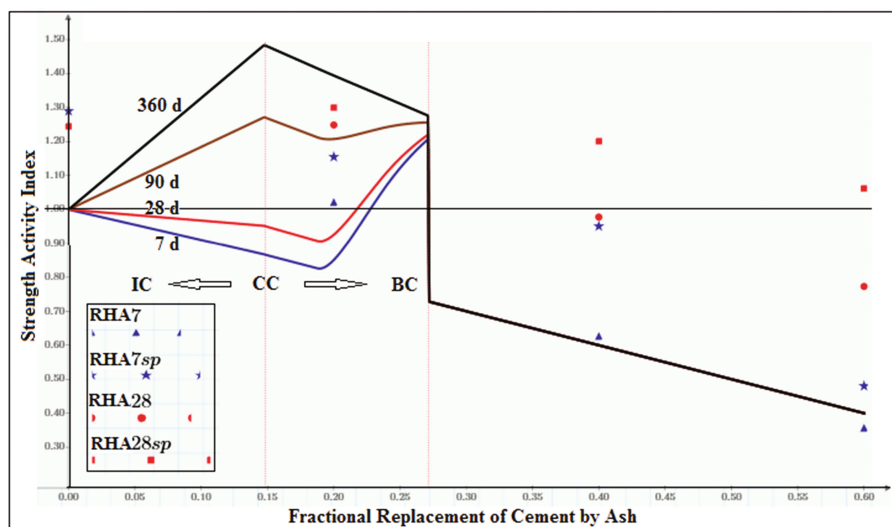


Fig. 24. Comparison between the tested results at the age 28 days by Chatveera and Nimityongskul (1994b) with the SAI diagram – fly ash



**Fig. 25.** Comparison between the tested results at the age 28 days by Chatveera and Nimityongskul (1994b) with the SAI diagram – rice husk ash

It could be seen clearly from Fig. 23 that at the cement replacement of 0.20 the values of SAI of the tested results were much higher than the corresponding values from the model. For the cement replacement at 0.4 and 0.6, the values of SAI from the results at the early ages of 3 and 7 days. Again this fact confirmed the threshold of forward pozzolanic reaction of silica. The tested results at the older age, however, showed that pozzolanic reaction of silica could move forward.

In Fig. 24 the predicted values of SAI tended to overestimate at the early ages; whereas they tended to underestimate at the older ages.

Sulphonated naphthalene formaldehyde condensed polymer was used as superplasticizer with the dose 1.25% of cement by weight. The specimens were tested at the age of 7, 14, 28, 60 and 90 days. The values of SAI for the specimens with superplasticizer were plotted against the short-term and long-term SAI diagrams for rice husk ash and fly ash as shown in Figs. 25 and 26, respectively. These two figures showed clearly that specimens with superplasticizer resulted in much higher values of compressive strength as well as SAI than those values of the corresponding specimens without superplasticizer. Furthermore with superplasticizer the pozzolanic reaction of silica could move forward beyond the threshold even at the early age.

### 3.6.6 Concrete - Rice Husk Ash

Habeeb and Mahmud (2010) studied the strength of concrete mixed with rice husk ash. The values of fractional replacement of cement were 0.05, 0.10, 0.15 and 0.20. The given contents of CaO, SiO<sub>2</sub> and Al<sub>2</sub>O<sub>3</sub> for rice husk ash and fly ash could be taken directly. The fractional contents of C<sub>3</sub>S, C<sub>2</sub>S, C<sub>3</sub>A and C<sub>4</sub>AF could be converted by Bouge's equation. However, for the sake of comparison, the optimum SAI indices for the compressive strength of concrete from the study at the ages of 28 days and 90 days

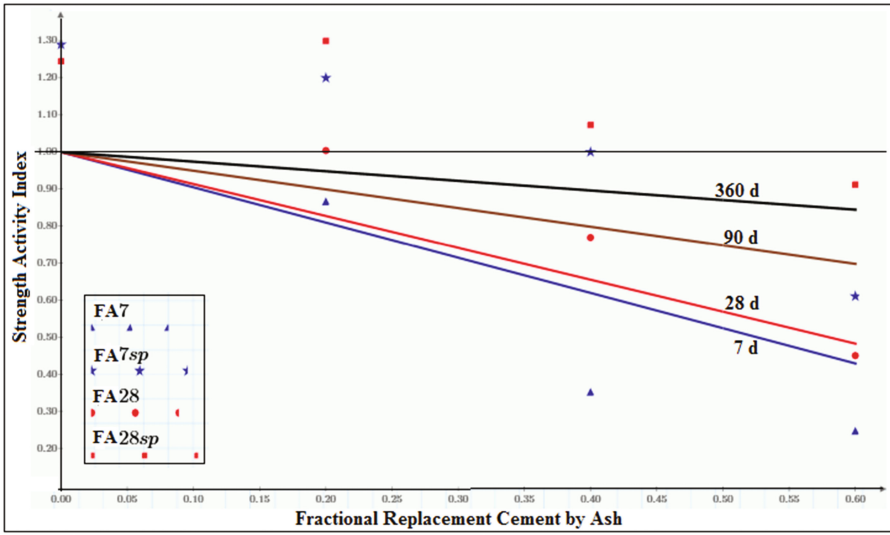


Fig. 26. Comparison between the tested results at the age 28 days by Chatveera and Nimityongskul (1994b) with the SAI diagram – fly ash

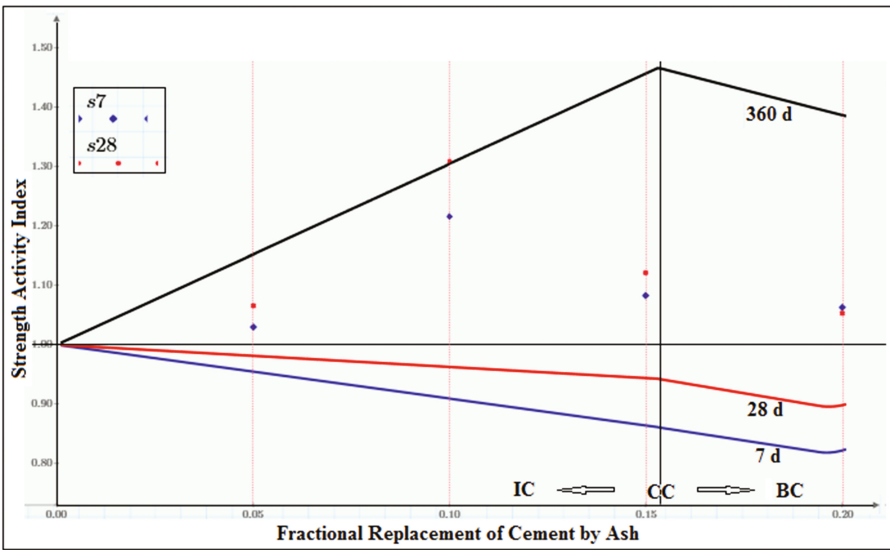
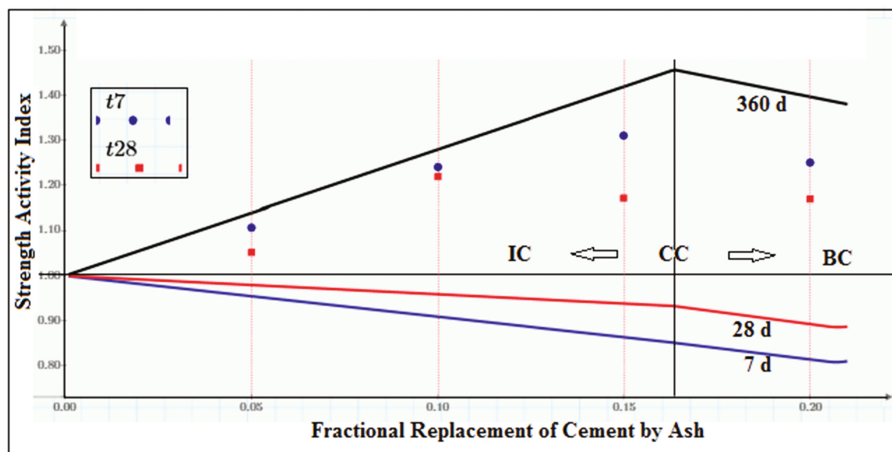


Fig. 27. Comparison of strength activity index with tested data by Habeeb and Mahmud (2010) - concrete mixed with rice husk as at the age of 28 days



**Fig. 28.** Comparison of strength activity index with tested data by Xu et al. (2016) - concrete mixed with rice husk ash and fly ash at the age of 7 and 28 days

were plotted against the corresponding SAI diagrams proposed the authors as shown in Fig. 27. It should be observed that the values of fractional replacement of 0.05, 0.10 and 0.15 lied within the range of incomplete consumption of calcium hydroxide, but the replacement 0.20 lied far beyond the complete consumption. The predicted values of the strength activity index at the age of 28 days were consistent with the tested results of concrete mixed with rice husk ash carried out by the researchers. It should be noted that the surface area of the grounded rice husk ash of the data points marked by solid squares (180 min.), solid asterisks (270 min.) and solid circles (360 min.) were lower in order, respectively. The values of SAI from the tested results were much higher than the corresponding values for the model for all cases. In cases of concrete the higher values of SAI from tested results might be much higher values of modulus of elasticity and strength of coarse aggregate than the corresponding values of the binder, especially at the early age.

The same trends were also observed from the studies of the other researchers such as results from Xu et al. (2016) as shown in Fig. 28.

## 4 Propagation of Uncertainty

### 4.1 Linear Functions

For a linear function of n random variables in form of:

$$g(\underline{X}) = a_0 + \sum_{i=1}^n a_i \cdot X_i \tag{40}$$

The correlation matrix of  $\underline{X}$  is symmetric in form of:



$$[C] = \begin{bmatrix} 1 & \rho_{12} & \cdot & \rho_{1n} \\ \rho_{12} & 1 & \cdot & \rho_{2n} \\ \cdot & \cdot & \cdot & \cdot \\ \rho_{1n} & \rho_{2n} & \cdot & 1 \end{bmatrix} \tag{41}$$

Where  $\rho_{ij}$  is the correlation coefficient between  $X_i$  and  $X_j$ . The covariance term  $\sigma_{ij}$  can be expressed in terms of the correlation coefficients:

$$\sigma_{ij} = \rho_{ij} \cdot \sigma_i \cdot \sigma_j \tag{42}$$

Where  $\sigma_i$  and  $\sigma_j$  are standard deviations of variables  $X_i$  and  $X_j$  respectively. Thus  $\sigma_i^2$  and  $\sigma_j^2$  are variance of variables  $X_i$  and  $X_j$ , respectively.

Then the variance of  $g(\underline{X})$  is:

$$\sigma_g^2 = \sum_{i=1}^n a_i \cdot \sigma_i^2 + \sum_{i=1}^n \sum_{j=1(j \neq i)}^n a_i \cdot a_j \cdot \rho_{ij} \cdot \sigma_i \cdot \sigma_j \tag{43}$$

In the case that variables  $\underline{X}$  are uncorrelated variables the variance and the standard variation of  $g(\underline{X})$  are reduced to:

$$\sigma_g^2 = \sum_{i=1}^n a_i^2 \cdot \sigma_i^2 \tag{44}$$

$$\sigma_g = \sqrt{\sum_{i=1}^n a_i^2 \cdot \sigma_i^2} \tag{45}$$

### 4.2 Nonlinear Functions and Monte-Carlo Simulations

For a nonlinear function of n uncorrelated random variables, the standard deviation of  $g(\underline{X})$  ( $\sigma_g$ ) to calculate error propagation, the variance formula (Ku 1966):

$$\sigma_g = \sqrt{\sum_{i=1}^n \left(\frac{\partial g}{\partial x_i}\right)^2 \cdot \sigma_{x_i}^2} \tag{46}$$

For other cases Monte-Carlo simulations may be applied. Then the suitable distributions for  $g(\underline{X})$  can be obtained by Goodness-Of-Fit Tests e.g. Chi-Square Errors Test and K-S Test (Ouypornprasert 2002).

### 4.3 Optimum Replacement of Rice Husk Ash for Cement

For the sake of further discussions: Let the value of a reduced variable  $y_i$  of a random variable  $X_i$  with mean  $(\mu_{X_i})$  and standard deviation  $(\sigma_{X_i})$  be:

$$y_i = \frac{x_i - \mu_{X_i}}{\sigma_{X_i}} \tag{47}$$

The partial derivative of a function  $g(\underline{X})$  with respect to a reduced variable  $y_i$  is  $\frac{\partial g(\underline{x})}{\partial y_i}$ . By applying the chain rule this term may be rewritten as:

$$\frac{\partial g(\underline{x})}{\partial y_i} = \frac{\partial g(\underline{x})}{\partial x_i} \cdot \frac{dx_i}{dy_i} = \frac{\partial g(\underline{x})}{\partial x_i} \cdot \sigma_{X_i} \tag{48}$$

From Eq. (29):

$$\frac{\partial r_r}{\partial yfC_3S} = \frac{r_{CH-C_3S} \cdot (fS'_r \cdot r_{SCH} + fA_r \cdot r_{ACH})}{[fCH + fS'_r \cdot r_{SCH} + fA_r \cdot r_{ACH}]^2} \cdot \sigma_{fC_3S} \tag{49}$$

$$\frac{\partial r_r}{\partial yfC_2S} = \frac{r_{CH-C_2S} \cdot (fS'_r \cdot r_{SCH} + fA_r \cdot r_{ACH})}{[fCH + fS'_r \cdot r_{SCH} + fA_r \cdot r_{ACH}]^2} \cdot \sigma_{fC_2S} \tag{50}$$

$$\frac{\partial r_r}{\partial yfC_4AF} = \frac{-r_{CH-C_3AF} \cdot (fS'_r \cdot r_{SCH} + fA_r \cdot r_{ACH})}{[fCH + fS'_r \cdot r_{SCH} + fA_r \cdot r_{ACH}]^2} \cdot \sigma_{fC_4AF} \tag{51}$$

$$\frac{\partial r_r}{\partial yfC_r} = \frac{fCH \cdot r_{SCH} \cdot r_{CS}}{[fCH + fS'_r \cdot r_{SCH} + fA_r \cdot r_{ACH}]^2} \cdot \sigma_{fC_r} \tag{52}$$

$$\frac{\partial r_r}{\partial yfS_r} = \frac{-fCH \cdot r_{SCH}}{[fCH + fS'_r \cdot r_{SCH} + fA_r \cdot r_{ACH}]^2} \cdot \sigma_{fS_r} \tag{53}$$

$$\frac{\partial r_r}{\partial yfA_r} = \frac{-fCH \cdot r_{ACH}}{[fCH + fS'_r \cdot r_{SCH} + fA_r \cdot r_{ACH}]^2} \cdot \sigma_{fC_r} \tag{54}$$

Thus:

$$\sigma_{r_r} = \sqrt{\sum_{i=1}^6 \left( \frac{\partial r_r}{\partial y_i} \right)^2} \tag{55}$$

Where  $y_i = yfC_3S, yfC_2S, yfC_4AF, yfC_r, yfS_r, yfA_r$ , for  $i = 1, \dots, 6$ , respectively.

#### 4.4 Optimum Replacement of Fly Ash for Cement

Similarly from Eq. (30):

$$\frac{\partial r_f}{\partial yfC_3S} = \frac{r_{CH-C_3S} \cdot (fS'_f \cdot r_{SCH} + fA_f \cdot r_{ACH})}{[fCH + fS'_f \cdot r_{SCH} + fA_f \cdot r_{ACH}]^2} \cdot \sigma_{fC_3S} \quad (56)$$

$$\frac{\partial r_f}{\partial yfC_2S} = \frac{r_{CH-C_2S} \cdot (fS'_f \cdot r_{SCH} + fA_f \cdot r_{ACH})}{[fCH + fS'_f \cdot r_{SCH} + fA_f \cdot r_{ACH}]^2} \cdot \sigma_{fC_2S} \quad (57)$$

$$\frac{\partial r_f}{\partial yfC_4AF} = \frac{-r_{CH-C_3AF} \cdot (fS'_f \cdot r_{SCH} + fA_f \cdot r_{ACH})}{[fCH + fS'_f \cdot r_{SCH} + fA_f \cdot r_{ACH}]^2} \cdot \sigma_{fC_4AF} \quad (58)$$

$$\frac{\partial r_f}{\partial yfC_f} = \frac{fCH \cdot r_{SCH} \cdot r_{CS}}{[fCH + fS'_f \cdot r_{SCH} + fA_f \cdot r_{ACH}]^2} \cdot \sigma_{fC_f} \quad (59)$$

$$\frac{\partial r_f}{\partial yfS_f} = \frac{-fCH \cdot r_{SCH}}{[fCH + fS'_f \cdot r_{SCH} + fA_f \cdot r_{ACH}]^2} \cdot \sigma_{fS_f} \quad (60)$$

$$\frac{\partial r_f}{\partial yfA_f} = \frac{-fCH \cdot r_{ACH}}{[fCH + fS'_f \cdot r_{SCH} + fA_f \cdot r_{ACH}]^2} \cdot \sigma_{fC_f} \quad (61)$$

Thus:

$$\sigma_{r_f} = \sqrt{\sum_{i=1}^6 \left(\frac{\partial r_f}{\partial y_i}\right)^2} \quad (62)$$

Where  $y_i = yfC_3S, yfC_2S, yfC_4AF, yfC_f, yfS_f, yfA_f$ , for  $i = 1, \dots, 6$ , respectively.

## 5 Reliability Analyses

### 5.1 Linear Limit-State Functions

For a linear function of  $n$  random variables  $g(\underline{X})$  as in form of Eq. (40), the mean ( $\mu_g$ ) and the standard deviation ( $\sigma_g$ ) of a vector of normal variables  $X$  can be calculated from the equations below:

$$\mu_g = a_0 + \sum_{i=1}^n a_i \cdot \mu_{X_i} \tag{63}$$

$$\sigma_g = \sqrt{\sum_{i=1}^n a_i^2 \cdot \sigma_{X_i}^2} \tag{64}$$

Then the reliability index ( $\beta$ ) may be defined as:

$$\beta = \frac{\mu_g}{\sigma_g} \tag{65}$$

Thus the failure probability ( $p_f$ ) can be calculated from the equation below:

$$p_f = \Phi(-\beta) \tag{66}$$

Where  $\Phi(z)$  is the cumulative probability of the standard normal variable of a z-score. For more details about reliability analyses it is referred to Ouyornprasert (1988).

### 5.2 Nonlinear Limit-State Functions and Monte-Carlo Simulations

For general applications where the functions  $g(\underline{X})$  are nonlinear and/or random variables are non-normal, then the statistical representation of a limit-state function may be obtained by Monte-Carlo simulations as discussed earlier. However the failure probability may be estimated efficiently by Monte-Carlo simulations together with an advanced variance reduction technique such as Importance Sampling Technique as shown below:

$$p_f \cong \frac{1}{N} \sum_{j=1}^N I(g(\underline{x})) \cdot \frac{f_{\underline{X}}(\underline{x}_j)}{h_{\underline{Y}}(\underline{x}_j)} \tag{67}$$

Where  $N$  is the number of simulations,  $f_{\underline{X}}(\underline{x})$  is the joint probability density function,  $h_{\underline{Y}}(\underline{x})$  is an importance sampling density function,  $I(g(\underline{x}))$  is an indicator function whose value equals 1 when  $g(\underline{x}) \leq 0$  and equals 0 otherwise.

## 6 Mass Production of Precast Concrete

The statistical data of cement, rice husk as and fly ash available in hands showed significant variation. On one hand the mass production of precast products should be of optimum cost. On the other hand the products should be qualified for all specifications with pre-specified criteria. Therefore the statistical data should be analyzed in advance.

For a concrete cast of cement mixed with rice husk ash, the statistical data available of the materials are summarized in Table 5.

## 7 Discussion

For preliminary analyses all related variables are assumed uncorrelated and normally distributed. The optimum fractional replacement of cement by rice husk ash is 0.1777.

The long-term strength activity index of the optimum replacement of cement by rice husk ash is 1.4252. The uncertainty of the long-term strength activity index can be obtained by simple Monte-Carlo simulations. Goodness-Of-Fit tests revealed that the long-term strength activity index can be represented well by normal distribution. For optimum replacement of cement by rice husk ash only the long-term strength activity index based on 8192 simulations can be represented well by normal distribution with mean value and standard deviation = 1.1232 and 0.0113, respectively. The goodness of fit is shown in Fig. 29.

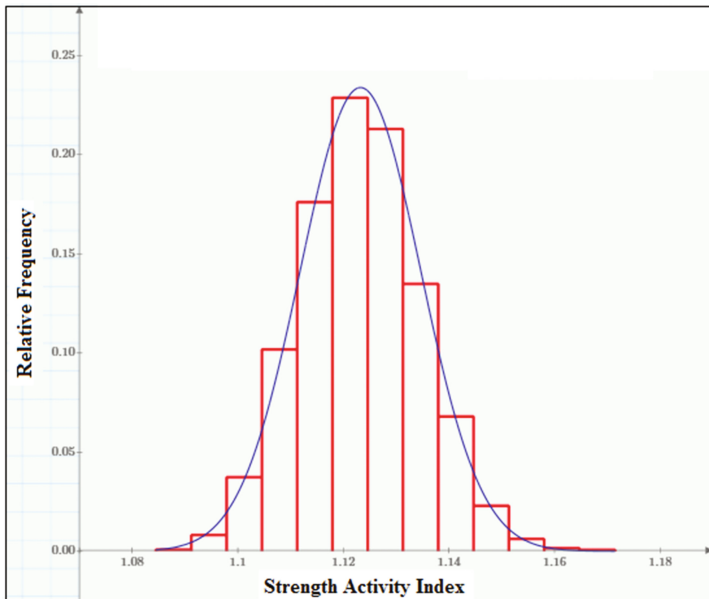


**Fig. 29.** Goodness-of-fit test (Chi-Square Error) for the optimum replacement of cement by rice husk ash

For the decision based on strength of the concrete the values of failure probability may play an important role. If the failure of the binder paste is defined as the value of the long-term strength activity index less than 1.1 (see Fig. 30), then the value of failure probability can be estimated. It can be seen from Eq. (31) that the cross multiplication for  $SAI = 1.1$  and forming the limit-state function from the difference of both sides of

the equation, then the limit-state function is linear in term of related random variables. Since all these variables are assumed normally distributed, then the reliability index and the corresponding value of failure probability can be obtained easily by using Eqs. (65) and (66), respectively. In other cases the Monte-Carlo simulations together with an Importance Sampling technique may be applied.

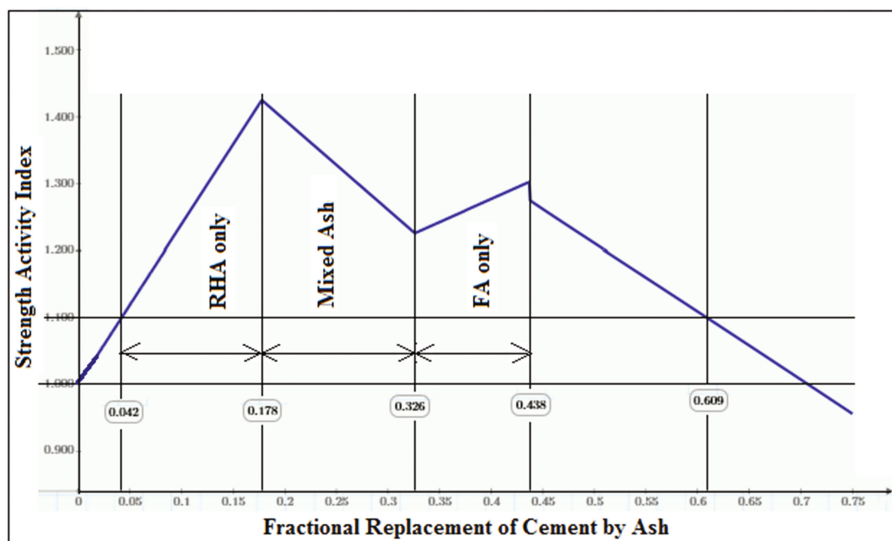


Fig. 30. Range of suitable fractional replacement of cement by rice husk ash and fly ash

For this particular case the reliability index (Fig. 30) and the value of failure probability for the optimum replacement of cement by rice husk ash are 2.021 and  $\Phi(-2.021) = 2.165 \times 10^{-2}$ , respectively. Theoretically SAI of the optimum replacement should yield the maximum SAI. Since the failure probability in term of SAI is very low for this particular case, a higher or lower value of replacement of cement by rich husk ash might be possible so that products could be qualified for all specifications.

Once this optimum replacement of cement by rice husk ash = 0.1777 is selected, then the propagation of uncertainty in terms of optimum ratio should be also considered. The corresponding standard deviation of this ratio is 0.0035. Again if the ratio is assumed normally distributed, then the interval of the applied ratio should be [0.1708,0.1846] with the confidence interval 95% ( $0.1777 \pm 1.96 \times 0.0035$ ). The more precise conclusion may be, again, estimated from Monte-Carlo Simulations and Goodness-Of-Fit tests.

The reliability indices based on long-term SAI = 1 within the range of partial replacement of cement by mixed ash of rice husk ash and fly ash were in the close interval of [0.753,10.862] and the corresponding values of failure probability were in the close interval of [ $8.75 \times 10^{-28}$ ,  $2.26 \times 10^{-1}$ ]. The relationship between the reliability index and the fractional replacement of cement by mixed ash was shown in Fig. 31.

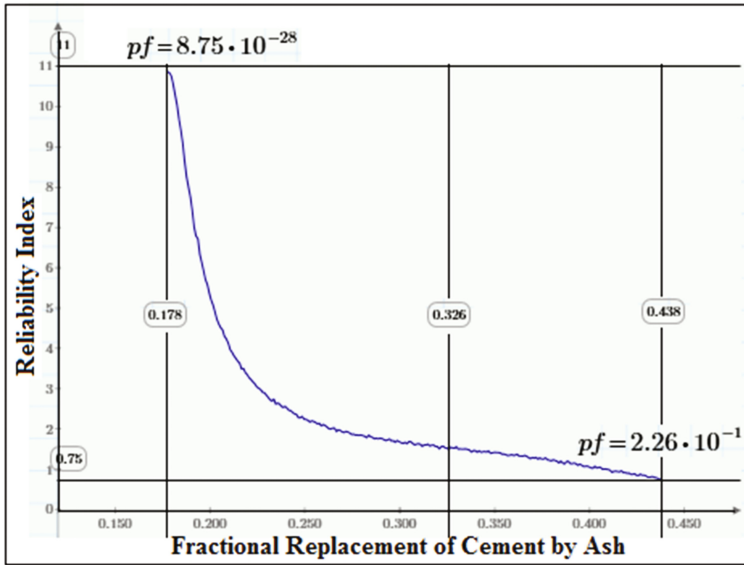


Fig. 31. Reliability index in the range of mixed ash of rice husk ash and fly ash

## 8 Conclusions

- (1) Hydration of main chemical compositions of cement and pozzolanic reactions of minerals in rice husk ash and fly ash were reviewed. Data necessary for stoichiometry of hydration- and pozzolanic reactions were also given,
- (2) Formula for the optimum replacement of cement by rice husk ash and fly ash based on the complete consumption of calcium hydroxide from hydration of cement was derived,
- (3) The long-term strength activity index (*SAI*) for the age of 360 days based on equivalent calcium silicate hydrate was proposed and the *SAI* diagrams could be constructed,
- (4) The strength activity index at any age could be modeled based on nano-structures depending on the  $\text{CaO}/\text{SiO}_2$  ratio and the scenario of *SAI* diagrams could be seen.
- (5) The proposed *SAI* diagrams were verified by a series of tests for specimens of mortars mixed with silica fume, rice husk ash and fly ash carried out by the authors, and were validated by results by other researchers. It should be noted that the proposed model was based on main chemical compositions in cement and ash only. Although other factors such as engineering properties of ash, heat evolution of hydration, relative mean particle size of cement to that of ash, type and dose of superplasticizer etc. showed influences on *SAI*, they were out of the scope of this technical paper. However they should be included in the refined models in the authors' prospective research projects.

- (6) The propagation of uncertainty of the partial replacement of cement by rice husk ash and fly ash in term of variation of main chemical compositions in cement and rice husk ash and fly ash were formulated.
- (7) Reliability analyses for utilizing the optimum replacement of cement by rice husk ash and fly ash were reviewed,
- (8) The applicability of the proposed concepts was demonstrated based on statistical data of materials available in hands,
- (9) All the concepts mentioned above could be extended to one other type of pozzolan as well as mixed pozzolan.

**Acknowledgments.** Full financial support and Granting a Professional License of Software Mathcad Prime for calculation throughout the authors' research projects by Asia Group (1999) Company Limited was cordially acknowledged.

## References

- Bogue, R.H.: Chemistry of Portland Cement. Reinhold, New York (1955)
- Chansawang, S., Ouypornprasert, W.: Rate of pozzolanic reactions of rice husk ash and fly ash. Intl. J. Mater. Struct. Reliab. (2017, Submitted for publication)
- Chatveera, B., Nimityongskul, P.: Influence of artificial pozzolanas on mechanical behavior of high strength concrete, Khonkaen Univ. J. Eng. **21** pp. 59–71 (1994a). (in Thai)
- Chatveera, B., Nimityongskul, P.: Portland cement containing rice husk ash, fly ash and superplasticizer. Suranaree J. Sci. Technol. **1**, 109–122 (1994b)
- Dumrongsil, S., et al.: Stiochiometry of pozzolanic reaction. J. Res. Training Rajmangala Inst. Technol. **4**(1), 28–34 (2000)
- Habeeb, G.A., Mahmud, H.B.: Study on properties of rice husk ash and its use as cement replacement material. Mat. Res. **13**(2), 185–190 (2010)
- James, J., Rao, M.S.: Reactivity of rice husk ash. Cement Concr. Res. **16**(3), 296–302 (1986)
- Jaturapitakkul, C., et al.: A study of strength activity index of ground coarse fly Ash with Portland cement. ScienceAsia **25**, 223–229 (1999)
- Kamollertvara, K., Ouypornprasert, W.: Determination of mean values of common distributions in civil engineering from the specifications for mass production. In: The Proceedings of the 7th International Conference on Engineering and Technology ICET-2015, Phuket, 19–20 June 2015, pp. 1-4. Prince of Songkla University, Faculty of Engineering, Hat Yai, Songkhla (2015)
- Kamollertvara, K., et al.: Statistical analyses of optimum partial replacement of cement by rice husk ash based on complete consumption of calcium hydroxide. In: The Proceedings of RSU International Research Conference 2016, Pathumthani (2016)
- Khalil, N.M., et al.: Beneficiation of the huge waste quantities of barley and rice husks as well as coal fly ashes as additives for Portland cement. J. Ind. Eng. Chem. **20**, 2998–3008 (2014)
- Ku, H.H.: Notes on the use of propagation of error formulas. Natl. Bureau Stand. **70C**(4), 262 (1966)
- Langan, B.W., et al.: Effect of silica fume and fly ash on heat of hydration of Portland cement. Cem. Concr. Res. **32**, 1045–1051 (2002)
- Le, H.T., Ludwig, H.M.: Effect of rice husk ash and other mineral admixtures on properties of self-compacting high performance concrete. Mater. Des. **89**, 156–166 (2016)



- Nawaz, A., et al.: Effect and limitation of free lime content in cement-fly ash mixtures. *Constr. Build. Mater.* **102**, 515–530 (2016)
- Ouypornprasert, W.: Methods to calculate structural reliability, Internal Working Report No.18 – Institute of Engineering Mechanics, University of Innsbruck, Austria (1988)
- Ouypornprasert, W.: Goodness-of-fit tests for common continuous distributions in civil engineering. In: *Proceedings of the International Conference on Computational Mathematics and Modeling (CMM-2002)*, 22–24 May 2002, pp. 117–126. Mahidol University and Curtin University of Technology, Century Park Hotel, Bangkok (2002)
- Ouypornprasert, W., et al.: Statistical analyses of optimum partial replacement of cement by fly ash based on complete consumption of calcium hydroxide. In: *The Proceedings of the International Conference of Advanced Engineering and Technology (ICAET2016)*, Bhai Gurdas Institute of Technology, Sangrur, Punjab, India (2016)
- Ouypornprasert, W., et al.: The use of rice husk ash and fly ash for partial replacement of cement for mass production of precast concrete products. Internal Working Report No.20 - Asia Research, Development and Innovation Center, Asia Expansion Concrete Product (1993) Co. Ltd., Bangkok (2017)
- Över, D.: Early heat evolution in natural pozzolan incorporated cement hydration. In: partial fulfillment of the requirements for the degree of Master of Science in Civil Engineering Department, Middle East Technical University (2012)
- Qing, Y., et al.: Influence of nano-SiO<sub>2</sub> addition on properties of hardened cement paste as compared with silica fume. *Constr. Build. Mater.* **21**, 539–545 (2007)
- Skinner, B., et al.: Nanostructure of CSH in cement. *Phys. Rev. Letters* **104**(19), 195502 (2010)
- Taylor, H.F.W.: *Cement chemistry*. J. Am. Ceram. Soc. **69**, 614–618 (1986)
- Taylor, H.F.W.: *Cement Chemistry*, 2nd edn. Thomas Telford Publishing, Thomas Telford Services Ltd., London (1997)
- Tokyay, M., et al.: Granüle Yüksek Fırın Cürufu, Tras ve Kalker İçeren Çimentolarda Mineral Katkı Türü, Öğütme Yöntemi ve Çimento İnceliğinin Hidratasyon Isısına Etkilerinin Araştırılması. vols. AR-GE 2010/01-A. Turkish Cement Manufacturers Association, Ankara, Turkey (2010)

# Freeze-Thaw Durability of Air-Entrained Concrete Incorporating Natural and Recycled Concrete Aggregate Mixtures

Prabir K. Kolay<sup>(✉)</sup>, Salman Sulaiman, Sanjeev Kumar,  
and Vijay K. Puri

Civil and Environmental Engineering Department,  
Southern Illinois University Carbondale,  
1230 Lincoln Drive, MC 6603, Carbondale, IL 62901, USA  
pkolay@siu.edu

**Abstract.** The present study investigates the effect of natural aggregate (NA) and recycled concrete aggregate (RCA) in concrete mixture on Freeze-Thaw (F-T) durability. Freeze-thaw action is considered to be one of the most destructive actions that can cause significant damage to concrete pavement structures. To check the F-T durability; various physical, chemical, mechanical properties test has been conducted on the virgin or natural aggregate (NA) and recycled concrete aggregate (RCA) collected from Illinois. The aggregate resistance for degradation has been measured by using micro-deval and sulphate resistance test. The F-T durability of standard concrete mix using various percentages of NA and RCA has been investigated with or without air-entraining admixtures (AEA). The internal damage of the concrete due to rapid freeze-thaw (F-T) has been evaluated by comparing the relative dynamic modulus (RDM) of elasticity of a specimen at the lab, after a specific amount of F-T exposure, to the dynamic modulus test prior to the start of F-T exposure. The results show that concrete sample prepared with air-entrains agent survived more number of F-T cycles and also concrete prepared using RCA samples shows better durability than NA.

## 1 Introduction

Construction Materials Recycling Association (CMRA) estimated that approximately 127 million tonnes of concrete recovered annually from the waste in USA (CMRA 2011). It also raises a concern in the depletion of non-renewable natural resources Ortiz et al. (2009). These concerns have encouraged researchers to study the possible potentials of recycled and demolished concrete materials to replace natural aggregates for construction purposes. Recycled crushed concrete may be used as aggregate in many applications, including new Portland cement concrete (PCC) pavement, bituminous concrete, lean-concrete or concrete bases, pavement sub-bases, roadway shoulder material, bulk fill for drainage layers, rip-rap for erosion control, and bedding for utilities trenches (Yrjanson 1989; Recycling Concrete and Masonry 1999; Chini and Monteiro 1999). According to the Federal Highway Administration (FHWA), 41 states in US uses recycle concrete as aggregate in new construction, primarily in base

applications (Gonzales and Moo-Young 2004). Out of these states, however, only 11 are reported as using Recycled Concrete Aggregate (RCA) in new Portland cement concrete (PCC).

According to Amorim et al. (2012) it is believed that with all other factors being equal, concrete made with natural aggregates will perform better than concrete made with recycled aggregates. Hansen and Narud (1983), Li (2008) reported that using recycled aggregates in concrete affects the durability of the concrete more than its mechanical properties. Durability of concrete is the ability of a construction material to withstand chemical attacks, actions due to abrasion or weathering or other processes of deterioration. When subjected to cyclic freeze-thaw, concrete possess the ability to deteriorate as the cycle increases. According to the American Concrete Institute (ACI), weather is considered cold if the temperature of three successive days falls below 40°F. This is a concern for in colder region of the world when using concrete because continuous deterioration increases surface scaling in the concrete that eventually leads to total collapse of structures. There has been concerning questions regarding the freeze-thaw durability of recycled aggregate concrete due to the varying difference in the quality and composition of crushed concrete. A research by Buck (1977) reported that the resistance of concrete containing recycled concrete aggregates having chert gravel as the original concrete increases the freeze-thaw resistance that could be due to the reduction of frost susceptibility of porous aggregates particles. Yemato et al. (1988) determined the freeze-thaw resistance of concrete made with recycled aggregates and concluded that the freeze-thaw resistance of concrete with recycled aggregates is lower than that of concrete made with natural aggregates. Kawamura and Torri (1988) carried out an investigation on the disintegrated surface of concrete made with frost susceptible RCA subjected to freeze-thaw. They found out that the deterioration due to freeze-thaw occurred within the adhered mortar. Hosokawa et al. (1997) determined the effect of adhered mortar content of RCA on the freeze-thaw durability of concrete and found out there was no significant effect of the adhered mortar on the freeze-thaw resistance. It is believed that addition of air entraining admixtures helps in increasing the freeze-thaw resistance of concrete. Richardson (2006) reported that air entrained concrete is 76 times more effective than plain cement concrete. According to America's Cement Manufacturers, the freeze-thaw resistance of concrete in moist condition was made better by intentionally entrained air. However, according to Shang and Yi (2013), very little work has been documented on the freeze-thaw durability of concrete.

Hence, the purpose of this study is to characterize natural coarse aggregate (NCA) and recycled concrete aggregate (RCA) obtained from old concrete pavement and replaced with various percentages of natural aggregate (by percent weight) to ascertain their suitability for freeze-thaw durable concrete. Tests were carried out on the RCA to determine whether it can be used for concrete mix design and durable concrete resistance to free-thaw. The durability parameter of the recycled aggregates was determined to ascertain the long-term strength of the aggregates on exposure to sodium sulfate and rapid freezing and thawing temperatures, and their resistance to Micro-Deval abrasion. The compressive strengths of concrete at different curing periods (i.e., 7, 14, and 28 days) were investigated for concrete mixes consisting of the replacement of conventional or natural coarse aggregate with coarse RCA at replacement percentages ranging from 20, 40, 60, 80, and 100%.

## 2 Materials and Description

In this study, the cementitious material used was a QUIKRETE Portland cement Type I/II. The physical properties of the Portland cement used in the present study are presented in Table 1.

**Table 1.** Physical properties of QUIKRETE Portland cement type I/II

Property	Description or Value
Appearance	Gray to gray-brown colored powder. Some products available in white and other colors
Specific gravity	2.6 to 3.15
Melting point	>2700° F
Boiling point	>2700° F
Vapor pressure	Not applicable
Vapor density	Not applicable
Evaporation rate	Not applicable
Solubility in water	Slight
Odor	Not applicable

## 3 Natural Coarse Aggregates and Recycled Concrete Aggregates

The Natural Coarse Aggregates (NCA) used in this research is a class CA 11 material with size ranging from 4.75 to 19 mm. The aggregate was produced by crushing limestone rock and was obtained from Anna Quarry in Southern Illinois, USA.

The Recycled Concrete Aggregates (RCA) used in this research was produced from demolished road pavement. It was obtained from Marion Excavating and Construction Inc., Marion, recycling plant in Southern Illinois. The demolished concrete pavement is transported to the recycling plant where it is crushed into different sizes of RCA. The sizes of the RCA used ranges from 0 to 25 mm.

## 4 Admixtures

The admixture used in this study was an Air Entraining Admixture (AEA). The AEA used was Polychem VRC from GRT, Inc. Admixtures manufacturer. The suggested dosage (recommended by the manufacturer) is 1/8 to 3 fl.oz per 100 lbs of cement. The properties of the AEA used in this study is presented in Table 2.

**Table 2.** Physical properties of polychem VRC

Property	Description and values
Physical state	Liquid
Appearance and color	Dark Green
pH	12.0
Melting point/Freezing point	N.A.
Relative density ( $\text{g}/\text{cm}^3$ )	1.06
Solubility in water	N.A.

## 5 Tests and Characterization of Aggregates

In this study, various tests have been performed using ASTM standard methods. Moisture content of the aggregates were determined in accordance with the ASTM C566-13 (2013) standard. The sieve analysis of the RCA, NCA and natural fine aggregates were determined using the ASTM C136/C136M-14 (2014) standard. The gradation analysis was then compared to the upper and lower limit of the ASTM standard for aggregate in concrete mix.

## 6 Specific Gravity and Absorption

The specific gravity and absorption of coarse aggregates were conducted using the procedure mentioned in ASTM C127-12 standards.

The specific gravity and absorption of fine aggregates were conducted using the procedure mentioned in ASTM C128 standards. The cone method was used to check if the sample has attained SSD (Saturated Surface Dry) condition. In this method, a cone mold was placed on a flat surface and filled with the aggregates until it over flows. Then the cone was lifted after 10 drops of tamping. When the fine aggregates reach SSD condition, the aggregates will slump but if it doesn't the sand will attain the shape of the cone mold.

## 7 Micro-Deval Degradation

This test was used to determine the ability of RCA and NCA to resist abrasion like studded tire damage. This test was carried out in accordance with the ASTM D6928 standards.

## 8 Concrete Mix Design

In present study, the concrete consisted of five components which are: cement, fine aggregates, coarse aggregates (i.e., natural and recycled), water and air entraining admixture (AEA) i.e., Polychem VCR. In this study, the Illinois Department of Transportation (IDOT) method of mixing concrete was used. At first starting with

100% natural coarse aggregates followed by 20, 40, 60, and 80% replacement (by weight) with recycled concrete aggregates. An Excel Spreadsheet template was used in designing the concrete mix. The variables used to calculate quantity of various aggregates were: specific gravity and absorptions, water to cement (w/c) ratio, cementation factor, fineness modulus of fine aggregates and volume of air entraining admixture. A cement factor of 6 bags (564 lb) per cubic yard was used for all the batches mixed. Batches of concrete were prepared by replacing the natural aggregates with recycled concrete aggregates at 20, 40, 60, and 80% (by weight) without air entraining admixture (AEA) and then repeated the same combination with air entraining admixture (AEA). The compressive strength of various concrete mixes was determined after 7, 14, and 28 days of curing period and the freeze-thaw durability test was conducted after 28 days of curing period. A constant water to cement (w/c) ratio of 0.45 was used in this study.

## 9 Slump and Air Content

The slump test was carried out in accordance with the ASTM C143 standards to determine the workability of the fresh concrete.

The air content test was performed to determine the amount of air voids in the mixed concrete. The test was carried out in accordance with the ASTM C231/C231M-14 (2014) standards.

## 10 Curing

Each batch of concrete mix was molded into cylindrical and beam samples in accordance with ASTM C192 standard. Cylindrical molds and beam molds were used to prepare the specimens. The dimensions of the cylindrical molds were 8 in. height and 4 in. diameter. For the beams, the dimensions were 4 in. × 3 in. × 16 in. The samples were prepared by placing fresh concrete immediately after mixing in the mold. The concrete is placed in three layers 1/3 each by volume. All the layers are rodded 25 times to ensure even distribution and the outside of the mold tapped 10 to 15 times. A trowel was then used to smoothen and even the surface. The samples were stored in a flat surface for 24 h at room temperature. The samples are demolded after 24 h and stored in a curing tank containing water at a room temperature of  $73 \pm 3.5^\circ\text{F}$ .

## 11 Compressive Strength

The compressive strength tests were performed on samples in accordance with the ASTM C39/C39M standards. Cylindrical samples at different curing period (i.e., 7, 14, and 28 days) were removed from the curing tank and kept in a moist condition.

## 12 Freeze-Thaw Resistance

Freeze-thaw resistance was carried out on concrete beam samples to check the durability of the concrete. In this study, the tests were carried out in accordance with the ASTM C666/ C666M-15 (2015) standards. The beams for the freezing and thawing were cured for 28 days as opposed to the ASTM standard of 14 days to that the samples could gain more strength. The mass, transverse frequencies, and effective length of the beams were recorded. The samples were then placed into a container with two metal rods underneath to ensure water touches all part of the sample.

The temperature of the freeze-thaw chamber was set to lower temperature from 40 to 0°F and rise from 0 to 40°F as recommended by ASTM C666 standard. After an approximately every 30 to 36 cycles, the specimens were removed from the chamber and the length change, mass change and transverse frequencies (RDM, Relative Dynamic Modulus) were checked.

## 13 Results and Discussions

In this study, sieve analysis was performed for both RCA and NCA samples. The results obtained were compared to each other and checked to see if they conform to the ASTM specifications. Results obtained for the fine aggregate is shown in Fig. 1. The result of sieve analysis for the coarse aggregates mixes (i.e., various percentage of NAC and RCA) used in this study are shown in Fig. 2. It can be observed that both RCA and NCA did not fall within the range specified by ASTM.

The apparent specific gravity of NCA and RCA found to be 2.71 and 2.67, respectively. The apparent specific gravity of RCA is 1.0% lower than that of NCA. The

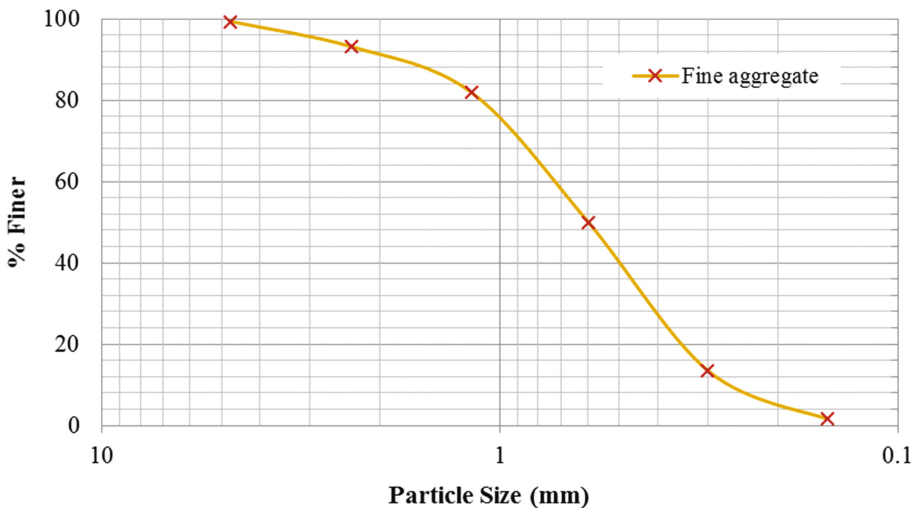


Fig. 1. Sieve analysis of fine aggregate

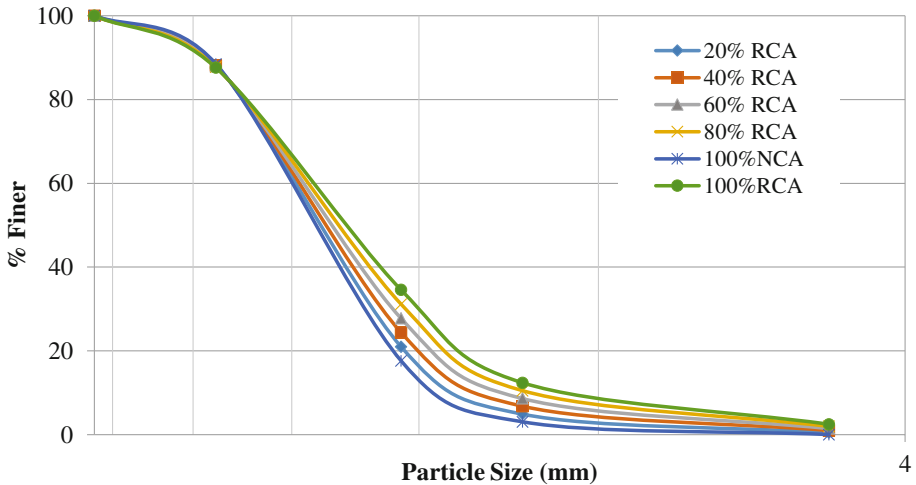


Fig. 2. Sieve analysis of different mix of RCA and NCA

apparent specific gravity obtained for the RCA falls outside the range reported by a few researchers. ACPA (2009) reported ranges of specific gravity between 2.1–2.4. Poon et al. (2004) reported ranges between 2.33–2.37 and Kou et al. (2007) 2.49–2.57. The bulk specific gravity (Oven Dry, OD) obtained, 2.64 for NCA and 2.37 for RCA also falls between the values reported by Gomez-Soberon (2002) for both RCA and NCA. He reported a value of bulk specific gravity (OD) that ranges between 2.59–2.67 for NCA and 2.35–2.42 for RCA. The bulk specific gravity (Saturated Surface Dry, SSD) of NCA, 2.67 and RCA 2.49 also fall in the range reported by Abbas et al. (2009) i.e., 2.71–2.74 for NCA and 2.42–2.5 for RCA.

The absorption value for NCA sample was found to be 0.98%. The absorption value for RCA sample obtained was 4.76%, which is almost 5 times greater than that of NCA. This falls within the range in a study by Limbachiya (2004). The reported absorption of RCA to be 3–5 times more than that of NCA. IDOT Bureau of Materials and Physical Research (2012) suggests that the specific gravity and absorption of aggregates shouldn't be used in determining the acceptability of construction aggregates but recommends using it in determining the design of Portland cement concrete.

The result of the Micro-Deval degradation test for NCA and RCA are 11.3% and 18.2%, respectively. Both Micro-deval abrasion loss can be said to be within the acceptable range specified by TRB (Transportation Research Board), which is  $\leq 18\%$ . A report by Gabr and Cameron (2011) reported a 28% and 30% Micro-deval loss for RCA from two different sources. Another research by Butler et al. (2011) also reported a 15.1% and 11.9% Micro-deval abrasion loss for RCA from two different sources.

In this study, the Portland cement concrete was made using NCA and RCA with and without AEA. The NCA is replaced in various percentages with RCA. The properties of the fresh or plastic state concrete were recorded by a slump test and checking the air content. The hardened concrete was also studied checking its compressive strength after



7, 14 and 28 days of curing. The development of compressive strength for various mix for without and with AEA are shown in Figs. 3 and 4, respectively.

From Figs. 3 and 4, it can be noticed that replacement of Natural Coarse Aggregates with Recycled Concrete Aggregates in Portland cement concrete caused a reduction in compressive strength of the concrete. In this study, an approximately 5, 6, 8, 10 and 11% reduction in compressive strength for 28 days was noticed when the NCA is replaced with 20, 40, 60, 80 and 100% RCA, respectively in the Portland cement concrete mix. Akentuna (2013) reported a 28-day compressive strength loss of 4, 5, 9, 11, 11 and 13% in concrete when the NCA in the concrete is replaced with 10, 20, 30, 40, 60 and 80% of RCA, respectively. A report by Yemato et al. (1998) showed a 20, 30, and 45% decrease in compressive strength of concrete with NCA replaced at 20, 30 and 50%, respectively. Also, a report by Buck (1977) showed a 20% reduction in compressive strength for concrete made with a 100% RCA. It can be observed from Figs. 3 and 4 that the compressive strength development of concrete without air entraining admixture and with air entraining admixture, respectively showed the same trend.

Figure 5 shows the loss of RDM with increase in number of freeze-thaw cycles for all samples tested. The samples with air entraining admixtures were found to perform better in freeze-thaw resistance. From Fig. 5, it can be noticed that all the concrete mix without air entrainment agent didn't last for more than 150 cycles. However, concrete mix with air entraining admixtures lasted even past 300 cycles. Shang and Yi (2013) reported that the RDM of concrete decreases slowly as the amount of air entrainment is increased. Li-Kun (2003) also concluded that for conventional concrete, the RDM reduces to about 62% after 100 cycles. Gokce et al. (2004) investigated at a

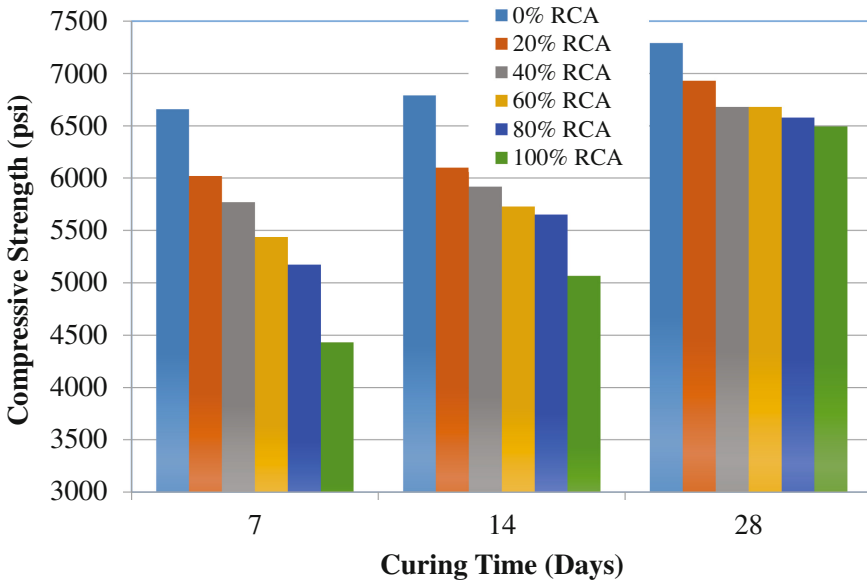


Fig. 3. Compressive strength of various proportion concrete mix without AEA

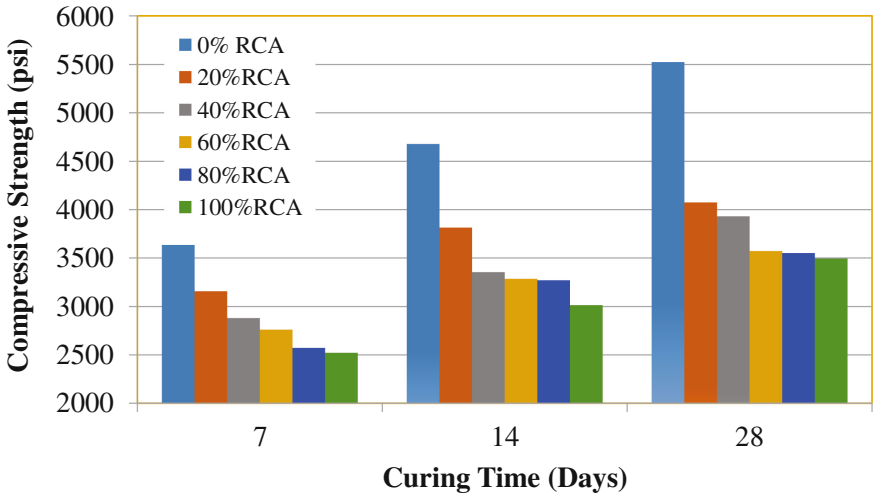


Fig. 4. Compressive strength for various proportion of concrete mix with AEA

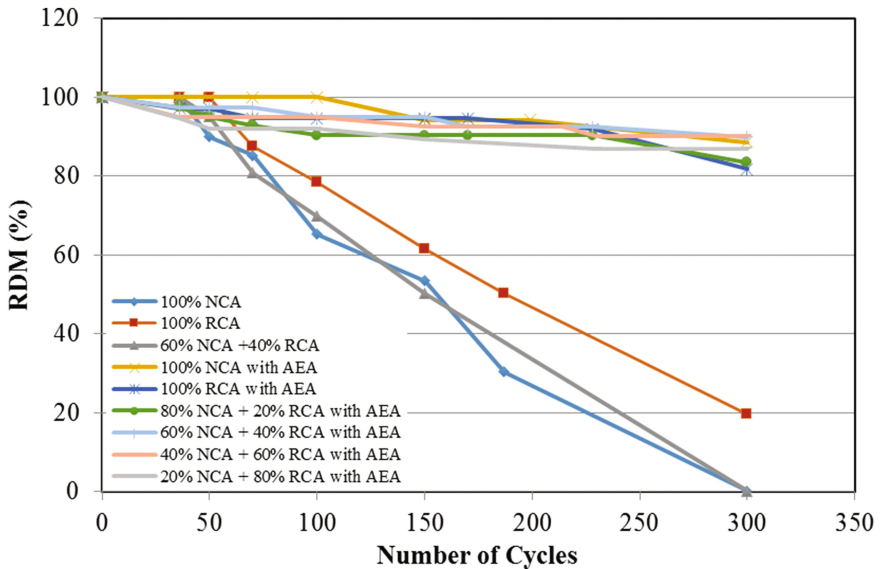


Fig. 5. RDM loss for various concrete mix with number of Freeze-Thaw cycles

microscopic level to determine the damage mechanism for concrete produced with non-air entrained RCA. They also found that the damaged adhered mortar with severe cracks causes the disintegration of the RCA and the damaged particles act as defects which distresses the new mortar hence causing the concrete to fail.

## 14 Conclusions

The present study characterizes natural coarse aggregate (NCA) and recycled concrete aggregate (RCA) and RCA replaced with various percentages of NCA (by percent weight) to ascertain their suitability in Portland cement concrete mix and freeze-thaw durable concrete. It also studies the effect of adding air entraining admixtures (AEA) to the durability mainly freeze-thaw property of Portland cement concrete. Based on the experimental investigation conducted at laboratory following conclusion can be made:

1. The grading characteristics of both coarse aggregates i.e., the NCA and RCA used did not meet the ASTM specifications. However, the fine aggregate conforms to the ASTM specifications. Coarse aggregates should be sieved so as to get rid of fine particles to meet the right specifications.
2. Specific gravity of the NCA and RCA were higher compared to IDOT specifications. The absorption for NCA is found to be lower than the IDOT specifications while that of RCA is higher than specified.
3. The Micro-Deval abrasion loss of RCA was found to be higher than that of NCA. However, the RCA meets the ASTM standards. The high abrasion loss by RCA can be attributed to presence of adhered mortar.
4. Replacement of NCA with RCA in concrete resulted in decrease workability of fresh concrete and increase in the air content of the concrete. The compressive strength of the concrete reduced as replacement of NCA with RCA increases.
5. All concrete mix showed considerable amount of compressive strength gain from 7 to 28 days of curing.
6. Samples without air entraining admixture (AEA) deteriorated severely before 150 cycles of freezing and thawing. Therefore, addition of air entrainment agent in Portland cement concrete is effective in reducing the weight loss and loss RDM of the concrete under increasing cycles of freezing and thawing. However, it is important to note that the addition of air entraining agent also reduced the compressive strength of the concrete.

**Acknowledgments.** Authors are thankful to Mr. Jerry Barras from Marion Excavating, Marion, Illinois, for providing the recycled aggregate samples.

## References

- Abbas, A., Fathizal, G., Isgor, O.B., Razaqpur, A.G., Fournier, B., Foo, S.: Durability of recycled aggregate concrete designed with equivalent mortar volume method. *Cement and Concrete Composites* (2009). doi:[10.1016/j.cemconcomp.2009.02.012](https://doi.org/10.1016/j.cemconcomp.2009.02.012)
- ACPA (American Concrete Pavement Association): *Recycling Concrete Pavement*. Engineering Bulletin, vol. 84 (2009)
- Akentuna, M.: *Characterization and utilization of Recycled Aggregates (RCA) for road pavement work*. M.S. Thesis, Southern Illinois University, Civil and Environmental Engineering, Carbondale, USA (2013)

- Amorim, P., de Brito, J., Evangelista, L.: Concrete Made with coarse concrete aggregate: influence of curing on durability. *ACI Mater. J.* **109**(2), 195–204 (2012)
- ASTM C136/C136M-14: Standard test method for sieve analysis of fine and coarse aggregates. In: *Annual Book of ASTM Standards*, Vol. 04.02, West Conshohocken, PA (2014)
- ASTM C231/C231M-14: Standard test method for air content of freshly mixed concrete by the pressure method. In: *Annual Book of ASTM Standards*, vol. 04.02 (2014)
- ASTM C566-13: Standard test method for total evaporable moisture content of aggregate by drying. In: *Annual Book of ASTM Standards*, vol. 04.02, West Conshohocken, PA (2013)
- ASTM C127-12: Standard test method for density, relative density (specific gravity), and absorption of coarse aggregate. In: *Annual Book of ASTM Standards*, vol. 04.02, PA (2012)
- ASTM C143/C143M-12: Standard Test Method for Slump of Hydraulic-Cement Concrete, *Annual Book of ASTM Standards*, vol. 04.02, West Conshohocken, PA (2012)
- ASTM C192/C192M-12a: Standard practice for making and curing concrete test specimens in the laboratory. In: *Annual Book of ASTM Standards*, vol. 04.02 (2012)
- ASTM C39/C39M-15a: Standard test method for compressive strength of cylindrical concrete specimens. In: *Annual Book of ASTM Standards*, vol. 04.02 (2015)
- ASTM C666/C666M-15: Standard test for resistance of concrete to rapid freezing and thawing. In: *Annual Book of ASTM Standards*, vol. 04.02 (2015)
- ASTM D6928-10: Standard test method for resistance of coarse aggregate to degradation by Abrasion in the Micro-Deval Apparatus. In: *Annual Book of ASTM Standards*, vol. 04.03 (2010)
- Buck, A.: Recycled concrete as a source of aggregate. *ACI Matter* **74**(5), 212–219 (1977)
- Butler, L., West, J.S., Tighe, S.L.: The Effect of Recycled Concrete Aggregate Properties on the Bond Strength between RCA Concrete and Steel Reinforcement. *Cement and Concrete Research* (2011). doi:[10.1016/j.cemconres.2011.06.004](https://doi.org/10.1016/j.cemconres.2011.06.004)
- Chini, A.R., Monteiro, F.: Use of recycled concrete aggregate as a base course. In: *Proceedings of the Associated School of Construction* (1999)
- CMRA: Construction Materials Recycling Association (2011). <http://www.concreterecycling.org>. Accessed 15 Dec 2016
- Gabr, A.R., Cameron, D.A.: Properties of recycled concrete aggregate for unbound pavement construction. *J. Mater. Civ. Eng.* (2011). doi:[10.1061/\(ASCE\)MT.1943-5533.0000447](https://doi.org/10.1061/(ASCE)MT.1943-5533.0000447)
- Gokce, A., Nagataki, S., Saeki, T., Hisada, M.: Freezing and thawing resistance of air-entrained concrete incorporating recycled coarse aggregate: the role of air content in demolished concrete. *Cement Concr. Res.* (2004). doi:[10.1016/j.cemconres.2003.09.014](https://doi.org/10.1016/j.cemconres.2003.09.014)
- Gomez-Soberson, J.M.: Porosity of recycled concrete with substitution of recycled concrete aggregate and experimental study. *Cement Concr. Res.* (2002). doi:[10.1016/S0008-8846\(02\)00795-0](https://doi.org/10.1016/S0008-8846(02)00795-0)
- Gonzales, G., Moo-Young, H.: *Transportation Applications of Recycled Concrete Aggregate. FHWA State of the Practice National Review*, Washington, D.C. (2004)
- Hansen, T., Narud, H.: Strength of recycled concrete made from crushed concrete coarse aggregate. *Concr. Int.* **5**(1), 79–83 (1983)
- Hosokawa, Y., Maeda, N., Hayasaka, T.: Influence of the time of removing mortar from recycled coarse aggregate on the properties of concrete products using recycled coarse aggregate from waste concrete. In: *Proceedings of CSCE/JSCE International Conference on Engineering Materials*, 775–788 (1997)
- Kawamura, M., Torii, K.: Reuse of recycled concrete aggregate for pavement. In: *Proceedings of the Second International Symposium (RILEM) on Demolition and Reuse of Concrete and Masonry*, vol. 2, pp. 726–735 (1988)

- Kou, S.C., Poon, C.S., Chan, D.: Influence of fly ash as cement replacement on the properties of recycled aggregate concrete. *J. Mater. Civ. Eng.* (2007) doi:[10.1061/\(ASCE\)0899-1561\(2007\)19:9\(709\)](https://doi.org/10.1061/(ASCE)0899-1561(2007)19:9(709))
- Li, X.: Recycling and reuse of waste concrete in china: part i. material behaviour of recycled aggregate concrete. *Resour. Conserv. Recycl.* (2008) doi:[10.1016/j.resconrec.2008.09.006](https://doi.org/10.1016/j.resconrec.2008.09.006)
- Li-Kun, Q.: Study on the strength and deformation of concrete under multiaxial stress after high-temperature of freeze-thaw cycling. Ph.D. Thesis, Dalian University of Technology Liaoning, China (2003)
- Limbachiya, M.C.: Performance of recycled aggregate concrete. In: *International Symposium of Environmental - Conscious Material and System for Sustainable Development*, pp. 127–136 (2004)
- Ortiz, O., Castells, F., Sonnemann, G.: Sustainability in the construction industry: a review of recent developments based on LCA. *Constr. Build. Mater.* (2009). doi:[10.1016/j.conbuildmat.2007.11.012](https://doi.org/10.1016/j.conbuildmat.2007.11.012)
- Poon, C.S., Shui, Z.H., Lam, L., Fok, H., Kou, S.C.: Influence of moisture states of natural and recycled aggregates on the slump and compressive strength of concrete. *Cement Concr. Res.* (2004). doi:[10.1016/S0008-8846\(03\)00186-8](https://doi.org/10.1016/S0008-8846(03)00186-8)
- Recycling Concrete and Masonry: Publication EV 22. Environmental Council of Concrete Organizations, Skokie, IL (1999). <http://www.ecco.org/pdfs/ev22.pdf>. Accessed 15 Apr 2005
- Richardson, A.E.: Compressive strength of concrete with polypropylene fibre additions. *Struct. Surv.* (2006). doi:[10.1108/02630800610666673](https://doi.org/10.1108/02630800610666673)
- Shang, H.-S., Yi, T.-H.: Freeze-Thaw durability of air-entrained concrete. *Sci. World J.* Article ID 650791, p. 6 (2013)
- Yamato, T., Emoto, Y., Soeda, M., Sakamoto, Y.: Some properties of recycled aggregate concrete. In: *Proceedings of the Second International Symposium (RILEM) on Demolition and Reuse of Concrete and Masonry*, vol. 2, pp. 643–651 (1988)
- Yrjanson, W.A.: *Recycling of Portland Cement Concrete Pavements*. National Cooperative Highway Research Program Synthesis of Highway Practice 154, TRB, Washington, D.C. (1989). ISSN: 0547-5570

# Use of Rice Husk Ash (RHA) as a Sustainable Cementitious Material for Concrete Construction

Mohammad Badrul Ahsan<sup>1</sup> and Zahid Hossain<sup>2</sup>(✉)

<sup>1</sup> Arkansas State University, Jonesboro, USA  
mohammad.ahsan@smail.astate.edu

<sup>2</sup> Civil Engineering, Arkansas State University,  
PO Box 1740, Jonesboro, AR 72467, USA  
mhossain@astate.edu

**Abstract.** Use of supplementary construction materials in concrete industries has become a great interest in recent years. Stringent guidelines of the United States Environmental Protection Agency (EPA) influence the use of recycled materials in construction industry. Furthermore, there is an eminent shortage of the predominately used fly ashes from local sources generated by coal plant industries in Arkansas. On the other hand, rice husk ash (RHA), a by-product of the rice milling process, has high potential of being a supplementary cementing material. The RHA generated by Riceland Foods, the largest grain processing industry in the United States located in Arkansas, is treated as waste materials. It has become a financial burden to local farmers due to its ever increasing handling, storage and disposal costs. The RHA consists of non-crystalline silica, which proves it as a very reactive pozzolanic material in mortar and concrete. To this end, laboratory-based experimental study investigated the performance of a locally available RHA as a supplement of Type-I Ordinary Portland Cement (OPC). Properties of concrete with different percentages of RHA (10% and 20% by weight) were investigated in this study. Fresh concrete properties (slump, unit weight, air entrainment etc.) as well as mechanical properties (compressive, tensile, flexural strength) of hardened concrete were determined. Additionally, alkali-silica reaction (ASR) test was conducted on mortar bars to evaluate cracking and expansion of concrete while exposed to adverse weather. It was found that, RHA particles were 13 times coarser than the cement particles. Use of this bulk RHA yielded significant strength reduction of the RHA modified concrete compared to the control sample. The maximum compressive strength gained by 10% RHA-modified concrete was 56% of that of the control specimen. Tensile and flexural strengths achieved by 10% replacement level were 76% and 96%, respectively, of those of the control samples. Moreover, the ASR test revealed that the bulk RHA was very reactive. Local construction industries can use this RHA as flowable fill as an alternative of cement and fly ash.

## 1 Introduction

The present world is focused on the use of waste material in a sustainable way to make a greener earth for the future generations. Different studies were incorporated to use industrial waste and agricultural by-product in modifying concrete. Rice husk ash (RHA), an agricultural byproduct, is yielded during the burning process of rice hull. RHA with more than 80% silica content in shape of non-crystalline silica is produced when it is burnt at less than 700 °C (Rashid et al. 2010). This high silica percentage can make RHA a sustainable replacement of ordinary Portland cement.

Rice hull is the outer shell of the rice grain. During the husking process of paddy, about 30% rice hulls is produced (Givi et al. 2010). It is used as biomass for energy production in paddy milling process as well as in various power plants. During the burning process, about 20% of it converts into RHA (Givi et al. 2010; Rashid et al. 2010). About 738.2 million tons of paddy is produced in the world each year of which about 40 million tons are RHA (Rice Market Monitor 2016). This huge amount of RHA is usually stored at temporary locations that may cause environmental havocs. Moreover, RHA cannot be naturally degraded due to its siliceous compositions (Zerbino et al. 2011). On the other hand, cement industries are responsible for about 7% of the total equivalent CO<sub>2</sub> emissions (Zerbino et al. 2011), and one ton of cement production is responsible for about one ton of equivalent CO<sub>2</sub> emission (Khan et al. 2012). The use of RHA in substitution of cement can reduce the CO<sub>2</sub> footprint as well as the ecological hazards (Ramesh and Kavitha 2014; Chakraborty and Goswami 2015; Swaminathen and Ravi 2016).

Riceland Foods, Inc., a farmer-family owned business, is the largest rice miller in the U.S. that produces 125 million bushels of paddy annually. A significant amount of that paddy produces a huge amount of RHA. Generally, Riceland Foods considers RHA as a waste product and disposes it to nearby custom-designed landfill, which is an economical burden to the company and may pose an environmental threat to local communities. This RHA contains about 70% amorphous silica that makes it a potential source of pozzolanic materials, and it can be used as a replacement of cementitious material. But, its application as a pozzolanic material has not been investigated yet other than the current study. The present study primarily focuses on the effects of silica content of RHA in RHA-modified concrete.

The strength development of concrete is primarily governed by the strength of cement gel. The cement gel is nothing but the crystallized compound of calcium silicate hydrate (C-S-H) and calcium aluminate hydrate (C-A-H). The Ordinary Portland Cement (OPC) generally consists of tricalcium silicate (C<sub>3</sub>S) and dicalcium silicate (C<sub>2</sub>S). During the hydration process, C<sub>3</sub>S and C<sub>2</sub>S react with water and produce C-S-H gel and calcium hydroxide (CH), as shown in Eqs. (1) and (2). The produced CH reacts with alumina (Al<sub>2</sub>O<sub>3</sub>) and generates C-A-H as shown in Eq. (3). Both C-S-H and C-A-H are responsible for strength development of cement paste. When a pozzolanic material having silica (SiO<sub>2</sub>) comes in contact with the CH produced from C<sub>3</sub>S and C<sub>2</sub>S contributes to the amount of cement paste by forming C-S-H gel as shown in Eq. (4)





## 2 Research Significance

RHA produced by Riceland Foods Inc. has the potential to be used in construction work, but its properties as construction material have not been investigated yet. This RHA could be an alternative cementitious material of cement or fly ash. The use of local RHA as a supplementary cementitious material (SCM) would aid local farmers to be economically sustainable by reducing its disposal cost and profiting from its sales to construction and paving contractors.

## 3 Materials Used

An OPC Type-I with a specific gravity of 3.15 was used in this research. Locally available stone sand with a fineness modulus (FM) of 2.2 and crushed stone having a nominal maximum size (NMS) of 25 mm (1 in.) were used as fine aggregate and coarse aggregate, respectively. The specific gravity values of fine aggregate and coarse aggregate were 2.58 and 2.61, respectively, and their absorption values were 0.3% and 0.9%, respectively. The volumetric mix design recommended in American Concrete Institute (ACI) 211.1 was followed. For a desired compressive strength of 31 MPa (4,500 psi), it yielded a mix proportion of 1.0, 1.3, and 3.0 of cement, fine aggregate and coarse aggregate, respectively. RHA was collected from Riceland Foods Inc. plant located in Stuttgart, Arkansas, and its selected chemical and physical properties are presented in Table 1. It is seen that this RHA contains more than 90% reactive oxides, which makes it a possible source of pozzolan. However, the loss on ignition (LOI) value is slightly higher than the American Society for Testing and Materials (ASTM) specification limit.

**Table 1.** Chemical and physical properties of RHA

Chemical properties	Tested RHA	AASHTO M 321-04
Reactive oxides ( $\text{SiO}_2 + \text{Al}_2\text{O}_3 + \text{Fe}_2\text{O}_3$ )	95.5%	75% (minimum)
Loss on ignition (LOI)	8.98%	6% (maximum)
Moisture content	3–5%	3% (maximum)
pH	9.4–9.8	
Physical properties		
Specific Gravity	0.35	
Bulk Density	12.39 lbs./cu. ft.	

## 4 Experimental Methods

In this study, two different percentages (10% and 20%) RHA were used to substitute the OPC. The control sample (0% RHA) was tested for comparing test data with the other two samples (10% and 20% RHA). Values of slump, air content and unit weight of fresh concrete were estimated in accordance with ASTM C143, ASTM C231 and ASTM C138, respectively. Apart from these, mechanical properties such as

compressive strength, tensile strength, flexural strength, modulus of elasticity, and Poisson’s ratio of hardened concrete cured for different days were also estimated in the laboratory. Compressive and tensile strength of concrete were determined using 150 mm × 300 mm (6 in × 12 in.) cylinders after 7, 14, 21 and 28 days of curing time in accordance with ASTM C39-04a. Two replicate specimens for each testing condition of the RHA-modified samples were casted in plastic molds and cured for 24 h in a moist condition at 24°C. For the flexural strength testing, a 600 mm (24 in.) long beam with a cross sectional area of 150 mm × 150 mm (6 in × 6 in) was casted for each RHA-modified concrete samples. Modulus of elasticity and Poisson’s ratio were measured after 28 days of curing period using the same specimens casted for the compressive strength. The test setup for measuring the Poisson’s ratio is shown in Fig. 1. To determine the Poisson’s ratio, an electrical strain gage and a compressometer were used to measure the lateral strain and the vertical strain, respectively. A portable strain indicator connected to the strain gages through wires displayed the lateral strains. The compressometer readings were noted from a dial gage. All cylinders and beams were demolded and kept in a water bath at room temperature of 24°C for curing until the age of testing (Fig. 2).

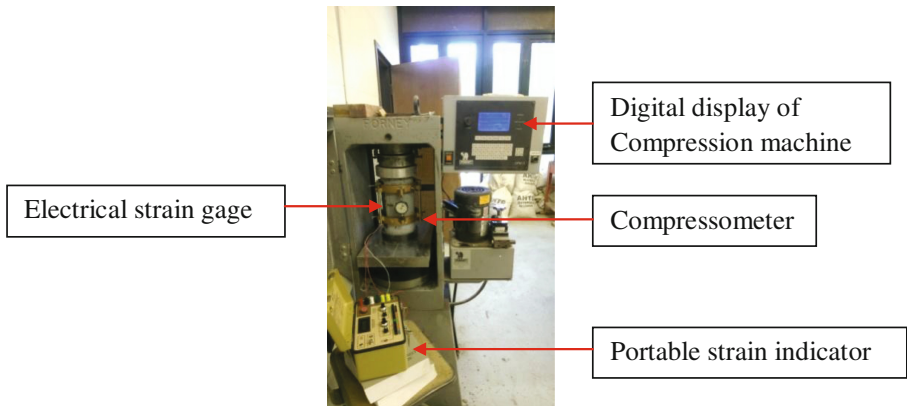


**Fig. 1.** Setup for measuring Poisson’s ratio with Compression machine.

The specific surface area, an indicator of fineness, of RHA was estimated by following the Brunauer, Emmett and Teller (BET) method, which used experimental data collected by a NOVA 2200e analyzer (Fig. 3). The BET surface area was calculated using Eq. (5).

$$\frac{1}{W\left(\frac{P}{P_0}\right)^{-1}} = \frac{1}{W_m C} + \frac{C - 1}{W_m C} \left(\frac{P}{P_0}\right) \tag{5}$$

Where,

- W = weight of gas adsorbed,
- P/P<sub>0</sub> = relative pressure,



**Fig. 2.** Water bath curing at room temperature

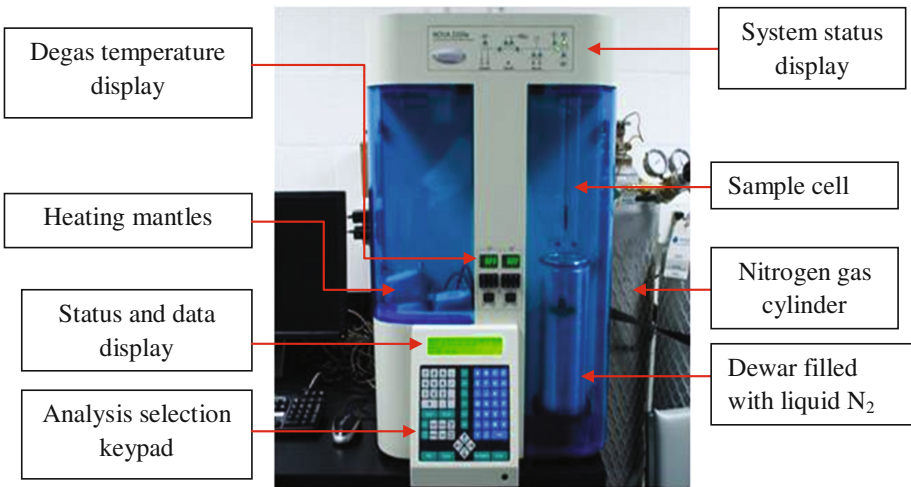


**Fig. 3.** NOVA 2200e multi-station high speed gas sorption analyzer version 10.05

- P = equilibrium adsorption pressure,
- $P_0$  = saturation vapor pressure,
- $W_m$  = weight of adsorbate as monolayer, and
- C = the BET constant.

To get more accurate results, the multi-point BET mode was used with nitrogen as the adsorbate gas. Liquid nitrogen was used to provide the required test temperature (77°K) for nitrogen adsorption isotherms (Sing 2011; Mohamed et al. 2015).

The ASR tests were conducted in accordance with the ASTM C1567 procedure. Three mortar bars with an effective gage length of 285 mm (11.25 in) were casted for

each RHA-modified (10% and 20%) samples. All the mortar bars were kept in a moist room for 24 h, and they were then immersed in tap water for another 24 h. Afterwards, the specimens were removed from water and immersed in 1 N NaOH solution for 14 days. Throughout this period, the change of length of each mortar bar was determined by taking four (4) consecutive readings at 4, 8, 12 and 14 days. Data were collected using a linear variable differential transformer (LVDT) connected with a data storage unit as shown in Fig. 4.

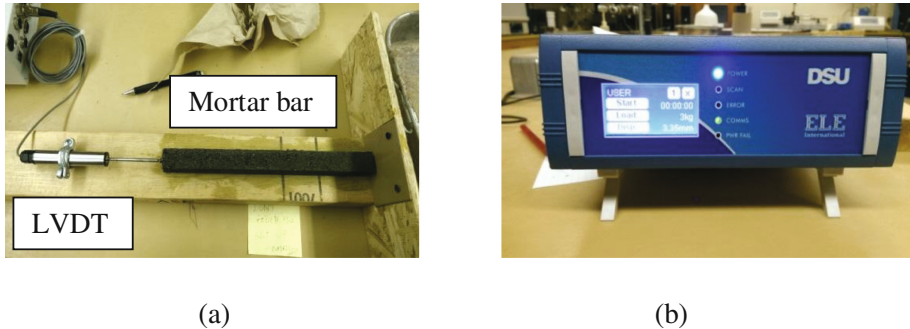


**Fig. 4.** (a) Use of LVDT to measure length change (b) Data storage unit (DSU)

## 5 Results and Discussion

### 5.1 Grain Size Distribution of RHA and BET Surface Area

The pozzolanic activity of RHA is very much dependent on the particle size and surface area (Cordeiro et al. 2011). The RHA sample was sieved in the Arkansas State University Materials laboratory with the ASTM standard sieves to find its grain size distribution (Fig. 5). From Fig. 5, it is observed that only 3% of the tested RHA sample are 45  $\mu\text{m}$  or smaller than 45  $\mu\text{m}$ . On the other hand, AASHTO M 321-04 requires that 90% of the sample should not be larger than 45  $\mu\text{m}$ . About 90% of the RHA used in this study has particle size 600  $\mu\text{m}$  indicating that it is about 13 times coarser than the specified limit. To use RHA as SCM, the particle size of RHA should be the same as cement. However, tests were continued with this coarser RHA to see the behavior of the RHA in concrete without any modification or chemical treatment since this RHA had not been previously used in concrete as SCM. To reduce the particle size of RHA, it is recommended to burn RHA further using a furnace or to grind it by the help of hammer mill or ball mill.

The BET surface area of the tested RHA sample was found to be 18.038  $\text{m}^2/\text{g}$ . Habeeb and Mahmud (2010) reported BET surface areas of 25.3  $\text{m}^2/\text{g}$ , 27.4  $\text{m}^2/\text{g}$ , 29.1  $\text{m}^2/\text{g}$ , and 30.4  $\text{m}^2/\text{g}$  for different sizes of RHA samples having average particle sizes of 63.8  $\mu\text{m}$ , 31.3  $\mu\text{m}$ , 18.3  $\mu\text{m}$ , and 11.5  $\mu\text{m}$ , respectively. Therefore, the higher the particle size, the lower the BET surface area. The RHA of the current study had a very low BET surface area, which indicated a coarse particle. Such a coarse RHA sample can affect the pozzolanic activity of RHA in the modified concrete (Xu et al. 2016).

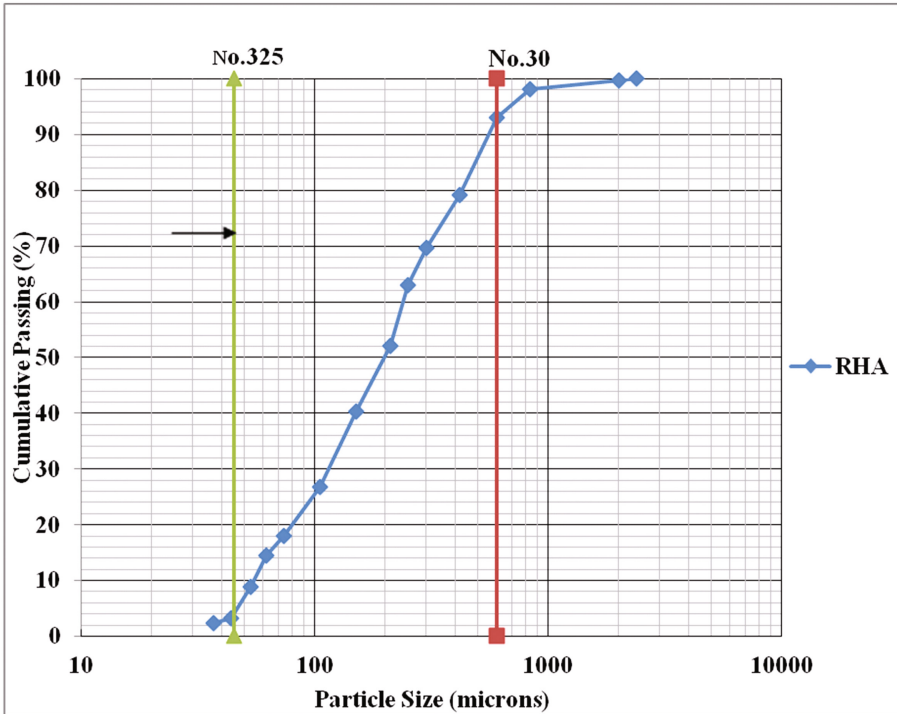


Fig. 5. Grain size distribution of RHA

### 5.2 Properties of Fresh Concrete

The properties of 0%, 10% and 20% RHA-modified fresh concrete samples are presented in Table 2. It is seen that slump values were about the same for 0% and 10% RHA concrete, whereas 20% RHA-modified concrete exhibited a higher slump value. A higher amount of air voids due to an increased RHA percentage could be the reason behind this phenomenon. An increment of the RHA percentage also increased the air voids, but it decreased the unit weight. It happened as the OPC was significantly finer than the RHA. Coarser particles of RHA created additional air voids in the concrete, which eventually decreased the unit weight of the fresh concrete, as presented in Table 2.

Table 2. Fresh properties of concrete

Sample	Slump (inch)	Air Content (%)	Unit Weight (pcf)
Control	3.5	1.3	152
10% RHA	3.5	2.1	141
20% RHA	4.5	3.2	136

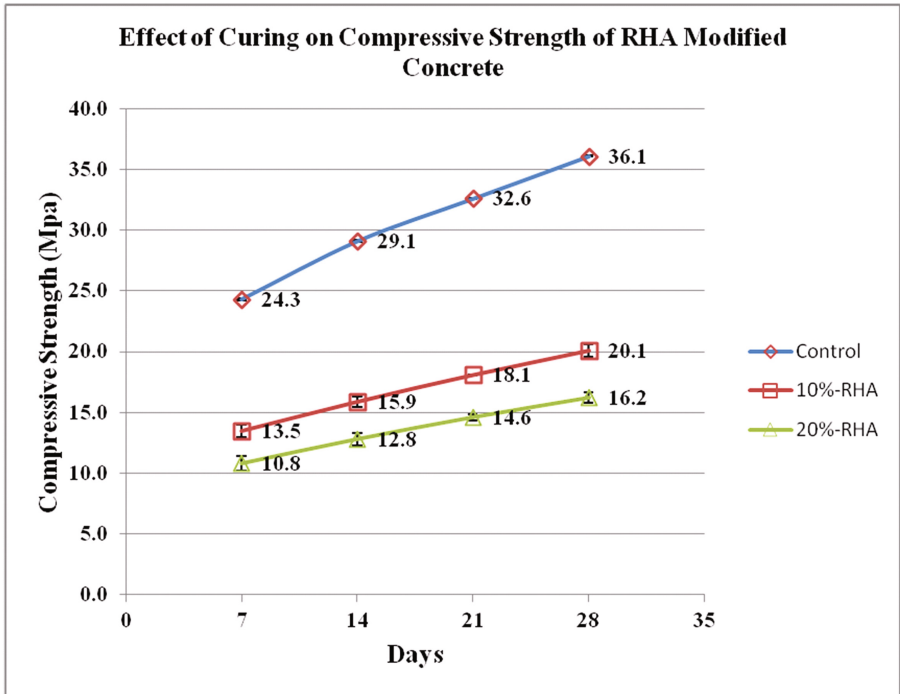


Fig. 6. Comparison of compressive strength of RHA-modified concrete

### 5.3 Compressive Strength

The compressive strength values of the tested concrete cylinders are shown in Fig. 6. It is observed that the control specimen gained compressive strength up to 36 MPa. On the other hand, the maximum compressive strength of 10% RHA-modified concrete was 20.13 MPa, which was only 56% of that of the control sample. A considerable amount of compressive strength 16.20 MPa was also gained by 20% RHA-modified concrete, and it was about 45% of that of the control sample. Bulk particle of RHA might not generate sufficient amount of C-S-H gel to fill up void spaces. The presence of high air voids in RHA-modified concrete due to bulk particles caused noticeable amount of strength reduction. This type of RHA-modified concrete can be used in controlled low strength materials such as flowable fill that requires a low compressive strength of 8.3 MPa (Ayers et al. 1994; Deng and Tikalsky 2008).

### 5.4 Tensile Strength

The tensile strength of RHA-modified concrete is shown in Fig. 7. It is seen that the rate of gain in tensile strength of RHA-modified concrete was similar to that of its compressive strength. Between the RHA-modified samples, the 10% RHA-modified concrete gained the highest tensile strength, which was 75% of that of the control specimen. The 20% RHA-modified concrete exhibited further reduction of tensile

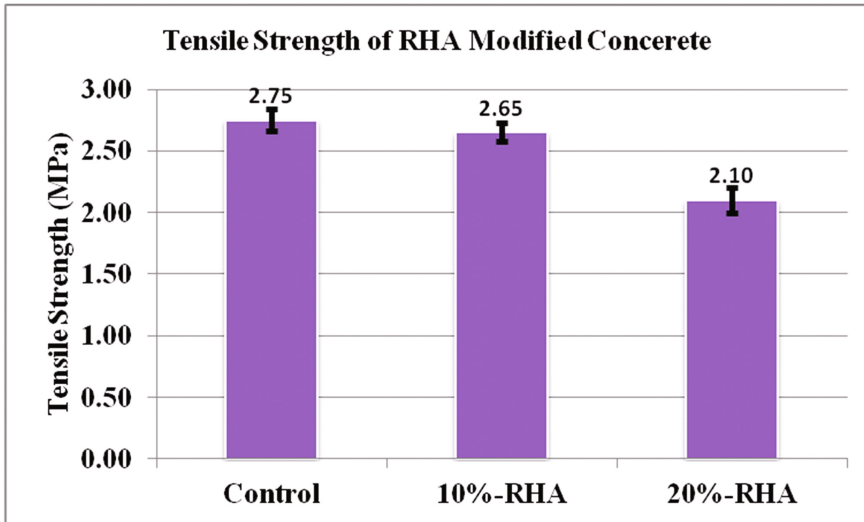


Fig. 7. Comparison of tensile strength of RHA-modified concrete

strength, which was 65% of that of the control specimen. It is seen that the effect of air voids in concrete has a significant role in reducing tensile strength of concrete.

### 5.5 Flexural Strength

Beam samples were tested after 28 days curing period to determine the modulus of rupture, which is often known as flexural strength. It is noticed that 10% and 20% RHA-modified concrete imparted 96% and 76%, respectively, of the flexural strength of the control specimen (Fig. 8). The use of RHA as a partial replacement of OPC reduced the flexural strength of RHA-modified concrete.

### 5.6 Poisson's Ratio and Modulus of Elasticity

The result of Poisson's ratio and Modulus of elasticity of RHA-modified concrete are presented in Table 3. Poisson's ratios increased with the increment of the RHA content. The rate of the gain of compressive or tensile strength of RHA concrete is highly correlated (negatively) with as the Poisson's ratio. Another important parameter of concrete is modulus of elasticity. While comparing the measured modulus of elasticity with the American Concrete Institute (ACI) equation ( $E_c = 4700\sqrt{f'_c}$ ) (Table 4), it is seen that the measured  $E_c$  value is within  $\pm 22\%$  of that obtained in the latter approach. In general, the modulus of elasticity values decreased with the increment of RHA percentage. It occurred due to less strength development in RHA concrete than the control specimen.

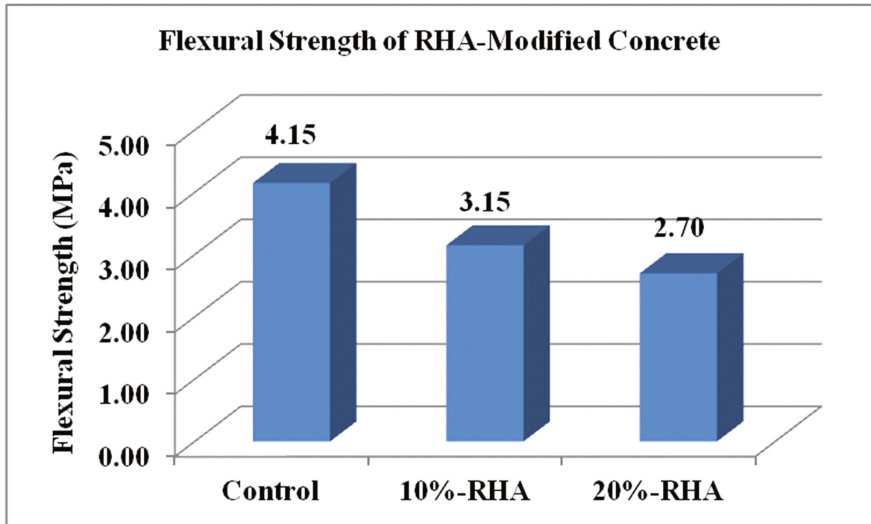


Fig. 8. Results of flexural strength of RHA-modified concrete

Table 3. Results of poisson's ratio

Sample	Measured value
Control	0.28
10%-RHA	0.40
20%-RHA	0.55

Table 4. Modulus of elasticity

Sample	Measured (MPa)	$E_c = 4700\sqrt{f_c}$ (MPa)
Control	$3.12 \times 10^4$	$2.83 \times 10^6$
10%-RHA	$2.56 \times 10^4$	$2.10 \times 10^6$
20%-RHA	$1.65 \times 10^4$	$1.89 \times 10^6$

## 5.7 ASR Test Results

The expansion of concrete mortar bars obtained from ASR tests is shown in Fig. 9. The expansion of the control and 10% RHA-modified concrete is 0.20% and 0.25%, respectively, which exceeded the ASTM C1567 specified expansion limit (0.10%). It happened as RHA containing bulk particle size imparts higher alkali-silica expansions (Attoh-okine and Atique 2006). Visible cracks were found in the control sample as well as in 10% RHA-modified sample. However, the 20% RHA-modified samples showed reduced expansion of mortar bars after 14 days of curing. This is possibly due to the production of less expansive alkali-silica gel during hydration process of cement (de Sensale 2010) or due to lower alkali/ reactive silica ratio. Further, micro level



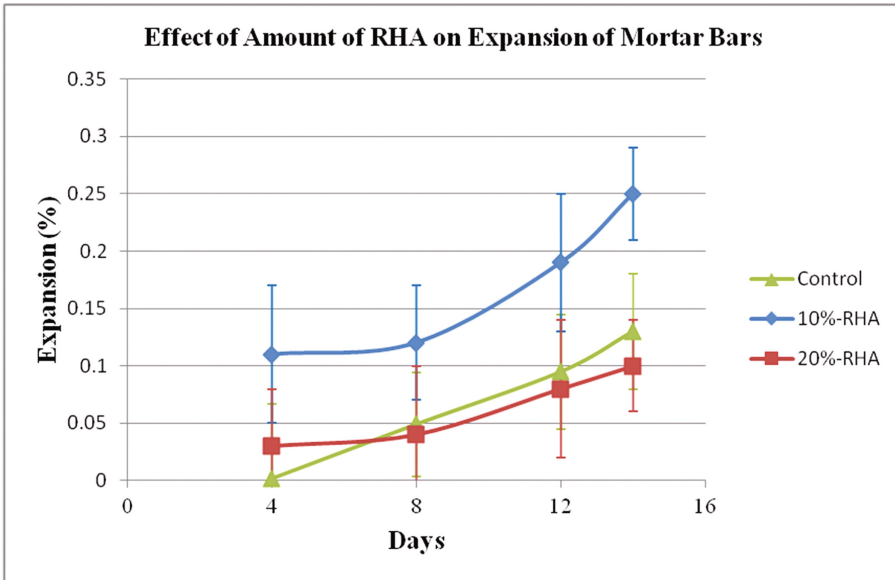


Fig. 9. Comparison of effect of ASR on RHA-modified concrete

investigation should be carried out on the RHA-modified mortar bars by scanning electron microscopy (SEM) in association with X-ray diffraction (XRD) to visualize the intermolecular bonding phenomena. This would help to describe more accurately the ASR expansion of RHA-modified mortar bar.

## 5.8 Summary

The maximum compressive, tensile and flexural strengths were gained by 10% RHA-modified concrete. The compressive, tensile and flexural strength gained by 10% RHA concrete were 20.13 MPa, 2.77 MPa and 4.16 MPa, respectively. Less cement gel production due to usage of bulk RHA could be a possible reason for the strength reduction in concrete. The modulus of elasticity of control, 10% and 20% RHA-modified concrete were  $3.12 \times 10^4$  MPa,  $2.56 \times 10^4$  MPa and  $1.65 \times 10^4$  MPa, respectively. It is observed that the control, 10% and 20% RHA-modified concrete samples had Poisson's ratio 0.28, 0.40 and 0.55, respectively. With the increment of RHA percentage, the modulus of elasticity decreased but the Poisson's ratio increased. The value ASR seemed to increase in the case of concrete with 10% RHA, but it did not vary significantly from the control sample when 20% RHA was used.

Based on the properties of fresh concrete and hardened concrete, it is observed that RHA-modified concrete of the current study is not suitable for typical structures such as foundation, floor, and pavement. This is mainly due to significant low strength of RHA-modified concrete even though the workability and ASR properties are favorable. The authors believe that the low strength gain in RHA-modified concrete is due to the

use of significantly large RHA particles, which is observed from the gradation analysis. Concretes with such low strength can be used as controlled low strength materials (CLSM), also known as controlled density fill, flowable fill, unshrinkable fill, or lean-mix backfill (NRMCA 2000). The CLSM does not require human to compact them, and it can be used in various constructions such as utility trenches, bridge abutment, abandoned mines, and underground storage tanks.

## 6 Conclusions

Engineering properties of RHA-modified concrete cylinders, beams and mortar bar samples were tested in the laboratory. Significant strength reduction was observed by partial replacement of cement by RHA. A 10% replacement of cement by RHA in concrete was found to be the optimum for this study based on mechanistic properties of concrete. However, ASR test indicated that 20% cement replacement by RHA will have less ASR-related cracks. It is concluded that this RHA can be used as supplementary cementitious material in controlled low strength materials such as flowable fill. Further, it is recommended to burn RHA further using a furnace at a higher temperature or to grind it by the help of a hammer or ball mill in a controlled environment to obtain finer than 45 microns RHA.

**Acknowledgement.** The authors acknowledge the financial support of the Office of the Provost of Arkansas State University for this study. The authors are also thankful to Riceland Foods, Inc. and Nettleton Concrete for providing test materials for this research.

## References

- Attoh-okine, N.I.I., Atique, F.: Service life assessment of concrete with ASR and possible mitigation. Delaware Center for Transportation, Newark, Delaware (2006)
- Ayers, M.E., Wong, S.Z., Zaman, W.: Optimization of flowable fill mix proportions. Spec. Publ. **150**, 15–38 (1994)
- Chakraborty, A., Goswami, A.: Conservation of environment by using fly ash and rice husk ash as a partial cement replacement in concrete. *J. Energ. Res. Environ. Technol.* **2**(1), 9–11 (2015)
- Cordeiro, G.C., Toledo Filho, R.D., Tavares, L.M., Fairbairn, E.D.M.R., Hempel, S.: Influence of particle size and specific surface area on the pozzolanic activity of residual rice husk ash. *Cement Concr. Compos.* **33**(5), 529–534 (2011)
- de Sensale, G.R.: Strength development of concrete with rice-husk ash. *Cement Concr. Compos.* **28**(2), 158–160 (2006)
- de Sensale, G.R.: Effect of rice-husk ash on durability of cementitious materials. *Cement Concr. Compos.* **32**(9), 718–725 (2010)
- Deng, A., Tikalsky, P.J.: Geotechnical and leaching properties of flowable fill incorporating waste foundry sand. *Waste Manag* **28**(11), 2161–2170 (2008)
- Dunstan, E.R.: How does pozzolanic reaction make concrete green? In: World of Coal Ash (WOCA) Conference-May 9–12, pp. 1–14 (2011)

- Givi, A.N., Rashid, S.A., Aziz, F.N.A., Salleh, M.A.M.: Contribution of rice husk ash to the properties of mortar and concrete: a review. *J. Am. Sci.* **6**(3), 157–165 (2010)
- Habeeb, G.A., Fayyadh, M.M.: Rice husk ash concrete: the effect of RHA average particle size on mechanical properties and drying shrinkage. *Aust. J. Basic Appl. Sci.* **3**(3), 1616–1622 (2009)
- Habeeb, G.A., Mahmud, H.B.: Study on properties of rice husk ash and its use as cement replacement material. *Mater. Res.* **13**(2), 185–190 (2010)
- Khan, R., Jabbar, A., Ahmad, I., Khan, W., Khan, A.N., Mirza, J.: Reduction in environmental problems using rice-husk ash in concrete. *Constr. Build. Mater.* **30**, 360–365 (2012)
- Mohamed, R.M., Mkhaliid, I.A., Barakat, M.A.: Rice husk ash as a renewable source for the production of zeolite NaY and its characterization. *Arabian, J. Chem.* **8**(1), 48–53 (2015)
- NRMCA: Concrete in Practice, what, why & how?: CIP 17- Flowable fill materials, p. 2000. National Ready Mixed Concrete Association, Silver Spring, Maryland (2000)
- Ramesh, S., Kavitha, S.: Experimental study on the behaviour of cement concrete with rice husk ash (RHA). *Int. J. Eng.* **6**(02), 8269 (2014)
- Rashid, M.H., Molla, M.K.A., Ahmed, T.U.: Durability of Mortar in Presence of Rice Husk Ash. *Development*, 158, 11106 (2010)
- Rice Market Monitor, vol. XIX, Issue No. 1, Food and Agriculture Organization of the United Nations, Rome, Italy, April 2016
- Sing, K.: The use of nitrogen adsorption for the characterisation of porous materials. *Colloids Surf. A* **187**, 3–9 (2001)
- Swaminathan, A.N., Ravi, S.R.: Use of rice husk ash and metakaolin as pozzolonas for concrete: a review. *Int. J. Appl. Eng. Res.* **11**(1), 656–664 (2016)
- Xu, W., Lo, T.Y., Wang, W., Ouyang, D., Wang, P., Xing, F.: Pozzolanic reactivity of silica fume and ground rice husk ash as reactive silica in a cementitious system: a comparative study. *Materials* **9**(3), 146 (2016)
- Zerbino, R., Giaccio, G., Isaia, G.C.: Concrete incorporating rice-husk ash without processing. *Constr. Build. Mater.* **25**(1), 371–378 (2011)
- Zhang, M.H., Lastra, R., Malhotra, V.M.: Rice-husk ash paste and concrete: some aspects of hydration and the microstructure of the interfacial zone between the aggregate and paste. *Cem. Concr. Res.* **26**(6), 963–977 (1996)

# Behavior of SCC Incorporating Granulated Blast Furnace Slag and Ground Clay Brick Powders at High Temperatures

M.H. Seleem<sup>(✉)</sup>, A.A.M. Badawy, S.A. Ahmed, and A.A. Elakhras

Engineering Materials Department, Faculty of Engineering,  
Zagazig University, Zagazig, Egypt  
mhseleem@yahoo.com

**Abstract.** Behavior of self-compacting concrete (SCC) produced from local waste powder materials was experimentally investigated at high temperatures. Two types of wastes powder, granulated blast furnace slag (GBFS) and ground clay bricks (GCB) were used as a partial replacement of cement by weight. Five concrete mixes were prepared with 0% wastes powder, 30% GBFS, 20% GBFS +10% GCB, 10% GBFS+20% GCB and 30% GCB. The total cementitious materials content and water/cementitious materials ratios were 450 kg/m<sup>3</sup> and 0.39 respectively for all mixes. After water curing for 28 days, the test specimens were dried at 105 °C for 24 h before exposure to the desired high temperatures of 200, 400, 600 and 800 °C for 2 h. After exposure to the desired target temperature, the test specimens were allowed to cool at room temperature (RT) before testing. Fresh properties of all SCC mixes were measured and evaluated. Weight loss, residual compressive and splitting tensile strengths were measured after exposure to high temperatures. Properties at RT were also measured for comparison. Changes in physicochemical properties were explained based on the results of mass loss and X-ray diffraction analysis. Test results indicated that most of the original strength was lost on exposure to temperature between 600 and 800 °C. The performance of SCC mixes incorporating high content of GCB was better than that with GBFS at high temperatures. Utilization of GBFS, GCB or a combination of them as 30% partial replacement of cement content can produce economically and environmentally friendly concrete mixes.

## 1 Introduction

Portland cement concrete is a major construction material worldwide. Unfortunately, the production of portland cement releases large amounts of CO<sub>2</sub> into the atmosphere (Bilodeau and Malhotra 2000). The increase in the cement production is expected to be in the developing countries. Therefore, increasing the use of supplementary cementitious materials (SCMs) in concrete is an obvious and necessary step to reduce carbon emissions and produce environmentally friendly concrete (Malhotra 2006). SCMs, such as silica fume, fly ash and slag are often waste materials from industrial processes. These wastes possess hydraulic and/or pozzolanic properties and, when used at optimal levels, enhance fresh state properties, mechanical performance and durability (Kuder et al. 2012).

Self-compacting concrete (SCC) is a new generation of concrete that can be compacted under its own weight without the need of external vibration. It is characterized by its ability to flow and fill narrow and deep members and produces uniform concrete mixes without any sign of segregation or bleeding. The development of SCC is considered to be one of the most significant developments in the building material domain. This is due to its advantages over the conventional concrete. One of the disadvantages of SCC is its cost, associated with the use of high volumes of Portland cement and use of chemical admixtures. Some researchers tried to reduce the cost of SCC by the use of mineral admixtures as a partial replacement of cement (Uysal and Sumer 2011; Uysal and Yilmaz 2011; Seleem et al. 2006; Ahmed et al. 2007). They found that, besides the decrease in the cost of cement, the use of mineral admixture may eliminate the need for viscosity-enhancing admixtures. Also, the use of mineral admixtures may improve the rheological properties of SCC and reduce thermally-induced cracking of concrete due to the reduction in the overall heat of hydration and increase in the workability and long-term properties of concrete (Dinker et al. 2008). Granulated blast furnace slags (GBFS) and ground clay bricks (GCB) are local industrial by-products mineral admixtures that can be used to reduce the cost of SCC.

In case of fire, concrete is exposed to high temperature that induces a material degradation: strength decrease, cracking and in some conditions spalling. Up to now, the effect of elevated temperatures has been studied mainly on vibrated ordinary and high performance concretes. The few studies on SCC subjected to high temperatures showed either a decrease in strength or an increase in the risk of spalling, or a behavior similar to that of vibrated concrete (Badawy et al. 2011a; Uysal 2012; Uysal et al. 2012). Using mineral admixture powders in the production of SCC mixes led to dense microstructure of mixes compared with those of normal concrete. The dense microstructure of SCC introduces a high strength and a very low permeability. However, the dense microstructure of SCC seems to be a disadvantage when exposed to fire (Fares et al. 2009). Therefore, the strength and durability characteristics after exposure to high temperatures of SCC containing mineral admixtures as partial replacements of cement should be investigated.

The objective of this study is to investigate the effect of high temperatures up to 800 °C on the properties of SCC incorporating two types of local wastes powder; GBFS, GCB or combinations of them as a partial replacement of cement weight. Fresh properties of the investigated SCC mixes were measured. Compressive and tensile strengths of the studied SCC mixes were also estimated at room and high temperatures. Moreover, weight loss and X-ray diffraction were used to explain the changes in physicochemical properties.

## 2 Experimentation

### 2.1 Materials

Ordinary Portland cement, conforming to Egyptian Standard Specifications (ESS 373/1991) and labeled as CEM I 42.5N was used. A natural well-graded river sand and dolomite with a maximum nominal size of 14 mm were used as fine and coarse

aggregates respectively. The specific gravity and water absorption of the used sand and dolomite were 2.63, 0.65%, and 2.61, 0.8%, respectively. Two different types of by-products namely; GBFS and GCB ground to pass 170  $\mu\text{m}$  sieve were used as mineral admixtures. Table 1 shows the chemical composition and specific gravities of cement, GBFS and GCB. A third generation super plasticizer, Sika Viscocrete-5930, based on modified polycarboxylate, was used as a viscosity enhancing admixtures (VEA). It has a dual action. It gives excellent flowability and in the same time enhances the stability (viscosity) of concrete. It meets the requirements for superplasticizers according to EN 934-2 and ASTM-C-494 type G and F.

**Table 1.** Chemical composition and specific gravity of cement and by-products

Component (%)	Cement	GBFS	GCB
SiO <sub>2</sub>	21.0	35.78	57.7
Al <sub>2</sub> O <sub>3</sub>	6.1	10.94	15.6
Fe <sub>2</sub> O <sub>3</sub>	3.0	0.43	8.16
CaO	61.5	34.22	4.65
MgO	3.8	6.52	1.38
SO <sub>3</sub>	2.5	3.01	7.02
Na <sub>2</sub> O	0.4	1.06	1.26
K <sub>2</sub> O	0.3	1.02	1.67
TiO <sub>2</sub>	–	0.02	0.19
Specific gravity	3.15	2.89	2.5

## 2.2 Experimental Program and Mix Proportions

One control SCC mix without waste powders and four SCC mixes incorporating waste powders were prepared with 0% wastes powder (CM), 30% GBFS (S-30), 20% GBFS +10% GCB, (SH20-10), 10% GBFS+20% GCB (SH10-20) and 30% GCB (H-30) as a partial replacement of cement, see Table 2. After trial mixes the total content of cementitious materials and water/cementitious materials ratio (w/cm) were kept at 450 kg/m<sup>3</sup> and 0.39 respectively. The VEA was added in the amount of 2% from the total cementitious materials.

**Table 2.** Concrete mix proportions of SCC mixes

Mix code	Materials, kg/m <sup>3</sup>									
	Cement	GBFS	GCB	W/CM	Water	Sand	Dolomite	VEA		
CM	450	–	–	0.39	175	883	883	9		
S-30	315	135	–			877	877			
SH20-10	315	90	45			874	874			
SH10-20	315	45	90			871	871			
H-30	315	–	135						868	868

### 2.3 Fresh and Hardened Concrete Tests

The slump-flow, V-funnel and L-box tests were conducted to assess the workability, filling and passing abilities of SCC mixes in the fresh state according to the European guidelines (EFNARC 2002). Cube specimens having dimensions of  $100 \times 100 \times 100$  mm were used to determine the compressive strength and cylindrical specimens having dimensions of  $75 \times 150$  mm were used to determine the splitting tensile strength. All specimens were cast after carrying out the fresh properties tests. The cast specimens were removed from moulds after 24 h and were cured in water for 28 days. After removing from water, the test specimens were air dried for the next day in the laboratory environment ( $30^\circ\text{C}$  temperature and 80% relative humidity). After that, the specimens were oven dried at approximately  $105^\circ\text{C}$  for 24 h. For the high temperature tests, the specimens were heated until reaching to the desired target temperatures of 200, 400, 600 or  $800^\circ\text{C}$  and held at that temperature for 2 h. The heated specimens were taken out from the furnace and left to cool at room temperature (RT). Fresh and hard properties were measured at room temperature (RT). Residual strength properties, weight loss due to high temperature exposure were also measured. XRD analysis and specimen surface examination due to exposure to high temperatures were conducted.

## 3 Results and Discussions

### 3.1 Properties of Fresh Concrete

The fresh properties of SCC mixes were measured in terms of slump flow diameter, slump flow time (T50), efflux time, flow time at T5 min, average flow velocity ( $V_{av}$ ) and blocking ratio (H2/H1). These properties were used to assess the workability, filling and passing ability of SCC mixes. The fresh properties of all investigated concrete mixes are given in Table 3. The properties of all investigated SCC mixes satisfy the requirements of the European guidelines for SCC (EFNARC 2002) as illustrated in Table 3. Based on the results of fresh properties of SCC mixes, it can be concluded that the inclusion of GBFS in SCC mixes led to a significant improvement in their fresh properties. In contrast there was worsening in the fresh properties of SCC mixes containing GCB compared to control mix.

**Table 3.** Fresh properties of SCC mixes

Mix code	Slump-flow test		V-funnel test		L - box test		
	Flow diameter (mm)	T50 (Sec)	Efflux time (Sec)	T5 Min (Sec)	Velocity (cm/sec)	H2/H1	
CM	730	2.85	7.28		8.73	24.29	0.94
S-30	765	1.90	6.00		7.12	29.82	0.97
SH20-10	740	2.45	6.46		7.7	24.90	0.94
SH10-20	720	2.71	6.82		7.64	23.80	0.87
H-30	695	3.15	7.8		8.40	21.94	0.85
EFNARC Req.	<b>650–800</b>	<b>2–5</b>	<b>6–12</b>		Efflux time increase <b>0–3</b>	–	<b>0.80–1</b>

## 3.2 Properties of Hardened Concrete

### 3.2.1 Mass Loss

Figure 1 shows the effect of high temperatures on the mass loss for the investigated SCC mixes. The figure shows a gradual increase in the mass loss with the increase in temperature. The increase in the mass loss for all mixes is more significant after 600 °C. Also, there was a marginal increase in the weight loss of specimens prepared from SCC mixes with GBFS and/or GCB compared to specimens of the control mix. The highest mass loss was observed for specimens containing 30% GBFS, (S-30). Causes of mass loss due to water evaporation from concrete specimens were discussed and illustrated based on XRD analysis in several previous works (El-Shihy et al. 2009; Piasta et al. 1984; Phan 2002; Peng and Huang 2008; Fares et al. 2010).

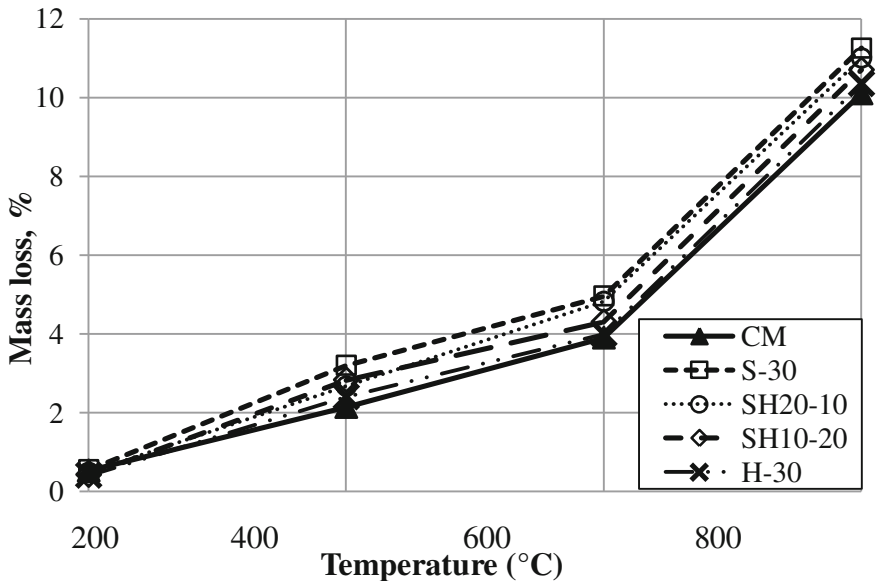


Fig. 1. Mass loss for SCC specimens after exposure to high temperatures

### 3.2.2 Compressive Strength

Results of compression strength test for the five investigated SCC mixes are given in Table 4. The results in Table 4 were represented in Figs. 2 and 3 in two forms; as values in MPa, Fig. 2, and as relative to the corresponding strength of the same mix at RT (without heating), Fig. 3. It is clear from Fig. 2 that, the control mix recorded the highest compressive strength among all SCC mixtures for different exposure temperatures. Comparing the results of compressive strength at 200 °C to those at RT indicates an increase in the strength for all specimens except mix containing 30% GCB, H-30, which showed a decrease in the compressive strength, see Fig. 3 at that temperature. With the increase in temperature above 200 °C, there was a gradual decrease in compressive strength. The percentage loss or gain in compressive strength for all



**Table 4.** Compressive strength results for SCC mixes at different exposure temperatures

Mix code	Temperatures									
	RT		200°C		400°C		600°C		800°C	
	MPa	%	MPa	%	MPa	%	MPa	%	MPa	%
CM	52.0	53.5	102.9	50.0	96.2	38.0	73.1	22.6	43.5	
S-30	46.0	48.2	104.8	44.6	97.0	31.5	68.5	17.9	38.9	
SH20-10	46.8	47.7	101.9	45.8	97.9	33.4	71.4	18.6	39.7	
SH10-20	47.8	48.2	100.8	46.0	96.2	34.3	71.8	19.5	40.8	
H-30	50.0	47.0	94.0	46.8	93.6	33.0	66.0	20.8	41.6	

SCC mixes due to exposure to high temperatures from 200 °C to 800 °C is given in Table 4. Specimens of the control mix exhibited the best performance when exposed to high temperatures, followed by mixes containing large amount of GCB, while the lowest strength was recorded for specimens containing 30% GBFS as shown in Fig. 2.

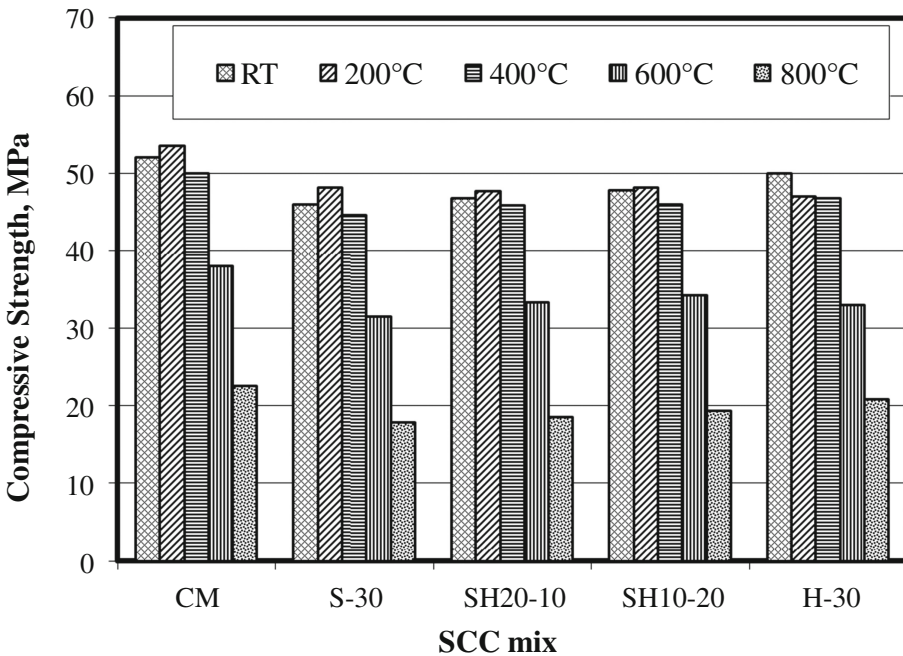


**Fig. 2.** Compressive strength of SCC specimens after exposure to high temperatures

The enhancement in the compressive strength of SCC specimens exposed to temperature from RT to 200 °C may be attributed to the formation of C-S-H from the reaction between the unhydrated cement particles and lime at these temperatures (Tanyildizi and Coskun 2008). Several hypotheses have been proposed to explain this

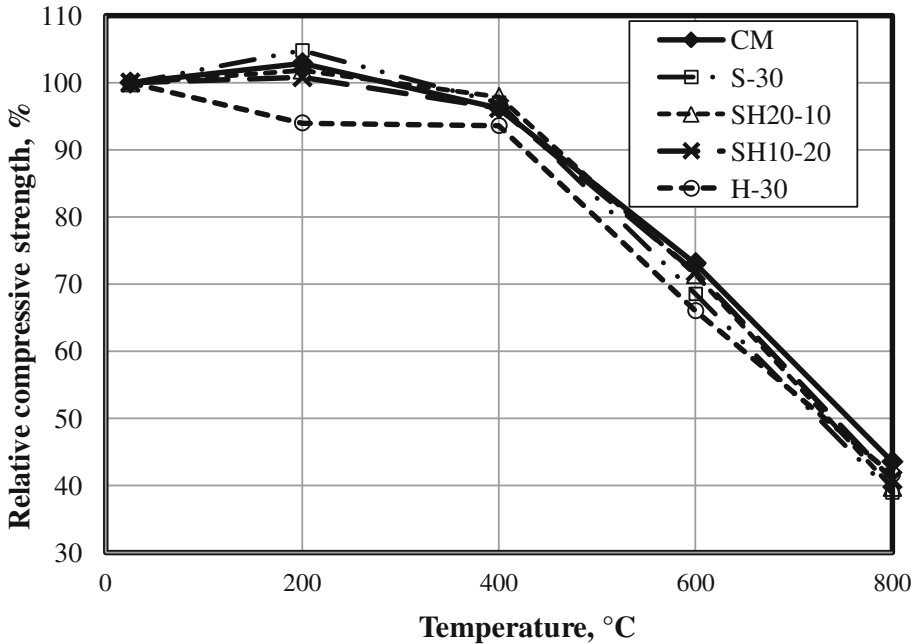


**Fig. 3.** Relative compressive strength of SCC specimens after exposure to high temperatures

increase in strength. Dias et al. (1990) attributed the increase in compressive strength at that temperature to a rehydration of the paste due to migration of the water in the pores. Also, it can be attributed to the increase in forces between the gel particles (Van der Waal's forces) due to the water removal (Behnood and Ziari 2008; Castillo and Durrani 1990).

From 200 to 400 °C, there was only a marginal decrease in the compressive strength of SCC mixes of about 2–7%. This may be due to the water loss from pores of the hydrates as well as the first stage of dehydration (Ye et al. 2007). Also, it may be due to the increase in the amounts of C-S-H and CH with the heating to 400 °C. It is postulated that the pore-structure coarsening can be regarded as the formation of equivalent cracks which should be responsible for the reduction in mechanical properties of concrete, especially as no chemical decomposition of hardener cement paste occurs below 400 °C (Peng and Huang 2008).

A severe loss in strength of about 27–34% was observed when the temperature increased to 600 °C. This great loss in compressive strength can be attributed to the dense microstructures of this type of concrete, that lead to the building up of high internal pressure during heating. Moreover, some researchers reported this strength loss is largely attributed to the decomposition of calcium hydroxide, which is known to occur between 450 and 500 °C (Zhang and Bicanic 2002). According to Peng and Huang (2008), the decomposition of CH and  $\text{CaCO}_3$  was initiated at 430 °C and 530 °C, respectively. Also, the main hydration product in hardened cement paste started to decompose to  $\text{C}_2\text{S}$  and  $\text{C}_3\text{S}$  at 560 °C. In addition, at 573 °C, the allotropic

transformation of  $\alpha$ -quartz into  $\beta$ -quartz occurs with an expansion in the volume (Fares et al. 2010).

Above 600 °C, the decomposition became significant and the C-S-H decomposition rate increased dramatically with temperature (Peng and Huang 2008). All SCC mixes showed severe deterioration in compressive strength at 800 °C, about 57–61%. This may be due to breaking down of bond between aggregate and cement paste as a result of expansion of aggregates and contraction of cement paste, that produce higher stress concentrations at the transition zone. In addition, the decomposition of the C-S-H gel may be another cause of this severe deterioration (Demirel and Kelestemur 2010)

### 3.2.3 Tensile Strength

Results of indirect tensile strength of the five SCC mixes are given in Table 5. The results in Table 5 were represented in Figs. 4 and 5 in two forms; as values in MPa and as relative to the corresponding strength of the same mix at RT (without heating). The results in Table 5 and Fig. 4 show that the control mix recorded the highest tensile strength among all mixtures. The control mix recorded the highest relative tensile strength up to 400 °C. Above 400 °C, the SCC mix contained 10% GBFS and 20% GCB showed the highest relative tensile strength, Fig. 5. In general there is a pronounced decrease in the tensile strength for the five SCC mixes with increasing exposure temperatures from RT to 800 °C. It is clear also that SCC mix incorporating 30% GBFS indicate the lowest tensile strength among other mixes at exposure temperature of 400 °C or more. The reduction in splitting tensile strength with the increase in heating temperature can be attributed to the thermal stresses induced in dense microstructure and thermal incompatibility between aggregates and cement paste that resulted in micro and macro cracks (Heikal 2008).

**Table 5.** Tensile strength results for SCC mixes at different exposure temperatures

Mix code	Temperature										
	RT		200 °C			400 °C		600 °C		800 °C	
	MPa	%	MPa	%	MPa	%	MPa	%	MPa	%	
CM	5.6	96.4	5.40	4.39	78.4	2.5	44.6	1.25	22.3		
S-30	4.8	95.8	4.60	3.30	68.8	2.0	41.7	0.97	20.2		
SH20-10	5.0	91.6	4.58	3.50	70.0	2.6	52.0	1.05	21.0		
SH10-20	5.0	96.0	4.80	3.79	75.8	2.7	54.0	1.20	24.0		
H-30	5.2	84.6	4.40	4.00	76.9	2.4	46.2	1.10	21.2		

Comparing the results of the relative tensile and compressive strengths, Figs. 3 and 5, for different SCC mixes clearly indicate excessive deterioration in the tensile strength compared to that of compressive strength after exposure to high temperatures. This behaviour can be explained as follows: On heating, a thermal stresses at the interface are occurred as a result of different coefficient of thermal expansion between mortar and coarse aggregate. These stresses break the bond at the interface between the mortar and aggregate and thus creating cracks. These cracks are more effective in the mode of failure under tension compared to those under compression.

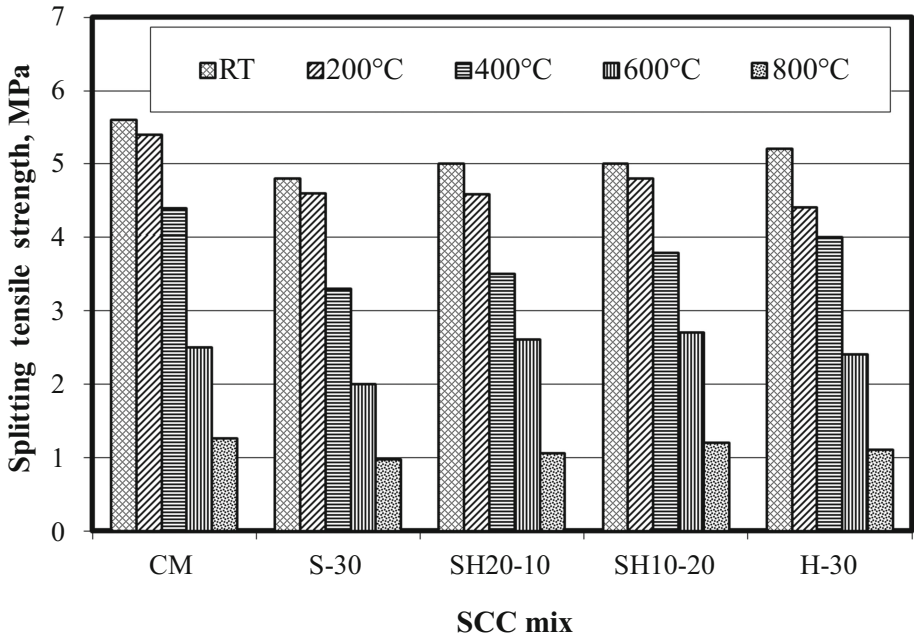


Fig. 4. Tensile strength of SCC specimens after exposure to high temperatures

### 3.3 XRD Analysis

X-ray diffraction technique was used to find changes in the mineralogy of hydration products of cement paste. Results from XRD of concrete samples were also used to verify the decomposition of C-S-H, CH and aggregates after exposure to high temperatures. Concrete samples were taken from specimens fractured during compression and splitting tension tests to carry out these tests.

The XRD diagrams of the control mix at RT and those after exposure to temperatures of 200, 600 and 800 °C for 2 h are shown in Fig. 6. The main phases in samples are C-S-H gel, portlandite  $\text{Ca}(\text{OH})_2$ , calcite  $\text{CaCO}_3$ , dolomite, quartz and microcline. Microcline is considered impurity in sand. It is observed that C-S-H and CH are still found at 200 °C. The intensity of the peaks characteristic of C-S-H increased while those of CH decreased with the increase in temperature up to 200 °C. This is because further hydration of cement residues occurred and C-S-H may simply have become more crystalline with heating. This may be the reasons of increasing the compressive strength at 200 °C.

Intensity of the peaks characteristic of C-S-H and CH phases disappeared in SCC samples subjected to 600 °C. This is due to a dehydration of  $\text{Ca}(\text{OH})_2$  into  $\text{CaO} + \text{H}_2\text{O}$ , where  $\text{H}_2\text{O}$  evaporated at this temperature. However, intensity of the peak characteristic for calcite increased. This may be due to the reaction of the free lime, CaO, with  $\text{CO}_2$  from the surrounding atmosphere during cooling. These results can explain the sharp drop in the values of compressive strength for specimens subjected to 600 °C temperature.

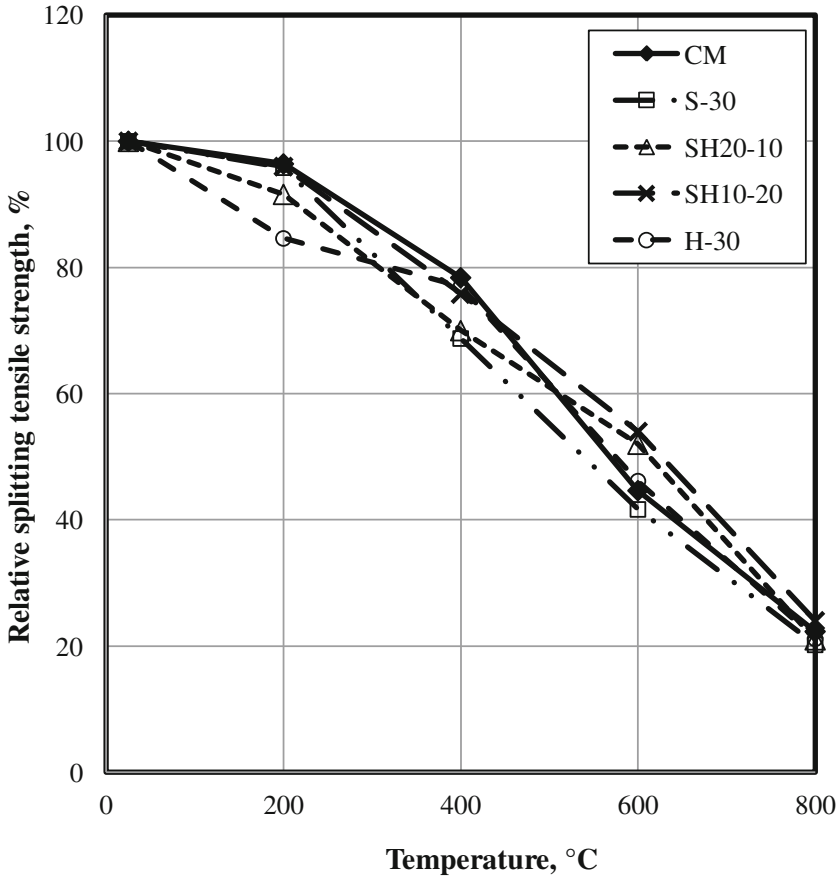


Fig. 5. Relative tensile strength of SCC specimens after exposure to high temperatures

The XRD diagram of the control specimen subjected to 800 °C, Fig. 6d, shows the presence of quartz and calcite in contrast to C-S-H and CH. The dolomite peaks intensity disappeared, which means the occurrence of the dolomite decomposition. The main components of dolomite are calcium and magnesium carbonate  $\text{CaCO}_3$  and  $\text{MgCO}_3$ . At high temperatures, there is partial transformation of  $\text{CaCO}_3$  and  $\text{MgCO}_3$  into oxides. Firstly  $\text{MgCO}_3$  in dolomite decomposes at 800 °C, and then the decomposition of  $\text{CaCO}_3$  occurs at 900 °C (Mitchell 1962). Therefore, the reduction in strength at 800 °C was due to the decomposition of the hydration products in cement paste in addition to the decomposition of dolomite.

Figure 7 shows the XRD diagrams of mix which contained 30% slag (S-30) at RT and after exposure to temperatures of 200, 600 and 800 °C for 2 h. Referring to Fig. 7a, it is clear that at RT, the intensities of C-S-H and CH are less than those for control mix at the same temperature, Fig. 6a. This may explain the increase in the strength of control mix compared to that of 30% slag (S-30) at RT. At temperatures of

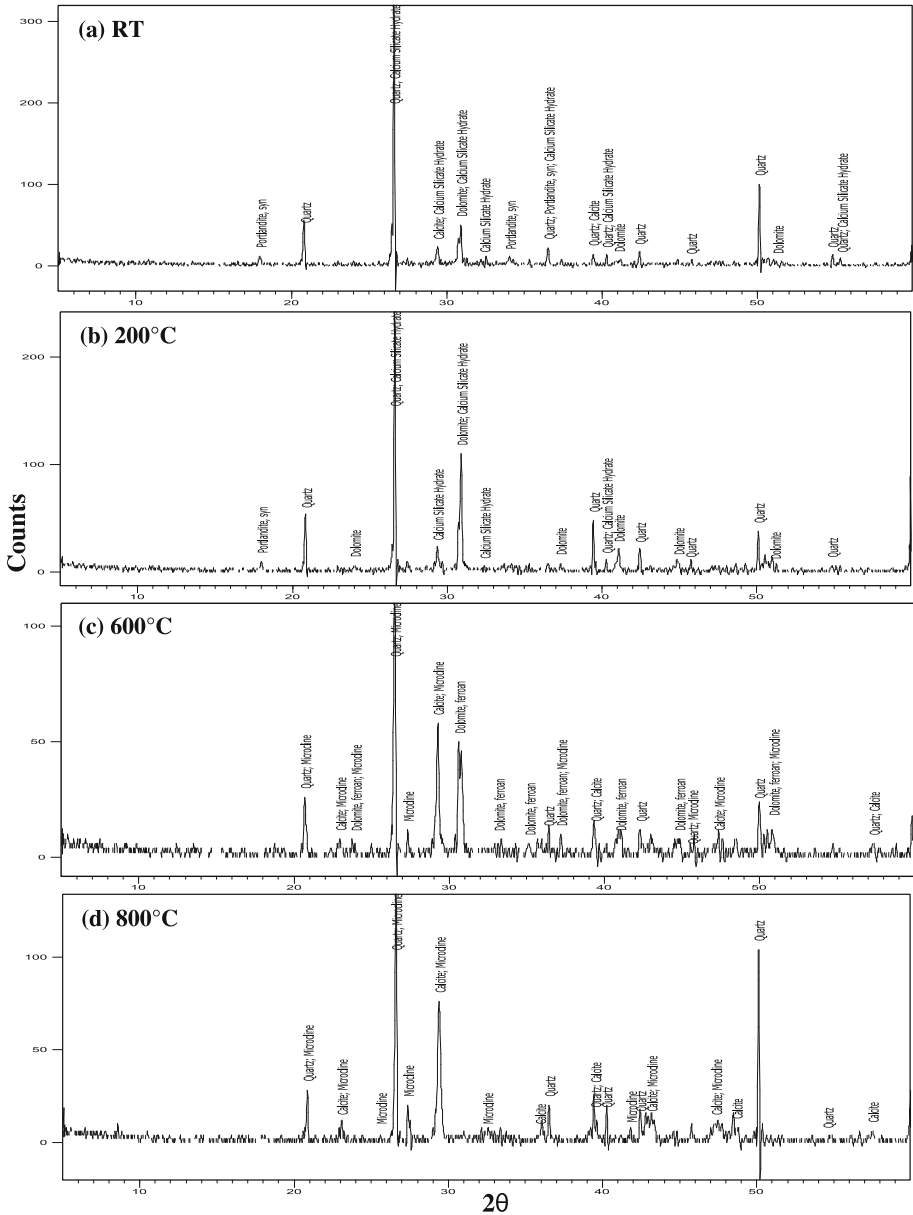


Fig. 6. XRD pattern of control mix at RT, 200, 600 and 800 °C

200, 600 and 800 °C, similar trends are observed between the XRD of the control mix and the mix containing 30% slag (S-30).

The XRD diagrams for mix containing 30% GCB (H-30) at RT and after exposure to temperatures of 200, 600 and 800 °C for 2 h are shown in Fig. 8. It is obvious that

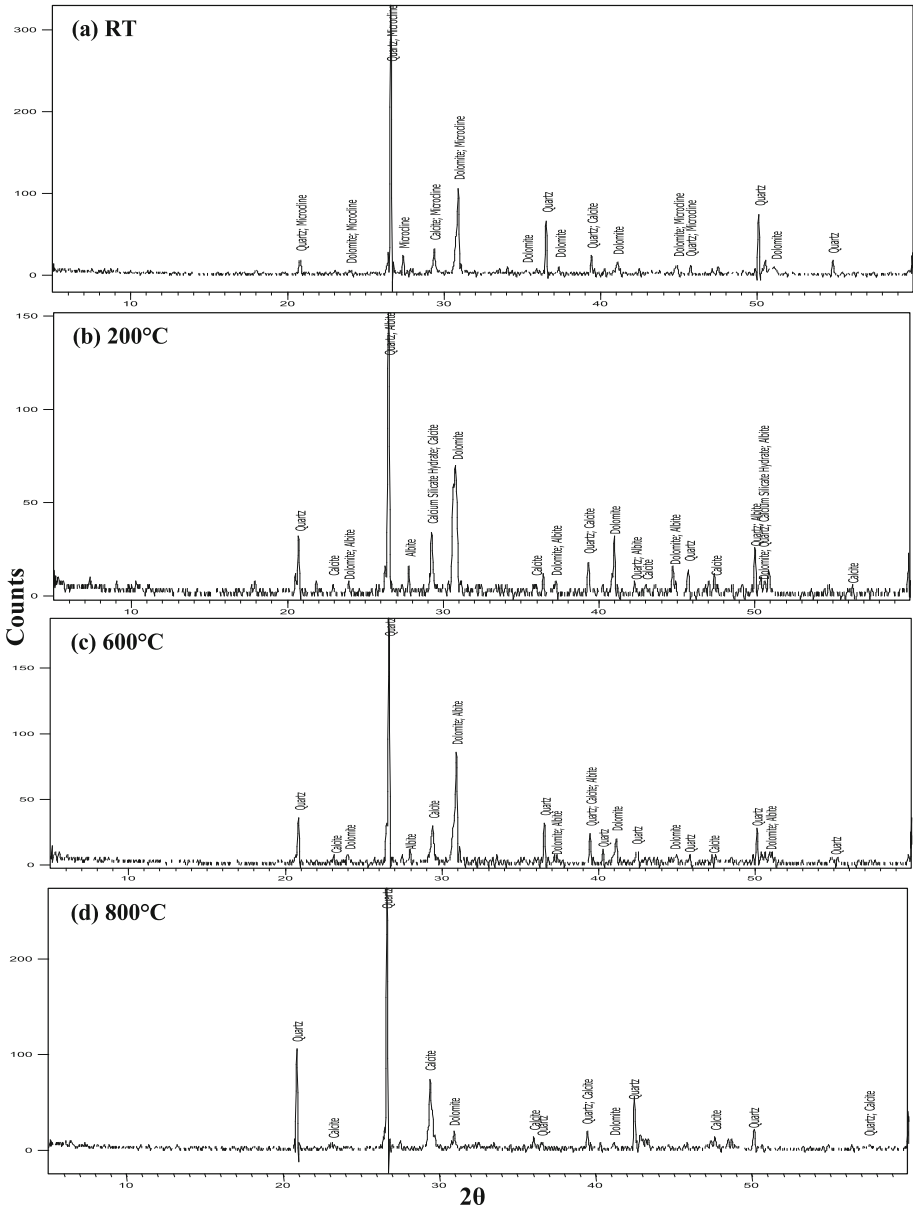
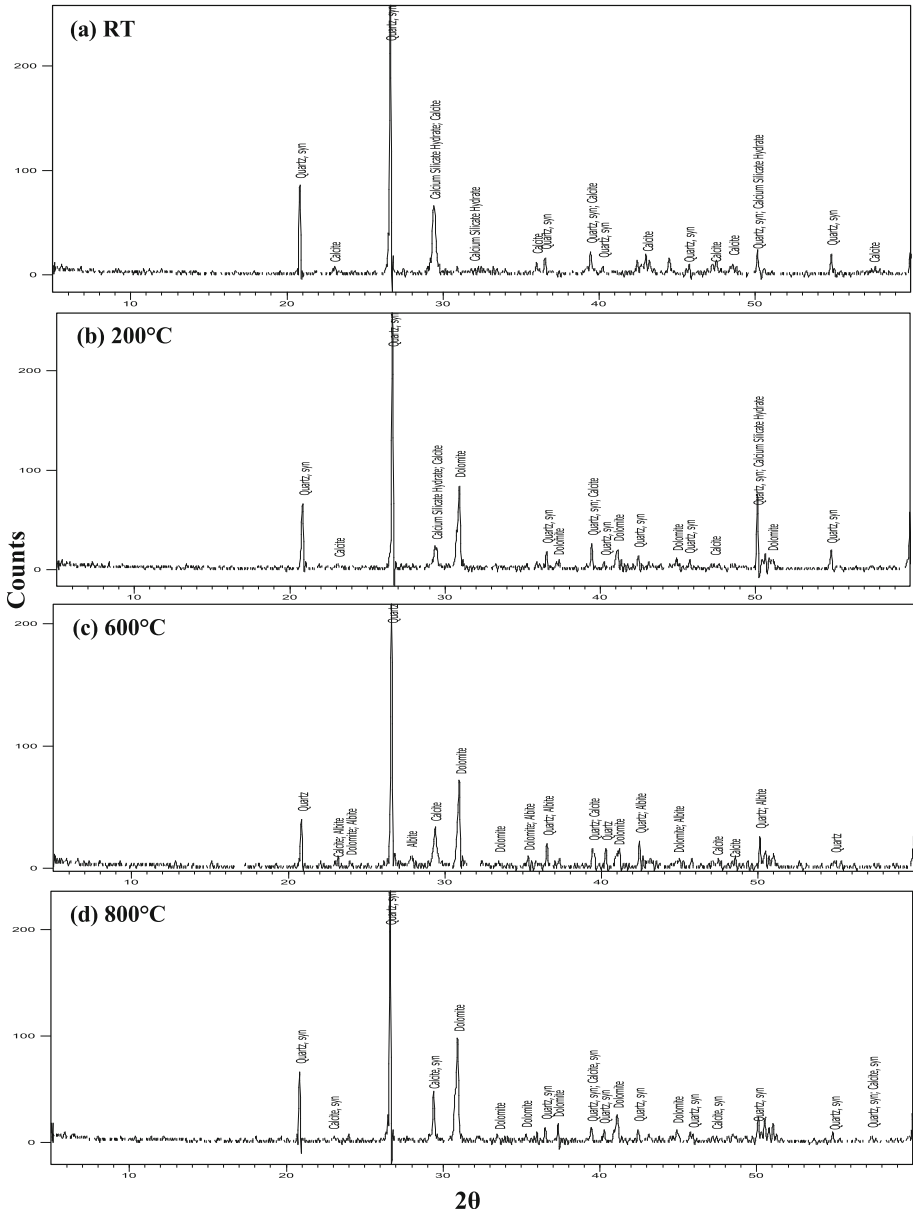


Fig. 7. XRD pattern of S-30 mix at RT, 200, 600 and 800 °C

there is difference between the XRD analysis of the control mix and the corresponding mix containing 30% GCB, (H-30) at 200 °C, Fig. 8b. The intensities of peaks characteristic of CSH and CH phases decreased with increasing temperature up to 200 °C, in contrast to the control mix and mix containing 30% GBFS. This may explain the



**Fig. 8.** XRD pattern of H-30 mix at RT, 200, 600 and 800 °C

reduction in the compressive strength at this temperature for mix containing 30% GCB. Also dolomite peak intensity still presented up to exposure to 800 °C. This is an indication to the good performance of this mix at 800 °C.



### 3.4 Surface Characteristics of SCC Samples

Visual inspection of the surfaces of SCC test specimens after exposure to high temperatures was performed to detect the signs of cracking and occurrence of spalling. No visible cracking or spalling was observed in SCC samples subjected to temperatures of 200 or 400 °C, as shown in Fig. 9. Hairline cracks appeared extensively at approximately 600 °C as shown in Fig. 10. In Fig. 11, the crack intensity increases as the temperature increases up to 800 °C. However, no spalling occurred for all SCC specimens heated to temperatures range from 200–800 °C. These result confirmed those found by Chan et al. (1999). They mentioned that the explosive spalling of HPC is governed by a vapour pressure mechanism. Spalling depends on both the strength

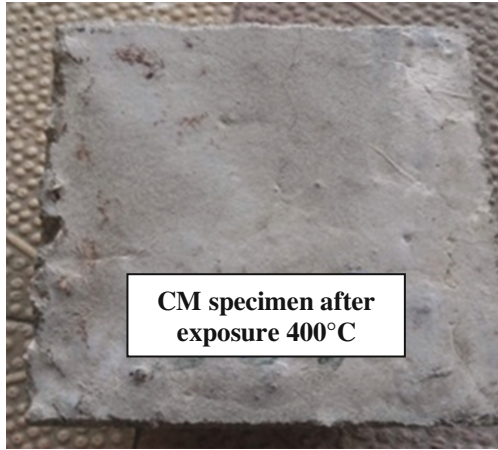


Fig. 9. Surface characteristic of SCC samples after exposure to 400 °C

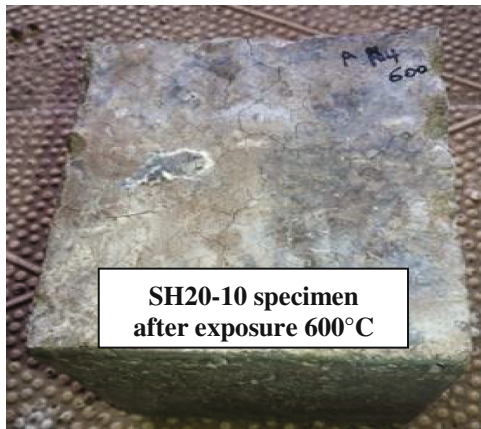
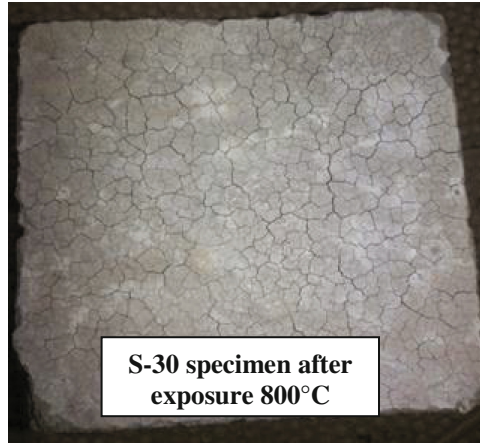


Fig. 10. Surface characteristic of SCC samples after exposure to 600 °C



**Fig. 11.** Surface characteristic of SCC samples after exposure to 800°C

and moisture content of concrete. For concrete strength less than 60 MPa, there was no spalling even with the concrete fully saturated.

#### **4 Conclusion**

Based on the results of fresh and hardened tests of SCC mixes at room and high temperatures, it can be concluded that:

1. All the mixtures had satisfactory self-compacting properties in the fresh state according to EFNARC requirements.
2. An improvement in the fresh properties was observed in SCC mixes incorporating higher contents of GBFS, in contrast to those containing high contents of GCB that showed worsening in the fresh properties compared to the control mix.
3. The use of GBFS and GCB as partial replacement of cement in SCC mixes produced slight decrease in the compressive strength ranging from 3.8–11.5%. For the tensile strength this reduction was in the range of 8.8–14% relative to the control mix.
4. The reduction in both compressive and tensile strengths due to high temperatures exposure was less with GCB than with GBFS as a result of its chemical composition.
5. After exposure to high temperatures, specimens of the control mix exhibited the best strength, followed by mixes containing large amounts of GCB, while the worst strength was recorded for specimens containing large amounts of GBFS, especially at 800 °C.
6. Utilization of GBFS, GCB or a combination of them as 30% partial replacement of cement content can produce environmentally friendly concrete mixes.

## References

- Ahmed, S.A., Khalil, H.S., Elmalky, A.A.: Use of ground glass powder in self-compacting concrete. In: Twelfth International Colloquium on Structural and Geotechnical Engineering (12th ICSGE). Ain Shams University, Faculty of Engineering, Department of Structural Engineering, Cairo, Egypt (2007)
- Badawy, A.A.M., Seleem, M.H., El-Shihy, A.M., Gabal, A.E.K.: Flexural capacity of high performance self compacting RC beams under direct fire. *Eng. Res. J.* **34**(3), 285–291 (2011a). Faculty of Engineering, Minoufiya University, Egypt
- Badawy, A.A.M., Seleem, M.H., El-Shihy, A.M., Gabal, A.E.K.: The mechanical behavior of fiber reinforced high performance self-compacted concrete at high temperatures. *Eng. Res. J.* **34**(3), 293–301 (2011b). Faculty of Engineering, Minoufiya University, Egypt
- Behnood, A., Ziari, H.: Effects of silica fume addition and water to cement ratio on the properties of high-strength concrete after exposure to high temperatures. *Cem. Concr. Compos.* **30**(2), 106–112 (2008)
- Bilodeau, A., Malhotra, V.M.: High-volume fly ash system: concrete solution for sustainable development. *ACI Mater. J.* **97**(1), 41–48 (2000)
- Castillo, C., Durrani, A.J.: Effect of transient high temperature on high-strength concrete. *ACI Mater. J.* **87**(1), 47–53 (1990)
- Chan, Y.N.: Behavior of high-performance concrete made with silica fume at various moisture contents. *ACI Mater. J.* **96**(3), 405–409 (1999)
- Demirel, B., Kelestemur, O.: Effect of elevated temperature on the mechanical properties of concrete produced with finely ground pumice and silica fume. *Fire Saf. J.* **45**, 385–391 (2010)
- Dias, W.P.S., Khoury, G.A., Sullivan, P.J.E.: Mechanical properties of hardened cement paste exposed to temperatures up to 700 °C. *ACI Mater. J.* **87**(2), 160–166 (1990)
- Dinakar, P., Babu, K.G., Santhanam, M.: Durability properties of high volume fly ash self compacting concretes. *Cem. Concr. Compos.* **30**(10), 880–886 (2008)
- El-Shihy, A.M., Seleem, M.H., Shoaib, M.M., Badawy, A.A.M., Gabal, A.E.K.: Effect of elevated temperatures on the mechanical and physico-chemical behavior of normal, high strength and light weight concrete. *Ain Shams J. Civil Eng.* **2**, 49–62 (2009)
- EFNARC, Specifications and guidelines for self-compacting concrete, EFNARC 2002, UK, pp. 1–32 (2002). <http://www.efnarc.org>
- Fares, H., Noumowe, A., Remond, S.: Self-consolidating concrete subjected to high temperature: mechanical and physicochemical properties. *Cem. Concr. Res.* **39**, 1230–1238 (2009)
- Fares, H., Remond, S., Noumowe, A., Cousture, A.: High temperature behaviour of self-consolidating concrete microstructure and physicochemical properties. *Cem. Concr. Res.* **40**(3), 488–496 (2010)
- Heikal, M.: Effect of elevated temperature on the physico-mechanical and microstructural properties of blended cement pastes. *Build. Res. J.* **56**, 2–3 (2008)
- Kuder, K., Lehman, D., Berman, J., Hannesson, G., Shogren, R.: Mechanical properties of self consolidating concrete blended with high volumes of fly ash and slag. *Constr. Build. Mater.* **34**, 285–295 (2012)
- Malhotra, M.: Reducing CO<sub>2</sub> emissions: the role of fly ash and other supplementary cementitious materials. *Concr. Int.* **28**, 42–45 (2006)
- Mitchell, L.L.: Thermal properties. *ASTM Spec. Tech. Publ.* **169**, 129–135 (1962)
- Peng, G.F., Huang, Z.S.: Change in microstructure of hardened cement paste subjected to elevated temperatures. *Constr. Build. Mater.* **22**, 593–599 (2008)

- Phan, L.T.: High-strength concrete at high temperature-an overview. In: 6th International Symposium on Utilization of High Strength/High Performance Concrete, Leipzig, Germany, vol. 1, pp. 501–518 (2002)
- Piasta, J., Sawicz, Z., Rudzinski, L.: Changes in the structure of hardened cement paste due to high temperature. *Materiaux et Constructions* **17**(100), 291–296 (1984)
- Seleem, M.H., Badawy, A.A.M., Shehabeldin, H.A.: Effect of sand aggregate ratio and type of coarse aggregate on the properties of self compacting concrete. *Eng. Res. J.* **29**(1), 105–112 (2006). Faculty of Engineering Minoufiya University
- Tanyildizi, H., Coskun, A.: The effect of high temperature on compressive strength and splitting tensile strength of structural lightweight concrete containing fly ash. *Constr. Build. Mater.* **22**, 2269–2275 (2008)
- Uysal, M., Sumer, M.: Performance of self-compacting concrete containing different mineral admixtures. *Constr. Build. Mater.* **25**, 4112–4120 (2011)
- Uysal, M., Yilmaz, K.: Effect of mineral admixtures on properties of self-compacting concrete. *Cem. Concr. Compos.* **33**, 771–776 (2011)
- Uysal, M.: Self-compacting concrete incorporating filler additives: performance at high temperatures. *Constr. Build. Mater.* **26**, 701–706 (2012)
- Uysal, M., Yilmaz, K., Ipek, M.: Properties and behavior of self-compacting concrete produced with GBFS and FA additives subjected to high temperatures. *Constr. Build. Mater.* **28**, 321–326 (2012)
- Ye, G., Liu, X., DeSchutter, G., Taerwe, L., Vandeveld, P.: Phase distribution and microstructural changes of SCC at elevated temperatures. *Cem. Concr. Res.* **37**, 978–987 (2007)
- Zhang, B., Bicanic, N.: Residual fracture toughness of normal-and high-strength gravel concrete after heating to 600 °C. *Mater. J.* **99**(3), 217–226 (2002)

# Investigation on the Effect of Anti Stripping Additives on the Moisture Sensitivity of Bituminous Concrete

A.U. Ravi Shankar<sup>1</sup>(✉), Goutham Sarang<sup>2</sup>, B.M. Lekha<sup>3</sup>,  
and Calvin Carlton-Carew<sup>4</sup>

<sup>1</sup> Department of Civil Engineering, NITK Surathkal, Mangaluru, India  
aurshankar@gmail.com

<sup>2</sup> School of Mechanical and Building Sciences, VIT University,  
Chennai Campus, Chennai, India  
goutham.sarang@vit.ac.in

<sup>3</sup> Department of Civil Engineering, KVG College of Engineering, Sullia, India  
lekhabm@gmail.com

<sup>4</sup> Edward Davies and Associates, Freetown, Sierra Leone  
calvintinto@gmail.com

**Abstract.** Moisture damage is one of the most common reasons for the premature deterioration of Hot Mix Asphalt (HMA) pavements. Over the years, extensive research has been carried out by scientists and engineers on this subject; however, pavements still succumb to early failure from infiltrating moisture. A very popular method of minimizing the moisture susceptibility of asphalt pavements is by the use of anti-stripping agents. These additives are chemical substances that alter the physicochemical properties of the asphalt by making it more hydrophobic. This study focuses on the effect of anti-stripping agents on the moisture susceptibility of Bituminous Concrete (BC) mixture. The anti-stripping agents used were hydrated lime and Zycosoil. Three mix types were studied, namely: BC mix without additive, BC mix with hydrated lime and BC mix with Zycosoil. Viscosity Grade (VG) 30 bitumen was used in all three groups of samples. Marshall mix design method was adopted and specimens were prepared at bitumen contents 4.5, 5.0, 5.5, 6.0, 6.5 and 7.0% by weight of mixture. Volumetric properties and Marshall characteristics were determined for each specimen, and using them, the Optimum Binder Content for each mixture was obtained. Moisture susceptibility of mixtures was assessed using Tensile Strength Ratio, Retained Stability and Stripping Value. From the experimental results, it is observed that the addition of anti-stripping agents had a significant positive influence on the results of the test properties being evaluated in each test.

## 1 Introduction

Asphalt has a long history as a binder in the construction of Hot Mix Asphalt (HMA) pavements. Generally, pavements are thought to be impervious but moisture-induced damage still adversely affects the longevity of HMA pavements. Over the

years, engineers and scientists have achieved tremendous feats in understanding the problem; however, pavements still yield to early failure from moisture infiltration.

The resistance of HMA to moisture damage is very critical to its long-term performance. Therefore, if an HMA mixture is susceptible to moisture damage, it could fail prematurely in due to low temperature cracking, ravelling, rutting or fatigue. Constructed HMA pavements that are in service are subjected to changing environmental conditions and traffic wheel loads. Conditioning of the pavement is done by the environment due to the presence of moisture, the fluctuations in temperature and aging of HMA mixtures. Coupled with the imposed stresses from the repeated traffic loads, detachment of the asphalt binder to the aggregate may begin to occur. As the binder is displaced, moisture moves in to capture the aggregate's surface. This phenomenon is referred to as "stripping". Based on research, the factors associated with stripping can be summarized the ability of asphalt to bond with aggregate, dust coating on aggregate, residual moisture in the HMAC during construction, moisture penetration into the pavement structure, traffic loads and freeze-thaw actions (Lottman et al. 1988; Hunter and Ksaibati 2002; Epps et al. 2000).

### 1.1 Antistripping Additives

When water sensitive pavements are exposed to moisture, deterioration to the pavement may be fast tracked. This would result in a pavement with reduced performance and service life and increases in the maintenance costs. Using clean, dustless and dry quality aggregates that are not hydrophilic will help minimize moisture damage by fostering a strong bond between the asphalt binder and aggregate surface. Paving in cool and wet conditions must also be avoided as it may lead to poor compaction and have significant effect on the sensitivity of the pavement to moisture damage.

The use of anti-stripping agents is a very effective and popular method for reducing the stripping potential of asphalt mixes. They usually minimize the moisture damage by increasing the adhesion at the aggregate-asphalt interface. The most important function of an anti-strip additive is to eliminate the moisture sensitivity of the HMA mixture by improving the bond between the asphalt binder and the aggregates, by maintaining desirable properties of the mixture. According to Hunter and Ksaibati (2002), experimental studies of the physical and compositional properties of asphalt cement with anti-stripping additives demonstrated that anti-stripping additives tend to soften asphalt, reduce temperature susceptibility, and improve the aging characteristics of asphalt cement. Also, the effect of the anti-stripping additive depends on the asphalt. Before deciding to include an anti-stripping additive to a mixture, it must first be ascertained that the mixture is susceptible to moisture damage. If an additive is used when it is not needed or if it is used incorrectly, adverse effects may occur, including early maintenance and an increase in economic cost.

Anti-strip additives can be categorized into two major groups: liquid and lime. Liquid anti-stripping additives are chemicals that reduce the aggregate's surface tension promoting better surface coverage. The liquid additive is usually added to the asphalt binder. Lime is generally added to the aggregates and it tends to change the surface chemistry or

molecular polarity of the aggregate surface. The resulting aggregate-asphalt interface in the mix is stronger as its adhesive properties are improved.

## 1.2 Liquid Anti-stripping Agents

Liquid anti-stripping agents are chemical compounds that generally contain amines and can affect the engineering properties of the aggregate, asphalt binder or the resulting asphalt mixture. The effectiveness of the liquid anti-strip on the water sensitivity of the hot mix asphalt mixture depends on the physicochemical properties of the asphalt binder and the aggregate, as well as on the amount of liquid anti-strip agent used. Most anti-stripping agents reduce surface tension between the asphalt and aggregate in a mixture. When surface tension is reduced, increased adhesion of the asphalt to the aggregate is promoted. Thus, most liquid anti-stripping agents are surface-active agents (Hunter and Ksaibati 2002). Aggregates have a natural affinity for water and hence untreated aggregates are much more likely to be damaged by water breaking the asphalt-aggregate bond. Liquid anti-stripping additives allow the asphalt cement to create a strong bond between the asphalt and aggregate. Most of the liquid anti-stripping additives are added to the heated asphalt binder prior to its application onto the aggregates and can be mixed with large amounts of asphalt and stored for use before mixing. A disadvantage of the liquid additives is that they are usually deteriorated with prolonged heating (Tayebali et al. 2003).

Various factors affect the effectiveness of the liquid anti-stripping additive including the chemistry of the asphalt binder, the chemistry and the concentration level of the liquid anti-strip, the types of dispersant used etc. The degree of aging and penetration of the asphalt cement can also be affected by the presence of a liquid anti-strip agent (TRB 2003).

## 1.3 Lime Anti-stripping Agents

The application of lime is one of the most common methods of minimizing moisture susceptibility of a mix but the mechanism with which lime eliminates stripping is not fully understood. More lime may be need if the aggregate surface area is increased by the presence of more fines (Hunter and Ksaibati 2002).

Both hydrated lime  $\text{Ca(OH)}_2$  and quick lime (CaO) are effective at preventing stripping in HMA mixes, although the former is most commonly used. Based on previous research, the addition of hydrated lime to asphalt mixtures improved the adhesive bond between the aggregate and bitumen, substantially reducing the occurrence of stripping. Further research identified chemical reactions that occurred between lime and most bitumen that reduced their affinity for water, in turn reducing the mixture's tendencies to strip. In addition, when aggregates are coated with clays, hydrated lime can react to remove the deleterious materials that would otherwise damage the mixture (TRB 2003). The effect of hydrated lime on the moisture sensitivity of asphalt mixes can also be viewed in a mechanical perspective. Hydrated lime, which is an extremely fine filler, helps to stiffen the asphalt mixture. Consequently, the

lime increases the rutting and fatigue resistance and also the ability of water to enter the system.

## 1.4 Objectives

The primary objective of this study was to determine the differences in the moisture susceptibility and stability of untreated HMA and HMA treated with various anti-stripping agents.

## 2 Materials Used

In this study, three bituminous concrete mixes were investigated. The type and gradation of the aggregate and bitumen are the same for the three mixes. However, Mix 1 had no anti-stripping additive while Mix 2 had hydrated lime and Mix 3 had Zycosoil anti-stripping additive. The mixture design criteria for BC as per the specification provided by the Ministry of Road Transport and Highways (MoRT&H), Govt. of India are listed in Table 1.

**Table 1.** Requirement for BC mixture specified by MoRT&H

Test property	Specified value
Marshall stability, kg	Min. 900 (for VG bitumen) Min. 1200 (for modified bitumen at hot climate)
Flow, mm	2–4
Percent air voids in the mix, %	3–5
Voids filled with bitumen, %	65–75
Voids in mineral aggregates, %	13

### 2.1 Aggregates

Crushed granite aggregates obtained from nearby quarry was used for the study and they were sufficiently strong, hard, tough, and well-shaped. The properties of these aggregates are presented in Table 2. Aggregate grading that satisfying the MoRT&H requirement for Grading I of Bituminous Concrete was selected and is shown in Table 3.

**Table 2.** Properties of aggregates

Property tested	Test methods	Results	MORT&H specifications
Aggregate impact value	IS:2386 (IV)	22%	24% maximum
Water absorption value	IS:2386 (III)	1.07%	2% maximum
Specific gravity	IS:2386 (III)	2.67	2.5–3.0
Combined flakiness and elongation index	IS:2386 (I)	27%	35% maximum



**Table 3.** Aggregate gradation of BC mixtures

IS sieve (mm)	Cumulative % passing
26.5	100
19	90–100
13.2	59–79
9.5	52–72
4.75	35–55
2.36	28–44
1.18	20–34
0.6	15–27
0.3	10–20
0.15	5–13
0.075	2–8

## 2.2 Mineral Filler

The mineral filler material used in the study was stone dust (ie, aggregates passing the 0.075 mm sieve) and constitutes 5% of the total aggregate weight. The grading limit for the filler is shown in Table 4.

**Table 4.** Gradation of mineral filler

IS sieve (mm)	0.6	0.3	0.075
Cumulative % passing by total weight of lime	100	95–100	85–100

## 2.3 Bitumen

The conventional Viscosity Graded 30 bitumen, with properties listed in Table 5, was used in the study.

**Table 5.** Physical properties of VG 30 bitumen

Property tested	Test method	Results
Penetration (100 g, 5 s at 25 °C) (1/10 <sup>th</sup> of mm)	IS 1203-1978	58
Softening point, °C (ring & ball apparatus)	IS 1205-1978	54
Ductility at 27 °C (5 cm/minute pull), cm	IS 1208-1978	93
Specific gravity	IS 1202-1978	1.00
Flash point, °C	IS 1209-1978	247

## 2.4 Antistripping Additives

In order to minimize the stripping potential of BC mixtures, hydrated lime and a commercial liquid chemical additive, named Zycosoil, were used. The mixture with lime is designated as Mix 2, in which 2% (by weight of aggregates) lime was added

**Table 6.** Properties of Zycosoil

Property	Description
Colour	Clear to pale yellow
Solid content	41 ± 2%
Solvent	Ethylene glycol
Viscosity at 25 °C	200–800 cps
Solubility	Forms water clear solution and soluble in bitumen

along with 3% quarry dust, as mineral filler. The hydrated lime used was also graded to satisfy the grading of mineral filler.

Zycosoil is an organosilane compound used as an additive for bituminous mixes, manufactured and supplied by M/s. Zydex Industries, Gujarat, India. Most of the aggregates contain silicates that form the silanol groups on the surface. Zycosoil reacts with these silanol groups to convert them and create an alkyl-siloxane surface. These changes to the surface characteristics of the aggregate allow for substantially improved bonding of the asphalt binder with the aggregate surface, hence reducing the stripping susceptibility of the binder. Also the alkyl-siloxane bond makes the asphalt more heat and UV stable. The properties of Zycosoil are listed in Table 6.

In this study, 1 g of concentrated Zycosoil was diluted in 10 g of Methanol, and the diluted chemical was added with bitumen at a dosage of 1% (by weight of bitumen) and mixed thoroughly. The properties of chemically modified bitumen are tabulated in Table 7. The penetration value decreased and the softening point increased by the addition of Zycosoil to the bitumen, implying the increase in stiffness of the bitumen.

**Table 7.** Properties of VG 30 bitumen with 0.1% Zycosoil

Property tested	Test method	Results
Penetration (100 g, 5 s at 25 °C) (1/10 <sup>th</sup> of mm)	IS 1203-1978	50
Softening point, °C (ring & ball apparatus)	IS 1205-1978	63
Ductility at 27 °C (5 cm/min pull), cm	IS 1208-1978	>100
Specific gravity	IS 1202-1978	1.03

### 3 Experimental Investigation

#### 3.1 Marshall Mixture Design

Marshall method of mix design was adopted in this study and specimens were prepared for all the three mixtures at bitumen contents 4.5, 5.0, 5.5, 6.0, 6.5 and 7.0% (by weight of mixture). Volumetric and Marshall properties were determined for each specimen as shown in Table 8.

**Table 8.** Properties of mixes using Marshall mix design

Bitumen content (%)	G <sub>b</sub> (g/cc)	V <sub>v</sub> (%)	VMA (%)	VFB (%)	Marshall stability (kg)	Flow (mm)	MQ (kg/mm)
<i>Mix 1 (without additive)</i>							
4.5	2.380	5.47	15.13	63.88	1032	2.6	397
5.0	2.392	4.33	15.08	71.27	1240	3.1	400
5.5	2.400	3.41	15.21	77.59	1559	3.4	459
6.0	2.410	2.39	15.26	84.32	1460	3.6	406
6.5	2.406	1.94	15.79	87.71	1407	4.1	343
7.0	2.396	1.75	16.53	89.44	1224	4.5	272
Optimum Bitumen Content, OBC = (5.5 + 6 + 5.2)/3 = <b>5.57%</b>							
<i>Mix 2 (with hydrated lime)</i>							
4.5	2.385	5.08	14.59	65.17	1116	2.5	446
5.0	2.401	3.83	14.42	73.42	1554	3.2	486
5.5	2.404	3.10	14.71	78.90	1728	3.5	494
6.0	2.420	1.83	14.52	87.38	1368	3.8	360
6.5	2.425	1.04	14.75	92.94	1262	4.1	308
7.0	2.416	0.83	15.46	94.65	1162	4.4	264
Optimum Bitumen Content, OBC = (5.5 + 6.5 + 4.9)/3 = <b>5.63%</b>							
<i>Mix 3 (with Zycosoil)</i>							
4.5	2.385	5.14	14.92	65.58	1345	2.6	517
5.0	2.403	3.82	14.71	74.06	1517	3.0	506
5.5	2.405	3.11	15.05	79.33	1654	3.4	486
6.0	2.414	2.10	15.11	86.12	1337	3.7	361
6.5	2.422	1.14	15.22	92.50	1254	4.1	306
7.0	2.416	0.78	15.84	95.05	1147	4.4	261
Optimum Bitumen Content, OBC = (5.5 + 6.5 + 4.85)/3 = <b>5.62%</b>							

### 3.1.1 Volumetric Properties

Density is an important factor for bituminous mixtures because proper density in the finished product is essential for lasting pavement performance. Table shows that the addition of anti-stripping additive increases the bulk density (G<sub>b</sub>) for the full range of percentage bitumen considered. The volume of air voids (V<sub>v</sub>) usually decreases with an increase in the percentage of bitumen for any given mix type. This is because, increasing the percentage of bitumen would provide more bitumen to fill the pore spaces and expel the air voids between the aggregates. It can be deduced from the results that, for the same magnitude of compaction, the addition of anti-stripping agent to the mix reduces the volume of air voids when the percentage bitumen and compaction temperature are the same. For any percentage of bitumen, VMA reduces when the anti-stripping agents used in this study are added to the mix. In any bituminous mix, an increase in the bitumen content would increase the percentage of VFB. It can be seen that, at any given bitumen content, the inclusion of an additive to the mix slightly increases the % of VFB. The improvement in the volumetric properties for mixtures with anti-stripping agent may be due to the improved bituminous binder properties.

### 3.1.2 Marshall Stability and Flow

The Marshall stability and flow test provides the performance prediction measure for the Marshall mix design method. The addition of anti-stripping agents increases the Marshall stability of the mix when the bitumen content is between 4.5–5.5%, however on further increase in the bitumen content, the stability decreases. Increased stability for mixtures with additives may be attributed to the improved moisture resistance, adhesion and binder properties. All three the mixes have the maximum stability at 5.5% bitumen content; with Mix 3 having the highest peak stability. The flow increases with increase in bitumen for all the mix types. Generally, in all three cases, the flow increases from 2.5 to 4.5 mm along the range of bitumen content considered. Marshall Quotient (MQ) is the ratio of Marshall stability to flow, and it was obtained to be in the specified range.

### 3.1.3 Optimum Bitumen Content

The Optimum Bitumen Content (OBC) was determined for each type of mix using the average of bitumen content corresponding to the maximum density, maximum stability and 4% air voids. The Marshall and volumetric properties of BC mixes at OBC are summarized in Table 9, and observed that all properties satisfied the requirements.

**Table 9.** Comparison of the various mix properties at OBC

Mix property	Mix 1	Mix 2	Mix 3
Optimum Bitumen Content (OBC), %	5.57	5.63	5.62
Marshall stability, kg	1,555	1,600	1,685
Flow, mm	3.40	3.40	3.60
Marshall quotient, kg/mm	457	471	468
Bulk density, $G_b$	2.401	2.404	2.406
Volume of air voids, %	3.22	3.03	3.07
Voids Filled with Bitumen (VFB), %	78.5	80	79.5
Voids in Mineral Aggregate (VMA), %	15.22	14.67	15.06

## 3.2 Moisture Susceptibility

While testing methods for determining the moisture susceptibility of asphalt mixtures are far from perfect, tests have been developed which help to characterize and compare how well various mixtures perform from a moisture susceptibility perspective.

### 3.2.1 Tensile Strength Ratio

The most common moisture susceptibility test currently conducted is based on AASHTO T 283 which results in a Tensile Strength Ratio (TSR). The test provides a method to determine how well a mixture performs after undergoing saturation, a freezing cycle, and soaking in a hot water bath to represent environmental conditioning that will occur over the lifecycle of the pavement. The TSR is a widely used concept to determine if an asphalt mixture will be susceptible to moisture damage. As a part of the test, Indirect Tensile Strength (ITS) of bituminous mixtures is determined along the

diametrical plane of cylindrical specimen. The specimens were prepared at OBC and were grouped into two subsets for each of the three bituminous mixes under investigation. Specimens in the first subset, called unconditioned specimens, were kept in a water bath for two hours at  $25 \pm 1$  °C. Each specimen in the other subset was kept in a water bath until 70–80% saturation. Then they were placed in a plastic bag with  $10 \pm 0.5$  ml of water and sealed and kept in freezer at temperature of  $-18 \pm 3$  °C for  $24 \pm 1$  h. The samples were then removed from the plastic wrapping and kept in water bath for  $24 \pm 1$  h at  $60 \pm 1$  °C. The specimens were then placed in a water bath for two hours at  $25 \pm 1$  °C. These specimens are called conditioned specimens. Both sets of specimens were tested for ITS and the ratio of conditioned ITS to unconditioned ITS is termed as TSR.

The ITS and TSR values obtained in the current investigation are presented in Table 10. Using the ITS values of Mix 1 (without additives) as a benchmark, it was found that for unconditioned samples, the addition of hydrated lime and Zycosoil improved the ITS values by 24 and 28% respectively. Also, for conditioned specimens, the addition of hydrated lime and Zycosoil to the mix improved the ITS values by 29 and 38% respectively when compared to those of the untreated mix. Mix 3 has the highest TSR ratio of 96% whilst mixes 2 and 1 have a TSR ratio of 93% and 89% respectively. All the mixtures satisfy the minimum TSR requirement of 85% suggested by MoRT&H.

**3.2.2 Retained Stability**

Retained stability test measures the loss of cohesion resulting from the action of water on compacted bituminous mixtures. A numerical index of reduced cohesion is obtained by comparing the Marshall stability of the freshly moulded and cured (unconditioned) specimens with that of the duplicate conditioned specimens that have been immersed in water under prescribed conditions.

**Table 10.** ITS and TSR values of BC mixtures

Specimen type	Unconditioned			Conditioned			TSR (%)	
	Mixture	ITS (MPa)		V <sub>v</sub> (%)	ITS (MPa)		Value	Minimum requirement
		Value	SD		Value	SD		
Mix 1	7.19	0.96	0.051	6.86	0.86	0.045	88.93	85
Mix 2	7.09	1.19	0.057	7.24	1.11	0.062	93.54	
Mix 3	6.98	1.23	0.066	7.04	1.19	0.067	96.48	

The specimens were prepared for all mix types in a similar manner as in the case of Marshall mixture design. Six samples were prepared for each of the three bituminous mixes being investigated and these six specimens were divided into two equal subsets. The first subset is the unconditioned sample set and the specimens were tested for Marshall stability. The specimens in the second subset, named conditioned subset, were cooled to room temperature and then immersed in a water bath for 24 h at 60 °C. The

specimens were then tested for Marshall stability. The ratio of average Marshall stability values of conditioned subset of specimens to that of unconditioned subset is represented as Retained Marshall Stability.

The stability of each subset for mixtures was tested and the retained Marshall stability values are tabulated in Table 11. Using the mean Marshall stability value of Mix 1 (without additive) as the benchmark, it was found that for conditioned samples, the addition of hydrated lime and Zycosoil improved the Marshall stability by 10 and 19% respectively. Mix 1 without any additive resulted into the minimum Retained stability ratio 83% whilst mixes 2 and 3 had the stability ratio of 89 and 92% respectively. MoRT&H specifies a minimum retained Marshall stability ratio of 75% for any BC mixture, and this was satisfied by all mixtures used in the study.

**Table 11.** Retained stability of BC mixtures

Specimen type	Unconditioned		Conditioned		Retained stability (%)	
	Marshall stability (kg)		Marshall stability (kg)		Value	Minimum requirement
	Value	SD	Value	SD		
Mix 1	1555	56.70	1298	48.87	89.58	75
Mix 2	1600	42.32	1432	50.29	93.28	
Mix 3	1685	39.68	1547	47.75	96.75	

### 3.2.3 Stripping Value

In order to determine the stripping value based on IS 6241, about 200 g loose mixtures were prepared for each case. The mixture was then cooled to room temperature for 2 h and transferred to a beaker. The beaker was then filled with water and kept in a water bath at 60 °C for 24 h. In this study, the test was extended for 48 h to properly observe the effect of the anti-stripping agents. The stripping value is expressed as a percentage of the uncovered or stripped area observed visually to the total area of aggregates for each test. From the results, tabulated in Table 12, it is clear that the addition of lime and Zycosoil reduces the stripping value of the mix. MoRT&H recommends an allowable maximum limit of 5% stripping after 24 h, and this criterion is satisfied by mixes with anti-stripping additives. When the test was extended for 48 h, the unmodified mixture was seriously damaged, but significant effect was not observed for other mixes.

## 4 Conclusions

The study compared the moisture susceptibility of three variations of bituminous concrete grade 1 mix: (1) Mix without anti-stripping additive (2) Mix with hydrated lime as an anti-stripping additive and (3) Mix with Zycosoil as an anti-stripping additive. Based on the results of the various tests performed in this study, the following conclusions are drawn:

- The addition of anti-stripping additives improves the bulk density of the bituminous concrete mix.
- The Marshall stability is significantly increased with the addition of anti-stripping additives.
- The addition of anti-stripping additive slightly lowers the volume of air voids of the mixes at OBC. Also, the values of the flow, VMA and VFB did not show any significant variation between samples with additives and those without.
- From the ITS results, for both conditioned and unconditioned samples, the addition of anti-stripping agent increases the ITS value. Using the untreated mix as a reference point, the addition of hydrated lime and Zycosoil improved the TSR ratio by 4% and 8% respectively.
- Using the untreated mix as a benchmark, the retained Marshall stability was improved by 7% and 10% in the mixes with hydrated lime and Zycosoil respectively.
- The addition of anti-stripping agents significantly reduces the stripping value of the bituminous concrete mix. After 24 h of conditioning, the strip value was 8%, 3% and 2% for Mixes 1, 2 and 3 respectively.

The current study resulted in improved bituminous mixtures with the use of anti-stripping additives, especially in the moisture resistance property of the mixture. Both the additives used, the hydrated lime powder and the Zycosoil liquid chemical, produced similar results, when the dosage of lime was 2% by weight of aggregates and that of Zycosoil (after diluting in methanol) was 1% by weight of bitumen.

## References

- AASHTO T 283: Resistance of compacted asphalt mixtures to moisture-induced damage, USA (2003)
- Epps, J.A., Sebaaly, P.E, Penaranda, J, Maher, M.R, McCann, M.B., Hand, A.J.: Compatibility of a test for moisture-induced damage with Superpave volumetric mix design. Transportation Research Board, NCHRP Report 444, Washington D.C (2000)
- Hunter, E.R., Ksaibati, K.: Evaluating moisture susceptibility of asphalt mixes. Department of Civil and Architectural Engineering, University of Wyoming, Laramie, Wyoming (2002)
- IS:2386: Methods of test for aggregates for concrete-part 1 particle size and shape. Bureau of Indian Standards, India (Part I) (1963a)
- IS:2386: Methods of test for aggregates for concrete-part 3 specific gravity, density, voids, absorption, bulking. Bureau of Indian Standards, India (Part III) (1963b)
- IS:2386: Methods of test for aggregates for concrete-part 4 mechanical properties. Bureau of Indian Standards, India (Part IV) (1963c)
- IS:1202: Methods for testing tar and bituminous materials; determination of specific gravity. Bureau of Indian Standards, India (1978)
- IS:1203: Methods for testing tar and bituminous materials; determination of penetration. Bureau of Indian Standards, India (1978)
- IS:1205: Methods for testing tar and bituminous materials; determination of softening point. Bureau of Indian Standards, India (1978)

- IS:1208: Methods for testing tar and bituminous materials; determination of ductility. Bureau of Indian Standards, India (1978a)
- IS:1208: Methods for testing tar and bituminous materials; determination of flash point and fire point. Bureau of Indian Standards, India (1978b)
- IS:6241: Determination of stripping value of aggregates. Bureau of Indian Standards, India (1971)
- Lottman, R.P., White, L., Frith, D.: Methods of predicting and controlling moisture damage in asphalt concrete. Transportation Research Record 1171, Washington D.C (1988)
- Ministry of Road Transport and Highways: Specification for roads and bridge works. New Delhi (2013)
- Tayebali, A.A., Fischer, W.K., Huang, Y.X., Kulkarni, M.B.: Effect of percentage baghouse fines on the amount and type of anti-stripping agent required to control moisture sensitivity. Department of Civil Engineering, North Carolina State University, Raleigh, North Carolina, Report No. FHWA/NC/2003-04 (2003)
- Transportation Research Board (TRB): Moisture sensitivity of asphalt pavements. A National Seminar, San Diego, California (2003)



# The Strength of Lightly Cemented Power Plant Ash

Felix N. Okonta<sup>(✉)</sup>, Thabo Falayi, and Roshuma Makhado

Department of Civil Engineering Science, University of Johannesburg,  
Johannesburg, South Africa  
fnokonta@uj.ac.za

**Abstract.** Coal ash from most of Eskom power plants consists of 70–85% fly ash and 15–30% bottom ash. A total of 25 million tons of ash is produced from approximately 109 million tons of coal per annum. Small percentage of the ash were used in cement production and other construction applications and almost 80% of the ash were disposed into ash dams. The need for high volume utilization is important because of the cost of disposal and associated environmental impact. The mechanical properties of Eskom ash that were stabilized with cement was investigated. Specimens of ash were stabilized with 2% to 10% of rapid hardening Portland cement (52.5R), and compacted at two different moulding water content; (a) the optimum moisture contents of stabilized specimens (15%–19%) and (b) moisture content wet of the OMC (30%). The unconfined compressive strength (UCS), soaked UCS, secant modulus and microstructure of the stabilized specimens were evaluated. The result indicated that specimens that were compacted at 30% moisture content mobilized greater UCS than those that were compacted at OMC. For specimens that were stabilized with high cement content of 8%–10% and compacted at OMC, soaking for 24 h only indicated a marginal reduction in UCS. The increase in secant modulus with cement content was nonlinear and indicated a decreasing rate with increase in cement content. The XRD and SEM results revealed that strength development was associated with the predominance of calcium silicate hydrate (CSH) and needle shaped ettringite in cement stabilized ash. Based on limited test data, only specimens that were stabilized at 30% moisture content and with greater than 4% cement met the SANS (2007) criteria for masonry and TRH (2010) criteria for pavement backfill.

## 1 Introduction

Coal is the major source of electricity in South Africa and approximately 92.8% of the electricity demand is generated by coal fired power stations (Bada et al. 2015). South Africa have a total of 18 coal fired power stations and 13 of them are in Mpumalanga province due to coal fields concentrated in that province. Currently a total of 16 power stations are operational while 2 stations are under construction. The 13 coal fired power stations in the Mpumalanga Province (coordinates 25:26:15 S/30:58:19 E), are Arnot, Camden, Duvha, Grootvlei, Hendrina, Kendal, Komati, Kriel, Majuba, Matla and Tutuka. The others are Lethabo power station in the Free State Province (coordinates 26:44:31 S/27:58/39 E), Matimaba power stations in the Limpopo province

(coordinates 23:40:06 S/27:36:38 E), Gauteng province (coordinates 25:45:28 S/28:08:49 E) have three power stations while the city of Tshwane have two in Pretoria West. Kusile power stations and Medupi power stations are under construction.

Up to 109 million tons of coal feedstock are produced per annum and this generates approximately 25 million tons of ash, and 70–85% of the total ash produced is fly ash while 15–30% is bottom ash (Nyale et al. 2013; Singh and Rafat 2015). The management of ash is a major concern in the country because annually millions of tons are disposed in ash dams which covers large area of land and there are potential ground water pollution problems (Kruger and Krueger 2005).

Sasol Synfuels by comparison consumes approximately 45 million tons of coal annually and yield over 4 million tons of fine ash (Nyale et al. 2013).

Bottom ash unlike fly ash, is coarse, porous, glassy, granular, greyish material with grain sizes ranging from fine sand to fine gravel, (Sivakumar and Kameshwari 2015). However, bottom ash is lighter and more brittle than natural fine aggregate. It has a specific gravity of 1.39–2.33 and contain more particles with diameter smaller than 75  $\mu\text{m}$  as compared to river sand or natural fine aggregates. In addition it has water absorption by mass of 31.58% while river sand has water absorption by mass of 2.46% (Singh and Siddique 2013). The major compound found in most power plant ash are silica, alumina and iron with small portion of calcium, magnesium sulfate. Both the physical and chemical properties makes coal ash a good candidate for cement additives and fine aggregate in concrete mixes for use in the construction industry (Singh and Siddique 2013).

This research was focused on the utilization of coal ash for civil engineering applications with the aim of reducing the use of natural river sand from main river channels and adjacent sandbanks. It is noted that currently the rate of sand utilization has exceeded the natural regenerative capacity of the sand, resulting in net loss of the sand. Thus there is a need to explore the use of large ash dump materials as potential replacement for natural sand as fine aggregate in concrete (Chevallier 2014).

Low cost construction rely on the use of cheap materials that are available locally. South Africa construction industry is growing at a rapid rate with both the private and public sectors investing 76% and 24% respectively in the industry, however there is scarcity of building and construction material especially river sand. In addition, the construction industry relies heavily on the transportation sectors for the distribution of construction materials locally (CIDB 2007). The use of waste for low cost construction is attractive since the growing demand of natural construction cannot be fully met (Sivakumar and Kameshwari 2015). Singh and Siddique (2013), Sivakumar and Kameshwari (2015) have demonstrated that large volume coal stabilized materials can be used for civil engineering construction.

In order to investigate the potential use of large volume of power plant derived coal ash for construction application, series of laboratory tests were conducted to determine the physical properties of coal ash as well as the mechanical properties and microstructure of cement stabilized coal ash after compaction and curing for 28 days.

## 2 Materials

The Eskom ash investigated was obtained from Eskom Camden Power Station. The station is located in the Mpumalanga province, with coordinates 26:37:13 S 30:5:38 E.

The cement used for stabilization of the coal ash was Afrisam 52.5R rapid hardening cement.

## 3 Experimental Methods

Specimens were compacted into moulds of 130 mm height and 58 mm diameter. The specimen height to diameter ratio is less than 2.5 and based on ASTM D2938 criteria, a significant variation in compression strength will not occur.

The major tests that were performed on the ash material was detailed in Table 1.

**Table 1.** Major geotechnical tests

Major tests	Specimens
Grain size analysis of coal ash (ASTM D422)	Eskom coal ash
Compaction tests using the modified proctor effort (ASTM D698)	(a) Eskom coal ash (b) Cement stabilized Eskom ash (2, 4, 6, 8, 10% cement)
Specific gravity (SG) The test was determined using ASTM D854	Eskom coal ash
Unconfined compressive strength after curing period for 28 days	(a) Eskom coal ash (b) Cement stabilized Eskom ash (2,4,6,8,10% cement)
X-ray power diffraction (XRD)	Cement stabilized Eskom ash (2, 4, 6, 8, 10% cement)
X-ray Fluorescence (XRF)	
Scanning Electron micrograph (SEM)	

## 4 Results

### 4.1 Physical Properties

The particle size distribution of the ash was detailed in Fig. 1 and Table 2. The ash consists of predominantly fine particles with more than 50% passing the 0.075 mm size. The large percentage of particles less than 0.075 mm implies high specific surface and obviates the need for mechanical activation by pulverization. The ash material is a good candidate for light weight construction material as the specific gravity is 2.35 which is lower than quartz and most clay particles. The pH is greater than 5.5 and thus the ash is not an acid generating material.

The compaction properties of Camden ash material was presented in Fig. 2. The shape of the curve is bell like and reflected the high content of particles less than 0.075 mm. The maximum dry density was 1244 kg/m<sup>3</sup> and the optimum moisture content was 22%, thus the ash materials can be compacted to lightweight materials that

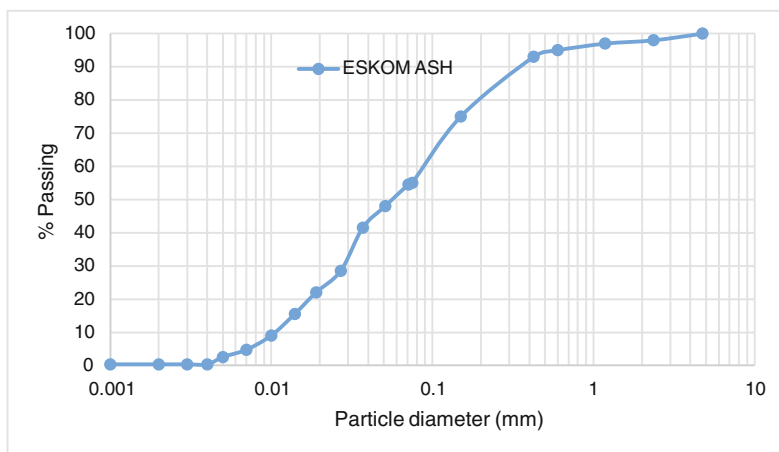


**Fig. 1.** Particle size curve of eskom ash

**Table 2.** Physical properties of camden ash

<b>D<sub>10</sub></b>	0.012 mm	<b>Cu</b>	7.5	<b>% Gravel</b>	0	<b>% Clay</b>	0.3
<b>D<sub>30</sub></b>	0.29 mm	<b>Cc</b>	78	<b>% Sand</b>	45	<b>Specific gravity</b>	2.35
<b>D<sub>50</sub></b>	0.055 mm	<b>&gt;4.75 mm</b>	100	<b>% Fine</b>	55	<b>Relative Density</b>	2.28–2.47
<b>D<sub>60</sub></b>	0.09 mm	<b>&gt;0.075 mm</b>	55	<b>% Silt</b>	54.7	<b>pH</b>	10.54–11.26

require some moisture for remoulding. Specimens of ash that were stabilized with cement did not exhibit a defined trend of increase or decrease of density with binder content.

The pozzolanic potential index of ash materials that were sampled from different location in the Ash dam in Eskom Camden station was presented in Table 3. There is no major difference in the glass content and quartz with respect to samples taken from the surface A and B, however samples taken at depth of 4 below the surface indicated significant difference in quartz and haematite ratio. All three samples have glass content and mullites ratio that supports pozzolanic reaction upon hydration and thus the ash materials requires chemical activation to increase the PPI.

The loss on ignition LOI was within the range of 4–9% SANS 50450 (2011) thus the material is category C ash and also by ASTM C618 classification. The major compound were presented in Table 4. The sum of oxides of aluminium, iron and silica was greater than 70% and thus the material was essentially pozzolanic (Cadersa et al. 2014; Menéndez et al. 2014). However because of the low calcium content, there is need for addition of more calcium from either lime or Portland cement to increase the amount of hydration products, especially the calcium hydrates.

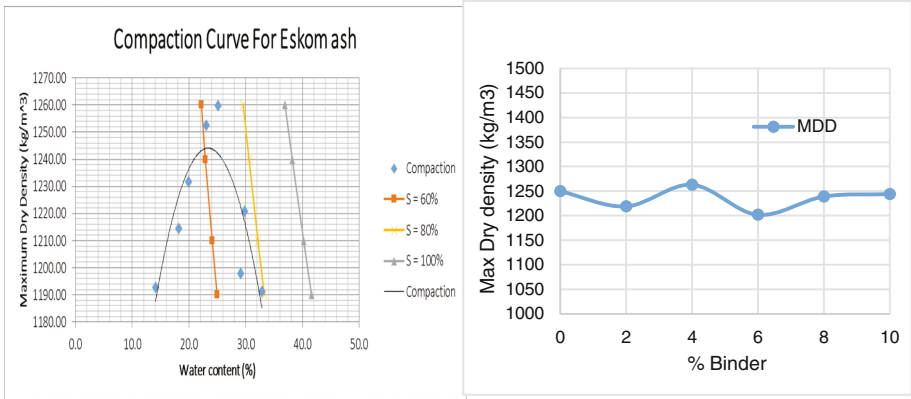


**Fig. 2.** (a) Compaction curves of eskom ash and (b) maximum dry density of cement stabilized ash.

**Table 3.** PPI of various camden ash samples %m/m

Sample	PPI	Glass content	LOI	Quartz	Mullite	Magnetite/maghemite	Haematite
A	0.46	47.52	7.22	20.96	20.96	2.85	0.44
B	0.4	45.82	7.82	21.02	21.43	3.45	0.46
C	0.54	49.97	10.76	5.17	20.48	8.61	5.02

**Table 4.** Chemical properties of eskom ash.

Content (% m/m)	Eskom ash	Content (% m/m)	Eskom Ash	Content (% m/m)	Eskom ash
Na <sub>2</sub> O	0.060333	CaO	7.311	Ga <sub>2</sub> O <sub>3</sub>	0.01161
MgO	0.538667	TiO <sub>2</sub>	2.403333	Rb <sub>2</sub> O	0.009333
Al <sub>2</sub> O <sub>3</sub>	24	Cr <sub>2</sub> O <sub>3</sub>	0.053233	SrO	0.202333
SiO <sub>2</sub>	43.43333	MnO	0.0591	Y <sub>2</sub> O <sub>3</sub>	0.181
P <sub>2</sub> O <sub>5</sub>	0.631	Fe <sub>2</sub> O <sub>3</sub>	9.833333	ZrO <sub>2</sub>	0.09
SO <sub>3</sub>	1.183	NiO	0.0178	BaO	0.138667
Cl	0.0225	CuO	0.0135	PbO	0.096667
K <sub>2</sub> O	1.106667	ZnO	0.015767	ThO <sub>2</sub>	0.009667

### 4.2 Mechanical Properties

Specimens of freshly mixed ash and different percentages of Portland cement with high liquid limit (52%–59%) and shrinkage limit of (2.6–2.29) were divided into two sets (1) Specimens were compacted at OMC and cured for 28 days at 20 °C (2) Specimens were compacted at 30% moulding water content and cured for 7 days at 35–40 °C.

Typical Ash containing 2% cement and typical 8% cement stabilized ash were presented in Fig. 3. Low cement composites were brittle, rough textured and cracks



**Fig. 3.** (a) Typical ash containing 2% cement (b) Typical 8% cement stabilized ash

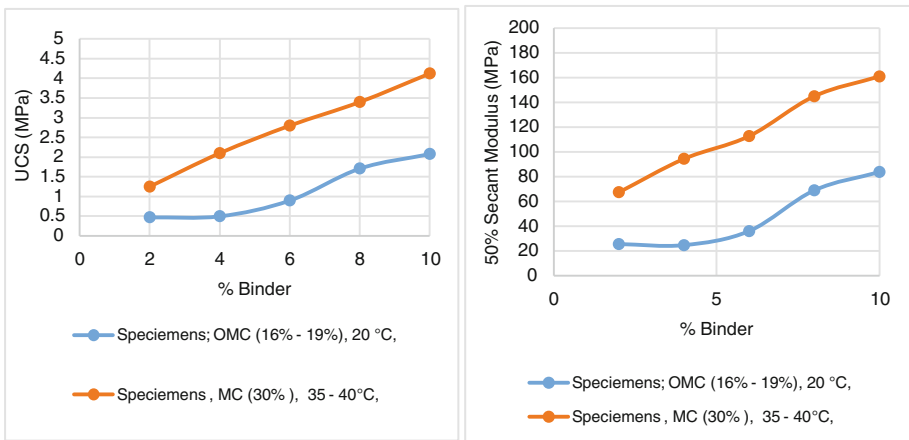


**Fig. 4.** (a) UCS of specimens cured for 28 days at 20 °C and 7 days at 35–40 °C (b) 50% Secant modulus of cement stabilized ash

easily. The UCS of specimens that were cured at the respective OMCs of 15%–19% for 28 days were presented in Fig. 4a. Also specimens that were compacted with moisture content of 30% and cured in a chamber with temperature of 35 °C–40 °C and humidity of 70% for 7 days was also presented in Fig. 4a. The specimens that were compacted at 30% and cured at 35 °C–40 °C mobilized greater UCS than specimens that were cured at their respective OMC. For specimens that were cured at OMC, there was no significant change in UCS for binder content between 2% and 6%. Thus while specimens containing 4% binder that were cured at OMC mobilized UCS less than 0.5 MPa, similar specimens that cured in chamber at 35 °C–40 °C mobilized UCS that were greater than 2 MPa. In addition only the specimens cured in the chamber mobilized UCS greater than the 3.5 MPa (SANS 2007) recommended for load bearing walls (Table 5).

**Table 5.** Atterberg limits of stabilized ash

% of cement	Liquid limit	Plastic limit (%)	Plastic index (%)	Linear shrinkage (%)
2	53.2	Nonplastic (N.P.)	Nonplastic (N.P.)	2.6
4	56.9	Nonplastic (N.P.)	Nonplastic (N.P.)	1.28
6	57.4	Nonplastic (N.P.)	Nonplastic (N.P.)	1.29
8	59.2	Nonplastic (N.P.)	Nonplastic (N.P.)	1.3
10	58.3	Nonplastic (N.P.)	Nonplastic (N.P.)	1.28

The 50% secant modulus of the stabilized ash were also presented in Fig. 4(b) and showed that irrespective of curing condition, the secant increase increased with binder content, due to the precipitation of dense calcium silicate gels. The ash cement reaction is beneficial for the development of material stiffness because bottom ash typically decreases the thermal expansion of concrete.

**4.3 Microstructure**

The XRD of ash showing Q = Quartz, M = Mullite, and H = Haematite was presented in Fig. 5(a) and (b) showed the XRD result of 8% cement stabilized ash indicating the presence of major hydration products calcium silicate hydrate CSH and Ettringite. In addition, in Fig. 6(a) the SEM of Eskom ash indicated the absence of needle shaped ettringite and Fig. 6(b) showed the SEM of 8% cement stabilized ash with strong evidence of spokes of hydration products ettringite. Similar results were obtained by Singh and Rafat (2015) in 28 days cured concrete containing 40% replaced cement.

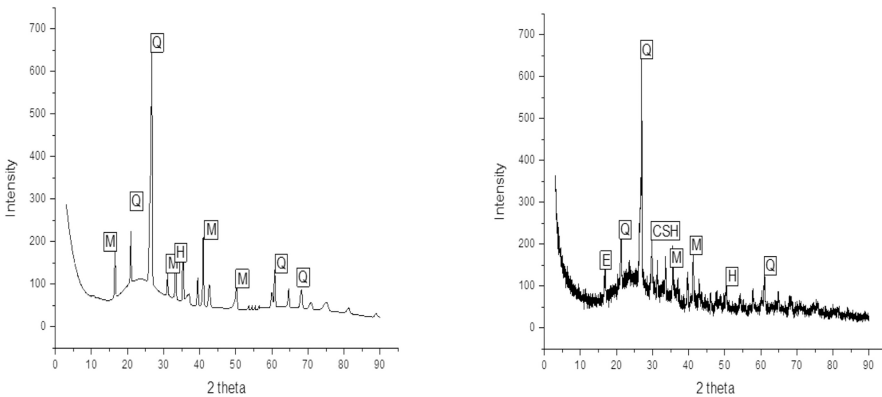


**Fig. 5.** (a) XRD graph of ash showing Q = Quartz, M = Mullite, and H = Haematite and (b) 8% cement stabilized ash indicating the presence of hydration products calcium silicate hydrate CSH and Ettringite

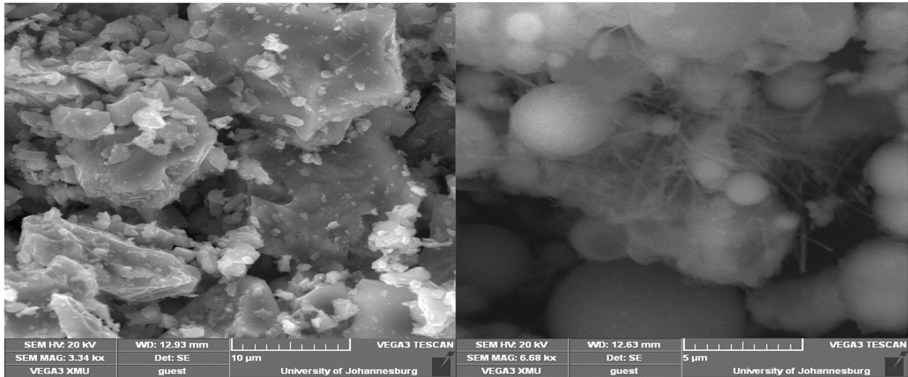


**Fig. 6.** SEM of Eskom ash and (b) SEM of Eskom+Cement: the spokes shows evidence of hydration

## 5 Conclusion

Camden power station ash materials was made up of more than 50% particles less than 0.075 mm and with specific gravity of 2.35, thus it is a good candidate for light weight construction. The PPI was below 0.5 but the sum of the oxides of iron, aluminium and silica were greater than 70% and thus the ash is a good candidate for pozzolanic induced strength development in the presence of external sources of calcium hydroxide.

The UCS of cement stabilized specimens was dependent on moulding water content and curing condition. Materials produced at curing conditions of temperature of 35–40 °C and moulding water content of 30% for 7 days developed greater compressive strength than those cured at optimum moisture content for 28 days. The strength development in cement stabilized ash was associated with the predominance of CSH and needle like ettringite.

## References

- Afrisam, n.d. Cement technical reference guide. Cement (2010)
- Bada, S., Falcon, R., Falcon, L.: Characterization and co-firing potential of high volume ash coal with Bambusa Balcooa, p. 9. School of Chemical and Metallurgical Engineering Faculty and the Built Environment, University of the Witwatersrand (2015)
- Chevallier, R.: Illegal sand mining in South Africa. Policy Brief. **11**(6), 6 (2014)
- Cadersa, A.S., Rana, J., Ramjeawon, T.: Assessing the durability of coal bottom ash as aggregate replacement in low strength concrete. *J. Emerg. Trends Eng. Appl. Sci. (JETEAS)* **5**(5), 344–349 (2014)
- Kruger, R.A., Krueger, J.E.: Historical development of coal ash utilisation in South Africa. In: *World of Coal Ash*, p. 8 (2005)



- Menéndez, E., Álvaro, A.M., Hernández, M.T., Parra, J.L.: New methodology for assessing the environmental burden of cement mortars with partial replacement of coal bottom ash and fly ash. *J. Environ. Manage.* **133**, 275–283 (2014)
- Naganathan, S., Linda, T.: Effect of fly ash fineness on the performance of cement mortar. *Jordan J. Civil Eng.* **7**(3), 326–331 (2013)
- Nyale, S.M., et al.: Synthesis and characterization of coal fly ash-based foamed. In: 2013 International Symposium on Environmental Science and Technology (2013 ISEST), pp. 722–730 (2013)
- Singh, M., Rafat, S.: Properties of concrete containing high volumes of coal bottom ash. *J. Cleaner Prod.* **91**, 269–278, 67 (2015)
- Singh, M., Siddique, R.: Effect of coal bottom ash as partial replacement of sand on properties of concrete. *Resour. Conserv. Recycl.* **72**, 20–32 (2013)
- Sivakumar, S., Kameshwari, B.: Influence of fly ash, bottom ash, and light expanded clay aggregate on concrete. *Adv. Mater. Sci. Eng.* **2015**, 9 (2015)
- South African National Standard: Burnt Clay Masonry Units. SABS, Pretoria (2007)
- The Construction Industry Development Board. The Building and Construction Materials Sector Challenges and Opportunities, s.l. Building Research Strategy Consulting Unit cc. (2007)

# Determination of Indirect Tensile Strength of Bituminous Concrete Mix Prepared Using Stone Dust and Cement as Filler Materials

Lokesh Gupta<sup>1</sup>(✉) and G. Suresh<sup>2</sup>

<sup>1</sup> Department of Civil Engineering, Sir Padampat Singhania University, Udaipur, India

lokeshgupta699@gmail.com

<sup>2</sup> Department of Civil Engineering, University Visvesvaraya College of Engineering, Bangalore University, Bangalore, India

gsuvce98@gmail.com

**Abstract.** Pavement engineers are too much concerned about the tensile properties of bituminous mix because of the problems associated with cracking. Hence tensile strength of bituminous concrete mix is important in pavement applications. The indirect tensile strength test is used to assess the tensile properties of the bituminous mix. The present research work, essentially emphasize to study the effect of filler materials, test temperature on the tensile properties and moisture susceptibility characteristics of bituminous concrete mix prepared using stone dust and cement as filler materials. For the preparation of bituminous concrete mix specimens using stone dust and cement as filler materials, optimum bitumen content was determined by adopting Marshall method of bituminous mix design. Bituminous mix properties were determined at optimum bitumen content. Indirect tensile strength (ITS) and Tensile strength ratio (TSR) of bituminous concrete mix were evaluated by varying test temperatures at 15 °C, 20 °C, 25 °C, 30 °C and 35 °C. Prediction model for Indirect tensile strength was developed by considering the temperature, Marshall stability and optimum bitumen content as independent variable for each filler material. As the test temperature increases the ITS and TSR values of bituminous concrete mix decreases irrespective of type of filler material. Based on the analysis of data, it was observed that at any test temperature, ITS and TSR values of bituminous concrete mix prepared using cement as filler material were higher when compared to bituminous concrete mix prepared using stone dust as filler material. It may be concluded that the behavior of bituminous concrete mix prepared using cement as filler material is superior in terms of mix properties, ITS and TSR.

**Keywords:** ITS · TSR · Stone dust · Cement

## 1 Introduction

The resistance of bituminous mixtures to fatigue cracking is dependent upon its tensile properties, notably its tensile strength and extensibility characteristics. The layers in a flexible pavement structure are subjected to continuous flexing as a result of the traffic

loads that they carry, resulting in tensile stresses and strains at the bottom of the bituminous layers of the pavement. The magnitude of the strain is dependent on the overall stiffness of the pavement. Indirect tensile strength test is an indicator of strength and adherence against fatigue, temperature cracking and rutting. Tensile strength is difficult to measure directly because of secondary stresses induced by gripping a specimen so that it may be pulled apart. Therefore, tensile stresses are typically measured indirectly by a splitting tensile test. As per the study of (Breen and Stephens 1966), the split cylinder test is preferred to assess the tensile strength of bituminous concrete mix at temperatures from 0 to 40 F. Many researchers (Ross et al. 1989, Sabnis et al. 1979, Chen et al. 1980) attest that tensile strength is inversely proportional to diameter of specimen (while a study made by Hondros (1959) represents vice versa that tensile strength increases with the increase in diameter of specimen. (Tunnickliff 1962) The application of filler material in a bituminous mix is primarily preferred to improve the characteristics of mix by minimizing the temperature susceptibility of binder.

Filler is a prime constituent of bituminous concrete mix and imparts a significant effect on its characteristics and performance (Anderson et al. 1992). A well-built backbone for the mixture is provided by the good packing of the coarse aggregate, fine aggregate and filler (Vavrik et al. 2002; Qiu 2006). The filler can improve the resistance of particle to move within the mix matrix and/or works as an active material when it interacts with the asphalt binder to change the properties of the mastic (Kalkattawi 1993). Zulkati et al. (2012) represents that performance of asphalt concrete mix is affected by the involvement of filler material in three traditions i.e. Firstly the amount of asphalt content in a mix largely depends upon filler material, Secondly workability during mixing and compaction, and lastly the resultant properties of asphalt-filler mastic contribute to the performance of mix.

Al-Sayed (1988) has done comprehensive investigation on the use of filler material type and recommended the utilization of the crushed limestone (fines passing than 0.975 mm) that improves the characteristics of asphalt mixes and accordingly, reduces cracking and rutting of pavements. The adding of filler material improves the resilient modulus of asphalt concrete mix (Anderson 1987). Excessive amount of filler material may result in a harsh mix as the high amount of asphalt would be needed to cover the aggregates (Elliot et al. 1991; Kandhal et al. 1998), which affect the workability of the mixture as well. According to the Craus et al. (1978), the interactive physio chemical features between the filler and bitumen are correlated to adsorption intensity at the filler-bitumen interface, and surface activity considerably contributes to better bonds at the filler-bitumen interface. It can be ascertain that the interactive role related with the physio chemical reaction, which is influenced by the type of bitumen and filler as well as the selection of filler material type in bituminous mix that would also modify its properties and improve the behavior of the bituminous mix. Wu et al. (2011) Filler material can improve the temperature susceptibility and durability performance of binder and asphalt concrete mixture.

## 2 Objective of Present Study

The objectives of the present study are-

- To study the effect of stone dust and cement as filler materials on the indirect tensile strength and tensile strength ratio of bituminous concrete mix at different temperatures viz., 15 °C, 20 °C, 25 °C, 30 °C and 35 °C.
- To develop a mathematical model for predicting the indirect tensile strength of bituminous concrete mix prepared using cement and stone dust as filler materials.

## 3 Material Characterization

Coarse aggregates, fine aggregates, mineral filler and binder are the general constituents of a bituminous mix. In the present study VG-30 as binder while Stone dust and cement are used as mineral filler.

### 3.1 Aggregates

Aggregates offers compressive and shear strength and shows good interlocking properties. To assess the properties of aggregates i.e. sufficient strength, hardness, toughness, specific gravity and shape, tests were conducted on aggregates in the laboratory and the test results are presented in Table 1. Aggregate gradation for Bituminous concrete mix (Grading-2) is adopted for the present study as per MORT&H (V<sup>th</sup> Revision) and is presented in Table 4.

**Table 1.** Aggregate test results

Test particulars	Test results	Requirements as per MORT&H (V <sup>th</sup> Revision)
Aggregate impact value (%)	21.40%	Max 24%
Los Angeles abrasion value (%)	23.34%	Max 30%
Flakiness and elongation index (Combined), (%)	27.69%	Max 30%
Aggregate stone polishing value	64	Min. 55
Water absorption (%)	0.25%	Max 2%
Aggregate specific Gravity		
• Coarse aggregate	2.663	Min 2.5
• Fine aggregate	2.65	

### 3.2 Mineral Filler

Mineral filler fills the voids, stiffens the binder and offers permeability. In the present study, stone dust and cement is used as mineral fillers. The specific gravity test and

**Table 2.** Gradation requirements of filler material

IS Sieve size (mm)	Cumulative %passing by weight of total aggregates		
	Obtained		Requirement as per MORT&H (V <sup>th</sup> Revision)
	Stone dust	Cement	
0.6	100	100	100
0.3	100	100	95–100
0.075	91.2	96.65	85–100

gradation requirement were tested in the laboratory and results obtained are presented in Table 2. Specific gravity of stone dust and cement are 2.60 and 3.09.

### 3.3 Bitumen

In the present study viscosity grade (VG-30) bitumen is used as binder material. In order to check the suitability of bitumen as binder material, tests were conducted in laboratory. The test results satisfy the requirements as per IS 73:2013 and are presented in Table 3. The specific gravity of bitumen (VG-30) is 1.01.

**Table 3.** Bitumen (VG-30) test results

Tests particulars	Test results	Requirement as per IS73:2013
Penetration at 25 °C, 100gm, 5 s, 0.1 mm	64	Min. 45
Softening point (Ring & Ball), °C	52.5	Min. 47
Flash point, °C	275	Min 220
Fire point, °C	295	Min 220
Ductility @27 °C, cm	88	Min 75
Specific gravity	1.014	Min 0.99
Kinematic viscosity @135 °C, CP	461	Min 350

**Table 4.** Aggregate gradation for bituminous concrete mix (Grading-2)

Sieve Size in mm	% Passing (Specified)	Obtained Gradation
19	100	100
13.2	79–100	89.5
9.5	70–88	79
4.75	53–71	62
2.36	42–58	50
1.18	34–48	41
0.6	26–38	32
0.3	18–28	23
0.15	12–20	16
0.075	04–10	7

## 4 Test Programme

### 4.1 Indirect Tensile Strength Test (ITS)

The Indirect Tensile Strength test is conducted in the laboratory by loading a cylindrical specimen with a single or repeated compressive load, which acts parallel to and along the vertical diametric plane. This loading configuration develops a relatively uniform tensile stress perpendicular to the direction of the applied load and along the vertical diametric plane, which ultimately causes the specimen to fail by splitting along the vertical diameter. Indirect tensile strength test mechanism is shown in Fig. 1.

Test Procedure for Conducting Indirect Tensile Strength test is-

- The test specimens are prepared at the optimum bitumen content using Marshall method of mix design for bituminous concrete mix (Grade-2) as per MoRT&H (V revision) specifications.
- The height of the specimens is recorded. Each set of specimens was tested at test temperature of 25 °C to determine their indirect tensile strength. This was achieved by using breaking head under a load applied at a rate of 50 mm per minute.

Load at failure is recorded and the indirect tensile strength is computed using the relation given below.

$$\sigma_x = (2 \times P) / (\pi \times D \times t) \quad (1)$$

Where:

- $\sigma_x$  = Horizontal tensile stress/tensile strength, N/mm<sup>2</sup>  
 P = Failure load, N  
 D = Diameter of the specimen, mm  
 t = Height of the specimen, mm.

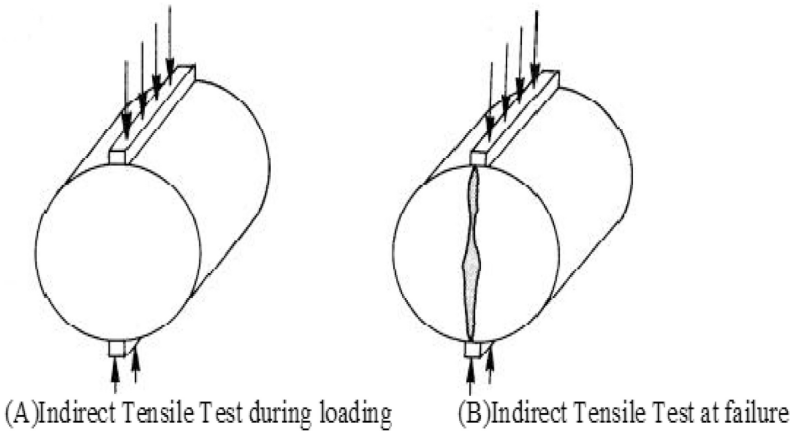


Fig. 1. Indirect tensile strength test mechanism

## 4.2 Tensile Strength Ratio (TSR)

Continuous contact of water with pavement causes premature pavement damage. Moisture induced distress may be considered as one of the most significant problem for bituminous pavement. Moisture susceptibility of bituminous mixes can be quantified by tensile strength ratio. Similar to Indirect Tensile Strength test procedure, Marshall specimens are prepared at optimum bitumen content. Procedure for evaluating the tensile strength as per ASTM D-1075 is-

Samples were divided into two groups i.e. Group-1 and group-2.

- The Group-1 of specimens are tested in a dry condition (unconditioned state), while the Group-2 specimen are tested in soaked condition.
- For the Group-1, specimens are treated as control specimens without any conditioning and then all specimens are tested for ITS at test temperature of 15 °C, 20 °C, 25 °C, 30 °C and 35 °C (by keeping them in a water bath maintained at test temperature for not less than 2 h) under the loading rate of 50 mm per minute. The load at failure is recorded and the indirect tensile strength is computed using the Eq. (1).
- For the Group-2, specimens were kept in water bath maintained at 60 °C for 24 h. The specimens were transferred to the second water bath maintained at 15 °C, 20 °C, 25 °C, 30 °C and 35 °C and kept for 2 h and then tested for ITS.
- Tensile strength ratio (TSR) can be determined using the following relation-

$$\text{TSR} = S_n / S_t \quad (2)$$

Where

TSR: Indirect Tensile Strength Ratio

$S_t$ : Average Indirect tensile strength of Group-1 specimens

$S_n$ : Average Indirect tensile strength of Group-2 specimens

## 5 Results and Discussion

Indirect Tensile Strength test is conducted on bituminous concrete mix (Grading-2) prepared using stone dust (1%), stone dust (2%), cement (1%) and cement (2%) as filler materials at optimum bitumen content. Specimens are conditioned at 15 °C, 20 °C, 25 °C, 30 °C, 35 °C in water bath for a duration of 2 h. The test results are presented in Tables 5, 6 and 7, Figs. 2 and 3.

### 5.1 Indirect Tensile Strength (ITS)

#### 5.1.1 Effect of Filler Material

It is observed from Table 5 that the indirect tensile strength (ITS) of bituminous concrete mix depends on filler content and also vary depending on filler type. At 25 °C

**Table 5.** Indirect tensile strength of bituminous concrete mix prepared using stone dust and cement as filler materials

Mix type	Filler content	Indirect tensile strength, N/mm <sup>2</sup>				
		15 °C	20 °C	25 °C	30 °C	35 °C
Bituminous concrete mix-II	S-1	0.878	0.863	0.849	0.802	0.79
	S-2	0.939	0.921	0.913	0.869	0.821
	C-1	0.972	0.963	0.954	0.923	0.910
	C-2	1.121	1.110	1.079	1.010	0.963

**Table 6.** Indirect tensile strength (Conditioned Specimen @ 60 °C) of bituminous concrete mix prepared using stone dust and cement as filler materials

Mix type	Filler content	Indirect tensile strength, N/mm <sup>2</sup>				
		15 °C	20 °C	25 °C	30 °C	35 °C
Bituminous concrete mix-II	S-1	0.775	0.7457	0.725	0.672	0.641
	S-2	0.839	0.813	0.796	0.739	0.674
	C-1	0.893	0.872	0.858	0.814	0.760
	C-2	1.153	1.041	0.995	0.925	0.862

**Table 7.** Tensile strength ratio of bituminous concrete mix prepared using stone dust and cement as filler materials

Test temperature, °C	Tensile strength ratio (TSR), %			
	Stone dust (1%)	Stone dust (2%)	Cement (1%)	Cement (2%)
15	88.35	89.84	91.91	95.34
20	86.41	88.31	90.56	93.78
25	85.19	87.28	89.93	92.25
30	83.71	85.1	88.24	91.58
35	81.22	82.1	83.51	89.51

test temperature, there is substantial increase in the indirect tensile strength value of bituminous concrete mix prepared using Cement 2% and Cement 1% by about 15% and 11% when compared to bituminous concrete mix prepared using stone dust 2% and stone dust 1% respectively. Similar trend can also be observed at 15 °C, 20 °C, 30 °C and 35 °C test temperature.

Further the ITS value of bituminous concrete mix prepared using stone dust as filler material is always lesser than cement as filler material. The difference among the results may be due to cement as filler material causes better stiffening or reinforcing effect in bituminous concrete mix as well as acting as an antistripping agent.



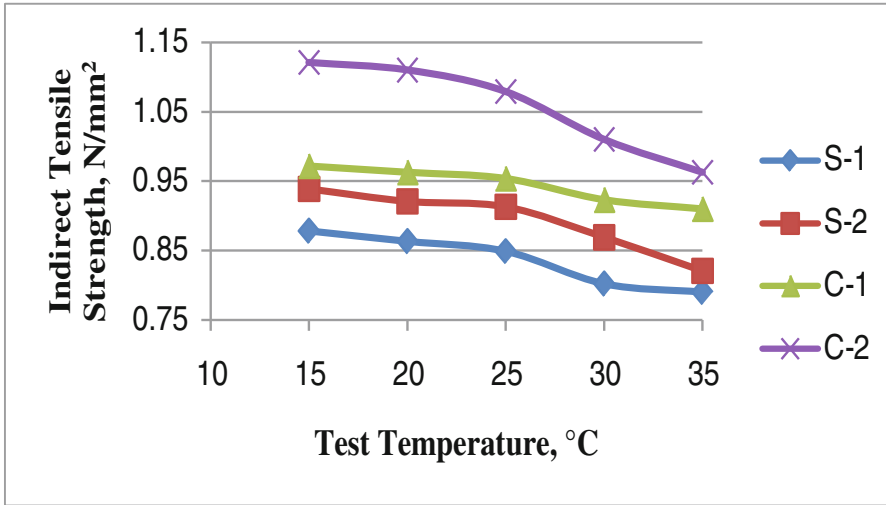


Fig. 2. Indirect tensile strength of bituminous concrete mixes prepared using stone dust and cement as filler materials.

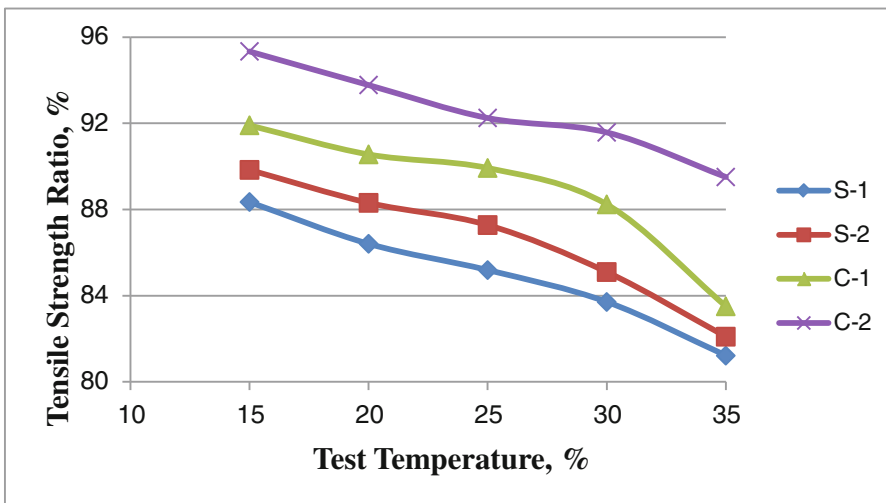


Fig. 3. Tensile strength ratio of bituminous concrete mixes prepared using stone dust and cement as filler materials.

**5.1.2 Effect of Test Temperature**

In Fig. 2 it is observed that as the temperature increases from 15 °C to 35 °C, there is substantial reduction in ITS value of bituminous concrete mix prepared using cement 2%, stone dust 2%, cement 1% and stone dust 1% as filler material by about 16%, 14%, 6% and 11% respectively.

Actually temperature is inversely proportional to viscosity. Therefore, with the elevation in temperature, the viscosity of bitumen reduces. This may be one of the factor that, as the test temperature increases from 15 °C to 35 °C, the ITS value of bituminous concrete mix reduces irrespective of type of filler material and filler content.

**5.2 Tensile Strength Ratio (TSR)**

Figure 3 shows the relationship between the tensile strength ratio (TSR) and different test temperature ranging from 15 °C to 35 °C for stone dust and cement as filler material. At 25 °C test temperature, there is marginal increase in tensile strength ratio of bituminous concrete mix prepared using cement 2% and cement 1% by about 6% and 5% when compared to bituminous concrete mix prepared using stone dust 2% and stone dust 1% respectively. Similar trend can also be observed at 15 °C, 20 °C, 30 °C and 35 °C test temperature.

As the test temperature increases from 15 °C to 35 °C, the TSR value of bituminous concrete mix reduces irrespective of type of filler material and filler content. This is observed in Table 7.

**6 Prediction Model**

Prediction model for indirect tensile strength (ITS) is developed by considering the temperature, Marshall stability and optimum bitumen content as independent variables for each filler material i.e. cement 2%, stone dust 2%, cement 1% and stone dust 1%. Prediction model is developed in the form of-

$$ITS_{X_n} = A_0 + A_1T + A_2S + A_3OBC \tag{3}$$

Where-

- ITS<sub>X<sub>n</sub></sub> = Indirect Tensile Strength, N/mm<sup>2</sup>
- X = Filler Material, Stone dust or Cement
- N = Filler Content, 1% or 2%
- A<sub>0</sub> = Constant
- A<sub>1</sub>, A<sub>2</sub>, A<sub>3</sub> = Regression Coefficient
- T = Temperature, °C
- S = Marshall Stability, Kg
- OBC = Optimum Bitumen Content, %

**6.1 Model for Stone Dust 1%**

Summary of prediction model for indirect tensile strength (ITS) of bituminous concrete mix prepared using stone dust 1% is presented in Table 8. Model developed for stone dust 1% is as-

$$ITS_{S_1} = -15.548 - 0.005T + 0.01S + 0.822OBC \tag{4}$$

Coefficient of correlation and adjusted R square ( $R^2$ ) values are 0.990 and 0.978 respectively.  $R^2$  is the coefficient of determination. Table 8 illustrate that independent variables i.e. temperature, Marshall stability and optimum bitumen content are able to explain the variation in indirect tensile strength (ITS) up to an extent of 97.8% ( $R^2 = 0.978$ ). Further analysis also indicates that temperature, Marshall stability and optimum bitumen content are statistically significant associated with the ITS value ( $p = 0.0000$ ) as p value is less than the predetermined  $\alpha$  value i.e. 0.05 (5%).

**Table 8.** Summary of prediction model for ITS value of bituminous concrete mix prepared using stone dust 1%

Model Summary (Stone dust 1%)									
Model	R	R square	Adjusted R square	Std. error of the estimate	Change statistics				
					R square change	F change	df1	df2	Sig. F Change (p)
1	0.990	0.980	0.978	0.005231	0.980	428.834	3	30	0.000

a. Predictors: (Constant), OBC, Temperature, Stability  
 b. Dependent Variable: ITS

**ITS<sub>s\_1</sub> = -15.548 - 0.005T + 0.01S + 0.822OBC**

**6.2 Model for Stone Dust 2%**

Summary of prediction model for indirect tensile strength (ITS) of bituminous concrete mix prepared using stone dust 2% is presented in Table 9. Model developed for stone dust 2% is as-

$$ITS_{s_2} = -29.248 - 0.006T + 0.025 S - 0.183 OBC \tag{5}$$

Coefficient of correlation and adjusted R square ( $R^2$ ) values are 0.988 and 0.972 respectively.  $R^2$  is the coefficient of determination. Table 8 illustrate that independent

**Table 9.** Summary of prediction model for ITS value of bituminous concrete mix prepared using stone dust 2%

Model summary (Stone dust 2%)									
Model	R	R square	Adjusted R square	Std. error of the estimate	Change statistics				
					R square change	F change	df1	df2	Sig. F Change (p)
1	0.988	0.976	0.972	0.014101	0.976	97.658	3	30	0.000

a. Predictors: (Constant), OBC, Temperature, Stability  
 b. Dependent Variable: ITS

**ITS<sub>s\_2</sub> = -29.248 - 0.006T + 0.025S - 0.183 OBC**

variables i.e. temperature, Marshall stability and optimum bitumen content are able to explain the variation in indirect tensile strength (ITS) up to an extent of 97.2% ( $R^2 = 0.972$ ). Further analysis also indicates that temperature, Marshall stability and optimum bitumen content are statistically significant associated with the ITS value ( $p = 0.0000$ ) as  $p$  value is less than the predetermined  $\alpha$  value i.e. 0.05 (5%).

### 6.3 Model for Cement 1%

Summary of prediction model for indirect tensile strength (ITS) of bituminous concrete mix prepared using cement 1% is presented in Table 10. Model developed for cement 1% is as-

$$ITS_{C\_1} = -15.246 - 0.002T + 0.012S - 0.159 OBC \tag{6}$$

Coefficient of correlation and adjusted R square ( $R^2$ ) values are 0.992 and 0.984 respectively.  $R^2$  is the coefficient of determination. Table 8 illustrate that independent variables i.e. temperature, Marshall stability and optimum bitumen content are able to explain the variation in indirect tensile strength (ITS) up to an extent of 98.4% ( $R^2 = 0.984$ ). Further analysis also indicates that temperature, Marshall stability and optimum bitumen content are statistically significantly associated with the ITS value ( $p = 0.0000$ ) as  $p$  value is less than the predetermined  $\alpha$  value i.e. 0.05 (5%).

**Table 10.** Summary of prediction model for ITS value of bituminous concrete mix prepared using cement 1%

Model summary (Cement 1%)									
Model	R	R square	Adjusted R square	Std. Error of the Estimate	Change Statistics				
					R square change	F change	df1	df2	Sig. F change (p)
1	0.992	0.985	0.984	0.0038502	0.985	1205.604	3	30	0.000
a. Predictors: (Constant), OBC, Temperature, Stability									
b. Dependent Variable: ITS									
<b><math>ITS_{C\_1} = -15.246 - 0.002T + 0.012S - 0.159 OBC</math></b>									

### 6.4 Model for Cement 2%

Summary of prediction model for indirect tensile strength (ITS) of bituminous concrete mix prepared using cement 2% is presented in Table 11. Model developed for cement 2% is as-

$$ITS_{C\_2} = -64.70 - 0.009T + 0.044S + 0.107 OBC \tag{7}$$

**Table 11.** Summary of prediction model for ITS value of bituminous concrete mix prepared using cement 2%

Model summary (Cement 2%)									
Model	R	R square	Adjusted R square	Std. error of the estimate	Change Statistics				
					R square change	F change	df1	df2	Sig. F change (p)
1	0.997	0.994	0.992	.001303	0.992	13806.86	3	16	.000

a. Predictors: (Constant), OBC, Temperature, Stability

b. Dependent Variable: ITS

$$ITS_{C_2} = -64.70 - 0.009T + 0.044S + 0.107 OBC$$

Coefficient of correlation and adjusted R square ( $R^2$ ) values are 0.997 and 0.992 respectively.  $R^2$  is the coefficient of determination. Table 8 illustrate that independent variables i.e. temperature, Marshall stability and optimum bitumen content are able to explain the variation in indirect tensile strength (ITS) up to an extent of 99.2% ( $R^2 = 0.992$ ). Further analysis also indicates that temperature, Marshall stability and optimum bitumen content are statistically significant associated with the ITS value ( $p = 0.0000$ ) as p value is less than the predetermined  $\alpha$  value i.e. 0.05 (5%).

## 7 Conclusions

On the basis of limited laboratory study carried out in the present study, the following conclusion are drawn-

- At the elevated temperature, indirect tensile strength (ITS) value of the bituminous concrete mix prepared using stone dust and cement as filler material decreases.
- ITS value of viscoelastic material is highly influenced by the test temperature.
- Substantial increase in indirect tensile strength value of bituminous concrete mix prepared using cement (2%) and cement (1%) as filler materials.
- Marginal increase in tensile strength ratio (TSR) of bituminous concrete mix prepared using cement (2%) and cement (1%) as filler materials.
- If the tensile strength of bituminous concrete mix is more and TSR is with in the permissible limit, then it can be concluded that bituminous concrete mix may be safe against fatigue.
- In the prediction model, temperature, Marshall stability and optimum bitumen content are statistically significant with the ITS value.
- It may be concluded that the behavior of bituminous concrete mix prepared using cement as filler material is superior in terms of mix properties, ITS and TSR value.

## References

- Al-Sayed, M.H.: The Effect funeral filler performance of tolled Asphaltic Mixes. Ph.D. Thesis, University of Leeds (1988)
- Anderson, D.A., Bahia, H.U., Dongre, R.: Rheological properties of mineral filler asphalt mastics and their relationship to pavement performance. In: Meininger, R.C. (ed.) ASTM STP 1147. American Society for Testing Materials, Philadelphia, U.S.A. (1992)
- Bazant, Z.P., et al.: Size effect in brazilian slip-cylinder tests: measurement and fracture analysis. *Mater. J.* **88**(3), 325–332 (1991)
- Breen, J.J., Stephens, J.E.: Split cylinder test applied to bituminous mixtures at low temperature. *J. Mater.* **1**(1), 66–76 (1966)
- Chen, W.F., Yuan, R.L.: Tensile strength of concrete: double-punch test. *J. Struct. Div. ASCE* **106 ST8**, 1673–1693 (1980)
- Craus, J., Ishai, I., Sides, A.: Some physico-chemical aspects of the effect and the role of the filler in bituminous paving mixtures. *J. Assn. Asphalt Paving Technol.* **47**, 558–588 (1978)
- Elliot, R.P., Ford, M.C., Ghanim, M., and Tu, Y.F.(1991), Effect of aggregate gradation variation on asphalt concrete mix properties, Transportation Research Record, 1317, National Research Council, Washington, D.C
- Gupta, L., et al.: A study on the marshall properties Of DBM mix prepared using Vg-30 and Crmb-55 as binder materials. *IJRET* **05**(3), 32–36 (2016). doi:[10.15623/ijret.2016.0503007](https://doi.org/10.15623/ijret.2016.0503007)
- Gupta, L., Suresh, G.: Effect of using cement and Fly Ash as filler material on The Marshall Properties of bituminous concrete mix. *Indian Highways*, April 2016, pp. 09–15 (2016). ISSN 0376-7256
- Hondros, G.: Evaluation of poisson ration and the modulus of materials of low tensile resistance by the Brazilian (Indirect Tensile) test with particular references to concrete. *Aust. J. Appl. Sci.* **10**(3), 243–268 (1959)
- IS: 73, 2013. Paving bitumen-specification. Bureau of Indian Standards, New Delhi, India
- Kalkattawi, H.R.: Effect of Filler on the Engineering Properties of Asphalt Mixes, M.S. Thesis, King Abdul Aziz University, Jeddah, Saudi Arabia (1993)
- Kandhal, P.S., et al.: Characterization tests for mineral fillers related to performance of asphalt paving mixtures. *Transp. Res. Rec. J. Transp. Res. Board* **1638**(1), 101–110 (1998)
- Ministry of Road Transport and Highways (MORTH): Specifications for Road and Bridge Works, Section 500, Fifth Revision, Indian Roads Congress, New Delhi, India (2013)
- Qiu, Y.: Design and performance of stone mastic asphalt in Singapore conditions, Ph.D. thesis, Nanyang Technological University, Singapore(2006)
- Ross, C.A., Thompson, P.Y., Tedesco, J.W.: Split-hopkinson pressure-bar tests on concrete and mortar in tension and compression. *ACI Mater. J.* **86**(5), 475–481 (1989)
- Sabnis, G.M., Mirze, S.M.: Size effects in model concrete. *J. Struct. Div. ASCE* **106 ST6**, 1007–1020 (1979)
- Taih, S.A.: The effect of additives in hot asphalt mixtures. *J. Eng. Dev.* **15**, 131–150 (2011)
- Tunnicliff, D.G.: A Review of Mineral Filler. *A.A.P.T.* **3** (1962)
- Vavrik, W.R., Pine, W.J., Carpenter, S.H., Bailey, R.: Bailey, Method For Gradation Selection in Hot-Mix Asphalt Mixture Design, Transportation Research Board, National Research Council, Washington, D.C. (2002)
- Wu, S., Zhu, J., Zhong, J., Wang, D.: Experimental investigation on related properties of asphalt mastic containing recycled brick powder. *Constr. Build. Mater.* **25**(6), 2883–2887 (2011)
- Zulkati, A. et al.: dpEffects of Fillers on Properties of Asphalt-Concrete Mixture. *J. Transp. Eng.* 902–910 (2012). [10.1061/\(ASCE\)TE.1943-5436.0000395](https://doi.org/10.1061/(ASCE)TE.1943-5436.0000395)

# Sustainable Application of Quarry Byproducts Mixed with Large Size Unconventional Aggregates for Improved Performance

Issam Qamhia, Hasan Kazmee, Erol Tutumluer<sup>(✉)</sup>, and Hasan Ozer

University of Illinois at Urbana-Champaign, Champaign, USA  
{qamhia2, kazmee2, tutumlue, hozer2}@illinois.edu

**Abstract.** With recent focus on sustainable construction practices and the ever-increasing transportation costs and scarcity of natural resources, integration of large-size unconventional and marginally acceptable aggregates, such as quarry by-products (QB), and making their routine use in construction specifications is becoming imperative. In this study, the stability of large-size aggregates is increased by adding QB as sand- and smaller-sized particles to fill up the voids. Adding QBs is expected to increase density and provide stability for better aggregate interlock, and therefore, to increase the subgrade strength and eventually improve the road's rutting performance. In order to determine the appropriate weight mix ratio of the large-size aggregates and the fine QB materials, a steel box with dimensions 610 mm by 610 mm by 533 mm was built to assess the packing of the two materials. One of the sides of the box was designed to have a transparent Plexiglas that enabled observation of the QB percolation into the voids of the large-sized aggregates, which were added in multiple lifts. The QB materials were then evenly spread on the surface of each lift and compacted with a laboratory-sized roller compactor. Different mix ratios, support conditions, and moisture contents of the QBs were investigated. The study concluded that 25% QB by the dry weight of the large aggregates is an appropriate amount to be used for both one- and two-lift construction practices of this composite weak subgrade replacement aggregate material, i.e., aggregate subgrade, in the field. The laboratory results will be implemented in the field by constructing test sections for unpaved construction platform and asphalt-paved low volume road applications and monitoring them for rutting performance using an accelerated pavement testing device.

## 1 Introduction

Adequate subgrade support is critical to proper compaction of overlain pavement layers and long term pavement performance. In the Midwestern United States, in-situ subgrade soils have predominantly silt content and stay saturated throughout the year and as a result, conventional chemical stabilization may often be deemed ineffective for subgrade stabilization and pavement working platforms. Achieving adequate subgrade stability becomes more challenging owing to the freeze-thaw effects followed by harsh winters. To this end, Illinois Department of Transportation (IDOT) frequently uses crushed rocks for weak subgrade remediation. Furthermore, IDOT has recently

introduced open-ended gradation bands allowing inclusion of large rocks with a maximum dimension in the range of 152 to 203 mm. These large rocks can be originated from both primary crushing stage at quarries and recycled sources and are often referred to as “aggregate subgrade.” Materials by IDOT. In a recent full scale accelerated pavement testing study, such application of large rocks was proven to be beneficial in terms of pavement rutting performance (Kazmee et al. 2016). However, the researchers also concluded that uniformly graded large rocks could exhibit variable performance in strength and deformation characteristics due to significant particle reorientation in presence of large voids in the granular matrix. For this, sufficient amount of fine materials is necessary for a stable unbound aggregate layer with uniformly graded large rocks.

Over the last few decades, transportation agencies have been using more and more recycled materials and industrial byproducts alternative to materials from primary sources. However, by-product variability, improper storage and/or stockpiling and lack of end-performance based specifications have been the major hurdles in environment-friendly construction practices. Quarry byproduct (QB) is one such material found abundantly all over the United States as an entailment to the vast network of crushed rock extraction facilities. According to a recent Federal Highway Administration report, 159 million metric tons of quarry byproducts are being generated in over 3000 quarries in United States each year, little of which is being put to use for highway applications (Chesner et al. 1998). Stroup-Gardiner and Wattenberg-Komas (2013) synthesized that only 4 states out of 50 use mill-tailings or screenings in flowable fill and embankment; whereas, 5 states out of 50 utilize such byproducts in hot mix asphalt.

Considering the open-ended gradation bands and abundance of fines from mineral aggregates extraction, IDOT recently initiated a research study at the University of Illinois with the goal to investigate effective use of a certain percentage of QB screenings as fine materials to be mixed with the aggregate subgrade large rocks over weak subgrade. To this end, a field study was undertaken at the Illinois Center for Transportation (ICT) to assess the rutting performance of blended primary crusher run aggregates and QB fines. However, no clear guidelines could be established as to dictate the appropriate percentage of QB filling up the voids in large rocks. Several previous studies have focused on the application of stabilized QB layers in pavement structures (Galetakis et al. 2012; Puppala et al. 2012; Tutumluer et al. 2015). Conversely, only a few studies in the past dealt with the packing perspective in typical base course and/or railway ballast granular materials (Boler et al. 2014; Xiao and Tutumluer 2016). However, none of these studies involved packing optimization of large rocks and QB-fines for sustainable applications in construction platforms. With this in mind, this paper focuses on a laboratory investigation conducted to ascertain the most stable blend of large rocks and QB. According to the ASTM size specifications, a customized compaction box was built to investigate the packing efficiency at varying percentages of QB materials, compactive effort with respect to lift thickness and support condition. The compaction box was designed such that compacted blends can be visually examined from a standard distance and height for meaningful qualitative assessment. The following sections discuss details of the designed compaction box, comparison of selected QB blends and the selection procedure for optimized QB percentage for field applications.



## 2 Objective and Scope

Based on the recent research at the University of Illinois on the use of large-size unconventional aggregates (up to 200 mm nominal aggregate size) for subgrade replacement applications, the penetration of large rocks into very soft subgrade (CBR 1) was effective in improving the weak subgrade and preparing a fairly stable working platform in pavement construction (Kazmee et al. 2016). The study also concluded some stability issues of those large primary crusher run aggregates and a wide variation in rutting performance due to the presence of inherent voids. The stability issues can be overcome by filling up some of the voids with QB. The main objective of this paper has been to study the maximum possible quantity of QB that can be practically used for this purpose and to investigate construction practices for mixing the QB with the large rocks using a steel box in the laboratory for vibratory compaction. The laboratory study is thereafter replicated in the field by building test sections of large aggregates with QB shaken and compacted from the top in one and two lifts to be used as stable pavement materials for both construction platforms and hot mix asphalt (HMA-paved) low volume road applications.

### 2.1 Aggregate Materials Used

The QB used in this study are the residual deposits from the production of required grades of primarily carbonatic crushed stone aggregate in the state of Illinois. These are usually less than 6 mm in size and are often stockpiled in excess quantities at the quarries. The chemical composition of the used QB material, as determined by X-ray fragmentation (XRF) technique is shown in Table 1, which shows that the rock type is mainly limestone. The typical QB grain size distribution is presented in Fig. 1.

**Table 1.** Chemical Composition of the QB Material

XRF analysis	CaO	MgO	SiO <sub>2</sub>	Fe <sub>2</sub> O <sub>3</sub>	SO <sub>3</sub>	K <sub>2</sub> O	Others
Quantity (%)	81.11	11.29	5.59	0.84	0.50	0.46	0.21

The unconventional large-size aggregates used are primary crusher run limestone aggregates intended to simulate a recently adopted aggregate subgrade IDOT gradation band known as CS02. For simplicity, the large aggregate materials will be referred to as ‘CS02’ in this paper hereafter. These aggregates have a nominal aggregate size of 150 mm, and are mostly larger than 12.5 mm in size. The grain size distribution of the used CS02 material, along with the IDOT gradation bands for CS02 are also shown in Fig. 1. The gradation of particles smaller than 76 mm was performed by traditional sieve analysis, while the size of the particles retained on the 76-mm or 3-in. sieve was obtained using a field imaging technique.

The Enhanced University of Illinois Aggregate Image Analyzer (E-UIAIA) was used to determine the morphological shape properties, namely: Angularity Index (AI), Surface Texture (ST) and Flat and Elongated Ratio (F&ER) (Moaveni 2015) for

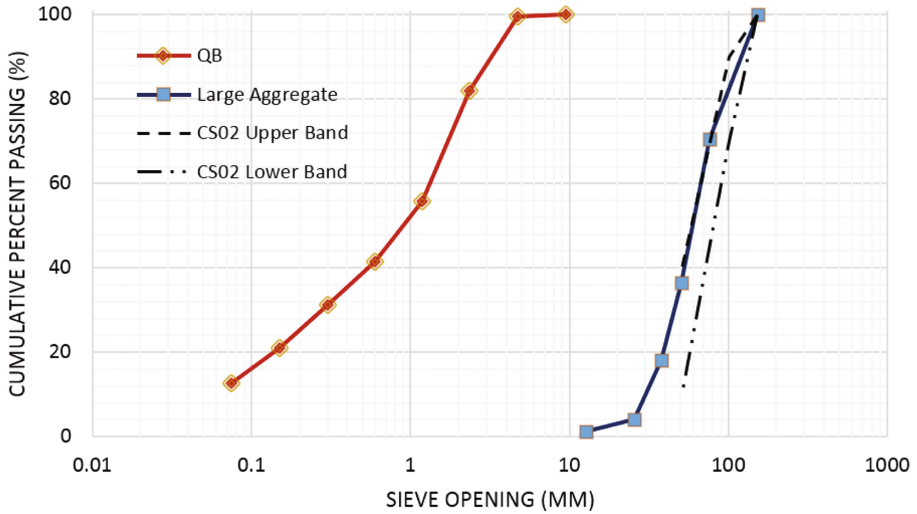


**Fig. 1.** Gradation curves for the QB and the large CS02 aggregates used in the box compaction study and field application

**Table 2.** Summary of the average morphological shape properties of the CS02 large aggregates

Sieve size		Number of scanned particles	Average angularity	Average F&E ratio	Average surface texture
mm	in.				
76.2	3.0	88	447.84	1.36	2.37
50.8	2.0	48	488.37	2.11	1.54
38.1	1.5	26	452.87	2.01	1.38
25.4	1.0	21	401.69	2.37	1.44
12.7	0.5	6	462.61	2.48	2.29

particle sizes smaller than 76 mm. The imaging based aggregate shape properties are summarized in Table 2. The number of particles is chosen based on the gradation curve to give a representative estimate of the shape properties. It can be seen that particles larger than 76 mm, which comprise around 30% of the total size and with an F&ER of 1.36 are relatively cubical in shape, which is expected to highly influence the void ratio and the packing of these aggregates.

## 2.2 Description of Test Setup and Test Procedure

To determine the appropriate weight mix ratio of the large-size aggregates and the fine QB materials, a steel box with dimensions 610 mm by 610 mm by 530 mm was built to assess the packing of the two materials. One side of the box has a removable steel door, which is pulled up to expose the cross section to a Plexiglas side, and an image is taken of the cross section (see Fig. 2) to study the packing and percolation of the QB through the large aggregates. In the earlier tests, the front sliding door was used, but

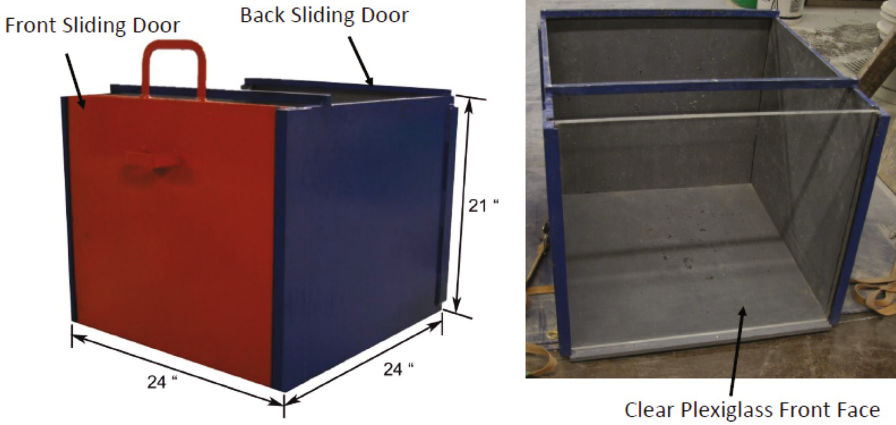


**Fig. 2.** UIUC compaction box showing the front and back sliding doors and the clear plexiglas face (1 in = 25.4 mm)

later on the vibration of the QB and compaction was performed directly against the Plexiglas in order to obtain more realistic images of the cross section, especially when it was concluded that compaction was not causing a serious damage to the Plexiglas. The purpose of the back sliding door is to assist with emptying the box after the test is completed.

The large aggregates were added in the box in one or two equal lifts, and the QB materials are evenly spread on the surface using a hand shovel and then compacted with a laboratory-sized roller compactor to the satisfaction of the operator such that no further movement and rearrangement of individual aggregate particles was possible. Since these large aggregates were dumped from previously weighed buckets, the final weights of the leftover aggregates in the buckets and therefore the weight of the large rocks placed in the box were recorded. Note that the heights of the loose large rocks, loose large rocks and QB on the surface, and the compacted mix were typically measured at nine locations (center, midpoint of each face, and each corner) in the box, and averaged for density calculations. To minimize variability, the same large aggregates were used in all tests.

### 3 Description of the Test Matrix

A total of fourteen (14) different tests were conducted using the UIUC compaction box. The test matrix included tests for variables including: the number of lifts for compaction (1 or 2 equal lifts), the quantity of the QB by weight of the large rocks, the moisture content of the QB, as well as the support conditions (a rigid steel bottom vs. compaction on top of a very soft subgrade soil). Table 3 summarizes the test matrix in the order the tests were conducted. The following sections will present detailed results and discuss the effects of the test variables studied.

**Table 3.** Summary of the Test Matrix for All Tests conducted using the UIUC Compaction Box

Test No.	Percentage of QB (%)	No. of lifts	Moisture content of QB (%)	Support condition	Achieved density $\text{kN/m}^3$ (pcf)
1	0 (CS02 only)	2	0 (oven dry)	Steel bottom	14.73(93.8)
2	0	2	0	Steel bottom	14.75 (93.9)
3	0	1	0	Steel bottom	14.15 (90.1)
4	0	1	0	Steel bottom	14.43 (91.9)
5	20	2	0	Steel bottom	17.80 (113.3)
6	40	2	0	Steel bottom	19.57 (124.6)
7	30	2	0	Steel bottom	18.95 (120.6)
8	30	1	0	Steel bottom	18.69 (119.0)
9	30	2	0	Steel bottom	19.07 (121.4)
10	40	2	0	Steel bottom	20.28 (129.1)
11	35	1	0	Soft loose subgrade	18.58 (118.3)
12	30	2	2.6	Steel bottom	18.91 (120.4)
13	25	2	2.5	Steel bottom	18.32 (116.6)
14	25	1	2.6	Soft compacted subgrade	18.58 (118.3)

### 3.1 Compaction Tests of CS02 Aggregate Subgrade Materials

Compaction tests were conducted for the large CS02 aggregates in order to study the packing conditions and assess their void ratios. Tests were conducted in the box for both the 1-lift and 2-lift construction cases of CS02 materials. The bulk specific gravity was measured as per ASTM C127 to be 2.67. Using this value of specific gravity, and based on the arrangement of the large rocks in the box, a void ratio of 77.5% and 83.1% were calculated for the large rocks compacted in two lifts and one lift, respectively. These correspond to porosity values of 43.6% and 45.4% for the two- and one-lift arrangements, respectively. Based on these calculations, and given that some of the voids will be isolated and cannot be filled with QB; the maximum possible QB quantity to be used was set to 40% of the weight of the dry large rocks. Cross sections of the compacted large rocks in the UIUC compaction box are shown in Fig. 3. The average compacted densities achieved are  $14.74 \text{ kN/m}^3$  and  $14.29 \text{ kN/m}^3$  for the two-lift and one-lift arrangements, respectively.

### 3.2 Effect of Varying Quantity of QB

As described in the test matrix, the quantity of the QB to be mixed with the CS02 was varied to determine the optimum quantity to be used in the field application. The quantity of the QB was varied between 20% and 40% of the dry weight of the large



**Fig. 3.** Cross sections of the compacted large aggregates in (a) One lift and (b) Two lifts

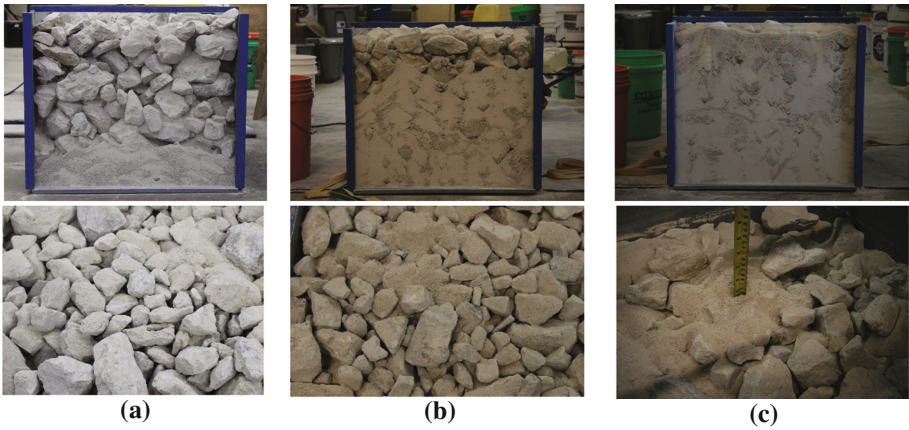


**Fig. 4.** Cross sections (Top) and top views (Bottom) of the compacted large aggregates with (a) 20% QB (b) 30% QB and (c) 40% dry QB by dry weight of CS02

rocks to study the maximum practical amount that can be added. Figure 4 shows an example of varying the quantity of QB between 20%, 30% and 40% for compaction in 2 lifts in the case of dry QB. By a visual assessment of the surface and the cross section, 20% and 30% of the dry weight of the large rocks are somewhat underestimating the amount of dry QB that can be packed within the CS02 large aggregates, while 40% leaves excessive quantity of the QB on the surface; indicating that the optimum dry quantity of QB is around 35%. In the case of wet QB, however, the optimum quantity was approximately 25% as explained later in this paper.



### 3.3 Effect of Varying Number of Lifts

The main construction variable to be studied in the field is the effect of the number of lifts for which the CS02-QB mix is to be constructed. The IDOT field application over a very weak, California Bearing Ratio of 1% ( $CBR = 1\%$ ), subgrade soil requires almost 533-mm thick CS02-QB mix and additional 76-mm of dense graded capping layer with a top aggregate size of 25-mm. Accordingly, the CS02-QB lift thickness will either be 533 mm for the one-lift construction or two equal lifts of approximately 267 mm. In both cases, the QB will be spread evenly on top of the lift and vibrated into the voids of the large aggregates. It is believed that constructing with two lifts will lead to a better quality control, more homogeneous mix, and will accommodate more of the QB needed for ensuring a stable improved subgrade layer. However, it is also believed that any excess QB left on the surface between the two lifts might result in loss of contact between the large aggregate particles, leading to loss of shear strength and a weaker shear plane that might jeopardize the layer performance. The mechanical performance will be later tested in the field, and the purpose of the lab study is to quantify the reasonable amount of QB to be added in both cases, as well as to qualitatively inspect the percolation of the QB with changing other variables.

Initial laboratory results have not shown a big difference in densities and percolation between the 1-lift and 2-lift experiments with dry QB. Figure 5 shows images of the top surface and the cross sections with 30% QB by weight for both 1 and 2 lifts experiments. However, the results are expected to differ for wet QB as higher moisture

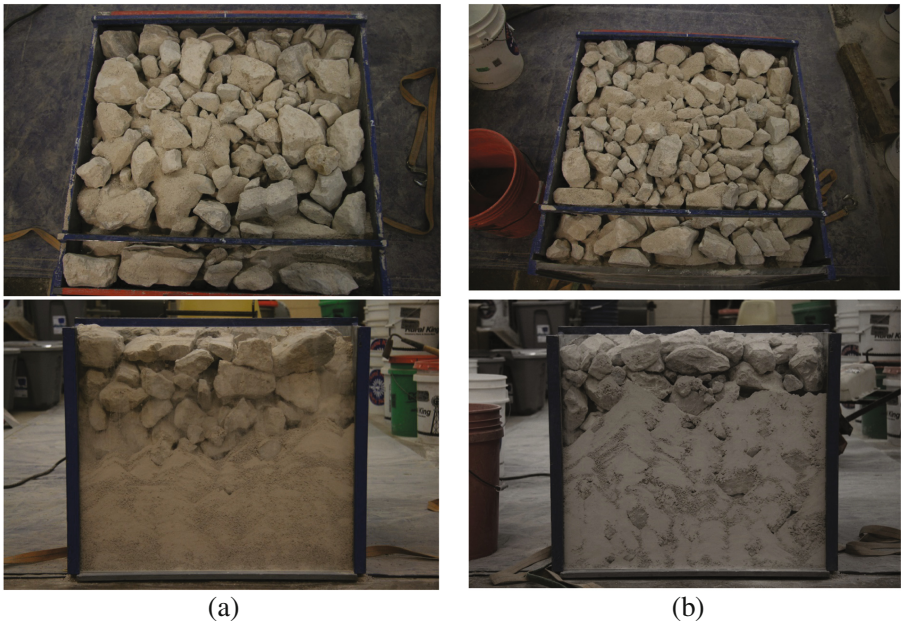


**Fig. 5.** Top views (Top) and cross sections (Bottom) of the compacted large aggregates with 30% dry QB by dry weight of CS02 in (a) 1 lift (b) 2 lifts

contents could make it more difficult for the QB to percolate and fill the voids at higher depths when constructing a 1-lift application. This was not tried in the laboratory, however, the field application eventually indicated that only two-thirds of the optimum quantity of QB that was used in a 2-lift construction could be used in a 1-lift application before starting to accumulate fine materials on the surface.

### 3.4 Effect of Moisture Content of QB

Two different moisture contents were studied in the laboratory. The first is the ideal condition of completely dry (oven dried for  $24 \pm 1$  h), which is expected to maximize the amount of QB that will fill the voids between the large rocks. The other moisture content is the as-received moisture content of the QB material from the source quarry, which was measured to be around  $2.5 \pm 0.2\%$ . The second moisture content is more realistic for field construction, and is considered a typical value for the moisture content to be encountered during the field construction, since several quarries reported a typical in-situ moisture contents of 2–3.5% in the state of Illinois on a dry day. Visual inspection of the cross section of the Plexiglas and the top surface after compaction showed roughly similar excess amount when 40% dry QB and 30% wet QB by weight of the large rocks were used (see Fig. 6). Thus, based on these results, even though 30% was found to be the optimum quantity of QB in the case of dry QB; the same quantity was found to lead to a relatively large amount of QB left on the surface when the QB had a moisture content of 2.5%. Accordingly, a maximum quantity of 25% of the weight of the large CS02 aggregates was proposed and tested, which ultimately led to good percolation, and a significantly smaller quantity left on the surface. Two final tests were performed with the 25% wet QB: the first is in two lifts on top of the rigid steel foundation, and the second is a one-lift test (approximately 292 mm height). Both tests with 25% showed that this quantity is the maximum reasonable quantity to be used for increasing the stability of the CS02 and reducing the amount of QB remaining on the surface and weakening the structure. Thus, the recommended QB quantity to be used for field construction is 25% of the weight of the large CS02 aggregates. The next section explains the effect of the type of foundation.

### 3.5 Effect of Foundation Rigidity

Initially, the compaction tests of the CS02 and the CS02-QB mixes were conducted on top of a rigid steel bottom in the box. To further simulate the field application, where the CS02-QB mix would be used for subgrade modification on top of a very soft subgrade with CBR = 1%, two tests were carried out in the UIUC compaction box for a CS02-QB mix compacted on top of a very soft subgrade. A representative sample (from a representative depth) of the low plasticity CL-ML subgrade on which the field test sections will be built was obtained and used for this study. The in-situ subgrade had a moisture content of 11.5% and an average CBR of 12% as estimated using the South African equation (Kleyn 1975) developed for interpreting the Dynamic Cone Penetrometer (DCP) field test results. The subgrade soil was modified to a CBR of approximately 1% in the laboratory



**Fig. 6.** Top views of the surface of the compacted large aggregates with (a) 40% dry QB and (b) 30% QB with 2.5% moisture content showing roughly similar quantities remaining on the surface

by increasing the water content to 16% (Mishra 2012), which enabled the achievement of the very low CBR as verified using the DCP equipment.

For the first test, the subgrade was left loose, and the quantity of the oven-dried QB used was 35% of the weight of the CS02. For the second test, QB 25% of the weight of the CS02 was used, and the QB had a moisture content of 2.6%, which is the moisture content of the QB as received from the quarry on a dry day. The subgrade was compacted in the box using a vibratory roller prior to adding the CS02. The 35% value for the dry test was chosen based on the previous results with the rigid steel bottom, which concluded that 40% was excessive while 30% left room for more QB to be added. For the wet results, the 25% value was chosen because 30% was found to be excessive in the case of wet QB as shown previously in Fig. 6. Figure 7 shows the cross sections of a CS02-QB mix with 25% wet QB by the dry weight of the CS02, compacted in two lifts on top of a rigid foundation and in one-lift on top of very soft subgrade. Based on the possibility of wet QB applications in the field, the amount of QB that is 25% by weight of the CS02 was found to be the optimum value to be recommended for use in the field application.



**Fig. 7.** Cross sections of the compacted large aggregates with 25% of wet QB by dry weight of CS02 on top of (a) Rigid steel bottom (b) Soft compacted subgrade soil



## 4 Conclusions

This paper presented the use of Quarry Byproducts (QB) that are intended to fill the voids of large rocks recently adopted in Illinois for subgrade replacement and subbase use as “aggregate subgrade” materials. The QB mixed with the primary crusher run type large-size aggregate subgrade materials can provide sustainable field applications for increased stability of working platforms and low volume road applications constructed on top of very soft, California Bearing Ratio of approximately 1% (CBR = 1%), subgrade soils. In this study, the appropriate weight mix ratio of the large-size aggregates and the fine QB materials was studied in the laboratory using a steel packing box having one transparent Plexiglas face. The optimum amount of QB was assessed visually by inspecting the surface and the cross section of the QB and large aggregates mix after the QB is shaken on the top. Several factors were found to affect the maximum quantity of QB that can be used to stabilize large rocks and fill the voids. The moisture content of the QB was found to be one of the most important factors. Other significant factors include the gradations of both materials, the number of lifts for construction, and the rigidity of the foundation on top of which the QB is vibrated. One important lesson learnt is that in order for the QB to percolate through the large rock, the compaction technique used should provide proper vibration; otherwise, a higher compactive effort will create a thin layer of QB on the surface, inhibiting any further QB from percolating and reducing the efficiency of void filling. Additionally, less QB could be accommodated as the moisture content of the QB increased, especially in the case of a one lift construction practice, where it becomes harder for the QB to percolate the full depth when vibrated from the surface. Future papers will follow up on this study with further details of the field construction.

**Acknowledgments.** The support for this study was provided by the Illinois Department of Transportation as part of the recent ICT R27-168 research project. The authors would like to acknowledge the members of IDOT Technical Review Panel (TRP) and especially Sheila Beshears as the TRP Chair for their useful advice at different stages of this research. The authors also acknowledge support from the Illinois aggregate producers for donating the aggregate materials. Special thanks go to Illinois Center for Transportation (ICT) research engineer James Meister as well as Marc Killion and the staff in the machine shop of the Newmark Civil Engineering Laboratory at the University of Illinois. Many thanks for John Hart and Dr. Maziar Moaveni for characterizing aggregate shape properties and the undergraduate student Lucas Chae for his help with conducting the laboratory tests. The contents of this paper reflect the views of the authors who are responsible for the facts and the accuracy of the data presented herein. This paper does not constitute a standard, specification, or regulation.

## References

- Boler, H., Qian, Y., Tutumluer, E.: Influence of size and shape properties of railroad ballast on aggregate packing. *Transp. Res. Record J. Transp. Res. Board Transp. Res. Board Nat. Acad.* **2448**, 94–104 (2014). doi:[10.3141/2448-12](https://doi.org/10.3141/2448-12)

- Chesner, W.H., Collins, R.J., MacKay, M.H.: User Guidelines for Waste and Byproduct Materials in Pavement Construction. Techreport, Washington DC (1998)
- Galetakis, M., Alevizos, G., Leventakis, K.: Evaluation of fine limestone quarry by-products, for the production of building elements – an experimental approach. *Const. Build. Mater.* **26**(1), 122–130 (2012). doi:[10.1016/j.conbuildmat.2011.05.011](https://doi.org/10.1016/j.conbuildmat.2011.05.011)
- Kazmee, H., Tutumluer, E., Beshears, S.: Pavement working platforms constructed with large-size unconventional aggregates. *Transp. Res. Rec. J. Transp. Res. Board Transp. Res. Board Nat. Acad.* **2578**, 1–11 (2016)
- Kleyn, E.G.: The use of the dynamic cone penetrometer (DCP). Transvaal Provincial Administration, Pretoria (1975)
- Mishra, D.: Aggregate characteristics affecting response and performance of unsurfaced pavements on weak subgrades. Doctoral dissertation, University of Illinois at Urbana-Champaign (2012)
- Moaveni, M.: Advanced image analysis and techniques for degradation characterization of aggregates. Doctoral dissertation, University of Illinois at Urbana-Champaign (2015)
- Puppala, A.J., Saride, S., Williammee, R.: Sustainable reuse of limestone quarry fines and RAP in pavement base/subbase layers. *J. Mater. Civil Eng.* **24**(4), 418–429 (2012). doi:[10.1061/\(ASCE\)MT.1943-5533.0000404](https://doi.org/10.1061/(ASCE)MT.1943-5533.0000404)
- Stroup-Gardiner, M., Wattenberg-Komas, T.: Recycled materials and byproducts in highway applications. *Transp. Res. Board* (2013)
- Tutumluer, E., Ozer, H., Hou, W., Mwumvaneza, V.: Sustainable aggregates production: green applications for aggregate by-products (Report No. FHWA-ICT-15-012). Illinois Center for Transportation/Illinois Department of Transportation, Springfield, IL (2015)
- Xiao, Y., Tutumluer, E.: Gradation and packing characteristics affecting stability of granular materials: aggregate imaging-based discrete element modeling approach. *Int. J. Geomech. Am. Soc. Civil Eng.* 4016064 (2016). doi:[10.1061/\(ASCE\)GM.1943-5622.0000735](https://doi.org/10.1061/(ASCE)GM.1943-5622.0000735)

# Membrane-Forming Performance and Application of Emulsion Wax Curing Agent (EWCA) for Cement Concrete Curing

Jian-Bo Yuan<sup>1</sup>(✉), Jia-Liang Yao<sup>1</sup>, Hui-Cong Wang<sup>2</sup>,  
and Ming-Jie Qu<sup>2</sup>

<sup>1</sup> Changsha University of Science and Technology,  
Changsha 410114, Hunan, China

yuanjb01@163.com, yao26402@126.com

<sup>2</sup> School of Traffic and Transportation Engineering, Changsha University  
of Science and Technology, Changsha 410014, Hunan, China  
{770692963, 352587764}@qq.com

**Abstract.** The research of the present paper explored the membrane-forming performance and application for a kind of emulsion wax curing agent (EWCA) used as the curing material during cement concrete construction, which passed through a series of tests that included tests for membrane forming on glass plates, tests for membrane forming on cement concrete test blocks, tests for membrane forming and thermal endurance and tests for appearance observation about membrane forming and water pouring. Those tests helped to optimize the formula for EWCA and establish the process parameters for production of EWCA and then produce an EWCA with high performance. Tests for cracking on slabs and engineering projects of cement concrete curing indicated that the EWCA studied in this paper can be applied to cure cement concrete which is cured by spraying water or under all kinds of weather condition.

**Keywords:** Emulsion wax curing agent · Membrane-forming performance · Components · Cement concrete · Curing

## 1 Introduction

After covering straws, geotextiles, corn stalks and so on concrete construction surface, this way is suitable for concrete construction conservation of which small quantities and plenty of water. But the above methods of conservation projects has these disadvantages that difficult to covered uniformly, uneven watering, difficult to guaranteed water conservation, wasted time and labor and difficult to controlled concrete construction quality which resulted in crack was unavoidable because of improper curing to large projects and dryland [1, 2]. The method that using concrete curing agent to replace traditional watering conservation concrete is a question that majority of scientific and technical personnel widespread concerning in the domestic and abroad [3, 4]. When using concrete curing agent can save time and labor, without limited the construction site, construction convenient, can solved the problems of concrete conservation to ensured the performance of concrete and prolonged life in dryland,

high-rise buildings, large-scale construction projects and bridge pier, girder and tunnel etc. concrete construction projects. Currently the curing agent was used to concrete construction mainly have four categories at home [5] which included type of sodium silicate modified, type of paraffin emulsion modified, type of polymer and inorganic and high polymer composite curing agent. The main problems of the prior EWCA is the membrane forming intolerant aging and it is easy to crack thereby it affected the effect of conservation [6].

In this regard, the author of this paper complexed fully refined paraffin wax, polymer materials and a variety of surfactants via formulation and process optimization, which was in order to improved the stability and membrane-forming performance of EWCA and produced the storage stability and excellent membrane-forming performance of EWCA. At present, EWCA is mainly used to cement concrete conservation at home and aboard, it also is used to spacer layer of lean concrete base as well as concrete surface on United States, Korea, Guangdong Province and Hunan Province at home and so on cement concrete pavement [7], This paper explored indoor experimental research about curing performance after scribble EWCA on concrete surface based on the results of lotus effect research [8–10].

## 2 Composition of Emulsion Wax Curing Agent (EWCA)

### 2.1 Technical Theory

This paper study on high-performance EWCA is a type of a new concrete curing materials that to fully refine paraffin wax (mixture of alkanes with carbon number of 18 to 36) as a primary membrane-forming component, which passed through designing formulation optimization and advanced manufacturing equipment as well as using reasonable industrial technology parameters to manufacture this new concrete curing materials.

EWCA with high performance actually is a type of emulsion that is polymer material combined with emulsifying wax, emulsifying fabricated wax is dispersed multiphase system. Generally this is called oil-in-water emulsifying wax (O/W) which fabricated of emulsion wax is dispersed tiny wax tablets in water and its dispersed phase particle size generally is less than 15  $\mu\text{m}$ . The formulations of emulsifying wax include waxes, oils, polymers, emulsifiers, water, and various additives. Emulsifiers which is commonly used include cationic emulsifiers, anionic emulsifiers and nonionic emulsifiers. EWCA has a wide range of applications and its main application areas included textile, paper making, leather, fiberboard, polishing, fruit preservation, construction engineering, gardening, ceramics and so on. EWCA as the water features of concrete curing because of emulsifying wax which has small particles that easy to permeate the concrete surface and effectively blocked the pores of the concrete, at the same time it can effectively prevent water evaporating of concrete because of it could formed continuous membrane in concrete surface which owing to air oxidation, the polymerization itself and polymer materials membrane-forming effect, therefore it can be used to curing after the construction of the concrete.

The emulsion of paraffin is aimed to dispersing it in water, it can change its surface tension via directional adsorption of emulsifier, and let paraffin turned into high dispersion, uniform, stable emulsion under the forces of external mechanical. Paraffin was a long chain hydrocarbon compound which had a linear structure and was not easy to emulsify. To produce a stable quality products of emulsifying wax, only through selecting a suitable emulsifier can it be achieved possibly [11]. Emulsifier is an amphoteric surfactant, Their molecules at one end hydrophilic and the other lipophilic. It can greatly reduce the interfacial tension. The key of emulsified paraffin is dispersed paraffin into tiny droplets and let its surface orientation adsorbed to molecules of the emulsifier. Forming the single molecule interfacial film of emulsifier with a bound mechanical strength and electric charge. Lipophilic group towards waxes, polar groups towards water, letting wax drop steady dispersed in water and be difficult to coalesce. The contact angle of paraffin with water is much greater than  $90^\circ$ , only using appropriate technology can it be manufactured to have both hydrophilic and hydrophobic wax emulsion. The project team did a research on the effect factors of emulsification and emulsion stability in the paraffin emulsification process. This research passed through formulation and process optimization to complexed fully refined paraffin wax, polymer materials and a variety of surfactants, which was in order to improve the stability and membrane-forming performance of EWCA, it produced the storage stability and excellent membrane-forming performance of EWCA high performance.

## 2.2 Equipment and Raw Materials

Equipment in the laboratory: constant temperature in the water bath, the error of temperature  $\pm 2^\circ\text{C}$ , electric mixer, glassware.

Pilot scale production equipment: FSA high-shear emulsifier, The main parameters of equipment: rated power 11 KW, rated working voltage  $\sim 380\text{ V}$ , the working rotating speed in rated power 4000 r/min, the working electric current in rated power 21.6 A, maximum capacity 1000 L.

Raw materials: 58# fully refined paraffin wax, industrial grade; polyvinyl alcohol 17-88, polyvinyl alcohol 20-88, polyvinyl alcohol 20-99, industrial grade; Polyacrylic acid polymer emulsion A, Polyacrylic acid polymer emulsion B, industrial grade; OP-10, OP-7, Tween-80, Span-80, industrial grade; The compound emulsifier C, self-made; defoamers, water is running water.

## 2.3 Process of Composition Crafts

Weighing paraffin wax, emulsifier, some of water according to the formulation metering, then placed them in a reaction apparatus and heated all wax melting. When it started stirring and then added a metering polyvinyl alcohol solution, an emulsion polymer, Finally added in a balance of water, followed by stirring down to ambient temperature, packaged them after filtered.

### 3 Tests for Membrane Forming on Emulsion Wax Curing Agent (EWCA)

When EWCA was used to conserve the construction, conservation, the membrane forming of EWCA should be stable and have some resist water erosion performance, at the same time it should have the workability (suitable for mechanical or electrical spray at normal temperature), and meet the requirements of conservating the concrete construction conservation, The primary component of EWCA included paraffin, polymer materials with a variety of surfactants which was the major factor of affecting the membrane-forming performance. The research primarily explored the different components of the tests for membrane forming on glass plates, tests for membrane forming on cement concrete testing blocks, tests for membrane forming and thermal endurance, tests for membrane forming and performance against water erosion, tests for stability in membrane forming under indoor normal temperature and tests for observing the microstructure through electron microscope. Via the testing of selecting optimally raw materials and mix proportion, it can take this to determine the materials formulation and performance standards when the EWCA was regarded as concrete conservation.

#### 3.1 Tests for Membrane Forming on Glass Plates

Observing the EWCA of different composition and content (coordinate proportion) under certain conditions (the time of membrane-forming and integrity of membrane-forming). When coated with different curing agents on a glass plate. Spaying the standard dose of  $0.25 \text{ kg/m}^2$  curing agent on the glass plate that was used, then making it as dried membrane. Observing the curing agent whether there was leaking gas pores bad emulsified particles or not after forming membrane. If membrane-forming were discontinuous, it had pores and did not form closed layer or the particles are coarse, which indicated the membrane-forming was rough and bad. The tests is given to Fig. 1, The result of tests is given in Table 1.

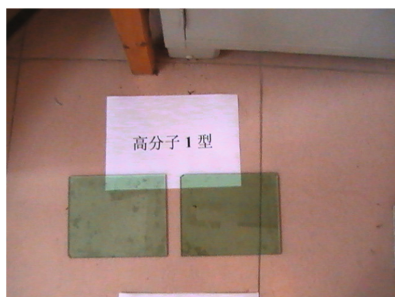


Fig. 1. Tests for time for membrane forming of EWCA on glass plates

**Table 1.** Test results of membrane forming of EWCA on glass plates

Type of emulsion alkane	Membrane forming test time (temperature: 16 °C)	Time of membrane forming
A type of EWCA	8:30–13:30	5 h
B type of EWCA	8:30–12:30	4 h
Type of paraffin	8:30–16:30	8 h

Note: A type of EWCA of which the mass ratio of polymer materials and paraffin was 1:3, B type of EWCA of which the mass ratio of polymer materials and paraffin was 1:3.

### 3.2 Tests for Membrane Forming on Cement Concrete Test Blocks

Based on the different compact situation of glass plate and concrete with the application properties of curing agent, The author of this paper coated different curing agent on concrete block based tests for membrane-forming on glass plate, Then observed the membrane-forming situation of different curing agent under certain conditions, The result of tests is given in Table 2.

**Table 2.** Test results of membrane forming of EWCA on cement concrete test blocks

Type of EWCA	Membrane forming test time (temperature: 23 °C)	Time of membrane forming
A Type of EWCA	8:30–12:30	4 h
B Type of EWCA	8:30–12:00	3.5 h
Type of paraffin	8:30–14:30	6 h

### 3.3 Tests for Membrane Forming and Thermal Endurance

Membrane forming and thermal endurance performance referring to the membrane did not melt flowing when the temperature of curing agent membrane surface reached to 60 °C and the membrane was exposed in the sun. The method of tests: Added it into 60 °C oven and heated 10 min after different curing agent forming membrane. Observing their thermal endurance performance. The tests is given to Fig. 2, the results is given to Table 3.

**Fig. 2.** Tests for membrane forming and thermal endurance of EWCA on glass plates

**Table 3.** Test results of membrane forming and thermal endurance of EWCA on glass plates

Type of EWCA	Time of tests for membrane forming (temperature: 60 °C)	Thermal endurance
A type of EWCA	20 min	Didn't melted
B type of EWCA	40 min	Didn't melted
Type of paraffin	10 min	Melted

### 3.4 Tests for Appearance Observation About Membrane Forming and Water Pouring

It could qualitatively judge the membrane forming quality of EWCA via the emulsion alkane of tests for appearance observation about membrane forming and water pouring on concrete surface. The membrane-forming surface was dense when membrane was well-formed and the surface of concrete was gray after membrane forming and was dispersed when membrane was not-well formed. The results of tests appearance observation about membrane forming and water pouring is given to Fig. 3.

It can observed the surface of concrete which sprayed curing agent formed a certain hydrophobic membrane via tests for water pouring after spraying curing agent on the surface of concrete and forming membrane, water will not soon dispersed and like drops of water. If membrane was formed on the inclined plane, in this case the water on the surface will flow to the lower and there was beads of water. While the water on the surface of concrete was easy to dispersed when the membrane-forming performance of spraying curing agent was not good and couldn't observed beads of water distribution. The results is given to Fig. 4.



**Fig. 3.** Surface conditions of formed membrane of EWCA: (a) powder present on surface if membrane is not well-formed; (b) dense surface of a well-formed membrane

## 4 The Formulation and Main Performance of EWCA

It determined the primary effect process parameters of the performance of EWCA membrane-forming via the research of this paper that is the emulsifying temperature, emulsifying time and emulsifying speed of EWCA via the orthogonal tests for process





**Fig. 4.** Water pouring tests: (a) water dispersed on a not-well-formed membrane; (b) water beads on a well-formed membrane

parameters and membrane forming performance. Paraffin is a solid state at normal temperature, only when paraffin is heated to the above of melting point will it form liquid. Forming a stable emulsion in the presence of an emulsion by the stirring of machine. The research of this paper about the results of tests for EWCA basic formulation and primary performance is given to Tables 4 and 5.

**Table 4.** Basic formula for EWCA

Raw materials	Quantity (%)
58# fully refined paraffin wax	30–40
Emulsifier	5–20
Polymer materials	0–10
Defoamers	0.1–5
Water	Margin
Summation	100

**Table 5.** Performance of EWCA

Project	JT/T522-2004 formulate criterion	The result of tests
Flooding solubility performance	Insoluble	Insoluble
Thermal endurance performance	Did not melting, deformation	Did not melting, deformation
Effective water retention (%)	≥ 90	97
The strength ratio of concrete compressive, %	7d ≥ 95	96
	28d ≥ 95	103

## 5 The Ice Mechanics Performance Test

Ice mechanics performance test refers to research all kinds of mechanical properties for ice, the article was mainly aimed to do researches about the ice layer Shear Bond Stress and Composite Friction Coefficient, the Pull-out, ice impact. Testing the change of various performance indicators after using wax curing agent. At present, most of researches on the anti-icing coating was still in the laboratory stage, but this means that there is no uniform standard test, and used icing time test method commonly, the bond strength test method are not the same. Based on this, the paper aimed at the important factors that affect the efficiency of mechanical de-icing: the degree of fragmentation of the ice sheet and the bond strength between the ice and the pavement surface, and the mechanical properties of the ice layer are proposed to characterize them. Through the ice layer shear test the horizontal bond stress, the pull-out bond stress was determined via pull-out tests, and the impact properties was determined impact tests.

### 5.1 Tests for Ice Layer Shear Bond Stress and Composite Friction Coefficient

In order to better evaluated the mechanical properties of the layers, the changes of shear bond stress and friction between concrete pavement and ice layer after EWCA were researched. In this paper, the author developed a direct shear test specimens, according to the structure and material properties of concrete pavement, the direct shear test specimens are prepared and given to Fig. 2.

Interlaminar shear stress and friction coefficient test were done in the laboratory, in accordance with the concrete pavement mix requirements in diameter cylinder for 110 mm mold casting of high 100 mm concrete specimens, the weight of 2.3 kg. On the standard of maintenance condition, to reach 30–35 MPa compressive strength (the pullout test strength requirements are the same). A group of specimen surface according to 0.2 L/m<sup>2</sup> meters the amount of spray EWCA, another group of parallel specimens do not apply, cold water poured over the ice 5 cm refrigerator to EWCA after drying the specimen under −18 °C, forming specimens as shown in Fig. 5.

When the test specimens are finished, the jack center, the center of the measuring ring and the center of the test specimens are arranged on the same horizontal plane. When the load is loaded, push the load slowly until the test piece is completely out of the bond with the concrete pavement. Record the maximum value of the force loop, this value is the maximum horizontal thrust. The test is given in Fig. 6.

The maximum shear stress was determined by the ratio of the maximum horizontal thrust  $T_{\max}$  to the shear area  $A$  ( $1/4\pi \times 110^2 \text{ mm}^2$ ).

$$\tau = T_{\max}/A \quad (1)$$

Composite friction coefficient  $f_h$  was the ratio of the maximum horizontal thrust of specimen  $T_{\max}$  to the dead weight of specimen  $m$ .

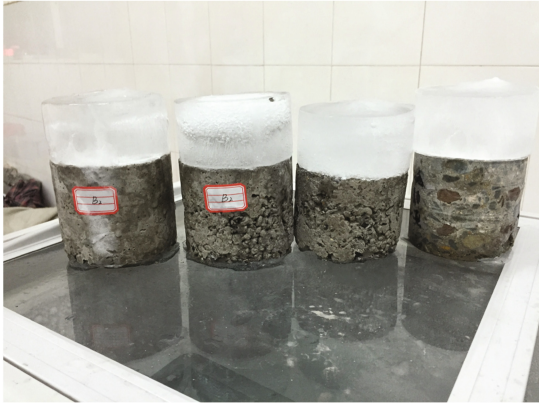


Fig. 5. Concrete - covered ice specimen



Fig. 6. Tests for interlayer shear bond stress and composite friction coefficient.

$$f_h = T_{\max}/m \quad (2)$$

The computed results were given in Table 6, It can be seen that the friction coefficient of EWCA is decreased by 61%, and the variation trend of shear bond strength between layers is the same as that the composite friction coefficient. The main reason of the decrease of water were adhesion with road surface, when the water freezes, EWCA coating to the waterproof layer in the isolation layer between water and ice road pavement, interlayer is smooth interface (there refers to the smooth and interlayer interface compared to continuous shear stress and horizontal friction) so inter layer decreases. The test results are shown in Table 6.

**Table 6.** Results of tests for bonding stress

Test item	Tests for ice layer shear bond stress	
	Test result/KN	Average value/KN
Have coating	1.6	1.3
	1.0	
	1.3	
No coating	3.2	3.5
	3.4	
	3.6	

## 5.2 Pull-Out Tests

The pull-out tests are shown in Fig. 7. The pull-out bond stress  $\sigma$  was defined as the ratio of the maximum pull-out force  $P_{\max}$  to the cross-sectional area  $A$  ( $1/4\pi \times 110^2 \text{ mm}^2$ ) of the test specimen for the pull-out tests.

$$\sigma = P_{\max}/A \quad (3)$$

The tensile bond stress test is mainly used for comparison with EWCA without ice and the surface coating of the tensile bonding force, tensile cohesive force differential analysis of the ice and the surface, their value can reflect the strength of concrete pavement deicing constraint. Test method with reference to ice shear test. In the test mode in the pouring cylinder diameter of 11 cm of the specimen, some of EWCA

**Fig. 7.** Tests for ice layer pull-out

**Table 7.** Results of Pull-out Tests

Test item	Pull-out tests	
	Test result/KN	Average value/KN
Have coating	1.5	1.4
	1.4	
	1.4	
No coating	2.2	2.3
	2	
	2.5	

parallel specimens without processing, and the surface with subcooled water freezing icing test. After they were freezing 12 h, the test specimens are placed on the production of a good drawing test instrument, the fixed position of the jack will be pushed slowly, until the test specimens of the ice completely and the concrete pavement out of bond. Record the maximum value of the process jack, its value is the maximum positive pull bond stress. The results of experiment shows that the drawing force is reduced by 48% after EWCA treatment. The results of the experiment indicates that the EWCA changes the interface conditions of ice and road surface, the change of stress on the bottom of the ice sheet is eased to fall off, which is conducive to mechanical of icing. The test results are shown in Table 7.

### 5.3 Ice Impact Tests

Impact performance test (shown in Fig. 8) reference ACI544 Committee of the United States to study the drop-weight method self-made experimental equipment. During the test, the steel ball is arranged in advance from the center of the board body height free fall, repeated impact, observe the plate body appear, and the data record. Test records of the two elements: the initial impact of the number of N1 (the corresponding impact times of the first crack appeared in the specimen), the final impact of the number of N2. On the basis of this, the difference between the number of final crack and initial crack and the impact work can be calculated separately.

The impact of the specimen is a cube, the hammer drop height  $h = 1000$  mm, weight 200 g, each made of 3 specimens. The difference between the number of final crack and initial crack that  $\Delta N$  and the impact work  $W$  can be calculated separately, as follows:

$$W = Nmgh \tag{4}$$

Where:

- W = impact work
- N = The number of final crack impact
- h = impact ball drop height
- m = the quality of the impact ball
- g = Acceleration of gravity,  $9.8 \text{ m/s}^2$



**Fig. 8.** Impact performance test diagram

The ice impact test results are shown in Table 8.

The results of experiments results shows that the impact work is reduced by 50% after EWCA treatment.

**Table 8.** Results of ice impact tests

Test item	N1		N2		$\Delta N$
	Test result	Average value	Test result	Average value	
Have coating	2	2	7	8	6
	2		8		
	2		7		
No coating	5	5	15	17	12
	6		18		
	5		17		

## 6 Conclusions

- (1) This paper produced a products of high-performance emulsion alkane via the research of emulsion alkane membrane forming performance and the parameters of manufacture process;
- (2) Ice shear stress test show that: the friction coefficient of EWCA is decreased by 61%, and the variation trend of shear bond strength between layers is the same as that of the composite friction coefficient;
- (3) The pull-out tests show that the drawing force is reduced by 48% after EWCA treatment;
- (4) The impact experimental show that the impact work is reduced by 50% after EWCA treatment.

**Acknowledgements.** This research was supported by the National Natural Science Foundation of China under Grant 51578080, Grant 51178064 and the Transportation Department of Hunan Province, No. 2013-01.

## References

1. Bao, J., Li, F., Zhao, T.: Research on the emulsifier to prepare the high-soild content wax emulsion. *Appl. Chem. Ind.* **38**(7), 1025–1029, 1045 (2009)
2. Jin, H., Zhao, H., Zhang, Z., Chen, S., Liu, Y.: Experimental study on the performance of a modified curing agent emulsifying wax. *Liaoning Build. Mater.* (6), 57–59 (2009)
3. Liu, K., Zhang, M., Zhai, J., et al.: Bioinspired construction of Mg-Li alloys surfaces with stable superhydrophobicity and improved corrosion resistance. *Appl. Phys. Lett.* **92**, 183103 (2008)
4. Nimittrakoolchai, O.-U., Supothina, S.: Deposition of organic-based superhydrophobic films for anti-adhesion and self-cleaning applications. *J. Eur. Ceram. Soc.* **28**, 947–952 (2008)
5. Shou, C., Zhang, Z., Xie, Z., Li, L., Chen, L., Fu, Z.: Research on curing agent based on polymer emulsions for cement concrete pavement. *J. Highw. Transp. Res. Dev.* **21**(1), 16–18 (2004)
6. Tian, Y., Zhang, J., Zuo, F., Zhang, Y., Hou, S., He, Y., Liu, Y., Kou, H.: Development and evaluation of emulsified paraffin. *Drill. Fluid Complet. Fluid* **25**(4), 29–30, 33 (2008)
7. Wang, W., Shi, J.: Advances in research and application of emulsifying wax in China. *Spec. Petrochem.* **25**(2), 79–83 (2008)
8. Wang, G., Fang, S., et al.: Latest advances concrete curing agent in China. *Shanghai Coat.* **43**(3), 16–19 (2005)
9. Wang, S., Zhu, Y., Xia, F., et al.: The preparation of a superhydrophilic carbon film from a superhydrophobic lotus leaf. *Lett. Editor Carbon* **44**, 1845–1869 (2006)
10. Yao, J., Yao, J., et al.: Research on mechanism of using emulsion wax curing agent as separation layer and its effectiveness. *China J. Highw. Transp.* **22**(6), 47–52 (2009). (in Chinese)
11. Zhang, Z., Zhao, H., Zhang, F., Chen, S., Zhou, X.: Experimental study on modified emulsified wax concrete curing agent component. *Liaoning Build. Mater.* (11), 41–43 (2009)

# Thermoelasticity, Superelasticity and Nanoscale Aspects of Structural Transformations in Shape Memory Alloys

Osman Adiguzel<sup>(✉)</sup>

Department of Physics, Firat University, 23169 Elazig, Turkey  
oadiguzel@firat.edu.tr

**Abstract.** Shape memory alloys have a peculiar property to return to a previously defined shape on heating after deformation in low temperature product phase region. These alloys take place in a class of functional materials due to the response to the variation of temperature, and they are used shape memory elements in a wide range of industry; in particular, they are used in the construction sector, aeronautical industry due to the energy dissipation properties. Shape memory effect is facilitated by martensitic transformation which is a solid state phase transformation and occurs in thermal manner in material on cooling from high temperature parent phase region. This transformation is governed by changes in the crystalline structure of the material. Thermal induced martensite occurs as martensite variants, twinned martensite, in self-accommodating manner on cooling from high temperature parent phase region. Mechanically deformation of these alloys in martensitic state proceeds through martensite variant reorientation by the detwinning process. Martensitic transition occurs as self-accommodated martensite with lattice invariant shears which occur in two opposite directions,  $\langle 110 \rangle$ -type directions on the  $\{110\}$ -type plane of austenite matrix. In addition, shape memory alloys can exhibit another property called superelasticity performed in only mechanical manner. These alloys can be deformed just over austenite finish temperature, and recover the original shape on releasing the stress in superelastic manner. Copper based alloys exhibit this property in metastable  $\beta$ -phase region, which has bcc-based structures at high temperature parent phase field and these structures martensitically turn into the layered complex structures following two ordered reactions on cooling.

**Keywords:** Thermoelasticity · Superelasticity · Shape memory effect · Lattice twinning · Lattice invariant shear

## 1 Introduction

Phase transformations are important factor in the processing of materials, like strengthening the steel and shape changes with variation of temperature. Shape memory alloys take place in a class of functional materials by exhibiting a peculiar property called shape memory effect. This property is characterized by the recoverability of desired shape on the material at different temperatures. Shape memory effect is performed in only thermal manner on heating and cooling after deformation at low



temperature martensitic condition, and this behavior can be called thermoelasticity. Shape memory effect is linked with martensitic transformation, and comprises a reversible transition from product martensite to parent austenitic phase. Martensitic transformations are first order lattice-distorting phase transformations and occur with the cooperative movement of atoms by means of lattice invariant shears in the materials on cooling from high temperature parent phase region. Martensitic transformation is evaluated by the structural changes in microscopic scale. Shape memory effect is based on martensitic transformation, and microstructural mechanisms are responsible for shape memory behaviour. In particular, the lattice twinning and detwinning processes are essential as well as martensitic transformation in reversible shape memory effect (Ma et al. 2010; Sun et al. 2012). Thermal induced martensite occurs by means of a shear-like mechanism as multivariant martensite in self-accommodating manner and consists of lattice twins. Also, this martensite is called twinned martensite or multivariant martensite. Martensitic transformations occur with cooperative movement of atoms by means of lattice invariant shears on a  $\{110\}$ -type plane of austenite matrix which is basal plane of martensite. The lattice invariant shears occurs, in two opposite directions,  $\langle 110 \rangle$ -type directions on the  $\{110\}$ -type basal planes. The  $\{110\}$ -plane family has 6 certain lattice planes;  $\{110\}$ ,  $\{1\bar{1}0\}$ ,  $\{101\}$ ,  $\{10\bar{1}\}$ ,  $\{011\}$ ,  $\{01\bar{1}\}$ . This kind of shear can be called as  $\{110\} \langle 110 \rangle$ -type mode and possible 24 martensite variants occur. Shape memory alloys can be deformed plastically in low temperature martensitic condition, and recover the original shape on heating over the austenite finish temperature. The material cycles between the deformed and original shapes on cooling and heating in reversible shape memory case. By applying external stress, martensite variants are forced to reorient into a single variant leading inelastic strains, and deformation of shape memory alloys in martensitic state proceeds through a martensite variant reorientation or detwinning of twins (Ma et al. 2010; Sun et al. 2012). The twinning occurs with internal stresses, whereas detwinning occurs with the external stresses. The basic mechanism phase transition and shape memory effect in crystallographic level is schematically illustrated in Fig. 1 (Sun et al. 2012). The deformed material recovers the original shape in bulk level, and crystal structure turns into the parent phase structure on first heating.

The parent phase structure returns to the multivariant martensite structures in irreversible shape memory effect on cooling below the martensite finish temperature; in contrast, the material returns to the detwinned martensite structure in reversible shape

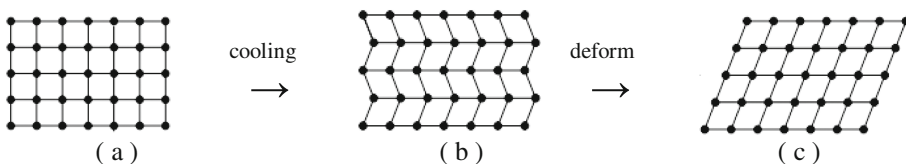


**Fig. 1.** Schematic illustration of the mechanism of the shape-memory effect: (a) atomic configuration on  $\{110\}$ -type planes of parent austenite phase, (b) twinned martensite phase occurring thermally on cooling, (c) detwinned martensite occurring with deformation (Sun et al. 2012)

memory case. Shape memory alloys exhibit another property, superelasticity (SE), which is performed by mechanical stress, in a constant temperature, just over austenite finish temperature. Shape memory alloys can be deformed just over austenite finish temperature, and recover the original shape on releasing the stress in superelastic manner. Deformation at different temperature exhibits different behaviour beyond shape memory effect and superelasticity.

Shape memory effect is performed in a temperature interval depending on the forward (austenite  $\rightarrow$  martensite) and reverse (martensite  $\rightarrow$  austenite) transformation, on cooling and heating, respectively. Superelasticity is performed in the parent austenite phase region, just over Austenite finish temperature. Superelastic materials are deformed in the parent phase region and, shape recovery is carried out instantly and simultaneously upon releasing the applied stress. This property exhibits rubber like behaviour or classical elastic material behaviour. Stress-strain behaviour is different in two cases, shape memory effect and super-elasticity. Deformation is performed plastically in product martensitic condition in shape memory case. Meanwhile, the material is deformed in parent phase region in superelasticity, and the material recover the original shaper after releasing the external stress. Superelasticity proceeds with only mechanical treatment. This behaviour is also result of stress induced martensitic transformation which is induced by applying external stress only in mechanical manner. With this stress, parent austenite phase structures turn into the fully detwinned martensite, and very large strain is observed; and a complete shape recovery is observed upon unloading, therefore, the material behavior resembles elasticity. This strain is maximum 8% in NiTi alloys (Sun et al. 2012). The loading and releasing paths demonstrating the shape memory effect and superelasticity and stress-strain diagram is shown in Fig. 2 (Barbarino et al. 2014).

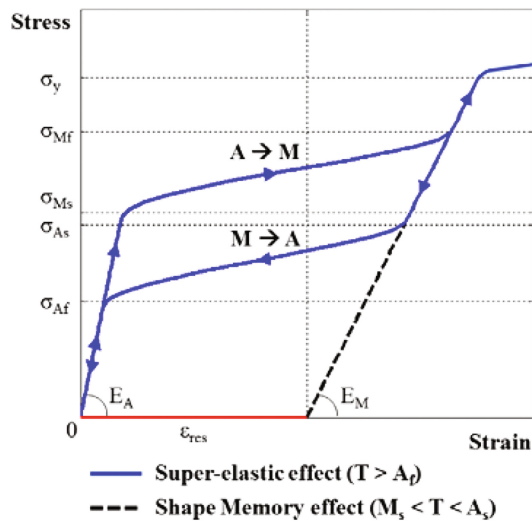


Fig. 2. Stress-strain diagram of shape memory effect and superelasticity (Barbarino et al. 2014)

Copper based alloys exhibit this property in metastable  $\beta$ -phase region, which has B2 or DO<sub>3</sub>-type ordered lattice at high temperature, and these structures martensitically turn into layered complex structures with lattice twinning process, on cooling from high temperature austenitic phase region. Martensitic transformations occur mainly in two steps in copper based ternary alloys.

First one is Bain distortion, and second one is lattice invariant shear. Bain distortion consists of an expansion of 26% parallel to the  $\langle 001 \rangle$ -type axes, and compression of 11% parallel to the  $\langle 110 \rangle$  and  $\langle 1 \bar{1} 0 \rangle$ -type directions (Adiguzel 2013). Lattice invariant shears occur with cooperative movement of atoms less than interatomic distances on  $\{110\}$ -type close packed planes of austenite matrix.

The lattice invariant shears occur, in two opposite directions,  $\langle 110 \rangle$ -type directions on the  $\{110\}$ -type basal planes and this type of shear can be called as  $\{110\}$   $\langle 110 \rangle$ -type mode and has 24 variants in self-accommodating manner (Zhu et al. 2003; Sutou et al. 2005; Adiguzel 2012; Riccardo Casati et al. 2014). These lattice invariant shears are not uniform in copper alloys and give rise to the formation of unusual complex layered structures called long period layered structures such as 3R, 9R or 18R depending on the stacking sequences on the close-packed planes of the ordered lattice. The periodicity and unit cell is completed through 18 layers in case of 18R martensite.

## 2 Experimental Details

In the present paper, two copper based ternary shape memory alloys were selected for investigation; Cu-26.1%Zn 4%Al and Cu-11%Al-6%Mn (in weight). The martensitic transformation temperatures of these alloys are over the room temperature and both alloys are entirely martensitic at room temperature. Specimens obtained from these alloys were solution treated for homogenization in the  $\beta$ -phase field (15 min at 830 °C for CuZnAl alloy and 20 min at 700 °C for CuAlMn alloy), then quenched in iced-brine to retain the  $\beta$ -phase and aged at room temperature after quenching (both alloys). Powder specimens for X-ray examination were prepared by filling the alloys with diamond file, and these specimens were heated in evacuated quartz tubes in the  $\beta$ -phase field (15 min at 830 °C for CuZnAl and 20 min at 700 °C for CuAlMn) for homogenization and quenched in iced-brine. These specimens were also given different post-quench heat treatments and aged at room temperature. X-ray diffraction studies carried out on these specimens, and x-ray diffraction profiles were taken from the quenched specimens using Cu-K $_{\alpha}$  radiation with wavelength 1.5418 Å.

## 3 Results and Discussion

X-ray powder diffractograms were taken from CuZnAl and CuAlMn samples. An x-ray powder diffractogram taken from the long term aged CuAlMn alloy sample is shown in Fig. 3. This diffractogram has been indexed on the monoclinic M18R basis. On the other hand, electron diffraction pattern were also taken from the samples of these alloys, the details were given elsewhere (Adiguzel 2013; Adiguzel 2012). X-ray diffractograms and electron diffraction patterns reveal that both alloys have the ordered

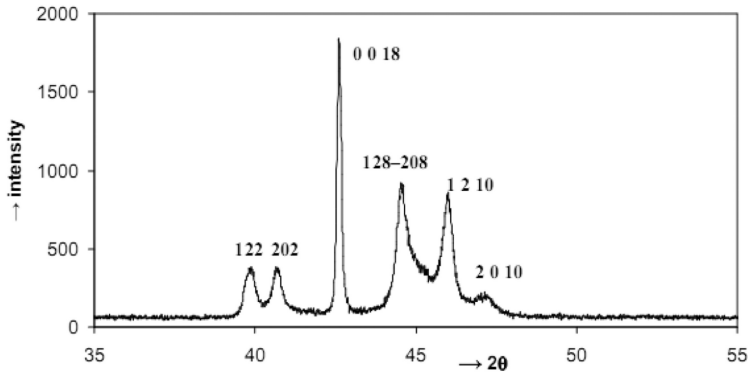


**Fig. 3.** An x-ray diffractogram taken from the long term aged CuAlMn alloy sample.

structure in martensitic condition, and exhibit superlattice reflections. A series of X-ray powder diffractograms and electron diffraction patterns were taken from both CuZnAl and CuAlMn alloy samples in a large time interval and compared with each other. It has been observed that electron diffraction patterns exhibit similar characteristics, but some changes occur at the diffraction angles and peak intensities on the x-ray diffractograms with aging duration. These changes occur as rearrangement or redistribution of atoms in the material, and attribute to new transitions in diffusive manner (Adiguzel 2013; Adiguzel 2012). The ordered structure or super lattice structure is essential for the shape memory quality of the material. In the shape memory alloys, homogenization and releasing the external effect is obtained by ageing at  $\beta$ -phase field for adequate duration (Guo et al. 2007; Aydogdu et al. 2004).

On the other hand, post-quench ageing and other processes in devices affect the shape memory quality, and give rise shape memory losses. These kinds of results lead to the martensite stabilization in the reordering or disordering manner. In order to make the material satisfactorily ordered and to delay the martensite stabilization, copper-based shape memory alloys are usually treated by step-quenching after homogenization. Metastable phases of copper-based shape memory alloys are very sensitive to the ageing effects, and any heat treatment can change the relative stability of both martensite and parent phases (Li 2008; De Castro et al. 2012). Martensite stabilization is closely related to the disordering in martensitic state. Structural ordering is one of the important factors for the formation of martensite, while atom sizes have important effect on the formation of ordered structures (Guo et al. 2007; Aydogdu et al. 2004; De Castro et al. 2012).

Although martensitic transformation has displacive character, martensite stabilization is a diffusion controlled phenomena, and this result leads to redistribution of atoms on the lattices sites. Stabilization is important factor and causes to memory losses, and changes in main characteristics of the material; such as, transformation temperatures, and diffracted angles and peak intensities.

Martensitic transformation in copper-based  $\beta$ -phase alloys is based on one of the  $\{110\}_\beta$  planes of parent phase called basal plane for martensite. The (110) basal plane

which has a rectangular shape in parent phase is subjected to hexagonal distortion and undergoes a hexagon.

The powder specimens were aged at room temperature after quenching process, and a series of x-ray diffractograms have been taken from both of the alloy samples in a large time interval. Although all of the diffractograms exhibit similar characteristics, some changes have been observed at diffraction angles and intensities of diffraction peaks on the diffractograms with aging duration. These changes are attributed to new transitions which have diffusive character. It means that some neighbour atoms change locations. In particular, some of the neighbour peak pairs have moved toward each other. It is interesting that miller indices of these plane pairs provide a special relation:

$$(h_1^2 - h_2^2)/3 = (k_2^2 - k_1^2)/n$$

where  $n = 4$  for 18R martensite (Adiguzel 2013). These plane pairs can be listed as follow; (122)–(202), (128)–(208), (1 2 10)–(2 0 10), (040)–(320). This result can be attributed to a relation between interplane distances of these plane pairs and rearrangement of atoms on the basal plane. In these changes, atom sizes play important role. The different sizes of atomic sites lead to a distortion of the close-packed plane from an exact hexagon and thus a more close-packed layered structure may be expected. In the disordered case, lattice sites are occupied randomly by the atoms, and atom sizes can be taken nearly equal each other, and martensite basal plane becomes an ideal hexagon, whereas, the lattice sites are occupied regularly by different atoms which have different sizes.

## 4 Conclusions

It can be concluded from the above results that the copper-based shape memory alloys are very sensitive to the ageing treatments. Diffraction angles and intensities of x-ray diffraction peaks gradually change with ageing time in martensitic condition. In particular, some successive peak pairs come close each other. These changes lead to the martensite stabilization in the redistribution or disordering manner, and stabilization proceeds by a diffusion-controlled process. The martensite stabilization is a diffusion controlled phenomena and leads to redistribution of atoms on the lattices sites, although martensitic transformation has displacive character. The basal plane of martensite turns into a hexagon by means of Bain distortion with martensite formation on which atom sizes have important effect. In case the atoms occupying the lattice sites have the same size, the basal plane of martensite becomes regular hexagon; otherwise the deviations occur from the hexagon arrangement of the atoms. The above mentioned peaks come close each other in the disordered case, and occur separately in the ordered case. The changes in the diffraction angles of the selected plane pairs can be a measure of the ordering degree in martensite.

## References

- Adiguzel, O.: Martensitic transformation and microstructural characteristics in copper based shape memory alloys. *Key Eng. Mater.* **510–511**, 105–110 (2012)
- Adiguzel, O.: Phase transitions and microstructural processes in shape memory alloys. *Mater. Sci. Forum* **762**, 483–486 (2013)
- Aydogdu, A., et al.: Long-term ageing behaviour of martensite in shape memory Cu–Al–Ni alloys. *J. Mater. Process. Technol.* **153–154**, 164–169 (2004)
- Barbarino, S., et al.: A review on shape memory alloys with applications to morphing aircraft. *Smart Mater. Struct.* **23**, 1–19 (2014)
- Casati, Riccardo, et al.: Thermal cycling of stress induced martensite for high performance shape memory effect. *Scripta Mater.* **80**, 13–16 (2014)
- De Castro, F., et al.: Improvements in the mechanical properties of the 18R ↔ 6R high hysteresis martensitic transformation by nanoprecipitates in CuZnAl alloys. *Mater. Sci. Eng., A* **543**, 88–95 (2012)
- Guo, Y.F., et al.: Mechanisms of martensitic phase transformations in body-centered cubic structural metals and alloys: molecular dynamics simulations. *Acta Mater.* **55**, 6634–6641 (2007)
- Li, Z., et al.: Macroscopic shape change of Cu<sub>13</sub>Zn<sub>15</sub>Al shape memory alloy on successive heating. *J. Alloy. Compd.* **452**, 307–311 (2008)
- Ma, J., et al.: High temperature shape memory alloys. *Int. Mater. Rev.* **55**, 257–315 (2010)
- Sun, L., et al.: Stimulus-responsive shape memory materials: a review. *Mater. Des.* **33**, 577–640 (2012)
- Sutou, Y., et al.: Effect of grain size and texture on pseudoelasticity in Cu–Al–Mn-based shape memory wire. *Acta Mater.* **53**, 4121–4133 (2005)
- Zhu, J.J., Liew, K.M.: Description of deformation in shape memory alloys from DO3 austenite to 18R martensite by group theory. *Acta Mater.* **51**, 2443–2456 (2003)

# Mechanical Behavior of Hydraulic Concrete to Extreme Service Temperatures: The Influence of the Particle Size

Kenouza Yamina<sup>(✉)</sup>

University of Bechar Algeria, Bécharr, Algeria

**Abstract.** The climate of the Saharan and sub-Saharan regions is characterized by low temperatures during the winter which can reach negative values during the night and high temperatures during the summer, sometimes exceeding 60 ° C. The behavior of the concrete to extreme service temperatures is currently not mastered since changes in strength depending on the local temperature is not taken into account in the design of structures. In this regard; the present work aims to study the sensitivity of hydraulic concrete in its thermal environment, such as cold regions, moderate and warm, taking into account the influence of the particle size of aggregates. The originality of this work lay in the study of different types of concretes (0/8, 0/16 and 0/25), mortars (0/3 and 0/5) and a micro-concrete (0/5). The results show a significant effect of particle size (Dmax) depending on the temperature, as well as each type of studied materials (concrete, mortar and micro-concrete) has its own behavior towards the temperature in the range studied.

## 1 Introduction

Concrete structures are still susceptible to thermal actions: for functional, climate and accidental reasons. For this, a lot of research was conducted on the influence of curing temperature on the strength of concrete at early age and long term such as Almusallam (2001), Gallucci et al. (2006), Husem and Gözütok (2005), Ortiz et al. (2005) and Topçu and Toprak (2005). There is also a lot of studies on the influence of the very high and very low temperatures on the cured concrete (beyond 28 days) such as Arvidson (1982), Carette and Malhotra (1985), Fares (2009), Khoury (1992), Lawson et al. (2000), Lee et al. (1988), Nasser and Evans (1989), Phan and Carino (2003) and Pliya et al. (2007). However, there is a lack of studies on the effects of intermediate temperatures on the cured concrete which is mentioned recently by Shoukry et al. (2011). According to these studies, it is found that the effect of temperature on the behavior of the hydraulic concrete is very complex, because of the heterogeneity of this material. However, to understand this effect, the most important factor is the age of concrete or rather the process of hydration of the cement paste. Thus, according to this criterion and their major role in the effect of temperature, there are two cases. The first case, the effect of the curing temperature, at early stages and during hydration whose effect of the ambient temperature is very significant. We noticed that an increase in ambient curing temperature accelerates the rate of hydration, and thus advantageously affects the resistance

young age; it had a detrimental effect on the subsequent strength. Extreme ambient temperatures can cause the stop of the hydration process and causing the resistance drop. The second case, the effect of temperature on the cured concrete, beyond 28 days, whose concrete takes more than 90% of its strength, and the hydration process is almost or even complete. Furthermore, in this case, the temperature range is very wide with respect to the first case, and a new term has been introduced, which is the extreme conditions of temperatures. In general, for very high temperatures; the concrete strength decreases when the temperature increases. The main reason for the strength decrease is the evolution of the microstructure due to the dehydration. The strength increases as the temperature decreases at very low temperatures, because of gel formation in the pores, the ice is more resistant than air or water. Between the lower and the higher temperatures, there is a temperature range, it comes to the intermediate temperatures; it is not discussed sufficiently, because of the remarkable lack in the literature.

For this reasons, the objective of this work is to contribute to the research undertaken to understand the mechanical behavior of hydraulic concretes subject to different local service temperatures in a temperature range [10 °C, 60 °C], who allowed an almost representative simulation of the climate of northern Africa.

In addition, several types of concretes and mortars were studied in order to take an overall idea about the effect of temperature. The parameter that distinguishes them is called the particle size (the size of the largest aggregate  $D_{max}$ ).

Moreover, the mechanical behavior of the mixtures studied in this study is reflected by measuring the compressive strength which is the most important property of concrete. In this context, an experimental device representing a thermal enclosure was designed and adapted to simulate and stabilize the temperatures during the test of the compressive strength.

## 1.1 Testing Program

The concrete specimens were prepared and cured in water at 20 °C for 28 days. Two types of tests corresponding to two states of thermomechanical loading are considered:

- Testing cold: thermal loading at low and moderate temperatures (–15 °C, 10 °C and 20 °C) using freezer (24 h), then an immediate crash in the equipped thermal chamber.
- The hot tests: thermal loads at high temperatures (30 °C, 40 °C, 50 °C and 60 °C) using an oven (24 h), and then a crash in the press equipped with a thermal chamber.

In both cases, four specimens were tested for each test temperature and the maximum load is recorded, from which we deduce the mean value.

We worked with the following variable parameters:

- The temperature (T): for all types of mixtures, the temperature that we have applied varies from 10 °C to 60 °C. A particular case of a temperature studied, –15 °C, was taken to assess the effect of the very low temperature (freezing temperature) on the strength of concrete.



- The type of mixture: three types of mixes were prepared; ordinary concrete; mortars and micro-concrete.
- The aggregate Dmax: depending on the size of the largest aggregate of each type of mixture, we have; the micro-concrete 0/5, very fine concrete 0/8, fine concrete 0/16 and medium concrete 0/25. For mortars, mortar 0/3 and 0/5.

The parameters and the experimental conditions set for this study:

- The consistency of all the mixtures was defined as normal, and carried out using the Abrams cone in the case of concrete in which the sag is 6.5 0.5 cm (plastic concretes), and with the plunger in the case of mortars where the value of penetration is 36 mm (conventional mortars);
- The origin of aggregates, including sand and gravel used are derived from the exploitation of river deposits;
- The type of cement used is CPJ CEM II/A 42.5 R;
- The maturation period (treatment) of mixtures was fixed at 28 days;
- The duration of exposure to different temperatures was set at 24 h from 28 days of maturation;
- The temperature conditions during implementation have been set for all the mixes;
- The dimensions and shape of the specimens tested: cubic specimens (10 × 10 × 10 cm);
- The loading speed is constant and equal to 0,5 MPa/s.

### 1.1.1 Concrete Mix Composition

The compositions found after using the Faury method for the three concretes are shown in Table 1.

**Table 1.** Compositions of ordinary concrete

Dosage (Kg/m <sup>3</sup> )	0/8	0/16	0/25
S (0/3)	608	624	548
G1 (3/8)	1140	157	152
G2 (8/16)	–	1056	363
G3(16/25)	–	–	780
C	350	350	350
W	200	186	179
W/C	0,57	0,53	0,51

### 1.1.2 Mortars Mix Composition

The mortar is compound by weight, of part of cement and three parts of sand. The W/C will be set according to the workability of the mortar.

Depending on the consistency that is already defined (normal consistency), and after the absolute density of components of mortar, dosages of these components have been found and they are indicated in Table 2.

**Table 2.** Compositions of mortars

Dosage (Kg/m <sup>3</sup> )	0/3	0/5
S (0/3)	1520	–
S (0/5)	–	1552
C	507	517
W	258	243
WC	0,51	0,47

### 1.1.3 Micro-concrete Mix Composition

According to the formulation mentioned by Dreux (2007), and taking into account the absolute densities of the micro-concrete components, the dosages of the latter were found, is kept, also in this case, the normal consistency concrete (slump equal to 6.5 0.5). The composition of the micro-concrete is shown in Table 3.

**Table 3.** Compositions of micro-concrete

Dosage (Kg/m <sup>3</sup> )	0/5
S1 (0/0,5)	308
S2 (0,5/1,6)	206
S3 (1,6/5)	1193
C	380
W	220
W/C	0,58

### 1.1.4 Designing a Thermal Enclosure

To achieve our objective to study the mechanical behavior of concrete at different temperatures, we developed a specific experimental device representing a thermal enclosure mounted on a compression machine. The design of the enclosure is designed to stabilize the temperature inside the testing machine during the crushing tests. Figures 1 and 2 show the steps and the material used for the design of the thermal enclosure.

## 1.2 Influence of Particle Size on the Compressive Strength of Hydraulic Concrete

To get a general idea about the influence of the largest aggregate dimension on the compressive strength of concrete, without considering the effect of temperature, tests were performed on cubic specimens (10 × 10 × 10 cm) immersed in water for 28 days.

### 1.2.1 Particle Size and Water Demand (Normal Consistency)

To obtain a normal consistency for different concretes; slump test were performed until obtaining the desired results.



Heating Plate



Heating plate mounted on the metal grid



Plywood for protection



Heating plate and plywood mounted on the metal grid



Two heating plates



Insulating lateral plate

**Fig. 1.** Thermal enclosure design: heating accessories and insulation lateral plate

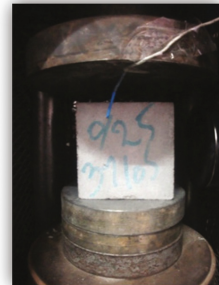


**Fig. 2.** Thermal enclosure design: temperature control and stabilization accessories

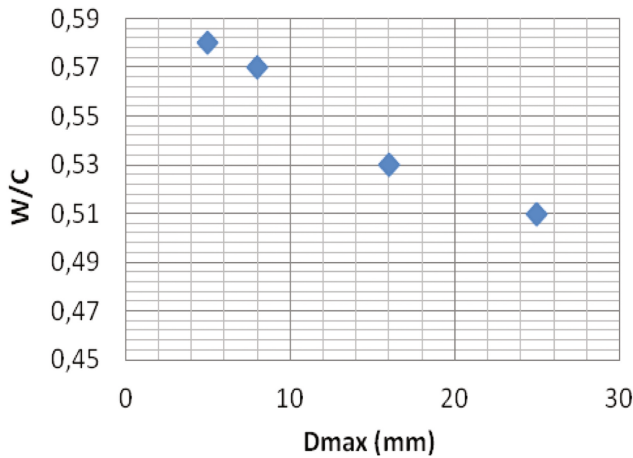


**Fig. 3.** Dmax effect on water demand of concretes

A relationship between the ratio W/C of the mixes and Dmax of the aggregates was deduced and illustrated in Fig. 3.

From Fig. 3, we notice that the increase in aggregate Dmax reduces the water demand of concrete, in this context, it should be mentioned that the water demand is the amount of water necessary to obtain a consistency normal of concrete.

### 1.2.2 Open Porosity and Bulk Density

The compactness of concrete is one of the most important properties which define the quality of concrete, and which can evolve by the porosity and the density of the hardened concrete. According to this, we will see later, the influence of Dmax on the open porosity and bulk density of concrete.

Results regarding the porosity and the bulk density concretes, depending Dmax are shown in Figs. 4 and 5.

From Fig. 4, we notice that the open porosity of the concrete decreases as Dmax increases. We also noticed that the porosity of the micro-concrete is greater compared to the other cases.

From Fig. 5, we see that the bulk density of concrete increases as Dmax increases.

Logically, the porosity decreases as the density increases, and these two criteria lead to the evaluation of compactness of concrete. Thus; we can say that the compactness of the concrete increases when Dmax increases.

### 1.2.3 The Compressive Strength

The results of the compressive strength are shown in Table 4 and illustrated in Fig. 6.

From Table 4 and Fig. 6, it is noticed that the strength of mortars and concretes increases as Dmax increases, which is a consequence of the decrease of water demand and augmentation of compactness. On the other way, it may be said that increasing the size of the largest aggregate Dmax reduces the water demand and improves the compactness and therefore increases the compressive strength of concretes and mortars.

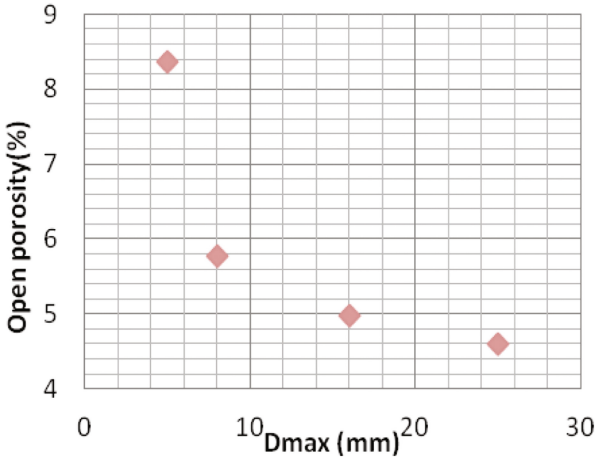


Fig. 4. Dmax effect on open porosity of concretes

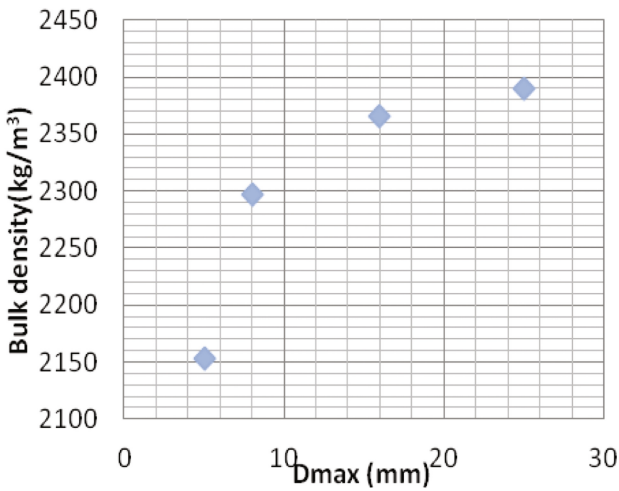


Fig. 5. Dmax effect on bulk density of concretes

### 1.3 The Temperature Influence on the Compressive Strength of Concrete and Mortars

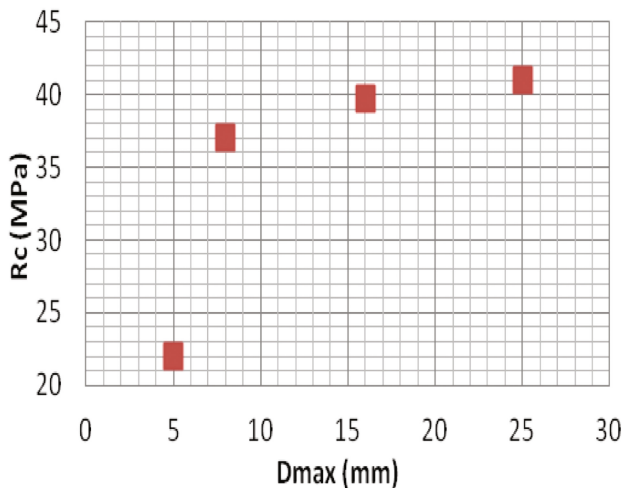
#### 1.3.1 Concretes

The results for the three types of concrete, very fine concrete 0/8, fine concrete 0/16 and medium concrete 0/25, are shown in Table 5 and illustrated in Fig. 7.

From the results shown in Table 5, it is noted that the influence of Dmax is the same; the strength increases when Dmax increases, except in a special case for the concrete 0/8 at T = 30 °C, where the strength is greater than the concrete 0/16.

**Table 4.** Compressive strength of concretes and mortars

Material	Compressive strength Rc(MPa)
<i>Mortars</i>	
0/3	40,37
0/5	44,83
<i>Concretes</i>	
0/5	22
0/8	37
0/16	39,75
0/25	41

**Fig. 6.** Dmax effect on the compressive strength of concretes

From the curves given in Fig. 7 it is noticed that:

- The curves of concrete 0/16 and 0/25 show similar pattern and the same behavior in different temperatures, with a difference of strength of the order 1 to 5 MPa;
- The three concretes show almost the same strength curve in the range from  $-15$  to  $20$  °C, so the same behavior in this latter;
- For the temperature range of  $20$  to  $60$  °C, the curve of the concrete 0/8 shows a different appearance to those of the two other concretes;
- For both concrete 0/16 and 0/25, the temperature  $T = 30$  °C is a critical temperature, the strength reaches its minimum value, whereas, the concrete 0/8 showed that the strength increased in this temperature point, and then decline to  $T = 40$  °C.
- According to the regression curves reported in Fig. 7; we noticed that:
- in the range of  $T = -15$  to  $30$  °C; three concrete show almost the same pattern of strength curves, and the difference was in the curvature and slope, the importance of

**Table 5.** Compressive strength of concretes at different temperatures

Temperatures (°C)	Compressive strength Rc(MPa)		
	0/8	0/16	0/25
-15	40	43,5	49
10	37,5	40	42
20	37	38	39,5
30	37	36	37,5
40	33,5	39	40
50	33,5	39,5	41
60	36,5	39	40

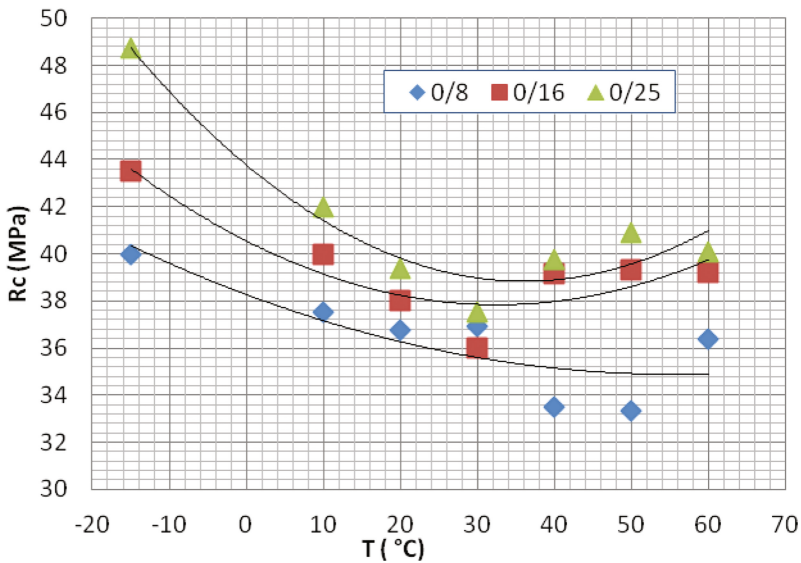


**Fig. 7.** Influence of temperature on the compressive strength of concretes

the latter increases with increasing of Dmax; where a very low slope is recorded for concrete 0/8;

- The pattern of the curves of the two concrete 0/16 and 0/25 was changed from T = 30 °C which undergoes an increase;
- The pattern curve of concrete 0/8 continues to decrease beyond T = 30 °C.
- The curve of the concrete 0/8 found at the bottom of the other curves, 0/16 in the middle and 0/25 at the top, indicating that the strength to different temperatures increases as Dmax increases.

### 1.3.2 Mortars

The results of the compressive strength at various temperatures of mortars 0/3 and 0/5 are shown in Table 6 and illustrated in Fig. 8.

**Table 6.** Compressive strength of mortars at different temperatures

Temperatures (°C)	Compressive strength Rc (MPa)	
	0/3	0/5
10	41	44
20	39,5	43,5
30	38	41
40	37	40,5
50	37	40,5
60	33,50	40

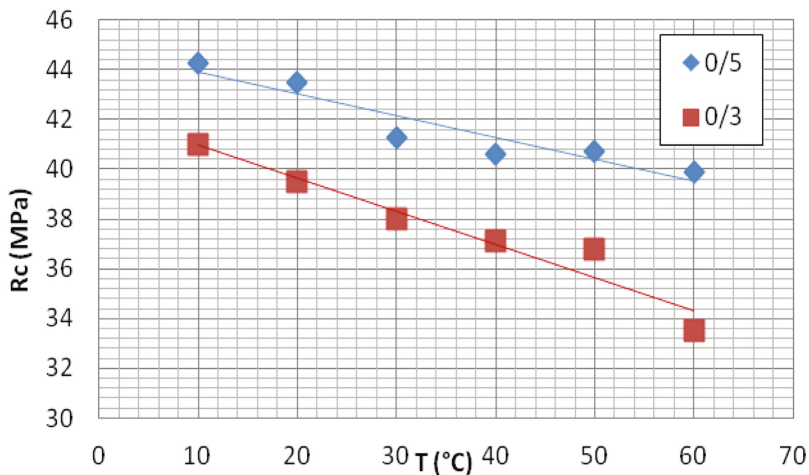


**Fig. 8.** Influence of temperature on the compressive strength of mortars

From Fig. 8, we noticed that for both mortars; the strength decreases with increasing temperature in the range of 10 °C to 60 °C.

In addition, it is clear in these curves the effect of  $D_{max}$  on the compressive strength of the mortars, which we find that strength at different temperatures increases when  $D_{max}$  increases.

### 1.3.3 Micro-concrete

The results of the compressive strength at various temperatures of micro-concrete 0/5 are shown in Table 7 and illustrated in Fig. 9.



**Table 7.** Compressive strength of micro-concrete at different temperatures

Temperatures (°C)	Compressive strength Rc(MPa)
10	19
20	20,5
30	22
40	29
50	30,5
60	27,5

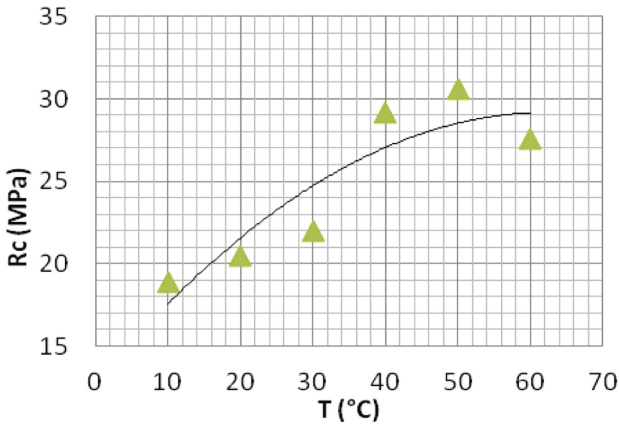


**Fig. 9.** Influence of temperature on the compressive strength of micro-concrete

From the Fig. 9, we noticed that the strength increases with increasing of temperature and reaches its maximum value at  $T = 50\text{ }^{\circ}\text{C}$  (peak strength) and then decreases to  $T = 60\text{ }^{\circ}\text{C}$ . Thus, the micro-concrete shows a different behavior of those mortars and concretes. However; from the regression, we see that the strength increases as the temperature increases to its maximum value  $T = 60\text{ }^{\circ}\text{C}$ .

## 2 Conclusions

Regarding the influence of  $D_{max}$  on the physical and mechanical properties of concretes and mortars, it was found that the increase of  $D_{max}$  leads to decrease of water demand, increased the compactness, therefore, compressive strength of concretes and mortars increases.

The mechanical behavior of concretes, mortars and micro-concrete varies from one material to another, which depends on the temperature; for concretes a concave parabolic curves (marking a critical temperature), a quasi-linear downward curves for mortars, and a convex parabolic curve (marking a peak strength) for micro-concrete.

For concretes, in general, the mechanical behavior was similar; the compressive strength drops with increasing temperature, the difference was in the position of the critical temperature in the range studied.

The behavior of mortars was the simplest; it was found that the compressive strength decreases with increasing temperature in all the temperatures range studied.

The micro-concrete was the most special case in this study, whose behavior is different from other cases where it was found that the temperature increases the compressive strength in the range studied, through peak of strength then decreased.

## References

- Almusallam, A.A.: Effect of environmental conditions on the properties of fresh and hardened concrete. *Cem. Concr. Compos. J.* **23**, 353–361 (2001)
- Arvidson, J.M.: Mechanical properties of concrete mortar at low temperatures. National Bureau of Standards (1982)
- Carrette, G.G., Malhorta, V.M.: Performance of Dolostone and Limestone Concretes at Sustained High Temperatures: Temperature Effects on Concrete. American Society for Testing and Materials, USA (1985)
- Dreux, G., Festa, J.: *Nouveau Guide du Béton et de ses Constituants*, 8ème édition, 3ème tirage, Eyrolles (2007)
- Fares, H.: Propriétés mécaniques et physico-chimiques de bétons autoplaçants exposés à une température élevée, Thèse de Doctorat, Université de Cergy-Pontoise, France (2009)
- Gallucci, E., Zhang, X., Scrivener, K.: Influence de la température sur le développement microstructural des bétons, Septième édition des Journées scientifiques du Regroupement francophone pour la recherche et la formation sur le béton, Toulouse, France (2006)
- Husem, M., Gozutok, S.: The effects of low temperature curing on the compressive strength of ordinary and high performance concrete. *Constr. Build. Mater. J.* **19**, 49–53 (2005)
- Khoury, G.A.: Compressive strength of concrete at high temperatures: a reassessment. *Mag. Concr. Res.* **44**, 291–309 (1992)
- Lawson, J.R., Phan, L.T., Davis, F.L.: Mechanical Properties of High Performance Concrete After Exposure to Elevated Temperatures. National Technical Information Service, USA (2000)
- Lee, G.C., Shih, T.S., Chang, K.C.: Mechanical properties of concrete at low temperature. *Cold Reg. Eng. J.* **2**, 13–24 (1988)
- Nasser, K.W., Evans, G.A.: The effects of cold on cured concrete. Canadian Research Council (1989)
- Ortiz, J., Aguado, A., Agulló, L., García, T.: Influence of environmental temperatures on the concrete compressive strength: simulation of hot and cold weather conditions. *Cem. Concr. Res.* **35**, 1970–1979 (2005)
- Phan, L.T., Carino, N.J.: Code provisions for high strength concrete strength-temperature relationship at elevated temperatures. *Mater. Struct. J.* **36**, 91–98 (2003)
- Pliya, P., Morais, M.V.G., Noumowe, A., Beaucour, A.L., Ortola, S.: Contraintes développées dans un élément en béton soumis à une température élevée. AUGC, France (2007)
- Shoukry, S.N., William, G.W., Downie, B., Riad, M.Y.: Effect of moisture and temperature on the mechanical properties of concrete. *Constr. Build. Mater. J.* **25**, 688–696 (2011)
- Topçu, İ.B., Toprak, M.U.: Fine aggregate and curing temperature effect on concrete maturity. *Cem. Concr. Res. J.* **35**, 758–762 (2005)

# Thermal Properties of Base-Course Material Containing Recycled Glass Under Dry and Wet Condition

Youness Berraha<sup>(✉)</sup>, Michel Vaillancourt, and Daniel Perraton

Ecole de Technologie Supérieure, Montreal, Canada  
youness.berraha.1@etsmtl.net,  
{michel.vaillancourt,daniel.perraton}@etsmtl.ca

**Abstract.** The increasing need to recycle waste and reduce the use of landfills has led to the reconsideration of the use of recycled glass aggregates in pavement construction. While the mechanical and hydraulic performances of recycled glass aggregates (RGA) in roadwork applications are well documented, their thermal performance is almost unexplored. However, in cold regions, the adequate thermal design of pavement relies on a good prediction of the thermal regime in the road structure. Glass is known for its insulating or heat-retention properties (low thermal conductivity). Aggregates and aggregate mixtures with low thermal conductivity can help decrease the depth of frost penetration. This experimental study aimed to evaluate the thermal properties of RGA blended with natural aggregate (NA). In this paper, we present the results of thermal conductivity and thermal diffusivity measurements on RGA, NA and NA blended with RGA (NA/RGA). Our methodology included the influence of particle size, moisture content and glass content. At a given moisture content, the thermal conductivity of RGA and NA decreased with increasing particle size. The results show that an increase of water content in any of the studied material increased its thermal conductivity but at relatively different rates. It was also found that increasing the percentage of glass in NA/RGA blends decreased their thermal conductivity.

## 1 Introduction

In 2012, more than 160 000 metric tons of glass entered the waste stream in the Canadian province of Quebec, but only 43% (69 000 Mt) of this material was recycled into new glass products (Eco-Entreprise Québec 2015). In other words, 91 000 Mt went to landfills, defeating the efforts and investments of environmental agencies to improve glass recovery and recycling from Quebec's single-stream collection program. Moreover, in 2013, Klareco, a facility that used to prepare about 70% of Quebec's glass for recycling, shut down, substantially affecting the province's overall waste management strategy. Meanwhile, current research and practice in road construction tend to concentrate on the use of recycled materials in the lower courses of the road (Lu et al. 2011). The use of

recycled glass, instead of virgin materials, may help ease landfill pressures and reduce demand of extraction.

The idea of using recycled glass as an aggregate in pavement material dates back to 1969 when the University of Missouri-Rolla undertook laboratory studies to determine the mechanical properties of asphaltic paving mixtures containing glass (glasphalt) (Lolias et al. 2012). Furthermore, recycled glass is perceived to have many strength and drainage applications (Lee and Landris (2007); Ooi et al. (2008); Wartman et al. (2004)). Yet, few studies have focused on the thermal properties of the material used in pavement design. This lack of thermal property data can be attributed partly to the complexity and variety of paving materials designs as well as to little interest in accurately determining the thermal regime in pavement structures (Carlson et al. 2010).

In research conducted by the Federal Highway Administration in 1998 (Chesner et al. 1998), it was reported that thermal conductivity is not only a function of glass content, but is also a function of the density of the compacted material. In 1993, laboratory tests compared the thermal conductivity of recycled glass with natural aggregates using 50 and 100% aggregate mixes, 3/4-inch minus cullet size, and both low and high contamination (Dames and Moores 1993). The results indicated that glass aggregate pavements would take a longer time to cool down due in part to the lower conductivity of glass, when compared to natural aggregates. Henry and Morin (1997) studied frost susceptibility of 100% and 30% of crushed glass by weight blended with two types of aggregates (stream gravel and crushed gravel). Their results suggest that crushed glass has negligible to very low frost susceptibility and did not increase the susceptibility of aggregates.

The aim of the present study is to evaluate the thermal properties of recycled glass and compare them with those of natural aggregates. This research project is composed of two phases of laboratory works: (1) thermal conductivity and diffusivity of pure glass aggregates and virgin limestone aggregates based on different particle size and moisture content; and (2) thermal conductivity and diffusivity of NA/RGA blends with various glass and moisture content.

## 2 Material

The RGA studied in this research are a mixture of different colored glass particles and are often comprised of a wide range of debris (mainly paper and plastic, up to 5%). This glass is supplied by Tricentris, a sorting center based in Lachute (Québec), and is usually collected from residential recycled. NA used is an excavated and crushed limestone rock from a quarry in Saint-Phillipe (Québec) and is approved for granular material base course. Samples were prepared by recombining the aggregate fractions to meet the average curve of the MG20 (0–20 mm base course material) specification of the ministry of Transportation of Quebec (MTQ). MG20 has a maximum particle size of 20 mm whereas RGA supplied by Tricentris is 5 mm (passing 5 mm). Therefore the present study was focused only on the part of the MG20 curve below 5 mm. Figure 1 gives the particle size distribution considered in this research project.

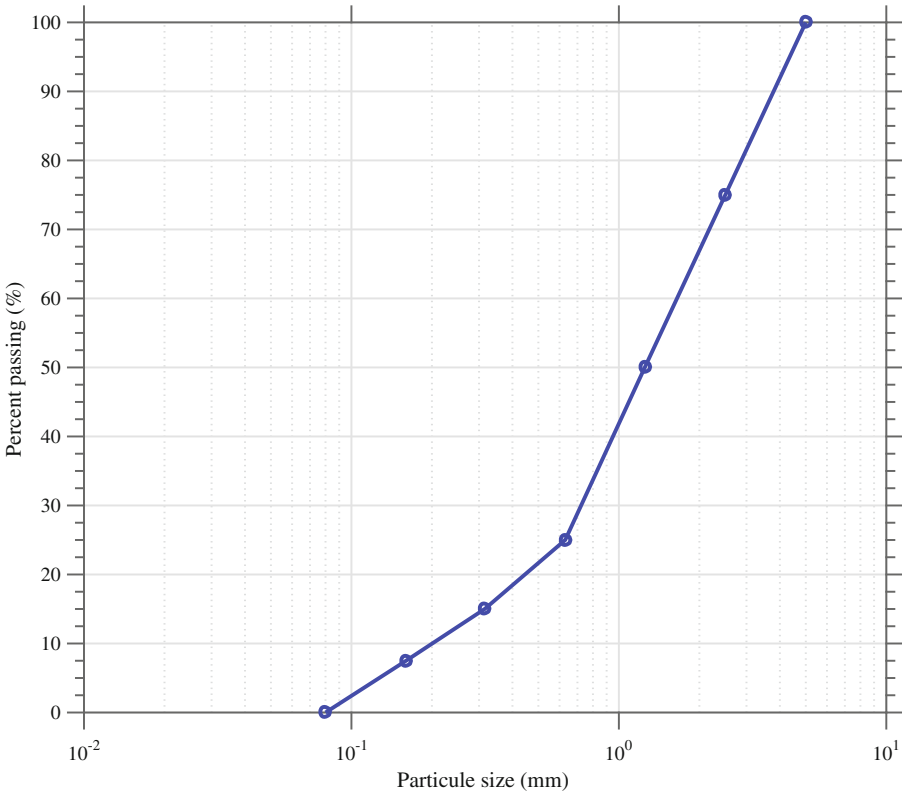


**Fig. 1.** Gradation considered for this study based on the MG20 specification of the MTQ

In order to evaluate the influence of particle size, the particle distribution considered in this study was subdivided into 3 classes: (1) [0.08–1.25 mm] (retained 0.08 mm, passing 1.25 mm); (2) [0.630–2.5 mm] (retained 0.630 mm, passing 2.5 mm) and (3) [1.25–5 mm] (retained 1.25 mm, passing 5 mm). Thermal conductivity and diffusivity test were conducted on each of these classes, for RGA and then for NA, and for various moisture contents.

Regarding the influence of glass content, the particle distribution presented in Fig. 1 was used to prepare RGA and NA materials. Once prepared, they were combined to make three different blends of NA and RGA. 25, 50 and 75% of NA fractions passing the 5 mm sieve of the MG20 material were substituted with RGA and each of these mixtures are referred to respectively as: 75NA/25RGA, 50NA/50RGA and 25NA/75RGA. For each of these blends, the impact of water content was also a part of the investigation.

### 3 Methods

For thermal conductivity measurements, samples were compacted in a cylindrical metal mold with a nominal capacity of 948.4 cm<sup>3</sup> while following the Canadian standard procedure for modified Proctor tests (CAN/BNQ (2013), method A). Figure 2 shows the experimental apparatus used for thermal conductivity measurements. A single needle sensor (TR-1) was employed to measure the thermal conductivity. This device creates a linear heat source and incorporates a thermistor, located midway along its length, to measure the variation of temperature. During measurements, the 100 mm long probe was put into the samples and the thermal data were collected using a CR1000 data-logger which records temperature measurements at 1 second intervals over a period of 120 s. For each sample, 5 different points of measurement were defined and 4 measurements were made at each of these points. In other words, 20 values of thermal conductivity were obtained for each sample, and the mean of all these values gave the thermal conductivity of the sample.

The CR1000 was loaded with a program containing the algorithms to analyze measurements made during the heating and the cooling phases. The algorithms are based on the transient line heat source analysis given in the international standard ASTM D5334 (ASTM 2005). Two different interpretation methods were used for the determination of thermal conductivity. The first method takes into account only the data which are recorded within the heating phase. The second approach uses both heating and cooling data for the analysis. According to Róžański and Sobótka (2013) and the ASTM D5334 standard, the difference between the two methods relies mainly on the fact that the second method's use of both phases minimizes the effects of thermal drifts, thus minimizing errors in estimating thermal conductivity. For each of these interpretation methods, the thermal conductivity is determined using Eqs. 1 and 2 for the first and the second method respectively.

$$\lambda_h = \frac{q}{4\pi S_h} \quad (1)$$

$$\lambda_{hc} = \frac{q}{2\pi(S_h + S_c)} \quad (2)$$

where  $q$  is the heat input (W/m),  $S_h$  and  $S_c$  the slope of temperature data for the heating and cooling phase respectively (ASTM 2005).

An experimental setup, inspired by Mrawira and Luca (2002), was conceived for the measurement of thermal diffusivity. This method is based on the assumption of one-dimensional heat-flow and uses a mathematical solution of the Fourier (Eq. 3).

$$\frac{\partial T}{\partial t} = \alpha \frac{\partial^2 T}{\partial z^2} \quad (3)$$

where  $\alpha$  is the thermal diffusivity of the specimen,  $T$  the temperature and  $z$  the direction of the heat flow.

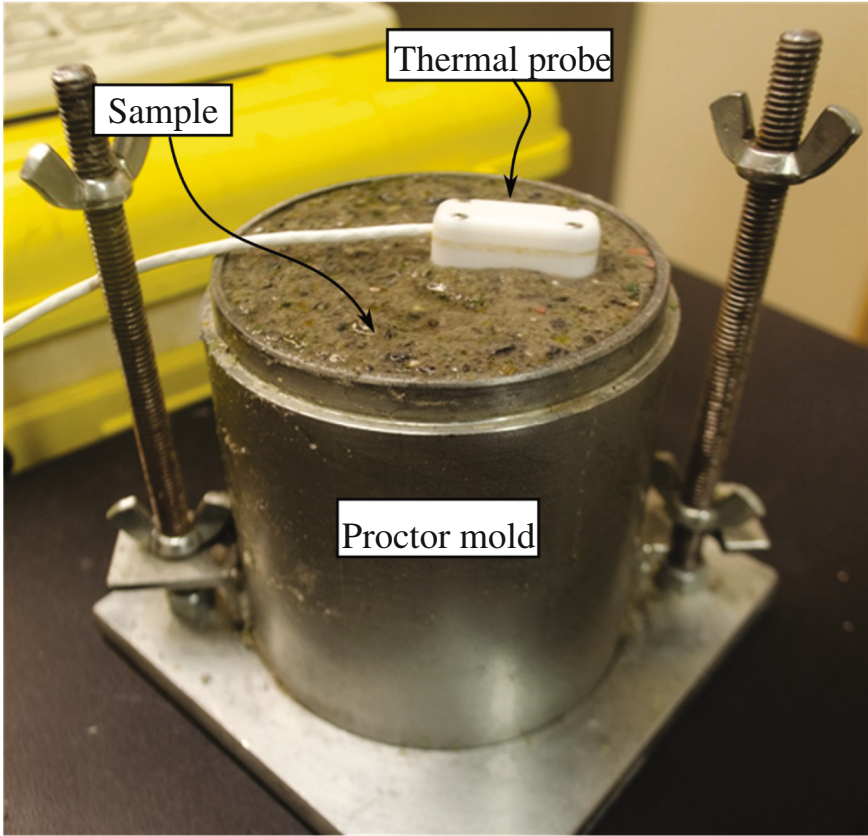


**Fig. 2.** Thermal conductivity apparatus

A thin-walled plastic cylindrical mold was used to enclose the samples which in turn were confined in a concrete mold during the compaction, using the same compaction technique as for the samples prepared for thermal conductivity experiments. After compacting to the desired density, one-dimensional heat flow was approximated by providing adequate insulation in the two other dimensions of the cylindrical sample. Three thermocouples were installed at distances of 50 mm, 71 mm and 92 mm along the axis of the sample from the top. A constant and uniform heat source, generated by a 200 W heat lamp bulb, was placed 30 mm above the top face of the sample (Fig. 3). The temperature data were collected by a data acquisition system. Using a discrete solution to Eq. 4 and using the early transient temperature-time profile, thermal diffusivity can be obtained by

$$\alpha = \frac{T(z, t + \Delta t) - T(z, t)}{T(z + \Delta z, t) - 2T(z, t) + T(z - \Delta z, t)} \frac{\Delta z^2}{\Delta t} \quad (4)$$



where  $T(z, t)$  is the temperature at the position  $z$  and time  $t$ ,  $\Delta z$  represents the space between the thermocouples and  $\Delta t$  is the increment of time between two measures of  $T(z, t)$ .

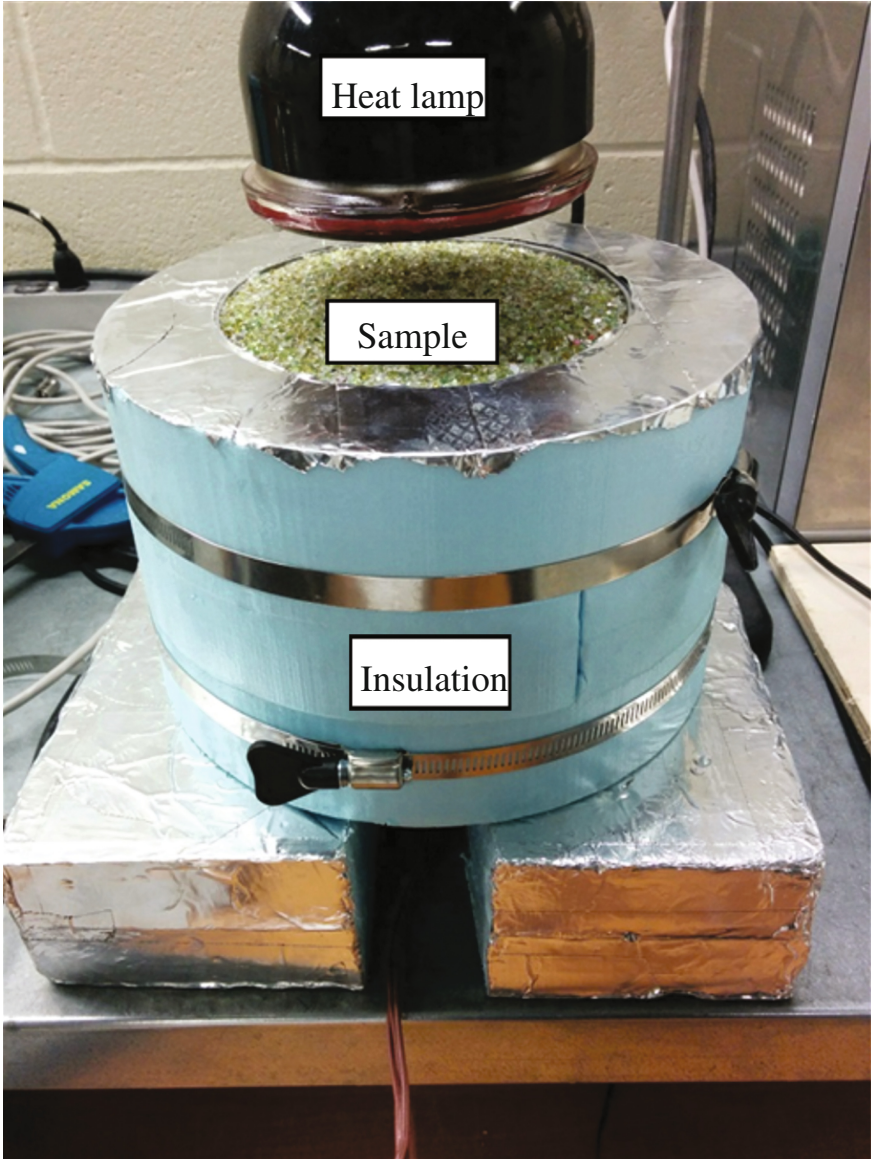


**Fig. 3.** Thermal diffusivity apparatus



## 4 Results and Discussion

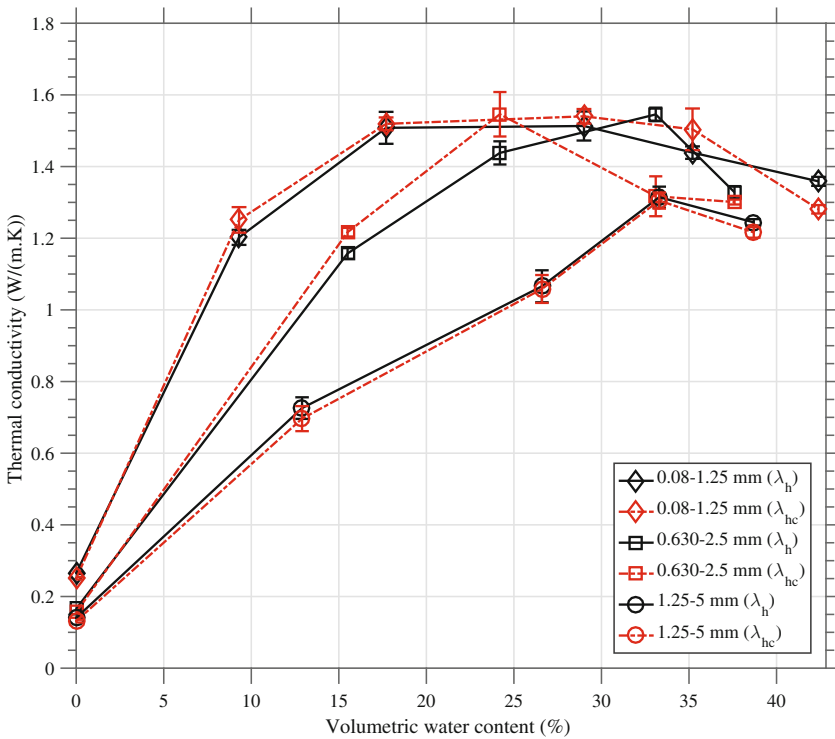
### Specific Gravity

Before thermal measurements, specific gravity of all tested blends was determined by means of a water pycnometer and according to ASTM D854-14 (ASTM 2014). Three different measurements were conducted for each blend and Table 1 presents the results of these tests. Overall, specific gravity of NA is higher than RGA and the increase of RGA content in NA/RGA blends decreases its specific gravity.

### Influence of Particle Size

Figures 4 and 5 show the variation of thermal conductivity of NA and RGA respectively as a function of volumetric water content ( $\theta$ ) with respect to different particle sizes. Volumetric water content is defined as:

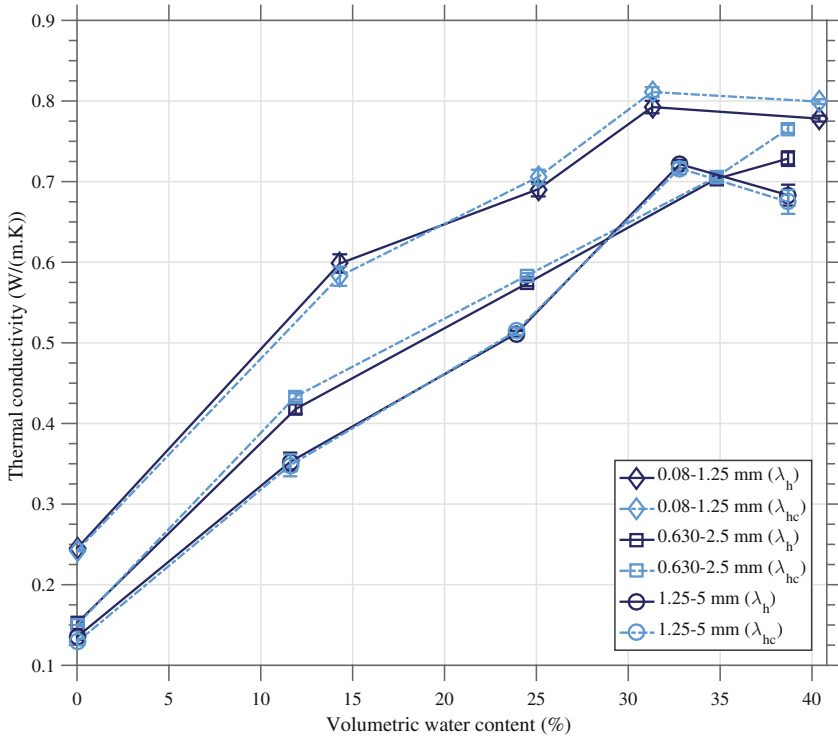
$$\theta = w \frac{\rho_d}{\rho_w} \quad (\%) \tag{5}$$



**Fig. 4.** Thermal conductivity of NA as function of volumetric water content and for different particle sizes

**Table 1.** Specific gravity of blends considered in this study

Blends		Specific gravity ( $\rho_s$ )	Standard deviation	Repetition
1.25–5 mm	RGA	2.453	0.103	3
	NA	2.765	0.012	3
0.630–2.5 mm	RGA	2.519	0.017	3
	NA	2.771	0.004	3
0.08–1.25 mm	RGA	2.524	0.007	3
	NA	2.774	0.004	3
75NA/25RGA		2.708	0.018	3
50NA/50RGA		2.615	0.006	3
25NA/75RGA		2.578	0.005	3

**Fig. 5.** Thermal conductivity of RGA as function of volumetric water content and for different particle sizes

**Table 2.** Average values of measured thermal conductivity of RGA for different particle size and other experimental parameters

RGA	$\rho_d$	$\theta$	$n$	$\lambda_c$	$\sigma^a$	$\lambda_{hc}$	$\sigma^a$
	g/cm <sup>3</sup>	%		W/(m.K)			
0.08–1.25 mm	1.80	0.0	28.7	0.245	0.003	0.242	0.001
	1.73	14.3	31.6	0.598	0.013	0.583	0.010
	1.73	25.1	31.5	0.691	0.010	0.706	0.008
	1.61	31.3	36.3	0.793	0.009	0.811	0.005
	1.41	40.4	44.3	0.778	0.004	0.799	0.003
0.630–2.5 mm	1.49	0.0	40.9	0.152	0.002	0.150	0.001
	1.50	11.9	40.4	0.418	0.007	0.434	0.003
	1.46	24.5	42.2	0.574	0.004	0.584	0.003
	1.50	34.8	40.4	0.703	0.004	0.706	0.004
	1.43	38.7	43.1	0.729	0.011	0.766	0.004
1.25–5 mm	1.52	0.0	38.0	0.135	0.005	0.129	0.004
	1.52	11.6	37.9	0.352	0.013	0.348	0.012
	1.54	23.9	37.2	0.512	0.004	0.515	0.004
	1.56	32.8	36.3	0.722	0.006	0.717	0.006
	1.43	38.7	41.6	0.683	0.015	0.675	0.013

<sup>a</sup>Standard deviation

where  $w$  is the mass-basic water content,  $\rho_d$  is the bulk density and  $\rho_w$  represents the water density.

At  $\theta=0\%$ , all samples have relatively close thermal conductivity, ranging from 0.135 to 0.245 W/(m.K), and from 0.131 to 0.251 W/(m.K) for RGA and NA respectively, with slightly higher values for class [0.08–1.25 mm]. This slight difference between class [0.08–1.25 mm] and the two other classes can be explained by looking at values of porosity ( $n$ ) given in Table 2 along with the thermal conductivity results. If we consider RGA, at  $\theta=0\%$ , we notice that for class [0.08–1.25 mm]  $n=28.7\%$  whereas the two other samples' porosity  $n=40\%$ . As has been shown in previous studies, a decrease in porosity leads to an increase in thermal conductivity mainly due to a better heat transfer across the contacts (Farouki 1981). Table 3 shows the thermal conductivity results obtained on NA.

As  $\theta$  increases, thermal conductivity also increases but at different rates dependent on the nature of the material (RGA or NA). Indeed, thermal conductivity of NA increases rapidly with increase of volumetric water content, in particular for class [0.08–1.25 mm] for which thermal conductivity rises from 0.265 to 1.202 W/(m.K) for respectively  $\theta=0\%$  and  $\theta=9.3\%$ . On the whole, thermal conductivity is higher for samples with small particles, and as particle size increases, thermal conductivity decreases. Compared with NA, the increase of  $\theta$  has a relatively lower impact on the increase of thermal conductivity of RGA. Otherwise, values of  $\lambda$  also decrease with increase of particle size, and the

**Table 3.** Average values of measured thermal conductivity of NA for different particle size and other experimental parameters

NA	$\rho_d$	$\theta$	$n$	$\lambda_c$	$\sigma^a$	$\lambda_{hc}$	$\sigma^a$
	g/cm <sup>3</sup>	%		W/(m.K)			
0.08–1.25 mm	1.94	0.0	30.1	0.265	0.003	0.251	0.003
	1.86	9.3	33.1	1.202	0.024	1.251	0.031
	1.86	17.7	32.8	1.508	0.052	1.519	0.015
	1.81	29.0	34.7	1.513	0.047	1.540	0.018
	1.68	35.2	39.5	1.439	0.020	1.504	0.050
	1.50	42.4	46.1	1.359	0.015	1.281	0.010
0.630–2.5 mm	1.71	0.0	38.3	0.166	0.001	0.156	0.001
	1.65	15.5	40.6	1.158	0.017	1.217	0.010
	1.67	24.2	39.8	1.438	0.038	1.546	0.053
	1.70	33.1	38.7	1.546	0.022	1.317	0.048
	1.63	37.6	41.0	1.328	0.020	1.301	0.006
1.25–5 mm	1.70	0.0	38.5	0.140	0.004	0.131	0.003
	1.68	12.9	39.2	0.726	0.035	0.697	0.030
	1.70	26.6	38.4	1.067	0.052	1.058	0.033
	1.70	33.6	38.6	1.315	0.034	1.305	0.019
	1.59	38.7	42.4	1.244	0.010	1.216	0.013

<sup>a</sup>Standard deviation

**Table 4.** Average values of measured thermal diffusivity of NA for different particle size and other experimental parameters

NA	$\rho_d$	$\theta$	$n$	$\alpha$	$\sigma^a$
	g/cm <sup>3</sup>	%		$\times 10^{-7} \text{ m}^2/\text{s}$	
0.08–1.25 mm	1.87	0.0	32.6	2.09	0.14
	1.81	13.8	34.7	4.88	0.16
	1.81	24.2	34.8	4.81	0.97
0.630–2.5 mm	1.65	0.0	40.5	2.28	0.25
	1.63	12.4	41.2	5.13	0.16
	1.62	23.6	41.7	4.21	0.36
1.25–5 mm	1.68	0.0	39.2	2.29	0.27
	1.67	13.2	39.7	4.83	0.14
	1.68	23.3	39.4	5.18	0.28

<sup>a</sup>Standard deviation

maximum value of 0.793 W/(m.K) is obtained for class [0.08–1.25 mm] at  $\theta = 31.3\%$ .

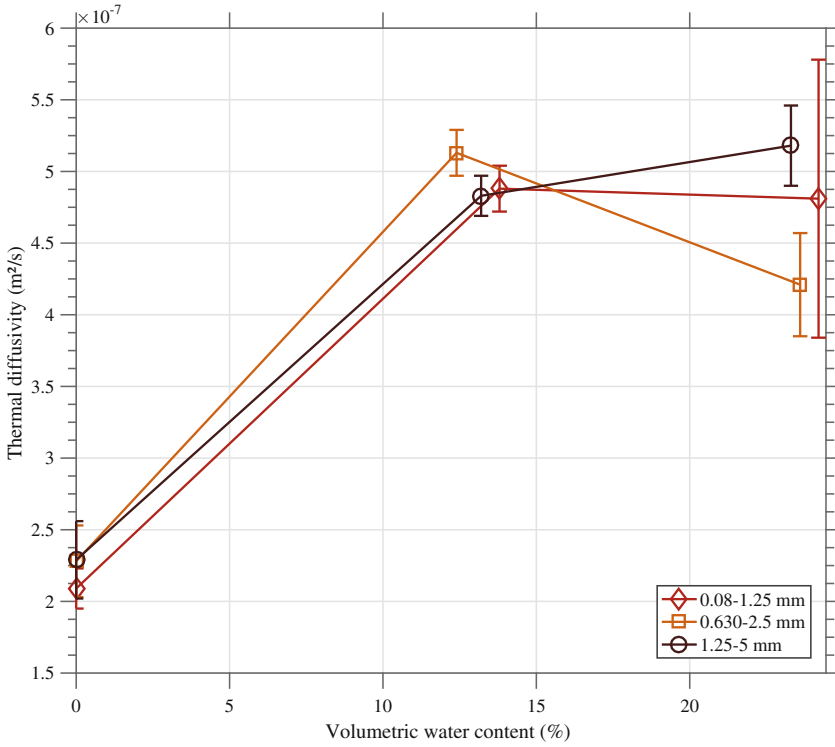


**Fig. 6.** Thermal diffusivity of NA as function of volumetric water content and for different particle sizes

Thermal diffusivity of NA was found to vary between  $2.09 \times 10^{-7}$  and  $5.18 \times 10^{-7} \text{ m}^2/\text{s}$ ,  $2.28 \times 10^{-7}$  and  $5.11 \times 10^{-7} \text{ m}^2/\text{s}$ , and  $2.29 \times 10^{-7}$  and  $5.18 \times 10^{-7} \text{ m}^2/\text{s}$  for particle sizes of [0.08–1.25 mm], [0.630–2.5 mm] and [1.25–5 mm] (Table 4). Thermal diffusivity increases with increase in volumetric water content but is not much affected by the variation of particle size as shown in Fig. 6.

The variation of thermal diffusivity of RGA ranged between  $2.70 \times 10^{-7}$  and  $2.89 \times 10^{-7} \text{ m}^2/\text{s}$ ,  $1.76 \times 10^{-7}$  and  $2.74 \times 10^{-7} \text{ m}^2/\text{s}$ , and  $1.77 \times 10^{-7}$  and  $3.11 \times 10^{-7} \text{ m}^2/\text{s}$  for particle sizes of [0.08–1.25 mm], [0.630–2.5 mm] and [1.25–5 mm] (Table 5). These results are presented in Fig. 7 and a similar observation can be drawn: the influence of particle size is not substantial here again. However, the increase of thermal diffusivity with increase of  $\theta$  is minor when compared with NA.

### Influence of Glass Content

Results regarding the influence of glass content on the thermal conductivity are presented in Fig. 8, thermal conductivities of all three blends being plotted

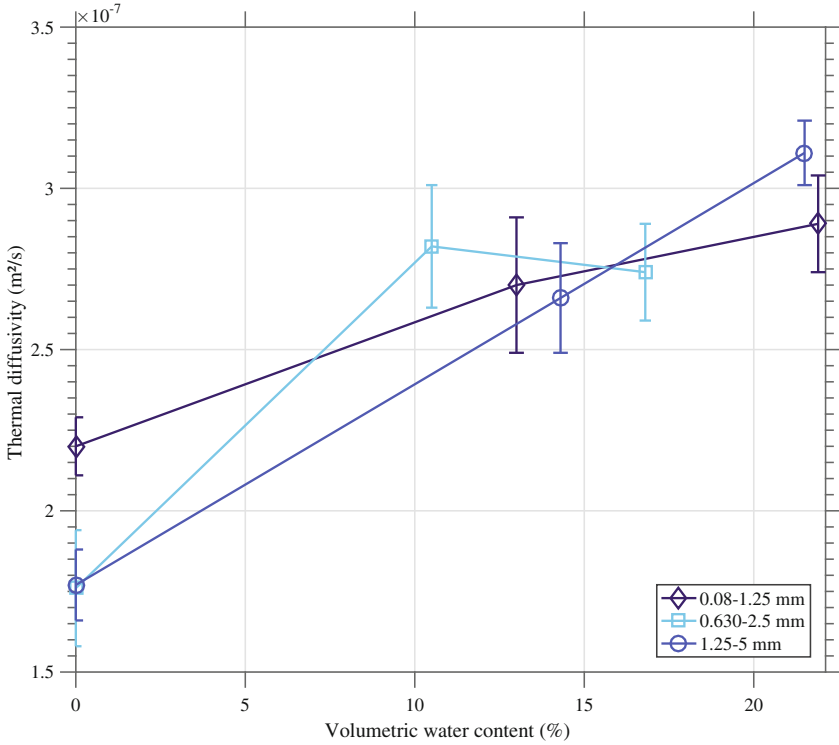


**Fig. 7.** Thermal diffusivity of RGA as function of volumetric water content and for different particle sizes

**Table 5.** Average values of measured thermal diffusivity of RGA for different particle size and other experimental parameters

RGA	$\rho_d$	$\theta$	$n$	$\alpha$	$\sigma^a$
	g/cm <sup>3</sup>	%		x10 <sup>-7</sup> m <sup>2</sup> /s	
0.08–1.25 mm	1.74	0.0	31.1	2.20	0.09
	1.64	13.0	35.0	2.70	0.21
	1.68	21.9	33.4	2.89	0.15
0.630–2.5 mm	1.42	0.0	43.6	1.76	0.18
	1.44	10.5	42.7	2.82	0.19
	1.41	16.8	44.0	2.74	0.15
1.25–5 mm	1.50	0.0	38.8	1.77	0.11
	1.51	14.3	38.6	2.66	0.17
	1.54	21.5	37.3	3.11	0.10

<sup>a</sup>Standard deviation

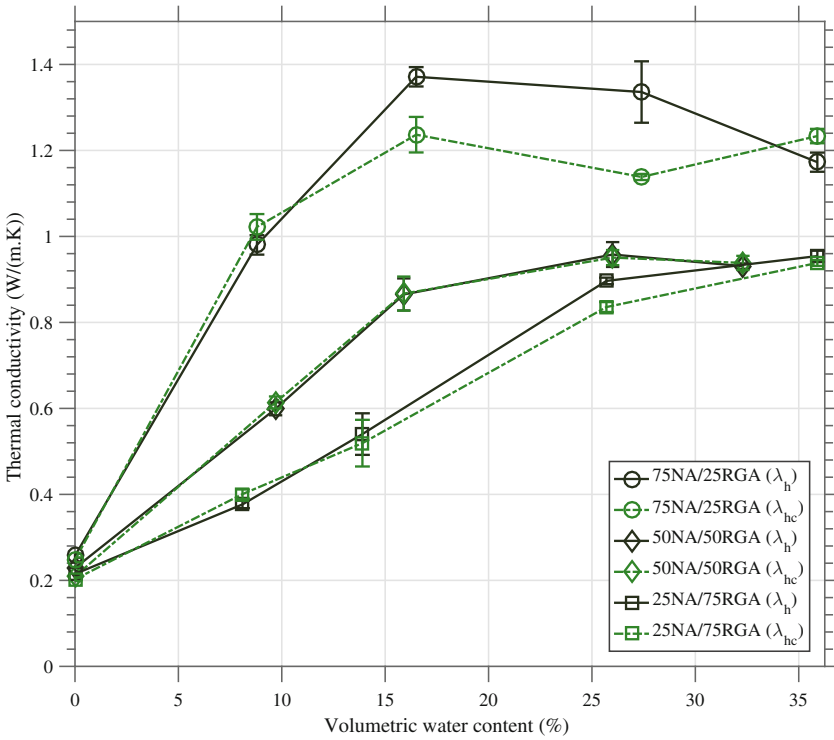


**Fig. 8.** Thermal conductivity of NA/RGA blends as function of volumetric water content and for different RGA content

against the volumetric water content. At  $\theta = 0\%$ , all three blends have similar thermal conductivity but as  $\theta$  increases the effect of RGA becomes noticeable. 75NA/25RGA exhibits the highest thermal conductivities (1.371 W/(m.K) at  $\theta = 31.3\%$ ) and when the RGA content increases relatively to NA, thermal conductivity decreases (Table 6). This is consistent with the fact that glass has lower thermal conductivity than NA (Gotoh 2001). Moreover, if we compare 50NA/50RGA results with the other two combinations, one can see that there is a larger difference between 50NA/50RGA and 75NA/25RGA than 50NA/50RGA and 25NA/75RGA. In other words, impact of glass content is more significant when RGA fraction increases from 25% to 50%; whereas when RGA fraction increases from 50% to 75%, the difference in thermal conductivity is less substantial.

Thermal diffusivity was also measured for various volumetric water contents, and the results are presented in Fig. 9. With the increase of  $\theta$ , thermal diffusivity was found to increase from  $2.32 \times 10^{-7}$  to  $4.21 \times 10^{-7}$  m<sup>2</sup>/s,  $2.20 \times 10^{-7}$  to  $5.03 \times 10^{-7}$  m<sup>2</sup>/s and  $3.16 \times 10^{-7}$  to  $3.72 \times 10^{-7}$  m<sup>2</sup>/s, for 75NA/25RGA, 50NA/50RGA and 25NA/75RGA respectively (Table 7). These results suggest that increasing RGA content in NA/RGA blends tend to decrease their ther-

**Table 6.** Average values of measured thermal conductivity of NA/RGA blends and other experimental parameters

NA/RGA blends	$\rho_d$	$\theta$	$n$	$\lambda_c$	$\sigma^a$	$\lambda_{hc}$	$\sigma^a$
	g/cm <sup>3</sup>	%		W/(m.K)			
75NA/25RGA	1.93	0.0	28.7	0.258	0.006	0.248	0.005
	1.92	8.8	29.0	0.980	0.026	1.022	0.026
	1.94	16.5	28.2	1.371	0.026	1.237	0.036
	1.87	27.4	31.1	1.336	0.083	1.138	0.006
	1.63	35.9	39.8	1.173	0.026	1.234	0.014
50NA/50RGA	1.91	0.0	27.0	0.229	0.007	0.209	0.005
	1.80	9.7	31.1	0.599	0.018	0.614	0.015
	1.91	15.9	26.9	0.865	0.043	0.867	0.034
	1.81	26.0	29.6	0.958	0.034	0.951	0.015
	1.66	32.3	36.6	0.931	0.007	0.938	0.014
25NA/75RGA	1.89	0.0	26.7	0.215	0.004	0.203	0.004
	1.85	8.1	28.3	0.377	0.010	0.401	0.009
	1.88	13.9	27.0	0.540	0.056	0.519	0.047
	1.81	25.7	29.7	0.897	0.009	0.836	0.010
	1.63	35.9	36.7	0.954	0.015	0.938	0.006

<sup>a</sup>Standard deviation

**Table 7.** Average values of measured thermal diffusivity of NA/RGA blends for different particle size and other experimental parameters

NA/RGA blends	$\rho_d$	$\theta$	$n$	$\alpha$	$\sigma^a$
	g/cm <sup>3</sup>	%		$\times 10^{-7} \text{ m}^2/\text{s}$	
50NA/50RGA	1.91	0.0	27.0	2.20	0.13
	1.86	13.2	28.9	3.37	0.26
	1.79	25.4	31.7	5.03	0.59
75NA/25RGA	1.90	0.0	29.8	2.32	0.17
	1.89	13.8	30.1	5.17	0.29
	1.82	24.0	32.8	5.11	0.30
25NA/75RGA	1.89	0.0	26.7	3.16	0.40
	1.84	14.3	28.8	3.42	0.13
	1.74	21.9	32.5	3.72	0.09

<sup>a</sup>Standard deviation



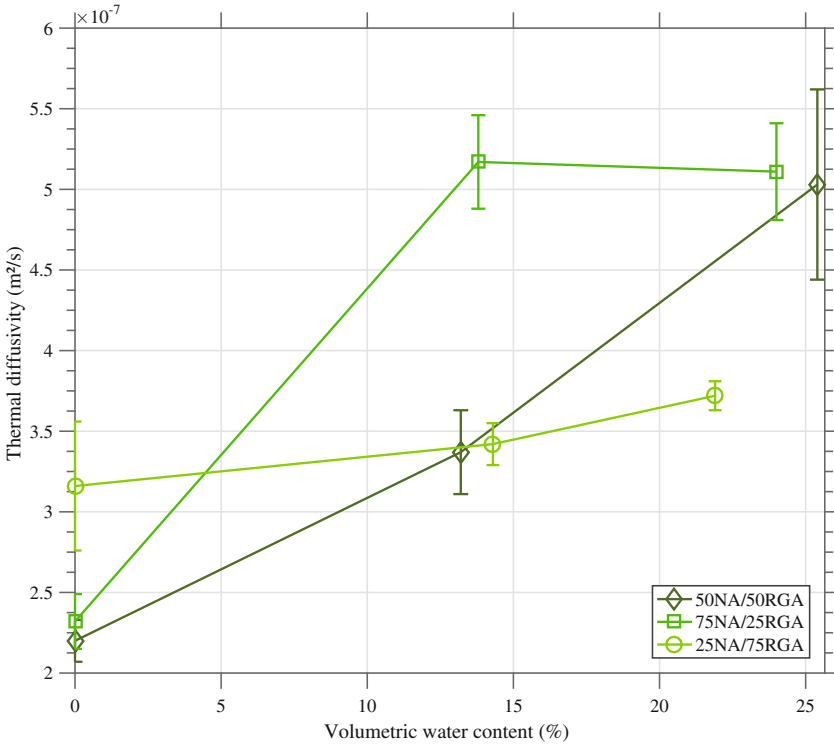


**Fig. 9.** Thermal diffusivity of NA/RGA blends as function of volumetric water content and for different RGA content

mal diffusivity; this trend can be observed by taking the results obtained with the 25NA/75RGA and comparing them with the results obtained with the 75NA/25RGA.

## 5 Conclusion

A laboratory study of thermal conductivity and diffusivity of natural aggregates, recycled glass aggregates, and blends of both these materials was conducted in order to evaluate the influence of particle size, glass content, and moisture content on thermal properties. Results showed that thermal conductivity is strongly influenced both by moisture content and particle size whereas thermal diffusivity is influenced only by moisture content. As anticipated, recycled glass has lower thermal properties when compared to natural aggregate, thus increasing glass content resulted in a decrease of thermal conductivity.

**Acknowledgments.** This work was supported by Eco Entreprise Québec, la Société des Alcools du Québec, Recyc Québec, the city of Montreal and by Mitacs Accelerate program.

## References

- ASTM: Standard test method for determination of thermal conductivity of soil and soft rock by thermal needle probe procedure (2005)
- ASTM: Standard test methods for specific gravity of soil solids by water pycnometer (2014)
- CAN/BNQ. 2501–250: Determination of the water content-dry density relation (2013)
- Carlson, J.D., Bhardwaj, R., Phelan, P.E., Kaloush, K.E., Golden, J.S.: Determining thermal conductivity of paving materials using cylindrical sample geometry. *J. Mater. Civil Eng.* **22**(2), 186–195 (2010)
- Chesner, W.H., Collins, R.J., MacKay, M.H.: User guidelines for waste and by-product materials in pavement construction. Technical report Rept. No. 480017, Federal Highway Administration (1998)
- Dames and Moores, Inc. Glass Feedstock Evaluation Project. Technical Report B6, Clean Washington Center, division of the Washington State Department of Trade and Economic Development, Seattle (1993)
- Eco-Entreprise Québec. Annual Report. Technical report (2015)
- Farouki, O.: Thermal properties of soils. Number Monograph 81–1. U.S. Army Corps of Engineers, Cold Regions Research and Engineering Laboratory, Hanover (N.H.) (1981)
- Gotoh, K.: Thermal and mechanical properties of glass cullet mixed with asphalt as low-exothermic pavement material. **31**(57), 111–114 (2001)
- Henry, K.S., Morin, S.H.: Frost susceptibility of crushed glass used as construction aggregate. Technical note. *J. Cold Regions Eng.* **11**(4) (1997)
- Lee, J., Landris, T.: Recycled glass and dredged materials (2007)
- Lolias, Y., Cameron, L., Cielo, A., Cordelia, M., Gethin, B., Josefa, T., Kenneth, K., Matthew, S.: Research report on the recycling and reuse of materials within civil construction. Technical report, Department of Construction and Infrastructure, Palmerston, Northern Territory (2012)
- Lu, H., Huang, W., Li, K., Liu, L., Sun, L.: Glasphalt Mixtures' Performance Research and Analysis, pp. 1427–1432. American Society of Civil Engineers (2011)
- Mrawira, D., Luca, J.: Thermal properties and transient temperature response of full-depth asphalt pavements. *Transp. Res. Rec. J. Transp. Res. Board* **1809**, 160–171 (2002)
- Ooi, P., Li, M., Sagario, M., Song, Y.: Shear strength characteristics of recycled glass. *Transp. Res. Rec. J. Transp. Res. Board* **2059**, 52–62 (2008)
- Rózański, A., Sobótka, M.: On the interpretation of the needle probe test results: thermal conductivity measurement of clayey soils. *Studia Geotechnica et Mechanica* **35**(1), 195–207 (2013)
- Wartman, J., Grubb, D.G., Nasim, A.S.M.: Select engineering characteristics of crushed glass. *J. Mater. Civil Eng.* **16**(6), 526–539 (2004)

# Evaluation of Using Waste Road Construction Materials with Additives in Warm Mix Asphalt

Abdelzاهر E.A. Mostafa<sup>(✉)</sup>, Mohamed S. Ouf,  
and Hala H. Abdel Fatah

Civil Engineering Department, Faculty of Engineering, Mattaria Branch,  
Helwan University, Cairo, Egypt  
zaher292@yahoo.com, eng.halahashem@yahoo.com,  
drmoamedouf@hotmail.com

**Abstract.** One of the hottest topics in asphalt pavement today is applying warm asphalt mix to reduce the mixing temperature with 20 to 40 °C, eliminate the greenhouse emissions and conserve the fuel required by less energy needed by using Zeolite and Sasobit additives with polymers to improve properties of the mixtures. Also, Nano Silica has been employed to enhance the asphalt mixture properties. The results revealed that using SBS with percentage of 3% by weight of asphalt binder increased stability with 33% at 0.75% of Zeolite and using 4% of SBS increased stability with 20% when adding 2% of Sasobit more than control mixture. Using EPF modified asphalt polymer to produce WMA has insignificant effect in control mixture performance. Rutting resistance was improved in case of using Zeolite with SBS polymer more than in case of using modified Sasobit with SBS polymer under WTT.

**Keywords:** RAP · Zeolite · Sasobit · Warm additives · SBS · EPF

## 1 Introduction

Due to the increase in asphalt binder, aggregate and fuel cost and the lack of natural resources parallel with the problem of waste by-product of construction materials, using reclaimed aggregate pavement to eliminate using of new aggregate resources and asphalt binder is very beneficial. Also to reduce the environmental pollution related to asphalt mixing temperature, using warm mix technology is very essential.

In this paper, many materials and techniques have been employed to produce warm mix asphalt (WMA). Aspha-min, which is a fine synthetic powder, Sasol wax commercially known as Zeolite and Sasobit respectively have been used. Expanded polystyrene foam (EPF) as a polymer has been used to improve the strength and enhance rutting resistance for asphalt mixes, Also, Styrene Butadiene Styrene (SBS) has been used as a thermoplastic polymer, can improve the elasticity, and stiffness index of the

---

The original version of the book was revised: For detailed information please see Erratum.  
The erratum to the book is available at [https://doi.org/10.1007/978-3-319-61633-9\\_25](https://doi.org/10.1007/978-3-319-61633-9_25)

mixes. SBS can reduce the potential rutting in summer and the cracking in winter (Tarefder and Zaman 2010).

Nano technology can produce materials with vast surface areas, less adsorption, has good dispersion, high chemical purity and good stability, thus, improve the strength and rutting resistance (Yao et al. 2012).

## 2 Background

Within the past two decades or so, the asphalt paving industry has responded positively to the need for sustainable practices within the industry through the development and deployment of (WMA) technologies. Warm-mix asphalt is an innovative asphalt produced at temperatures about 20 °C–40 °C less than traditional hot mix asphalt (HMA) (Miller and Bahia 2009). (Barthel et al. 2005) pointed out that, it is important that the synthetic Zeolite particles are foamed and losing their water in several steps and not all at once and the asphalt mixture can be compacted until the temperature fall down below 120 °C. In their promotional material, Eurovia indicates that Aspha-min can give a reduction in mixing temperature more than 30 °C, save 30% of energy, and satisfy all commonly used asphalt and polymer-modified binders as well as the addition of RAP.

The (RAP) is one of the most recycled materials in the world, recent researches (Celauro et al. 2010; Shirodkar et al. 2011) have investigated that, adding RAP at percentage above 50% is feasible to produce new (HMA), obtaining satisfactory results in the mechanical properties. Studies in Europe and the United States have concluded that over 80% of the recycled materials is reused in the construction of roads, but regulations are still restricted, allowing using of RAP in percentages between 5 and 50% to produce new (HMA) (Mengqi et al. 2012).

(Mostafa 2016) pointed out that, adding RAP at percentage above 80% of the asphalt mix with Sasol wax commercially known as Sasobit at mixing temperatures between (120–140) °C produced satisfactory results in the mechanical properties at mixing temperature of 130 °C. A nanomaterials are a miniaturized particle that is measured in nanometers (nm) and is defined as a particle with at least one dimension that is less than 100 nm. The physics and chemistry of nano-sized particles are different from conventional materials, primarily due to the increased surface area-to-volume ratio of nano-materials (Teizer et al. 2012).

## 3 Objectives

The primary objective of this paper is to investigate the performance of the asphalt mixtures containing reclaimed aggregate pavement (RAP).

Investigate the performance of WMA after adding additives with RAP mixture.

Evaluate the economic and environmental benefits of using recycled materials in roadways with additives.

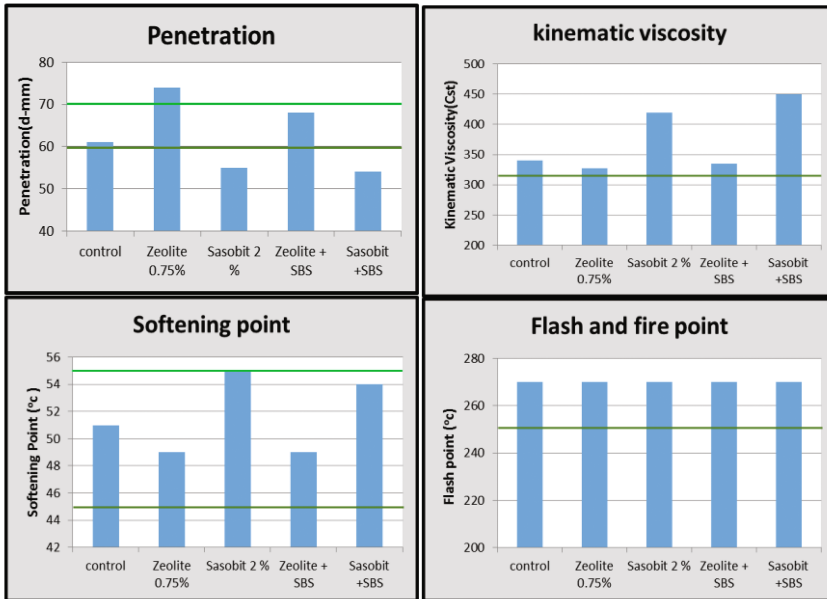


Fig. 1. Asphalt binder Tests with additives mixtures

## 4 Experimental Tests and Results

### 4.1 Asphalt Binder Tests

Asphalt tests have been carried out to compare the effect of WMA and modified asphalt polymer on asphalt used in RAP mixture. Figure 1 shows an increase in penetration with an increase in Zeolite percentages in both cases of Zeolite only and modified with SBS, but the increase in case of Zeolite only was more than the limits of the Egyptian code specifications (ECP). Adding Sasobit in both forms significantly reduced the penetration. All the penetration test results refer to the best additive was Zeolite with modified polymer SBS while, Sasobit has no significant effect on the properties of asphalt binder. Also, adding Sasobit to bitumen increases the kinematic viscosity due to the remaining of Sasobit particles in the asphalt binder at low temperatures which leads to an increase in viscosity. While, adding Zeolite reduces the kinematic viscosity of bitumen due to the foaming effect of Zeolite in the asphalt binder. The penetration test results show an increase in penetration with an increase in Zeolite percentages in both cases of Zeolite only and modified with SBS, but the increase in case of Zeolite only was more than the limits. Also, adding Zeolite to mixture reduces the softening point of bitumen due to lesser viscosity than in case of adding Sasobit to RAP mixture.

## 4.2 Marshall Test (AASHTOT 245)

### 4.2.1 Marshall Mix Design

Mix design was carried out for “RAP” with asphalt binder percentage of 4.25% by total weight of aggregates melded from surface layer with 5% of silica fume powder to accomplice with specifications at the temperature of 150 °C. Five mixes of different bitumen rations (4.75: 5.75) were prepared with an increment of 0.25% to determine (OBC) for RAP mixture. Marshal test was carried out for all specimens, stability and flow were recorded; material stiffness index can be calculated which indicated to the material resistance to shear stresses.

**Table 1.** Marshal mix design results for RAP mix at temperature 150 °C.

Volumetric properties	Values
Stability	1964 (Ib)
Flow	10.3 (0.01”)
AV	3.2%
VMA	13.8%
Unit weight	2.367
Stiffness	191

Table 1 revealed that, the (OBC) for RAP mixture was 5.5%, while the original bitumen content existing in RAP was 4.25%, therefore 1.25% bitumen was needed to satisfy the (OBC). It was observed that, the mixture satisfied the minimum requirements for most volumetric properties.

In this paper, the above mixture has been used as a control mixture at 150 °C and additives have been used to improve the performance of the asphalt mixture.

### 4.2.2 Results of Marshall Test for Warm Mixes

#### 4.2.2.1 Zeolite and Sasobit Additives Mixture

Zeolite and Sasobit have been used with RAP mixes, between 0.25 to 1.25% with an increment of 0.25% and between 1 to 3% with an increment of 0.50% by binder weight respectively to investigate the improvement in the mixture properties (Fig. 2).

##### 4.2.2.1.1 Effect of Adding Zeolite on Stability and Flow on RAP Mixture

In Fig. 3, it was found that, stability increases with an increase in Zeolite percentage until a maximum value of 20% at 0.75%, while flow decreases with an increase in Zeolite percentage to achieve the control limit at 0.75% of Zeolite and further decrease below control limit with further increase in zeolite percentage was found but still in the specification ranges.

##### 4.2.2.1.2 Effect of Adding Sasobit on Stability and Flow on RAP Mixture

In Fig. 4, it was found that, an increases in stability with an increase in Sasobit percentage until a maximum value of 15% more than control sample at 2% of Sasobit and then decreased. while, flow decreases with an increase in Sasobit percentage to achieve control limit at 2% of Sasobit and further decrease below control limit with further increase in Sasobit percentage was found but still in specification range.

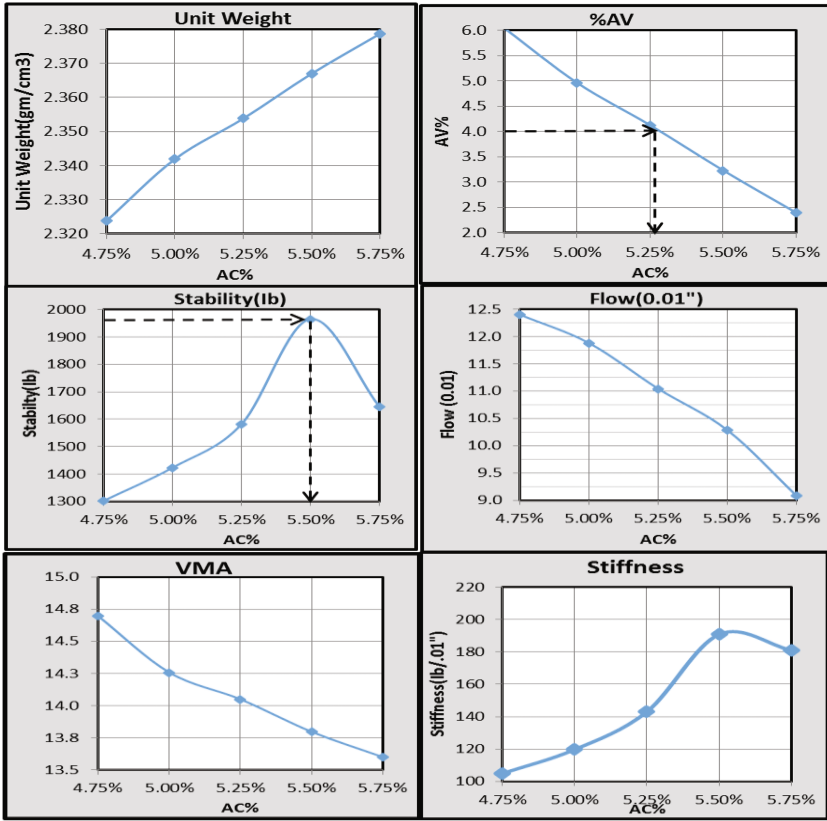


Fig. 2. Mix design of RAP mixtures

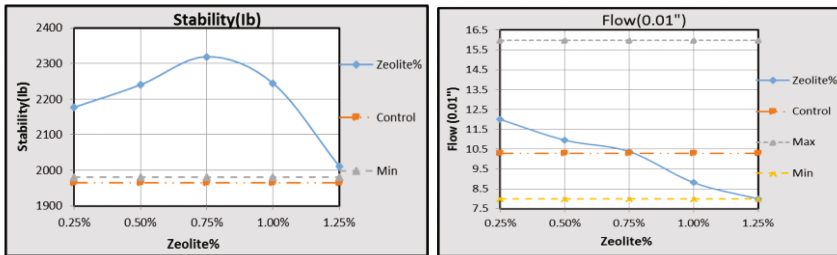


Fig. 3. Stability and flow of mixture with Zeolite warm additive.

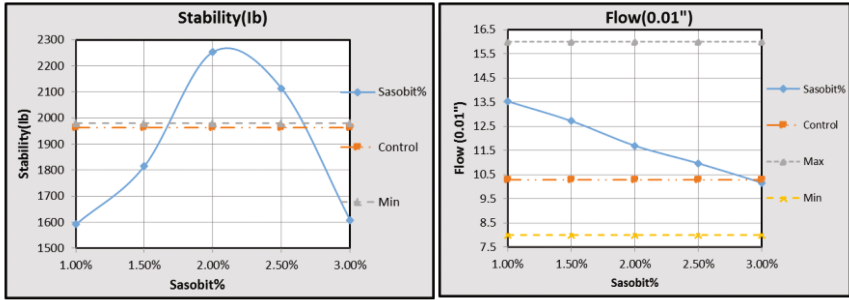


Fig. 4. Stability and flow of mixture with Sasobit warm additive.

4.2.3 Result of Marshal Tests for Modified Asphalt Mixtures

4.2.3.1 Warm Additives with (SBS) and (EPF) Polymers Modified Asphalt

4.2.3.1.1 Effect of Adding SBS on Stability and Flow on RAP Mixture

In Fig. 5, stability of mixes containing zeolite increased to 33% more than the control sample with an increase in SBS up to 3% then decreased. While the increase in stability was only 15% more than in case of using zeolite only. Adding SBS to mixes containing Sasobit increased the stability up to 20% more than the control sample at 4% and no significant effect was observed with Sasobit only.

In Fig. 5, the flow of mixes containing zeolite with SBS was increased to 15% more than the control sample with an increase in SBS up to 3% then insignificantly decreased. Adding SBS to mixes contain Sasobit increased the flow to a maximum limit of 26% at 4% of SBS then decreased, but still in specification ranges.

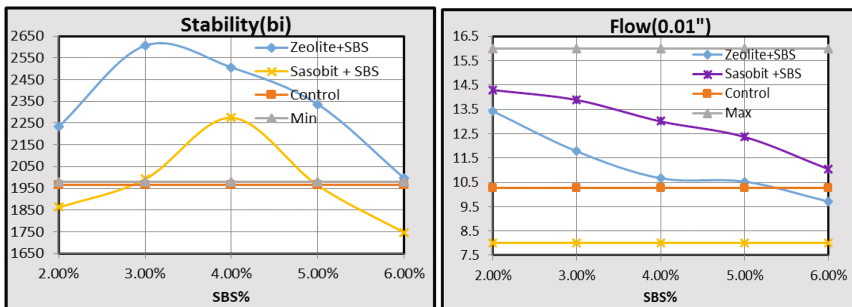


Fig. 5. Stability and flow of SBS with warm additives.

4.2.3.1.2 Effect of Adding EPF on Stability and Flow on RAP Mixture

In Fig. 6, stability of mixes containing zeolite increased to 5% more than the control sample with an increase in EPF up to 1.75%, then decreased. Adding EPF to mixes containing Sasobit increased the stability up to 6% more than the control sample at 1.5% EPF.



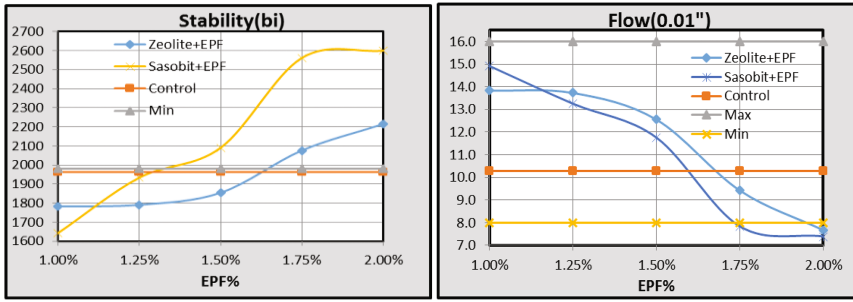


Fig. 6. Stability and flow of EPF with warm additives.

In Fig. 6, flow of mixes containing zeolite with EPF was decreased to 9% less than the control sample with an increase in EPF up to 1.75% then insignificantly decreased. Adding EPF to mixes containing Sasobit increased the flow to a maximum limit at 1.5% of EPF of 15% then decreased, but still in specification ranges.

**4.2.4 Result of Marshal Tests for Modified Warm Mixes with Nano Silica (Sio2)**

*4.2.4.1 Effect of Adding Nano Silica (Sio2) on Stability and Flow on RAP Mixture* In Fig. 7, stability of optimum mix containing zeolite increased to 29% more than the control sample with an increase in Sio<sub>2</sub> up to 1.75% then decreased. Adding Sio<sub>2</sub> to mix containing Sasobit increased the stability up to 16% more than the control sample at 1% Sio<sub>2</sub>.

In Fig. 7, the flow of optimum mixes containing zeolite with Sio<sub>2</sub> increased to 47% more than the control sample with an increase in Sio<sub>2</sub> up to 1.75% then insignificantly decreased. Adding Sio<sub>2</sub> to mixes containing Sasobit increased the flow to a maximum limit at 1% of Sio<sub>2</sub> then decreased.

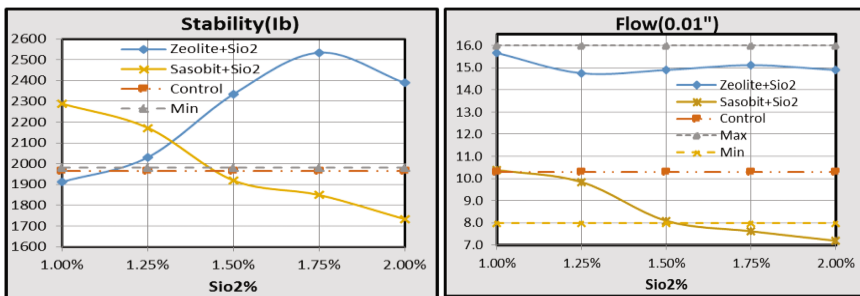


Fig. 7. Stability and flow of Nano Silica with modified asphalt warm additives.

Figure 8 shows the stability and flow comparison for RAP mixes contain additives.

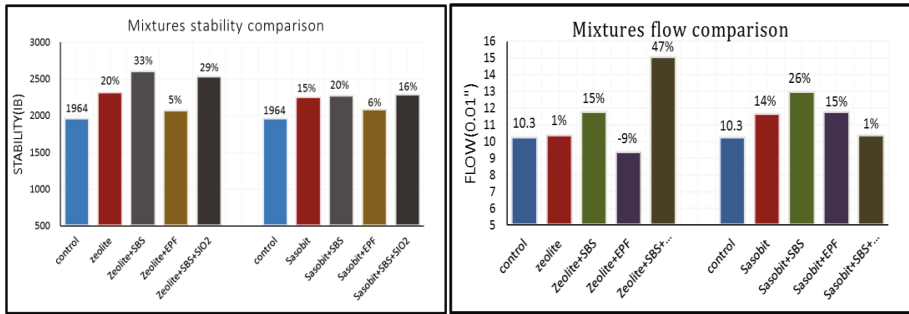


Fig. 8. Stability and flow of RAP mixtures comparison.

**4.2.5 Result of Indirect Tensile Strength (ITS) for RAP Mixes**

In Fig. 9, ITS of mixes containing zeolite and SBS polymer increased to 37% more than the control mixture. While, ITS for mixes containing Sasobit and SBS revealed an increase of 31% more than the control mixture.

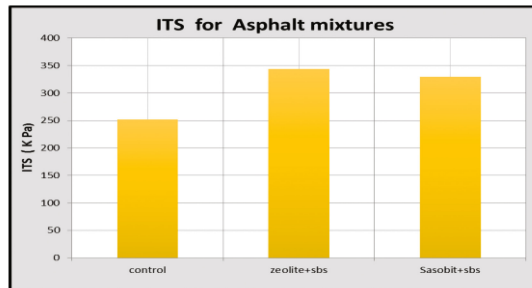


Fig. 9. ITS results.

**4.2.6 Result of Wheel Track Test (WTT) for RAP Mixes**

Figure 10, shows the component of wheel tracking equipment including its tray and the roller compactor. The equipment able to simulate the traffic loads effect on slab asphalt specimen.

Figure 11, describes the relationship between rutting depth and the number of cycles load, WTT was carried out for three specimens, control specimen (mix1) and the best two combinations that revealed the best stability and flow. The first combination containing 0.75% zeolite and 3% SBS (mix2), while the second combination containing 2% Sasobit and 4% SBS (mix3). In Fig. 11, it was observed that, generally rutting depth increased with an increase in cycle load number, the maximum rutting



Fig. 10. Wheel track process.

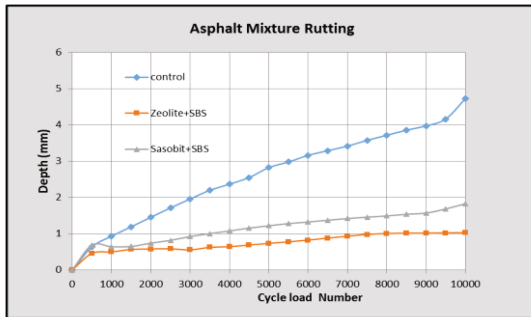


Fig. 11. Asphalt mixtures rutting results.

depth for mix1 was 4.7 mm, while significant decrease in rutting depth was found to be 1 and 1.8 mm for mix 2 and mix 3 respectively.

**4.2.7 Result of Compressive Strength for RAP Mixes**

Compressive strength test was used to estimate and evaluate the compressive stress with the strain which leads to the calculation of Modulus of elasticity (M E) to investigate the resistance to failure load.

Figure 12 shows a reduction in modulus of elasticity (M E) with 11% less than control mixture for mixture included modified Zeolite, while in case of modified Sasobit there was a significant reduction in (M E) with 25% less than control mixture. The low compressive strength tends to show low bond behavior of mixture which leads to low rutting resistance and increase moisture cracks in the asphalt paving with age.

**4.2.8 Economic Study**

This phase of work was carried out to investigate the benefits of using waste materials to produce WMA in the presence of modified asphalt in cost of highway construction industry.

Table 2 compares the benefit of reduction in temperature with range of 20 to 30 °C with adding 100% RAP of HMA with virgin aggregate and RAP mixes, while Table 3 compares between the cost of producing WMA in case of adding Zeolite and Sasobit

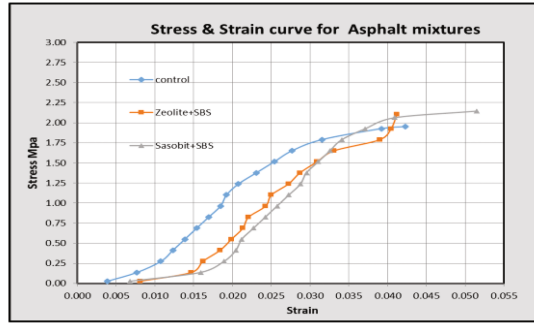


Fig. 12. Compression test results.

Table 2. HMA cost with virgin and RAP aggregate mixture at temperature 150 °C.

Component	Amount	Price/ton	Total cost (L.E/ton)	Component	Amount	Price/ton	Total cost (L.E/ton)
virgin aggregate	1 ton	535	535	RAP	1 ton	200	200
Asphalt binder as 5.5% by mixture weight	0.055	3000	165	Asphalt binder as 1.25% by mixture weight	0.0125	3000	37.5
Fuel consumed at temperature 150 °C	15	1.8	27	Fuel consumed temperature 150 °C	15	1.8	27
Total cost / ton	727			Total Cost/ton	≈265		

Table 3. WMA cost of modified asphalt binder with Zeolite and Sasobit additives mix with RAP mixture at temperature 130 °C.

Component	Amount	Price/ton	Total cost (L.E/Ton)	Component	Amount	Price/ton	Total cost (L.E/Ton)
RAP	1 ton	200	200	RAP	1 ton	200	200
Asphalt binder as 1.25% by mixture weight	0.0125	3000	37.5	Asphalt binder as 1.25% by mixture weight	0.0125	3000	37.5
Fuel consumed at temperature 130 °C	11.7	IE	21	Fuel consumed at temperature 130 °C	11.7	1.8	21
Zeolite additive at 0.75% of binder weight	0.09 kg	100/kg	9	Sasobit additive at 2% of binder weight	0.25 kg	20	5
SBS polymer at 3% of binder weight	0.375 kg	20/kg	7.5	SBS polymer at 4% of binder weight	0.50 kg	20	10
Total cost	≈275			Total cost	≈274		

**Table 4.** Cost comparison of HMA and WMA using additives.

Component	Total cost (L. E/ton)
HMA with virgin aggregate mixture at temperature 150 °C	727
HMA with RAP aggregate mixture (Control mixture) at temperature 150 °C	265
Modified asphalt binder (SBS) with Zeolite additive	275
Modified asphalt binder (SBS) with Sasobit additive	274

respectively. In Table 4 cost comparison was carried out between HMA and WMA with SBS polymer as modified binder in mixes to compare between HMA and WMA techniques.

It was observed that, saving in cost in control mixture asphalt was 64% of construction cost price, while, in case of using SBS modified asphalt binder with additives to produce WMA saving was 62% of construction cost price.

**4.2.9 Environmental Study**

The main purpose of this paper was reusing of waste materials to reduce using of virgin aggregates to save the main asphalt components in asphalt mixtures which has a significant effect in reducing landfill wastes to consume the environmental resources. Also, a reduction in mixing temperature between 20 to 30 °C controls the emission of gasses causing from heating the asphalt mix component to conventional temperature.

Emission tests have been carried out using drager equipment that was borrowed from National Center for Occupational Safety and Health and secure work environment. Results of emission test for RAP mixes using emission tubes as shown in Fig. 13, was illustrated in Table 5.

Test results revealed that using Zeolite in asphalt mix eliminates emission gases more than using Sasobit with SBS polymer



**Fig. 13.** Drager equipment and emissions tubes.

**Table 5.** Emissions test results for RAP mixtures.

Emission gases (ppm)	0.75% Zeolite with 3% KBS		Reduction%	2% Sasobit with 4% SBS		Reduction% 3 > PC
	130 °C	165 °C		130 °C	165 °C	
Carbon monoxide (CO)	20	32	37.5	25	32	22
Nitrogen dioxide (NO <sub>x</sub> )	<0.50	2	75	<0.50	2	75
Sulphur dioxide (SO <sub>i</sub> )	<1	<1	–	<1	<1	–
Volatile organic compounds (VOCs)	<50	75	33.3	<50	75	33.3

## 5 Conclusions

The following conclusions can be extracted:

1. Using RAP in asphalt mixtures at temperature of 150 °C as control mix wasn't reach the limitations of the Egyptian code specifications(ECP).
2. Adding additives to produce WMA, such as Zeolite and Sasobit to RAP mixture enhanced the performance of mixture more than control mix at temperature of 130 °C
3. Using SBS with percentage of 3% by weight of asphalt binder increased stability with 33% at 0.75% of Zeolite more than control mixture and using 4% of SBS increased stability with 20% when adding 2% of Sasobit more than control mixture.
4. Using EPF modified asphalt polymer to produce WMA has insignificant effect in control mixture performance.
5. Rutting resistance was improved in case of using Zeolite with SBS polymer more than in case of using modified Sasobit with SBS polymer under WTT.
6. There was insignificant effect of using Nano Silica with both Zeolite and Sasobit with SBS polymer mixture.
7. Using Zeolite and Sasobit with modified SBS polymer produced a reduction in cost of HMA of 62%.

### Recommendations for future studies

1. RAP with WMA technology, should be encouraged for road construction projects in Egypt.
2. Field study for RAP mixes with additives needs to be carried out.

## References

- Barthel, W.; Marchand, J.P., Von Devivere, M.: Warm asphalt mixes by adding a synthetic zeolite. Eurovia (2005). [www.asphamin.com](http://www.asphamin.com). Accessed 2 2016
- Celauro, C., Bernardo, C., Gabriele, B.: Production of innovative, recycled and high performance asphalt for road pavements. *Conserv. Recycl.* **54**, 337–347 (2010). doi:[10.1016/j.resconrec.2009.08.009](https://doi.org/10.1016/j.resconrec.2009.08.009)

- Mengqi, W., Haifang, W., Muhunthan, B., Kalehiwot, N.: Influence of RAP content on the air void distribution, permeability and moduli of the base layer in recycled asphalt pavements. In: Proceedings of the 91st Transportation Research Board Meeting (2012)
- Miller, T., Bahia, H.: Sustainable Asphalt Pavements: Technologies, Knowledge Gaps and Opportunities. Modified Asphalt. Research Center, University of Wisconsin, Madison (2009)
- Mostafa, E.A.: Development of environmentally sustainable warm mix asphalt using sasobit and nanomaterials. *IJEI* **6**(2), 44–58 (2016)
- Shirodkar, P., Mehta, Y., Nolan, A., Sonpal, K., Norton, A., et al.: A study to determine the degree of partial blending of reclaimed asphalt pavement (RAP) binder for high RAP hot mix asphalt. *Construct. Build. Mater.* **25**, 150–155 (2011). doi:[10.1016/j.conbuildmat.2010.06.045](https://doi.org/10.1016/j.conbuildmat.2010.06.045)
- Tarefder, R.A., Zaman, A.M.: Nanoscale evaluation of moisture damage in polymer modified asphalts. *J. Mater. Civil Eng.* **22**(7), 714–725 (2010)
- Teizer, J., Venugopal, M., Teizer, W., Felkl, J.: “Nanotechnology and its impact on construction” bridging the gap between researchers and industry professionals. *J. Constr. Eng. Manage.* **138** (5), 594–604 (2012)
- Yao, H., You, Z., Li, L., Lee, C.H., Wingard, D., Yap, Y.K., Shi, X., Goh, S.W.: Rheological properties and chemical bonding of asphalt modified with nanosilica. *J. Mater. Civil Eng.* **25** (11), 1619–1630 (2012)

# Developing New Design Criteria of Asphalt Pavement Mix Using Nano-Materials and Polymer-Materials

Abdelzaher E.A. Mostafa<sup>1</sup>(✉), Waleed M.F. Tawhed<sup>1</sup>,  
Mohamed R. Elshahat<sup>2</sup>, and Alaa G. Sherif<sup>1</sup>

<sup>1</sup> Civil Engineering Department, Faculty of Engineering-Mataria,  
Helwan University, Cairo, Egypt  
zaher292@yahoo.com, waleed.tawhed@m-eng.helwan.edu.eg,  
Alaa\_Sherif@m-eng.helwan.edu.eg

<sup>2</sup> Construction Engineering Department, School of Engineering,  
Egyptian Russian University, Cairo, Egypt  
vitch\_2004@yahoo.com

**Abstract.** In the context of the wide demand of high quality of bitumen, this research was initiated with the objective of enhancing the asphalt mix properties. Variable additives percentages of nano-materials and polymer materials were, experimentally, investigated to determine their effect on asphalt properties. Three nano materials (namely; nano-silica, nano-kaolinite and nano-montmorillonite) and three polymer materials (namely; styrene butadiene styrene (SBS), polypropylene, and polyethylene) were considered. Modified specimens (with 1, 3, 5, 7, and 9% of nano and polymer materials) were prepared. Rheological properties tests were conducted (namely; penetration, softening, flash point and viscosity). In addition, mechanical properties tests were carried out (namely; Marshall, compression, and indirect tensile tests). Results were obtained and analyzed. They indicated that both types of additives enhanced rheological and mechanical properties of asphalt mix.

**Keywords:** Hot asphalt mix · Nano-Materials · Polymer-Materials

## 1 Introduction

Asphalt is a binder material that should resist environmental conditions, rutting, heavy stresses and low temperatures. Accordingly, it should be enhanced (Asphalt Institute; Eurobitume 2011). Road development, new cities construction, expanding highway network led to a rapid increase in bitumen demand. Becker et al. (2001), reported that bitumen consumption reached 102 million tons per year, 85% of which are utilized in pavements.

Bitumen production is a complex process that depends on the raw materials quality (crude oil properties, and refinery process). Accordingly, more attention is directed

---

The original version of the book was revised: For detailed information please see Erratum.  
The erratum to the book is available at [https://doi.org/10.1007/978-3-319-61633-9\\_25](https://doi.org/10.1007/978-3-319-61633-9_25)



towards enhancing bitumen properties to improve its performance (e.g. adhesion, sensitivity to temperature, oxidation resistance, friction properties, durability and aging resistance) (Shen et al. 2011). There are many asphalt modifiers (i.e. resins, sulfur, metal complexes, rubbers, polymers, fibers and chemical agents) (Abdel-Lateef et al. 2009).

In the context of the wide demand of high quality of bitumen, this research was initiated with the objective of enhancing the asphalt mix properties. Accordingly, an experimental research program was designed to determine the optimum percentages of nano-materials and polymer additives to optimize and enhance bitumen quality. Further, the optimum dosages were used to propose a new design criteria for the asphalt pavement mix.

## 1.1 Objectives

The objectives set forth for this research effort are:

1. to compare the performance of the nano-modified asphalt mixtures with those which are polymer-modified.
2. to investigate the enhancement of modified HMA with both nano-materials and polymer-materials.
3. to perform a feasibility study to determine the impact of increasing the traditional HMA cost by adding those relatively new material additives.

## 2 Background

Many researchers were involved in investigating the enhancement of bitumen using numerous materials. For example, Abdel-Lateef et al. (2009), investigated the effect of different percentages of polyethylene terephthalate (PET) to hot mix asphalt (HMA) on the mix properties. Marshall, indirect tensile strength, rutting and bending tests were carried out to assess the properties enhancement. Their results indicated that using PET enhanced the stability, indirect tensile strength, stiffness, and rutting. Their documented that there was a decrease in flow, failure strain, and rutting depth. In addition, the results indicated that 13% PET provided an optimum ratio.

Qing et al. (2009), reported that softening and ductility enhanced the bitumen by adding 10% weight of mechano-chemically devulcanized tire rubber (m-GTR) and SBS. This percentage decreased road deformation and increased the viscous modulus ( $G''$ ) and elastic modulus ( $G'$ ).

Romeo et al. (2010), examined the impact of SBS modifiers on the hot asphalt mix properties. SUPERPAVE IDT (Indirect Tensile) and the SCB (Semi Circular Bending) tests were carried out to evaluate the change in the product characteristics. The results indicated that polymer modifications do not induce significant effects on the resilient modulus at intermediate temperatures. On the other hand, the tensile creep test provided a decrease in the rate of creep, which implied the occurrence of reduced accumulations of micro-damage.

Ghasemi et al. (2012), investigated the impact of nano-SiO<sub>2</sub> and SBS on asphalt mixtures. Five asphalt binders, with polymer modified bitumen by 5% SBS were investigated using different nano-SiO<sub>2</sub> percentages (namely 0, 0.5, 1, 1.5, and 2%). The mixtures (bitumen with SBS and SiO<sub>2</sub>) were prepared in a high shear mixer.

They investigated the rheological properties (e.g. modified bitumen softening point, penetration and ductility). In addition, Marshall test was applied to all specimens. The results indicated that the asphalt mixture with 5% SBS and 2% nano-SiO<sub>2</sub> powder provided the best results among all the tested specimens. Accordingly, this modification was perceived to enhance the physical and mechanical properties of asphalt binder as well as the mixtures.

Walters (2014), investigated the bio-char and nano-clay effect on asphalt rheological properties, where two nano-materials (nano-clay and bio-char) were examined. Rotational Viscometer (RV) tests were carried out, at 120, 135 and 150°C, to evaluate the enhancement in their properties. The results indicated that using nano-particles and bio-modified materials enhanced the high temperature performance and aging resistance. X-Ray Diffraction (XRD) ascertained that the reason was the alteration of the layer spacing in nano-clay.

### 3 Methodology

The scope of this study based on the stat of art combined to investigate the performance of modified asphalt mix with both nano-materials and polymer-materials as shown in Fig. 1. as the following:

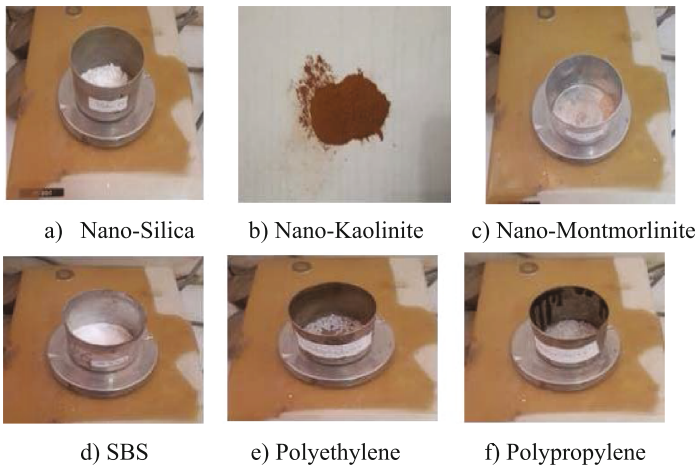


**Fig. 1.** Nano-Materials and Polymer-Materials

#### 1. Modified Asphalt Binder Tests

Asphalt tests were made to compare the effect of both nano-materials and polymer-materials on the rheological properties of modified asphalt binder. Nano-materials were nano-silica, kaolinite nano-clay, and montmorillonite nano-clay while polymer materials were SBS, polypropylene, and Polyethylene. Modified asphalt binders were prepared by adding five different percentages of both nano-materials and polymers (1, 3, 5, 7, 9% by weight).

### 1.1. Penetration Test Results

Penetration test results as show in Fig. 2. show that, for all types of nano- modified asphalt binder or polymer-modified asphalt binder increase both nano-materials or polymer materials decrease the penetration degree. Also, increase in nano-materials or polymer-materials change the grade of bitumen. 9% nano-materials or polymer-materials change the grade from 60–70 to 50–60 except 9% SBS which change the grade to 40–50. The best modified material was SBS.

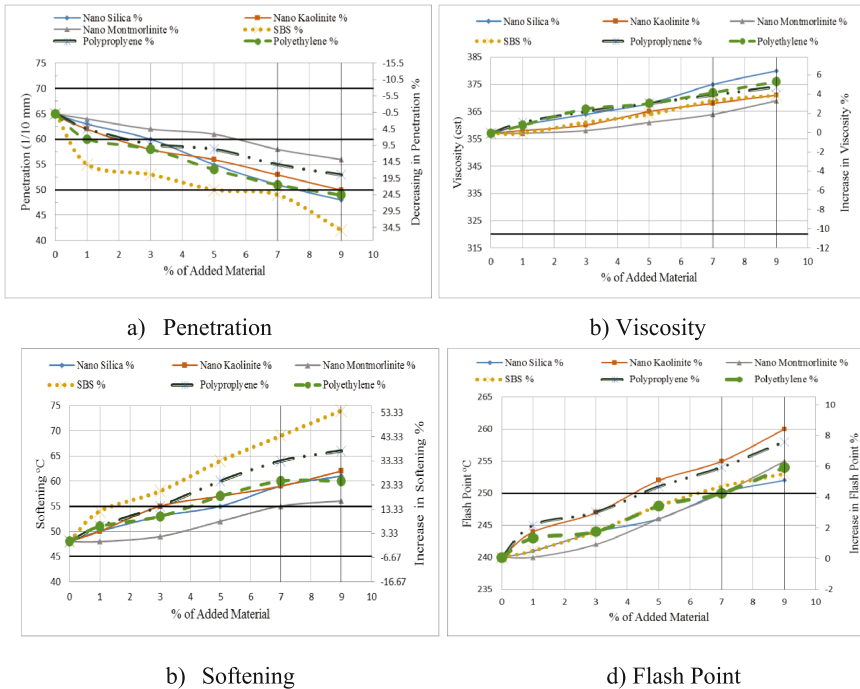


**Fig. 2.** Asphalt binder tests with modified materials

### 1.2. Kinematic Viscosity Test Results.

As shown in Fig. 2. increase in nano-materials or polymer-materials percentages leads to increase in kinematic viscosity. The best modified material was nano-silica.

### 1.3. Softening Point Test Results

Also, as shown in Fig. 2. Increase in additives leads to increase in softening point, the best modified materials was SBS.

### 1.4. Flash Point Test Results

As shown in Fig. 2. for all the modified materials, flash point increase by increasing the percentages of modified materials. The best modified material was nano-kaolinite.

At final Fig. 2. show that there are interference between lines represents polymer-modified materials and lines represents nano-modified materials which mean that polymer-materials are not better than nano-materials or verse. It is depend on the material type not on the material group.

2. Marshall Test (ASTM D5581)

2.1. Marshall mix design for Conventional Asphalt Mix

Marshall mix design were conducted to determine the optimum bitumen content, five different asphalt mixes were prepared and tested with bitumen percentages of (4.5, 5, 5.5, 6, and 6.5%). Relations between the bitumen content and each of stability, flow, air voids, voids in mineral aggregate (VMA), unit weight were obtained as shown in Fig. 3.

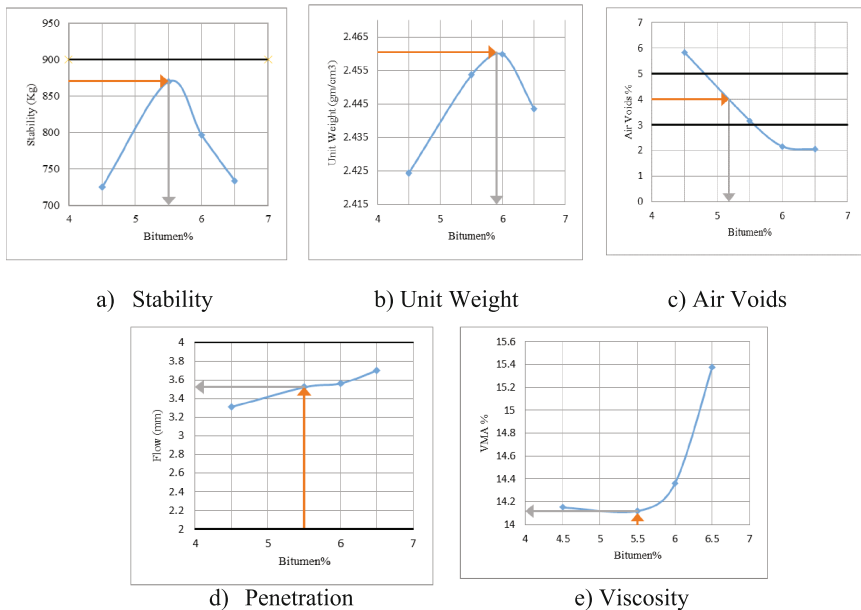


Fig. 3. Mix design of RAP mixtures

2.2. Marshall Test for Modified Asphalt Mix

To study the mechanical properties, asphalt mix specimens were prepared from the previous modified asphalt binder. From the results, optimum percent of nano-silica is 7%, while optimum percent of both kaolinite nano-clay and montmorilinite nano-clay is 9%. Percent of 11% was added to check the optimum point in case of nano-clay. There was no optimum point for polymer-materials therefore 9% will be as the optimum point.

As in Fig. 4, at optimum percentages, the stability increased by 60.78%, 50.5%, 37.5%, 31.75%, 17.6%, and 17% for polypropylene, polyethylene, nano-kaolinite, nano-silica, nano- montmorlinite and SBS, respectively. While the flow decreased by 21.75%, 21%, 19.22%, 13.65%, 13%, and 13.4% for polypropylene, nano-kaolinite, polyethylene, nano-montmorlinite, nano-silica and SBS, respectively.

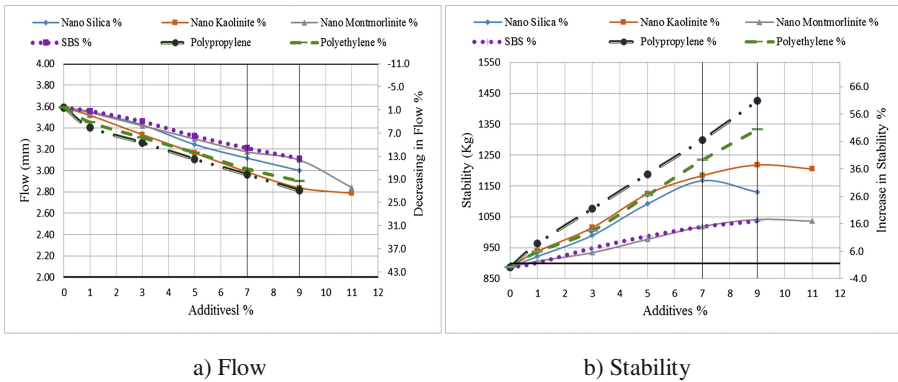


Fig. 4. Stability and flow of modified asphalt mix

As in Fig. 5, air voids decreased by 17.13%, 16.85%, 15.5%, 13%, 6.5%, and 3.65% for nano-kaolinite, SBS, nano- montmorlinite, nano silica, polyethylene and polypropylene, respectively while, VMA decreased by 3.7%, 3.66%, 3.4%, 3.3%, 1.38%, and 0.76% for nano-kaolinite, SBS, nano-silica, nano- montmorlinite, polyethylene and polypropylene, respectively.

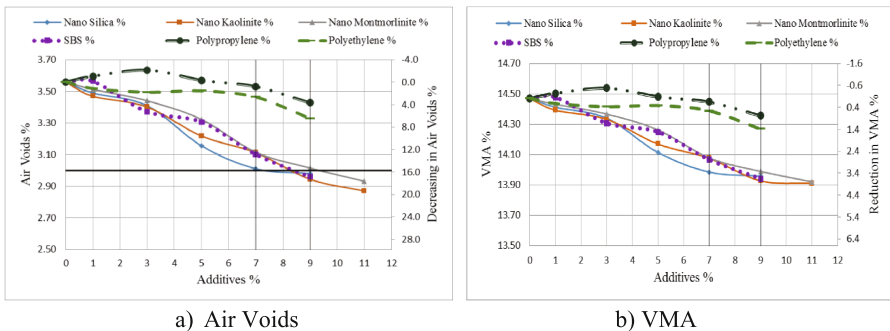


Fig. 5. Air Voids and VMA of modified asphalt mix

As in Fig. 6, unit weight increased by 0.61%, 0.61%, 0.57%, 0.53%, 0.2%, and 0.12% for SBS, nano-kaolinite, nano-silica, nano- montmorlinite, polyethylene and polypropylene, respectively while rigidity increased by 105%, 86%, 73.8%, 51.6%, 36.2%, and 35% for polypropylene, polyethylene, nano-kaolinite, nano-silica, nano- montmorlinite and SBS, respectively.



polyethylene, respectively but it decreased by 5.9% in case of SBS, and is not significant for nano-montmorlinite.

Indirect tensile strength increased by 200.8%, 174%, 93.5%, 60.16%, 50%, and 40.65% for polypropylene, polyethylene, nano-kaolinite, SBS, nano-silica and nano-montmorlinite, respectively.

Modulus of resilience increased by 93%, 32.5%, 32.5% for nano-silica, nano-kaolinite and nano-montmorlinite, respectively, while it decreased by 23%, 32.5%, and 32.5% for SBS, Polypropylene and polyethylene, respectively.

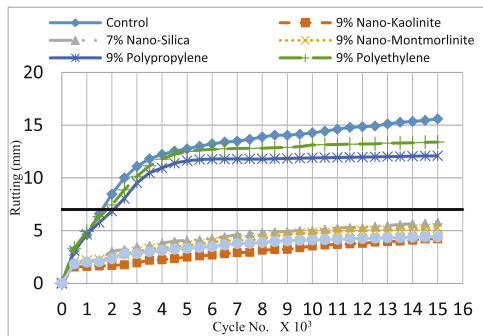
Modulus of toughness increased by 0%, 47.6%, and 19% for nano-silica, nano-kaolinite and nano-montmorlinite, SBS, respectively. Polyethylene decreased modulus of toughness by 19% while polypropylene increased it by the same percent.

4. Result of Wheel Track Test (WTT)

Figure 8 present the wheel track test for nano-materials modifying asphalt mix under wheel weighting 70 kg in temperature 60°c, Also it present the rutting test results. They indicated the behavior of modified asphalt mix compared to the conventional asphalt mix, as follows:



a) Wheel Track Test



b) Rutting Results for Modified Asphalt Mix

Fig. 8. wheel track test

For conventional asphalt mix, the maximum rutting was 15.589 mm, which occurred mostly in the first 4000 cycle. For the first 4000 cycle, rutting is 12 mm, which mean that about 75% of rutting happened in the first 4000 cycle and 25% of rutting happened in subsequent cycles. For all types of nano-materials, the rate of rutting increased during all cycles. Maximum rutting was 4.228 mm, 5.247 mm, and 5.808 mm for nano-kaolinite, nano-montmorlinite and nano-silica, respectively. Nano-materials decreased the rutting depth by 72.9%, 66.34%, and 62.75% for nano-kaolinite, nano-montmorlinite and nano-silica, respectively. According to BS 598-110 the maximum allowable rutting is 7 mm. Conventional asphalt mix reached this limit at 1500 cycle while nano-materials reached it at 1500 cycle.

Polypropylene and polyethylene nearly have the same behavior of conventional asphalt mix. Maximum rutting are 12.092 mm and 13.4 mm for polypropylene and polyethylene, respectively. For the first 4000 cycle rutting was 10.945 mm and 11.769 mm for polypropylene and polyethylene, respectively, which means that about 90% of rutting occurred within the first 4000 cycle after that they become stable, compared to the conventional asphalt mix. For SBS, the maximum rutting depth is 4.416 mm and the rate of increase in rutting for polypropylene and polyethylene occurred after 5000 cycles. Polymer-materials decrease the rutting depth by 71.7%, 22.4%, and 14% for SBS, polypropylene and polyethylene, respectively. Polyethylene and polypropylene reached to the maximum rutting depth after 2000 cycles. They increased the rutting life with 33%.

5. Fatigue Life

Table 1 is presented to encompass the number of cycle that provided the maximum rutting depth for nano-materials and the equations of the trend lines, for all types.

**Table 1.** Equations of trend lines for nano-materials rutting

Nano-Material Type	Equation	R	Cycle No.
Silica	$y = -2E-23x^6 + 8E-19x^5 - 2E-14x^4 + 2E-10x^3 - 8E - 07x^2 + 0.0025x + 0.2511$	0.9904	21000
Kaolinite	$y = -2E-23x^6 + 9E - 19x^5 - 2E-14x^4 + 2E-10x^3 - 7E - 07x^2 + 0.0017x + 0.3319$	0.9804	33000
Montmorlinitite	$-2E-23x^6 + 8E-19x^5 - 2E-14x^4 + 2E-10x^3 - 9E-07x^2 + 0.0023x + 0.3947$	0.9806	28000

According to Eq. (1) the number of load repetition is calculated and tabulated in Table 2. From the results, the maximum increase of load repetition is attained for nano-kaolinite with 6.24%.

**Table 2.** Number of Load Repetition (NLR) for Modified Asphalt Mix

Material	E (kg/cm <sup>2</sup> )	Strain $\epsilon_t$	NLR	NLR Increase %
Conventional	950	$7 \times 10^{-4}$	5497605	–
7% Nano-Silica	1050	$6.8 \times 10^{-4}$	5552450	1
9% Nano-Kaolinite	1250	$6.4 \times 10^{-4}$	5840737	6.24
9% Nano-Montmorlinitite	1150	$6.6 \times 10^{-4}$	5667768	3.1
9% SBS	820	$7.2 \times 10^{-4}$	5681838	3.35
9% Polypropylene	1150	$6.6 \times 10^{-4}$	5667768	3.1
9% Polyethylene	1175	$6.6 \times 10^{-4}$	5564622	1.22



$$N_f = f_1 \varepsilon_t - f_2 EI - f_3 \tag{1}$$

Where;  $f_1 = 0.0795$ ;  $f_2 = 3.291$ ;  $f_3 = 0.854$ ,

According to Eq. (1) the number of load repetitions are calculated and tabulated in Table 2. From results the maximum increase in number of load repetitions is for nano-kaolinite with 6.24%.

$$N_f = f_1 \varepsilon_t^{-f_2} EI^{-f_3} \tag{2}$$

Where;  $f_1 = 0.0795$ ;  $f_2 = 3.291$ ;  $f_3 = 0.854$

### 6. Economic study

The objective of this study is to compare the cost of using nano-or polymer-materials as additives in contrast to modifying the asphalt mix proportions. Figure 9 presents the variance in construction costs for the different materials. These are the actual material cost used in this study:

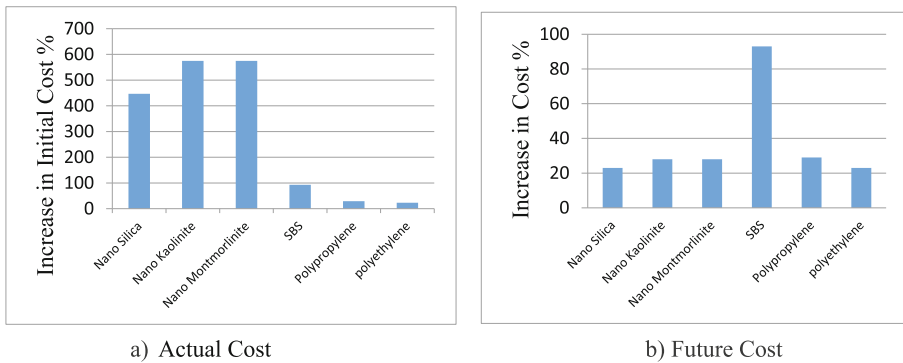


**Fig. 9.** Increase in cost for modified asphalt mix

Material	Cost (LE/kg)
Bitumen	3
Aggregates	90
Nano-materials	250
Polypropylene	25
Polyethylene	20
SBS	80

From Fig. 9 and for comparison purposes, the cost of a conventional mix is considered as baseline and the following is provided: For nano-modified asphalt mix, nano-silica, kaolinite nano-clay and montmorillonite nano-clay the increase in the cost

was 447%, 575%, and 575%, while for polymer modified asphalt mix, SBS, polypropylene, and polyethylene increase the cost by 93, 29, and 23%, respectively. It is expected in the future that the price of nano-materials to be similar to cement or slightly higher than it. The raw materials of manufacturing nano-materials are not expensive. After constructing many factories for producing nano-materials, the traditional price will be normal price. Figure 9 presents the increase in cost for asphalt pavement if the cost of nano-materials is more than 10 times of cement cost. For the sake of the argument, cement cost will be assumed to be 0.6 LE/kg and nano-material will be 10 LE/kg. The increase in cost for nano-materials will not exceed 28%. It gives increase in fatigue life about 6% and in addition the very high resistance for rutting therefore it will decrease the final cost of nano-materials modified asphalt mix.

7. New Design Criteria Based on The Outcomes of The Results

For roads acquire high resistance to rutting with 30% increasing in stability, nano-kaolinite and nano-silica are suitable in addition. Nano-kaolinite will extend the fatigue life time by 6% while nano-silica will not.

Nano-montmorlinitite and SBS are suitable for roads that acquire high resistance to rutting with increasing in stability by 15% and an extend in fatigue life time by 3%.

For roads that acquire high stability and high strength, regardless rutting, polypropylene and polyethylene are suitable. They increased the stability and compressive strength by 55% and 30%. In addition, slight improvement in rutting occurred. Furthermore, polypropylene extended the fatigue life more than polyethylene.

The new design criteria are presented in Table 3, where the best material in enhancing the performance of asphalt mix is nano-kaolinite with optimum percentage 9%. Although, it is not economic, it is expected to be within the norm in the future.

**Table 3.** New Design Criteria for Modified Asphalt Mix

Material	Optimum percent %	Fatigue and compression		Crack	Best material
		NLR %	Rutting Life Time %	ITS (kg/cm <sup>2</sup> )	
Polypropylene	9	3.1	6	200	Nano-Kaolinite
SBS	9	3.35	1900	60	
Nano-Kaolinite	9	6.24	1841	93	
Mix	9 (P.P) + 5 (N-K)	4.46	1847	273	

Accordingly, this research suggested that asphalt pavement design should include rutting depth and use SBS so as nano-materials, as additives. This would extend its life time by 5% and its cost would be reduced by 25% in the future.

## 4 Conclusions

Based on the results obtained from this research, the following conclusions are provided:

1. Both nano- and polymer-materials improve the mechanical properties of the asphalt mix namely (stability, unit weight, modulus of elasticity (E), compressive strength, and indirect tensile strength) while it reduces flow, air voids, and voids in mineral aggregates.
2. Polymer-materials do not necessarily perform better than nano-materials or vice-versa.
3. SBS has the highest effect on each of penetration, and softening by 54.17%, and 35.38%, respectively while nano-kaolinite has the highest effect on flash point by 8.33% and viscosity by 6.44%.
4. Polypropylene has the highest effect on stability and flow by 60.78% and 21.75%, respectively, while nano-silica has the highest effect on air voids, VMA and unit weight by 13%, 3.4%, and 0.61%, respectively.
5. Nano-kaolinite has the highest effect on compressive strength and modulus of elasticity by 41.14%, and 41.8%, respectively, while polypropylene has the highest effect on indirect tensile strength by 200.8%
6. Using nano-kaolinite, as an additive for polymer modified asphalt, improves all properties but it should not exceed 5%, which causes a decrease in the air voids and flow greater than the acceptable code specifications.
7. Using nano-materials increase modulus of resilience and toughness in contrast to polymer-materials.
8. Both nano-materials and SBS reduce rutting depth by more than 60% while, polymer-materials only reduce it by up to 20%.
9. Service life is extended by 6.24%, 3.1%, 3.35%, 3.1%, 1.22%, and 4.46% for nano-kaolinite, nano- montmorlinite, SBS, polypropylene, polyethylene and mixture of polypropylene with nano-kaolinite, respectively.
10. Initial cost increased by 447% for nano-silica and 575% for nano-kaolinite and nano-montmorlinite, while SBS, polypropylene, and polyethylene increased the initial cost by 93%, 29%, and 23%, respectively.
11. For roads that require high resistance to rutting with 30% increasing in stability, nano-kaolinite and nano-silica is suitable in addition nano-kaolinite will extended the service life by 6% while nano-silica would not.
12. Nano-montmorlinite and SBS are suitable for roads that acquire high resistance to rutting with increasing in stability by 15% and increased the service life by 3%.
13. For roads that require high stability and high strength regardless of rutting, polypropylene and polyethylene are suitable. Using them improve the stability and compressive strength by 55% and 30% with a slight improvement in rutting.

## 5 Recommendations

1. Study the effect of nano-materials and polymer-materials on asphalt mix design.
2. Examine the nano-materials modified bitumen and polymer-modified bitumen behavior under dynamic loads.
3. Use nano-kaolinite and nano-silica as they are suitable for roads that require high resistance to rutting.

## References

- Abdel-Lateef, T.H., El-Hamrawy, S.A., Mahmoud, A.A.H., Naglaa, M.K.: The use of additives in improved pavement mix design. PhD. Thesis in Civil Engineering (2009)
- Asphalt Institute; Eurobitume: The Bitumen Industry - A Global Perspective, 2nd edn. Asphalt Institute, Lexington, Kentucky; Eurobitume, Brussels, Belgium (2011)
- Becker, Y., Méndez, M.P., Rodriguez, Y.: Polymer modified asphalt. *Vision Technol.* **9**(1), 39–50 (2001)
- BS, 598-110: Sampling and examination of bituminous mixtures for roads and other paved areas. Methods of test for the determination of wheel-tracking rate and depth (1998)
- Ghasemia, M., Marandia, S.M.B., Tahmoosib, M., Kamalia, R.J., Taherzadec, R.: Modification of stone matrix Asphalt with Nano-Sio<sub>2</sub>. *J. Basic. Appl. Sci. Res.* **2**(2), 1338–1344 (2012). ISSN 2090-4304, A civil Engineering Department, Shahid Bahonar University, Kerman, Iran, international Center For Science
- Mostafa, A.E.: Examining the performance of hot mix asphalt using nano- materials. *Int. Organ. Sci. Res. (IOSRJEN)* **06**(02), 25–34 (2016)
- Lewandowski, L.H.: Polymer modification of paving asphalt binders. *Rubber Chem. Technol.* **67**(3), 447 (1994)
- Qing, X.Z., Hui, C.L., Mei, L.: Rheological property of bitumen modified by the mixture of the mechanochemically devulcanized tire rubber powder and SBS. *J. Materials Civil Engg. ASCE* **21**(11), 699–705 (2009)
- Romeo, E., Birgisson, B., Montepara, A.: The effect of polymer modification on hot mix asphalt fracture at tensile loading conditions. *Int. J. Pavement Eng.* **11**(5), 403–413 (2010). Taylor & Francis
- Shen, J.A.: Pavement Performance of Asphalt and Asphalt Concrete. China Communication Press, Beijing (2011)
- Walters, R.C., Fini, E.H., Abu-Lebdeh, T.: Enhancing asphalt rheological behavior and aging susceptibility using Bio-Char and Nano-Clay. *Am. J. Eng. Appl. Sci.* **7**(1), 66–76 (2014). doi:[10.3844/Ajeassp.2014.66.76](https://doi.org/10.3844/Ajeassp.2014.66.76). ISSN 1941-7020, Department of Civil, Architectural and Environmental Engineering, North Carolina A and T State University, Greensboro, Nc 27411, USA, ©2014 Science Publication

# The Application Analysis of Fly Ash in Magnesium Phosphate Cement

Rui Huang<sup>(✉)</sup> and Xiangxing Kong

The First Highway Survey and Design Institute  
of China Communications Construction Company Ltd., Xi'an, China  
{254438803, 103121153}@qq.com

**Abstract.** The addition of fly ash into magnesium phosphate-base material will reduce the original compressive strength, flexural strength and abrasion resistance of magnesium phosphate cement, the expansion character of it will increase as the amount of fly ash increase. With the increase of the dosage of fly ash, the compressive strength of pure magnesium phosphate cement will reduce after the first increases, and the flexural strength and abrasion resistance of magnesium phosphate cement will decrease with the increase of the dosage of fly ash. But the ultimate strength could meet the need of practical engineering if the dosage is appropriate. The addition of fly ash can help reduce the cost and improve the properties of phosphate cement-based repair material. Propriate dosage of fly ash into the cement could help improve its liquidity, adjust the setting time and improve the bonding degree of magnesium phosphate cement with portland cement concrete. So it could be better used in many areas such as patching material, oil well cement and waste disposal and so on.

## 1 Introduction

Magnesium phosphate cement is made up of burnt magnesia and phosphoric acid or acid phosphate and some cementitious materials in a certain proportion. The chemical reactions between magnesia and phosphoric acid is very quickly, usually within a few minutes of rapid condensation, half an hour creates a certain strength, which contributes to its high early strength. In order to facilitate the construction, some certain retarder will be needed, which is mainly the boric acid or sodium borate. Magnesium phosphate cement hydration reaction is essentially an acid - alkali reaction, which will release a lot of heat. Therefore, magnesium phosphate cement can rapidly congeal at a low temperature.

In addition, magnesium phosphate cement also has peculiarities of wonderful bonding performance while splicing old concrete, good abrasion resistance and freeze resistance as well as the dry shrink (Jiang 2004). Based on the above characteristics of magnesium phosphate cement, it has a good prospect in application to both civil buildings and military facilities. It can be used in the mending and repairing of airport runway, bridges, roads and other civil and military engineering (Wang 2005). In addition, it also can be used as a precision casting of coated materials, dental and bone cement binder and so on (Chen 2006; Wu 2006). Adding suitable amount of fly ash to the magnesium phosphate cement can improve the performance of it while making use

of a lot of fly ash which used to be a waste. Fly ash has the advantages of low price and rich source, and adding it into magnesium phosphate cement can reduce the cost of the cement and improve its performance. After mixed with fly ash, magnesium phosphate cement base material cost could be greatly reduced, which provides economic feasibility for the popularization and application of magnesium phosphate cement base material (Zhang 2009a).

## **2 Influence of Fly Ash on Magnesium Phosphate Cement Base Composite Material's Performance**

### **2.1 Mechanical Property**

Under the similar conditions, with the increasing dosage of fly ash, the strength of the repaired phosphate cement base material is basically showed a trend of decrease, but when the dosage of fly ash reached 25%, 1 d and 28 d compressive strength of the magnesium phosphate cement reached 41.0 MPa and 63.2 MPa, which is enough to meet the engineering requirements. Due to the role of shape effect, fine grinding fly ash in repair material can rise to adjust the grading and close-grained filling effect, thus increase the compactness of cement mortar, it can also reduce the water cement ratio, increase strength, its micro aggregate effect of fly ash also enhanced effect of phosphate cement-based repair material. At the same time, the addition of fly ash will "dilute" the paste, influence the crystal structure of the network formed between hydration product particles, the fly ash contains fairly coarse, porous and loose particles (such as carbon particles) will have adverse impact on the liquidity and strength. Results and Discussion.

### **2.2 Compressive Strength**

Under the same age, with the increase of dosage of fly ash, the strength of magnesium phosphate cement net pulp first increases and then decreases, and when the dosage of fly ash reaches 10%, the compressive strength is the largest. With the increase of age, the strength of the same dosage of fly ash net slurry of magnesium phosphate cement increases gradually. When mixed with 10% of fly ash, the cement reaches its highest compressive strength. That is because of the micro aggregate effect of fly ash, the particle could fill the wool stoma of the cement paste and refine the capillary porosity of the cement paste, which is beneficial to the increase of the compressive strength of the material. When the dosage of fly ash was increased further, a number of porous particles in fly ash can absorb part of the moisture so that the water needed for the reaction of the material will be reduced, inhibiting the development of magnesium ammonium phosphate crystal. Simultaneously, the fly ash and magnesium phosphate cement base material are not obviously chemically combined, making the adhesion strength of the fly ash with magnesium phosphate cement base material poor. This affected the continuity of magnesium ammonium phosphate crystal network, thus to reduce the compressive strength of magnesium phosphate cement base material.

### 2.3 Flexural Strength

With the increasing dosage of fly ash, the flexural strength of magnesium phosphate cement base material gradually decreases; with the increase of age, the flexural strength of the same amount of fly ash using material increases. Under the same age, the flexural strength of the material will decrease with the increase of dosage of fly ash, and the main reason for the increase is that the chemical bond between fly ash and magnesium phosphate cement matrix has not been formed so that the connection is very weak. And the increasing dosage of fly ash will seriously damage the crystallization the matrix network, therefore, under the action of shear force, its strength is on the decline.

### 2.4 Wear-Resisting Performance

As the magnesium phosphate cement base material is often used to repair roads, the wear resistance of materials is particularly important. The research based on that taking the wear resistance of pure magnesium phosphate cement mortar as a measurement of that of the material have found that the magnesium phosphate cement base material without fly ash had the least wear loss, and the more the dosage is, the greater the wear lose is and the worse the wear resistance is, and also, the speed of the wear resistance to be worse is gradually faster. This is related to that the connection between fly ash and magnesium phosphate cement matrix is weak, and the wear resistance of fly ash is not high in itself.

### 2.5 Expansion Properties

With the increase of fly ash content, inflation rate increased gradually. After 7th d, the inflation rate of magnesium phosphate cement base material which contained 30% of fly ash surpassed that with 40% of fly ash (Zhang 2009b). The expansion rate of magnesium phosphate cement base material increases along with the growth of the age. This is related to the exothermic reaction of magnesium phosphate cement base material, and the heat of the reaction is released mainly in its early stages during which the temperature rises rapidly. Therefore, the inflation rate of magnesium phosphate cement base material increased quickly before 7~14 d stage but increased slowly later. The reason that the base material containing 30% and 40% of fly ash has larger inflation rate is that with large dosage of fly ash, the number of porous particle in fly ash will increase, and after mixed with water, these particles can absorb a large number of moisture, which decreases the amount of the water involving in reaction and makes the concentration of  $Mg^{2+}$  in the solution increases. From the perspective of reaction dynamics, the increasing of the concentration of reactants will speed up chemical reaction so that large amount of heat is released in a short time, thereby making the material undergo large amount of expansion.

### **3 Influence of Fly Ash on Magnesium Phosphate Cement Base Composite Material's Performance**

The latest test showed that fly ash can significantly improve the interfacial bonding strength of magnesium phosphate cement and ordinary cement. In the repairing of the concrete, it is a key factor to successful repair (Su). When the fly ash content was 20%, the highest bonding strength can be obtained, and its 3th d bonding strength can achieve 50 MPa. When the fly ash content increased to 30%, the bonding strength will decrease.

The main reason for this phenomenon may be the reaction between the hydration products of ordinary cement mortar and MPC; Secondly, the active SiO<sub>2</sub> and Al<sub>2</sub>O<sub>3</sub> in fly ash react with Ca(OH)<sub>2</sub> in ordinary cement mortar to generate the C-S-H gel, which improves the bonding strength with both physical bond and chemical bond. Along with the continuous increasing use of fly ash, hydration rate slowed, the hydration products decreased and the strength decreased. Excellent adhesive performance between MPC mortar and ordinary cement mortar can make bonding strength reach 6.3 MPa after 1 day. The bonding strength reaches 10 MPa when the amount of fly ash is 10% and reaches 5.6 MPa even if the amount of fly ash is as high as 50% after 1 day. Researchers have analyzed and believed that three effects play a great role in enhancing the bonding strength. The micro aggregate effect makes fly ash effectively fill pores on the interface and get the old and new interface region more compact. That the micro fly ash particles filled within the MPC matrix uniformly and the porosity decreases significantly make the interface zone structure more compact and effectively improve the pore structure of the transition zone. Fly ash has ball effect in slurry which can decrease the internal frictional resistance of inter particles, reduce the porosity, improve the compactness and effectively increase the interfacial bonding strength.

### **4 Conclusions**

According to the research results above, it can be seen that although magnesium phosphate cement with the addition of fly ash would reduce the strength of the cement to some extent, but the final strength does not affect its normal usage in the general engineering. And it can also improve other properties. The appropriate addition of fly ash can prolong the setting time of magnesium phosphate cement itself, increase the liquidity, reduce the unit volume weight itself and improve the adhesion with ordinary cement products. These improvements can make better application of magnesium phosphate cement to the real work. We can choose the appropriate amount of fly ash according to the actual needs to make it better adaptable to the need of practical engineering so that the material can be fully utilized and its cost can be reduced at the same time.

As an early strength rapid hardening cement, magnesium phosphate cement can be widely applied to roads, bridges and other civil and military engineering repair. Magnesium phosphate cement can also be used as coating materials, dental cement and bone adhesive. As repairing materials, magnesium phosphate cement needs to have



good adhesiveness with raw materials in engineering and can improve its bonding strength with the ordinary cement products after adding fly ash into it to meet the project requirements. Because of the high cost, magnesium phosphate cement is not suitable for large-scale application to the general construction engineering.

A large amount of fly ash to mingle with the magnesium phosphate cement can not only improve its property, but also greatly reduce the material cost. This largely broadens out the way of application of magnesium phosphate cement based materials. Fly ash modified magnesium phosphate cement not only can be used as engineering repair materials, but also can be used as a treatment of oil well cement and toxic and radioactive waste Chen (2006). For the improvement of the material property, or for the economic and environmental protection point of view, the addition of fly ash in magnesium phosphate cement is a way worthy of developing.

## References

- Chen, Y., Tang, Y.: Magnesium phosphate coating lithium cobalt nickel manganese oxide synthesis and performance research. Chinese chemical society academic conference paper sets the 25th session(I) (2006)
- Jiang, H., Zhou, H., Yang, H.: Super fast repair hard phosphate cement hydration hardening mechanism research. *J. Wuhan Univ. Technol.* (4), 18–20 (2004)
- Keller, G.H.: Organic matter and the geotechnical properties of submarine sediments. *Geo-Marine Lett.* **2**(5), 191–198 (1982)
- Su, L., Huang, Y., Qian, J.: Fly ash modified magnesium phosphate cement and Portland cement matrix adhesion performance research. In: *The Third International Symposium on High Performance Concrete: Hong Kong, Macau, Taiwan*, pp. 78–85
- Wang, H., Qian, J., Cao, J., Tang, C.: The effect of fly ash on the properties of phosphate cement-based repair materials. *J. New Build. Mater.* (12), 41–43 (2005)
- Wu, Z., Zhang, J.: The experimental study of magnesium phosphate bone cement adhesive fracture. *Chinese J. Reconstr. Surg.* **20**(12), 912–915 (2006)
- Yan, L., Lei, N., Yan, X.: The mechanism of the physical and mechanical properties of peat soil organic matter analysis. *Chinese J. Geotech. Eng.* **33**(4), 655–660 (2011)
- Zhang, S., Shi, H., Huang, S.: The influence of the dosage of fly ash has on the mechanics performance of magnesium phosphate cement base composite material. *J. Nanchang Univ.* **31** (1), 80–82 (2009a)
- Zhang, S., Shi, H.: The application of fly ash modified magnesium phosphate cement base material. *J. Compr. Utilization Fly Ash* (1), 54–56 (2009b)

# Erratum to: Materials for Sustainable Infrastructure

Leslie Struble<sup>1</sup>(✉) and Gabriele Tebaldi<sup>2</sup>

<sup>1</sup> University of Illinois at Urbana-Champaign, Urbana-Champaign, IL, USA  
lstruble@illinois.edu

<sup>2</sup> Department of Civil and Environmental Engineering and Architecture,  
University of Parma, Parma, Italy

**Erratum to:**  
**L. Struble and G. Tebaldi (eds.),**  
***Materials for Sustainable Infrastructure,***  
**Sustainable Civil Infrastructures,**  
<https://doi.org/10.1007/978-3-319-61633-9>

In the original version of the book, the following corrections have to be incorporated:

In Chapter 7, author's email id and name have to be updated.

The two missed out chapters in the book have to be included now.

The erratum book has been updated with the changes.

---

The updated online version for these chapters can be found at:

[https://doi.org/10.1007/978-3-319-61633-9\\_7](https://doi.org/10.1007/978-3-319-61633-9_7)

[https://doi.org/10.1007/978-3-319-61633-9\\_22](https://doi.org/10.1007/978-3-319-61633-9_22)

[https://doi.org/10.1007/978-3-319-61633-9\\_23](https://doi.org/10.1007/978-3-319-61633-9_23)

# Author Index

## A

Abdel Fatah, Hala H., [322](#)  
Abdull-Hussain, Rusul Raed, [96](#)  
Adiguzel, Osman, [287](#)  
Ahmed, S.A., [211](#)  
Ahsan, Mohammad Badrul, [197](#)  
Al-Ridha, Ahmed S.D., [96](#)  
Ali, Ayman W., [1](#)  
AL-Kaissi, Zainab A., [96](#)

## B

Badawy, A.A.M., [211](#)  
Bautista, Emil G., [80](#)  
Benešová, Lucie, [46](#)  
Berraha, Youness, [306](#)  
Bhuyan, Prasanta Kumar, [65](#)

## C

Carlton-Carew, Calvin, [228](#)  
Celaya, Manuel, [1](#)  
Cloutier, Clayton, [80](#)

## D

Davis, Mark, [16](#)

## E

Elakhras, A.A., [211](#)  
El-Hakim, Ragaa Abd, [16](#)  
Elshahat, Mohamed R., [335](#)

## F

Faheem, Ahmed F., [80](#)  
Falayi, Thabo, [240](#)

## G

Gupta, Lokesh, [249](#)

## H

Hossain, Zahid, [197](#)  
Huang, Rui, [348](#)

## I

Inés, Beltrán Calvo Gloria, [27](#)

## J

Jena, Subhashree, [65](#)  
Jing, Wu, [121](#)

## K

Kamollertvara, Kong, [145](#)  
Kazmee, Hasan, [262](#)  
Kolay, Prabir K., [185](#)  
Kong, Xiangxing, [348](#)  
Kumar, Sanjeev, [185](#)

## L

Lekha, B.M., [228](#)  
Li, Wu, [121](#)  
Luis, Mercado Pérez José, [27](#)

## M

Makhado, Roshuma, [240](#)  
Mehta, Yusuf, [1](#)  
Mostafa, Abdelzaher E.A., [322](#), [335](#)

## O

Okonta, Felix N., [240](#)  
Ouda, Ahmed S., [130](#)  
Ouf, Mohamed S., [322](#)  
Ouypornprasert, Winai, [145](#)  
Ozer, Hasan, [262](#)

**P**

Panda, Mahabir, [65](#)  
Perraton, Daniel, [306](#)  
Puri, Vijay K., [185](#)

**Q**

Qamhia, Issam, [262](#)  
Qu, Ming-Jie, [274](#)

**R**

Ravi Shankar, A.U., [228](#)

**S**

Sarang, Goutham, [228](#)  
Seleem, M.H., [211](#)  
Sherif, Alaa G., [335](#)  
Sobolev, Konstantin, [80](#)  
Souliman, Mena, [16](#)  
Sulaiman, Salman, [185](#)  
Suresh, G., [249](#)

**T**

Tawhed, Waleed M.F., [335](#)  
Traitsuengtatsana, Narong, [145](#)  
Tutumluer, Erol, [262](#)

**V**

Vaillancourt, Michel, [306](#)  
Valentin, Jan, [46](#)  
Valentová, Tereza, [46](#)  
Venkiteela, Giri, [1](#)

**W**

Walubita, Lubinda, [16](#)  
Wang, Hui-Cong, [274](#)

**Y**

Yamina, Kenouza, [294](#)  
Yao, Jia-Liang, [274](#)  
Yuan, Jian-Bo, [274](#)